# University of Southampton

Faculty of Environmental and Life Sciences

Ocean and Earth Science

**Cold-Water Coral Habitat Mapping in Submarine Canyons**

by

**Tabitha Rosemary Rainbow Pearman**

B.Sc., University of Plymouth  M.Sc., Imperial College London

ORCID ID 0000-0003-4213-4464

Thesis for the degree of Doctor of Philosophy

August 2020

# University of Southampton

## Abstract

Faculty of Environmental and Life Sciences

Ocean and Earth Science

Thesis for the degree of Doctor of Philosophy

Cold-Water Coral Habitat Mapping in Submarine Canyons

by

Tabitha Rosemary Rainbow Pearman

Submarine canyons, are geomorphological features of high ecological importance that require detailed faunal distribution maps and an advanced understanding of the processes influencing faunal distribution to ensure effective management. Faunal patterns are influenced by environmental heterogeneity in water mass characteristics, seafloor characteristics and food availability. The high structural complexity of canyon geomorphology, coupled with canyon-modified hydrodynamics (such as internal tides) are important phenomena that generate environmental heterogeneity in these variables. However, few faunal studies in canyons explicitly include physical oceanographic data (water mass characteristics and hydrodynamics) or fine-scale structural complexity as explanatory variables of faunal distribution and assemblage structure. This thesis applies a range of statistical approaches to a novel interdisciplinary dataset to increase our understanding of what drives faunal patterns, including cold-water corals, over a range of spatial scales using Whittard Canyon, North-East Atlantic as a model system. More specifically, this thesis aims to 1) assess the relative importance of physical oceanography in explaining faunal patterns across the canyon by estimating its effect on predictive modelling performance, 2) investigate if spatial patterns in temporal oceanographic variability induced by the internal tide explain variation in spatial patterns of faunal diversity and assemblage structure on canyon walls, and 3) explore the relationship between structural complexity at various spatial scales and faunal diversity/assemblage within mound provinces occurring on canyon interfluves. The research presented shows how structural complexity and internal tides influence faunal patterns by generating environmental heterogeneity at various spatial scales. Predictive distribution modelling demonstrates that including physical oceanographic data improves predictive accuracy and that the omission of these data can lead to an overestimated cold-water coral occurrence. The thesis demonstrates the importance of the internal tide in generating both spatial and temporal gradients in physical oceanography and food supply that influences faunal patterns in diversity, abundance and assemblage composition. The thesis further illustrates how structural complexity at various scales influences faunal patterns by generating environmental heterogeneity in fine-scale substratum characteristics and at broader-scales interacting with internal tides to concentrate food, both of which act to increase faunal diversity. The thesis also demonstrates that even when broad-scale structural complexity of the terrain is reduced, fine-scale structural complexity may still be present and acting to increase faunal diversity.

# Table of Contents

# Table of Tables

# Table of Figures

Table of Figures

# Research Thesis: Declaration of Authorship

Print name: Tabitha Rosemary Rainbow Pearman

Title of thesis: Cold-Water Coral Habitat Mapping in Submarine Canyons

I declare that this thesis and the work presented in it are my own and has been generated by me as the result of my own original research.

I confirm that:

1. This work was done wholly or mainly while in candidature for a research degree at this University;
2. Where any part of this thesis has previously been submitted for a degree or any other qualification at this University or any other institution, this has been clearly stated;
3. Where I have consulted the published work of others, this is always clearly attributed;
4. Where I have quoted from the work of others, the source is always given. With the exception of such quotations, this thesis is entirely my own work;
5. I have acknowledged all main sources of help;
6. Where the thesis is based on work done by myself jointly with others, I have made clear exactly what was done by others and what I have contributed myself;
7. Parts of this work have been published as:-

Pearman, T.R.R., Robert, K., Callaway, A., Hall, R., Lo Iacono, C., Huvenne, V.A.I. (2020) Improving the predictive capability of benthic species distribution models by incorporating oceanographic data – towards holistic ecological modelling of a submarine canyon, *Progress in Oceanography*, 18, 4102338.

Signature: ..... Date: August 2020

# Acknowledgements

This work was funded by NERC (National Environmental Research Council) through the SPITIRE (Southampton Partnership for Innovative Training of Future Investigators Researching the Environment) Doctoral Training Partnership (DTP) studentship grant NE/L002531/1 and The National Oceanography Centre, UK, together with the CASE partner Centre for Environment, Fisheries and Aquaculture Science (CEFAS).

I would like to thank my supervisors, Dr. Veerle Huvenne, Dr. Alex Callaway, Dr. Robert Hall, Dr. Claudio Lo Iacono and Dr Antony Jenson for their support, guidance and encouragement over the past three and a half years. I thank my panel chair Dr. Philip Fenberg for his advice throughout. I also thank Dr. Katleen Roberts for her guidance and data and Dr. Tom Ezard for introducing me to the world of statistical modelling in R!

Over the course of this PhD, I have had the opportunity to travel and work in a variety of places and would like to thank Dr. Ashley Rowden and Dr. Malcom Clark for hosting me during my research placement at NIWA, New Zealand.

I am extremely grateful for the PhD community we have at NOC, where I have made many friendships through the years. I am also grateful to my friends from home (Cornwall) and Norfolk. In particular I am thankful for the encouragement, friendship and support given by Koko Kunde, Christina Wood, Emmie Broad, David Price, Guillem Corbera, Michael Faggetter, Louisa Fennelly, Helen Johnson, Tammy Noble-James, Gemma Nichols, Lynsey Nichols, Jessica Wilson and Billy Barnes.

I would like to thank my partner, Ryan Irvine and my parents, Stephanie and Peter Pearman for cultivating my love of nature and always believing in me. To my mum for her support throughout my career, writing to radio 4 shows to get advice on marine biology and always thinking of ways to help. To my dad, for opening my eyes to the wonderment of the sea, inspiring me with his stories to explore the world and encouraging my lifelong passion for learning by always having a book on any subject.

And it is in memory of my dad, Peter Pearman that I dedicate this thesis.

“Sew a button in that!”

# Definitions and Abbreviations

ROV: Remotely Operated Vehicle

AUV: Automated Underwater Vehicle

GLM: Generalised Linear Model

GAM: Generalised Additive Model

RDA: Canonical Redundancy Analysis

MBES: Multibeam echosounder

SSS: Sidescan Sonar

AIC: Akaike's Information Criterion

AUC: Area Under the Receiver operating Curve

VIF: variance inflation factor

ANOVA: Analysis of variance

ANOSIM: Analysis of similarities

SIMPER: Similarity percentage analysis

nMDS: non-metric Multi-Dimensional Scaling

# Chapter 1 Introduction

The deep sea is the most extensive and remote biome on Earth (Thistle, 2003; Danovaro et al., 2014). Submarine canyons, are important geomorphological features that connect the deep sea to coastal and shelf environments, make disproportionate contributions to deep-sea processes (Allen and Durrieu de Madron, 2009; Huvenne and Davies, 2014; Puig et al., 2014; Amaro et al., 2016; Fernandez-Arcaya et al., 2017) and provide key ecosystem services (Yoklavich et al., 2000; Epping et al., 2002; Canals et al., 2006; Masson et al., 2010; Fernandez-Arcaya et al., 2017). Canyons are ecologically important because they support high biological diversity, including vulnerable marine ecosystems such as cold-water coral habitats (De Leo et al., 2010; Miller et al., 2015; Fernandez-Arcaya et al., 2017; van den Beld et al., 2017). The steep canyon walls provide refuge for cold-water corals (Huvenne et al., 2011) that coincide with local peaks in biodiversity (Robert et al., 2017). Despite their ecological importance, canyons face threats from anthropogenic stressors, such as fishing (Martín et al., 2014b; Puig et al., 2012), pollution (Kane et al., 2020) and mining (Ramirez-Llodra et al., 2015). Effective management of canyons and the features of conservation interest that they support requires an increased understanding of the processes driving faunal distributions from which accurate faunal distribution maps can be made (Guisan and Zimmermann, 2000; Huvenne and Davies, 2014). However, due to the technological difficulties of sampling remote and complex canyon environments our understanding of these processes is limited (Huvenne and Davies, 2014). Environmental heterogeneity has been proposed to be a major driver of faunal patterns that contributes to driving the high biodiversity observed in canyons (Levin et al., 2010; 2001; Cunha et al., 2011; Fabri et al., 2017; Chauvet et al., 2018). However, there is a lack in our understanding of how environmental heterogeneity acting at different spatial scales influences spatial patterns of deep-sea fauna. Structural complexity and canyon-modified hydrodynamics are key phenomena associated with increased environmental heterogeneity in canyons (Wang et al., 2008; Lee et al., 2009; Liu et al., 2010; Levin and Sibuet, 2012; Amaro et al., 2015; 2016; Wilson et al., 2015b; Hall et al., 2017; Ismail et al., 2018). Yet, few studies looking at environmental drivers of faunal distributions and assemblages explicitly include physical oceanographic data (water mass characteristics and hydrodynamics) (Liao et al., 2017; Bargain et al., 2018) or finer-scale structural complexity as explanatory variables (Robert et al., 2017; Price et al., 2019). Consequently, there is a need to conduct research to further advance our understanding of how these environmental factors influence faunal patterns in canyons. To address this knowledge gap this thesis applies a range of statistical approaches and novel datasets to increase our understanding of what drives epibenthic megafaunal patterns, including cold-water corals, over a range of spatial scales using Whittard Canyon, North-East Atlantic as a model system.

## 1.1 Background

### 1.1.1 The deep sea

The deep sea, comprising the seabed and water column below 200 m water depth, represents the largest biome on earth (Thistle, 2003), covering >60 % of the earth's surface (Thistle, 2003; Smith et al., 2009; Danovaro et al., 2014). The deep sea is considered the last natural frontier (Ramirez-Llodra et al., 2010; Danovaro et al., 2014), where life unfolds in total darkness, under high hydrostatic pressures and far from the often productive surface waters above (Danovaro et al., 2014). Yet, despite the environmental extremities, the deep sea hosts a variety of unique and vulnerable habitats, each with specific biotic and abiotic characteristics (Ramirez-Llodra et al., 2010).

The study of deep-sea habitats has been intrinsically linked to technological advancements in marine robotics and ship borne acoustics (Danovaro et al., 2014; Huvenne and Davies, 2014). Research has progressed from the first lead weighted hand lines that were deployed to determine water depths, to sophisticated multibeam echosounders capable of generating large swathe bathymetry datasets (Wilson et al., 2007), and remotely operated vehicles (ROVs) capable of sampling and relaying images from thousands of meters below the sea surface (Johnson et al., 2013). These technological advancements have enabled the ever more precise characterisation of fauna and associated environmental conditions. However, so far only 5 % of the deep sea has been surveyed remotely with less than 0.01 % sampled and studied in any detail (Ramirez-Llodra et al., 2010). As a result, the deep sea is considered the least studied biome (Ramirez-Llodra et al., 2010) and questions remain regarding the habitats that occur in the deep sea and the processes that determine their spatial distribution.

The deep sea encompasses the continental slope (200 – 3000 m), continental rise (3000 – 4000 m) abyssal zone (4000 – 6000 m) and hadal zone (>6000 m). Originally the deep sea was thought to be inhospitable and incapable of supporting life, however, with technological advancements aiding increased deep-sea sampling it is now apparent that the deep sea supports a diversity of life (Danovaro et al., 2014) and several large scale biological patterns have been observed (Carney, 2005).

Biogeographical zones have been proposed that relate common faunal assemblages of shared evolutionary history to regions that capture large scale variation in physical oceanography, productivity and historical events (Watling et al., 2013). Additionally, large scale bathymetric patterns in faunal assemblage (Carney et al., 1983; 2005), diversity (Rex, 1973; 1983) and abundance (Rowe, 1983) have been documented.

Depth zonation of deep-sea fauna, whereby distinct faunal assemblages separated by transitional zones occur at specific depths, was first described during the Challenger expeditions of the 19$^{th}$

century (Agassiz, 1888; Murray, 1895). These early works described a shelf assemblage separated from a distinct abyssal assemblage by a transitional zone (Murray and Hjort, 1912). Technological advancements in the mid-20$^{th}$ century enabled the integration of acoustic data with faunal sampling facilitating the accurate characterization of these zones. However, there was debate concerning the rationale for delimiting the boundaries (Ekman, 1953; Bruun, 1957; Menzies, 1973) until a review by Carney et al. (1983) showed general consistency in the occurrence of shelf fauna to just beyond the shelf break, followed by a transitional zone between 300 - 1700 m with the abyssal zone starting at 1400 - 1700 m. Further research has confirmed the prevalence of depth zonation (Gage and Tyler, 1999; Howell et al., 2002; Carney, 2005; Olabarria, 2005) with transitional zones marking the depth zonation of fauna documented between the shelf and slope fauna at ~200 m - 1000 m, and between the slope and abyssal fauna at 2000 m - 3000 m (Carney, 2005; Rex and Etter, 2010). Depth zonation has been attributed to competition (Rowe and Menzies, 1969) and gradients in environmental variables (i.e. light, temperature, pressure, oxygen and food availability) that co-vary with depth and limit faunal distributions due to physiological tolerances of fauna (Rowe and Menzies, 1969; Rex, 1976; Lampitt et al., 1986; Howell et al., 2002; Carney, 2005; Olabarria, 2005; Wei et al., 2010; Brown and Thatje, 2014).

Large scale bathymetric trends in deep-sea biodiversity have also been described that parallel depth gradients in pressure, physical oceanography (hydrodynamics and water mass characteristics such as temperature, salinity, oxygen etc.), food availability and seafloor characteristics (Levin et al., 2001). Negative diversity-depth gradients have been attributed to reducing productivity with depth (Rex et al., 2005a; Stuart and Rex, 2009; Brault et al., 2013a; Hernández-Ávila et al., 2018) and metabolic constraints of decreasing temperature (O'Hara and Tittensor, 2010; Yasuhara and Danovaro, 2016) and increasing hydrostatic pressure with depth (Brown and Thatje, 2014). Decreased diversity with depth has also been explained by theories of 'extinction and replacement' whereby deep-sea fauna became extinct as a result of catastrophic anoxic events, with subsequent invasion and radiation of shallow-water species into the deep (Wilson, 1999; Rogers et al., 2000). On the other hand, studies based upon abyssal molluscs from the North Atlantic suggest that the continental margin and abyss constitute a source-sink system in which many abyssal populations are maintained by immigration from the bathyal zone (Rex et al., 2005b).

Diversity-depth gradients with unimodal patterns peaking at mid depths are common in deep-sea studies of the North-Atlantic (Rex, 1973; Rex, 1983; Carney, 2005). The peaks in species diversity have been attributed to the high species turn over associated with transitional zones (Brault et al., 2013b) that occur at similar depths ( ~1000 m and 3000) and mark the depth zonation of fauna on the continental slope (Carney, 2005; Rex and Etter, 2010). Additionally, unimodal diversity patterns have been attributed to environmental gradients in productivity and food availability (Rex, 1981), temperature (O'Hara and Tittensor, 2010; Yasuhara and Danovaro, 2016), disturbance, increased substratum heterogeneity and topographic complexity (Levin et al., 2001), together with source- sink

dynamics of abyssal fauna (Rex et al., 2005b; Brault et al., 2013b) and the evolutionary history of faunal assemblages with depth (Etter et al., 2005; Stuart and Rex, 2009). It is likely that these processes interact at varying spatial and temporal time scales to generate the patterns of depth zonation and resultant diversity-depth gradients observed in the deep sea (Levin et al., 2001).

Unimodal gradients are not universal and can vary between taxa and regions (Stuart and Rex, 2009). Where unimodal patterns of diversity are absent it is often attributed to past historical events (Danovaro et al., 2010) or where depth gradients of oceanographic conditions are not consistent, for example where oxygen minimum zones occur at specific depths (Levin et al., 2001; Rex and Etter, 2010). Additionally, large geomorphologic features such as trenches, seamounts and canyons generate further heterogeneity in environmental conditions, irrespective of depth (Levin et al., 2010; Fanelli et al., 2018). The increased structural complexity provided by the geomorphological features effects hydrodynamics, food availability and the spatial distribution of substratum that in turn modify bathymetric trends in biodiversity (Levin et al., 2001; 2010; Levin and Sibuet, 2012; Fernandez-Arcaya et al., 2017).

Complex features such as ridges, seamounts and canyons are associated with increased habitat heterogeneity (i.e. substratum type) and as a result increased biodiversity (Levin et al., 2010; Robert et al., 2015; Victorero et al., 2018). Hutchinson and MacArthur (1959) proposed that organisms were adapted to an environmental niche, so that a greater variety of environmental conditions (environmental heterogeneity) at a site would enable more species to coexist resulting in high biodiversity. MacArthur and MacArthur (1961) took the next step by relating species diversity to the number of niches associated with the structural complexity of a location. In marine settings, intertidal studies from rocky shores demonstrated that structural complexity can also influence diversity by affecting species interactions (predation and competition) by providing refuge and spatial separation between organisms (Menge and Sutherland, 1976; Menge et al., 1985; Hixon and Menge, 1991). Rocky shore studies also showed that increased structural complexity may also increase the available surface for sessile species, so that increased diversity is a function of the species–area relationship (Heck and Wetstone, 1977; Matias et al., 2010). However, it has also been shown that diversity in structurally complex environments increase regardless of surface area (Beck, 2000; Taniguchi et al., 2003; Warfe et al., 2008). Although the mechanisms behind the observed positive relationship between structural complexity and diversity are unresolved (Kovalenko et al., 2011), it is likely that the influence of these mechanisms in generating the observed relationship depends on the scale of study and relative spatial ‘patchiness’ of the structural complexity (Tews et al., 2004).

Positive relationships between structural complexity and species richness and abundance has been demonstrated in a number of settings (Tews et al., 2004; Kovalenko et al., 2011) including terrestrial (Lawton, 1983), lentic (fresh water) (Downes et al., 1998; Willis et al., 2005; Verdonschot et al., 2012) and marine settings such as mangroves (Crook and Robertson, 1999; Bond and Lake, 2003; O’Connor, 1991), rocky shores (Menge et al., 1985; Dean and Connell, 1987; Loke and Todd, 2016;

Menge and Sutherland, 1976), seagrass beds (Heck and Wetstone, 1977; Hyman et al., 2019), mussel beds (Seed, 1996; Borthagaray and Carranza, 2007) and shallow coral reefs (Risk, 1972; Luckhurst and Luckhurst, 1978; Graham and Nash, 2013). In the deep sea positive relationships have been found between species diversity and structural complexity provided by cold-water corals (Buhl-Mortensen et al., 2010; Price et al., 2019; Robert et al., 2017; Robert et al., 2019) and sponges (Bell and Barnes, 2001; Beazley et al., 2013) and by that provided by complex geomorphological structures at broader spatial scales (Buhl-Mortensen et al., 2012; Levin et al., 2010; Levin et al., 2001; Ismail et al., 2018) .

In the deep sea biodiversity hotspots often coincide with complex geomorphological features, such as canyons (De Leo et al., 2010; Vetter et al., 2010), ridges and seamounts (Clark et al., 2010; Morato et al., 2010). Early theories proposed high endemism as driving observed peaks in biodiversity associated with complex features such as seamounts (de Forges et al., 2000). However, increased sampling now indicates that deep-sea genera, and often species, are widely distributed, regardless of habitat (Howell et al., 2010; McClain and Hardy, 2010; Priede et al., 2013) and that peaks in diversity are driven by high species turnover of regionally shared species pools (Victorero et al., 2018). The observed depth zonation of many fauna (Carney et al., 1983; 2005) coupled with higher species turnover (Longhurst, 1998) and greater genetic differentiation along bathymetric gradients as opposed to horizontal distances (Zardus et al., 2006) suggests that bathymetric gradients in environmental conditions constrain species vertical ranges relative to horizontal distances. The result is that fauna on steep slopes will have smaller geographical distributions, which will promote higher species turnover in complex geomorphological environments compared to abyssal plains where environmental conditions are relatively constant over great distances and fauna have broader geographical distributions (McClain and Hardy, 2010).

The increased structural complexity of large geomorphological features is also believed to support more species by increasing environmental heterogeneity (Raymore, 1982; Levin et al., 2010; Ismail et al., 2018). Additionally local hydrodynamics can be modified by the complex topography (Boehlert, 1988; Khripounoff et al., 2001; Laurent and Thurnherr, 2007; White et al., 2007; Chen et al., 2014; Kämpf, 2018) which can result in modified larval dispersal (Mullineaux and Mills, 1997; Clavel-Henry et al., 2019; Metaxas et al., 2019; de Forges et al., 2000), increased upwelling (Kämpf, 2007; Laurent and Thurnherr, 2007; Chen et al., 2014; Clément and Thurnherr, 2018; Laurent et al., 2020), productivity (Hasegawa et al., 2009; Leitner et al., 2020) and lateral transport of surface derived organic matter (White et al., 2007; Harris and Whiteway, 2011; Wilson et al., 2015b; Turnewitsch et al., 2016) that can modify depth-productivity gradients so that they differ from the open slope (López et al., 2012; Turnewitsch et al., 2016). As a result, unlike the biogeographic patterns of the open slope that often exhibit unimodal diversity gradients, diversity-depth gradients associated with complex topographic features can be more variable (Genin et al., 1986; Bett, 2001;

McClain et al., 2010; Cunha et al., 2011; Clark and Bowden, 2015; Gambi and Danovaro, 2016; Morgan et al., 2019)

Increasingly submarine canyons are being advocated as deep-sea biodiversity hotspots (De Leo et al., 2010). Like seamounts and ridges, canyons are structurally complex and encompass large depth ranges and associated environmental gradients in physical oceanography and their complex topography modifies local hydrodynamics disrupting depth-productivity gradients (Martín et al., 2006; DeGeest et al., 2008; López et al., 2012; Lopez-Fernandez et al., 2013) resulting in bathymetric faunal patterns that contradict broader biogeographic patterns observed from less complex open slope (Maciolek et al., 1987; Duineveld et al., 2001; Gunton et al., 2015b; Covazzi Harriague et al., 2019). Consequently, improving our understanding of what drives faunal distributions and biodiversity in canyons provides valuable insight to contribute toward our understanding of deep-sea biodiversity patterns and ecology.

### 1.1.2 Submarine canyons

#### 1.1.2.1 Ecological role and conservation importance of canyons

Submarine canyons are ubiquitous features of the continental margins, with over 9000 large canyons estimated to occur globally, covering 11.2 % of the continental slope and 1.21 % of the seafloor (Harris et al., 2014). Despite their relatively small spatial extent, canyons make a disproportionate contribution to deep-sea processes by acting as conduits between the shelf and deep-sea (Allen and Durrieu de Madron, 2009; Huvenne and Davies, 2014; Puig et al., 2014; Amaro et al., 2016; Fernandez-Arcaya et al., 2017) and by providing major sources of heterogeneity in continental margin settings (Levin et al., 2001; 2010; Schlacher et al., 2007; 2010; De Leo et al., 2010).

Submarine canyons are important deep-sea features that substantially contribute to key ecosystem services via their regulation of cross-shelf exchanges, nutrient cycling, geophysical processing and carbon sequestration and storage (Epping et al., 2002; Canals et al., 2006; Masson et al., 2010). Canyons can be deep-sea biodiversity hotspots (Kelly et al., 2010) that promote regional species and habitat diversity, provide nursey grounds for economic species, refuge for vulnerable marine ecosystems (VMEs) (Schlacher et al., 2007; Huvenne et al., 2011; Davies et al., 2014) and support economically important fisheries (Yoklavich et al., 2000; Sanchez et al., 2013). As such, canyons represent “keystone structures” in the deep sea (Vetter et al., 2010) and meet criteria of ecologically or biologically significant marine areas (CBD, 2009). Consequently, furthering our understanding of canyon systems links with UN Millennium sustainable development goal 14, to ensure sufficient food supply and a healthy physical marine environment for the promotion of human wellbeing (MA, 2005).

Canyons have been proposed as priority areas for conservation on many continental margins (Davies et al., 2014). Canyons are listed as topographical features that may support VMEs (FAO, 2009), which UN member states have an obligation to identify, map and protect from anthropogenic activities such as trawling (UNGA, 2006; FAO, 2008). Cold-water coral habitats are listed as VMEs and also occur under regional protection initiatives, including deep-sea habitat types of threatened and declining species and habitats listed under Annex V of the OSPAR (OSPAR, 2008) and Annex 1 habitats under the Habitats Directive (92/43/EEC, 1992).

#### 1.1.2.2 The canyon environment

##### 1.1.2.2.1 Canyon formation and geomorphology

Submarine canyons are steep sided sinuous valleys with "V" or, "U" shaped profiles that incise continental margins (Shepard, 1981; Pratson et al., 2007; Amblas et al., 2018) (Figure 1.1). Canyons form through either the head-ward erosion of the continental shelf and slope by retrogressive sediment failures or, by down slope extension caused by erosive processes associated with turbidity currents and sediment laden gravity flows (Shepard, 1981; Pratson et al., 2007; Amblas et al., 2018). As a canyon evolves adjacent canyons may join to form dendritic canyon systems (Harris and Whiteway, 2011). The characteristics of a canyon are largely attributed to the activity of the margin that the canyon incises and its proximity to riverine inputs (Harris and Whiteway, 2011). Harris and Whiteway (2011) have used these associations to classify canyons into three types: (1) canyons that incise a shelf and have a head that is clearly connected to a major river system, and evolve by erosive turbidity flows from fluvial, shelf and upper slope sources, (2) canyons that incise a shelf, but do not have a clear connection to a river system, but also evolve by erosive currents, and (3) blind canyons incising the continental slope that evolve by slumping and slope failure processes.

Axial profiles can vary between canyons, but in general canyons are characterised by steep and complex topography comprised of vertical walls, outcrops, ridges, gullies and crevices (Figure 1.1) (Mortensen and Buhl-Mortensen, 2005; De Leo et al., 2014). The complex topography arises from canyons experiencing and exhibiting features of both erosion and deposition (Canals et al., 2006; Arzola et al., 2008). Differential erosion can generate disparity in the morphology of opposing flanks (Mortensen and Buhl-Mortensen, 2005; Van Rooij et al., 2010; Fabri et al., 2014) and influence the spatial distribution of substrata, whereby erosional features such as vertical walls and headwall scarps are associated with bedrock (Mortensen and Buhl-Mortensen, 2005; Stewart et al., 2014), while soft substrata dominate flatter areas that experience depositional regimes.

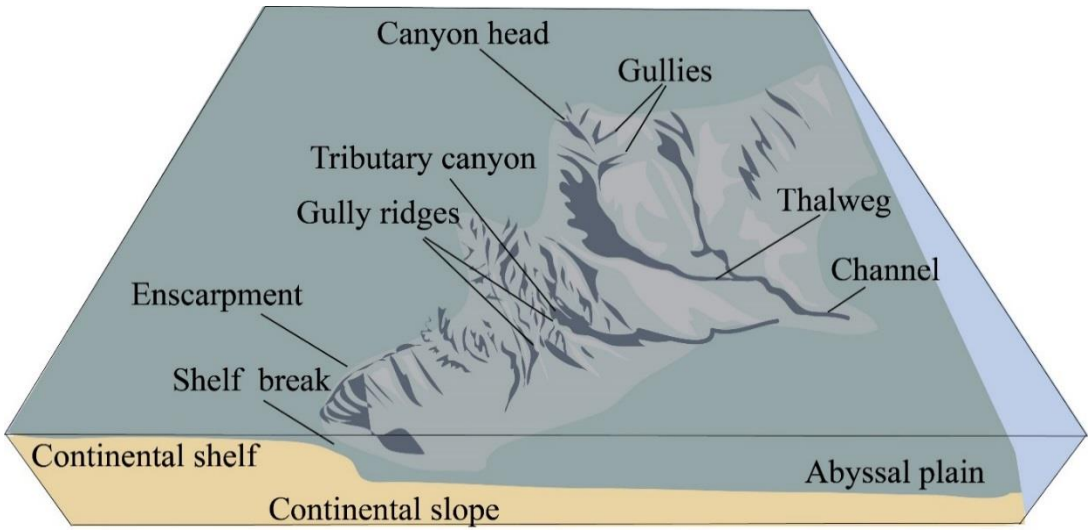


Figure 1.1 Schematic of a dendritic submarine canyon The canyon incises the continental slope and shelf to form a pathway between the shelf and deep-sea. Adapted from Amblas et al. (2018).

#### 1.1.2.2.2 Canyon-modified hydrodynamics

Canyon topography can modify local circulation and hydrodynamics (Chen et al., 2014; Hall et al., 2014; Kämpf, 2018). The incising canyon distorts the morphology of the continental margin, altering the along-slope current flow, which facilitates the exchange of water between the shelf and deep-sea (Allen and Durrieu de Madron, 2009; Saldías and Allen, 2020). Under certain conditions, the canyon topography can restrict the current flow resulting in modified vertical vorticity, which, depending on the direction of the current, leads to either locally enhanced up- (Kämpf, 2007; Chen et al., 2014) or downwelling (Allen and Durrieu de Madron, 2009). In some circumstances, under stratification, the interaction of the current flow with the canyon rim can lead to the formation of a cyclonic eddy over the canyon (Kämpf, 2007; Allen and Hickey, 2010). Additionally, surface (barotropic) tides interacting with the steep canyon topography convert some of their energy into internal (baroclinic) tides (Allen and Durrieu de Madron, 2009; Hall et al., 2017).

##### 1.1.2.2.2.1 Internal tides

Internal waves occur when there is a disturbance between layers of different density that the water column tries to counteract, forming an oscillation or ‘wave’. Internal waves with tidal frequencies are termed internal tides (Wunsch, 1975). Internal tides interact with complex canyon topography causing enhanced current speeds, and via their reflection and wave breaking, increased mixing and resuspension of material (Lee et al., 2009; Hall et al., 2017; Aslam et al., 2018).

Internal wave–topography dynamics are influenced by the characteristics of the internal wave, the density structure of the water column through which it propagates and the angle of the slope with which it comes into contact (Hall and Carter, 2011; Hall et al., 2014). The bathymetric slope

criticality to the dominant semi-diurnal internal tide (α) provides an indication of how up-slope propagating internal tides coming into contact with slopes will behave. α is the ratio of the topographic slope to the internal wave characteristic slope, $\alpha = \frac{\partial H/\partial x}{[(\omega^2 - f^2)/(N^2 - \omega^2)]^{\frac{1}{2}}}$

Where: $x$ is across-slope distance (m), $H$ is the total depth (m), ω is the angular frequency of the wave (Hz), $f$ is the inertial frequency (Hz), and $N$ is the buoyancy frequency (Hz). A supercritical angle (α >1) can result in the up-slope propagating wave being reflected back down-slope toward the canyon floor, when subcritical (α <1), the wave can be focussed toward the head of the canyon and when near-critical (α ≃ 1), the wave can become trapped resulting in wave breaking (Figure 1.2) (Hall et al., 2014). In this way, submarine canyons may also trap internal waves originating from outside the canyon, reflecting their energy toward the canyon floor (Gorden and Marshall, 1976) and head (Hotchkiss and Wunsch, 1982) as the waves come into contact with the sloping topography.

Internal tides can be prevalent within canyons due to their incision of the continental margin that facilitates interactions with ocean dynamics, their depth ranges that incorporate density gradients of the water column and their steep complex topography that promotes internal tide generation, reflection and wave breaking.

Canyon enhanced hydrodynamics, including internal tides, are important in generating spatio-temporal environmental heterogeneity throughout the canyon. In canyons, tidal current direction and speed, physical oceanography (i.e. temperature, oxygen, salinity) and areas of increased suspended material (nepheloid layers) have been observed to fluctuate at semidiurnal tidal frequencies of the internal tide (de Stigter et al., 2007; Wang et al., 2008; Lee et al., 2009; Liu et al., 2010; Amaro et al., 2015; 2016; Addamo et al., 2016; Hall et al., 2017).

Internal tides drive turbulent mixing (Lee et al., 2009; Wilson et al., 2015b; Hall et al., 2017; Aslam et al., 2018) which modifies gradients of physical oceanography (i.e. temperature, density and oxygen). Additionally, the propagation of the internal tide along a canyon causes vertical isopycnal displacement ranging from 10s to 100s m, which can generate temporal variability in physical oceanographic conditions (Wang et al., 2008; Hall et al., 2017).

Internal wave driven turbulent mixing is associated with increased concentrations of particulate organic matter (POM) and nepheloid layer production (Wilson et al., 2015b; Hall et al., 2017; Aslam et al., 2018). Nepheloid layers are layers with enhanced levels of suspended material (including POM) (Demopoulos et al., 2017). Spatial distributions of nepheloid layers have been linked to the semidiurnal frequencies of internal tides in a number of canyons. For example in Nazaré Canyon, increases in bottom water turbidity appear synchronised with increases in current speed at the semidiurnal frequency of the internal tide (de Stigter et al., 2007), in Gaoping Canyon characteristics of the benthic nepheloid layer, including thickness, flow and composition fluctuated at the semidiurnal frequency of the internal tide (Wang et al., 2008) and in Whittard Canyon, nepheloid

layer distribution exhibited vertical modulation in the water column at the semidiurnal frequency of the internal tide (Hall et al., 2017).

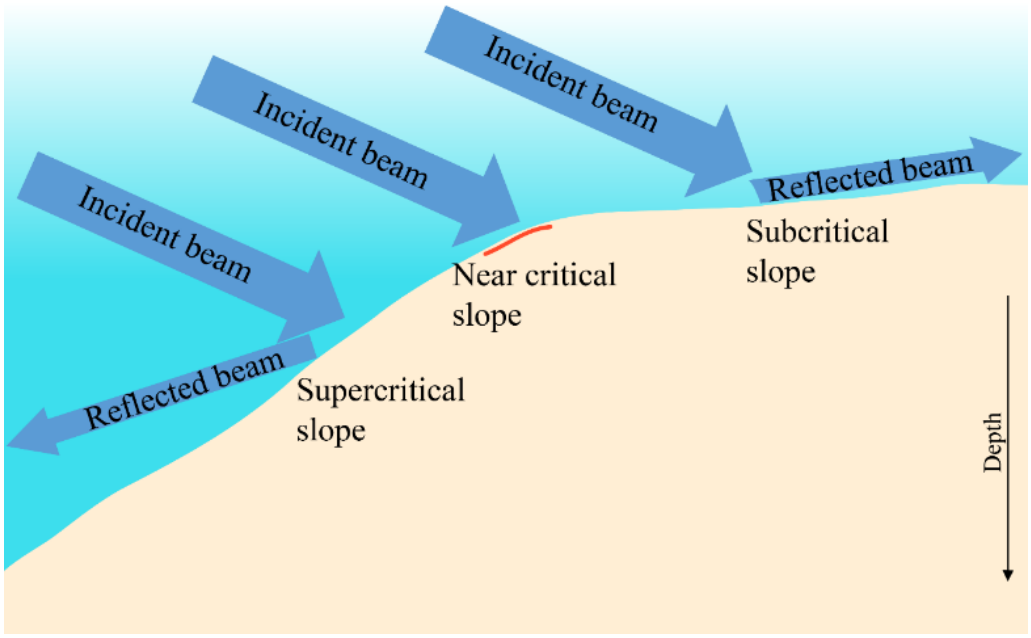


Figure 1.2 Schematic showing different scenarios of the bathymetric slope criticality to the dominant semi-diurnal internal tide (α). If the angle of the slope is larger than that of the propagating wave (α >1), supercritical reflection occurs and the wave is reflected downwards. If the angle of the slope is less than that of the propagating wave (α <1), subcritical reflection will occur and the wave will be propagated up toward the canyon head. When the angle of the slope and the propagating wave are near equal (α ≃ 1) the wave may become trapped and break. Adapted from Lamb (2014) and Pratson et al. (2007).

#### 1.1.2.2.3 Canyon mediated cross shelf exchange

The canyon incision of the continental margin forms a pathway between the shelf and deep-sea. The movement of material along the canyon pathway facilitates cross-shelf exchange (Allen and Durrieu de Madron, 2009). The movement of material can be both down- and up-canyon and is largely mediated by the canyon modified hydrodynamics that are important in keeping material in suspension (Lopez-Fernandez et al., 2013; Lo Iacono et al., 2020). Bottom current speeds of 40 cm $s^{-1}$ to 70 cm $s^{-1}$, capable of transporting finer grained material, as well as coarse grained material at higher speeds, have been recorded from canyons (de Stigter et al., 2007; Lopez-Fernandez et al., 2013) and evidence that internal tides may mediate the up-canyon transport of material has been presented (Wilson et al., 2015b). Larger material is more often transported down-canyon via turbidity currents and gravity flows, comprising a high sediment load that increases the density of the flow causing its rapid descent down the canyon axis (Puig et al., 2014). Turbidity currents can be triggered by excessive riverine discharges (Arzola et al., 2008), the rapid resuspension of sediments stored on

the shelf (Palanques et al., 2006) by processes such as storms (Canals et al., 2006), or tectonic activity causing slope failures and mass wasting (Heezen and Ewing, 1952; Mountjoy et al., 2018).

The remobilisation of material, including nutrients via upwelling and internal tides, promotes increased surface productivity toward canyon heads (Harris and Whiteway, 2011). Canyon enhanced hydrodynamics then facilitate the rapid delivery of this organic matter, from the surface to depth (Allen and Durrieu de Madron, 2009; Campanyà-Llovet et al., 2018). The rapid transportation of material to depth is important in the sequestration and storage of carbon (Masson et al., 2010). It also reduces exposure time to microbial breakdown and remineralisation, providing high quality POM to the deep sea benthos (Masson et al., 2010; Campanyà-Llovet et al., 2018), often concentrating in nepheloid layers (Wilson et al., 2015b; Demopoulos et al., 2017).

The funnelling effect of the canyon generally results in higher particle fluxes recorded from within canyons, compared to that at comparative depths on the open slope (Martín et al., 2006; DeGeest et al., 2008; López et al., 2012; Lopez-Fernandez et al., 2013). The flux of organic material into the canyon can be affected by seasonal inputs from riverine discharges (where canyons are connected to rivers), plankton blooms, aeolian inputs of mineral dust plus the resuspension and remobilisation of material by dense-shelf water cascading, storms and trawling (Lopez-Fernandez et al., 2013; Arjona-Camas et al., 2019). The relative influences of these processes on the flux of organic material into the canyon is often dependent on whether the canyon occurs on a passive or active margin.

The movement and spatial distribution of organic material through the canyon is influenced by hydrodynamics (Amaro et al., 2015; 2016; De Leo et al., 2010), canyon topography (Campanyà-Llovet et al., 2018) and benthic utilisation (Amaro et al., 2010). Together these processes interact across multiple scales to generate spatio-temporal heterogeneity in the quantity and quality of organic material in the canyon (Amaro et al., 2015; Campanyà-Llovet et al., 2018). In general, there is a spatial trend of decreased quality of organic matter with depth, which is consistent with that on the slope. However, local peaks occur where canyon topography and hydrodynamics facilitate the rapid delivery of surface derived material to depth (Demopoulos et al., 2017; Campanyà-Llovet et al., 2018) or where material accumulates as branches coalesce, sustaining high quantities of lower quality organic material at depth.

#### 1.1.2.3 Faunal patterns in canyons

Canyons support a diverse range of habitats. Here, "habitat" refers to the spatial extent over which a particular species assemblage and its associated environment (physical and chemical) occurs (MESH, 2008; Costello, 2009; Brown et al., 2011) and "assemblage" refers to a discrete group of reoccurring species that share a common attribute of habitat or taxonomic similarity and occur together in space and time (Pyron, 2010; Stroud et al., 2015).

The distribution of fauna and assemblages across canyon settings tends to be patchy, leading to high beta and regional diversity (Conlan et al., 2015; Robert et al., 2015; Covazzi Harriague et al., 2019). Broad-scale bathymetric trends in fauna and assemblages are commonly observed (Duineveld et al., 2001; Buhl-Mortensen et al., 2010; Cunha et al., 2011; Baker et al., 2012; Braga-Henriques et al., 2013; Currie and Sorokin, 2013; Kenchington et al., 2014; Conlan et al., 2015; Sigler et al., 2015; Pierdomenico et al., 2016) and often relate to distance along the canyon axis (Kelly et al., 2010). The bathymetric trends in fauna and assemblages vary between and within canyons and according to the size and life strategy of the fauna sampled. For example, Cunha et al. (2011) found increased species richness of macro- infauna was expected from the upper and middle sections of the Cascais Canyon, while lower species richness was expected from the middle sections of the Nazaré and Setúbal Canyons. On the other hand, a review of canyons within the Gulf of Maine by Kelly et al. (2010) reported highest diversity of combined faunal sizes, in the middle section of the canyon. Despite variable bathymetric trends, generally infaunal diversity is observed to decrease in areas of steep complex topography (Conlan et al., 2015) and epifaunal diversity is observed to increase in areas of steeper hard substratum and decrease in areas of soft substrata encountered on gentler slopes (Robert et al., 2015). For both epi and infauna low diversity and biomass is observed on the canyon axis (Cunha et al., 2011; Paterson et al., 2011) that is generally less hospitable due to the high disturbance associated with the movement of sediments along the axis (Johnson et al., 2013).

In the deep sea there is a general bathymetric trend of decreasing biomass or abundance with depth (Rex et al., 2006). Similarly, a decline in biomass with depth has been observed in megafauna in Bonney and du Couedic Canyons (Currie and Sorokin, 2013) and in meiofauna in the Western branch of Whittard Canyon (Gambi and Danovaro, 2016). However, this trend was not consistent across all the branches of Whittard Canyon, where instead no clear pattern was observed (Gambi and Danovaro, 2016), which is consistent with meiofaunal studies from Blanes Canyon (Romano et al., 2013). Further still, studies of macro- and megafauna show a different bathymetric trend whereby increased biomass or abundance is observed at intermediate depths. For example, in Whittard Canyon there are peaks in biomass at 2715 m for mega- and macro- infauna (Duineveld et al., 2001) and multiple peaks at ~1200, 2200, 3000 and 3700 m in abundance for epibenthic megafauna (Robert et al., 2015), while in Barkely Canyon epibenthic peaks in megafauna abundance occur at 300 and 2000 m. Peaks in macro- infauna abundance are reported in Nazaré Canyon at 2894 m (Cúrdia et al., 2004) and at 3461 – 3522 m (Cunha et al., 2011), in Cascais Canyon at 3199 – 3219 m, in Setúbal Canyon at 3224 – 3275 m (Cunha et al., 2011) and in Baltimore and Norfolk canyons at 800 - 900 m (Robertson et al., 2020).

Studies comparing faunal assemblage, richness and abundance at comparative depths between canyons and adjacent slope have reported inconsistent results. Higher species richness has been reported in canyons compared to the slope for epibenthic megafauna, both increased and decreased species richness and abundance for macro- infauna (Maciolek et al., 1987; Duineveld et al., 2001;

Gunton et al., 2015b; Covazzi Harriague et al., 2019) and either increased, decreased or similar species richness and abundance for meiofauna (Ingels et al., 2009; Gambi and Danovaro, 2016; Bianchelli and Danovaro, 2019; Carugati et al., 2019).

Macro- infaunal assemblages sampled from canyons are characterised by a high representation of Annelids and Arthropods (Cunha et al., 2011; Conlan et al., 2015; Campanyà-Llovet et al., 2018). Assemblages can vary between branches (Gunton et al., 2015a) and assemblages toward the middle and upper canyon reaches are often dominated by opportunistic deposit feeding species (Cunha et al., 2011; Conlan et al., 2015). Increased opportunist or early colonising meiofauna have also been observed toward the head of Whittard Canyon (Gambi and Danovaro, 2016). Epibenthic megafaunal assemblages are characterised by various representation of Cnidarians, Echinoderms and Foraminiferan xenophyophores (Robert et al., 2015; Pierdomenico et al., 2019). Assemblage composition varies along the canyon and between branches and flanks (Mortensen and Buhl-Mortensen, 2005; De Mol et al., 2011; Morris et al., 2013; Fabri et al., 2014; van den Beld et al., 2017).

#### 1.1.2.3.1 Canyon habitats as deep-sea biodiversity hotspots

There is a general association of increased diversity with habitats that include bio-engineers that modify the environment (Jones et al., 2010). These organisms frequently constitute the characterising species of the habitat in which they occur (MESH, 2008). Examples from canyons include sea pens (Baker et al., 2012; Fabri et al., 2014), sponges (Bertolino et al., 2019) and cold-water corals (De Mol et al., 2011; Morris et al., 2013; Fabri et al., 2017; van den Beld et al., 2017; Price et al., 2019).

Xenophyophores, seapen meadows and tulip sponge fields have been observed from soft substrata (Robert et al., 2015) and dense aggregations of the cold water corals, *Lophelia pertusa* (recently synonymised to *Desmophyllum pertusum* (Addamo et al., 2016)) and *Madrepora oculata* (Huvenne et al., 2011; Gori et al., 2013; Morris et al., 2013; Davies et al., 2014; Fabri et al., 2014; Robert et al., 2019) and deep water bivalves, *Acesta excavata* and *Neopycnodonte zibrowii* have been observed from hard substrata, often in association with vertical walls and overhangs (Johnson et al., 2013; Robert et al., 2019).

##### 1.1.2.3.1.1 Cold-water corals

Cold-water corals are a polyphyletic group of solitary or colonial azooxanthellate filter-feeding organisms belonging to the order Cnidaria and are defined by the presence of a calcium carbonate or proteinaceous axis or skeleton (Cairns, 2007). Cold-water corals comprise representatives of the subclass Octocorallia (soft corals), the orders Antipatharia (black corals), Scleractinia (stony corals), and the family Zoanthidae within the Hexacorallia, and the family Stylasteridae (hydrocorals) within the Hydrozoa. The three main reef framework forming Scleractinian cold-water corals are *D. pertusum*, *M. oculata* and *Solenosmilia variabilis*, (hereafter referred to as CWCs).

CWCs occur globally and have been recorded from continental margins (Davies et al., 2017; van den Beld et al., 2017), sea-mounts (Rowden et al., 2020) and canyons (Huvenne et al., 2011) across a depth range from 39 m, within Norwegian fjords to 2000 m in canyons (Roberts et al., 2009b; Lo Iacono et al., 2018). *D. pertusum*, is the most widespread and generally abundant species. However, in warmer waters such as the Mediterranean Sea *M. oculata* is more abundant (Fabri et al., 2014; Corbera et al., 2019) and in the South Pacific Ocean *S. variabilis* is more common (Rowden et al., 2020). These three CWCs can occur as isolated colonies, in small patch reefs several metres across or aggregate to form large reef systems (Roberts et al., 2006; Buhl-Mortensen et al., 2010; Corbera et al., 2019; Price et al., 2019) and ultimately through geological time can grow to form carbonate mounds several km across and exceeding 300 m in height (De Mol et al., 2002; Wheeler et al., 2006; Duineveld et al., 2007; Mienis et al., 2012). In canyons, CWCs occur as single colonies, large framework reefs and dense aggregations on vertical walls (Huvenne et al., 2011; Lo Iacono et al., 2018; Price et al., 2019; Robert et al., 2019). Recently small mound features (named 'mini-mounds') comprised of coral rubble that represent relict reef have been described from canyon interfluves (Stewart et al., 2014). Although no longer living, the degraded coral rubble still provides increased structural complexity compared to the surrounding seabed.

Cold-water corals can form key habitats such as reefs and coral gardens (Roberts et al., 2006; 2009b; Buhl-Mortensen et al., 2010; Robert et al., 2017; 2019; Price et al., 2019). Coral reefs can support high diversity, comparable to tropical reef systems (Henry and Murray, 2017). In canyons, the CWC habitats found on vertical walls represent biodiversity hotspots that constitute outliers in the general bathymetric trends of decreasing diversity with depth (Robert et al., 2015). The correlation of increased diversity with CWC habitats has led to CWCs becoming the focus of many deep-sea habitat mapping and ecological studies (Roberts et al., 2009a; Howell et al., 2011; Lo Iacono et al., 2018; Corbera et al., 2019; Rowden et al., 2020). However, few detailed studies of CWCs in canyons have been undertaken (Fernandez-Arcaya et al., 2017; Robert et al., 2017; Price et al., 2019) with still fewer studies of vertical wall CWC habitats (Robert et al., 2017; 2019), leaving gaps in our understanding of biodiversity hotspots in canyons.

#### 1.1.2.4 Environmental drivers of faunal patterns in canyons

##### 1.1.2.4.1 Environmental heterogeneity

The spatial distribution of fauna, assemblages and habitats is the result of a complex interplay between the physiological constraints of the environment (physical and chemical environment, size and relative distance to surrounding patches of similar environmental condition), food availability, biological processes (dispersal, competition and predation) and disturbance (Levin et al., 2001).

Environmental heterogeneity has been proposed as one of the key factors influencing deep-sea assemblages and diversity (Levin et al., 2001; 2010; Bianchelli and Danovaro, 2019) in structurally

complex environments, such as canyons (Ismail et al., 2018). Here, environmental heterogeneity refers to the variation in the spatial or temporal arrangement of environmental conditions at a given site. The idea that environmental heterogeneity can influence spatial patterns in fauna is based upon the principles of niche theory. Niche theory proposes that species adapt to exploit certain environmental conditions (fundamental niche) so that spatial patterns in faunal distribution and diversity are driven by the spatial structuring of species' environmental requirements (e.g. temperature, substrata). In reality, species may only occur within a portion of suitable sites (realised niche), as a result of biological interactions, such as dispersal, competition or predation, and disturbance effects (Hutchinson and MacArthur, 1959). As such, areas supporting greater environmental heterogeneity can support more niches and through associated resource partitioning, reduce competition, leading to higher coexistence of 'specialised' species and diversity (MacArthur and MacArthur, 1961).

In canyons, the patchy distribution of environmental conditions generates a heterogeneous landscape capable of supporting diverse habitats and assemblages (Schlacher et al., 2007; Robert et al., 2014) that leads to the observed high beta (Corinaldesi et al., 2019) and regional diversity (Bianchelli and Danovaro, 2019). Despite the recognised role of environmental heterogeneity in influencing faunal patterns, our understanding of the relative importance of the environmental conditions in which heterogeneity occurs is less understood. Our limited understanding stems from the difficulty of surveying such remote and heterogeneous environments (Amaro et al., 2016) and the lack of consistency in faunal bathymetric trends or slope-canyon comparisons, which makes identifying common causal processes difficult.

Canyon activity (Pierdomenico et al., 2016), continental shelf setting (Conlan et al., 2015), proximity to riverine inputs (Pierdomenico et al., 2016), trophic surrounding (Vetter et al., 2010) and prevailing oceanographic conditions have been shown to influence the relative importance of the environmental variables influencing habitat distribution (Pierdomenico et al., 2016). Even within canyons, the high spatial and temporal heterogeneity makes predictions of species responses to environmental variables difficult. For example, assemblages can vary between (De Mol et al., 2011) and within branches of the same canyon (Huvenne et al., 2011; Johnson et al., 2013; Robert et al., 2015). Further still, responses of fauna to environmental variables can vary, depending on successional stage of a community, mobility of fauna (Roberts et al., 2009a) or other unknown factors.

The methodological approaches can also influence the relative importance of the environmental variables. Depending on the scale of integration, the explanatory contribution and combination of environmental variables can change (Kenchington et al., 2014). However, published canyon studies principally assess the effects of factors in isolation over limited spatial and temporal scales (Huvenne and Davies, 2014; Robert et al., 2015) and rely on the use of acoustic proxies to quantify environmental heterogeneity. The use of proxies means that measured environmental variables are in fact indirect references of possible factors driving faunal patterns (Levin et al., 2001). This is

further confounded by the interconnected nature of environmental variables (Levin et al., 2001; Baker et al., 2012; Currie and Sorokin, 2013; Robert et al., 2015) and the technological constraints (Huvenne and Davies, 2014) and methodological inconsistencies (Amaro et al., 2016) of studies that limit comparability of results.

Despite the challenges that deep-sea canyon studies face, including the variability in methodological approaches and faunal patterns, some generalisations regarding processes influencing faunal patterns can be made.

#### 1.1.2.4.2 Environmental variables correlated with faunal patterns

In general, the distributions of habitats and fauna are believed to be driven by a complex interplay of multiple factors acting at different scales. Environmental heterogeneity is proposed to explain spatial patterns at broader spatial scales (McClain and Barry, 2010; Robert et al., 2015; Ismail et al., 2018), while biotic processes commonly act at finer spatial scales (Robert et al., 2019) and disturbance acts across a range of scales (Pierdomenico et al., 2016; Frutos and Sorbe, 2017).

##### 1.1.2.4.2.1 Seafloor characteristics (topography and substratum)

In benthic settings, at the regional scale, environmental heterogeneity is often spatially arranged in relation to seafloor characteristics (notably topography) (Wilson et al., 2007; Daly et al., 2018), so that increased structural complexity is associated with increased environmental heterogeneity and subsequently niche diversification, species coexistence and diversity (Willis et al., 2005; Graham and Nash, 2013). Structural complexity refers to "the irregularity in arrangement of structural elements which comprises the bathymetric contours of a given site" (Taniguchi et al., 2003; Yanovski et al., 2017) and represents the three-dimensional component of the seafloor.

Faunal patterns have been correlated with structural complexity at various spatial scales (MacArthur and MacArthur, 1961; Menge and Sutherland, 1976; Lawton, 1983; Willis et al., 2005; Buhl-Mortensen et al., 2010). In canyons, faunal patterns are commonly correlated with the broad-scale structural complexity of the canyon terrain (Domke et al., 2017; Bianchelli and Danovaro, 2019; Covazzi Harriague et al., 2019). The broad-scale structural complexity increases environmental heterogeneity not only by creating three-dimensional substratum morphology, but also by influencing sediment dynamics (de Stigter et al., 2011; Martín et al., 2011; Puig et al., 2017), food supply (Campanyà-Llovet et al., 2018) and local hydrodynamics (Hall et al., 2014). At finer spatial scales (<1 km) bio-engineers, including CWCs, increase the structural complexity of the seafloor. The increased fine-scale structural complexity increases fine-scale environmental heterogeneity in sediment dynamics, food supply and hydrodynamics within and around the bioengineers framework (Buhl-Mortensen et al., 2010; Price et al., 2019). Additionally, fine-scale structural complexity influences faunal patterns by providing shelter from predation and nursey grounds for fauna (Costello et al., 2005). The positive relationship between structural complexity and environmental

heterogeneity results in areas of increased structural complexity being correlated with increased diversity (Costello, 2009; Buhl-Mortensen et al., 2010; Robert et al., 2015).

Spatial distributions of faunal assemblages are also often associated with particular substratum types, (Hargrave et al., 2004; De Mol et al., 2011; Baker et al., 2012; 2019; Huvenne et al., 2012; Miller et al., 2012; Currie and Sorokin, 2013; Kenchington et al., 2014; Pierdomenico et al., 2016). The association of fauna with particular substrata is reflective of their life history traits (Baker et al., 2012). In canyons, the observed difference in the spatial patterns of epi- and infauna, whereby epibenthic fauna are associated with steep complex topography, reflect their differential preferences in colonisation substratum (Baker et al., 2012). For example, sessile epibenthic fauna predominantly require hard substratum upon which they can settle and grow (Baker et al., 2012), and the hard substratum occurs in association with steep complex topography (Stewart et al., 2014) which, is more commonly encountered toward the upper and middle sections of a canyon (Amblas et al., 2018). Faunal adaptations to particular substrata promote niche partitioning along substratum gradients, which enables more species to co-occur in areas of increased substratum heterogeneity (Hargrave et al., 2004; Levin et al., 2001; Baker et al., 2012; De Leo et al., 2014). However, in canyons, different faunal assemblages are often observed from the same substratum, indicating that in canyons substratum alone cannot determine faunal distributions and assemblages (Lacharité and Metaxas, 2017).

#### 1.1.2.4.2.2 Food availability

Variability in faunal patterns between and within canyons have been attributed to heterogeneity in the quantity and quality of food (McClain and Barry, 2010; De Leo et al., 2010; 2014; Cunha et al., 2011; Gunton et al., 2015a; Gambi and Danovaro, 2016; Demopoulos et al., 2017; Campanyà-Llovet et al., 2018; Carugati et al., 2019). Heterogeneity in the quantity and quality of food between canyons results from differing regional productivity, canyon activity (Lopez-Fernandez et al., 2013) canyon morphology, hydrodynamics and water mass characteristics (Paterson et al., 2011), while within canyons, faunal bathymetric trends are often attributed to a reduction in food availability with depth (Duineveld et al., 2001; Cunha et al., 2011; Miller et al., 2012; Currie and Sorokin, 2013; Gunton et al., 2015a; Sigler et al., 2015).

Infaunal assemblage composition is influenced by food quantity and quality (McClain and Barry, 2010; Ingels et al., 2013; Romano et al., 2013; Gambi and Danovaro, 2016) and often opportunistic species dominate at high abundance in organically enriched settings (Vetter and Drayton, 1998 ; Cúrdia et al., 2004; Cunha et al., 2011). High epifaunal richness, abundance and assemblages characterised by filter and suspension feeders are observed to coincide with areas of increased food input in the form of nepheloid layers (Huvenne et al., 2011; Johnson et al., 2013). Nepheloid layers represent an important food resource for deep-sea fauna (Demopoulos et al., 2017). The delivery of high quality POM with enhanced currents has been shown to sustain a variety of filter and suspension

feeder assemblages in other settings (White et al., 2005; Mienis et al., 2007; Miller et al., 2012; Demopoulos et al., 2017). For example, internal tides interacting with complex topography have been proposed as mediating efficient food supply mechanisms to CWCs on continental shelf settings where CWCs occur preferentially on supercritical slopes (Frederiksen et al., 1992; Mohn et al., 2014). In canyons, areas of high epibenthic megafaunal abundance, including CWCs, also occur on supercritical slopes coincident with nepheloid layers (Huvenne et al., 2011; Johnson et al., 2013; Wilson et al., 2015b). These observations have led authors to postulate the role of the internal tides in determining faunal distributions in canyons (Huvenne et al., 2011; Johnson et al., 2013; Robert et al., 2015). However, few studies explicitly modelling the relationship between canyon fauna and internal tide dynamics have been undertaken (Liao et al., 2017; Bargain et al., 2018).

#### 1.1.2.4.2.3 Water mass characteristics

Internal tides may also influence faunal patterns by generating temporal variability in water mass characteristics as they propagate along the canyon (Wang et al., 2008; Hall et al., 2017) . Bathymetric trends in fauna are often attributed to changes in water mass characteristics (Levin et al., 2001; Roberts et al., 2009a; De Mol et al., 2011; Currie and Sorokin, 2013; Johnson et al., 2013; Flögel et al., 2014; Conlan et al., 2015) that vary with depth. Fauna are known to respond to gradients in physical oceanography, and internal tide induced variability in water mass characteristics has been connected to faunal patterns in a seamount setting (van Haren et al., 2017). However to date, no study has been undertaken to assess the structuring force of internal-tide induced variability on faunal assemblages and diversity in a canyon. The lack of knowledge regarding how internal tides influence canyon fauna represents a limit to canyon ecology.

#### 1.1.2.4.2.4 Disturbance

Canyons are dynamic environments, subject to periodic mass wasting events and subsequent sediment laden flows, as such, disturbance represents an important factor influencing faunal distributions in canyons. Disturbance can be of natural, or anthropogenic origin. Sediment transport, turbidity currents, gravity flows, hydrodynamics or excess organic enrichment represent natural forms of disturbance that can influence the spatio-temporal distribution of assemblages (McClain and Barry, 2010; Cunha et al., 2011; Currie and Sorokin, 2013; Gunton et al., 2015a; 2015b; Amaro et al., 2016; Gambi and Danovaro, 2016), while fishing, waste dumping and climate change represent anthropogenic forms of disturbance (Levin et al., 2001; Puig et al., 2012; Pusceddu et al., 2014).

Disturbance influences faunal patterns either directly by physically damaging or removing organisms (Baker et al., 2019) or indirectly, by altering the environmental conditions so that they are no longer hospitable (McClain and Barry, 2010; Puig et al., 2012). The altered environmental conditions can change faunal assemblage composition to comprise more opportunistic or mobile species (McClain and Barry, 2010; Cunha et al., 2011; Miller et al., 2012; Fabri et al., 2014; Amaro et al., 2015;

Pierdomenico et al., 2016). Alternatively in areas where disturbance becomes too frequent, for example along the canyon axis that experiences high current speeds, frequent sediment transport, scour or sedimentation rates, conditions become too inhospitable and no or few fauna occur (Cunha et al., 2011; Paterson et al., 2011; Johnson et al., 2013).

Differences in infaunal assemblage composition observed between canyons and slopes has been attributed to differing disturbance regimes, whereby the periodic disturbance encountered within canyons and toward canyon heads results in assemblages dominated at high abundance by opportunistic and early colonising species (Cunha et al., 2011; Conlan et al., 2015; Gambi and Danovaro, 2016). Additionally, between and within canyons differences in observed infaunal assemblages are also attributed to varying disturbance regimes (Pierdomenico et al., 2016).

The stochastic nature of natural disturbance events has limited its incorporation into canyon studies. Consequently, the influence of disturbance is mostly inferred from data that is caught opportunistically by landers (de Stigter et al., 2011) or from the interpretation of bed forms after a disturbance event has occurred (Arzola et al., 2008; Mountjoy et al., 2018).

Fishing represents the most studied anthropogenic disturbance affecting canyon systems (Miller et al., 2012; Puig et al., 2012; Fabri et al., 2014; Pierdomenico et al., 2016). Fishing gear causes physical disturbance to habitats by removing, damaging and killing species (Puig et al., 2012). Additionally, contact fishing gear modifies the environment, usually leading to increased sedimentation and reduced structural complexity of the seafloor (Puig et al., 2012; Fabri et al., 2014; Pierdomenico et al., 2016). The remobilisation of sediments effects sediment flow and flux through canyons (Arjona-Camas et al., 2019). The steep and vertical walls of canyons are prohibitive to contact fishing gear and as such have been proposed as refuges from bottom trawling (Huvenne et al., 2011).

## 1.2 Motivation for study

Despite the ecological importance of canyons and recent protection initiatives, many canyons and the features that they support are increasingly under threat from anthropogenic disturbance. Fishing (Puig et al., 2012; Martín et al., 2014b), oil and gas (Hooker et al., 1999), the depositing of mine tailings (Ramirez-Llodra et al., 2015), the accumulation of litter (including discarded fishing gear (micro) plastics (Cau et al., 2017; van den Beld et al., 2017; Kane et al., 2020) and pollutants (Azaroff et al., 2020) plus climate change all potentially impact canyon systems (Fernandez-Arcaya et al., 2017) and have negative impacts on biodiversity, habitats, ecosystem functioning and consequently services (Pusceddu et al., 2014; Ramirez-Llodra et al., 2015; Fernandez-Arcaya et al., 2017).

The establishment of marine protected areas (MPAs) or equivalents to protect features of conservation interest requires knowledge of faunal distributions and species-environment relationships, of which a gap exists for deep-sea species, including cold-water corals (Davies et al.,

2007; Auster et al., 2011). Filling this knowledge gap is important because the typical characteristics of submarine canyons give them potential to support a disproportionate amount of diversity and VMEs, including cold-water corals. Additionally, the relatively high diversity of habitats and species within one defined geomorphological feature makes canyons key features for spatial management. However, due to the difficulty of surveying such remote and heterogeneous environments the distribution and understanding of processes influencing faunal patterns is relatively limited (Amaro et al., 2016). Furthermore, despite the widespread distribution of canyons (De Leo et al., 2010; Harris and Whiteway, 2011), De Leo et al. (2014) reported that faunal studies have only been conducted in a small fraction (~ 0.5%) of the world's canyons. In the case of epibenthic megafaunal studies, many have been descriptive (Brooke and Ross, 2014) or in cases where epibenthic megafauna have been enumerated, the information has usually become condensed into diversity metrics (i.e. species richness, diversity, abundance and biomass) (Robert et al., 2015), which limits the ecological inferences that can be drawn.

Due to the limited availability of deep-sea data, modelling techniques have increasingly been used to extrapolate relationships between and beyond a smaller number of data points to further our knowledge of deep-sea ecology (Robert et al., 2015; Rowden et al., 2020). In particular, predictive modelling techniques have been used to generate continuous spatial distribution maps of fauna from a smaller number of ground-truthed samples (Robert et al., 2015; Anderson et al., 2016a; Bargain et al., 2018). Predictive distribution modelling is a method by which continuous species or habitat distributions can be produced from limited sample data by modelling species – environment relationships using available samples and environmental information from which predictions beyond sampled areas can be made (Guisan and Zimmermann, 2000). Predictive modelling is increasingly being recognised as an important tool to facilitate deep-sea management where data are limited and models can identify suitable locations for species or habitats (Howell et al., 2011; Ross and Howell, 2013; Anderson et al., 2016a; Gullage et al., 2017). However, any models that inform ecology or the prioritisation of areas for protection can only be effective if the major drivers of faunal patterns are understood and incorporated, and their relative importance is adequately represented by the available datasets (Guisan and Zimmermann, 2000).

The difficulties of surveying the deep sea result in the use of environmental proxies or simulated models of environmental conditions both derived at broad spatial resolutions (Davies and Guinotte, 2011). Environmental conditions in canyons can vary over short spatial scales (McClain and Barry, 2010; Hall et al., 2017; Robert et al., 2017), so that the use of broad resolution data may fail to capture environmental gradients that are ecologically important to the fauna, which affects model precision and/or accuracy (Lecours et al., 2015; Miyamoto et al., 2017). Additionally, the omission of key environmental drivers could lead to predictive inaccuracies (Guisan and Thuiller, 2005).

Submarine canyons are characterised by increased structural complexity (Harris and Whiteway, 2011) and internal tides (Hall et al., 2014), which generate environmental heterogeneity within the

canyon at various spatial scales (Amaro et al., 2016; Hall et al., 2017; Campanyà-Llovet et al., 2018). However, despite the importance of structural complexity and internal tides, there is a lack of information regarding how exactly these phenomena influence faunal patterns in canyons. Structural complexity at various spatial scales is known to influence faunal patterns (Robert et al., 2017; Fanelli et al., 2018; Price et al., 2019). To date, canyon studies have predominately focussed upon broad-scale structural complexity as a proxy of environmental heterogeneity (Robert et al., 2015; Ismail et al., 2018). However, peaks in canyon diversity often coincide with features of finer-scale structural complexity that are not discernible in broad-scale acoustic datasets (Robert et al., 2015; Price et al., 2019). Consequently, there is a lack in our understanding of how structural complexity interacts at various spatial scales (specifically finer-scales) to influence faunal patterns in canyons.

Physical oceanography (water mass characteristics and hydrodynamics) is known to influence faunal patterns, including CWCs (Frederiksen et al., 1992; Thiem et al., 2006; Davies, 2009; Mienis et al., 2009; White and Dorschel, 2010). However, these data have rarely been explicitly included in faunal models from canyons settings (Liao et al., 2017; Bargain et al., 2018), despite the fact that canyons are characterised by strong gradients in water mass characteristics and internal tides (Hall et al., 2017; Aslam et al., 2018). The omission of spatially explicit internal tide data from predictive distribution models may lead to predictive inaccuracies because internal tides are important phenomena generating environmental heterogeneity in canyon settings (de Stigter et al., 2007; Wang et al., 2008; Lee et al., 2009; Liu et al., 2010; Amaro et al., 2015; 2016; Hall et al., 2017; Aslam et al., 2018) and hence could represent a key environmental driver of faunal patterns.

Internal tides generate physical oceanographic gradients by their movement along the canyon, which generates spatial and temporal variability in physical oceanographic conditions (Wang et al., 2008; Hall et al., 2017). Faunal patterns in other settings have been correlated with variability in physical oceanographic conditions (Levin et al., 2001; Dullo et al., 2008; Fabri et al., 2017). However, no study has been undertaken to determine if spatial patterns in temporal oceanographic variability induced by the internal tide explain variation in faunal patterns in a canyon setting.

Recent studies from other settings have highlighted that integrating data from spatially explicit hydrodynamic models with high resolution bathymetry can improve our understanding of multiscale interactions and predictions of habitat suitability (Rengstorf et al., 2013; 2014; Mohn et al., 2014; Bargain et al., 2018). The incorporation of high-resolution bathymetry also allows the influence of structural complexity at various spatial scales to be assessed (Robert et al., 2014). Studying the influences of both structural complexity and internal tides can further our understanding of canyon ecology because in canyons the variability in environmental conditions is often spatially arranged in relation to the canyons' complex topography and hydrodynamics (Lopez-Fernandez et al., 2013; Campanyà-Llovet et al., 2018).

## 1.3 Scientific objectives and research questions

Canyons are of high ecological importance and support increased diversity including VMEs. To ensure effective management of canyons and the assemblages within them, there is a need to increase our understanding of how variability in environmental conditions linked to internal tides and finer-scale structural complexity influence canyon faunal patterns in diversity and assemblage. This thesis applies a range of statistical approaches to novel datasets, in order to identify how environmental heterogeneity operating at various spatial scales drives epibenthic megafaunal patterns, including CWCs using Whittard Canyon, North-East Atlantic as a model system.

### 1.3.1 Chapter 2

The aim of this chapter is to identify which environmental variables best predict canyon-wide epibenthic megafaunal patterns in Whittard Canyon and to assess if including physical oceanographic data (internal tide data) improves predictions of biodiversity, species richness, abundance and CWC occurrence. General Additive Models, Random Forests and Boosted Regression Trees are used to compare predictions and build final ensemble predictive maps for CWC occurrence, epibenthic megafaunal abundance, species richness and biodiversity. The chapter highlights the importance of including oceanographic data and processes by which local hydrodynamics interact with topography to concentrate food resources in canyons.

### 1.3.2 Chapter 3

The aim of this chapter is to investigate if spatial patterns in temporal oceanographic variability induced by the internal tide explain variation in spatial patterns of diversity and assemblage composition on deep-sea canyon walls. The main questions addressed are: (1) Does epibenthic megafaunal assemblage composition change across physical oceanography and substratum gradients on vertical walls and (2) which environmental variables exert the strongest influence on epibenthic megafaunal diversity and assemblage structure? Multivariate analysis and Generalised Liner Models are used to relate epibenthic megafaunal assemblage and diversity to internal tide induced variability in oceanographic conditions. The chapter shows that the internal tide is a structuring force influencing faunal diversity and assemblages on canyon walls by generating both spatial and temporal gradients in physical oceanography and food supply.

### 1.3.3 Chapter 4

The aim of this chapter is to explore the relationship between structural complexity and epibenthic megafaunal assemblages within mini-mound provinces occurring on canyon interfluves. Multivariate analysis, Generalised Additive Models and Random Forests are used to relate epibenthic megafaunal assemblages, richness and density to derived proxies of substratum characteristics and structural

complexity at various spatial scales. The chapter provides evidence that substratum characteristics and structural complexity influence faunal patterns and emphasises the importance of fine-scale structural complexity in promoting increased diversity.

### 1.3.4 Chapter 5

In this final chapter, the results from the thesis are brought together and synthesised to show how internal tides and structural complexity influence faunal patterns by interacting at varying scales to generate environmental heterogeneity in canyons. The contribution of the thesis toward canyon research is discussed, as well as its limitations and future research directions.

# Chapter 2 Including oceanographic data improves predictive benthic species distribution models in a submarine canyon setting

This chapter is a reproduction of the text published as **Pearman, T.R.R.,** Robert, K., Callaway, A., Hall, R., Lo Iacono, C., Huvenne, V.A.I. (2020) Improving the predictive capability of benthic species distribution models by incorporating oceanographic data – towards holistic ecological modelling of a submarine canyon. Progress in Oceanography. 184, 102338. 10.1016/j.pocean.2020.102338

Author contributions: T.P, V.H, K.R conceptualised the chapter, T.P annotated ROV imagery, generated environmental rasters, conducted statistical analysis and wrote the manuscript. V.H and R.H acquired the data during the JC124_JC125 CODEMAP2015 cruise and supervised in the generation of environmental rasters. K.R contributed annotations from ROV imagery and code for predictive modelling. All authors reviewed and commented on the chapter.

## 2.1 Abstract

Submarine canyons are associated with increased biodiversity, including cold-water coral (CWC) colonies and reefs which are features of high conservation value that are under increasing anthropogenic pressure. Effective spatial management and conservation of these features requires accurate distribution maps and a deeper understanding of the processes that generate the observed distribution patterns. Predictive distribution modelling offers a powerful tool in the deep sea, where surveys are constrained by cost and technological capabilities. To date, predictive distribution modelling in canyons has focussed on integrating ground-truthed acoustically acquired datasets as proxies for environmental variables thought to influence faunal patterns. Physical oceanography is known to influence faunal patterns but has rarely been explicitly included in predictive distribution models of canyon fauna, thereby omitting key information required to adequately capture the species-environment relationships that form the basis of predictive distribution modelling. In this study, acoustic, oceanographic and biological datasets were integrated to undertake high-resolution predictions of benthic megafaunal diversity and CWC distribution within Whittard Canyon, North-East Atlantic. The main aim was to investigate which environmental variables best predict faunal patterns in canyons and to assess whether including oceanographic data improves predictive modelling. General Additive Models, Random Forests and Boosted Regression Trees were used to build predictive maps for CWC occurrence, megafaunal abundance, species richness and biodiversity. To provide more robust predictions, ensemble techniques that summarise the variation in predictions and uncertainties between modelling approaches were applied to build final maps. Model performance improved with the inclusion of oceanographic data. Ensemble maps identified areas of elevated current speed that coincided with steep ridges and escarpment walls as the areas most likely to harbour CWCs and increased biodiversity, probably linked to local hydrodynamics interacting with topography to concentrate food resources. This study shows how incorporating oceanographic data into canyon models can broaden our understanding of processes generating faunal patterns and improve the mapping of features of conservation, supporting effective procedures for spatial ecosystem management.

## 2.2 Introduction

Submarine canyons are environmentally complex geomorphological features that incise continental margins and act as conduits between the shelf and the deep sea (Allen and Durrieu de Madron, 2009; Huvenne and Davies, 2014; Puig et al., 2014; Amaro et al., 2016). Canyons are characterised by high spatial and temporal heterogeneity in environmental conditions (De Leo et al., 2014; Amaro et al., 2016; Fernandez-Arcaya et al., 2017), often resulting in enhanced regional and local productivity, biodiversity, and faunal abundance (De Leo et al., 2010; Vetter et al., 2010; De Leo et al., 2014). Reef-forming cold-water coral colonies (from here indicated as CWC) and reefs in particular represent features of high conservation value that can occur within canyons and are under increasing anthropogenic pressure (92/43/EEC, 1992; OSPAR, 2008; Davies et al., 2017). Accurate distribution maps of these features, in addition to an understanding of the processes that drive the observed spatial patterns, can support their effective spatial management and conservation (Huvenne and Davies, 2014; Buhl-Mortensen et al., 2015; Anderson et al., 2016a). In the deep sea, where surveys are constrained by costs and technological capabilities, predictive mapping offers a powerful tool for such studies. (Robert et al., 2015; Anderson et al., 2016a; Robert et al., 2016). Predictive mapping is based upon models of species–environment relationships that enable predictions of the likely occurrence of species beyond where they have been sampled (Guisan and Zimmermann, 2000; Guisan and Thuiller, 2005). These techniques are based upon concepts of niche theory, whereby species' distributions are determined by the environmental dimensions of their ecological niche (Guisan and Zimmermann, 2000). Therefore, accurate predictions rely upon the incorporation of ecologically relevant environmental data collected at resolutions which capture the scale at which these variables influence species spatial patterns (Lecours et al., 2015; Miyamoto et al., 2017; Misiuk et al., 2018; Porskamp et al., 2018).

In submarine canyons, acoustically derived environmental variables (e.g., depth, slope) are routinely used as indirect proxies for direct and resource variables (sensu Guisan and Zimmermann, 2000) including, water mass characteristics (temperature, salinity, potential density, dissolved oxygen concentration, aragonite compensation level and pH), substratum, seafloor characteristics, current exposure and food supply (Wilson et al., 2007; Robert et al., 2015); all of which have been shown to act at multiple scales to influence faunal patterns in canyons (De Mol et al., 2011; Howell et al., 2011; Baker et al., 2012; De Leo et al., 2014; Bargain et al., 2018). For example, water mass characteristics tend to influence canyon fauna at spatial scales of 10 - 1000 km (Dullo et al., 2008; Fabri et al., 2017) at which resolution they often co-vary with depth (Henry et al., 2014). On the other hand, spatial variation in seafloor characteristics and substratum are influential at finer resolutions of <1 - 10 km (Howell et al., 2011; Robert et al., 2015; Fabri et al., 2017), which can be captured by terrain derivatives such as slope and rugosity (Wilson et al., 2007; Howell et al., 2011). Equally at

this resolution, aspect can provide insights into areas that may be more exposed to currents (Wilson et al., 2007; Robert et al., 2015).

However, the sole use of indirect variables as proxies can hinder ecological interpretation, as a single proxy can be collinear with multiple direct and/or resource variables across varying scales (Wilson et al., 2007; Porskamp et al., 2018) and because the measured proxy does not influence organisms' distributions directly, it can lead to further predictive inaccuracies. In addition, environmental data are often acquired at low resolutions that reflect technological constraints rather than being ecologically meaningful (Verfaillie et al., 2009; Huvenne and Davies, 2014; Ismail et al., 2015; Lecours et al., 2015; Porskamp et al., 2018). These data are then incorporated into models at a pre-determined single fixed resolution as opposed to the increasingly advocated approach of incorporating data at multiple resolutions to then statistically identify the resolution that best captures the variability in the environment to which fauna are responding (Wilson et al., 2007; Fourniera et al., 2017; Porskamp et al., 2018). Consequently, the use of indirect variables together with the mismatch of resolution between ecological processes and data sampling represent key limitations of predictive model and map accuracy and precision (Brown et al., 2011; Lecours et al., 2015; Lo Iacono et al., 2018; Porskamp et al., 2018).

Physical characteristics of the water column and oceanographic processes are known to influence faunal patterns, including those of CWCs (Dullo et al., 2008; De Mol et al., 2011; Flögel et al., 2014; Fabri et al., 2017) but have rarely been included in predictive models of canyon fauna, one exception being Bargain et al. (2018). In canyons supporting intense hydrodynamic processes (Hall and Carter, 2011; Aslam et al., 2018) variability in faunal patterns has been observed and attributed to the increased heterogeneity in physical oceanography (Huvenne et al., 2011; Johnson et al., 2013). As such, canyons represent model systems for testing the role of physical oceanography in controlling faunal distribution patterns.

Here we develop predictive distribution models for CWCs and epibenthic megafaunal biodiversity using a multiscale approach integrating bathymetric and oceanographic datasets and their derivatives in the Whittard Canyon (North-East Atlantic) to investigate which environmental variables best predict faunal patterns. Finally, we aim to assess how the inclusion of oceanographic variables affects model performance, testing the null hypothesis that the inclusion of physical oceanographic variables in distribution models has no effect on model accuracy or precision.

## 2.3 Methods

### 2.3.1 Study Area

Whittard Canyon is located along the Celtic Margin, south-west of the British Isles in the Northern Bay of Biscay and extends >200 km (Figure 2.1). It is a dendritic canyon system comprised of four

main tributaries, the Western-, Western Middle-, Eastern Middle- and Eastern- branches, incising the shelf edge at a depth of ~200 m and coalescing at ~3700 - 3800 m water depth, then developing as Whittard Channel up to a depth of ~4500 m, where it joins the Celtic Fan that leads onto the Porcupine Abyssal Plain (Hunter et al., 2013; Amaro et al., 2016). Intensified bottom currents and internal tides have been associated with the canyon, making it a good candidate for investigating the impact of physical oceanography on faunal patterns (Reid and Hamilton, 1990; Hall et al., 2017; Aslam et al., 2018). Within the canyon system are the Dangaard and Explorer Canyons that together constitute the only deep-sea marine conservation zone (MCZ) within English waters. The Canyons MCZ designation is based upon the presence of the 'Deep-sea bed' broad-scale habitat and 'Cold-water coral reefs', 'Coral gardens' and 'Sea-pen and burrowing megafauna communities' habitat features of conservation interest (DEFRA, 2013; DEFRA, 2019a). Accurate predictive maps of these features based on key environmental predictors are essential to assist effective management of the MCZ. This study focuses on the Eastern branch of Whittard Canyon and the adjoining Dangaard and Explorer Canyons (Figure 2.1). This region of the Whittard Canyon system was chosen as the Eastern branch has been identified as the most hydrodynamically energetic while the Dangaard and Explorer Canyons incise the Brenot Spur, which is postulated to be a generation site for the internal tide that propagates into the Eastern branch (Aslam et al., 2018).

Whittard Canyon exhibits heterogeneity in both physical and oceanographic attributes. The geomorphology and substrata of the canyon are complex, with variability observed along the canyon axis and between branches (Stewart et al., 2014; Robert et al., 2015; Amaro et al., 2016; Ismail et al., 2018). The heads of the canyons are characterised by steep-sided walls and coarser substrata (outcropping bedrock, boulders and cobbles) (Carter et al., 2018).(Carter et al., 2018) Where the branches coalesce, the Whittard Channel leads further downslope to the depositional fan comprised of finer grained substrata (fine sand, silt and hemiplegic ooze). Sediment dynamics within the canyon are poorly understood. Although developing on a passive margin, Whittard Canyon does experience sediment dynamics (Amaro et al., 2016; Carter et al., 2018). Resuspension by intensified bottom currents and local slope failures within the canyon facilitate the availability of fine grained material (Reid and Hamilton, 1990; Amaro et al., 2015; Amaro et al., 2016; Hall et al., 2017; Carter et al., 2018) which is then transported via active down-slope transport in the form of turbidity currents and mud-rich sediment gravity flows (Cunningham et al., 2005; Amaro et al., 2016). On the other hand, up-canyon transport of material may be mediated by internal tides (Wilson et al., 2015b; Lo Iacono et al., 2020)

As it descends, the canyon intersects several water masses, including the Eastern North Atlantic Water (ENAW) (~100 - 600 m), the Mediterranean Outflow Water (MOW) (800 - 1200 m) and the Northeast Atlantic Deep Water (NEADW) (1500 - 3000 m), within which occurs a core of Labrador Sea Water (LSW) (~1800 - 2000 m) (Pollard et al., 1996; Van Aken, 2000). Mixing occurs along the water mass boundaries (Van Rooij et al., 2010). Barotropic tidal currents interact with the steep

canyon topography converting some of the energy into baroclinic internal waves (Allen and Durrieu de Madron, 2009; Hall et al., 2017) and partly standing internal waves have been observed within the Eastern branch (Hall et al., 2017). Internal wave driven turbulent mixing is associated with increased concentrations of particulate organic matter (POM) and nepheloid layer production within the canyon (Wilson et al., 2015b; Hall et al., 2017; Aslam et al., 2018).

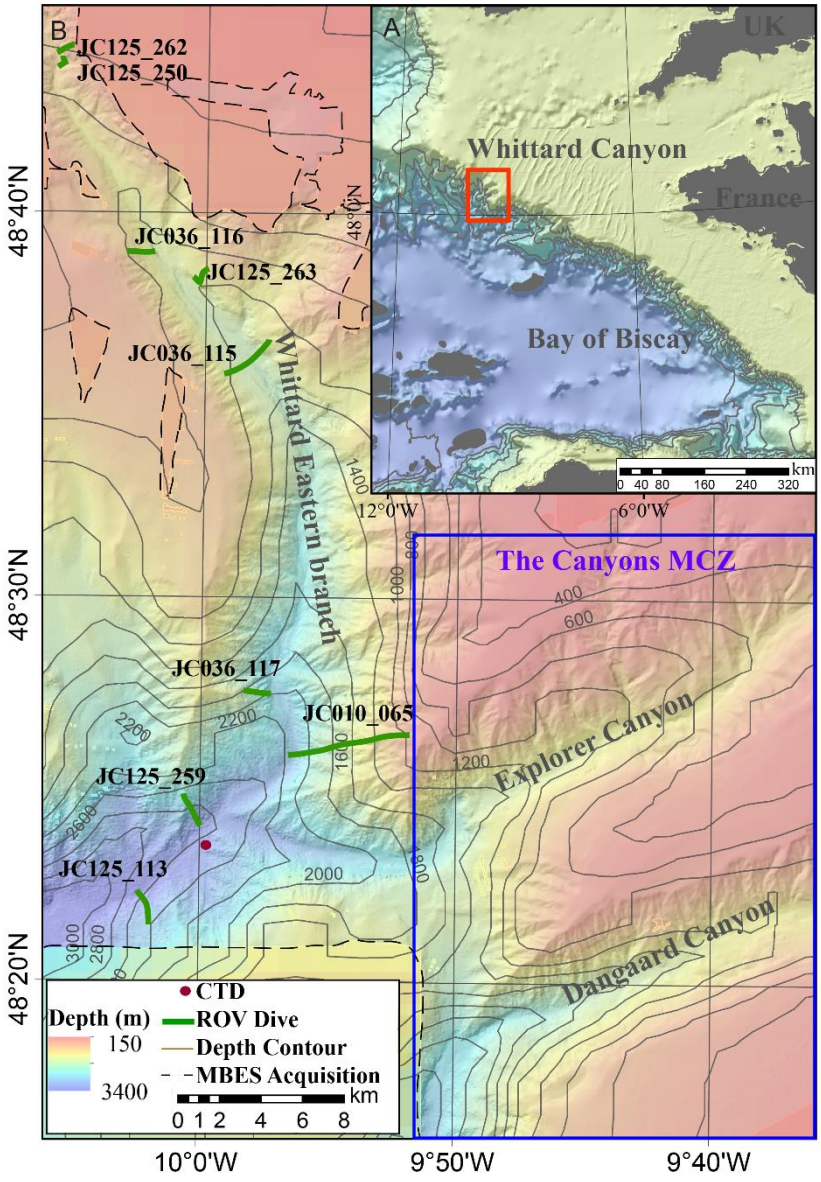


Figure 2.1 Location map of (A) Whittard Canyon and (B) data acquisitionduring the JC010, J036 and JC125 cruises over Whittard Canyon Eastern branch and the adjoining Dangaard and Explorer Canyons. Background bathymetry from GEBCO Compilation Group (2019).

### 2.3.2 Data acquisition and analysis

Data were collected during (1) the JC124_JC125 expedition funded by the ERC CODEMAP project (Starting Grant no 258482), the NERC MAREMAP programme and the Department of Environment, Food & Rural Affairs (DEFRA), (2) the JC010, JC035 and JC036 expeditions funded by the NERC core programme OCEANS2025 and the EU FP7 IP HERMIONE, and (3) the MESH expedition funded by the European Union INTERREG IIIb Community Initiative, and DEFRA.

#### 2.3.2.1 Video data acquisition and analysis

During the JC010 and JC036 cruises, video data were acquired using the remotely operated vehicle (ROV) *Isis* equipped with a standard definition video camera (Pegasus, Insite Tritech Inc. with SeaArc2 400 W, Deep sea Power & Light illumination) and stills camera (Scorpio, Insite Tritech Inc., 2048 x 1536 pixels). For the JC125 cruise, the ROV *Isis* was equipped with a dual high definition stills and video camera (Scorpio, Insite Tritech Inc., 1920 x 1080 pixels). Positional data were derived from the ROV's ultra-short baseline navigation system (USBL). A total of nine dives were completed in the Eastern branch (Figure 2.1 and Table 2.1) at an average speed of ~0.08 m $s^{-1}$ and an average camera height of 3 m from the seafloor (Robert et al., 2015). Video footage from the dives was analysed with all epibenthic megafauna >10 mm annotated and georeferenced, organism size was estimated from a laser scale with parallel beams positioned 10 cm apart. Due to limited species taxonomic knowledge for the area, fauna were identified to the lowest taxonomic level possible and identified as morphospecies (visually distinct taxa). To ensure consistency in nomenclature and improve comparability of annotations, the developed morphospecies catalogue (Appendix D) was based upon the CATAMI nomenclature (Althaus et al., 2015) and cross-referenced against the Howell and Davies (2010) morphospecies catalogue for the North-East Atlantic Deep-Sea. Those sections where the ROV altitude was >4 m for extended periods, prohibiting annotations, were noted by time and not considered in subsequent analysis. Video data annotations from the JC010, JC036 (previously annotated by Robert et al. (2015)) and JC125 cruises were combined into a single data matrix with possible annotator bias in the combined dataset assessed following the protocol set out in Durden et al. (2016)(see supplementary materials 2.1.1). Transects were subdivided into 50 m length sections and the morphospecies records within each section consolidated, with Species richness, Simpson's reciprocal index ($1/D$) (Simpson, 1949) and megafaunal abundance calculated for each 50 m section sample. These metrics were chosen as together they capture the key faunal responses to environmental heterogeneity (McClain and Barry, 2010; Amaro et al., 2015). Presence-absences for three scleractinian reef forming species, *Desmophyllum pertusum* (formerly *Lophelia pertusa)*, *Madrepora oculata* and *Solenosmilia variabilis* were combined to provide a CWC presence-absence value. This was recorded because reef forming scleractinians represent features of high conservation value that are often associated with increased diversity (OSPAR, 2008; 92/43/EEC, 1992; Davies et al., 2017). Additionally, as long-

lived immobile filter feeders that are associated with sustained hydrodynamics (Dullo et al., 2008; Howell et al., 2011; Fabri et al., 2017), CWCs represent good candidates for investigating the role of physical oceanography on faunal distributions.

All statistical analyses were conducted using the open source software R (R_Core_Team, 2014), packages "sp", "maptools", "rgeos", "vegan", "clustersim" and "MASS".

Table 2.1 ROV dives in Whittard Canyon analysed in the study: Dive code, start and end position (degrees and decimal minutes), dive length (m) and depth range across dive (m).

| Dive | Start Position | | End Position | | Length (m) | Depth Range (m) |
|---|---|---|---|---|---|---|
| JC125_113 | 48° 22.296' N | 10° 2.374' W | 48° 22.296' N | 10° 2.374' N | 1850 | 2619 - 3199 |
| JC125_250 | 48° 43.803' N | 10° 5.842' W | 48° 43.803' N | 10° 5.842' N | 600 | 751 - 886 |
| JC125_259 | 48° 24.049' N | 9° 59.867' W | 48° 24.049' N | 9° 59.867' N | 2000 | 2148 - 2987 |
| JC125_262 | 48° 44.149' N | 10° 5.965' W | 48° 44.149' N | 10° 5.965' N | 965 | 464 - 879 |
| JC125_263 | 48° 38.331' N | 10° 0.514' W | 48° 38.331' N | 10° 0.514' N | 1600 | 1138 - 1422 |
| JC_10_065 | 48° 25.908' N | 9° 56.432' W | 48° 25.908' N | 9° 56.432' N | 6585 | 464 - 2634 |
| JC_036_115 | 48° 36.742' N | 9° 57.297' W | 48° 36.742' N | 9° 57.297' N | 3000 | 1222 - 1667 |
| JC_036_116 | 48° 39.251' N | 10° 1.903' W | 48° 39.251' N | 10° 1.903' N | 1500 | 910 - 1407 |
| JC_036_117 | 48° 27.646' N | 9° 56.958' W | 48° 27.646' N | 9° 56.958' N | 2050 | 1762 - 2470 |

#### 2.3.2.2 Acoustic data acquisition and processing, and extraction of terrain derivatives

Multibeam echosounder (MBES) data were acquired during the MESH, JC035 and JC125 cruises with the ship-board Kongsberg Simrad EM120 MBES system of RRS *James Cook* (Masson, 2009; Huvenne et al., 2016) and Kongsberg Simrad EM1002 MBES system of RV *Celtic Explorer* (Davies et al., 2008b). Bathymetry data were processed utilising CARIS HIPS & SIPS v.8 and combined utilising the mosaic to new raster tool in ArcGIS 10.4.1, to produce a new grid at a resolution of 50 m (WGS1984, UTM Zone 29N).

Terrain derivatives previously identified as useful in predictive mapping (Wilson et al., 2007; Brown et al., 2011) were extracted from the bathymetry using the ArcGIS extension Benthic Terrain Modeler v. 3.0 (Walbridge et al., 2018). Slope, eastness, northness, curvature, fine and broad bathymetric position index (BPI) and rugosity (VRM = Vector Ruggedness Measure) were calculated. The bathymetric position index is a derived metric of a cell's position and elevation relative to its surrounding landscape/cells within a user defined area (Wright, 2005). A combination of broad and fine scale BPI metrics were derived to enable features at varying scales to be identified (Wilson et al., 2007). Broad-scale BPI was calculated using a neighbourhood analysis based upon an annulus with an inner radius of 2 pixels and an outer radius of 20 pixels with a scale factor of 1000. Fine-scale BPI was calculated using a neighbourhood analysis based upon an annulus with an inner

radius of 1 pixel and an outer radius of 2 pixels with a scale factor of 100. Rugosity is a measure of the ratio of the surface area to the planar area and was calculated with a neighbourhood size of 3 x 3 pixels (Wilson et al., 2007). Slope is a measure of change in elevation and was derived from a neighbourhood size of 3 x 3. Aspect (subsequently converted to eastness and northness) measures the orientation of maximum change along the slope. Curvature is a measure of the shape of the slope, with values indicating whether a slope is convex or concave. Three types of curvature were calculated: profile, planar and general. Each accentuates different aspects of slope shape and can provide indirect measures of different processes relating to flow, erosion and deposition within the canyon (Wilson et al., 2007).

To capture the range of spatial scales at which the terrain derivatives may affect faunal distributions, a multiscale approach was implemented, whereby terrain variables were derived from bathymetry gridded at 50, 100 and 500 m. Statistical modelling (following the same protocol to assess predictive value of variables as detailed in section 2.3.3) was then applied to identify the most ecologically meaningful resolution to use for each variable, identified as those derivatives contributing the greatest to variance explained. Terrain derivatives from bathymetry gridded at 50 m were found to be optimal (Supplementary 2.1.2), and were exported as rasters at 50 m resolution (Figures 2.2 and 2.3) for further modelling.

Bathymetric slope criticality to the dominant semi-diurnal internal tide was calculated (Supplementary 2.1.3) from the processed bathymetry gridded at 50 m and the potential density derived from a ship-based CTD cast acquired during JC125 (Figure 2.1). Bathymetric slope criticality to the dominant semi-diurnal internal tide ($\alpha$) can identify potential areas within the canyon where up-slope propagating waves could be reflected back down-slope toward the canyon floor (supercritical, $\alpha > 1$), be focussed toward the head of the canyon (subcritical, $\alpha < 1$) or, become trapped (near-critical, $\alpha \simeq 1$) resulting in waves breaking and mixing (Hall et al., 2017).

#### 2.3.2.3 Oceanographic data processing and derived environmental variables

Near bottom values for absolute salinity and conservative temperature were extracted from the Forecasting Ocean Assimilation Model 7 km Atlantic Margin model (FOAM AMM7) (O'Dea et al., 2014). The FOAM AMM7 is a coupled hydrodynamic-ecosystem model, nested in a series of one-way nests. Values were averaged from daily means over a three-year period to account for interannual seasonal variability.

Near bottom values for tidal current variables (R.M.S, Root mean squared near-bottom baroclinic and barotropic current speed) over an $M_2$ tidal cycle were calculated from velocity components extracted from a 500 m resolution canyon region hydrodynamic model based on a modified version of the Princeton Ocean Model, used to simulate the dominant semi-diurnal internal tide in the Whittard Canyon region for 32 $M_2$ tidal cycles (Aslam et al., 2018). Both R.M.S baroclinic and

barotropic current speed were calculated to differentiate between the influences of the two tides that exhibit different spatial patterns across the canyon system (Figure 2.3).

In order to represent the physical oceanographic conditions experienced by the benthos and match the resolution of the depth and terrain derivatives, the oceanographic data were interpolated into rasters at 50 m resolution in ArcGIS (Figure 2.3). Interpolation was based upon spatial variograms calculated in Golden Software Surfer V 8 and undertaken by kriging using the Spatial Analyst tool box in ArcGIS. To account for discrepancies in bathymetric resolution between the physical oceanographic models and the bathymetry gridded at 50 m, bathymetry from the models was also exported and rasters created. Depth discrepancies between the datasets were accounted for by extracting oceanographic and current values from the nearest corresponding depths to that of the bathymetry gridded at 50 m.

### 2.3.3 Modelling

#### 2.3.3.1 Modelling approaches

Modelling was conducted in the open source software R using a variety of packages as detailed in Hijmans and Elith (2017) and Zuur et al. (2014a) including “randomForest”, “mgcv” and “gbm”.

Environmental variables coinciding with the mid-point of each 50 m video transect segment were extracted from each of the environmental rasters and combined with the corresponding values for abundance, species richness, 1/*D* and CWC occurrence to form a single data matrix. Data exploration was undertaken following Zuur et al. (2010) and indicated non-linear relationships between the response and environmental predictor variables.

To fulfil model assumptions of independence and improve interpretation of results, collinearity between environmental variables was tested and correlated variables removed. Collinearity was tested with Pearson’s correlation coefficient (pairwise correlations), variance inflation factor (VIF) scores and pair plots (Zuur et al., 2010; Zuur et al., 2014a) (Supplementary 2.2.1). Variable pairs with Pearson’s correlation coefficients >0.5 and VIF scores >5 were deemed correlated (Zuur et al., 2014a). For each group of correlated environmental variables, modelling using various techniques was undertaken (as described below) with a representative of each group added in turn to assess its predictive value by reviewing diagnostic plots of residuals and when model assumptions were met, retaining those that explained the greatest variance and gave the lowest Akaike’s Information Criterion (AIC) score (Table 2.2). The AIC score is commonly applied to compare model performance and measures the goodness of fit and model complexity reflecting the variance explained penalised by the number of explanatory variables. A lower AIC score indicates a better model fit (Zuur et al., 2014a). This resulted in four of the 12 environmental variables being retained.

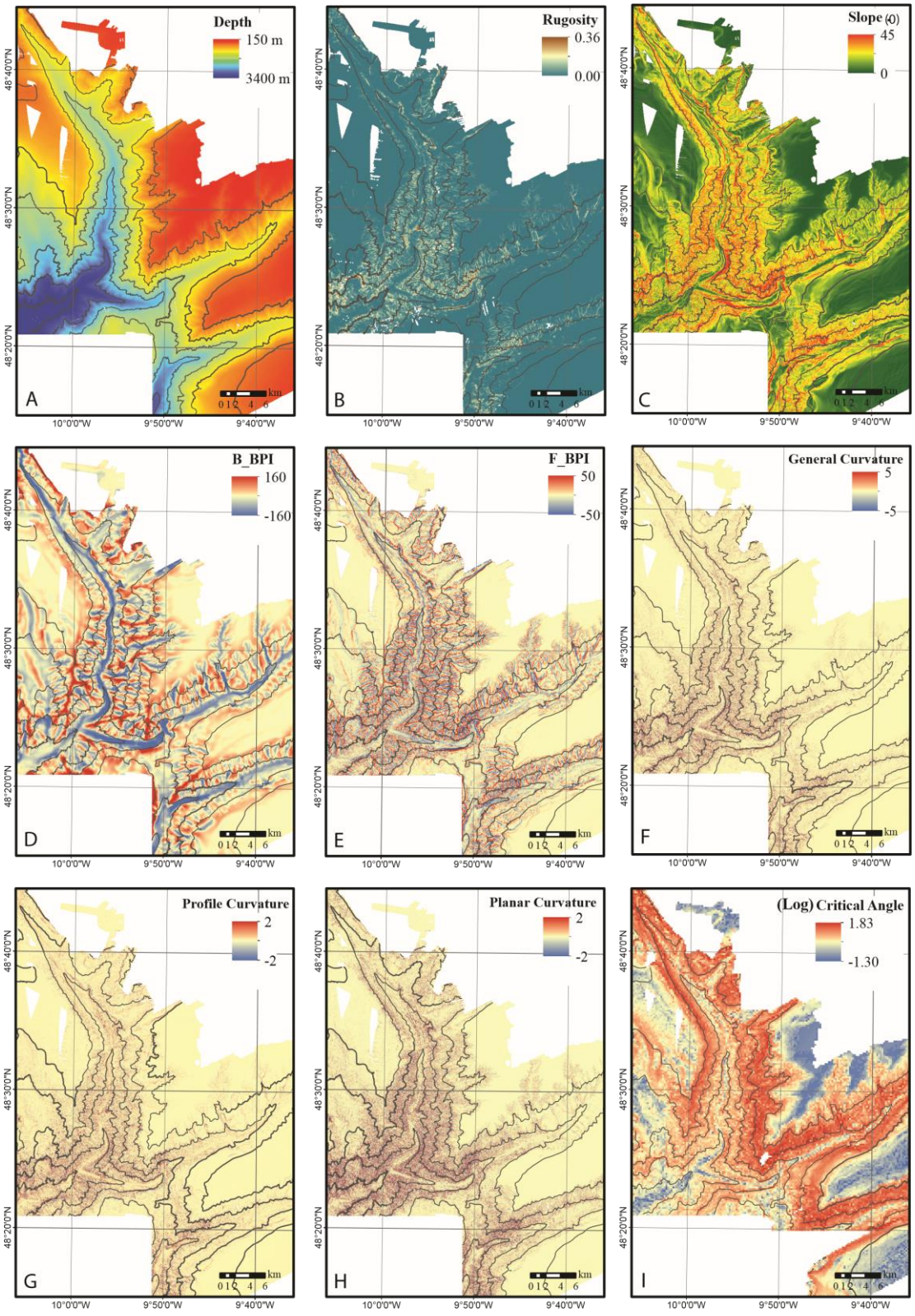


Figure 2.2 Maps (50 m pixel resolution) of the bathymetric derivatives used as environmental variable proxies in the predictive models: (A) Depth (m), (B) Rugosity, (C) Slope (ɵ), (D) Broad bathymetric positioning index, (E) Fine bathymetric positioning index, (F) Curvature, (G) Profile curvature, (H) Planar curvature, (I) Log of bathymetric slope criticality to the dominant semi-diurnal internal tide (α).

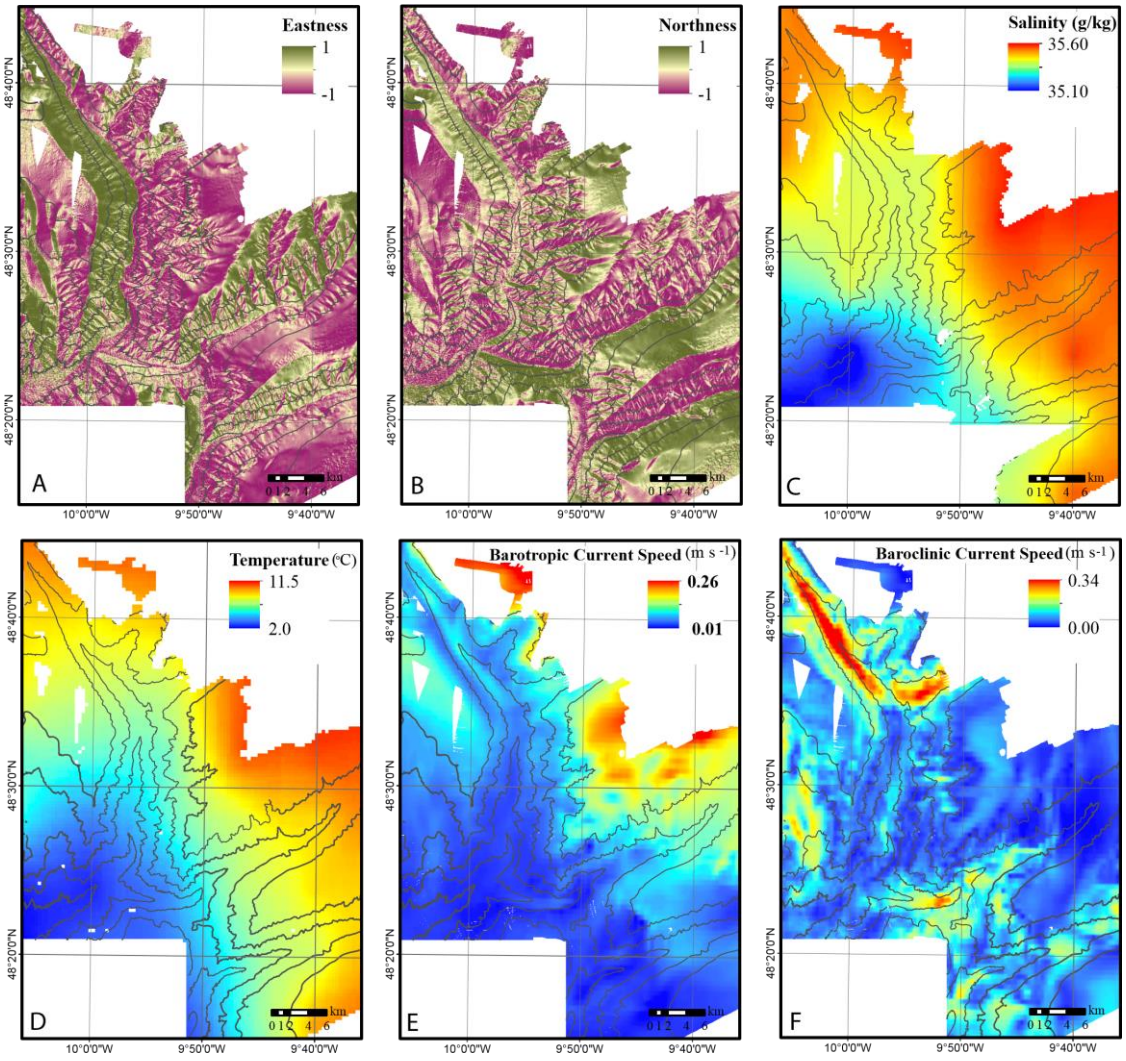


Figure 2.3 Maps (50 m pixel resolution) of the bathymetric and physical oceanographic derivatives used as environmental variable proxies in the predictive models. The physical oceanographic environmental variables were derived from the FOAM AMM7 ocean model and a canyon specific hydrodynamic model published by Aslam et al., 2018: (A) Northness, (B) Eastness, (C) Salinity (g/kg), (D) Temperature (°C), (E) R.M.S current speed for the barotropic tide (m $s^{-1}$), (F) R.M.S current speed for the baroclinic tide (m $s^{-1}$).

Table 2.2 Groups of correlated environmental variables. For each group, the variable retained for the models in indicated in bold

| Groups of correlated variables |
|---|
| • **Rugosity**, F_BPI, B_BPI |
| • **Slope**, General curvature, Profile curvature, Planar curvature |
| • **Depth**, Temperature, Salinity |
| • **R.M.S current speed for the baroclinic tide**, R.M.S current speed for the barotropic tide |

Generalized Additive Models, Random Forests and Boosted Regression Trees were used to determine which environmental variables explained the greatest variance in observed spatial patterns in CWC presence-absence, species richness, 1/*D* and abundance. To assess the influence of physical oceanographic variables, model performance with and without these environmental predictor variables was compared. Spatial autocorrelation in model residuals was assessed with semi-variograms and correlograms. Low spatial autocorrelation was observed in model residuals due to the sub-sampling of the data into training and test datasets (see section 2.3.2), together with the fact that sections of video transect were omitted due to data quality. Predicted probability of CWC occurrence, species richness, 1/*D* and abundance were mapped by applying each of the model algorithms to the full spatial extent of the selected environmental variable rasters.

Random Forests (RF) is a classification method that builds multiple trees based upon splitting rules that maximise homogeneity in response to predictors within branches, starting each time with a randomised subset of data points and predictor variables (Breiman, 2001). RF was chosen because it makes no underlying assumption of the distribution of the response variable, is robust to overfitting, allows for interactions between environmental variables and nonlinear relationships between the response and environmental variables (Prasad et al., 2006; Cutler et al., 2007). RF was run in classification mode for CWC presence-absence data and regression mode for the continuous response variables. Abundance was log+1 transformed. Each random forest was run with 1500 trees and the number of variables chosen at each node split set to default (square root of the number of variables in the model for classification and two for regression) with the out of bag (OOB) settings set as default (Breiman and Cutler, 2018).

Boosted Regression Trees (BRT) is a combined classification and regression method that builds a sequence of regression trees, with the initial tree fitted to the entire dataset and subsequent trees added to fit the remaining residuals (Elith, 2008). BRT was chosen as this method is robust to differing resolutions of data input and accommodates interactions and nonlinear relationships (Elith, 2008). BRT models were developed with cross validation on data using a tree complexity of 3 and learning rate of 0.001 with the optimum number of trees determined using a step forward function using k-fold cross validation. These parameter settings were chosen to ensure a minimum of 1000 trees were created and that the models did not overfit the data (Elith, 2008; Elith and Leathwick, 2009). For CWC presence-absence, a Bernoulli distribution was assumed, for species richness a Poisson distribution was assumed. Abundance was log+1 transformed to improve normality and modelled with a Gaussian distribution. Environmental variables were assessed using the inbuilt gbm.simplify function that specifies the optimum number of variables by dropping the least contributing variables and comparing deviance minimum error and model variance with and without that variable (Elith, 2008).

Generalized Additive Models (GAMs) are generalised models with smoothers and link functions based on an exponential relationship between the response variable and the environmental predictor

variables (Zuur et al., 2014b). This method was chosen because it can accommodate nonlinear relationships and produces ecologically intuitive outputs (Zuur et al., 2014a). GAMs have successfully been applied to model the distribution of marine species and habitats (Robert et al., 2015). The degree of smoothing for the environmental variables was selected based on the generalized cross validation (GCV) method and a log link function was used for all models except CWC presence-absence where a logit link function was used for the binary response. For CWC presence-absence, a Binomial distribution was assumed. For species richness and 1/*D* a Gamma distribution was assumed after exploring several alternative distributions (Gaussian, Poisson, quasi-Poisson and Negative-Binomial). Abundance was log+1 transformed to improve normality and modelled with a Gaussian distribution. Environmental variables were assessed by a backward-step selection, whereby the environmental variables resulting in the lowest deviance explained were dropped one at a time and the model refitted until only statistically significant (p value <0.05) variables remained in the models. Overall model fit was then compared and the most parsimonious model, identified as that containing those environmental variables that explained the maximal amount of variance whilst giving the lowest AIC score, was selected.

#### 2.3.3.2 Model performance

Model performance was assessed using a cross-validation procedure in which models were trained using a random partition of data (70 %) and tested against the remaining portion (30 %) (Guisan and Zimmermann, 2000). Model accuracy was assessed in terms of the model fit to the training dataset using AIC scores, diagnostic plots and variance explained (Adjusted $R^2$). Predictive performance was assessed using the Area Under the Receiver operating Curve (AUC) score for CWC presence-absence (Elith and Leathwick, 2009). The AUC score indicates how well the model discriminates presences and absences. An AUC score <0.5 indicates that the model is no better than random and an AUC score >0.7 can be considered as adequately discriminating presences from absences (Lobo et al., 2008). Due to the equal weighting of misclassification errors by the AUC, measures of sensitivity and specificity were also used to assess performance. Sensitivity is the fraction of correctly predicted CWC presences, while specificity is the fraction of correctly predicted CWC absences (Lobo et al., 2008). Predictive performance for the remaining models was assessed with correlation coefficients (linear regression) between the predicted and observed values.

#### 2.3.3.3 Ensemble Models

To provide more robust predictions, ensemble techniques that summarise the variation in predictions and uncertainties between modelling approaches were applied to build final maps. Ensemble models are important when optimal models cannot be identified. Ensemble model maps based upon weighted AUC scores or correlation coefficients of each of the algorithms were produced for each response variable.

## 2.4 Results

### 2.4.1 Morphospecies and observed patterns in diversity

A total of 280 morphospecies were annotated from the video data. Xenophyophores (representing ~17 % of individuals) were the most abundant morphospecies, followed by *Acanthogorgia* sp. (~10 %), Brachiopoda sp. 1 (~9 %), *Pentametrocrinus atlanticus* (~8 %) and Cerianthidae (~7 %). Due to poor video quality, Brachiopoda were not annotated from the data collected during JC010 and JC036 and so are omitted from further analysis. The predominant functional groups observed were suspension (filter) feeders, followed by detritivores and carnivores. Highest species richness (48) was sampled from a 50 m transect segment of vertical wall hard substratum observed during the dive JC125_262. This dive investigated a vertical wall community, comprising filter feeders (Cerianthidae, Scleractinia, Alcyonacea, Crinoidea, Actinaria, Porifera, Hydrozoa) detritivores (*Echinus*) and carnivores (Asteroidiea and Galatheoidea) (Figure 2.4). Highest diversity (1/*D*) (12.6) was recorded from the same dive JC125_262. Highest abundance (2149) was recorded from a 50 m transect segment on a different vertical wall observed during dive JC036_116, with the highest contributing taxa being *D. pertusum* (866 individual colonies) and *Acanthogorgia* sp. CNI14 (882).

Reef-forming CWCs, varying from single colonies to reefs were observed on seven dives amounting to 62 sample points out of 404. CWCs occurred on hard substratum with steep to vertical topography between water depths of 464 - 1892 m, temperature ranges of 5.6 - 9.6 °C, salinity 35.3 - 35.5 g/kg and R.M.S near bottom current velocities 0.09 - 0.29 m $s^{-1}$. CWCs were observed from a broad depth and associated temperature and salinity range because presence records represented the combination of three Scleractinia reef forming species (*M. oculata*, *D. pertusum* and *S. variabilis*) that occur across varying depth ranges.

### 2.4.2 Modelling

#### 2.4.2.1 Model performance

AUC scores for models of CWC presence-absence ranged from 0.96 - 0.99 (training dataset) to 0.82 - 0.93 (test dataset) indicating that all models adequately discriminate presences from absences, with RF performing the best (Table 2.3). Model sensitivity ranged from 0.35 - 0.87 (training dataset) to 0.21 - 0.60 (test dataset) and model specificity ranged from 0.97 - 1.00 (training dataset) to 0.98 - 0.99 (test dataset) with RF generally performing the best and GAM showing higher sensitivity in test datasets (Table 2.3). Lower sensitivity values and similar specificity and AUC values suggest a degree of over prediction of CWC occurrences by the models (Table 2.3). Correlation coefficients (Adjusted $R^2$) between predicted and observed species richness, 1/*D* and abundance ranged between 0.17 - 0.87 (training dataset) and 0.07 - 0.46 (test dataset) and were highest for RF, followed by BRT

and GAM (Table 2.4). The superior performance of RF could result from the inadequacy of available modelling distributions for the response variables assumed for BRT and GAM (Zuur et al., 2014a).

#### 2.4.2.2 Variable contribution in the predictive models

The environmental variables used for optimal models of CWC presence-absence, species richness, 1/*D* and abundance are shown in Tables 2.3 and 2.4. The importance of the environmental variables varied between the modelling algorithms. The models for CWC presence-absence ranked depth, rugosity and R.M.S baroclinic current speed as important predictor variables (Table 2.3). Models of species richness and abundance ranked depth as the most important predictor variable, whilst models for 1/*D* rank the predictor variables inconsistently (Table 2.4). The inconsistent rankings of environmental variables between models could result from the similarity in their contributing explanatory power and presence of interactions between the environmental variables. For example, the BRT model including R.M.S baroclinic current speed for 1/*D*, gave similar explanatory value to depth (26 %) followed by slope (23 %), and then rugosity (17 %), northness (17 %) and R.M.S baroclinic current speed (15 %). Furthermore, BRT pairwise interaction terms indicated interactions between depth and R.M.S baroclinic current speed.

### 2.4.3 Influence of oceanographic data

The physical oceanographic variables were highly collinear and only R.M.S baroclinic current speed was retained in the optimum models. Overall model performance was improved with the inclusion of R.M.S baroclinic current speed as an environmental predictor variable (Tables 2.3 – 2.4). Spatial predictions from the ensemble model including R.M.S baroclinic current speed showed increased diversity and increased probability of CWCs in areas of elevated current speed that coincided with steep topography (Figures 2.5 – 2.8), while the extent of suitable CWC habitat predicted decreased (Figure 2.5). For a CWC occurrence threshold >60 %, the suitable habitat reduced from 387 $km^2$ to 174 $km^2$, a decrease of 55 %; for a threshold of >70 % the habitat reduced from 125 $km^2$ to 13 $km^2$, a decrease of 89 % (thresholds consistent with those applied by Bargain et al. (2018).

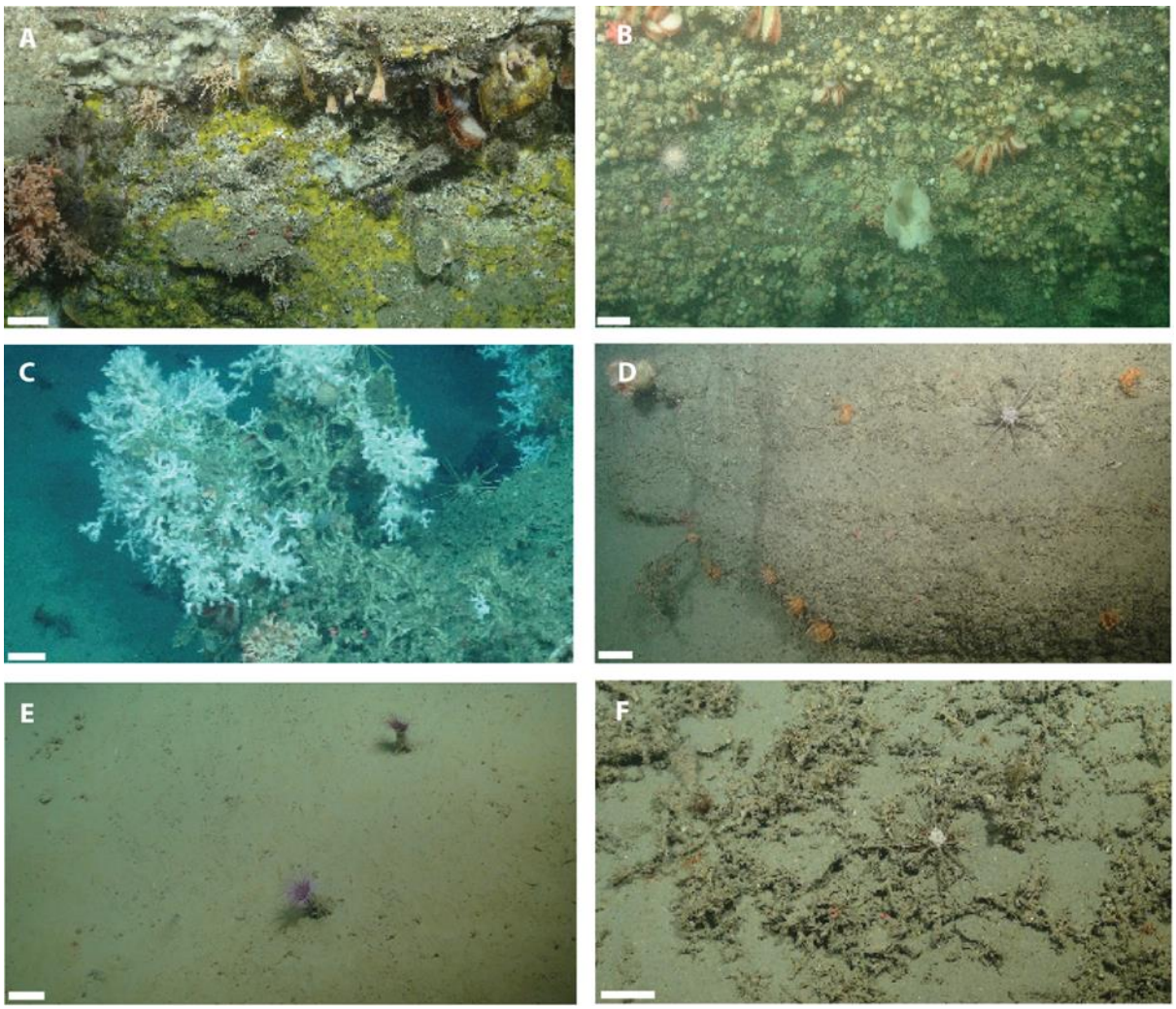


Figure 2.4 ROV video images showing organisms and substrata encountered: (A) *Acesta excavata*, *Neopycnodonte* sp., Porifera, Scleractinian corals and crinoids from vertical wall substratum during dive JC125_262 at 477 m, (B) Brachiopod sp. 1, *A. excavata*, *Psolus squamatus*, Porifera and echinoids from hard substrata during dive JC125_263 at 1400 m, (C) *Desmophyllum pertusum* reef during dive JC125_262 at 790 m, (D) *Brisingida* sp. and *Cidaris* from hard substratum during dive JC125_262 at 879 m, (E) Cerianthidae and Paguroidea from soft substratum during dive JC125_262 at 767 m, (F) Cerianthidae, Ophiuroidea, *C. cidaris*, *Munida* sp., *Bathynectes* sp., crinoids, and epifaunal turf from coral rubble during dive JC125_250 at 751 m. Scale bars = 10 cm.

Table 2.3 Modelling results for cold-water coral presence/absence based upon each of the modelling algorithms (Boosted Regression Tree (BRT), Random Forests (RF) and General Additive Models (GAMs)) that integrate variables including baroclinic current speed (BC_RMS) and excluding baroclinic current speed. Model performance was assessed using a cross-validation procedure in which models were trained using a random partition of data (70 %) and tested against the remaining portion (30 %). Model accuracy was assessed in terms of the model fit to the training dataset using variance explained (Adjusted $R^2$) and for GAMs the Akaike's Information Criterion score (AIC) and for RF the out of bag (OOB) test misclassification error rate. Predictive performance was assessed based upon the test dataset using measures of sensitivity, specificity and the Area under the receiver operating Curve (AUC).

| Model | Excluding BC_RMS | | | | | | | | | | | Including BC_RMS | | | | | | | | | | |
|---|---|---|---|---|---|---|---|---|---|---|---|---|---|---|---|---|---|---|---|---|---|---|
| | Variable importance | Variance explained | | OOB error rate | AIC | AUC | | Sensitivity | | Specificity | | Variable importance | Variance explained | | OOB error rate | AIC | AUC | | Sensitivity | | Specificity | |
| | | Train | Test | | | Train | Test | Train | Test | Train | Test | | Train | Test | | | Train | Test | Train | Test | Train | Test |
| BRT | Depth, Rugosity, Eastness, Slope | 26% | 28% | | | 0.96 | 0.88 | 0.48 | 0.21 | 1 | 0.98 | Rugosity, Depth, BC_RMS, Slope, Eastness | 34% | 27% | | | 0.97 | 0.89 | 0.66 | 0.43 | 0.98 | 0.89 |
| RF | Depth, Rugosity, Eastness, Slope, Northness | 25% | | 13% | | 0.99 | 0.89 | 0.82 | 0.26 | 1 | 0.98 | BC_RMS, Depth, Rugosity, Eastness, Slope | 32% | | 12% | | 0.99 | 0.93 | 0.87 | 0.52 | 0.99 | 0.94 |
| GAM | Rugosity, Eastness, Depth, Northness, Slope | 61% | | | 139 | 0.89 | 0.82 | 0.35 | 0.34 | 0.97 | 0.96 | Rugosity, BC_RMS, Depth, Slope | 58% | | | 130 | 0.97 | 0.87 | 0.74 | 0.60 | 0.98 | 0.89 |
| | | (Adj $R^2$ 55%) | | | | | | | | | | | (Adj $R^2$ 53%) | | | | | | | | | |

Table 2.4 Modelling results for species richness, Simpsons' reciprocal index (1/*D*) and abundancebased upon each of the modelling algorithms (Boosted Regression Tree (BRT), Random Forests (RF) and General Additive Models (GAMs)) that integrate variables including R.M.S baroclinic current speed (BC_RMS) and excluding R.M.S baroclinic current speed. Model performance was assessed using a cross-validation procedure in which models were trained using a random partition of data (70 %) and tested against the remaining portion (30 %). Model accuracy was assessed in terms of the model fit to the training dataset using variance explained (Adjusted $R^2$) and for GAMs the Akaike's Information Criterion score (AIC). Predictive performance was assessed based upon the test dataset using correlation coefficients (Adjusted $R^2$).

| Model | Excluding R.M.S baroclinic current speed | | | | | Including R.M.S baroclinic current speed | | | | |
|---|---|---|---|---|---|---|---|---|---|---|
| | Variable importance | Variance explained (Train) | AIC | Correlation Adj R² (Train) | Correlation Adj R² (Test) | Variable importance | Variance explained (Train) | AIC | Correlation Adj R² (Train) | Correlation Adj R² (Test) |
| Species Richness | | | | | | | | | | |
| BRT | Depth, Northness, Rugosity, Eastness, Slope | 31% | | 0.72 | 0.27 | Depth, Rugosity, Northness, BC_RMS, Slope, Eastness | 39% | | 0.78 | 0.31 |
| RF | Depth, Rugosity, Northness, Slope, Eastness | 35% | | 0.87 | 0.43 | Depth, BC_RMS, Rugosity, Northness, Slope, Eastness | 37% | | 0.87 | 0.46 |
| GAM | Depth, Rugosity, Northness, Eastness, Slope | 27.8% Adj R² (33%) | 1384 | 0.39 | 0.29 | Depth, Rugosity, BC_RMS, Northness, Eastness, Slope | 49% Adj R² (43%) | 1358 | 0.51 | 0.36 |
| Abundance | | | | | | | | | | |
| BRT | Depth, Eastness, Rugosity, Slope, Northness | 32% | | 0.77 | 0.31 | Depth, BC_RMS, Rugosity, Eastness, Slope | 35% | | 0.73 | 0.34 |
| RF | Depth, Eastness, Rugosity, Slope, Northness | 36% | | 0.87 | 0.36 | Depth, BC_RMS, Eastness, Rugosity, Slope | 40% | | 0.87 | 0.40 |

| Model | Excluding R.M.S baroclinic current speed | | | | | Including R.M.S baroclinic current speed | | | | |
|---|---|---|---|---|---|---|---|---|---|---|
| | Variable importance | Variance explained (Train) | AIC | Correlation Adj $R^2$ (Train) | Correlation Adj $R^2$ (Test) | Variable importance | Variance explained (Train) | AIC | Correlation Adj $R^2$ (Train) | Correlation Adj $R^2$ (Test) |
| GAM | Depth, Rugosity, Eastness, Slope | 19% Adj $R^2$ (15%) | 858 | 0.19 | 0.14 | Depth, BC_RMS, Rugosity, Eastness, Slope | 38% Adj $R^2$ (33%) | 802 | 0.38 | 0.27 |
| 1-*D* | | | | | | | | | | |
| BRT | Northness, Slope, Depth, Rugosity, Eastness | 14% | | 0.44 | 0.20 | Depth, Slope, Northness, Rugosity, BC_RMS | 15% | | 0.58 | 0.25 |
| RF | Slope, Depth, Rugosity, Northness | 18% | | 0.85 | 0.32 | Depth, Slope, BC_RMS, Rugosity, Northness | 20% | | 0.86 | 0.31 |
| GAM | Northness, Depth, Rugosity, Slope | 27% Adj $R^2$ (12%) | 862 | 0.17 | 0.07 | Depth, Rugosity, Northness, Slope, BC_RMS | 26% Adj $R^2$ (12%) | 862 | 0.17 | 0.08 |

### 2.4.4 Model predictions

Model predictions were made across the full extent of available environmental rasters. However, as the models were trained from samples within the canyon branches, model predictions beyond this extent are deemed less reliable. Therefore, we limit further analysis of model predictions to within the canyon branches.

Ensemble models predicted increased probability of CWCs, and increased species richness, 1/*D* and abundance at specific depths in areas of increased terrain complexity that coincided with relatively elevated current speed of the internal (baroclinic) tide.

Rugosity and slope were derived from 3 x 3 windows at a 50 m cell size and captured spatial heterogeneity in terrain features over 150 m resolution. Within the canyon, these relate to ridges between gullies and steep to vertical wall escarpments. Gullies occur on the canyon flanks and steep to vertical wall escarpments occur on the north-eastern flank of Whittard Canyon's Eastern branch as well as in association with the amphitheatre rims and headwall scars at tributary heads throughout the canyon (Figure 2.5). Highest probability of CWCs, and highest species richness, 1/*D* and abundance are predicted to occur in association with the increased terrain complexity provided by these features. Furthermore, the ensemble models emphasise areas of increased biological prevalence associated with elevated RMS baroclinic current speed and coincident topography. These areas predominantly occur toward the canyon head and north-eastern flank of the Eastern branch and a dog leg region towards the lower reaches of Explorer Canyon (Figures 2.3, 2.5 – 2.8).

CWCs exhibited a negative response with increasing depth beyond ~2000 m (Supplementary 2.3.1) and an overall positive response with increasing R.M.S baroclinic current speed, slope and seafloor ruggedness. Ensemble models predicted increased probability of CWCs in association with increased terrain complexity with highest probability of CWCs predicted on the slopes of ridges and escarpments above ~2000 m (Figure 2.5). Lowest probability of CWCs, was predicted in areas of low terrain complexity below ~2000 - 2500 m and at shallow depths along sections of the canyon axis and on the southern flanks of the Explorer and Dangaard Canyons (Figure 2.5).

Species richness and 1/*D* exhibited similar relationships with the environmental variables. Both species richness and 1/*D* exhibited an overall negative response with increasing depth with peaks at ~1200 m (Supplementary 2.3.1). They showed a positive response with increasing R.M.S baroclinic current speed which became negative at speeds greater than 0.25 m $s^{-1}$ and an overall positive response to increased slope and seafloor ruggedness. Ensemble models predicted increased species richness and 1/*D* in areas of increased terrain complexity with highest values predicted on escarpments and the crests and south facing slopes of ridges, peaking at 1200 m (Figure 2.6 and 2.7, respectively). Lower species richness and 1/*D* was predicted in areas of low terrain complexity below

~2000 - 2500 m and at shallow depths along sections of the canyon axis and on the southern flanks of the Explorer and Dangaard Canyons (Figure 2.6 and 2.7, respectively).

Abundance increased with depth although below 1600 m, the response became negative. (Supplementary 2.3.1). The response of abundance to R.M.S baroclinic current speed was variable, becoming negative at speeds greater than 0.25 m $s^{-1}$ whilst increased slope and seafloor ruggedness resulted in an overall positive abundance response. Ensemble models predicted increased abundance in association with greater terrain complexity. Peaks in abundance were predicted to occur on crests of the ridges between 800 - 1600 m (Figure 2.8). In areas of low terrain complexity below ~2000 - 2500 m, on the Southern flanks of the Explorer and Dangaard Canyons as well as at shallow depths along sections of the canyon axis, lower abundance was predicted by the ensemble model (Figure 2.8).

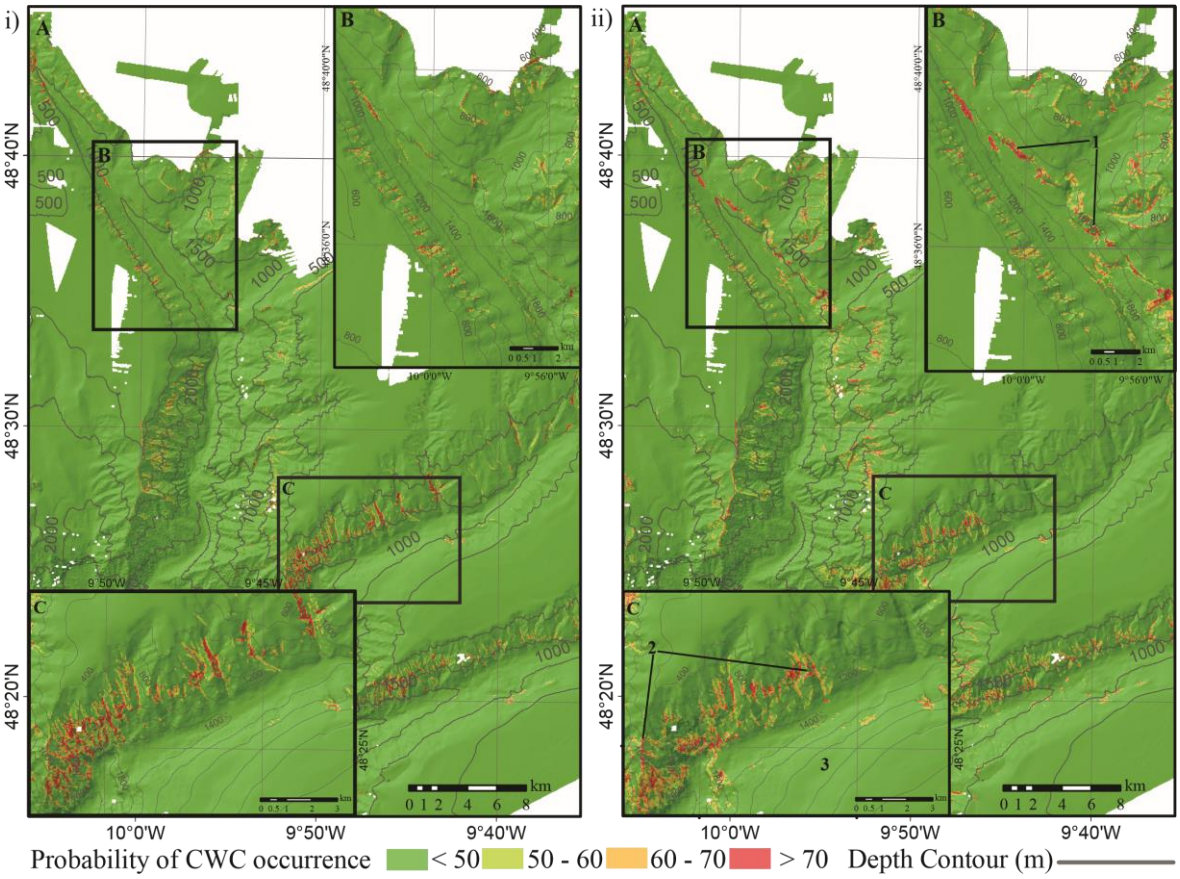


Figure 2.5 Ensemble model predictive maps for probability of cold-water coral occurrence (A) across the extent of the survey area and (B and C) insets zoomed in on canyon flanks. (i): Predictive map based upon bathymetry and its derivatives. (ii): Predictive map based upon bathymetry and its derivatives with physical oceanographic data (R.M.S current speed of the baroclinic tide). Increased probability of CWCs is predicted on escarpments (1) and slopes of ridges (2) and lower probability is predicted in areas of low terrain complexity (3). Model predictions beyond canyon branches (i.e. on the interfluves and the shelf) are less reliable because training datasets did not include these environments. We have excluded them from our interpretation.

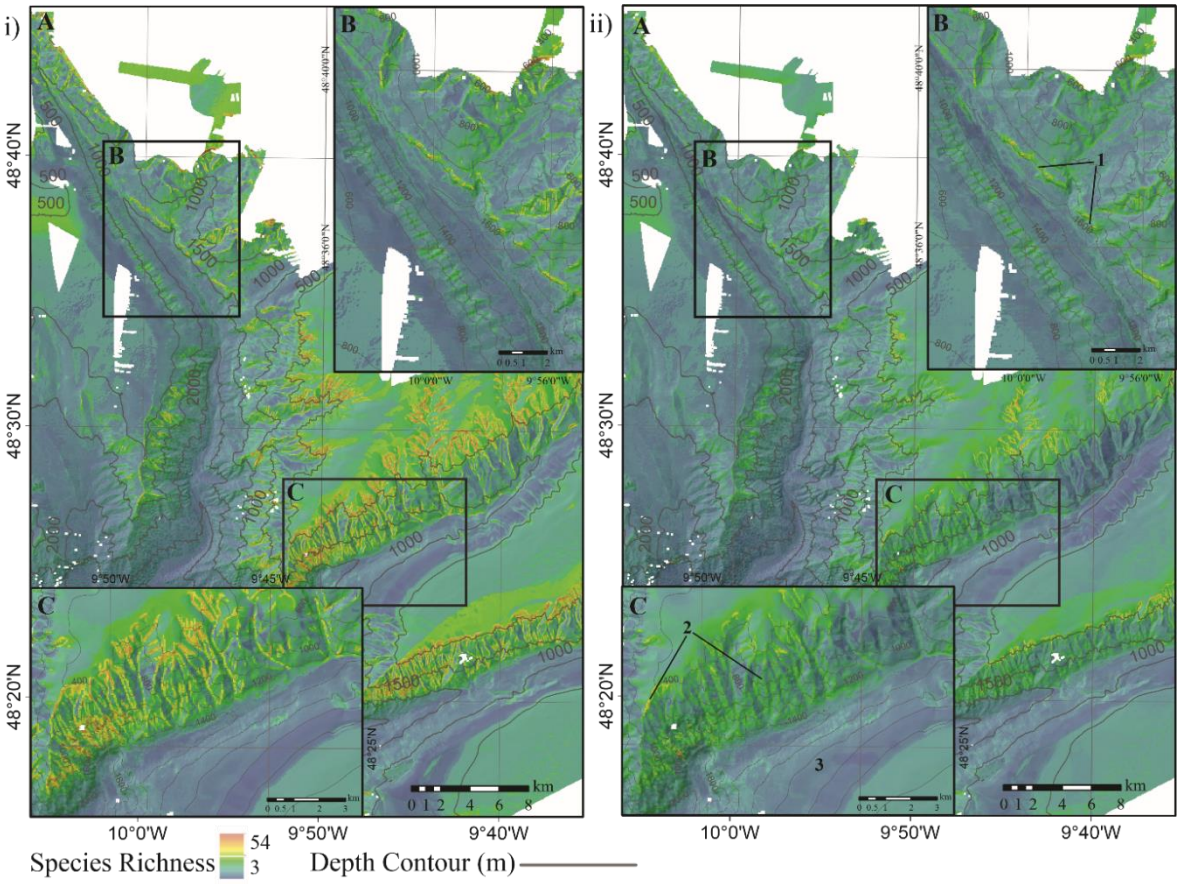


Figure 2.6 Ensemble model predictive maps for species richness (A) across the extent of the survey area and (B and C) insets zoomed in on canyon flanks. (i): Predictive map based upon bathymetry and its derivatives. (ii): Predictive map based upon bathymetry and its derivatives with physical oceanographic data (R.M.S current speed of the baroclinic tide). Increased species richness is predicted on escarpments (1) and the crests and south facing slopes of ridges (2) while lower species richness is predicted along sections of the canyon axis and of low terrain complexity (3). Model predictions beyond canyon branches (i.e. on the interfluves and the shelf) are less reliable because training datasets did not include these environments. We have excluded them from our interpretation.

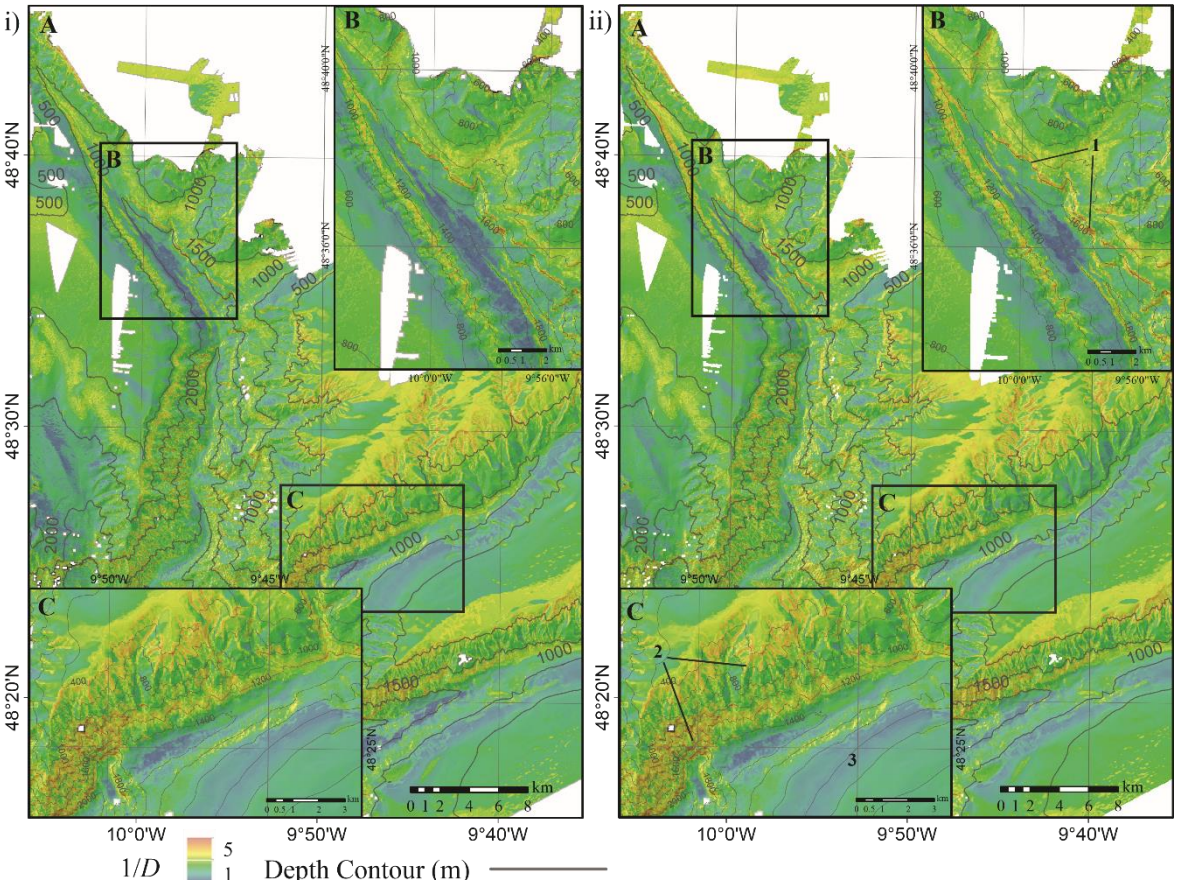


Figure 2.7 Ensemble model predictive maps for Simpsons' reciprocal index (1/*D*) (A) across the extent of the survey area and (B and C) insets zoomed in on canyon flanks. (i): Predictive map based upon bathymetry and its derivatives. (ii): Predictive map based upon bathymetry and its derivatives with physical oceanographic data (R.M.S current speed of the baroclinic tide). Increased 1/*D* is predicted on escarpments (1) and the crests and south facing slopes of ridges (2) while lower 1/*D* is predicted along sections of the canyon axis and of low terrain complexity (3). Model predictions beyond canyon branches (i.e. on the interfluves and the shelf) are less reliable because training datasets did not include these environments. We have excluded them from our interpretation.

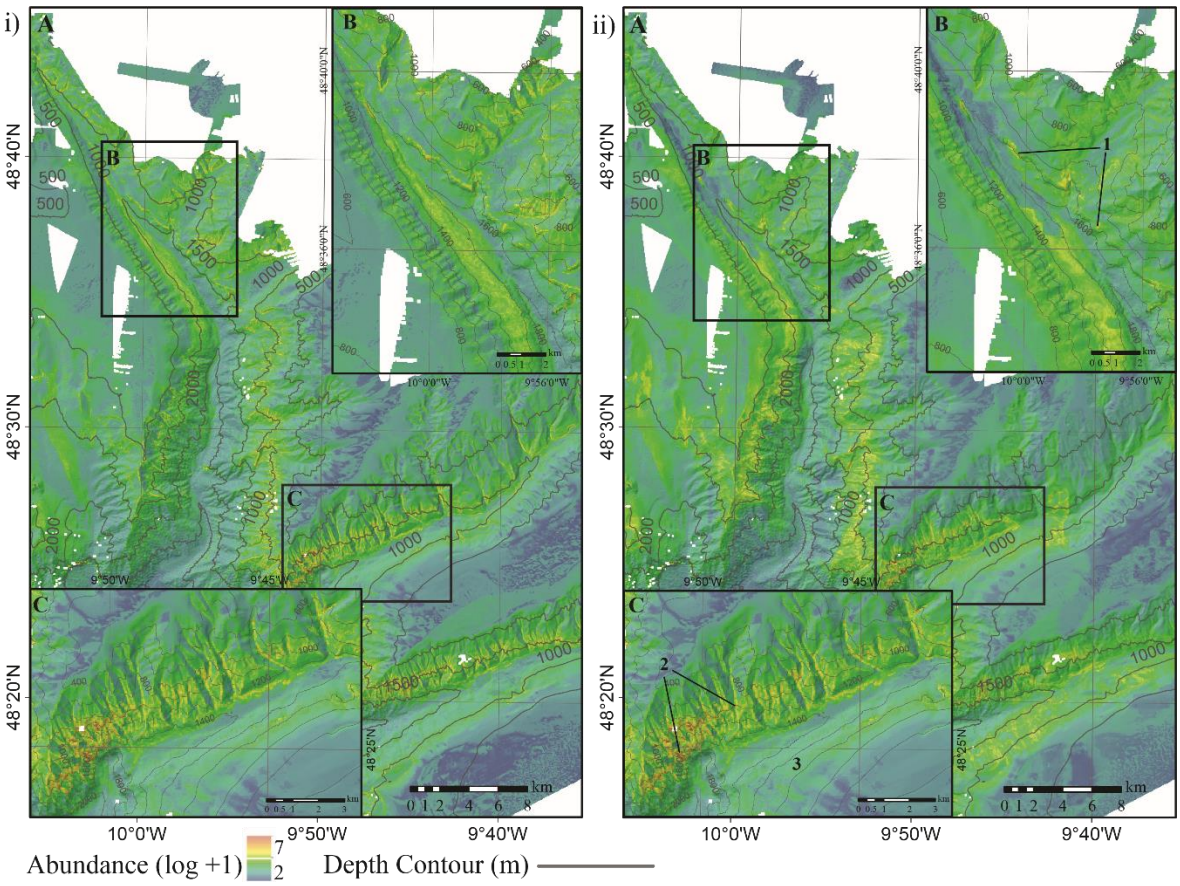


Figure 2.8 Ensemble model predictive maps for abundance (log+1) (A) across the extent of the survey area and (B and C) insets zoomed in on canyon flanks. (i): Predictive map based upon bathymetry and its derivatives. (ii): Predictive map based upon bathymetry and its derivatives with physical oceanographic data (R.M.S current speed of the baroclinic tide). Highest abundance is predicted on the crests of ridges between 800 - 1600 m (2) and lower abundance is predicted along sections of the canyon axis and of low terrain complexity (3). Model predictions beyond canyon branches (i.e. on the interfluves and the shelf) are less reliable because training datasets did not include these environments. We have excluded them from our interpretation.

## 2.5 Discussion

### 2.5.1 Environmental variables influencing faunal patterns in canyons

We have identified that depth, terrain complexity and hydrodynamics are important environmental factors influencing faunal patterns in submarine canyons and demonstrated that incorporating physical oceanographic data into predictive models improves their performance.

Spatial heterogeneity in these environmental conditions drives spatial patterns in fauna by providing a greater variety of niches with the potential to support increased species richness and diversity (Levin et al., 2010; De Leo et al., 2014).

#### 2.5.1.1 Terrain complexity

Terrain complexity is a proxy of seafloor heterogeneity that is positively correlated with diversity (Levin et al., 2010; De Leo et al., 2014). The high terrain complexity of canyons generates spatial heterogeneity in sediment dynamics (de Stigter et al., 2011; Martín et al., 2011; Puig et al., 2017), substratum composition (Huvenne et al., 2011; Huvenne and Davies, 2014; Stewart et al., 2014) and current exposure (Ismail et al., 2015). Filter feeders, including CWCs, show a preference for such increased terrain complexity (De Mol et al., 2011; Howell et al., 2011; Huvenne et al., 2011; Gori et al., 2013; Rengstorf et al., 2013; Robert et al., 2015; Pierdomenico et al., 2016; Fabri et al., 2017; van den Beld et al., 2017; Bargain et al., 2018). They colonise topographic highs to exploit local current regimes, and so increase food encounter rates (Mohn et al., 2014; Fabri et al., 2017; Lo Iacono et al., 2018). In our study, increased probability of CWC occurrence, species richness, 1/*D* and abundance were associated with areas of high terrain complexity (slope and rugosity) over similar spatial scales predicted for macrobenthic diversity in canyons off Hawaii (De Leo et al., 2014). These predictions are supported by previous studies within the canyon system that also predicted CWCs in areas of complex topography (Robert et al., 2015) and observed CWCs and increased epibenthic diversity and abundance in association with steep walls and topographic highs (Huvenne et al., 2011; Johnson et al., 2013; Davies et al., 2014; Robert et al., 2015). Our models predicted asymmetric distributions (where a higher prevalence of different taxa is predicted for one or the other canyon flank) between the opposing flanks of both Dangaard and Explorer Canyons. The flanks of the canyons differ in complexity, with higher species richness and probability of CWCs predicted for the more complex northern flanks. Unfortunately the spatial extent of predictive mapping in previous studies does not enable further confirmation of the asymmetric distributions predicted (Robert et al., 2015), but fauna are predicted and observed in association with complex terrain which would support our model predictions (Davies et al., 2014; Robert et al., 2015). In other canyons, asymmetric distributions have been attributed to the different geomorphology and hydrodynamics of canyon flanks, with one side more subject to intense hydrodynamics and the other dominated by depositional regimes (De Mol et al., 2011; Fabri et al., 2017; Pierdomenico et al., 2017; Lo Iacono et al., 2018). Our data suggest, more specifically, that it is the differences in terrain complexity between flanks that result from these processes, together with variation in baroclinic current speeds which generate the observed asymmetric patterns in fauna distribution.

Slope acts as a proxy for substratum type, which is correlated with faunal distributions. The steep slopes of Whittard Canyon are generally associated with hard substratum (Huvenne et al., 2011; Johnson et al., 2013; Stewart et al., 2014; Robert et al., 2015; Robert et al., 2017; Carter et al., 2018), which is positively correlated with sessile epibenthic diversity as it provides a suitable surface for epifauna to adhere to (Baker et al., 2012). In addition, steep slopes prevent sediment deposition and subsequent smothering of epifauna in these environments affected by high sedimentation rates (Howell et al., 2011; Baker et al., 2012). Steep slopes may also provide refuge for fauna from

anthropogenic disturbance caused by fishing gear (Huvenne et al., 2011; Johnson et al., 2013; Pierdomenico et al., 2016). A positive relationship between slope and diversity has been observed previously from Whittard and other canyons (Huvenne et al., 2011; Johnson et al., 2013; Robert et al., 2015; van den Beld et al., 2017; Chauvet et al., 2018). In our study, although highest diversity was recorded from vertical walls, some sections of the walls supported low diversity. This observation suggests that other processes and/or resources are acting together with terrain complexity to influence faunal distributions in canyons.

#### 2.5.1.2 Food supply and the internal tide

Variability in quality and amount of food supply influences canyon faunal distributions (De Leo et al., 2010; McClain and Barry, 2010; Cunha et al., 2011; Chauvet et al., 2018). Many benthic species within canyons rely on surface derived POM as their main food supply (Cunha et al., 2011; Miller et al., 2012). Generally, availability of surface derived POM decreases with depth (Lutz et al., 2007). However, in active canyons sediments can regularly be flushed to the deep. In parallel, local hydrodynamics (including internal tides) can cause resuspension of material and generate nepheloid layers at specific depths (Puig et al., 2014; Wilson et al., 2015b). Nepheloid layers are concentrations of suspended material (including POM) that represent an important food resource for deep-sea fauna (Demopoulos et al., 2017).

Within Whittard Canyon, nepheloid layers and centres of resuspension have been previously observed 1) where the MOW interacts with areas of complex canyon topography resulting in baroclinic internal wave motion, causing turbulent mixing (Wilson et al., 2015b), and 2) associated with the internal tide at depths of 400 - 500 m, 900 - 1600 m and 1700 - 1800 m as well as where internal waves propagate at the boundary between the permanent thermocline 600 - 900 m and upper boundary of the MOW (Wilson et al., 2015b). In our study, high probability of CWCs occurrence and peaks in species richness, 1/*D* and abundance are predicted at depths of 800 - 1600 m, coinciding with some of the above mentioned areas of resuspension and nepheloid layer production (Figures 5 - 8). Previous studies have also observed high diversity in association with nepheloid layers in Whittard Canyon (Huvenne et al., 2011; Johnson et al., 2013; Robert et al., 2015). The correlated spatial patterns between canyon fauna and nepheloid layer distributions support the importance of food availability, in the form of nepheloid layers, in influencing fauna distributions.

We found that internal tide dynamics correspond to an important factor influencing faunal patterns in canyons, contributing to increased spatial heterogeneity in environmental conditions. Faunal distributions are influenced by the internal tide both directly and indirectly. The internal tide directly influences fauna distributions by current speed and indirectly via its role in the production and distribution of nepheloid layers.

Current speeds exceeding 0.15 m $s^{-1}$ can cause resuspension of material (Thomsen and Gust, 2000), an important stage in nepheloid layer production. In our study, increased probability of CWC

occurrence, species richness, 1/*D* and abundance coincide with areas of elevated current speed for the internal tide. CWC occurrences have been linked to intensified bottom currents in a number of settings (Davies, 2009; Howell et al., 2011; Mohn et al., 2014; Rengstorf et al., 2013; van Oevelen et al., 2016), including canyons (Bargain et al., 2018). However, our data show that above 0.25 m $s^{-1}$ species richness and abundance are predicted to decrease. Species vary in their feeding strategies and efficiency under different hydrodynamic regimes (Järnegren and Altin, 2006; van Oevelen et al., 2016). For filter feeders, increased current flow increases food encounter rate up to a limit after which the speed of the current exceeds that at which fauna can extract particles and/or causes physical disturbance (Johnson et al., 2013; Orejas et al., 2016). Our models predict low diversity on relatively flat sections of the canyon floor that experience current speeds exceeding (0.25 m $s^{-1}$), located toward the canyon head of the Eastern branch, and also where the adjoining Dangaard and Explorer canyons intersect the main axis (Figure 2.3, 2.6-2.8). These are areas expected to experience higher disturbance regimes as mobile sandy sediments are routinely reworked over the tidal cycle, forming an unsuitable substratum for colonisation and abrasing the lower canyon walls. Additionally stochastic/episodic turbidity currents and mud-rich sediment gravity flows travel along the canyon's axis representing major disturbance events (Puig et al., 2014; Amaro et al., 2016). Johnson et al. (2013) also attributed low diversity toward the bottom of canyon walls to increasing disturbance toward the canyon floor. It is therefore likely that disturbance is restricting faunal patterns across the canyon floor, and could explain the negative relationship of species richness and abundance with high current speed.

As the internal tide wave propagates, it generates vertical displacement of the isopycnal surfaces and associated nepheloid layers (Hall et al., 2017). The periodic vertical movement of the nepheloid layer in the water column replenishes food to canyon fauna over the tidal cycle and has been linked to the distributions of antipatharians and gorgonians in canyons of the Bay of Biscay (van den Beld et al., 2017). In our study, CWCs are also associated with locations where the internal tide is proposed to propagate (Wilson et al., 2015b; Aslam et al., 2018) and isopycnal displacements caused by the internal tide with amplitudes measuring up to 80 m have been recorded within the Eastern branch of Whittard Canyon (Hall et al., 2017). However, fine scale studies investigating the influence of the vertical variations in environmental conditions generated by the internal tide on fauna are still lacking.

Internal waves, turbulent mixing and downslope displacement of water can generally be associated with enhanced resuspension of POM and can control the development of nepheloid layers (Allen and Durrieu de Madron, 2009; Hall et al., 2017; Aslam et al., 2018). Examples of the internal tide interacting with topography enhancing local hydrodynamics to form efficient food supply mechanisms to the benthos, have previously been documented in the Baltimore Canyon (Demopoulos et al., 2017). In other settings the reliance of CWCs on local current regimes to deliver food from the surface has been stressed (Rengstorf et al., 2013; Mohn et al., 2014; Davies, 2009;

Mienis et al., 2009; Soetaert et al., 2016). It is probable that a similar process is occurring in Whittard Canyon. Our models predict high diversity and probability of CWCs in areas of complex terrain, especially steep slopes that are critical and supercritical to the dominant semi-diurnal internal tide and experience moderate internal tide current speeds. In their study of nepheloid layers within Whittard Canyon, Wilson et al. (2015b) found the distribution of nepheloid layers was associated with the criticality of the slope to the dominant semi-diurnal internal tide. Intermediate nepheloid layers were associated with critical conditions, whilst supercritical conditions, that reflect wave energy back down slope to suspend material, were linked to the formation of intermediate nepheloid layers at greater depths. These correlated spatial patterns between canyon fauna, nepheloid layer distributions and criticality support the theory of the interactive processes of the internal tide (local hydrodynamics) and topography in generating spatial heterogeneity in food supply to which fauna respond.

#### 2.5.1.3 Physical oceanography in canyon modelling

Despite hydrodynamics having been related to epibenthic fauna distributions in canyons (Hargrave et al., 2004; Cunha et al., 2011; Huvenne et al., 2011; Johnson et al., 2013; Fabri et al., 2017; Bargain et al., 2018), there is a paucity of work which really quantifies this relationship as we have done here. Of the few studies that have incorporated hydrodynamics into predictive models, authors also found current speed to be an important environmental predictor (Bargain et al., 2018). In other studies the variable aspect, or its derivative components eastness and northness, used as a proxy for current exposure, have been identified as an important predictor variable (Lo Iacono et al., 2018).

Our work has shown that by integrating high-resolution hydrodynamic data into predictive models we are able to capture greater environmental heterogeneity beyond that solely represented by terrain proxies (specifically areas of resuspension and nepheloid layer production), and in turn improved the precision of the predicted distribution maps.

Future modelling efforts would benefit from incorporating physical oceanography data. However, high-resolution hydrodynamic models have only been developed for a subset of canyons and previous studies that integrated oceanographic data at low resolutions found it difficult to discriminate different environmental conditions (Davies et al., 2008a; Davies and Guinotte, 2011). Consequently, integrating oceanographic data at an appropriate scale currently represents the main challenge of high-resolution canyon mapping.

### 2.5.2 Model limitations

Field validations of deep-sea predictive models have demonstrated that caution should be applied not to over-interpret results (Anderson et al., 2016b). In particular, high spatial heterogeneity in environmental conditions and localised faunal distributions can be difficult to model accurately

(Anderson et al., 2016b). As such, model results should be viewed as representing suitable locations rather than actual distributions. The outputs from models are constrained by the data inputs (Lecours et al., 2015; Miyamoto et al., 2017; Misiuk et al., 2018; Porskamp et al., 2018), as demonstrated by our results which differed depending upon the inclusion of hydrodynamics (Table 2.3 and 2.4). Consequently, increased sample size, data resolution of the environmental variables and the inclusion of environmental variables that capture variability in food availability could improve our model predictions by further characterising environmental gradients and resolving the species – environment relationship of canyon fauna.

The dependence of model performance on data resolution represents a limitation for deep-sea models (Lecours et al., 2015; Miyamoto et al., 2017; Misiuk et al., 2018; Porskamp et al., 2018). In our study the environmental variables temperature and salinity were extracted and interpolated from the FOAMM model that outputted the data at 7 km, which is too coarse a grid size to resolve the fine-scale heterogeneity that influences species distributions in Whittard Canyon. As a result these variables were not retained in the models. The inclusion of finer resolution temperature and salinity data would enable environmental heterogeneity in water mass characteristics to be better characterised. Unfortunately, such fine-scale modelling outputs are rarely available for canyons. Additionally, incorporating oceanographic data metrics of higher temporal resolution that capture temporal variability in addition to mean values, could further improve the predictive value of oceanographic variables, since species distributions are often limited by environmental extremes (Vasseur et al., 2014; Stuart-Smith et al., 2017). Our results suggest that food supply is an important factor influencing species distributions, as such, the inclusion of environmental variables that capture variability in food availability could provide further insights and improve variance explained by models. Lastly, increasing the number of ground-truthed samples, from across the different canyon environments could reduce heterogeneity in the dataset and enable more accurate modelling of species- environment relationships, so improving prediction outside the originally sampled area.

Despite the limitations of predictive modelling, as mentioned above, and despite the limitations of our specific dataset in Whittard Canyon, the results of this study still provide new insights in the functioning of submarine canyons, and in the processes that drive benthic faunal distributions in canyons.

## 2.6 Conclusion

In conclusion, our study has shown that the inclusion of high-resolution oceanographic data into predictive models of CWCs and epibenthic megafaunal biodiversity improves their performance. Our work builds upon previous studies that solely used indirect variables to capture information regarding physical oceanography and provides further evidence within a statistical modelling framework for the role of hydrodynamics, and principally the internal tide, in influencing faunal

patterns in canyons. Highest probability of CWCs and epibenthic diversity occur in areas of complex terrain that are subject to elevated current speed. These areas coincide with areas of probable resuspension and nepheloid layer distribution that represent enriched food resources for epibenthic canyon fauna. Future predictive modelling efforts would benefit from incorporating physical oceanography data at ecologically meaningful resolutions, based upon prior multiscale analysis, helping to ensure accurate habitat mapping of features of conservation interest, which will facilitate effective spatial management.

## 2.7 Acknowledgements

The authors would like to thank the Captains, crews, and scientific parties of expeditions JC010, JC036, JC125 and MESH. We are particularly grateful to the Isis ROV team for the collection of groundtruthing data in the challenging submarine canyon terrain. We would also like to thank Tim Le Bas and Catherine Wardell for help with the bathymetry data processing, Dr Tom Ezard for his support with statistics and Michael Faggetter for his support with Matlab. We are very grateful to the two anonymous reviewers for their truly considerate and constructive reviews.

This work was funded by the NERC MAREMAP programme, the ERC CODEMAP project (Grant no 258482), the EC FP7 IP HERMIONE, DEFRA and the NERC CLASS programme (Grant No NE/R015953/1). Tabitha Pearman is a PhD student in the NERC-funded SPITFIRE Doctoral Training Programme (Grant number NE/L002531/1) and receives further funding from the National Oceanography Centre and the CASE partner CEFAS. Veerle Huvenne currently receives funding from the NERC CLASS programme and from the European Union’s Horizon2020 research and innovation programme iAtlantic project (grant agreement No 818123).

# Chapter 3 Spatial and temporal environmental heterogeneity generated by internal tides influences faunal patterns observed from vertical walls within a submarine canyon

This chapter is in preparation for submission to a peer-reviewed journal as **Pearman, T.R.R.,** Robert, K., Callaway, A., Hall, R., Lo Iacono, C., Mienis, F., Huvenne, V.A.I. Spatial and temporal environmental heterogeneity generated by internal tides influences faunal patterns observed from vertical walls within a submarine canyon

Author contributions: T.P conceptualised the chapter, annotated ROV imagery, processed and calculated vertical displacement of the internal tide from CTD data and associated variance in oceanographic conditions at all dive sites, conducted statistical analysis and wrote the manuscript. V.H and R.H acquired the ROV image and glider data during the JC124_JC125 CODEMAP2015 cruise. F.M provided CTD data from the 64PE421, 64PE453 and 64PE437 cruises. R.H provided vertical displacement measures of the internal tide from the Seaglider and supervised in the calculation of physical oceanographic variables. K.R contributed annotations from ROV imagery. All authors reviewed and commented on the chapter.

## 3.1 Abstract

Vertical walls of submarine canyons represent features of high conservation value that can provide natural areas of protection for vulnerable marine ecosystems under increasing anthropogenic pressure from deep-sea trawling. Wall assemblages can vary between and even within canyon branches, in part attributed to the nature of canyons that can exhibit high environmental heterogeneity over short spatial scales. Effective spatial management and conservation of these assemblages requires a deeper understanding of the processes that generate the observed faunal distribution patterns. Canyons are recognised as sites of intensified hydrodynamic regimes, with internal tides enhancing mixing and nepheloid layer production, which influence faunal distribution patterns. These patterns also respond to physical oceanographic (water mass characteristics and hydrodynamics) gradients. Internal tides can generate such gradients by their movement along the canyon. Here we take an interdisciplinary approach using biological, oceanographic and bathymetric derived datasets to undertake high-resolution analysis of a subset of wall assemblages within Whittard Canyon, North-East Atlantic. We investigate if, and to what extent, spatial patterns in diversity and epibenthic assemblages on deep-sea canyon walls can be explained by spatial and temporal variability induced by/of internal tides. Vertical displacement of the internal tide and associated variance in physical oceanographic conditions was calculated from Seaglider and CTD data. Spatial patterns in faunal assemblage structure was determined by cluster analysis and non-metric Multi-Dimensional Scaling plots. Canonical Redundancy Analysis and Generalised Linear Regression was then used to explore relationships between faunal diversity and assemblage structure and the different environmental variables. Our results support the role of the internal tide as a structuring force influencing wall faunal diversity and assemblages by generating both spatial and temporal gradients in physical oceanography and consequently food supply.

## 3.2 Introduction

Submarine canyons are complex geomorphological features that incise continental margins to form pathways between the shelf and deep-sea. (Huvenne and Davies, 2014; Amaro et al., 2016). The movement of water masses, sediments and organic matter through the canyon generate environmental gradients of physico-chemical characteristics that occur both horizontally along the canyon axis and vertically with depth (Obelcz et al., 2014; Fernandez-Arcaya et al., 2017; Hall et al., 2017; Ismail et al., 2018). As a result, environmental conditions can vary over short spatial scales, such that different branches within a single canyon, or even opposing flanks of the same branch can experience different topography, hydrodynamics and sedimentary regimes (McClain and Barry, 2010; Aslam et al., 2018; Bargain et al., 2018; Ismail et al., 2018; Pearman et al., 2020). The high spatial and temporal heterogeneity in environmental conditions often results in enhanced regional and local productivity, biodiversity, and faunal abundance (De Leo et al., 2010; 2014; Vetter et al., 2010).

Submarine canyons are listed as topographical features that may support vulnerable marine ecosystems (VMEs) (FAO, 2009).Vertical walls situated in submarine canyons can represent features of high conservation value, providing natural areas of protection for VMEs under increasing anthropogenic pressure from deep-sea trawling (Huvenne et al., 2011; Johnson et al., 2013). Vertical walls can support a range of faunal assemblages (which make up VMEs) that exhibit high diversity (Robert et al., 2015; 2017; Pearman et al., 2020). For example, vertical walls supporting dense benthic aggregations, such as the reef forming scleractinian corals, *Lophelia pertusa* (recently synonymised to *Desmophyllum pertusum* (Addamo et al., 2016)) (Huvenne et al., 2011; Fabri et al., 2014; Brooke and Ross, 2014) and *Madrepora oculata* (Fabri et al., 2014), the stony coral *Desmophyllum dianthus*, the octocorals *Paragorgia arborea* and *Duva florida* (Brooke et al., 2017), the deep-sea oyster, *Neopycnodonte zibrowii* (Fabri et al., 2014), and the fire clam, *Acesta excavata* (Johnson et al., 2013). On the other hand, other sections of vertical walls can be almost devoid of life (Robert et al., 2015; Pearman et al., 2020). Consequently, vertical walls contribute to a canyon's habitat diversity in various ways.

*D. pertusum* reefs and coral gardens are listed as 'threatened or declining' under Annex V of the Oslo-Paris convention (OSPAR, 2008) agreement, Annex 1 under the Habitats Directive (92/43/EEC, 1992) and as VMEs (FAO, 2008), requiring protection. Effective spatial management and conservation of vertical wall assemblages requires a deeper understanding of the processes that generate the observed faunal distribution patterns (Huvenne and Davies, 2014). However, despite the likely importance of canyon vertical walls in supporting and protecting diversity hotspots and protected habitats, few ecological studies of canyon wall fauna have been conducted (Robert et al., 2017; 2019) and our understanding of the processes that generate spatial patterns along them is limited.

This is, in part, attributed to the extremely challenging environment of deep-sea canyon vertical walls which stayed largely unsampled prior to recent advancements in remote technologies (e.g. ROVs) that enabled their study (Huvenne and Davies, 2014). Additionally, the limitations in the resolution of ship-borne bathymetry prevents accurate delineation of vertical walls (Huvenne et al., 2011). Consequently, despite their likely importance, vertical walls remain under-represented and under-sampled environments of canyons, limiting our knowledge of canyon ecology.

This is further confounded by the predominance of canyon studies which only model the probability of epibenthic species presence-absence (Robert et al., 2015; Bargain et al., 2018; Lo Iacono et al., 2018) or univariate faunal responses that condense faunal information into an index (Robert et al., 2015; Ismail et al., 2018), rather than representing wider, multivariate species assemblage data.

In general, the responses of canyon fauna are regulated by a complex interplay of multiple factors acting at different scales. Environmental factors (water mass characteristics, seafloor characteristics and food supply) are most likely to explain species patterns at broader spatial scales (McClain and Barry, 2010; Robert et al., 2015; Ismail et al., 2018) while biotic processes (i.e. competition) more often act at finer spatial scales (Robert et al., 2019), while stochastic events (disturbance) act at multiple scales (Pierdomenico et al., 2016). The interaction of these processes across different spatial and temporal scales makes identifying key factors that drive faunal patterns within heterogeneous canyon landscapes challenging.

Canyons are recognised as sites of intensified hydrodynamics, including internal tides (Liu et al., 2010; Hall et al., 2017) that are increasingly advocated as key environmental factors influencing species patterns in the deep sea (Huvenne et al., 2011; Johnson et al., 2013; van Haren et al., 2017; Davison et al., 2019; Pearman et al., 2020). For example, research focussing on scleractinian cold-water coral (CWC) assemblages has highlighted the importance of local hydrodynamics (including internal tides) in supplying nutrients and food to sustain CWC populations and preventing sedimentation on the hard substratum that the corals colonise (Frederiksen et al., 1992; Thiem et al., 2006; Davies, 2009; Mienis et al., 2009; White and Dorschel, 2010). Through interactions with topography, internal tides occurring within canyons may enhance near-bed flows and turbulent mixing forming efficient food supply mechanisms to benthic communities (Johnson et al., 2013). Internal tides also influence the resuspension and advection of suspended material in nepheloid layers (White et al., 2005; Liu et al., 2010; Puig et al., 2014; Wilson et al., 2015b). Nepheloid layers are layers where suspended material (including particulate organic matter) aggregates and represent an important food resource for deep-sea fauna (Demopoulos et al., 2017). Internal tide modulation of nepheloid layers can result in replenishment of food to the benthos over the tidal cycle (Davies, 2009) and has been linked to spatial distributions of antipatharians and gorgonians in canyons of the Bay of Biscay (van den Beld et al., 2017).

The vertical displacement of the water column, associated with internal tides, also results in temporal variability in physical oceanographic conditions on the canyon flanks. For example, in Whittard Canyon internal tides with amplitudes up to 80 m have been observed, generating twice daily 1°C temperature fluctuations and dissolved oxygen concentration changes of 12 μmol $kg^{-1}$ on certain sections of the canyon walls (Hall et al., 2017). Fauna respond to such physical oceanographic gradients (water mass characteristics and hydrodynamics) (Levin et al., 2001; Howell et al., 2002; Dullo et al., 2008; Fabri et al., 2017) and spatial patterns in temporal oceanographic variability have been linked to species richness and assemblage patterns (Henry et al., 2014). However, to date no studies investigating faunal responses to spatial patterns in temporal oceanographic variability (i.e. temperature, salinity and oxygen) induced by the internal tide have been conducted in submarine canyons.

Here we investigate if spatial patterns in temporal oceanographic variability induced by the internal tide explain variation in spatial patterns of faunal diversity and assemblage composition on deep-sea canyon walls. We take an interdisciplinary approach utilising biological, oceanographic and bathymetric derived datasets to undertake high-resolution analysis of wall assemblages within Whittard Canyon, North-East Atlantic. We ask the following questions: (1) Does epibenthic megafaunal assemblage composition change across physical oceanography and substratum gradients on vertical walls and (2) which environmental variables exert the strongest influence on epibenthic megafaunal diversity and assemblage structure?

## 3.3 Methods

### 3.3.1 Study Area

Whittard Canyon extends over >200 km and incises the shelf break of the passive Celtic Margin, south-west of the British Isles in the Northern Bay of Biscay, at ~200 m depth (Figure 3.1). It is a dendritic canyon system comprised of four main tributaries, the Western-, Western Middle-, Eastern Middle- and Eastern- branches that coalesce at ~3700 - 3800 m water depth. The Whittard Channel continues to a depth of ~4500 m, where it joins the Celtic Fan that leads onto the Porcupine Abyssal Plain (Hunter et al., 2013; Amaro et al., 2016). This study focusses on the Eastern branch of Whittard Canyon (Figure 3.1).

Several water masses occur in the region, including the Eastern North Atlantic Water (ENAW) (~100 - 600 m), the Mediterranean Outflow Water (MOW) (800 - 1200 m) and the Northeast Atlantic Deep Water (NEADW) (1500 - 3000 m) within which a core of Labrador Sea Water (~1800 - 2000 m) can be found (Pollard et al., 1996; Van Aken, 2000). The influence of each water mass on the water column characteristics varies along the canyon axis as depth decreases and mixing increases toward the canyon head (Hall et al., 2017).

Intensified bottom currents and internal tides have been documented from Whittard Canyon (Reid and Hamilton, 1990; Hall et al., 2017; Aslam et al., 2018) and attributed to generating spatial heterogeneity in environmental conditions (Wilson et al., 2015b; Hall et al., 2017; Aslam et al., 2018; Pearman et al., 2020). Baroclinic (internal) waves are generated when barotropic tidal currents interact with the steep canyon topography (Allen and Durrieu de Madron, 2009; Vlasenko et al., 2016; Hall et al., 2017). The internal waves drive turbulent mixing, which is associated with increased concentrations of particulate organic matter (POM) and nepheloid layer production within the canyon (Wilson et al., 2015b; Hall et al., 2017; Aslam et al., 2018).

Whittard Canyon is characterised by complex geomorphology and variable substrata that is observed to differ along the canyon axis and between branches (Stewart et al., 2014; Robert et al., 2015; Amaro et al., 2016; Ismail et al., 2018). The distribution of substrata is linked to the canyon geomorphology: increasingly fine substrata are associated with flat terrain whilst hard substrata are mostly associated with steep slopes (Stewart et al., 2014; Ismail et al., 2018). The hard substrata constitutes bedrock outcrops and escarpments (vertical walls) as well as boulders and smaller fractions of hard rock originating from slope failures (Carter et al., 2018). Due to the remobilisation and deposition of sediment in the canyon hard substratum is often coated in a sediment veneer of varying thickness.

Sediment dynamics within Whittard Canyon are poorly understood, and although developing on a passive margin and far from coastal sediment inputs, a certain amount of sediment dynamics has been recorded (Amaro et al., 2016). Local slope failures within the canyon and resuspension by intensified bottom currents (including internal tides) source fine grained material (Reid and Hamilton, 1990; Amaro et al., 2015; Amaro et al., 2016; Hall et al., 2017) which is transported down-canyon via turbidity currents and mud-rich sediment gravity flows (Cunningham et al., 2005; Amaro et al., 2016; Carter et al., 2018), while there is evidence that internal tides may act to transport material up-canyon (Wilson et al., 2015b; Lo Iacono et al., 2020).

### 3.3.2 Data acquisition

Data were collected during the JC125 expedition funded by the ERC CODEMAP project (Starting Grant no 258482), the NERC MAREMAP programme, the JC035_JC036 expedition funded by the NERC core programme OCEANS2025 and the EU FP7 IP HERMIONE; the MESH expedition funded by the European Union INTERREG IIIb Community Initiative, and DEFRA; and the 64PE421, 64PE453 and 64PE437 expeditions funded by the NICO initiative by NOW and NIOZ and the NWO-VIDI, grant agreement 016.161.360.

#### 3.3.2.1 Acoustic data acquisition and processing, and extraction of terrain derivatives

Multibeam echosounder (MBES) data were acquired during the MESH, JC035 and JC125 cruises with the ship-board Kongsberg Simrad EM120 MBES system of RRS *James Cook* (Masson, 2009;

Huvenne et al., 2016) and Kongsberg Simrad EM1002 MBES system of RV *Celtic Explorer* (Davies et al., 2008b). Bathymetry data were processed utilising CARIS HIPS & SIPS v.8 and combined utilising the mosaic to new raster tool in ArcGIS 10.4.1, to produce a new grid at a resolution of 50 m (WGS1984, UTM Zone 29N).

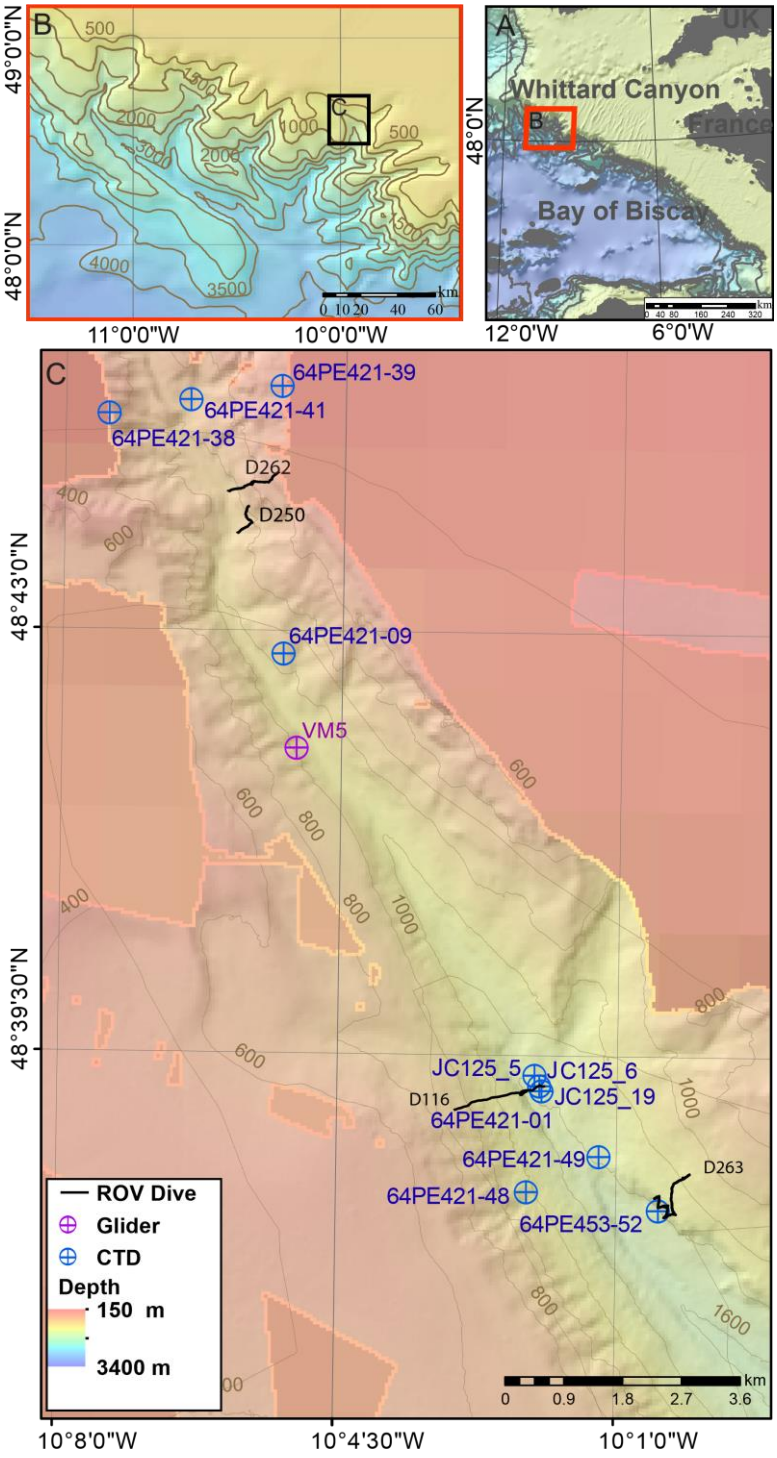


Figure 3.1 Location map of (A) Whittard Canyon and (B) the data acquired from the Eastern branchduring the J036, JC125, 64PE421, 64PE435 and 64PE437 cruises. Background bathymetry from JC125 and GEBCO compilation group (2019).

The terrain derivatives slope, eastness, northness and rugosity were derived from bathymetry data using the ArcGIS extension Benthic Terrain Modeler v. 3.0 (Walbridge et al., 2018). Bathymetric slope criticality to the dominant semi-diurnal internal tide (α) was also calculated from the bathymetry and observed stratification in MATLAB (Supplementary 3.1.1). The environmental variables were exported as rasters at 50 m resolution (Supplementary 3.1.2).

Rugosity is a measure of the ratio of the surface area to the planar area and was calculated with a neighbourhood size of 3 x 3 pixels (Wilson et al., 2007). Slope is a measure of change in elevation and was derived from a neighbourhood size of 3 x 3. Aspect (subsequently converted to eastness and northness) measures the compass orientation of the maximum change along the slope. The terrain derivatives were chosen as they have previously been shown to be informative explanatory variables of canyon fauna distribution within Whittard Canyon (Robert et al., 2015; Price et al., 2019; Pearman et al., 2020). Bathymetric slope criticality to the dominant semi-diurnal internal tide (α) can provide an indication of spatial variability in internal tide behaviour, by identifying potential areas within the canyon where up-slope propagating internal waves could be reflected back down-slope toward the canyon floor (supercritical, $\alpha > 1$), be focussed toward the head of the canyon (subcritical, $\alpha < 1$), or become trapped at the boundary (near-critical, $\alpha \simeq 1$) resulting in wave breaking and mixing (Hall et al., 2014; 2017).

#### 3.3.2.2 Model-derived oceanographic data

Near-bottom values for tidal current variables (root mean squared (R.M.S) near-bottom baroclinic, barotropic and their summed total current speed (m $s^{-1}$) over an $M_2$ tidal cycle) were calculated from horizontal velocity components extracted from a 500 m resolution canyon region hydrodynamic model based on a modified version of the Princeton Ocean Model, used to simulate the semi-diurnal internal tide in the Whittard Canyon region (see Aslam et al. (2018) for further details). To better represent tidal current speeds experienced by the benthos and match the resolution of the terrain derivatives, tidal current speeds were horizontally interpolated into rasters with 50 m resolution (Supplementary 3.1.2). Interpolation was undertaken by kriging using the Spatial Analyst tool box in ArcGIS, and based upon spatial variograms calculated in Golden Software Surfer V 8. To account for discrepancies in bathymetric resolution between the hydrodynamic model and the MBES bathymetry gridded at 50 m, bathymetry from the two datasets was compared and oceanographic and current values were extracted that corresponded to the nearest depth to that of the MBES bathymetry gridded at 50 m.

### 3.3.3 Oceanographic data acquisition and processing

Seaglider and shipboard CTD data were acquired along the Eastern canyon branch (Figure 3.1) and used to characterise its physical oceanography. Glider data were acquired with an iRobot 1KA Seaglider operated at station VM5 (Figure 3.1) in virtual mooring mode for 36 hours (see in Hall et

al. (2017) for further details). Temperature, salinity, dissolved oxygen concentration (µmol $kg^{-1}$), and optical backscatter measured at two wavelengths (470 nm and 700 nm) were measured. Temperature and salinity were sampled every 5 seconds, and averaged into 5 m vertical bins. Oxygen concentration and optical backscatter were sampled every 5 seconds in the upper 200 m and every 30 seconds between 200 m and 1000 m (or the seabed). The CTD data were acquired from 11 stations (Figure 3.1) with a Seabird Electronics Sea-Bird SBE 911plus, sampling at a rate of 24 Hz and averaged in 1 m depth bins. Temperature, salinity, dissolved oxygen concentration (µmol $kg^{-1}$) and turbidity (NTU) were measured. Conservative temperature (ºC), absolute salinity (g $kg^{-1}$), and potential density (kg $m^{-3}$), were calculated from the CTD and glider data using the Gibbs Salt Water Oceanographic Toolbox in MATLAB.

Depth profiles and temperature-salinity (T-S) plots from the CTD data were used to assess spatial and temporal variability within the dataset (Supplementary 3.1.3) and confirm consistency below the seasonal thermocline between profiles within spatial proximity but taken at different times. Consistency below the seasonal thermocline between profiles enabled profiles within proximity of ROV dive locations (Figure 3.1) to be combined to create mean depth profiles and for the local extrapolation of these depth profiles to ROV dive locations, all of which occurred below the seasonal thermocline (Supplementary 3.1.3). The mean of the combined profiles coincident with the ROV dive locations was then used to derive environmental variables for the multivariate analysis.

#### 3.3.3.1 Oceanographic data derived environmental variables

CTD and glider data were used to calculate vertical isopycnal displacement caused by the $M_2$ tide. Amplitude for vertical isopycnal displacement of the $M_2$ tide was calculated from the glider data at VM5 (Figure 3.1) by Hall et al. (2017). Amplitudes at depths below 817 m were linearly extrapolated assuming a linear decay of the wave amplitude to zero at the seabed. For fauna samples at sites deeper than the glider profiles (>1000 m), vertical isopycnal displacement of the $M_2$ tide was calculated from CTD profiles taken during the JC125 cruise (Figure 3.1). To justify the use of vertical isopycnal displacement amplitude derived from the datasets acquired by the glider and CTD, consistency between the density profiles from which vertical amplitude was calculated, was confirmed between the different datasets (Supplementary 3.1.3).

#### 3.3.3.2 Calculation of vertical isopycnal displacement of the $M_2$ internal tide from CTD profiles

The time averaged density profile, $\bar{\rho}(z)$, was calculated from CTD profiles JC125_05, JC125_06 and JC125_16. The time averaged density profile was used to calculate the density anomaly, $\rho'(z, t) = \rho(z, t) - \bar{\rho}(z)$, from which the vertical isopycnal displacement was calculated, $\xi(z, t) = -\rho'(\partial \bar{\rho}/\partial z)^{-1}$. An $M_2$ harmonic analysis was applied to the vertical isopycnal displacement

on each depth level to yield amplitudes for $M_2$ displacement ($\xi_A^{M2}$) every 5 m in the vertical using t-tide (Pawlowicz et al., 2002) in MATLAB.

#### 3.3.3.3 Estimation of temporal variability induced by the $M_2$ internal tide

To infer temporal oceanographic variability over the $M_2$ tidal cycle we took the time averaged profile of each of the oceanographic variables (conservative temperature, absolute salinity, potential density, absolute salinity and dissolved oxygen) from the three CTD casts and at each depth level calculated the range of values; from above and below that depth which were coincident with the amplitude of the vertical isopycnal displacement of the $M_2$ internal tide.

### 3.3.4 Seafloor Imagery

#### 3.3.4.1 Imagery data acquisition

Video data were acquired during the JC036 and JC125 cruises, using the remotely operated vehicle (ROV) *Isis*. During JC036 *Isis* was equipped with a standard definition video camera (Pegasus, Insite Tritech Inc. with SeaArc2 400 W, Deep sea Power&- Light illumination) and stills camera (Scorpio, Insite Tritech Inc., 2048 x 1536 pixels). For the JC125 cruise, the ROV *Isis* was equipped with a dual high definition stills and video camera (Scorpio, Insite Tritech Inc., 1920 x 1080 pixels). Positional data were derived from the ROV's ultra-short baseline navigation system (Sonardyne USBL). A total of four dives were completed in the Eastern branch to depths of 1420 m (Figure 3.1 and Table 3.1) (Robert et al., 2015). Epibenthic morphospecies (visually distinct taxa) >10 mm were annotated from the video, using a laser scale with parallel beams positioned 10 cm apart to estimate organism size. Those sections where the seabed was out of view for extended periods, prohibiting annotations, were noted by time and excluded from subsequent analysis.

Composition of substrata was visually assessed from images and assigned a class based on the CATAMI classification (Althaus et al., 2015) (Table 3.2). Additionally, occurrences of coral reef and dead coral reef framework was annotated (example images are provided in supplementary 3.1.4). Due to the patchy distribution of substrata, substratum type was coded based upon the dominant substratum type followed by the subordinate, for example hard substratum with coral rubble was coded as H_CR. Vertical walls were identified visually from video data, and defined as topography oriented at an angle >50º to horizontal, and of a height >3 m from the seabed.

#### 3.3.4.2 Imagery data analysis

Annotations from the JC036 (previously annotated by Robert et al. (2015) and JC125 cruises were combined into a single data matrix and nomenclature standardised. Transects were subdivided into 10 m length sections and the morphospecies records within each section consolidated. Species richness and Simpson's reciprocal index (1/*D*) (Simpson, 1949) were then calculated for each 10 m

section sample. A 10 m sample length was chosen after data exploration revealed that distinct bands of fauna usually occurred in linear extents < 50 m so that 10 m sample units would enable structure in assemblages on walls to be identified (Borcard et al., 2011).

#### 3.3.4.3 ROV derived depth

Depth values for the seabed were derived by combing the ROV's altitude and depth to obtain a seabed depth value (m). These data were cross-referenced with annotations to identify sections of vertical wall and for these sections ROV depth alone was used in the calculation. A smoothing average with a window size of 3 was applied to the new depth variable.

### 3.3.5 Statistical analyses

Univariate and multivariate analysis techniques were used to identify spatial patterns in faunal diversity and assemblages along each dive. Highly mobile taxa such as fish that can be 'double counted' were removed prior to analysis. Samples with <2 taxa present were also excluded from multivariate analysis. Environmental data coincident with the midpoint co-ordinate of each transect sample were extracted from the rasters and combined with oceanographic data extracted from depth profiles coincident with the depth of the sample. Samples D263_108 and D263_109 were removed as CTD data did not extend to the water depths of these samples. Data exploration was undertaken following the protocol described in Zuur et al. (2010).

Generalised Linear Models (GLMs) were used to explore the relationships between diversity (species richness and 1/*D*) and the environmental variables. Species richness and 1/*D* was assessed using GLMs with link functions based on an exponential relationship between the response variable and the environmental predictor variables (Zuur et al., 2014b). A Poisson distribution was assumed for species richness and a Gamma distribution was assumed for 1/*D*, based upon the distribution of the response variable, together with a log link function. Environmental variables were selected by forward selection under parsimony after Pearson's correlation and Variance Inflation Factor (VIF) scores were used to remove highly correlated variables (correlation coefficients >0.7) (Zuur et al., 2014b). Model assumptions were verified by plotting residuals versus fitted values, versus each covariate in the model and each covariate not in the model (Zuur et al., 2014a). Residuals were assessed for spatial dependency via variograms (Zuur et al., 2014a). To further account for inherent spatial autocorrelation in the data an additional predictor variable, the residual autocovariate (RAC) was calculated and added to the optimal model. The RAC represents the similarity between the residual from the optimal model at a location compared with those of neighbouring locations. This method can account for spatial autocorrelation without compromising model performance (Crase et al., 2012).

Multivariate species data were assessed with non-metric Multi-Dimensional Scaling (nMDS) and hierarchal cluster analysis with group-averaged linkage, using a Hellinger dissimilarity matrix derived from the Hellinger transformed data matrix. Data were Hellinger transformed to enable the use of linear ordination methods (Legendre and Gallagher, 2001; Legendre and Legendre, 2012). The optimal number of interpretable clusters was determined with fusion level and mean silhouette widths (Legendre and Legendre, 2012). Characteristic morphospecies contributing to similarity among clusters were identified using the Similarity percentage analysis (SIMPER) routine (Clarke, 1993).

Canonical Redundancy Analysis (RDA) was used to explore relationships between the multivariate species data and the different environmental variables. RDA combines the outputs of multiple regression with ordination (Legendre and Legendre, 2012). Prior to RDA, environmental data were standardised (i.e. transformed to zero mean, and unit variance). Forward selection was then carried out on the environmental variables to obtain the most parsimonious model and Pearson's correlation together with VIF scores were used to exclude environmental variables that showed strong collinearity with others present within the model (Correlation coefficients >0.7) (Borcard et al., 2011).

Spatial correlation in the multivariate species data was assessed by incorporating sample coordinates into the RDA of species data and by means of a Mantel correlogram on the detrended species data. Variance partitioning was then performed to assess how much of the variance explained in the species data by the environmental variables was spatially structured. Variance partitioning was performed using the environmental variables from the parsimonious model and sample coordinates, after forward selection (Legendre and Legendre, 2012).

During model selection for GLM and RDA, high collinearity was observed between certain environmental variables and depth. Depth per se does not influence fauna, but in canyons depth is correlated with measured and unmeasured environmental factors (i.e. current speed, water mass characteristics) that have been shown to influence faunal patterns (Robert et al., 2015; Pearman et al., 2020). Consequently, depth was retained in analysis, for ease of interpretation though in later sections we also discuss potential effects of correlated environmental factors.

All statistical analyses were conducted using the open source software R (R_Core_Team, 2014), packages "Packfor" "vegan", "cluster", "ape", "ade4", "gclus", "AEM", "spdep" and "MASS".

Table 3.1 Characteristics of ROV dives in Whittard Canyon analysed in the study: cruise number, total transect length (m), transect length (m) coincident with vertical walls, maximum and minimum water depth (m) coincident with vertical walls and number of samples extracted from each dive that represent vertical walls.

| Dive | Cruise | Total Transect Length (m) | Transect Length (m) (V. wall) | Min Depth (m) (V. wall) | Max Depth (m) (V. wall) | Samples (V. wall) |
|---|---|---|---|---|---|---|
| 262 | JC125 | 1030 | 226 | 486 | 836 | 21 |
| 250 | JC125 | 620 | 400 | 753 | 895 | 15 |
| 116 | JC036 | 1780 | 490 | 1291 | 1369 | 29 |
| 263 | JC125 | 1785 | 350 | 1260 | 1420 | 50 |
| Total | | 5215 | 1466 | | | 115 |

Table 3.2 Substratum classification used in annotation of image data. Substratum was annotated based upon the CATAMI classification. Additionally, coral reef and dead coral reef framework were added.

| | | CATAMI Classification | | | |
|---|---|---|---|---|---|
| Substratum Description | Substratum Code | Level 2 | Level 3 | Level 4 | Level 5 |
| Sand | S | Unconsolidated (soft) | Sand/mud (<2 mm) | Coarse sand (with shell fragments)<br>Fine sand (no shell fragments) | |
| Mud | M | | | Mud/silt (<64 µm) | |
| Biogenic gravel | BG | | Pebble/gravel | Biogenic | Shellhash |
| Coral rubble | CR | | | | Coral rubble |
| Hard | H | Consolidated (hard) | Rock | | |
| Dead coral reef framework | DCRF | | | | |
| Coral reef | CRF | | | | |

## 3.4 Results

### 3.4.1 Oceanographic data

Glider and CTD measurements show several water masses in the Eastern branch of Whittard Canyon (Figure 3.2 and Supplementary 3.2.1). The ENAW (ɵ range: 27.1 - 2 7.25 kg $m^{-3}$) occurs below the seasonally warmed surface waters to approximately 600 m water depth (Figure 4.2). The influence of the MOW (ɵ 27.5 - 27.6 kg $m^{-3}$), seen as increased salinity, can be observed from measurements taken further down the canyon axis, between 800 - 1200 m water depth, but is absent from those towards the canyon head (Figure 3.2 and Supplementary 3.2.1). Similarly, large gradients in dissolved oxygen (DO) concentration (µmol $kg^{-1}$) that are observed from measurements taken further down the canyon axis are absent from those toward the canyon head (Supplementary 3.2.1).

Increased optical backscatter, 8 - 10 x$10^{-4}$ $m^{-1}$ from 470 nm channel and 7 - 9 x$10^{-4}$ $m^{-1}$ from 700 nm channel, was observed from glider profiles at 400 m water depth and then below 600 - 700 m water depth (Supplementary 3.2.1). Increased turbidity was also observed from CTD profiles below depths of 400 - 600 m (upper canyon, 0.2 - 0.9) and below depths of 800 - 1150 m (mid canyon, 0.2 - 3.0). Higher turbidity was measured from the mid canyon, with the values measured in the vicinity of Dive 116 three times higher than the upper canyon (3.0) (Supplementary 3.2.1).

Vertical isopycnal displacement derived from the glider (Hall et al., 2017) and CTD data show variability across the Eastern branch and with depth. The highest displacement amplitude from the glider data (VM5, upper canyon) was 53 m at 617 m water depth (Figure 3.3), resulting in tidal temperature variations of 0.53 °C, salinity variations of 0.004 g $kg^{-1}$, potential density variations of 0.09 kg $m^{-3}$ and dissolved oxygen variations of 9.2 µmol $kg^{-1}$. The highest amplitude calculated from the CTD data (mid canyon) was 140 m at 942 m water depth (Figure 3.4), resulting in tidal temperature variations of 1.55 °C, salinity variations of 0.1 g $kg^{-1}$, potential density variations of 0.16 kg $m^{-3}$ and dissolved oxygen variations of 5.8 µmol $kg^{-1}$.

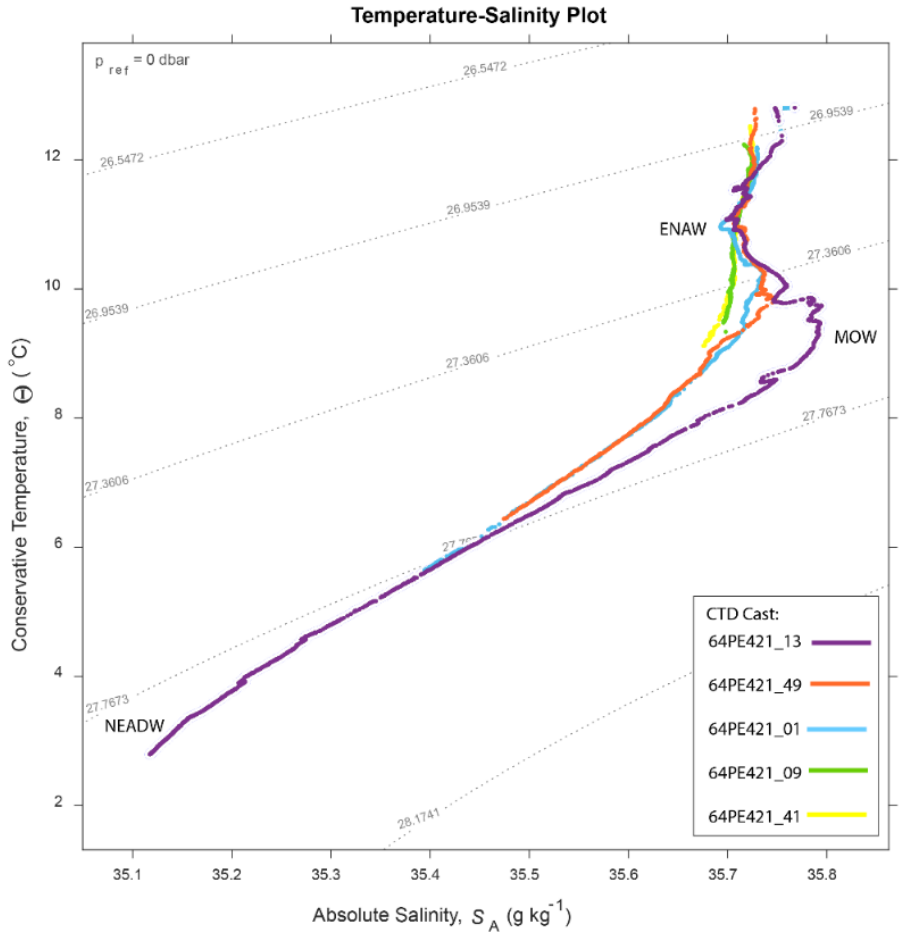


Figure 3.2 Temperature – Salinity Plot for 5 CTD casts along the canyon branch axis, collected during the 64PE21 cruise. See supplementary materials 3.2 for CTD locations. The influence of the MOW reduces toward the head of the canyon, until it is no longer distinguishable.

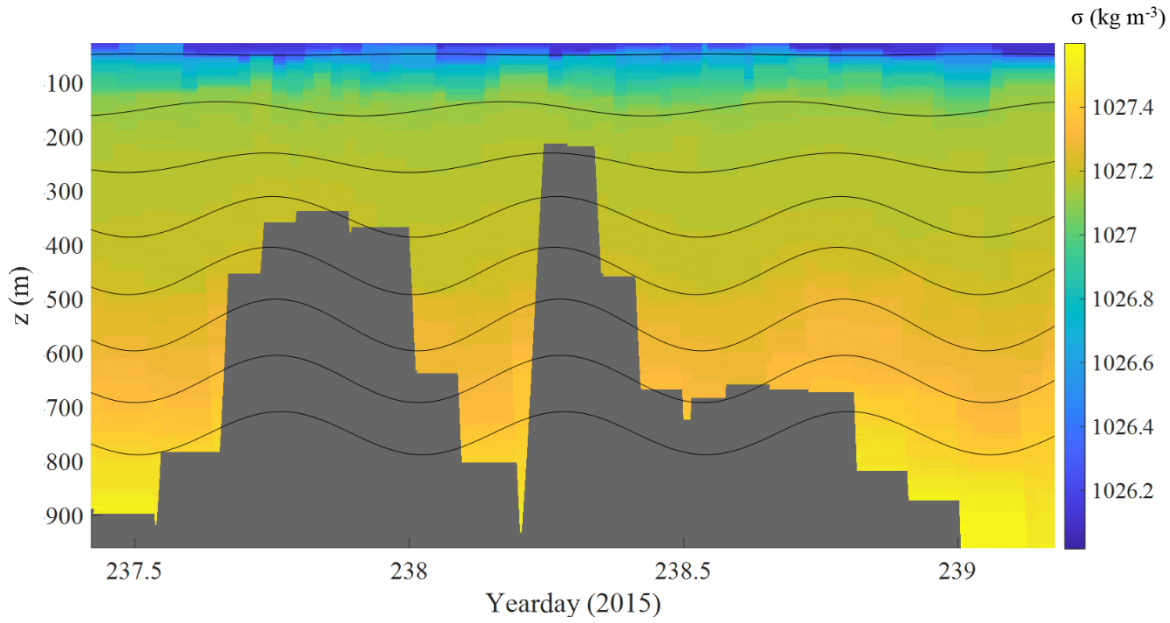


Figure 3.3 Time series of potential density at VM5 overlaid with $M_2$ harmonically filtered vertical isopycnal displacement every 100 m. When occupying the station in virtual mooring mode the glider maintained position within 2.5 km of the station during which it manoeuvred over different topography (grey).

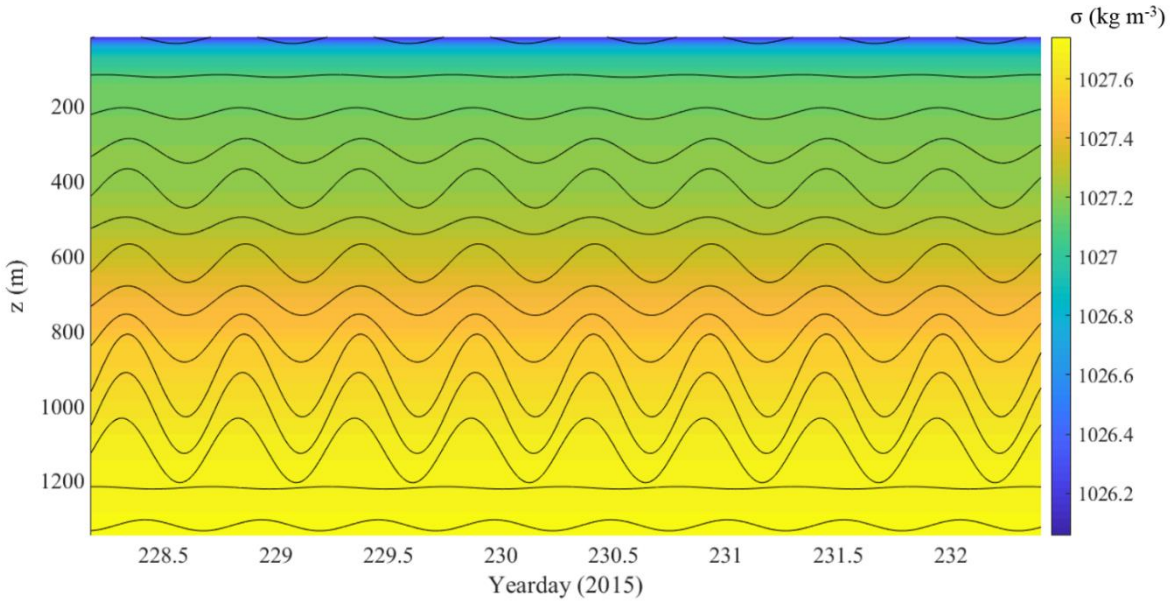


Figure 3.4 240 hour time series of potential density from combined CTD profiles overlaid with a $M_2$ harmonically filtered vertical isopycnal displacement every 100 m.

### 3.4.2 Fauna results

A total of 14701 individuals assigned to 150 morphospecies were annotated. Most morphospecies were rare (Supplementary 3.2.2), whilst others were abundant in specific locations and occurred at low density across the rest of the samples. The most abundant morphospecies was Brachiopoda sp. 1(4440). The most common morphospecies recorded across dives was Caryophylliidae sp. 1 (in 69.2 % of total samples). Highest species richness (29/10 m transect) and 1/*D* (10.87) was observed from dive 262 on hard substratum vertical wall with coral rubble.

Walls toward the head of the canyon (dives 262 and 250) were steep and comprised of an alternation of geological strata resistant to erosion, and friable, less competent sedimentary units of varying thickness with occasional ledges, all of which was covered in a mud veneer of varying thickness. The bivalves *Neopycnodonte* sp. 1 and *Acesta excavata*, stony corals *Madrepora oculata* and Caryophylliidae sp. 1 and crinoids were observed to aggregate beneath ledges (Figure 3.5). On other sections of wall the black coral Antipathidae sp. 1 or the sea star Brisingidae sp.1 reached relatively high abundances (Figure 3.5) and Cerianthidae sp. 1 occurred where soft sediment accumulated (Figure 3.5). The walls toward the canyon head were supercritical to the $M_2$ tide and although the area is exposed to relatively weaker currents 0.17-0.23 m $s^{-1}$ (Supplementary 3.1.2) it experiences similar short-term temporal variability to that of walls sampled in the mid canyon (dives 116 and 263), despite the water temperature being up to 5 ° C warmer.

Dense aggregations of *D. pertusum* framework were observed between 1301 and 1369 m water depth from walls comprised of alternations of strong and weak, thinly bedded sedimentary units that resulted in a 'stepped' relief (dive 116) (Figure 3.5) and were covered in a mud veneer of varying thickness. The walls were supercritical to the $M_2$ tide in a region exposed to high currents speeds 0.42 - 0.46 m $s^{-1}$.

Brachiopods, large erect sponges and arborescent gorgonians were observed between 1261 - 1406 m water depth from walls that comprised brown rocky strata resistant to erosion and covered in a mud veneer of varying thickness (dive 263) (Figure 3.5). The walls were critical to the $M_2$ tide and experienced currents of 0.27 - 0.29 m $s^{-1}$.

### 3.4.3 Statistical analysis results

High collinearity was present within the environmental dataset (Supplementary 3.2.2). Density, temperature, salinity and current speed were highly correlated with depth, as on occasion were values for the $M_2$ amplitude and associated ranges in density, temperature and salinity.

#### 3.4.3.1 Species diversity

The GLM analysis of the vertical wall dataset identified slope, depth and substratum as significant variables explaining 98 % variation in species richness across the dives (< 0.001 (79 df =107,114)) and 99 % variation in 1/*D* across dives (<0.001 (11 df = 96,103)). Species richness and 1/*D* have a positive relationship with slope and a weak negative relationship with depth and increasing soft sediment (Table 3.3).

#### 3.4.3.2 Canyon wall assemblages

Hierarchical clustering identified nine clusters (Figure 3.6 and Table 3.4) that separated into three regions of the nMDS plot (Figure 3.7). From review of clustering (Figure 3.6) and SIMPER results (Table 3.4 and supplementary 3.2.1) it is likely that clusters 1, 2 and 3 represent the three main assemblages with the remaining clusters representing transitionary components (Figures 3.6 and 3.7).

Cluster 1 represents the *D. pertusum* assemblage observed from dive 116, cluster 2 (and transitionary cluster 5) represents the Brachiopoda sp. 1 assemblage observed from dive 263 and cluster 3 (and transitionary clusters 4, 6 and 7) represents the general mixed assemblage comprised of Cerianthidae sp.1, *C. cidaris* and Antipathidae sp. 1 observed from dives 262 and 250 (Figures 3.5 - 3.9 and Table 3.4). Clusters 8 and 9 were only represented by a single sample, limiting conclusions that can be drawn and so are omitted from further discussion.

Walls toward the head of the canyon (between 500 - 900 m) support a wider variety of assemblages with some observed across both dive 250 and dive 262 (Figure 3.8). In contrast, lower down the

canyon at approximately 1350 m, single assemblage types dominated the walls of opposite canyon flanks (dives 116 and 263) (Figure 3.8).

The RDA analysis demonstrated assemblage-environment relationships, showing that species aggregations are driven by depth, $M_2$ amplitude, criticality of the slope and substratum type (thickness of sediment veneer and coral framework) (Adjusted $R^2$ 48 %) (Figure 3.10 and Table 3.5). The first axis of the RDA plot represents a gradient from reef to non-reef substrata and from supercritical to critical conditions, and the second axis represents a gradient in depth and $M_2$ amplitude (Figure 3.10).

The vectors representing species scores (Figure 3.10) separate into three subgroups: upper left quadrant, characterized by the predominance of the anemone Cerianthidae sp. 1, the urchin *C. cidaris*, the deep water oyster *Neopycnodonte* sp. 1, the black coral Antipathidae sp. 1, the squat lobster Munididae sp. 1, Brisingidae sp. 1 and the stony coral *M. oculata*; within which there is further differentiation depending on the relative abundance of Cerianthidae sp. 1, Antipathidae sp. 1, *Neopycnodonte* sp. 1 and Brisingidae sp. 1; the lower right quadrant represented by a predominance of Brachiopoda sp. 1, the stony coral Caryophylliidae sp. 1, Isididae sp. 3, the holothurian *P. squamatus*, the chalice sponge and *Echinus* sp. 1; and the lower left quadrant, represented by the predominance of the stony coral *D. pertusum*, the deep water bivalve *A. excavata*, the anemone morphospecies Actiniaria sp. 10, two coral morphospecies (Anothozoa sp. 1 and Cnidaria sp. 129) and Crinoidea sp. 11.

The clustering and nMDS plots showed a similar trend by identifying nine clusters that separated into three regions of the nMDS plots (Figure 3.6 and 3.7) comprised of the same characterising morphospecies as those in the RDA plot (Table 3.4). Cluster 1 relates to the lower left quadrant; cluster 2 relates to the lower right quadrant and cluster 3 relates to the upper left quadrant, with cluster 6 representing the increasingly Antipathidae sp. 1 dominated assemblage to the central upper quadrant and cluster 4 representing the *Neopycnodonte* sp. 1 dominated assemblage.

Results of the spatial analysis show that fauna samples are spatially structured showing both a general trend at a broad scale (Supplementary 3.2.2) and then greater similarity at distances <200 m and dissimilarity at distances >450 m that represents the difference between dives (Supplementary 3.2.2). Variance partitioning shows that 45.3 % of variance explained in species data by environmental variables is also spatially structured in relation to the sample coordinates (Figure 3.11). Together these results suggest spatial patterns in species are driven by environmental variables which themselves are spatially organised and so exhibit a degree of induced spatial dependence.

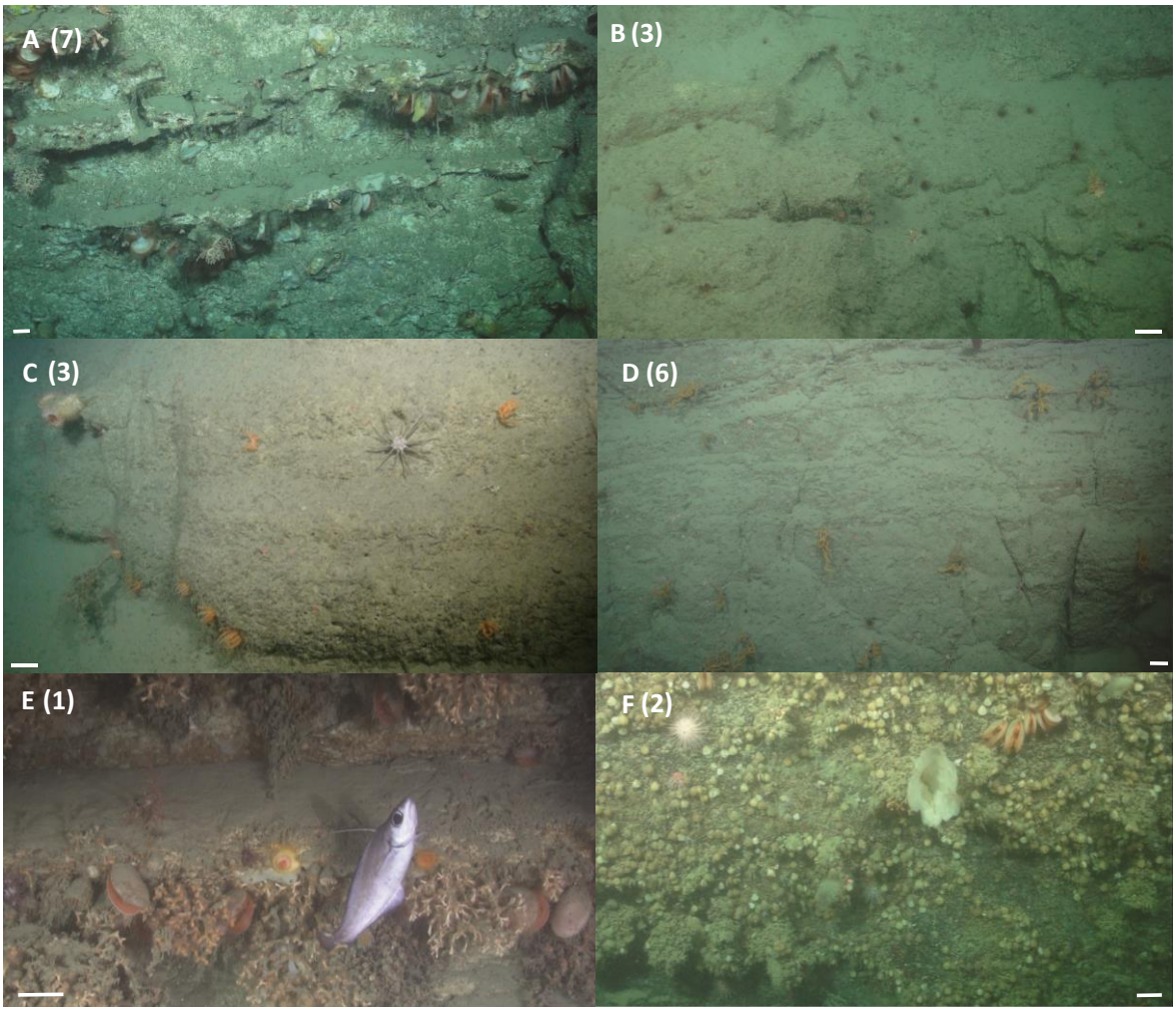


Figure 3.5 Example images of vertical wall assemblages observed from ROV video data. (A) The deep water oyster *Neopycnodonte* sp. 1 and the deep water bivalve *Acesta excavata*, the stony corals *Madrepora oculata* and Caryophylliidae sp. 1, the squat lobster Munididae sp. 1, the urchin *Cidaris* and crinoids, were observed aggregating beneath ledges, image taken during dive 262 at 637 m. (B) The anemone Cerianthidae sp. 1 occurs wherever there is sufficient soft sediment, image taken during dive 250 at 849 m. (C) The urchin *C. cidaris* and the seastar Brisingidae sp. 1, the anemone *Phelliactis* sp. 1, image taken during dive 262 at 826 m. (D) The black coral Antipathidae sp. 1, the urchin *C. cidaris*, the anemone Cerianthidae sp. 1, image taken during dive 262 at 733 m. (E) The stony coral *Desmophyllum pertusum*, the deep water bivalve *A. excavata*, the coral morphospecies Anthozoa sp. 1, the anemones morphospecies Actinaria sp. 2 and *Actinernus michaelsarsi*, and the fish *Lepidion eques*, image taken during dive 116 at 1362 m. (F) Brachiopoda sp. 1, sponge morphospecies chalice sponge, the deep water bivalve *A. excavata*, the holothurian *Psolus squamatus*, the stony coral Caryophylliidae sp. 1 and the urchin *Echinus* sp. 1, image taken during dive 263 at 1344 m. Scale bars = 10 cm. Numbers denote cluster membership after cluster analysis.

Table 3.3 Results from Generalised Linear Model for species richness and the selected environmental variables. Significance of individual terms tested by analysis of variance (ANOVA) ***p ≤ 0.001, **p ≤ 0.01, *p ≤ 0.05, • p ≤ 0.1

| Model | Environmental Variables - Significance of individual terms by ANOVA | Adjusted $R^2$ | F-value | p-value | ANOVA of model p-value |
|---|---|---|---|---|---|
| S | Slope 0.0199470 ***, depth -0.0004673 *, RAC 1.4144485 ***, Substrate H_V.MS -0.2589899 **, H_V.MS_BG -0.1892338, H_V.MS_R 0.0163835, V.MS_CRF -0.9036104 ** | 0.98 | 1289, df = 7,96 | < 0.001 | <0.001 (79.001 df=107,114) |
| 1/*D* | Slope -0.006666 ***, depth 0.0001939 ***, RAC -1.767***, Substrate H_V.MS 0.0654 •, H_V.MS_BG 0.05817, H_V.MS_R 0.04200, V.MS_CRF 0.07071 | 0.99 | 7413, df = 7,96 | < 0.001 | <0.001 (11.081 df=96,103) |

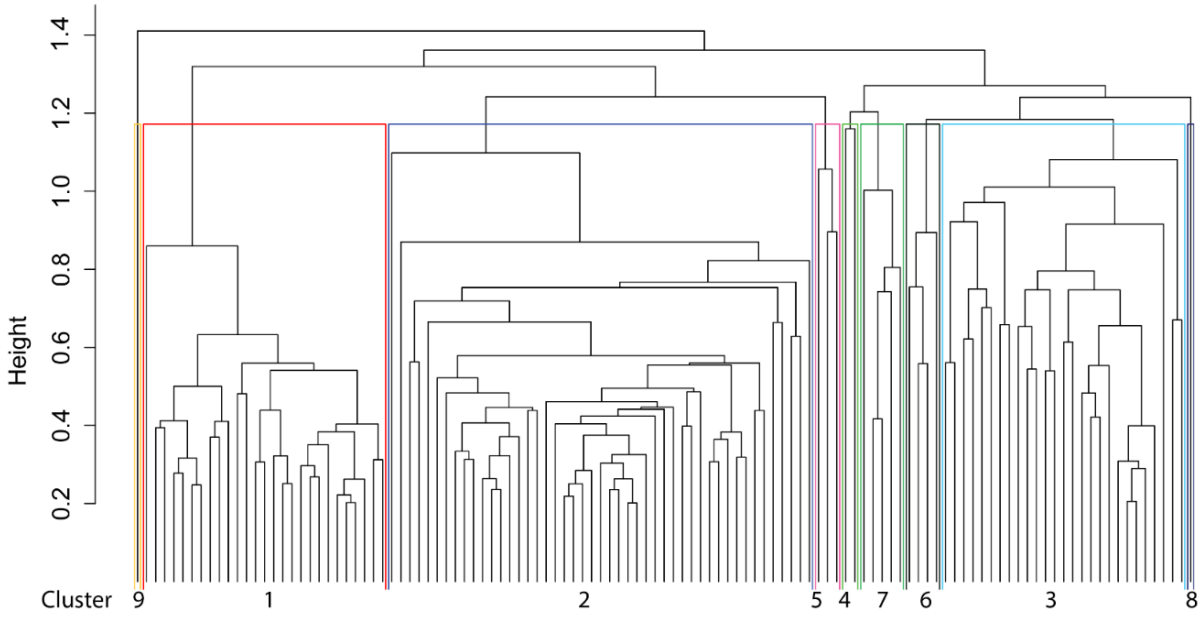


Figure 3.6 Dendrogram showing results of multivariate hierarchal clustering analysisof Hellinger transformed species data. Nine clusters (denoted by different colour overlays) were identified by silhouette and fusion level plots (Cluster: 1 2 3 4 5 6 7 8 9).

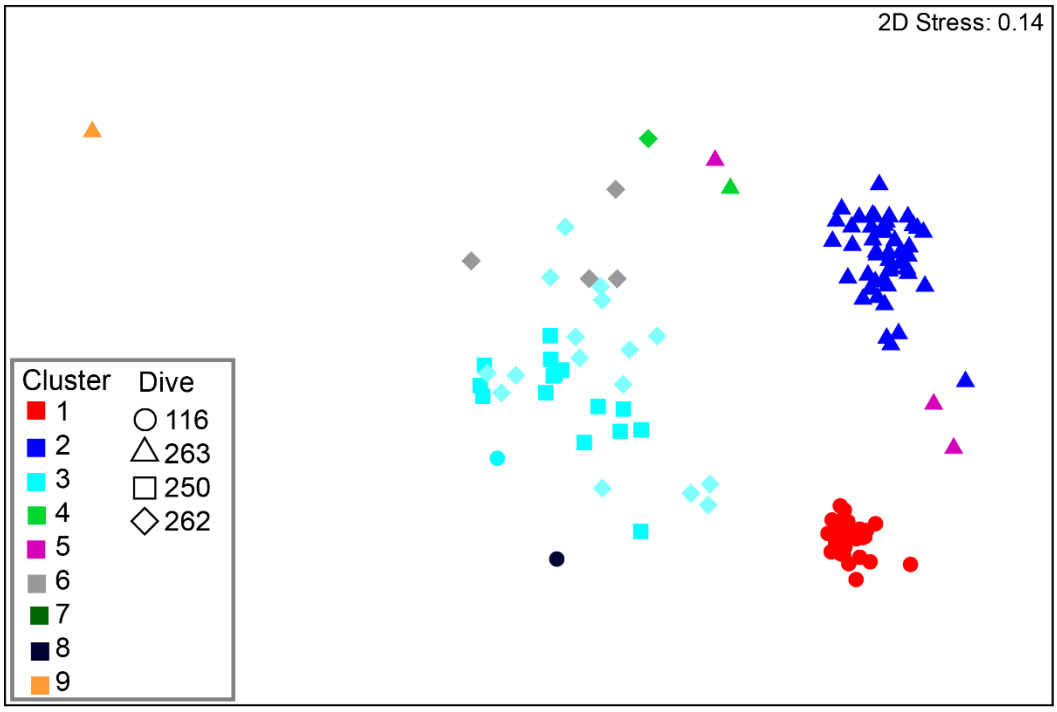


Figure 3.7 nMDS plot of multivariate Hellinger transformed species data. Samples are coloured to represent the nine clusters identified by hierarchal clustering analysis.

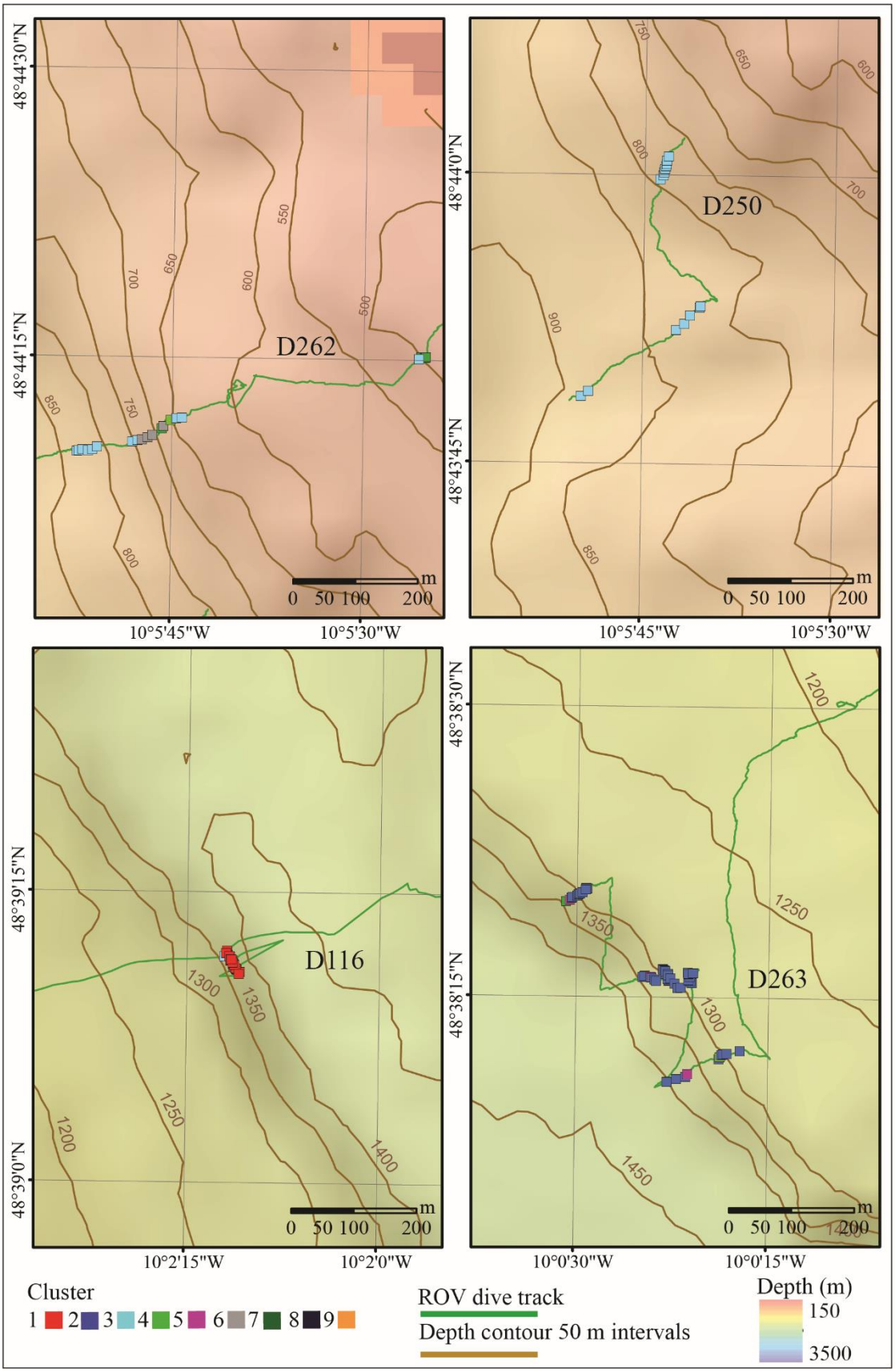


Figure 3.8 Spatial plot of sites (samples) from vertical walls across all dives plotted over MBES bathymetry. Samples are coloured to represent the nine clusters identified by hierarchal clustering analysis.

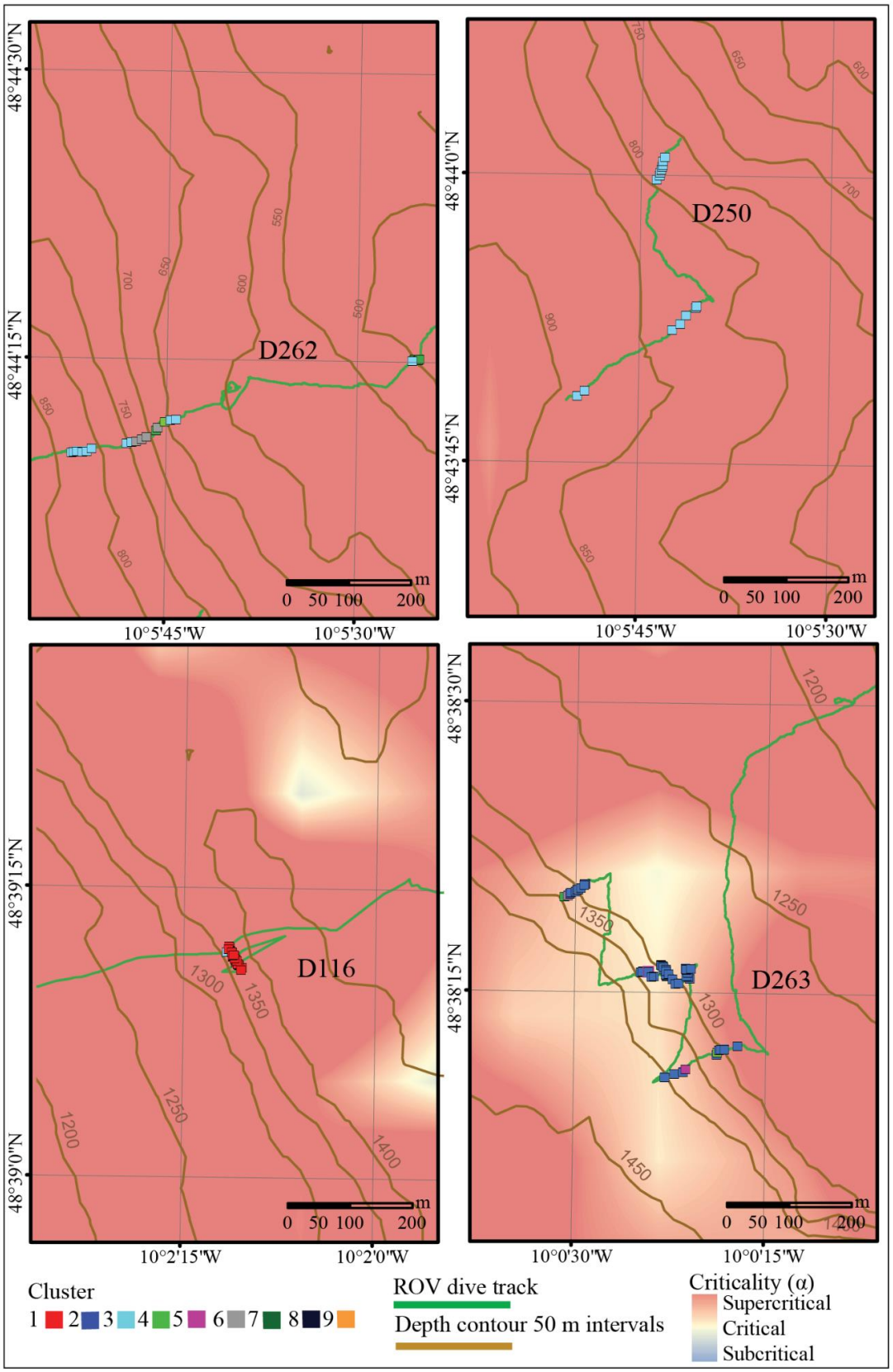


Figure 3.9 Spatial plot of sites (samples) from vertical walls across all dives plotted over bathymetric criticality to the $M_2$ tide. Samples are coloured to represent the nine clusters identified by hierarchal clustering analysis.

Table 3.4 Clusters identified from multivariate hierarchal clustering analysis with associated environmental parameters, and SIMPER resultsidentifying the morphospecies that characterise the clusters (70 % accumulative contribution cut off).

| Cluster | Characterising Species | Water Depth (m) | Substrate | Criticality | $M_2$ Amplitude (m) | Current Speed ($ms^{-1}$) | Temp Range (ºC) |
|---|---|---|---|---|---|---|---|
| 1 | *Desmophyllum pertusum, Acesta excavata,* coral morphospecies Anthozoa sp. 1 and Cnidaria sp. 129, Actiniaria sp. 10 | 1301-1369 | H.CRF.V.M | Supercritical | 0-58 | 0.42-0.46 | 5.6-7.1 |
| 2 | Brachiopoda sp.1, Caryophylliidae sp. 1, *Psolus squamatus*, Isididae sp. 3, Porifera morphospecies chalice sponge | 1261-1406 | H.V.M, H_V.MS_BG | Critical | 0-42 | 0.27-0.29 | 5.7-7.3 |
| 3 | Cerianthidae sp. 1, *Cidaris cidaris,* Antipathidae sp. 1, Ophiuroidea | 514-636 | H_V.M, H_V.M_R | Supercritical | 0-44 | 0.17-0.23 | 9.6-10.9 |
| 4 | Caryophylliidae sp. 1 | 639 and 1330 | H_V.M | Supercritical | 27-45 | 0.19-0.28 | 5.8-10.6 |
| 5 | *Echinus* sp. 1, *Acanella* sp. 1 | 1323-1368 | H_V.M | Supercritical | 0-28 | 0.28-0.29 | 5.7-6.9 |
| 6 | Porifera sp. 15, Antipathidae sp. 1, Actinaria sp. 14, *Cidaris cidaris, Serpulidae* sp. 1,Cyclostomatidae sp. 1, Cerianthidae sp. 1 | 660-731 | H_V.M_R, H_V.M | Supercritical | 44-47 | 0.19 | 9.2-10.6 |
| 7 | *Neopycnodonte* sp. 1, Crinoidea sp. 13, Munididae sp. 1, Caryophylliidae sp. 1, *Cidaris, Madrepora oculata*, Asterinidae sp. 1, Porifera sp. 11 | 486-1336 | H_V.M_R, H_V.M | Supercritical | 22-44 | 0.17-0.29 | 5.7-11 |
| 8 | Penatulacea sp. 1, *Actinoscyphia* sp. 1 | 1317 | V.MS_CRF | Supercritical | 13 | 0.4 | 6.4-6.4 |
| 9 | Asteriodea sp. 1, Actiniidae sp. 5 | 1363 | H_V.M | Critical | 0 | 0.29 | 6.2 |

Table 3.5 Results from Canonical Redundancy Analysis of Hellinger transformed species data and selected environmental variables. Significance of individual terms by analysis of variance (ANOVA) on RDA including spatial structure. ***$p \leq 0.001$, **$p \leq 0.01$, *$p \leq 0.05$, •$p \leq 0.1$

| Model | Environmental Variables - Significance of individual terms by ANOVA | Adjusted $R^2$ | Significance of RDA Plot by ANOVA | |
|---|---|---|---|---|
| | | | F-value | p- value |
| V.Walls | Depth***, $M_2$.Amp***, Criticality ***, Substrate*** | 48 | 14.305, df= 8,105 | 0.001 |

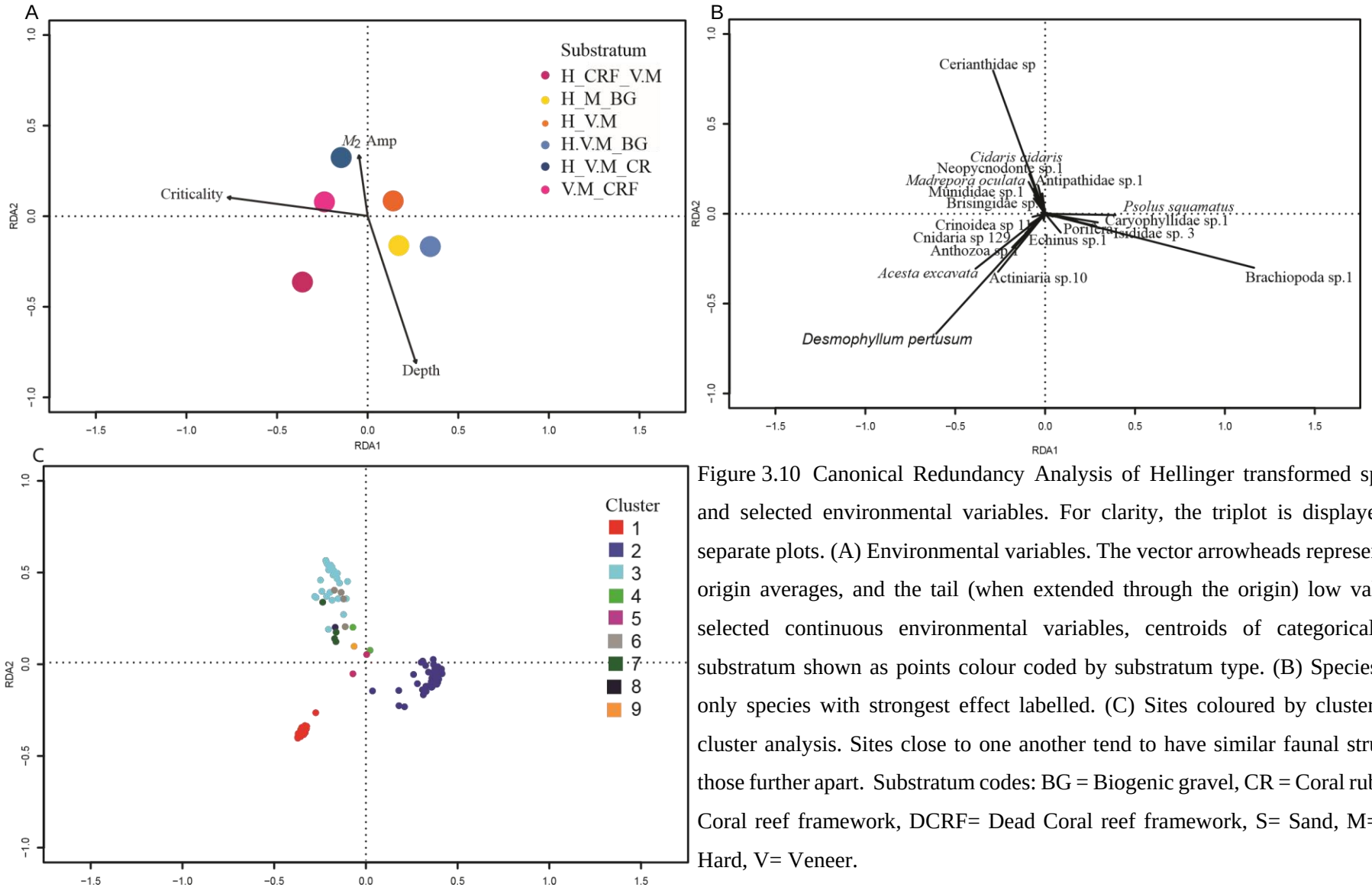


Figure 3.10 Canonical Redundancy Analysis of Hellinger transformed species data and selected environmental variables. For clarity, the triplot is displayed in three separate plots. (A) Environmental variables. The vector arrowheads represent high, the origin averages, and the tail (when extended through the origin) low values of the selected continuous environmental variables, centroids of categorical variables substratum shown as points colour coded by substratum type. (B) Species data with only species with strongest effect labelled. (C) Sites coloured by cluster following cluster analysis. Sites close to one another tend to have similar faunal structure than those further apart. Substratum codes: BG = Biogenic gravel, CR = Coral rubble, CRF= Coral reef framework, DCRF= Dead Coral reef framework, S= Sand, M= Mud, H= Hard, V= Veneer.

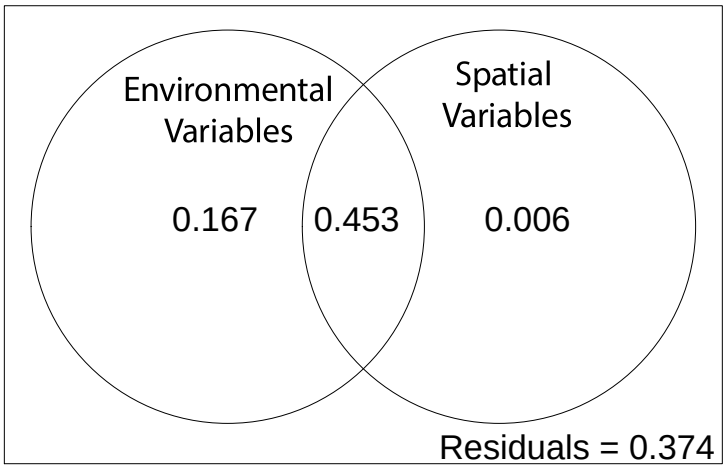


Figure 3.11 Variation partitioning plot for the Hellinger transformed species data, the selected environmental variables (depth, substratum, bathymetric criticality to the $M_2$ tide and amplitude of the $M_2$ tide) and spatial variables (sample coordinates).

## 3.5 Discussion

There have been a number of studies examining environmental drivers of faunal patterns in submarine canyons but until now, no study of canyon wall assemblages integrating both spatial and temporal oceanographic variability induced by the internal tide has been conducted. Using a multi-disciplinary approach, we have been able to further quantify spatial patterns in environmental variables and wall faunal assemblages, and have identified depth, substratum and proxies of internal tide dynamics as important factors driving species patterns on canyon walls.

### 3.5.1 Spatial gradients in oceanographic variables

Several oceanographic gradients in Whittard Canyon are correlated with depth and vary in intensity along the canyon (Figure 3.2, 3.3 and 3.4 and supplementary 3.1.3 and 3.2.1). The oceanographic data showed an increased homogenisation of the water column towards the canyon head, exemplified by decreased gradients in oceanographic variables (Figure 3.2 and supplementary 3.2.1) such as dissolved oxygen and temperature. The increased homogenisation is postulated to be the result of elevated levels of turbulent mixing due to internal tide dissipation (Hall et al., 2017). The reduced influence of the MOW toward the canyon head illustrates its progressive collapse onto a mixing line between the ENAW and NEADW, as previously described by Hall et al. (2017). The temporal variability induced by the internal tide was the result of the amplitude of the isopycnal displacement by the $M_2$ internal tide and the characteristics of the water it displaced. Concordantly, the temporal variability (over the $M_2$ tidal

cycle) was lower in more mixed areas toward the canyon head compared to locations toward the middle canyon where the water is more stratified (Figure 3.2 and 3.3 and supplementary 3.2.1).

### 3.5.2 Wall assemblages

In our study, the greatest variance in species richness, diversity and assemblages was explained by depth (and its covariates) followed by criticality of slope and substratum (presence of sediment veneer, presence of coral framework) (Figure 3.9 and Tables 3.3 and 3.5). Although the amplitude of the $M_2$ internal tide played a subordinate role, it nevertheless significantly explained variance in species assemblages (Table 3.5).

Studies investigating epibenthic assemblages in a variety of deep-sea settings (Levin et al., 2001; Howell et al., 2002; 2010), including seamounts (Kaufmann et al., 1989; Clark et al., 2010; Henry et al., 2014; Serrano et al., 2017; De la Torriente et al., 2018; Ramiro-Sánchez et al., 2019) and canyons (Vetter and Drayton, 1998 ; Mortensen and Buhl-Mortensen, 2005; Schlacher et al., 2007; Robert et al., 2015; Pierdomenico et al., 2016; Pearman et al., 2020) have identified the same environmental variables as significant factors influencing assemblage structure (depth, slope and substratum) as our study. As well as representing environmental parameters in their own right, depth and slope act as proxies for environmental parameters such as water mass characteristics or seafloor complexity, respectively(Levin et al., 2001; Wilson et al., 2007; Stewart et al., 2014; Carter et al., 2018; Ismail et al., 2018) that act at broad spatial scales to determine faunal patterns in distribution and abundance (Levin et al., 2001; Kenchington et al., 2014; McClain and Lundsten, 2015; Robert et al., 2015; Du Preez et al., 2016; Ismail et al., 2018). In our study, the influence of environmental variables (principally depth and its covariates) acting at a broader scale was manifested as a spatial trend (Figure 3.10 and supplementary 3.2.2).

Depth zonation of assemblages in the deep sea has been attributed to biological processes (competition and dispersal) and environmental factors (substratum, productivity and water mass characteristics including temperature, oxygen and pressure) that co-vary with depth (Rowe and Menzies, 1969; Lampitt et al., 1986; Levin et al., 2001; Howell et al., 2002; Carney, 2005; Olabarria, 2005). On topographically complex features such as seamounts depth zonation has been attributed to substratum, food availability and topographically modified hydrodynamics that vary with depth (Clark et al., 2010; McClain et al., 2010; McClain and Lundsten, 2015; Du Preez et al., 2016; Ramos et al., 2016). Despite assemblage responses in our study being linked to substratum changes (Figure 3.10, Table 3.5 and supplementary 3.2.2), different assemblages were observed from the same substratum type across different depths (Table 3.4 and supplementary 3.2.2) and even within similar depth ranges the assemblages observed varied (Table 3.4 and supplementary 3.2.2), indicating that other processes are working in concert at smaller spatial scales to drive spatial patterns in species assemblages on canyon walls.

#### 3.5.2.1 Hydrodynamics

Our results suggest that spatial variation in local hydrodynamics (amplitude of vertical isopycnal displacement of the $M_2$ internal tide and internal tide current speed) drives spatial patterns in species diversity and assemblages on canyon walls.

##### 3.5.2.1.1 Internal tides and nepheloid layer influence on canyon fauna

In our study, peaks in species diversity coincided with depths/areas of increased amplitude of vertical isopycnal displacement of the $M_2$ internal tide and turbidity (Figures 3.3 and 3.4 and supplementary 3.2.1). The increased turbidity is indicative of nepheloid layers, which have previously been reported at similar depths in Whittard Canyon (Huvenne et al., 2011; Johnson et al., 2013; Wilson et al., 2015b). These observations further support the link between increased epifaunal diversity and internal tide influenced nepheloid layers (Huvenne et al., 2011; Johnson et al., 2013; Pearman et al., 2020). However, our results go further to show that within these areas of high diversity, the species composition of assemblages varied, demonstrating that other processes are acting to determine assemblage contribution and that the sole use of univariate measures may miss key aspects of species – environment relationships in canyons and so limit our understanding of processes driving spatial patterns.

##### 3.5.2.1.2 Internal tide behaviour and quality of food in nepheloid layers

The content of nepheloid layers has been shown to vary across Whittard Canyon (Huvenne et al., 2011; Wilson et al., 2015b) and variability in the quality and amount of food supply is known to influence canyon faunal distributions (De Leo et al., 2010; McClain and Barry, 2010; Cunha et al., 2011; Chauvet et al., 2018). Internal tides interacting with supercritical slopes can form an efficient food supply mechanism to deliver high quality POM from surface waters to benthic assemblages at depth (Johnson et al., 2013). However, internal tides interacting with critical slopes may result in wave breaking and resuspension, and the mobilisation of older material from the seafloor that is often degraded and reworked material of lower quality POM.

We observed brachiopods, large sponges and arborescent gorgonians on walls where the slope was near critical (Figure 3.5). In contrast, the *D. pertusum* assemblage was observed at similar depth, from a wall that was supercritical (Figure 3.8). Huvenne et al. (2011) found that the composition of nepheloid layers within the vicinity of the *D. pertusum* assemblage was nutritionally higher compared to that of other sites measured in the canyon. Isotopic analysis shows that *D. pertusum* has a broad trophic niche (Demopoulos et al., 2017) having been known to feed on both POM and zooplankton (Duineveld et al., 2007; 2012) with a preference for high quality POM. On the other hand, isotopic signatures indicative of lower quality POM have been documented from brachiopods (Valls, 2017). Consequently, our results suggest that potential differences in internal tide behaviour between the sites could generate variability

in the quality of POM within nepheloid layers. This could further influence spatial patterns in faunal assemblages by processes of resource partitioning and specialisation of fauna targeting specific material within the nepheloid layers. These findings further support the role of hydrological and geomorphological processes in influencing the supply and resuspension of particulate organic carbon to canyon environments thus driving trophic structure, faunal assemblage composition and diversity as previously proposed by Dell'Anno et al. (2013) and Demopoulos et al. (2017).

#### 3.5.2.1.3 Internal tide current speed

Although R.M.S near-bottom baroclinic, barotropic and total current speed was removed from statistical analysis (due to collinearity with depth), data exploration showed that assemblages distributed along a gradient of baroclinic (internal) current speed (Supplementary 3.2.2). Separation of species along a gradient of current speed could reflect feeding and morphological adaptations. Species vary in their feeding strategies and efficiency under different hydrodynamic regimes (Järnegren and Altin, 2006; van Oevelen et al., 2016). Species may exploit exposed localities to increase food encounter rates (Davies, 2009; Howell et al., 2011; Mohn et al., 2014; Rengstorf et al., 2013; van Oevelen et al., 2016; Bargain et al., 2018) or, conversely avoid high current speeds that may exceed food capture rates, damage feeding apparatus (Johnson et al., 2013; Orejas et al., 2016) or topple large arborescent species (Weinbauera and Velimirov, 1996). Current speed is a primary driver of coral distributions and in our study the *D. pertusum* assemblage occurred in a region exposed to the highest speeds, which is consistent with published observations (Davies, 2009; Mohn et al., 2014; Rengstorf et al., 2013) including those from vertical walls (Brooke and Ross, 2014). On the other hand, larger gorgonians and sponges were observed in areas exposed to lower current speeds. Intensified currents are also linked to resuspension (Thomsen and Gust, 2000) and increased turbidity. Higher turbidity was measured from mid canyon sites (Supplementary 3.2.1). Both brachiopods and *D. pertusum* are noted to tolerate high turbidity (James et al., 1992; Brooke et al., 2009) that may enable them to exploit these conditions where other species cannot.

#### 3.5.2.1.4 Internal tide induced short term temporal variability

Amplitudes of up to 140 m were calculated for the $M_2$ tide resulting in maximum tidal temperature variations of 1.55 °C. Unfortunately these areas of high temporal variably were not coincident with vertical walls and the temporal variability in oceanographic variables experienced by wall fauna was relatively consistent between dives, even if the absolute values differed (Table 3.4). However, assemblages still differentiated across a gradient of $M_2$ internal tide amplitude (Figure 3.9, Table 3.4 and supplementary 3.2.2). Temperature has been linked to physiological responses and spatial patterns in species (Hutchins, 1947; Rowe and Menzies, 1969; Tietjen, 1971; Menzies, 1972; Van Den Hoek, 1982; Jeffree and Jeffree, 1994; Southward et al., 1995). In our study *D. pertusum* occurred across the

canyon but only obtained high abundances along dive 116. At this location the *D. pertusum* colonies were periodically exposed to cooler waters than at other supercritical settings. Laboratory experiments have shown *D. pertusum* to tolerate better sudden temperature variability and colder temperatures when compared to *M. oculata* (Brooke et al., 2013; Naumann et al., 2014). These eco-physical responses of *D. pertusum* may enable it to dominate vertical walls that experience temporal variability, including colder temperatures. Such species-specific thermal acclimatisation has been postulated to significantly affect the occurrence and abundance of CWCs (Brooke et al., 2013).

#### 3.5.2.2 Fine-scale structural complexity

In our study, increased species richness was observed from vertical walls that supported coral framework or coral rubble substratum and the amount of coral substratum explained variation in assemblages (Table 4.5). CWC species including arborescent gorgonians and scleractinians are considered ecosystem engineers capable of forming complex structures that provide substratum for settlement, food and refuge for many benthic species (Buhl-Mortensen et al., 2010). The organism structure can modify local current flow, sedimentation and subsequent food availability (Guihen et al., 2013) and so increase fine-scale environmental heterogeneity (Buhl-Mortensen et al., 2010). Increased environmental heterogeneity leads to a higher diversity of associated species (Frederiksen et al., 1992; Henry and Roberts, 2007; Lessard-Pilon et al., 2010). In our study species richness was highest where coral substrata occurred with mud on vertical walls whereby accumulations of mud supported additional soft sediment species, further increasing diversity.

We observed that some species aggregated in association with small scale geomorphological features such as ledges (Figure 3.5). Similar observations have been made from other vertical wall environments where the increased fine-scale structural complexity provided by ledges is proposed to provide some protection from sedimentation and allow species to position themselves further into the flow (Huvenne et al., 2011), contribute to fine-scale environmental heterogeneity and so promote niche differentiation (Robert et al., 2019). The fragile nature of the ledges has also been proposed as a limiting factor on maximum colony size of corals observed (Brooke et al., 2017; Robert et al., 2019). This postulation could explain the occurrence of the *D. pertusum* assemblage on the wall with wider stronger ‘steps’, observed from dive 116 that are capable of supporting greater weight and higher coral densities, compared to the thinner ledges observed elsewhere. However, the existence of different communities associated with ledges in ours (dive 262, 250 and 116) and other studies of Whittard Canyon (Johnson et al., 2013; Robert et al., 2019) suggests that these features act to influence species patterns at fine spatial scales whilst other factors beyond substratum availability (e.g. depth, current speed and food supply) influence assemblage patterns across walls at the canyon scale.

## 3.6 Conclusion

Our results show that species diversity and assemblage composition on vertical walls change in response to environmental gradients of depth (and its covariates), substratum type and internal tide dynamics. We demonstrate that multivariate analysis of species data provides greater sensitivity than univariate indices, providing further insight into how the environmental factors interact at different scales to generate variability in environmental conditions that control species abundances and which species become characteristic of assemblages. Specifically, we highlight the likely link between internal tides and their associated vertical displacement in generating both spatial and temporal gradients in food supply and water mass characteristics that in turn influence faunal patterns.

## 3.7 Acknowledgements

The authors would like to thank the Captains, crews, and scientific parties of expeditions JC036, JC125, 64PE421, 64PE453 and 64PE437. They are particularly grateful to the Isis ROV team for the collection of groundtruthing data in the challenging submarine canyon terrain. We would also like to thank Tim Le Bas and Catherine Wardell for help with the bathymetry data processing, Dr Brett Hosking for code to extract values from CTD casts and Michael Faggetter for his support with Matlab. Tabitha Pearman is a PhD student in the NERC-funded SPITFIRE Doctoral Training Programme (Grant number NE/L002531/1) and receives further funding from the National Oceanography Centre and the CASE partner CEFAS. Dr Veerle Huvenne was funded by the ERC Starting Grant project CODEMAP (Grant No 258482), by the NERC National Capability programme CLASS (Grant No NE/R015953/1); and the EU H2020 research and innovation programme project iAtlantic (grant agreement No 818123).

# Chapter 4 Structural complexity provided by coral rubble mounds influences faunal patterns on submarine canyon interfluves

This chapter is in preparation for submission as **Pearman, T.R.R.,** Callaway, A., Hall, R., Lo Iacono, C., Wardell, C., Marsh, L., Davies, J., Huvenne, V.A.I. Structural complexity provided by small mound features influences faunal patterns on submarine canyon interfluves.

Author contributions: T.P conceptualised the chapter, annotated the JC166 ROV imagery data, derived textual indices and terrain derivatives, conducted statistical analysis and wrote the manuscript. T.P, L.M and J.D annotated the CEND0917 imagery data. T.P and A.C were part of the team with who acquired the Drop-down imagery data during the CEND0917 cruise. T.P and V.H were part of the team that acquired the ROV imagery and AUV data during the JC166 cruise. V.H acquired the AUV data during the JC124_JC125 CODEMAP2015 cruise and C.W processed the AUV acquired side-scan sonar data. A.C and V.H reviewed and commented on the chapter.

## 4.1 Abstract

Environmental heterogeneity is a primary driver of faunal distributions. The structural complexity of the seafloor is an important factor promoting increased environmental heterogeneity in marine benthic settings. Small mound features 3 m high and 50 - 150 m in diameter occur on the interfluves between the Dangaard and Explorer Canyons, North-East Atlantic. The mounds are predominantly comprised of coral rubble and are structurally complex compared to the surrounding seafloor. The interfluves (and hence also the coral mounds) are subject to trawling pressure, which acts to reduce structural complexity by modifying seafloor morphology. Establishing the role of structural complexity as an environmental driver of faunal patterns across the mounds is fundamental to enable effective management of these features. This study aims to assess the link between environmental heterogeneity, particularly caused by structural complexity at multiple spatial scales, and faunal patterns across mound provinces of the two interfluves.

Autosub6000 AUV high-resolution sidescan sonar data, multibeam echosounder data, Drop-down camera and ROV Isis HD still imagery data were acquired to characterise the substrata, topography and epibenthic megafauna of the interfluves. Sidescan sonar image texture indices and a suite of terrain derivatives were calculated and integrated with still imagery data to explore the relationship between structural complexity, substratum characteristics and species richness, density and assemblage. Hierarchal clustering, Non-metric Multi-Dimensional Scaling and canonical Redundancy Analysis were applied to relate faunal assemblage composition to the environmental variables and Generalised Additive Models were applied to relate species richness and density to the environmental variables. To explore how structural complexity may influence spatial distributions of faunal assemblages Random Forests was used to build predictive distribution maps of faunal assemblages across the interfluves.

Our results demonstrate the importance of structural complexity in influencing species richness, density and assemblage structure at various spatial scales. Structural complexity influences faunal patterns on canyon interfluves by mediating spatial distributions of substratum characteristics and increasing environmental heterogeneity. In particular, fine-scale structural complexity provided by coral rubble appears to be important in explaining faunal patterns within mound provinces. We propose that coral rubble may act as a key stone structure on interfluves that supports a coral rubble assemblage distinct from that previously described from the coral rubble zone adjacent to living coral reefs. Furthermore, our results indicate that even if the broad-scale terrain complexity appears reduced (low ruggedness), fine-scale complexity may still be present and acting to increase diversity. Therefore, it is important that fine-scale structural complexity be taken into account when studying environmental drivers of faunal patterns and assessing impacts of trawling on canyons.

## 4.2 Introduction

Spatial patterns in fauna are intrinsically linked to environmental heterogeneity (Stein et al., 2014). Environmental heterogeneity is the variation in the spatial arrangement of environmental conditions at a given site. Niche theory states that species adapt to exploit certain environmental conditions (fundamental niche), although they may only occur within a portion of suitable sites (realised niche), as a result of biological interactions, such as dispersal, competition or predation (Hutchinson and MacArthur, 1959), or the impact of disturbance. As such, areas supporting greater environmental heterogeneity can support more niches and through associated resource partitioning reduce competition, leading to higher coexistence of 'specialised' species and diversity (MacArthur and MacArthur, 1961). Increased environmental heterogeneity has been linked to increased diversity in marine environments (McQuaid and Dower, 1990; Menge and Sutherland, 1976; Schlacher et al., 2007; Firth et al., 2013; Robert et al., 2014; Loke and Todd, 2016; Zeppilli et al., 2016), which has led to the use of environmental heterogeneity as a proxy of faunal diversity (Mumby, 2001; Buhl-Mortensen et al., 2012; Fontaneto et al., 2013; Meager and Schlacher, 2013; Mellin et al., 2014; Robert et al., 2014; Ismail et al., 2018).

In marine settings environmental heterogeneity in oceanography, food availability and seafloor characteristics interact at multiple scales, together with biological interactions to influence faunal patterns (Levin et al., 2001; McClain and Barry, 2010; De Mol et al., 2011; Howell et al., 2011; Baker et al., 2012; De Leo et al., 2014; Bargain et al., 2018; Pearman et al., 2020). Most studies assessing the influence of environmental heterogeneity on faunal patterns have focussed on seafloor characteristics (topography and substratum) (Brown et al., 2011; Robert et al., 2014; Ismail et al., 2018). The common use of seafloor characteristics is based on the observation that environmental heterogeneity is often spatially arranged in relation to topography (Wilson et al., 2007; Daly et al., 2018), coupled with the comparative ease of collecting broad-scale acoustic datasets (with multibeam echosounders (MBES)) from which seafloor characteristics can be inferred and used to model habitat (Kostylev et al., 2001; Wilson et al., 2007; Brown et al., 2011) and faunal distributions (Robert et al., 2014).

Seafloor characteristics influence faunal distributions by providing substratum for colonisation (Baker et al., 2012; Lacharité and Metaxas, 2017). On the other hand, topography influences sediment dynamics (de Stigter et al., 2011; Martín et al., 2011; Puig et al., 2017) and the degree of exposure to currents and waves fauna may experience (Wilson et al., 2007; Ismail et al., 2015; Robert et al., 2015). Additionally, complex topography can interact with local hydrodynamics to form efficient food supply mechanisms to the benthos (Demopoulos et al., 2017).

Seafloor characteristics contribute to the physical structural complexity of habitats (Graham and Nash, 2013). Structural complexity, refers to " the irregularity in arrangement of structural elements which

comprise the bathymetric contours of a given site" (Taniguchi et al., 2003; Yanovski et al., 2017) and represents the three-dimensional component of seafloor characteristics. Increased structural complexity is associated with increased environmental heterogeneity and subsequently niche diversification and species coexistence (Willis et al., 2005; Graham and Nash, 2013). Increased structural complexity has the ability to influence ecological interactions and community dynamics by providing refuges from predation and decreasing encounter rates between competitors, predators and prey (Stevenson et al., 2015; Price et al., 2019). Consequently, studies have shown positive relationships between structural complexity and diversity (Lingo and Szedlmayer, 2006; Moore and Hovel, 2010; Price et al., 2019; Mazzuco et al., 2020).

Substratum characteristics capture qualities of the substratum, including substratum composition (i.e. grain size), and fine-scale patchiness in the consistency and spatial arrangement in substratum composition (Lacharité et al., 2015). Substratum characteristics influence faunal distributions because many benthic species are associated with particular substratum characteristics, so that their spatial distributions are correlated with the spatial distribution of the substratum with which they affiliate (Baker et al., 2012; Pierdomenico et al., 2019). Consequently, substratum characteristics have been incorporated into benthic studies of faunal patterns and assemblage structure (Warwick and Davies 1977; Schneiderl et al., 1987; Robert et al., 2014; Post et al., 2016; Michaelis et al., 2019), as well as forming a key component of hierarchal habitat classification schemes (EUNIS, 2019).

Terrain derivatives, such as ruggedness and slope that are derived from MBES data can capture variability in topography, which can be used to quantify structural complexity and consequently act as a proxy of environmental heterogeneity (Robert et al., 2015; Ismail et al., 2018; Price et al., 2019) and be incorporated in to benthic mapping (Wilson et al., 2007). On the other hand, acoustic signatures in sidescan sonar (SSS) and MBES backscatter can indicate changes in substratum characteristics (Huvenne et al., 2002).

Image textural indices are second order derivatives of backscatter that can identify variation in image tone and contrast to provide a proxy for substratum patchiness and pattern that is independent of bathymetry (Blondel et al., 1998; Zelada Leon et al., 2020). Textural indices can delineate substratum types, such as sand that is more homogeneous compared to coarser substratum i.e. gravels (Blondel et al., 1998; Prampolini et al., 2018), and geomorphological features such as sand waves that exhibit regular structural complexity in contrast to the irregular patterns of rocky outcrops (Blondel et al., 1998). Due to the ability of textural indices to highlight areas of difference and similarity in the acoustic signatures of backscatter and so discriminate seafloor characteristics they have been incorporated at varying resolutions in studies of environmental heterogeneity (Huvenne et al., 2007; Ismail et al., 2018) and in automated benthic and habitat mapping (Ierodiaconou et al., 2007; Montereale-Gavazzi et al., 2017; 2018; Janowski et al., 2018; Prampolini et al., 2018).

With the increased use of Automated Underwater Vehicles (AUVs) in the deep sea enabling the acquisition of data at a resolution comparable to that of hull-mounted systems on continental shelf areas, we can now visualise fine-scale variability in seafloor characteristics (including structural complexity) over km-scale areas (Wynn et al., 2014; Zelada Leon et al., 2020), offering an opportunity to quantify its importance in driving faunal patterns.

Understanding the role of structural complexity is especially poignant on canyon interfluves that are under fishing pressure from bottom trawling (Wilson et al., 2015a; Daly et al., 2018), which reduces structural complexity by modifying the seafloor (Bahn_McGill, 2012; Puig et al., 2012; Martín et al., 2014a; 2014b; Daly et al., 2018). Contact between trawl gear and the seafloor can cause damage, resuspension, resorting and modified layering of the substrata present (Martín et al., 2014c). Trawling induced modification of seafloor characteristics can affect ecosystems by reducing environmental heterogeneity with subsequent reduction in diversity and abundance (O'Neill and Summerbell, 2011; Puig et al., 2012; Pusceddu et al., 2014).

We aim to explore the relationship between environmental heterogeneity, particularly caused by structural complexity acting at different spatial scales, and epibenthic megafaunal species richness, density and assemblage structure across mound features that have been described on the interfluves between the Dangaard and Explorer Canyons, North-East Atlantic (Stewart et al., 2014). The mounds comprise aggregations of coral rubble, pebbles and shell (Stewart et al., 2014), which make the mounds structurally complex compared to the surrounding seafloor. We calculate textural indices based on Grey level co-occurrence matrices (GLCM) derived from AUV-acquired SSS backscatter data, together with a suite of terrain derivatives to ascertain what drives patterns in species richness, density and assemblage across the interfluves. Our working hypothesis is ‘Epibenthic megafaunal assemblages are driven by environmental heterogeneity caused by structural complexity acting at different spatial scales and that increased species richness and density are associated with increased seafloor complexity as it promotes increased fine-scale patchiness in substratum characteristics, allowing more species to co-occur’.

## 4.3 Methods

### 4.3.1 Study Area

The Explorer and Dangaard Canyons incise the shelf break of the western flank of Brenot Spur, on the Celtic Margin, south-west of the British Isles in the Northern Bay of Biscay (Aslam et al., 2018) (Figure 4.1). They are located at a water depth ranging from approximately 200 m to 2200 m and 3600 m, respectively, where they join the Whittard Canyon system. Explorer Canyon trends north-east and Dangaard Canyon trends east north-east (Davies et al., 2014; Stewart et al., 2014).

Interfluves, representing relict parts of continental shelf and slope, separate the two canyons (Figure 4.1). The interfluves are named corresponding to the canyon branch located north of them, following the convention of Stewart et al. (2014) (Figure 4.1). The interfluves occur at approximate water depths of 250 m to 450 m (Stewart et al., 2014) where they are overlaid by the Eastern North Atlantic Water (ENAW) (~100 - 600 m) (Pollard et al., 1996; Van Aken, 2000). The slope current flows predominantly to the north-west at velocities of ~ 0.05 – 0.10 $ms^{-1}$ (Pingree and Cann, 1990). Estimated near-bed tidal currents are lower (0.02 - 0.17 $ms^{-1}$) on the interfluves compared to the intensified hydrodynamic regime within the canyon branches (Aslam et al., 2018).

The interfluves are characterised by slope angles of < 3º (Stewart et al., 2014) and are comprised of mixed substrata with areas of biogenic gravel composed of coral rubble and shell fragments associated with mound features (termed 'mini mounds'; (Stewart et al., 2014)). To date over 2800 mounds have been identified, and they are more numerous and pronounced on the Dangaard interfluve compared to the Explorer interfluve (Stewart et al., 2014; Stewart and Gafeira, 2016). The mounds measure up to 3 m in height with diameters of 50 – 150 m. Although the surface of the mounds is mainly comprised of coral rubble, to date no live cold-water corals have been observed (Davies et al., 2014; Stewart et al., 2014). The lack of subsurface expression of the mounds has led authors to propose their possible origination in the Holocene, during a period of live coral growth contributing to mound formation (Stewart et al., 2014).

The mounds are situated within the U.K designated 'The Canyons Marine Conservation Zone' (MCZ) that encompasses Dangaard and Explorer Canyons. The MCZ designation is based upon the presence of the 'Deep-sea bed' broad-scale habitat and 'Cold-water coral reefs', 'Coral gardens' and 'Sea-pen and burrowing megafauna communities', habitat features of conservation interest (DEFRA, 2013; DEFRA, 2019b).

An assemblage comprised of 'Ophiuroids and *Munida sarsi* associated with coral rubble' has previously been described from a limited dataset covering the mounds (Davies et al., 2014). This classification relates to 'coral rubble zone' described from other settings, where a coral rubble assemblage has been found close to live coral reef (Mortensen et al., 1995). Elsewhere on the interfluves an assemblage comprised of '*Munida sarsi* and *Leptometra celtica* on mixed substratum' has been described (Davies et al., 2014).

### 4.3.2 Data acquisition

Data were collected during (1) the JC124_JC125 expedition funded by the ERC CODEMAP project (Starting Grant no 258482), the NERC MAREMAP programme and the Department of Environment, Food & Rural Affairs (DEFRA), (2) the JC166 expedition funded by the NERC CLASS programme (Grant No NE/R015953/1) (3) the MESH expedition funded by the European Union INTERREG IIIb

Community Initiative, and the (4) CEND0917 cruise funded by DEFRA 2017 Marine Protected Areas Group.

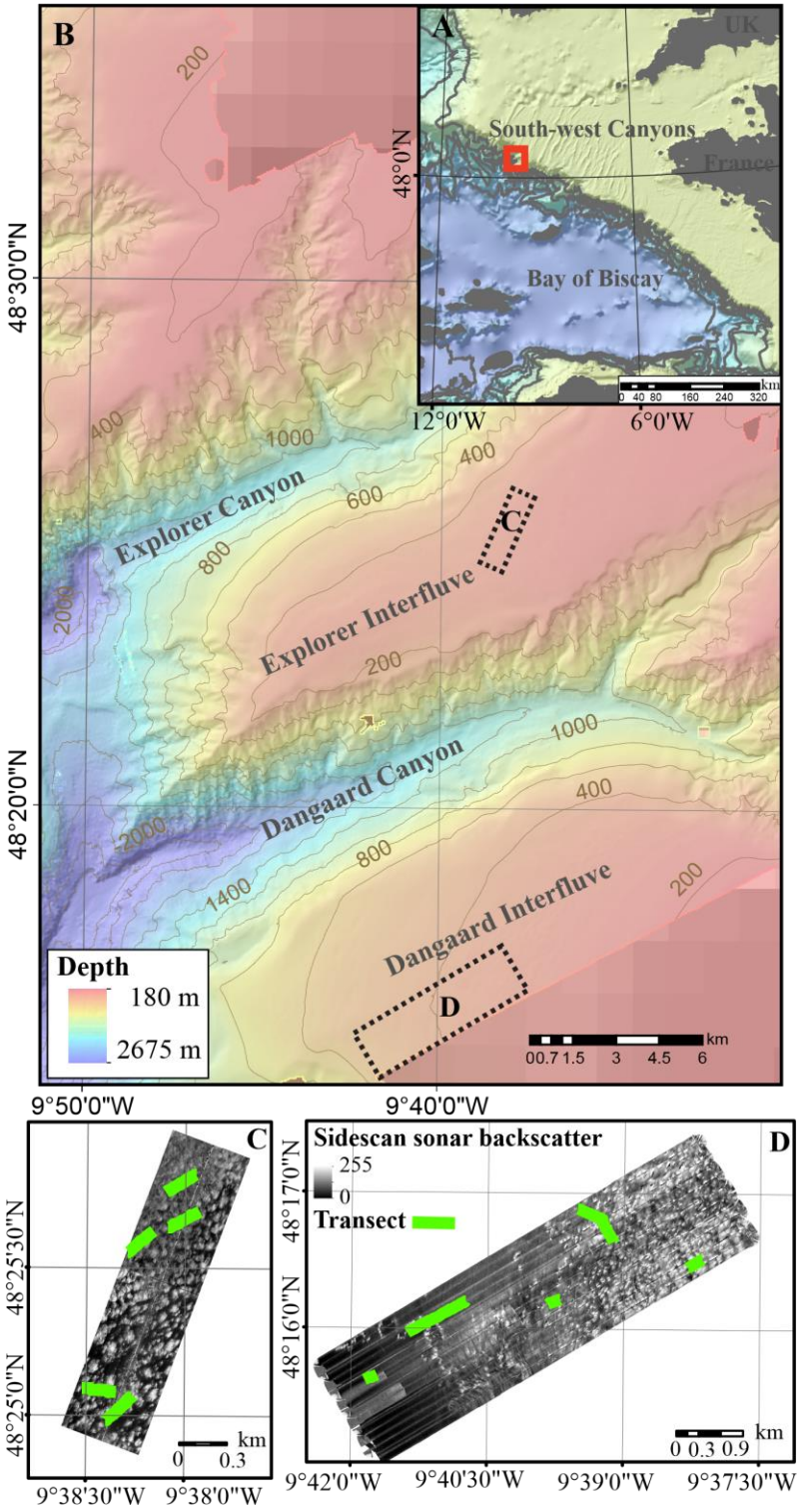


Figure 4.1 Location map of (A) Dangaard and Explorer Canyons and (B) of bathymetry data acquired from the interfluves during the MESH cruise. Background bathymetry from GEBCO compilation group (2019). Sidescan sonar and imagery data acquired from the (C) Dangaard and (D) Explorer interfluves during the JC125, JC166 and CEND0917 cruises.

### 4.3.3 Acoustic data acquisition and processing, and extraction of terrain derivatives

MBES data were acquired during the MESH cruise with the ship-board Kongsberg Simrad EM1002 MBES system of RV *Celtic Explorer* (Davies et al., 2008b). Bathymetry data were processed utilising CARIS HIPS & SIPS v.8 and exported at a resolution of 25 m (WGS1984, UTM Zone 29N)(Davies et al., 2008b). The terrain derivatives slope, curvature, eastness, northness, ruggedness (VRM = Vector Ruggedness Measure) and both broad and fine bathymetric position index (BPI) were derived from bathymetry data using the ArcGIS extension Benthic Terrain Modeller v. 3.0 (Walbridge et al., 2018) and exported as rasters at 25 m resolution (Supplementary 4.1.1).

The BPI is a derived metric of a cell's position and elevation relative to its surrounding landscape within a user defined neighbourhood (Wright, 2005). Ruggedness is a measure of the variation in three-dimensional orientation of grid cells within a neighbourhood. Slope quantifies the maximum rate of change in elevation within a neighbourhood, and aspect (subsequently converted to eastness and northness) measures the compass orientation of the maximum change along the slope (Wilson et al., 2007). Together these terrain derivatives can capture variation in seafloor characteristics, including structural complexity.

To further our understanding of the resolution at which structural complexity influences faunal assemblages, BPI and ruggedness were derived at pixel neighbourhoods ($_{nh}$) of 3, 5, 9, 17 and 33 and a multi-scale analysis was performed to identify which resolution explains most variation in the species data (Misiuk et al., 2018; Porskamp et al., 2018) (see supplementary 4.1.2). In summary, species data was modelled with each terrain derivative separately but at all resolutions, in order to rank the contribution of each terrain derivative at the different resolutions (Misiuk et al., 2018). Additionally, all terrain derivatives, at all resolutions were modelled simultaneously with species data to account for potential interactions or correlation between the variables. Results were reviewed and following Misiuk et al. (2018) terrain variables that contributed > 10 % to overall variance explained by the model and < 0.7 correlated were retained.

### 4.3.4 Textural derivatives

SSS backscatter data were collected with the Edgetech 2200-M system (120 - 410 kHz) mounted on the Autosub6000 AUV during the JC124_125 (Huvenne et al., 2016) and JC166 cruises (Huvenne and Furlong, 2019) (Figure 4.1). SSS backscatter data were processed utilising the NOC in-house PRISM software (Le Bas, 2002) and the mosaic from each interfluve exported at a resolution of 0.5 m (WGS1984, UTM Zone 29N). Due to internal navigation inconsistencies of the AUV during JC125, SSS lines were manually georeferenced against overlapping features on the MESH bathymetry using the ArcGIS georeferencing tool box. The corrected SSS lines were exported as a mosaic using the

ArcGIS mosaic to new raster tool box. The SSS backscatter mosaics from the two interfluves were standardised by bringing the histograms of grey scale values to an averaged mean calculated from both mosaics with the same standard deviation.

To obtain textural derivatives, GLCMs (Blondel et al., 1998) with 32 grey levels were derived from the SSS backscatter. GLCMs are an adaptable method for textural analysis of SSS backscatter (Blondel et al., 1996) that have been widely applied in benthic mapping (Huvenne et al., 2007; Montereale-Gavazzi et al., 2016; Prampolini et al., 2018; Zelada Leon et al., 2020). The GLCM represents the frequencies of probabilities of each tonal combination from 32 grey level tones of pixel pairs. 32 grey levels were chosen as a compromise between texture detection and computation time (Blondel et al., 1996; Huvenne et al., 2002). To account for the influence that pixel comparison distance and orientation can have on the GLCM frequencies of probabilities (due to spatial autocorrelation), GLCMs were calculated at various window sizes (11, 21 and 51) with a range of inter pixel distances (minimum 5 up to a maximum of half the window size) across all directions and a multi-scale analysis performed (following the same protocol as that for terrain derivatives) to identify which combination explains most variation (Supplementary 4.1.3). The importance of studying different spatial scales when analysing textural patterns from backscatter has been demonstrated by Montereale-Gavazzi et al. (2016) and Zelada Leon et al. (2020). Windows sizes ($_{w}$) and inter pixel distances ($_{ipd}$) were chosen to match the size of morphological features influencing textural contrast (mounds), whilst still capturing variation in seafloor characteristics at comparable resolutions to that captured by the still imagery data and terrain derivatives. Co-occurrence matrices were averaged for all directions to account for variation in heading affecting the angle at which features were insonified (Blondel et al., 1996; Huvenne et al., 2002).

The second order textural indices entropy, homogeneity, contrast and correlation were derived from the GLCM (Blondel et al., 1996) and exported as rasters at a 0.5 m resolution in the open source software R (R_Core_Team, 2014), packages "raster" and "glcm". Textural indices quantify spatial arrangements of grey level tones among pixels (Haralick et al., 1973) can provide an indication of seafloor characteristics, including substratum type (Blondel et al., 1998; Huvenne et al., 2002; 2007; Janowski et al., 2018; Prampolini et al., 2018). Homogeneity is measure of similarity in grey levels within the moving window (Blondel et al., 1998; Huvenne et al., 2002), entropy is a measure of spatial disorder in grey levels of the moving window, contrast is a measure of differences of the intensities of the grey levels within the moving window (Montereale-Gavazzi et al., 2017) and correlation is a measure of grey-level linear-dependencies in the moving window (Blondel et al., 1998).

### 4.3.5 Seafloor Imagery

#### 4.3.5.1 Imagery data acquisition and processing

Imagery data were acquired during the CEND0917 cruise (Figure 4.1 and Table 4.1), using a Drop-down camera system equipped with high definition stills (18 mega pixel) and video camera (1080 pixels). Positional data were derived from an ultra-short baseline navigation system (USBL) using a beacon attached to the camera frame. Still imagery data were also acquired during the JC166 cruise (Figure 4.1 and Table 4.1), using the remotely operated vehicle (ROV) *Isis* equipped with a dual high definition stills and video camera (Scorpio, Insite Tritech Inc., 1920 x 1080 pixels). Positional data were derived from the ROV's USBL (Huvenne and Furlong, 2019).

Overlapping images and those exceeding 2 m altitude or of low visibility (due to sediment or lighting) were removed. To reduce the influence of spatial autocorrelation 'sample images' were extracted at a minimum distance of 7 m. To account for the oblique angle of the ROV that could lead to bias counts, images were cropped and the area of each image was calculated. The area of each image was calculated following a JNCC procedure implemented during the analysis of CEND0917 images (Turner et al., 2006), whereby pixel dimension of each image together with the pixel and actual distance between lasers were used to give the approximate area of each still image (Supplementary 4.1.4). Percent composition of the substratum was visually assessed from images, substratum type was described and assigned a broader EUNIS habitat classification (EUNIS, 2019). Epibenthic morphospecies (visually distinct taxa) > 10 mm were annotated from the stills in BIIGLE, with organism size estimated from a laser scale with parallel beams positioned 10 cm apart. Taxa were assigned to morphospecies using a modified version of the Howell and Davies (2010) species catalogue that was developed specifically for the CEND0917 analysis. All individuals were enumerated except for encrusting and colonial fauna where area cover was used (by overlaying a grid on to images). To account for the differences in camera field of view, the area of each image was calculated and used to convert species counts to densities per $m^2$. Annotations from the two cruises were combined into a single data matrix and annotation consistency between cruises assessed following Durden et al. (2016) (Supplementary 4.1.4). Species richness and density was calculated for each sample image.

Table 4.1 Transects from Explorer and Dangaard interfluve analysed in the study. List of transects, cruises during which transect was complete, transect location (degrees and decimal minutes), transect length (m) and maximum and minimum water depth (m) from each transect.

| Transect | Cruise | Interfluve | Start Position | | End Position | | Length (m) | Depth Range (m) |
|---|---|---|---|---|---|---|---|---|
| CYN_042_STN_195 | CEND0917 | Explorer | 48° 25.695' N | 9° 37.927' W | 48° 25.634' N | 9° 38.092' W | 240 | (299 - 305) |
| CYN_047_STN_192 | CEND0917 | Explorer | 48° 25.077' N | 9° 38.246' W | 48° 24.981' N | 9° 38.398' W | 230 | (299 - 305) |
| CYN_051_STN_196 | CEND0917 | Explorer | 48° 25.818' N | 9° 37.942' W | 48° 25.756' N | 9° 38.103' W | 230 | (306 - 312) |
| CYN_054_STN_193 | CEND0917 | Explorer | 48° 25.080' N | 9° 38.338' W | 48° 25.091' N | 9° 38.521' W | 230 | (305 - 312) |
| CYN_058_STN_194 | CEND0917 | Explorer | 48° 25.634' N | 9° 38.149' W | 48° 25.550' N | 9° 38.294' W | 220 | (306 - 311) |
| CYN_082_STN_231 | CEND0917 | Dangaard | 48° 16.519' N | 9° 38.134' W | 48° 16.460' N | 9° 38.294' W | 230 | (321 - 333) |
| CYN_083_STN_229 | CEND0917 | Dangaard | 48° 16.218' N | 9° 39.700' W | 48° 16.177' N | 9° 39.877' W | 180 | (372 - 384) |
| CYN_091_STN_226 | CEND0917 | Dangaard | 48° 15.655' N | 9° 41.710' W | 48° 15.614' N | 9° 41.883' W | 190 | (485 - 495) |
| CYN_110_STN_227 | CEND0917 | Dangaard | 48° 15.968' N | 9 41.383' W | 48° 16.211' N | 9° 40.714' W | 930 | (450 - 416) |
| 340 | JC166 | Dangaard | 48° 16.644' N | 9 39.114' W | 48° 16.886' N | 9° 39.509' W | 710 | (362 - 372) |

### 4.3.6 Statistical analyses

Multivariate analysis was used to identify and relate faunal assemblage composition to structural complexity. Highly mobile taxa such as fish that can be 'double counted' and encrusting or colonial fauna that were estimated by percent cover and not readily comparable with our density measurements, were removed prior to analysis. Samples with < 3 taxa present were also excluded from the multivariate analysis.

Environmental data coincident with each sample image was extracted from the rasters and standardised (i.e. transformed to zero mean, and unit variance). Species data were Hellinger transformed to enable the use of linear ordination methods (Legendre and Gallagher, 2001; Legendre and Legendre, 2012) and data exploration was undertaken following the protocol described in Zuur et al. (2010).

Non-metric Multi-Dimensional Scaling (nMDS) and hierarchal cluster analysis was performed to identify faunal assemblages, using a Hellinger dissimilarity matrix derived from the transformed data matrix. Cluster analysis was based upon group average linkage. The optimal number of interpretable clusters was determined by mean silhouette widths (Legendre and Legendre, 2012). Silhouette widths are based upon comparisons of dissimilarity measures between objects within a cluster and those in the next closest cluster and can be useful in determining clustering performance based on different cut off levels for cluster interpretation (Legendre and Legendre, 2012). Characteristic fauna contributing to similarity among clusters were identified using the Similarity percentage analysis (SIMPER) routine (Clarke, 1993). Differences in faunal composition between interfluves, mounds and substratum type were tested via analysis of similarities (ANOSIM).

To explore relationships between faunal assemblages and seafloor structural complexity, canonical Redundancy Analysis (RDA) was performed. RDA combines the outputs of multiple regression with ordination (Legendre and Legendre, 2012). Forward selection was carried out on the environmental variables to obtain the most parsimonious model. Pearson's correlation and variance inflation factor (VIF) scores, which detect multicollinearity in regression analysis, were used to exclude environmental variables that showed strong collinearity with others present within the model and are therefore redundant (Correlation coefficients > 0.7 and VIF scores > 5) (Borcard et al., 2011; Zuur et al., 2014a). Spatial correlation in the multivariate species data was assessed by incorporating sample co-ordinates (Borcard et al., 2011).

Variance partitioning via partial RDA was performed to assess the combined and shared variance explained in the species data by the environmental variables. Variance partitioning was performed using the retained environmental variables and sample co-ordinates (Legendre and Legendre, 2012).

Generalised Additive Models (GAMs) were used to determine if species richness and density are associated with increased structural complexity, influenced by the same environmental drivers as assemblages, and to identify any potential thresholds for species richness and density with complexity. GAMs are generalised models with smoothers and link functions based on an exponential relationship between the response variable and the environmental variables (Zuur et al., 2014b). GAMs produce ecologically intuitive outputs (Zuur et al., 2014a) and have previously been applied to identify ecological response thresholds (Foley et al., 2015; Large et al., 2015; Rowden et al., 2020). The degree of smoothing in the fitting of the environmental variables was based on the Generalized Cross Validation (GCV) method and a log link function. A gamma distribution with no transformation was chosen after exploring several alternative distributions. Significance of terms in the model was tested with analysis of variance (ANOVA). Model accuracy was assessed by variance in species richness or density explained by each model (Adjusted $R^2$) and model fit was assessed by Akaike's Information Criterion score (AIC) and residual plots (Zuur et al., 2014a).

#### 4.3.6.1 Predictive distribution modelling of assemblages

To explore how structural complexity may influence spatial distributions of faunal assemblages, predictive distribution maps of faunal assemblages were built based upon the environmental variables identified as important after the multi-scale analysis (Supplementary 4.1.2 and 4.1.3) and for which spatial rasters existed. Random Forests (RF) were used to build predictive distribution maps of assemblages that had been defined during the multivariate analysis, and were subsequently modelled as a univariate response. RF is a classification method that builds multiple trees based upon splitting rules that maximise homogeneity in response to predictors within branches, starting each time with a randomised subset of data points and predictor variables (Breiman, 2001; Prasad et al., 2006). RF is commonly employed in predictive habitat mapping (Collin et al., 2011; Bučas et al., 2013; Piechaud et al., 2015; Robert et al., 2015; Zhang et al., 2019; Pearman et al., 2020), due to its high performance based upon lack of assumptions concerning the response variable, robustness to overfitting, allowance for interactions between environmental variables and nonlinear relationships between the response and environmental variables (Cutler et al., 2007). Each RF was run with 1500 trees and the number of variables chosen at each node split and the out of bag (OOB) set as default (Breiman and Cutler, 2018; Prasad et al., 2006). Model performance was assessed using a cross-validation procedure in which models were trained using a random partition of data (70 %) and tested against the remaining portion (30 %) (Guisan and Zimmermann, 2000). Predictive performance was assessed with the out of bag error rate of the training data and confusion matrices between the predicted and observed values within the test dataset.

All statistical analyses were conducted using Primer V7 and the open source software R (R_Core_Team, 2014), packages "Packfor" "vegan", "cluster", "ape", "ade4", , "gclus", "AEM", "spdep", "mgcv", "raster", "RandomForest", and "MASS".

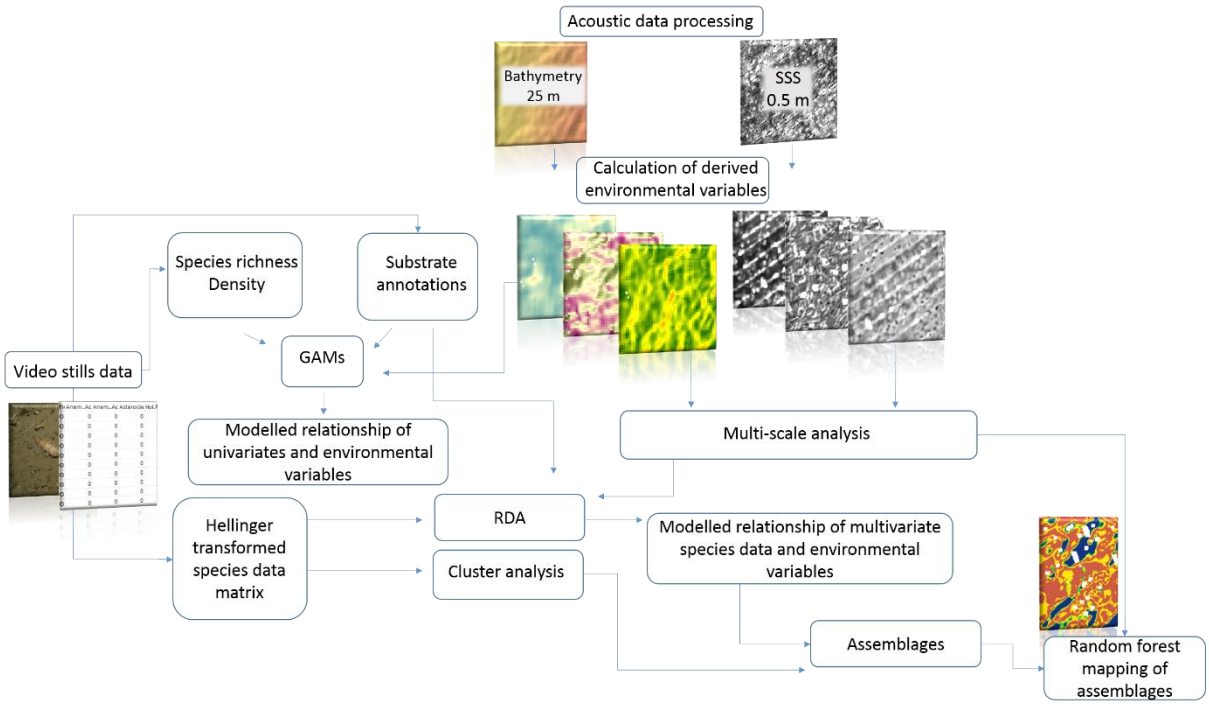


Figure 4.2 Overview of methodology applied during analysisEnvironmental variables were derived from the processed bathymetry and sidescan sonar (SSS) backscatter data. Multi-scale analysis of the terrain and textural environmental variables was undertaken separately (reported in supplementary 4.1.2 and 4.1.3). The best uncorrelated predictors for both the terrain and textural indices were incorporated into a canonical Redundancy Analysis (RDA) to discern which environmental variables explain the greatest variation in the Hellinger transformed species data. Predictive distribution mapping of the faunal assemblages, identified after review of clustering and RDA, was undertaken by Random Forest (RF). General Additive Models (GAMs) of species richness and density with uncorrelated environmental variables chosen by forward selection was undertaken to assess if they exhibit a positive response to increased structural complexity and are driven by similar environmental variables as assemblages

## 4.4 Results

### 4.4.1 Acoustic data results

The terrain derivatives captured variation in topography related to the bathymetry across the entire site and were only able to distinguish prominent mounds that occurred in relatively flat surroundings.

(Supplementary 4.1.1). The SSS backscatter data and textural indices captured variation in the patchiness of substratum characteristics (Supplementary 4.1.3), but were unable to distinguish fine-scale substratum characteristics (i.e. presence of coral fragments or pebbles) identified in still images.

The SSS survey of the Explorer interfluve covered an area of mini-mounds and comprised two acoustic facies (Figure 4.1). Patches of higher reflectivity backscatter were surrounded by areas of lower reflectivity backscatter. The SSS survey of the Dangaard interfluve covered an area of mini-mounds to the north-east that extended south-west to a depth of approximately 380 m (Figure 4.1). The mounds were more discrete on the Dangaard interfluve, with acoustic shadows indicating elevation (Figure 4.1 and 4.3). On the Dangaard interfluve three acoustic facies were identified. Patches of high reflectivity were surrounded by 'halos" of medium reflectivity in areas of lower reflectivity (Figure 4.3). The density of mounds decreased toward the south-west and higher reflectivity patches trending north-west associated with a bathymetric ridge were observed (Figure 4.1 and supplementary 4.1.1). Between water depths of 390 m and 450 m striations were present (Figure 4.1). The remaining area surveyed to the south-west comprised lower acoustic reflectivity with ripples (Figure 4.1). Acoustic signatures indicative of trawl marks were evident from the backscatter and confirmed in the imagery data (Figure 4.3).

The textural indices derived from the SSS backscatter captured variation in substratum characteristics (Supplementary 4.1.3), which appeared to be spatially arranged in relation to mound features evident in the SSS backscatter (Figure 4.1 and 4.3) and a bathymetric rise on the Dangaard interfluve that was evident in both the SSS backscatter (Figure 4.1) and MBES data (Supplementary 4.1.1). Substratum patchiness was higher within the mound provinces compared to that of the non-mound province area (Supplementary 4.1.3). Textural indices indicated that areas of more homogeneous substrata occurred toward the south-west of the Dangaard interfluve coincident with the lower backscatter reflectivity (Figure 4.1 and supplementary 4.1.3). Less homogeneous substrata occurred between areas of different acoustic reflectivity coincident with areas directly surrounding the mounds and the bathymetric rise on the Dangaard interfluve (Supplementary 4.1.1 and 4.1.3). These areas also showed high correlation values (Supplementary 4.1.3).

Ground-truth imagery showed that substrata within the mound provinces comprised muddy sand with varying quantities of pebbles, shell and coral fragments, with patches of coral rubble often coinciding with high reflectivity backscatter of mound features (Figure 4.3). Muddy sand with pebbles and shell fragments coincided with the "halos" of medium reflectivity (Figure 4.3) and higher reflectivity patches associated with the bathymetric rise on the Dangaard interfluve. Substratum to the south-west of the Dangaard mound province mainly comprised muddy sand coincident with low reflectivity backscatter and increased homogeneity (Figure 4.1 and supplementary 4.1.3).

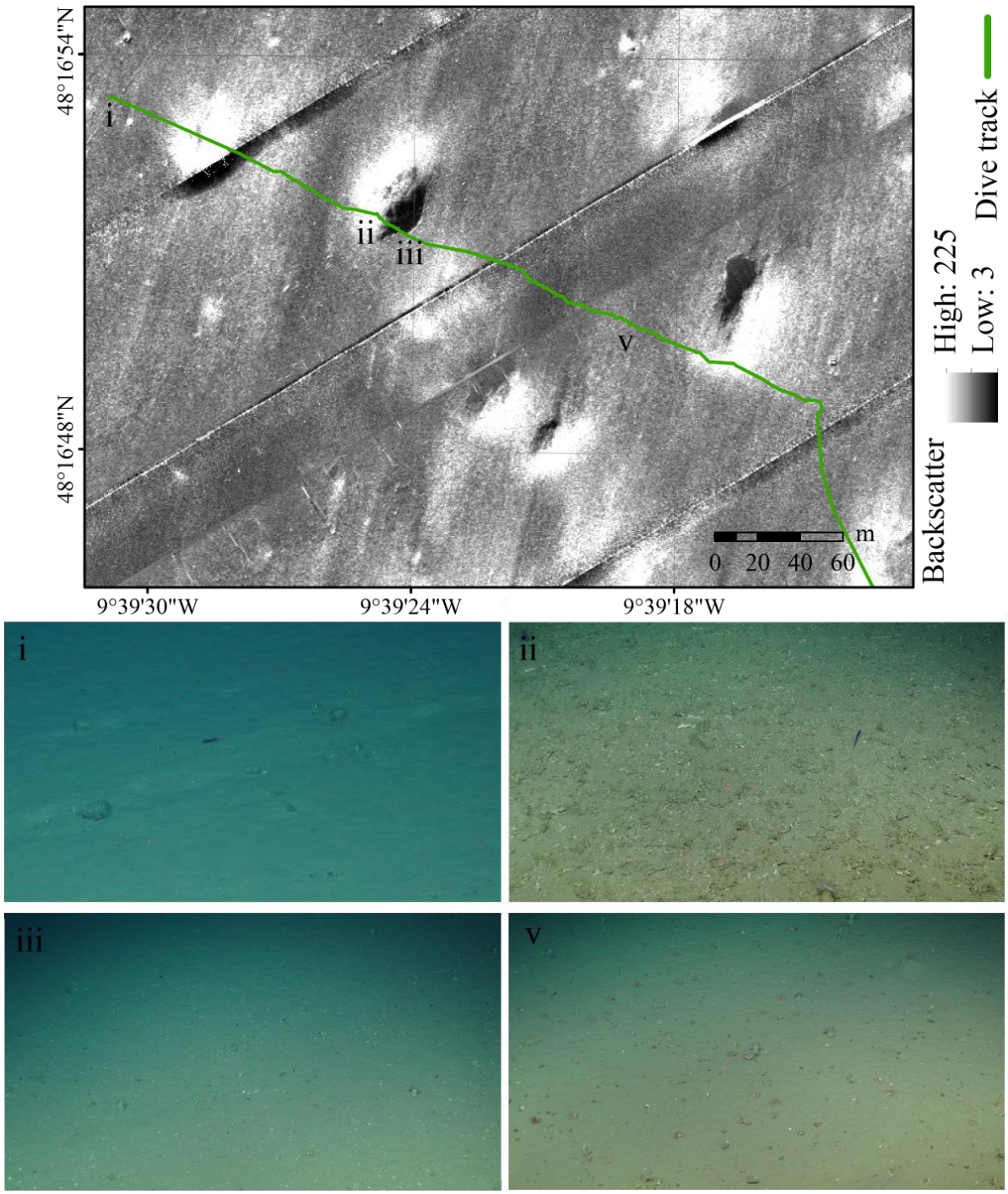


Figure 4.3 Example of sidescan sonar (SSS) backscatteracquired from the Dangaard interfluve. The partial track of the ROV during transect JC166_340 is illustrated in green. Letters denote the locations of ground-truthed backscatter: i) A trawl mark evident by a straight line of higher reflectivity ii) Coral rubble coincides with areas of high reflectivity iii) Muddy sand with pebbles and shell fragments coincide with a mottled pattern of moderate reflectivity iv) Muddy sand with pebbles, shell fragments and cup corals (with hard skeletons) coincide with a mottled pattern of moderate reflectivity.

### 4.4.2 Multi-scale analysis

Following the multi-scale analysis and model selection (detailed in supplementary 4.1.2 and 4.1.3), the terrain derivatives depth, slope, northness, eastness and ruggedness derived at neighbourhoods of 17 or 3 pixels, together with the textural indices correlation with a window size of 51 and inter-pixel distance of 20 and homogeneity with window size of 51 and inter-pixel distance of 25 were retained.

### 4.4.3 Fauna results

A total of 7492 individuals assigned to 71 morphospecies were annotated. Most morphospecies occurred at low abundance (Supplementary 4.2.1). The three most abundant morphospecies were brittlestars, OTU246 *Ophiactis balli*/ Ophiuroidea (2663), the cup coral OTU6 *Caryophyllia* sp. 2 (2537) and the anemone OTU499 *Actinauge richardi* (1200). The most common morphospecies recorded across transects was *A. richardi* (in 79.2 % of total samples). Highest species richness (13 from image CNYN_CEND0917_CNYN051_STN_196_A1_021) was observed from a mound feature comprised of coral rubble, shell fragments and muddy sand.

*A. richardi*, ophiuroids and squat lobsters, OTU200 *Munida* sp. were observed in association with coral rubble substratum of the mound features (Figure 4.4). The ophiuroids occurred within and beneath coral fragments, and *Munida* sp. occupied crevices beneath aggregations of coral rubble (Figure 4.4). Between the mounds, coral and shell fragments were more dispersed. Here, *A. richardi*, the polychaete, Serpulidae and the solitary cup coral, *Caryophyllia* sp. 2 were observed (Figure 4). *A. richardi*, the solitary cup coral, *C. smithii* and burrowing anemones of the Cerianthidae were observed on muddy sand with varying amounts of pebbles, shell and coral fragments in association with areas directly surrounding the mounds. Away from the mound province, substratum mostly comprised muddy sand where a variety of anemones, including cerianthids were observed. On the Dangaard interfluve patches of muddy sand with pebbles and shell fragments occurred in association with a bathymetric rise to the south-west and *A. richardi* were observed among this coarser material. In general, where coarser material was encountered it also provided a hard substratum for morphospecies of the Serpulidae and Hydrozoa to adhere to (Figure 4.4).

#### 4.4.3.1 Benthic assemblages

Following hierarchal clustering, mean silhouette widths identified an optimum of eight interpretable clusters that gave an average silhouette width per class of 0.28 (Figure 4.5). Silhouette widths for the classes varied between 0.00 and 0.37, indicating that the distinctness of clusters varied. The nMDS plot showed samples formed two aggregations with the remaining samples dispersed to the left (Figure 4.6). From review of the hierarchal clustering (Figure 4.5), nMDS (Figure 4.6) and SIMPER results (Table 4.2 and supplementary 4.2.1) it is likely that clusters 1, 2 and 3 represented three assemblages associated

with the mound provinces and clusters 4, 5 and 7 separated, representing less defined non-mound province assemblage(s). Clusters 6 and 8 were only represented by a single sample, limiting conclusions that can be drawn and so are omitted from further discussion (Table 4.2 and supplementary 4.2.1).

Cluster 1 represented an *A. richardi, C. smithii* and cerianthid assemblage observed on muddy sand with varying amounts of pebbles, shell and coral fragments in association with the area directly surrounding the mounds. Cluster 2 represented an *A. richardi*, ophiuroid, serpulid and *Munida* sp. assemblage observed on coral rubble in association with mounds. Cluster 3 represented an *A. richardi*, *Caryophyllia* sp. 2 and serpulid assemblage observed on muddy sand with varying amounts of pebbles, shell and coral fragments that occurs between mounds in the mound province. Clusters 4, 5 and 7 were less defined and comprised a mix of anemone species observed predominantly from muddy sand outside the mound province (Figures 4.4 and 4.7 and Table 4.2).

Results from the ANOSIM showed that fauna did not differentiate across the interfluves (R value 0.38, P 0.01) with two of the assemblages, represented by clusters 1 and 2, observed across both interfluves (Figure 4.7). Fauna showed a degree of differentiation between the mound and non-mound provinces (R value 0.47, P 0.01) but not necessarily between mounds and non-mounds (R value -0.077, P 0.98). Fauna also showed a degree of differentiation between substratum types that was greater for the more detailed substratum classification (R value 0.41, P 0.01) than that using the EUNIS classification (R value -0.025, P 0.75).

The RDA analysis demonstrated assemblage-environment relationships, indicating that faunal assemblage composition was driven by depth, substratum characteristics and structural complexity of the seafloor at various spatial scales (Adjusted $R^2$ 23%) (Figure 4.8 and Table 4.4). The first axis of the RDA plot represented a gradient from coral rubble (mound) to non-coral rubble substrata (non-mound) and increasing ruggedness $17_{nh}$. The percent cover of coral rubble acted as a proxy of fine-scale structural complexity, whereas the increase in ruggedness was a proxy of broader scale changes in structural complexity related to the bathymetry across the site (Supplementary 4.1.1). The second axis represented a gradient in homogeneity and eastness (Figure 4.8). Homogeneity captured fine-scale variability in substratum characteristics, and eastness captured the broader scale variation in the orientation of bathymetry across the site (Supplementary 4.1.1).

The vectors representing species scores separated into three main subgroups (Figure 4.8). The lower right quadrant was characterised by A. *richardi, Caryophyllia* sp. 2 and to a lesser extent *C. smithii* and the brittlestar OTU451 *Ophiothrix fragilis.* The lower left quadrant was characterised by the predominance of Ophiuroidea, *Munida* sp. and the polychaete OTU228 Serpulidae sp. 2 The upper right quadrant was represented by anemones, including an unidentified anemone and a variety of Actinaria morphospecies, OTU510 Actinaria sp. 17, OTU1255 Actinaria sp. 32 and OTU605 Actinaria sp. 20,

plus the molluscan morphospecies OTU1219 Bivalivia sp. 3 and OTU113 *Colus* sp. 2. Lastly, the upper left quadrant was characterised by a predominance of the polychaete OTU106 Serpulidae sp. 1.

The results from the RDA, corroborated those from the nMDS plot, whereby samples formed two main aggregations (Figure 4.6) that related to the lower left and right quadrants in the RDA plot (Figure 4.8). The remaining samples that dispersed, forming less well defined muddy sand assemblage(s) (Figure 4.6) related to by the upper quadrants of the RDA plot (Figure 4.8). The agreement in aggregation was primarily driven by the same morphospecies, except that the RDA highlighted OTU106 Serpulidae sp. 1 as contributing to sample differentiation (Figure 4.8 and Table 4.2).

Variance partitioning showed that 17 % of variance in species data explained by the environmental variables was spatially structured in relation to the sample co-ordinates (Figure 4.9). Pearson's correlation coefficients and VIF scores showed that sample co-ordinates were highly correlated with depth (Supplementary 4.2.3). Together these results suggested that observed spatial patterns in fauna are driven by the environmental variables which themselves are spatially organised in relation to depth and so exhibit a degree of induced spatial dependence.

The spatial structuring of the influential environmental variables expressed itself as spatial structure in the data, whereby samples exhibited a general spatial trend related to depth and greater similarity at distances < 14 m (Mantel correlation coefficient 0.02) that decreased with increasing distance, until samples exhibited greater dissimilarity than expected by chance at distances > 2.7 km (Mantel correlation coefficient - 0.09) (Supplementary 4.2.3). The similarity in samples was most likely driven by assemblages 1 – 3, which within each mound province were positioned on average 14 m apart. On the other hand, sample distances between the mound and non-mound provinces were larger and likely contributed to the broad-scale dissimilarity.

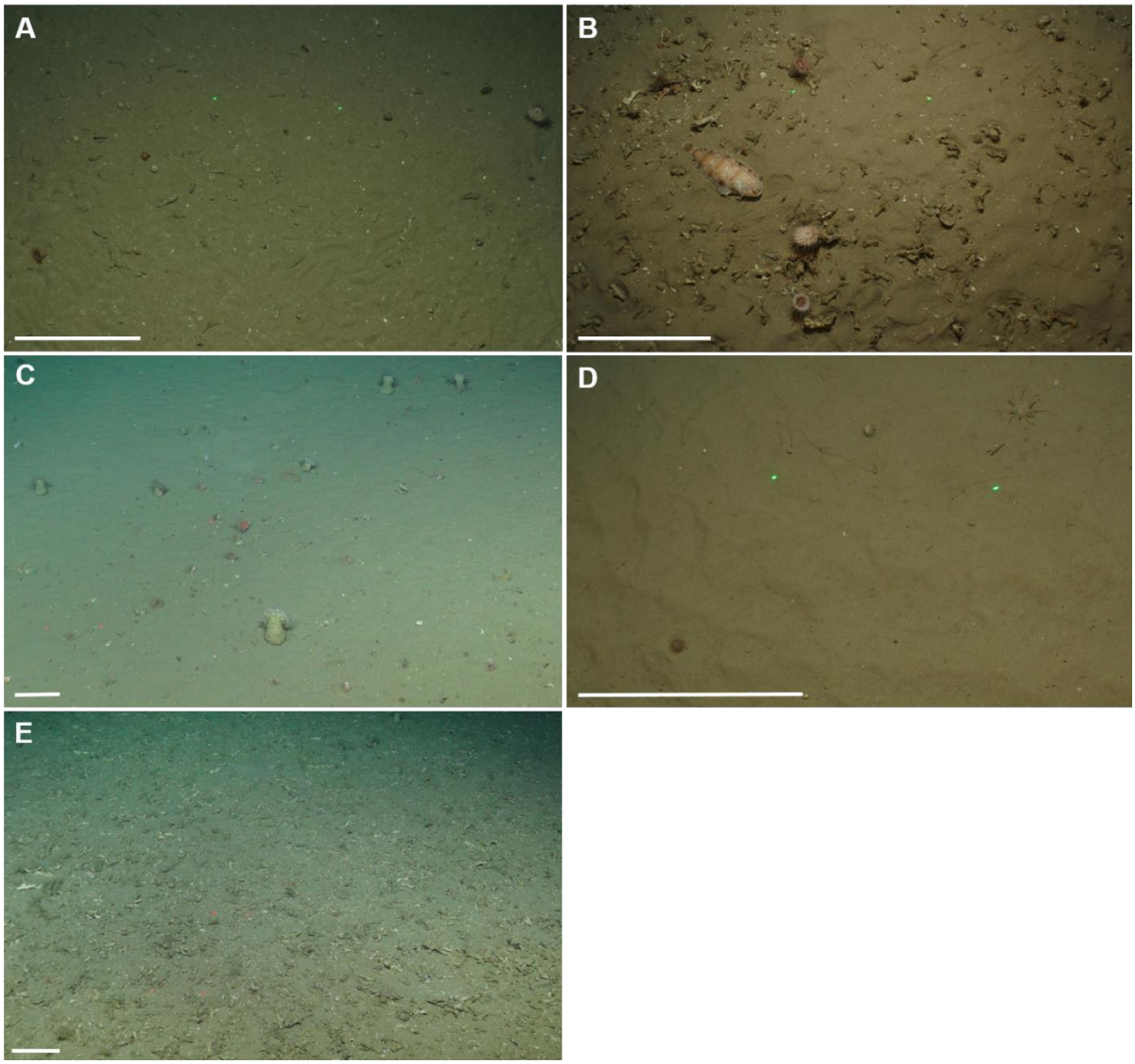


Figure 4.4 Example images of the fauna and substrataof (A) observed from the imagery data. (A) OTU510 Actiniaria sp.17, OTU499 *Actinauge richardi* and OTU500 *Caryophyllia smithii* observed from image CNYN_CEND0917_CNYN082_STN_231_A1_056 at 330 m water depth. (B) OTU200 *Munida* sp., Unidentified Actiniaria sp., OTU499 *Actinauge richardi*, OTU246 *Ophiactis balli* / Ophiuroidea, OTU228 Serpulidae sp. 2 and OTU447 *Microchirus variegatus* observed from image CNYN_CEND0917_ CNYN047_STN_192_A1_014, at a water depth of 300 m. (C) OTU6 *Caryophyllia* sp. 2, OTU499 *Actinauge richardi* and OTU228 Serpulidae sp. 2 observed from image JC166_STN340_607 at a water depth of 366 m. (D) OTU499 *Actinauge richardi*, OTU1219 Bivalvia sp. 3 and Unidentified Actiniaria sp. observed from image CNYN_CEND0917_CNYN110 _STN_227_A1_017 at a water depth of 440 m. (E) uncropped image of coral rubble observed from image JC166_STN340_376, at a water depth of 300 m Scale bars = 10 cm.

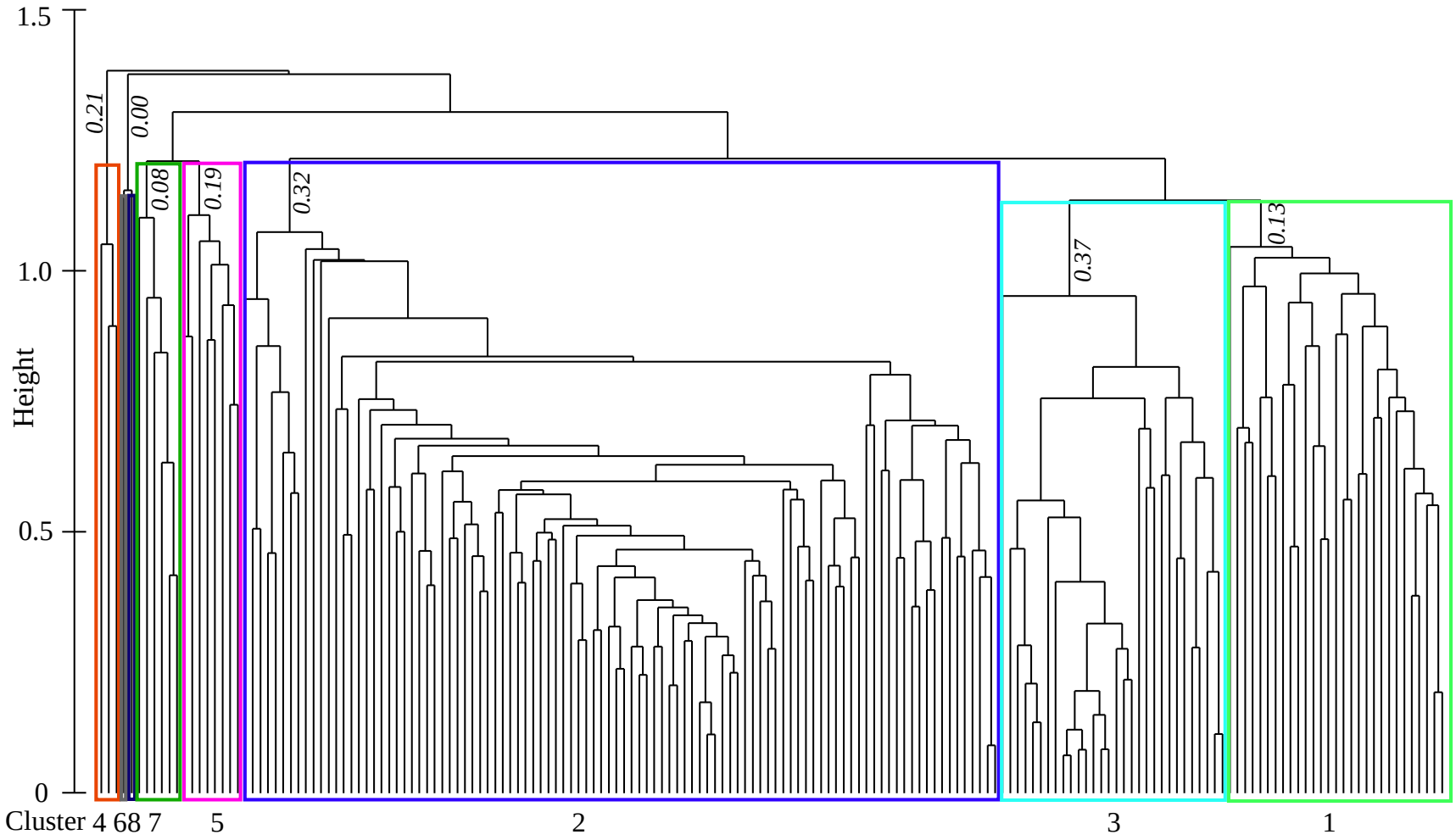


Figure 4.5 Dendogram showing results of multivariate hierarchal clustering of Hellinger transformed species dataSilhouette widths for each cluster are denoted in italics. Eight interpretable clusters were identified as producing the highest average Silhouette width (denoted by different colour overlays Cluster: 1 2 3 4 5 6 7 8).

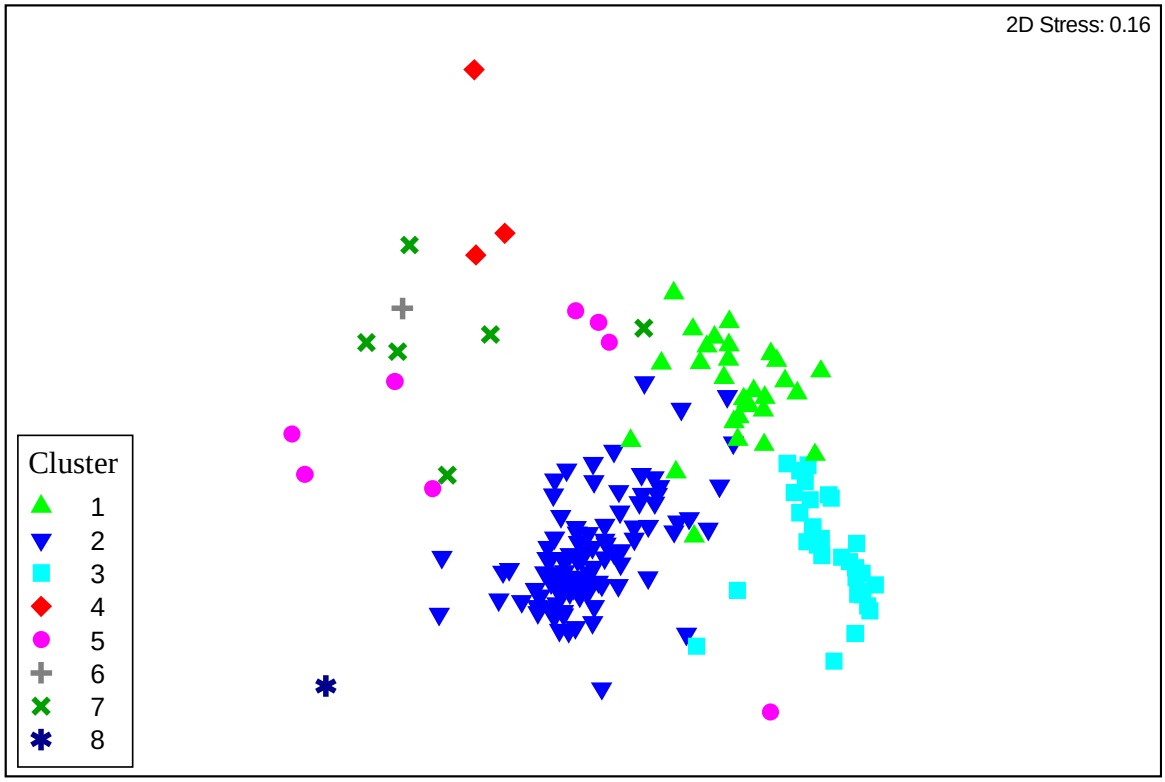


Figure 4.6 nMDS plot of multivariate Hellinger transformed species dataSamples are coloured to represent the eight clusters identified by hierarchical clustering analysis.

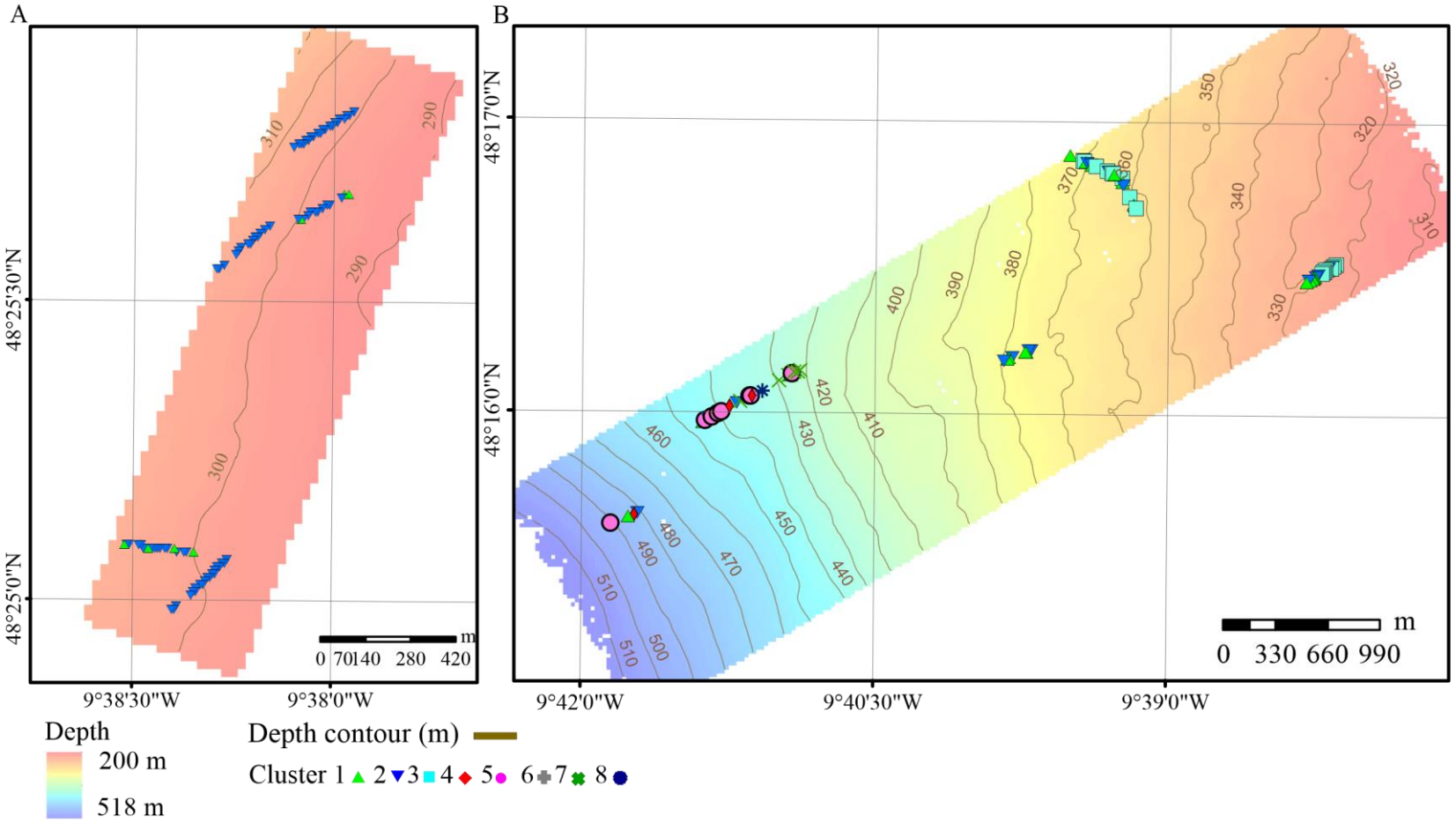


Figure 4.7 Spatial plot of clusters: Sample are coloured to represent the eight clusters identified by hierarchal clustering analysis.

Table 4.2 Clusters identified from multivariate hierarchical clustering analysis with associated environmental parameters, and SIMPER resultsidentifying the morphospecies that characterise the clusters (90% accumulative contribution cut off).

| Cluster | Characterising species | Water depth (m) | EUNIS Substratum | Substratum | Mound Province | Feature |
|---|---|---|---|---|---|---|
| 1 | OTU499 *Actinauge richardi*, OTU500 *Caryophyllia smithii*, OTU2 Cerianthidae sp. 1 | 296 - 484 | Mud and sandy mud, Coarse sediment | Muddy sand with varying amounts of pebbles, shell and coral fragments | Yes | In between mounds |
| 2 | OTU246 *Ophiactis balli*/ Ophiuroidea , OTU499 *Actinauge richardi*, OTU228 Serpulidae sp. 2, OTU200 *Munida* sp. | 296 - 481 | Mud and sandy mud, Sandy and muddy sand, Coarse sediment, Mixed sediment | Coral rubble, muddy sand with varying amounts of pebbles, shell and coral fragments | Yes | On and in between mounds |
| 3 | OTU6 *Caryophyllia* sp. 2, OTU499 *Actinauge Richardi*, OTU228 Serpulidae sp. 2 | 321 - 371 | Mud and sandy mud | Muddy sand with varying amounts of pebbles or coral fragments | Yes | In between mounds |
| 4 | OTU605 Actiniaria sp. 20 | 435 - 482 | Mud and sandy mud | Muddy sand with varying amounts of shell fragments | No | Flat |
| 5 | Unidentified Actiniaria sp., OTU1219 Bivalvia sp. 3, OTU499 *Actinauge richardi* | 424 - 490 | Mud and sandy mud, Mixed sediment | Muddy sand with varying amounts of pebbles and shell fragments | No | Bathymetric rise |
| 6 | Less than 2 samples in group | 440 | Mud and sandy mud | Muddy sand with shell fragments | No | Bathymetric rise |
| 7 | OTU1255 Actiniaria sp. 32, OTU510 Actiniaria sp. 17, Unidentified Actiniaria sp. | 421 - 435 | Mud and sandy mud, Mixed sediment | Muddy sand with varying amounts of pebbles and shell fragments | No | Flat |
| 8 | Less than 2 samples in group | 433 | Mud and sandy mud | Muddy sand | No | Flat |

Table 4.3 Analysis of Similarity results. Analysis of similarity was calculated between six categories based on Hellinger distance matrices. Each pairwise comparison of two groups was performed using 999 permutations. * 11 out of 42 pairwise comparisons < 999. Global R values > 0.75 are generally interpreted as clearly separated, R >0.5 as separated, R <0.25 as groups that are hardly separated and negative values suggest that dissimilarities are greater within than between groups (Chapman and underwood 1999).

| Factor | Number of levels in factor | Global R | p value |
|---|---|---|---|
| Interfluve | 2 | 0.38 | 0.01 |
| Province/Non-province | 2 | 0.47 | 0.01 |
| Mound/Non-mound | 2 | -0.08 | 0.98 |
| Substrata * | 10 | 0.41 | 0.01 |
| EUNIS Substrata | 4 | -0.03 | 0.75 |

Table 4.4 Results from Canonical Redundancy Analysis (RDA) of Hellinger transformed species data and selected environmental variables. Significance of individual terms by analysis of variance (ANOVA) on RDA including spatial structure. ***$p \leq 0.001$, **$p \leq 0.01$, *$p \leq 0.05$. ♦ amended significance taking into account spatial structure.

| Model | Environmental Variables - Significance of individual terms by ANOVA | Adjusted $R^2$ | Significance of RDA Plot by ANOVA | |
|---|---|---|---|---|
| | | | F-value | p - value |
| RDA | Depth***, Ruggedness (3)***, Ruggedness (17)**, Homogeneity**, Northness***, Eastness***, Coral rubble **, Correlation ***, Slope** | 23 | 6.70, df= 9,160 (♦ 7.24, df=11,158) | 0.001 |

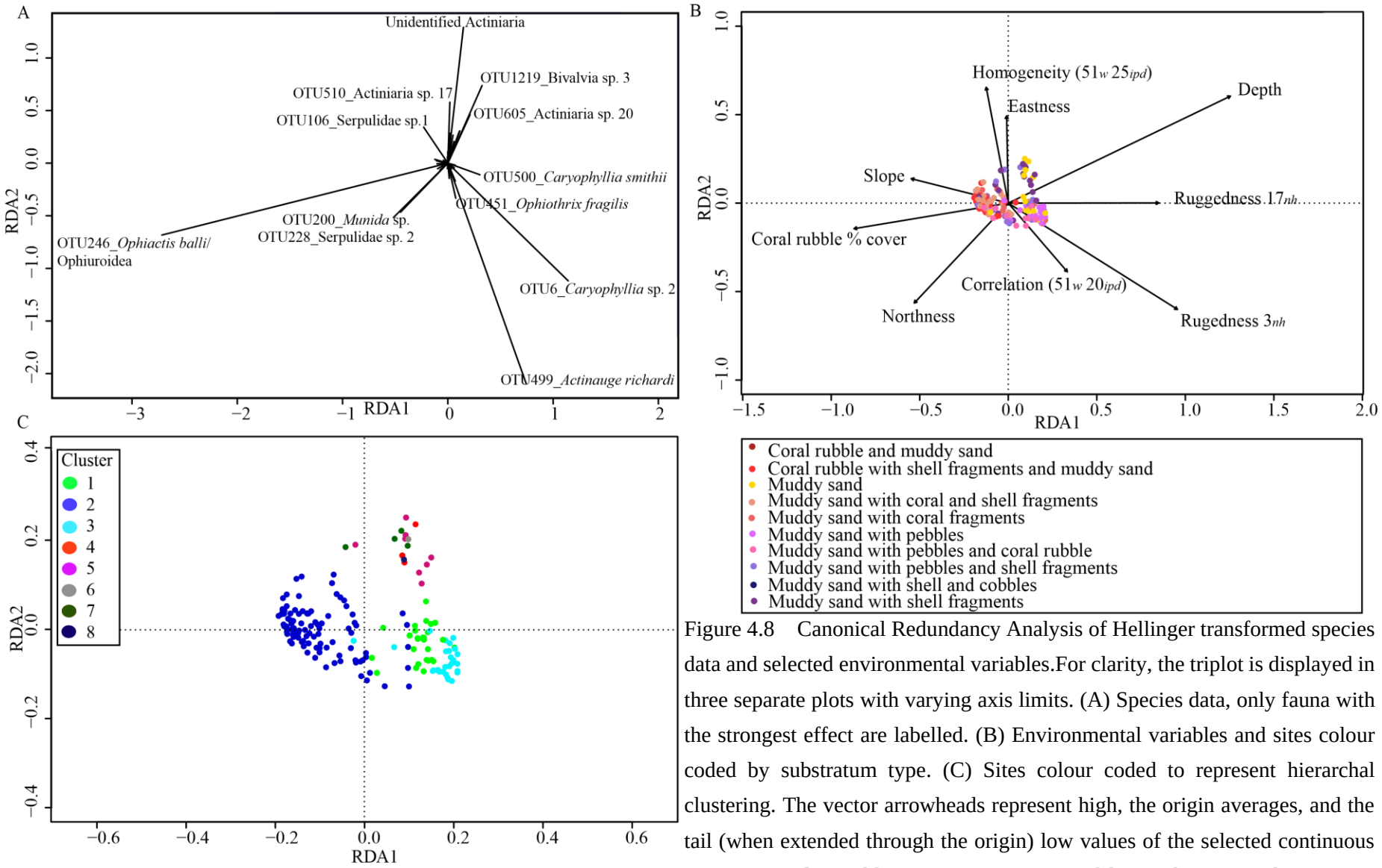


Figure 4.8 Canonical Redundancy Analysis of Hellinger transformed species data and selected environmental variables.For clarity, the triplot is displayed in three separate plots with varying axis limits. (A) Species data, only fauna with the strongest effect are labelled. (B) Environmental variables and sites colour coded by substratum type. (C) Sites colour coded to represent hierarchal clustering. The vector arrowheads represent high, the origin averages, and the tail (when extended through the origin) low values of the selected continuous environmental variables. Sites are represented by circles. Sites close to one another tend to have similar faunal structure than those further apart.).

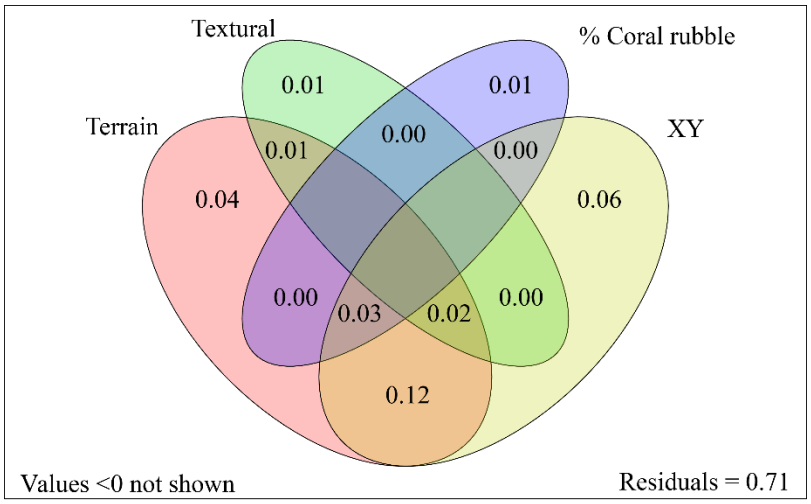


Figure 4.9 Variation partitioning plotplot for the Hellinger transformed species data, the selected environmental variables (Terrain = depth, northness, eastness, slope, ruggedness derived at neighbourhoods of three and 17, textural = homogeneity (51w 25ipd) and correlation (51w 20ipd), percent coral rubble and spatial variables (sample co-ordinates).

#### 4.4.3.2 Predictive distribution modelling of assemblages

Predictive distribution maps of the assemblages were built using RF. The predicted distributions represented the three mound province assemblages that corresponded to clusters 1-3 of the hierarchal clustering and a fourth assemblage that represented the combination of the less defined non-mound province samples belonging to clusters 4-8 of the hierarchal clustering. Predictive models based upon the variables depth, northness, eastness, homogeneity ($51_w$ $25_{ipd}$), correlation ($51_w$ $20_{ipd}$), slope and ruggedness at neighbourhoods of three and 17 were generated across the full extent of the available environmental rasters for the two interfluves (Figure 4.10). RF outputs showed that while terrain variables explained higher variance in assemblages, the textural indices were important for node purity (Supplementary 4.2.3).

Model accuracy estimated by the out of bag error rate using the training data, indicated that the model adequately discriminated the assemblages (30.36 %). However, the confusion matrix of the predicted and observed classification using the test data showed variable accuracy in assemblage predictions. Confusion matrices showed that most of the error was in the misclassification of assemblage 1 (misclassification error rate 0.91), which was inaccurately predicted where assemblage 2 or 3 occurred. Prediction accuracy of assemblage 2 and 4 was higher (misclassification error rate 0.06 and 0.00, respectively). Review of the predicted distributions (Figure 4.10) against spatial plots of clusters (Figure

4.7) showed that the predictive inaccuracy of assemblage 1 resulted in the overestimation of its extent. For example, assemblage 1 was predicted to occur to the north-east of the area surveyed on the Explorer interfluve (Figure 4.10), when in reality assemblage 2 (synonymous with cluster 2) was observed in the ground-truth data (Figure 4.7).

Assemblage 1 and 2 were predicted across both interfluves generally in areas with northern aspects (Figure 4.10 and supplementary 4.1.1). Assemblage 3 was predicted in areas of moderate ruggedness between areas straddling low and high homogeneity, observed in association with the bathymetric rise toward the south-west of the Dangaard survey area and between or surrounding mounds within the mound provinces (Figure 4.10 and supplementary 4.1.3). Assemblage 4 was predicted toward the south-west of the Dangaard survey area, coincident with homogeneous areas of low ruggedness and southern aspects in water depths > 390 m (Figure 4.10 and supplementary 4.1.1 and 4.1.3).

#### 4.4.3.3 Species Richness and Density

Highest species richness and density was observed from samples belonging to assemblage 2 that was observed from coral rubble substratum (Figure 4.11). GAMs analysis of the species richness data identified depth, slope, ruggedness $9_{nh}$ and coral rubble as important variables explaining 41% variation in species richness across the samples (< 0.001 (11.08 df =157,169)) (Table 5). GAMs also identified coral rubble, depth, ruggedness $17_{nh}$, slope and in addition correlation $11_{ws}$ $5_{ipd}$ as important variables explaining 28 % variation in density across samples (<0.001 (16.8 df = 150,167)) (Table 4.5). Both species richness and density exhibited an overall positive relationship with slope and an overall negative relationship with depth, although density showed a peak at 450 m water depth (Figures 4.12 and 4.13). Species richness exhibited a positive relationship with coral rubble (Figure 4.12), whereas density showed a positive relationship which peaked at ~ 22 % beyond which it became negative (Figure 4.13). Species richness showed a variable but overall negative relationship with ruggedness $9_{nb}$ (Figure 4.12), whereas density exhibited weak relationships with both ruggedness $17_{nh}$ and correlation $11_{w}$ $5_{ipd}$ (Figure 4.13). No obvious threshold for species richness or density was observed in the modelled environmental variables (Figures 4.12 and 4.13).

The relationships identified from the GAMs corroborate the analysis of faunal assemblages, where increased species richness and density was recorded from samples belonging to assemblage 2 (Figure 4.11), which the RDA analysis showed to exhibit a negative relationship with depth and positive relationship with percent cover of coral rubble and slope (Figure 4.8).

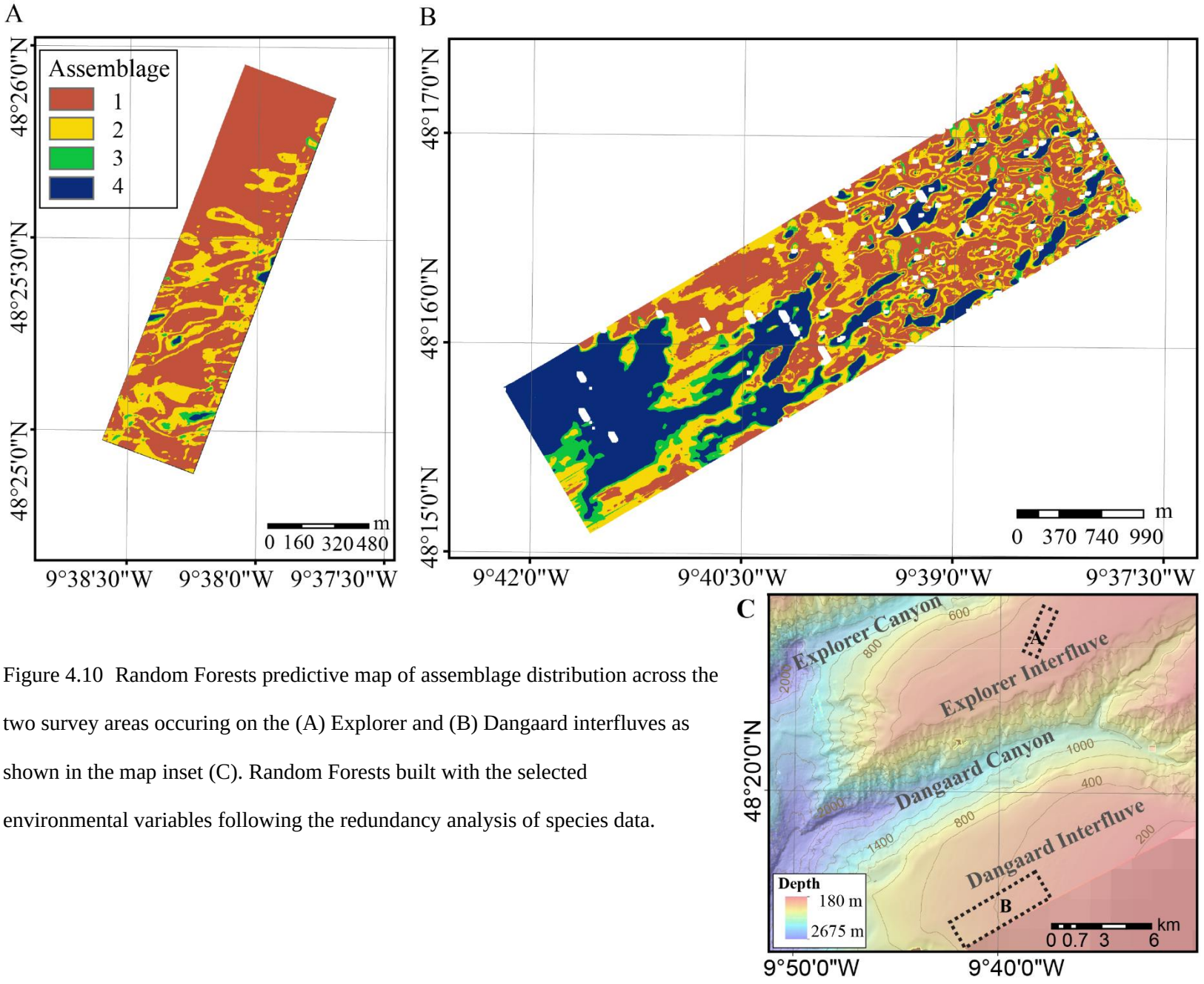


Figure 4.10 Random Forests predictive map of assemblage distribution across the two survey areas occuring on the (A) Explorer and (B) Dangaard interfluves as shown in the map inset (C). Random Forests built with the selected environmental variables following the redundancy analysis of species data.

Table 4.5 Results from Generalised Additive Models for species richness and density and the selected environmental variables. Significance of individual terms tested by analysis of variance (ANOVA) ***p ≤ 0.001, **p ≤ 0.01, *p ≤ 0.05, • p ≤ 0.10.

| Model | Environmental Variables - Approximate significance of individual terms by ANOVA | Variance explained (Adjusted $R^2$) | ANOVA of model p-value |
|---|---|---|---|
| Species richness | Intercept***, Ruggedness (9) ***, Slope ***, Coral rubble ***, Depth *** | 41% | <0.001 (11.08, df 157.169) |
| Density | Depth ***, Coral rubble **, Ruggedness (17)•, Correlation ($11_w$_$5_{ip}$)*, Slope ** | 28% | <0.001 (16.8, df = 150,167) |

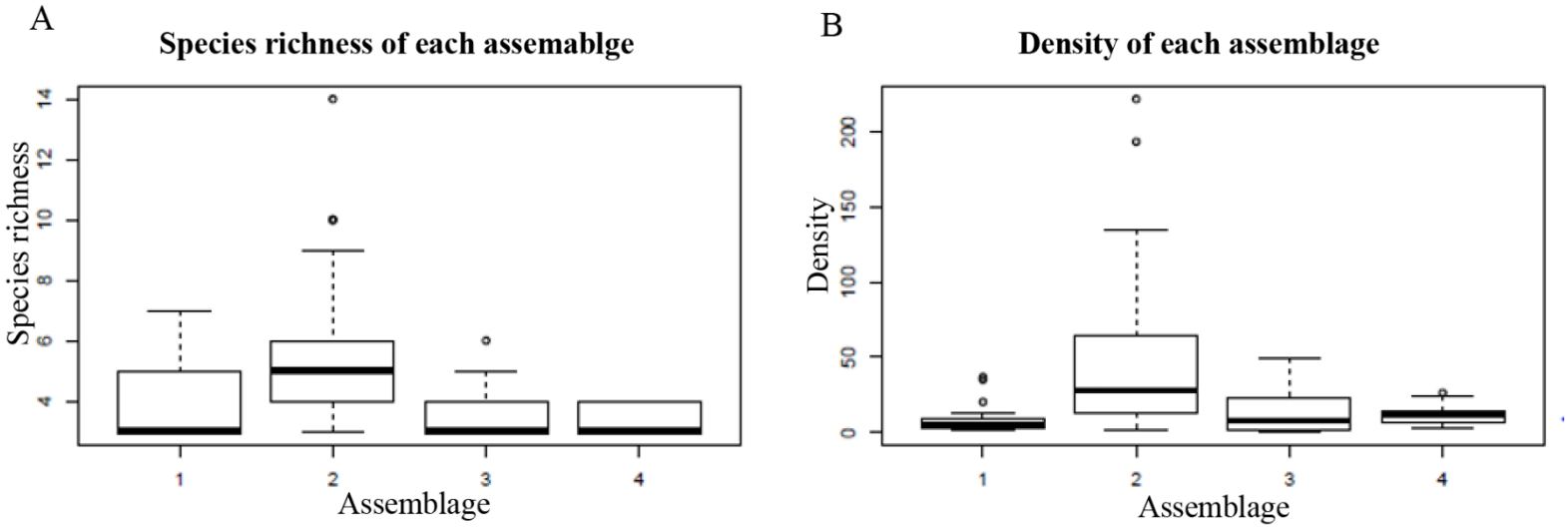


Figure 4.11 Boxplots showing (A) species richness and (B) densityrecorded from samples belonging to the four assemblages.

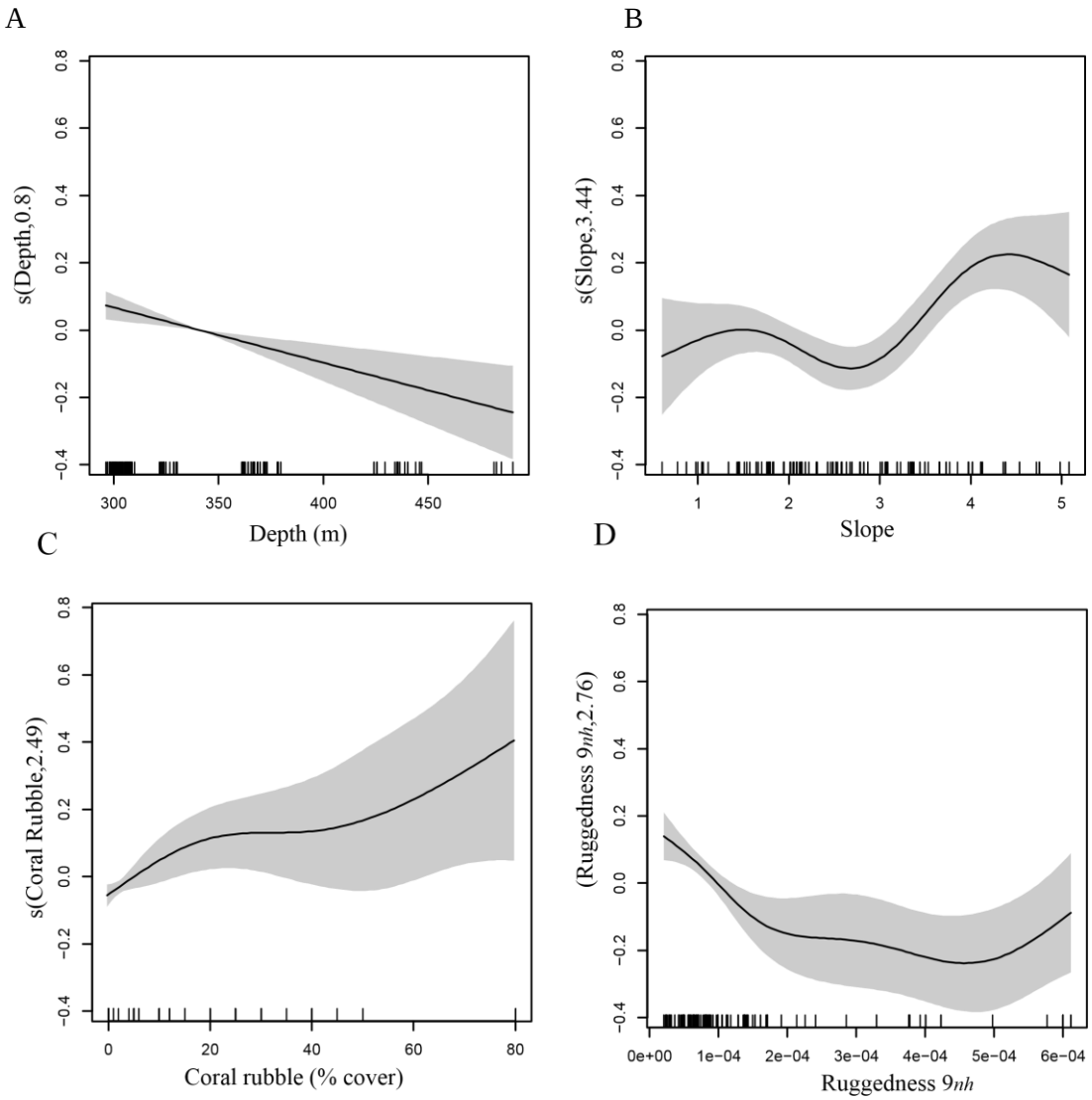


Figure 4.12 General Additive Models smoother outputs showing the relationship between species richness and the selected environmental variables. Centred smooth component and estimated degrees of freedom, black line. Grey shade represents standard error estimates for the smoothers. A) Depth (m), B) Slope º, C) Coral rubble as percent cover and D) Ruggedness $9_{nh}$.

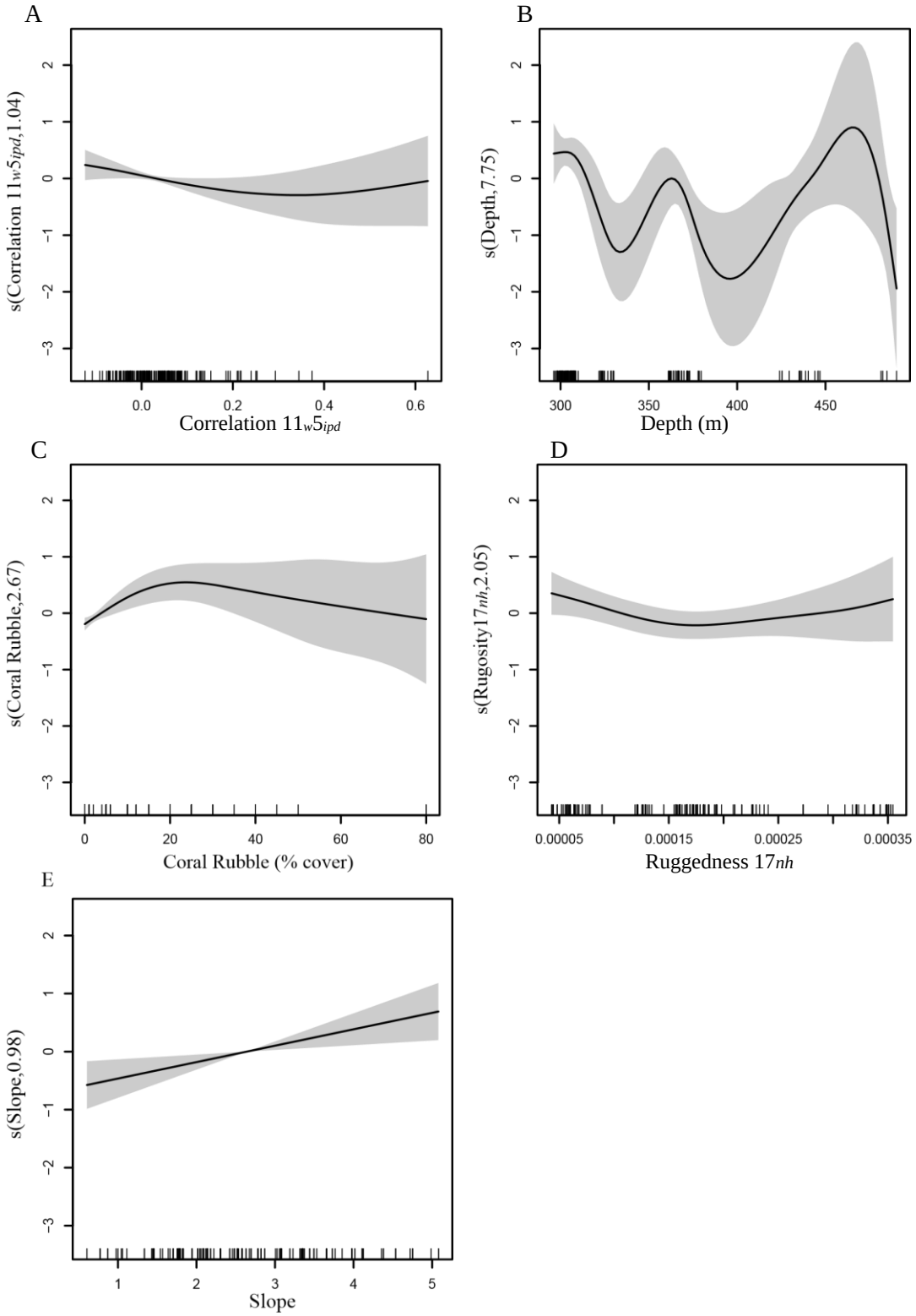


Figure 4.13 General Additive Models smoother outputs showing the relationship between density and the selected environmental variables. Centred smooth component and estimated degrees of freedom, black line. Grey shade represents standard error estimates for the smoothers. A) Correlation $11_{ws}$ $5_{ipd}$, B) Depth (m), C) Coral rubble as percent cover and D) Ruggedness $17_{nh}$, E) Slope º.

## 4.5 Discussion

Understanding how structural complexity influences spatial patterns in deep-sea species richness, density and assemblage is fundamental for understanding processes that drive faunal patterns in areas subject to seafloor modification by trawling.

### 4.5.1 The influence of seafloor heterogeneity and complexity

Our results show that depth and seafloor characteristics (topography and substratum) derived at spatial scales of 25 to 825 m, explain variation in observed species richness, density and assemblage. These variables relate to structural complexity, seafloor orientation and distribution of substratum.

Our results show that species richness, density and assemblage are influenced by variations in substratum characteristics linked to structural complexity at different scales. Faunal assemblage are influenced by substratum characteristics (Figure 4.8 and Tables 4.2 and 4.3), which exhibit a degree of spatial correlation with structurally complex geomorphological features (i.e. mounds and bathymetric ridge) that occur at specific depths on canyon interfluves (Figure 4.1). Species richness and density are likely influenced by heterogeneity in environmental conditions (notably variations in substratum characteristics), which are positively correlated with increased structural complexity, particularly at finer scales (i.e. coral rubble) rather than broader scales (i.e. Ruggedness $17_{nb}$)

In our study, depth was identified as an important factor explaining variation in species richness, density and assemblage (Tables 4.4 and 4.5). Depth is commonly identified as a prominent explanatory variable of deep-sea faunal patterns (Rex, 1976; 2006; 2010; Levin et al., 2001; Howell et al., 2002; Carney, 2005; Braga-Henriques et al., 2013; Kenchington et al., 2014; Robert et al., 2015), where in addition to substratum characteristics, it acts as a broad-scale proxy for water mass characteristics, food availability and hydrodynamics (Clark et al., 2010; McClain et al., 2010; 2015; Du Preez et al., 2016; Ramos et al., 2016; Pearman et al., 2020). On the interfluves, broad-scale gradients in water mass characteristics, food availability and hydrodynamics are not expected to vary (Aslam et al., 2018; Pearman et al., 2020). In our study, coral rubble and increased fine-scale patchiness (reduced homogeneity) of substratum characteristics was observed in association with the mound provinces that occur in water depths <380 m (Figure 4.1 and supplementary 4.1.3). Therefore, on the interfluves studied here, depth most likely acts as a broad-scale proxy of substratum characteristics, as well as the factors mentioned above.

Faunal patterns have been correlated with substratum characteristics in numerous benthic studies (Baker et al., 2012; Hallenbeck et al., 2012; Braga-Henriques et al., 2013; Currie and Sorokin, 2013; Robert et al., 2014; 2015; Durden et al., 2015; Sigler et al., 2015; Carvalho et al., 2017; Pearman et al., 2020). In canyon settings, substratum was the dominant factor driving assemblages at The Gully (eastern Canada

margin) (Mortensen and Buhl-Mortensen, 2005; Baker et al., 2012) and canyons in the Bay of Biscay (van den Beld et al., 2017), and sponge diversity was positively correlated with variation in substratum in five canyons off the south-eastern Australian margin (Schlacher et al., 2007).

Our results suggest that spatial patterns in faunal assemblage reflect the spatial arrangement of substratum characteristics in relation to the structural complexity of geomorphological features, which occur at specific water depths. Characteristic fauna of each assemblage show positive correlations with different seafloor characteristics (Figure 4.8). Ophiuroids, serpulids and *Munida* sp. are characteristic of assemblage 2, and are positively correlated with coral rubble, northness and slope (Figure 4.8). Review of SSS backscatter and MBES bathymetry shows that mound features occur at certain depths (< 380 m) (Figure 4.1 and supplementary 4.1.1) and aggregate above underlying bathymetry with high slope values (supplementary 4.1.1). The relationship with northness is less obvious and may reflect the general trend of increased variability in the orientation of the seafloor within the mound provinces, compared to outside the provinces, which is predominately southern (supplementary 4.1.1). On the other hand, *A. richardi*, *Caryophyllia* sp. 2 and *C. smithii*, which characterise assemblages 1 and 3, are positively correlated with ruggedness $3_{nh}$ and less homogeneous substrata with higher correlation indices (Figure 4.8). Review of the acoustic data shows that such conditions are concurrent with areas between the mounds and on the bathymetric ridge observed on the Dangaard interfluve (supplementary 4.2.1 and 4.2.2). Lastly, substrata characterised as being more homogeneous and occurring in deeper water, with eastern aspects are correlated with the remaining morphospecies (Figure 4. 8), which are associated with assemblage 4, and review of acoustic data shows that these conditions are coincident with the deeper muddy sand toward the south-west of the Dangaard interfluve (Figure 4.1 and supplementary 4.1.1 and 4.1.2). Similar patterns, where faunal distributions have been related to the spatial structuring of substratum characteristics in relation to geomorphological features have been observed at similar scales for iceberg plough marks (Robert et al., 2014) and sand ripples (Hallenbeck et al., 2012). Studies in canyons have also correlated faunal distributions with both substratum and/or topography (Robert et al., 2015; Pearman et al., 2020). However, these studies focussed on canyon branches, that differ from interfluves in that they occur in deeper water depths and often experience sharper environmental gradients and enhanced hydrodynamics (Stewart et al., 2014; Aslam et al., 2018; Pearman et al., 2020), which can affect the ability to isolate the direct influence of structural complexity.

In our study, species richness was positively correlated with the presence of the mounds. GAMs analysis for species richness identified a negative relationship with depth, an overall positive relationship with coral rubble and slope, and a variable but overall negative relationship with ruggedness $9_{nh}$ (Figure 4.12). The relationships identified from the GAMs corroborates the analysis of assemblages, where increased species richness and density was associated with assemblage 2 (Figure 4.11), which like species richness exhibited a negative relationship with depth and ruggedness $9_{nh}$, and positive relationship with slope and coral rubble (Figure 4.8). As such, increased species richness appears to be

associated with the mounds, which are aggregated at shallower depths, above underlying seabed with steep slopes (Supplementary 4.2.4). The overall negative relationship between species richness and ruggedness $9_{nh}$ may reflect the scale at which ruggedness was derived. Ruggedness derived at larger neighbourhoods than slope, captured broader scale variation in bathymetry, which did not relate to the distribution of mounds and coral rubble (Supplementary 4.2.4). High ruggedness calculated at neighbourhoods > 9 pixels highlighted areas coincident with broad-scale distributions of substratum characteristics (i.e. availability of pebbles) (Figure 4.1 and supplementary 4.2.4). Consequently, these results suggests that faunal patterns in species richness on the interfluves are influenced by the increased structural complexity provided by the presence of the mound provinces in conjunction with broader scale variability of the underlying bathymetry across the site.

Positive correlations between structural complexity and diversity have been documented in benthic studies across various scales (Levin et al., 2010; De Leo et al., 2014; Robert et al., 2017). At broad-scales environmental heterogeneity resulting from the structural complexity provided by topographic features has been linked to variations in faunal diversity and biomass on seamounts (McClain, 2007), abyssal hills (Durden et al., 2015) and in canyons (De Leo et al., 2010; McClain and Barry, 2010; Pearman et al., 2020). In canyons, broad-scale structural complexity generates environmental heterogeneity in substratum characteristics (Huvenne et al., 2011; Huvenne and Davies, 2014; Stewart et al., 2014), hydrodynamics (Hall et al., 2014; Hall et al., 2017) and food availability (Campanyà-Llovet et al., 2018) which have been linked to spatial patterns in fauna (Robert et al., 2015; Campanyà-Llovet et al., 2018; Pearman et al., 2020). In our study, the broad-scale distribution of substratum appeared correlated with the underlying bathymetry (Figure 4.1 and supplementary 4.1.1). On the other hand, increased fine-scale patchiness of substratum characteristics, which generate variations in backscatter image texture (i.e. contrast, entropy,) was associated with the increased structural complexity provided by the mini-mound provinces (Figure 4.3 and supplementary 4.1.3), which likely promotes increased species richness by enabling fauna with different substratum preferences to co-occur (Schlacher et al., 2007).

In our study, coral rubble was positively correlated with increased species richness and density (up to a point) (Figure 4.12 and 4.13) and highest species richness and density was observed from assemblage 2 (Figure 4.11), which was positively correlated with percent cover of coral rubble (Figure 4.8). The fine-scale structural complexity provided by coral framework or, rubble has been linked to high diversity observed from coral habitats (Frederiksen et al., 1992; Roberts et al., 2008; Buhl-Mortensen et al., 2010; Price et al., 2019). Coral rubble provides fine-scale structural complexity by the accumulation of hollow coral fragments that lay on top of one another to generate topographic irregularity in the seafloor surface (evident in image stills, Figure 4.3). The increased structural complexity promotes increased epi-benthic species richness and density because the accumulation of coral fragments provides increased surface area of hard substratum for colonisation (Buhl-Mortensen

et al., 2010) and increased elevation from the seafloor (Figure 4.3), which can enable fauna to better exploit currents to increase food encounter rates (Mohn et al., 2014; Fabri et al., 2017; Lo Iacono et al., 2018). Additionally, the interstitial spaces within and between coral fragments provide refuge from predation (Buhl-Mortensen et al., 2010; Price et al., 2019). In contrast to our work, previous studies exploring the influence of the fine-scale structural complexity provided by coral rubble have been conducted where coral rubble occurs in proximity to live reef (Buhl-Mortensen et al., 2010; Robert et al., 2017). Such locations are likely to experience enhanced hydrodynamics facilitating the growth of cold-water corals and associated filter and suspension feeding assemblages (Davies, 2009; Roberts et al., 2009a; Duineveld et al., 2007; 2012; Moreno Navas et al., 2014) promoting increased diversity (Kazanidis et al., 2015). In contrast the coral rubble setting of our study is quite different, to date no live coral reef or intact framework has been observed (Howell et al., 2010; Davies et al., 2014; Stewart et al., 2014) and there is no evidence of enhanced hydrodynamics across the study area (Aslam et al., 2018; Pearman et al., 2020). Thus our work provides unique insights into how fine-scale structural complexity provided by coral rubble influences faunal patterns on interfluves, independent of the presence of live coral cover, and confirms that coral rubble could be acting as a 'key stone structure' (Tews et al., 2004) to promote increased species richness and density on the interfluves.

### 4.5.2 Predictive distribution modelling of assemblages

Consistent with the RDA results, faunal assemblages were predicted in localities reflecting variability in structural complexity and associated patchiness in distribution of substratum characteristics (Figures 4.8 and 4.9). However, in our study, the inability of acoustic derivatives to differentiate the fine-scale substratum characteristics (i.e. presence of coral fragments), which image data could detect may have led to predictive inaccuracies. The association between coral rubble and mounds, and between mounds and the underlying geomorphology (i.e. depth, slope and northness) enabled terrain derivatives to act as proxies of mound occurrence and finer scale structural complexity. However, where the mounds on the Explorer interfluve were less discrete and the correlation between mound distribution and the underlying bathymetry was weaker, the effectiveness of terrain derivatives to act as a proxy of fine-scale structural complexity or indicate the presence of coral rubble was reduced, resulting in predictive inaccuracies in the form an overestimation of assemblage 1 on the Explorer interfluve (Figures 4.7 and 4.10). The predictive inaccuracy highlights the potential importance of fine-scale structural complexity in influencing faunal assemblage distribution on the interfluves and that predictive models based solely on broader resolution ship-based acoustic data may miss or inadequately represent this information.

Overall, our results indicate that faunal assemblages are influenced by substratum characteristics that are spatially arranged in respect to geomorphological features (i.e. mounds and bathymetric ridge) and the underlying bathymetry upon which they occur. Terrain derivatives capture variation in broad-scale structural complexity that reflects changes in the bathymetry across the site and potentially a gradation

in availability of coarser substrata. The increased structural complexity provided by the mini-mound provinces increases the fine-scale patchiness of substratum characteristics and the fine-scale structural complexity provided by coral rubble increases fine-scale environmental heterogeneity as well as influencing biological interactions by providing shelter for associated species, both resulting in increased species richness.

### 4.5.3 Ecological importance of mini-mounds

We have described three faunal assemblages from the mound provinces, and due to limited sampling have been unable to adequately describe those from outside (Figure 4.4 and Table 4.2). The *A. richardi*, ophiuroid and *Munida* sp. assemblage associated with coral rubble is consistent with the 'Ophiuroids and *Munida sarsi* associated with coral rubble' assemblage previously described from coral rubble on the interfluves (Davies et al., 2014; Stewart et al., 2014). However, in contrast to previous studies our results show that *A. richardi* was also a characteristic species and abundant across the mound provinces (Table 4.2 and supplementary 4.2.2). High abundances of *A. richardi* have been recorded from trawl surveys over coarse substratum of the canyons and the surrounding Celtic margin (Ellis et al., 2007). Additionally, in contrast to previous studies we did not observe the crinoid, *Leptometra celtica* that was a characteristic taxon observed on mixed substratum of the Dangaard interfluve (Stewart et al., 2014). Instead, we observed two other assemblages occurring between the mounds characterised by either the cup coral *Caryophyllia* sp. 2 or *C. smithii* (Figures 4.4 and 4.7 and Table 4.2). Elsewhere in the canyons an assemblage characterised by *Munida* sp. and caryophyllids on mixed substrata (including biogenic gravel) has been observed (Howell et al., 2010), as has another assemblage characterised by *Carophyllia* sp. 2, encrusting Porifera and Hydrozoa (Davies et al., 2014). Although not observed from the interfluves it is possible that these assemblages correspond to or represent, variations of the Caryophyllid assemblages observed in our study.

The differences in assemblages observed from interfluves between studies could reflect the differences in survey location and spatial extent that resulted in different environments being sampled. For example the *L. celtica* assemblage was observed from a mixed substratum (shell hash), that was not observed during our study. In contrast to our transect locations, previous transects where the *L. celtica* assemblage was observed were undertaken toward the north-east of the mound province of the Dangaard interfluve where substrata have been interpreted to be coarser (Stewart et al., 2014). The differences in assemblages observed across the mound provinces and surrounding interfluves highlights the spatial heterogeneity of assemblages associated with the mounds and illustrates the importance of the mound provinces for regional diversity by increasing habitat heterogeneity on the interfluves, which is positively correlated with increased diversity in associated species (Frederiksen et al., 1992; Henry and Roberts, 2007; Lessard-Pilon et al., 2010).

Observed fauna and assemblages in our study are also known from the wider North-East Atlantic, incorporating the Celtic margin, Rockall Bank and Wyville-Thomson Ridge (Howell et al., 2010; Davies et al., 2014). Solitary scleractinian fields on a range of Atlantic upper bathyal sediments and *Caryophyllia smithii* and *Actinauge richardi* assemblage on Atlantic upper bathyal coarse sediment, are described biotopes from Rockall Bank (Parry et al., 2015) that correspond to the assemblage in our study that was characterised by OTU499 *C. smithii, A. richardi* and OTU2 *Cerianthidae* sp. 1. An Ophiuroid and squat lobster (*Munida* sp.) assemblage has been observed from coral rubble substrata across the North-East Atlantic (Howell et al., 2010) and corresponds to the Squat lobster assemblage on Atlantic upper bathyal coarse sediment (*Lophelia* rubble) biotope (Parry et al., 2015). However, these assemblage descriptions are associated with 'the *Lophelia* rubble zone' or, 'coral rubble apron' that comprise the eroded fragments of coral framework that accumulate to surround living reefs (Mortensen et al., 1995), which differs from the environmental setting of coral rubble among the mini-mounds where no life reef is present. Consequently, Howell et al. (2010) has proposed that coral rubble assemblages that are separate from life reef systems represent a variant of the *Lophelia* rubble assemblages formerly described. Our results further support the differentiation between the coral rubble assemblages of the mini-mounds from coral rubble aprons of living reefs, based upon the presence of *A. richardi* which is absent from other descriptions (Mortensen et al., 1995; Howell et al., 2010; Parry et al., 2015). If the coral rubble associated assemblage observed in our study were to be considered a variant then its distribution would be more restricted, possibly to canyon interfluves, which would need to be considered in environmental management.

### 4.5.4 Fishing

The canyon interfluves have been historically fished for decades and in our study trawl marks were evident across the mini-mound provinces (Figure 4.3). Daly et al. (2018) reported that the 'Whittard Canyon area likely experiences the same effects from seafloor ploughing as those found at La Fonera Canyon in the North-West Mediterranean by Puig et al. (2012) albeit at a slower rate and wider geographical area'. Such studies of trawling impact have emphasised the reduction in seafloor complexity caused by contact fishing gear (Bahn_McGill, 2012; Puig et al., 2012; Martín et al., 2014a; 2014b; Daly et al., 2018).

The reduced expression of the mounds on the Explorer interfluve have been attributed to higher fishing intensity compared to that experienced by the Dangaard interfluve (Stewart et al., 2014). This could also account for the mounds being less discrete on the Explorer interfluve. However, despite differences in the expression of the mounds between the interfluves, mound assemblages in our study did not differ. We propose that this is because of the of importance fine-scale structural complexity, provided by the coral rubble, in influencing faunal assemblages within the mound provinces, even when broader scale structural complexity is reduced.

## 4.6 Conclusion

Our results have shown that faunal assemblages are influenced by substratum characteristics that are spatially arranged in relation to structurally complex geomorphological features (i.e. mounds and bathymetric ridge). Increased species richness and density are associated with increased patchiness in substratum characteristics in relation to increased structural complexity provided by the mini- mound provinces and fine-scale environmental heterogeneity and shelter provided by coral rubble. The fine-scale structural complexity provided by coral rubble is an important factor influencing faunal patterns even when the broader scale structural complexity of the mounds is reduced. Further, excluding or inadequately capturing variation in structural complexity of mounds or coral rubble may lead to predictive inaccuracies of assemblage distribution. Consequently, coral rubble may be acting as a key stone structure on interfluves that supports a coral rubble assemblage distinct from that previously described from the coral rubble zone adjacent to living coral reefs.

## 4.7 Acknowledgments

Thanks goes to the Captains, crews, and scientific parties of expeditions JC166 and CEND0917. They are particularly grateful to the Isis ROV team for the collection of groundtruthing data in the challenging submarine canyon terrain. We would also like to thank Tim Le Bas and Catherine Wardell for help with the sidescan sonar data processing, Michael Faggetter for his support with Matlab, Jamie Davie and Leigh Marsh who annotated the CEND0917 images used in the study and CEFAS personnel who provided guidance in the processing of CTD data. Tabitha Pearman is a PhD student in the NERC-funded SPITFIRE Doctoral Training Programme (Grant number NE/L002531/1) and receives further funding from the National Oceanography Centre and the CASE partner CEFAS. Dr Veerle Huvenne was funded by the ERC Starting Grant project CODEMAP (Grant No 258482), by the NERC National Capability programme CLASS (Grant No NE/R015953/1); and the EU H2020 research and innovation programme project iAtlantic (grant agreement No 818123).

# Chapter 5 Synthesis

## 5.1 Thesis Motivation

Submarine canyons are complex geomorphological features that incise continental margins and act as conduits between the deep sea and coastal and shelf environments. (Huvenne and Davies, 2014; Amaro et al., 2016). The complex geomorphology coupled with cross-shelf exchanges and canyon-intensified hydrodynamics, generates high spatio-temporal heterogeneity in environmental conditions (Fernandez-Arcaya et al., 2017; Hall et al., 2017; Campanyà-Llovet et al., 2018; Ismail et al., 2018). The high environmental heterogeneity is proposed to promote the high biological and habitat diversity observed within canyons (Bianchelli and Danovaro, 2019). In particular, the complex topography of canyons can lead to intensified hydrodynamics, including internal tides (Hall et al., 2014) that are hypothesised to influence faunal distributions (Huvenne et al., 2011; Johnson et al., 2013) and favour vulnerable marine ecosystems (VMEs) such as cold-water coral (CWC) habitats (De Leo et al., 2010; Robert et al., 2015). CWC habitats are associated with increased biodiversity (Roberts et al., 2009b; Buhl-Mortensen et al., 2010). Technological advancements have revealed CWC habitats occurring on the vertical walls of canyons (Huvenne et al., 2011; Robert et al., 2017) and small mounds comprised of coral fragments have been described from canyon interfluves (Stewart et al., 2014). Understanding the connection between faunal patterns, including CWCs, environmental heterogeneity, local hydrodynamics and fine-scale structural complexity like that provided by coral rubble mounds, is needed to support the effective management of canyons and the features of conservation that they support (Huvenne and Davies, 2014; Buhl-Mortensen et al., 2015). However, studies explicitly incorporating internal tide data into ecological modelling of canyon fauna are limited (Liao et al., 2017; Bargain et al., 2018). Furthermore, despite the importance of structural complexity in generating environmental heterogeneity, few studies assessing the influence of finer- scale structural complexity have been undertaken (Robert et al., 2017; Price et al., 2019). This thesis applied a range of statistical approaches to increase our understanding of what drives epibenthic megafaunal patterns, including CWCs, over a range of spatial scales, and specifically advances our understanding of how internal tides influence epibenthic megafaunal patterns in canyons, using Whittard Canyon, North-East Atlantic as a model system.

## 5.2 Thesis objectives

### 5.2.1 Overall thesis objective

The overall aim of this thesis was to (1) investigate how environmental heterogeneity acting at different spatial scales influences spatial patterns of epibenthic megafauna, including CWCs and (2) assess the role of the internal tide and fine-scale structural complexity in influencing faunal patterns in Whittard Canyon, North- East Atlantic.

This aim was achieved through: (1) comparative predictive habitat modelling with and without physical oceanographic data (including internal tide data) and (2) by multivariate statistical analyses to investigate the influence of spatial and temporal environmental heterogeneity on species diversity and assemblage structure.

The following sections aim to address each of these objectives and summarise the main scientific findings of each chapter.

### 5.2.2 Main scientific findings

#### 5.2.2.1 Chapter 2

The objective of this chapter was to identify which environmental variables best predict canyon-wide epibenthic megafaunal patterns in Whittard Canyon and to assess if including physical oceanographic data (internal tide data) improved predictions of biodiversity, abundance and CWC occurrence.

Submarine canyons represent deep-sea biodiversity hotspots that are associated with CWCs reefs (De Leo et al., 2010; Fabri et al., 2014; Robert et al., 2015; Price et al., 2019). Effective spatial management and conservation of these features requires accurate distribution maps and a deeper understanding of the processes that generate the observed distribution patterns (Huvenne and Davies, 2014; Buhl-Mortensen et al., 2015; Anderson et al., 2016a). Despite physical oceanography, including internal tides, being advocated as important phenomena influencing faunal patterns in canyons (Huvenne et al., 2011; Johnson et al., 2013; Liao et al., 2017), these data had rarely been incorporated into predictive mapping (Bargain et al., 2018). The work carried out within Whittard Canyon identified depth, terrain complexity and hydrodynamics as important environmental factors influencing faunal patterns in submarine canyons. The work demonstrated that incorporating internal tide data improved model predictions and that excluding internal tide data could lead to an over-estimate of CWC occurrence. The inclusion of internal tide current speeds, together with terrain derivatives, identified those areas where the internal tide is likely to interact with complex topography to suspend and concentrate food in the form of nepheloid layers. These areas of resuspension and nepheloid layer production coincided with CWC and diversity hot spots within the canyon.

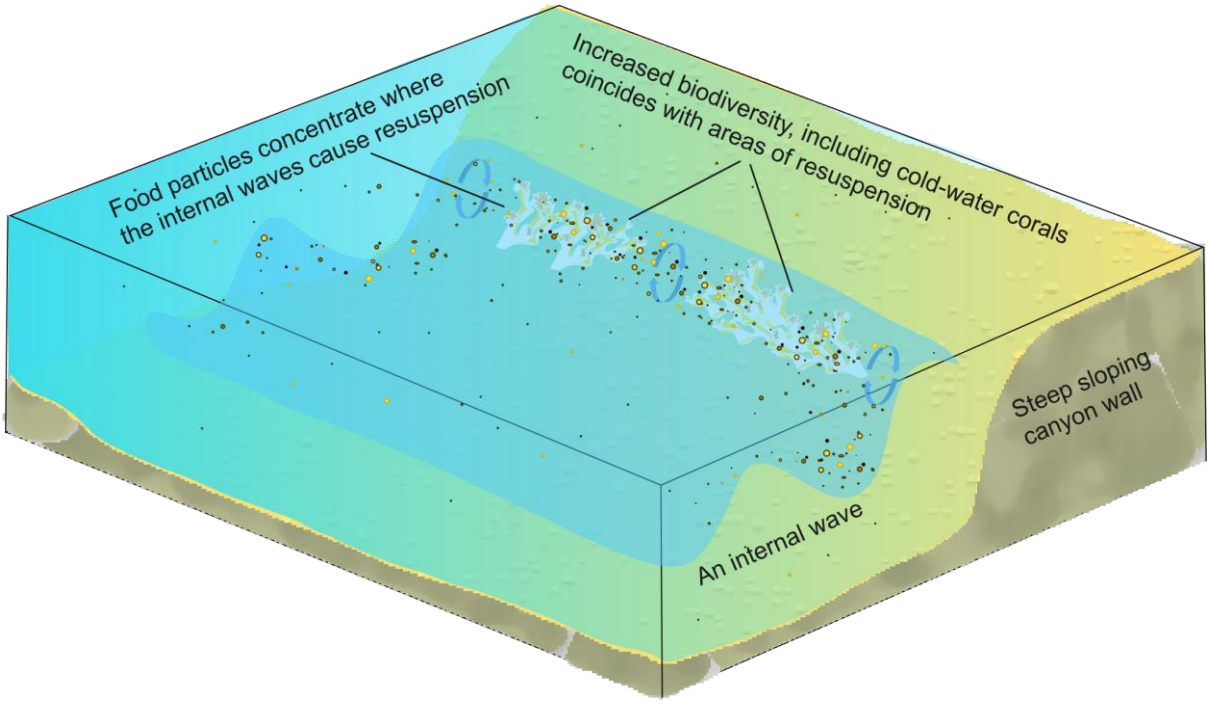


Figure 5.1 Schematic showing how internal tide dynamics influence food availability. Food particles from the surface sink down through the water column and concentrate where the internal waves re-suspend material as they come in to contact with the steep and complex topography of the canyon walls. Deep-sea filter feeding species, including cold-water corals take advantage of the increased food resources, promoting increased diversity in these areas.

#### 5.2.2.2 Chapter 3

The aim of this chapter was to investigate if spatial patterns in temporal oceanographic variability induced by the internal tides explained variation in spatial patterns of diversity and assemblage composition on deep-sea canyon walls. The objectives were achieved by asking: (1) Does epibenthic megafaunal assemblage composition change across physical oceanography and substratum gradients on vertical walls and (2) which environmental variables exert the strongest influence on epibenthic megafaunal diversity and assemblage structure?

The movement of the internal tide along the canyon causes the vertical displacement of isopcynals which in turn generates temporal variability in water mass characteristics on sections of canyon wall (Wang et al., 2008; Hall et al., 2017). The degree of variation experienced by canyon fauna on a section of wall is dependent on the amplitude of the internal tide and the characteristics of the water it displaces. Amplitudes of up 80 m had previously been observed within Whittard Canyon, generating twice daily 1°C temperature fluctuations and dissolved oxygen concentration changes of 12 µmol $kg^{-1}$ on certain sections of the canyon walls (Hall et al., 2017). However, no studies assessing the structuring force of this variability on benthic assemblages in canyons had been conducted. The work carried out showed that temporal oceanographic variability induced by the internal tide explained variation in spatial patterns of diversity and assemblage composition on canyon walls.

Assemblages were linked to the water depth and criticality of the canyon wall to the internal tide. Assemblages comprised of larger arborescent species occurred where internal tides potentially break, whereas vertical CWC reefs occurred on supercritical walls where internal tide energy is reflected back down toward the canyon floor. Heterogeneity in fine-scale substratum features influenced diversity patterns, with increased diversity associated with increased structural complexity provided by stepped features on walls and by CWC framework.

#### 5.2.2.3 Chapter 4

The aim of this chapter was to explore the relationship between structural complexity and epibenthic megafaunal assemblages within mini-mound provinces occurring on canyon interfluves that are subject to trawling pressure.

Understanding the role of structural complexity on deep-sea faunal assemblages and diversity at comparative scales is fundamental for the accurate impact assessment of seafloor modification by trawling and to assist effective spatial management. In general, spatial patterns in epibenthic megafauna are intrinsically linked to heterogeneity in environmental conditions at multiple scales (Levin et al., 2001; 2010; Robert et al., 2017). However, species-environment relationships are often modelled from broad resolution shipborne acoustic datasets from which bathymetric derivatives are used as proxies of environmental heterogeneity and complexity (Robert et al., 2015). The mis-match between scale of study and scale of biological response could lead to inaccuracies when quantifying anthropogenic impact. The thesis undertook a high-resolution study of the mini-mounds and demonstrated that species richness, density and assemblage are influenced by variations in fine-scale patchiness in substratum characteristics linked to structural complexity at different scales. The work supported the role of structural complexity in driving spatial patterns of species richness and density within the mound provinces of the canyon interfluves. The work emphasised the ecological role of mini-mounds in increasing regional diversity by increasing habitat heterogeneity on the interfluves and supported the proposed differentiation between the coral rubble assemblages of the mini-mounds from coral rubble aprons of living reefs (Mortensen et al., 1995; Howell et al., 2010). The predictive modelling illustrated the importance of fine-scale structural complexity in influencing faunal distributions and showed that if the ecologically important heterogeneity cannot be acoustically distinguished between classes that are to be mapped it can lead to predictive inaccuracies. The implication of these findings is that studies exploring environmental drivers for the purposes of habitat mapping should consider if environmental heterogeneity or complexity can be distinguished in the available datasets as part of the model selection process. Furthermore, the results of the study showed that when broad-scale structural complexity of the terrain is reduced, fine-scale structural complexity may still be present and acting to increase diversity. The implication of this finding is that a change detected in broad- complexity, which is often reported as an indication of fishing impact, does not necessarily reflect a change in fine-scale complexity or fine-scale variability of the substratum, which is equally if not more influential to faunal patterns on interfluves. This further

highlights the need for multi-scale and multi-loci approaches in detecting species – environment relationships to establish anthropogenic drivers and pressure specific effects on faunal assemblages to support effective management.

## 5.3 Thesis contributions

### 5.3.1 Scientific contributions

This thesis provided a contribution toward our understanding of how environmental heterogeneity generated by seafloor complexity and internal tides, acting at different spatial scales influences spatial patterns of deep-sea epibenthic megafauna, including CWCs in canyon settings. These findings can be used to propose a model, whereby the high variability in epibenthic megafaunal patterns observed within canyon systems can be attributed to variability in topography and internal tide behaviour between and within canyon branches.

The work represented one of a few studies that have explicitly investigated how the internal tide influences faunal patterns in a deep-sea canyon environment. The work provided further evidence for the ecological role of internal tides, which by interacting with complex topography generate environmental heterogeneity in food supply and water mass characteristics. Studies from other settings have shown that internal tides influence fauna by mediating food supply (Davies, 2009; Duineveld et al., 2012; Mohn et al., 2014; Demopoulos et al., 2017) and generating variability in water mass characteristics (Jantzen et al., 2013; Henry et al., 2014; van Haren et al., 2017; Hanz et al., 2019). In contrast to our study, the few deep-sea studies looking at the role of the internal tide in generating temporal variability in water mass characteristics have emphasised the importance of internal tides in ensuring efficient food and oxygen supply to support fauna in hostile oxygen minimum zones (van Haren et al., 2017; Hanz et al., 2019). Consequently this thesis furthered our knowledge of faunal responses to internal tide induced variability within a canyon setting.

Consistent with the findings of the thesis, assemblages in both deep and shallow water settings have been observed to differ between areas experiencing different degrees of internal tide induced variability (Jantzen et al., 2013; Henry et al., 2014), or behaviour (i.e. wave breaking) (van Haren et al., 2017). In particular, our results corroborate previously reported distribution patterns of deep-water CWCs that have been observed to thrive in areas experiencing increased internal tide driven variability and food supply (Henry et al., 2014; van Haren et al., 2017; Hanz et al., 2019). CWCs are opportunistic feeders (Duineveld et al., 2007; Mueller et al., 2014), capable of adjusting their metabolism in response to temperature and food supply, which has been proposed as an adaptation to periodic fluxes (van Oevelen et al., 2016; Maier et al., 2019). Consequently, by linking CWC distributions to internal tide dynamics in canyons, this thesis has contributed to our growing

understanding of the association between CWCs and internal tides (Frederiksen et al., 1992; White et al., 2005; Thiem et al., 2006; Roberts et al., 2009a; Mohn et al., 2014).

This thesis provided updated and improved distribution maps of diversity and CWC occurrence within the Eastern branch of Whittard Canyon and Dangaard and Explorer Canyons. Dangaard and Explorer Canyons constitute the Canyons Marine Conservation Zone (MCZ). Updated and improved maps can support the effective management of the MCZ. Furthermore, the predictive distribution modelling illustrated that incorporating internal tide data captured additional information to that provided by terrain derivatives alone. The incorporation of internal tide data enabled areas of possible resuspension and concentrated food resources to be better identified, which improved map accuracy and demonstrated that maps based upon terrain derivatives alone could lead to an overestimation of CWC occurrence. The improvement in predictive accuracy, provided by including high-resolution hydrodynamic data corroborated recent studies that have found that integrating data from spatially explicit hydrodynamic models with high resolution bathymetry can improve our understanding of multiscale interactions and predictions of habitat suitability, and adds to the growing argument to include spatially explicit hydrodynamic models into predictive distribution modelling (Rengstorf et al., 2013; 2014; Mohn et al., 2014; Bargain et al., 2018).

By using a suite of statistical approaches including different predictive mapping methods, this thesis has identified and confirmed different spatial scales at which environmental heterogeneity influences epibenthic megafaunal diversity and assemblage structure in the deep sea. The thesis has illustrated that substratum characteristics influence the spatial distribution of assemblages, while structural complexity at varying spatial scales is important in determining spatial patterns in diversity, species richness and abundance. For example, at the canyon scale, highest species diversity and CWC occurrence is associated with the increased structural complexity of canyon escarpments and ridges. Here internal tides interact with the complex topography causing enhanced current speeds or modified internal wave behaviour (i.e. wave breaking) resulting in the resuspension of particulate matter and nepheloid layer production. Nepheloid layers represent important food resources for deep-sea fauna, promoting increased diversity. At finer spatial scales, increased structural complexity, provided by lithologic features such as ‘steps’ or coral framework and rubble, is associated with local peaks in diversity. The increased structural complexity provided by lithology and coral increases fine-scale environmental heterogeneity, which in turn promotes increased diversity by the diversification of niches and provision of shelter from predators (See Figure 5.2 for a schematic over view).

These findings corroborate those from other deep-sea settings that have incorporated multi-scale data to show that heterogeneity in fine-scale substratum characteristics represents a principal driver of variation in assemblage structure and diversity at spatial scales of < 50 m (Robert et al., 2014) and that structural complexity across a range of spatial scales (including fine-scale complexity provided by coral colonies) may be important in determining spatial patterns in diversity (Robert et al., 2017). Similar to our study these authors also noted that fine-scale variability is largely undetected by ship-acquired MBES (Robert et al., 2017; Lacharité and Metaxas, 2017).

The utilisation of AUV acquired datasets allowed the characterisation of the mini-mound provinces at the metric scale, which, combined with ROV and Drop-down camera imagery data, allowed for the most detailed characterisation of the mounds yet. The results demonstrated the positive relationship between fine-scale structural complexity and diversity across a new canyon setting (i.e. mini-mounds on interfluves) and that fine-scale structural complexity may be an important factor acting to influence faunal patterns even when broader-scale complexity is not detected. The importance of fine-scale structural complexity and variability in substratum characteristics to the overall biodiversity of a system has also been demonstrated on the continental shelf (Post et al., 2016) and margin (Lacharité and Metaxas, 2017). The implications of these results is that trawling impact studies based solely on evidence of broad-scale reductions in seafloor complexity could be misrepresenting species-environment relationships and impacts. Consequently, the application of multi-scale approaches to understand and monitor the impacts of seafloor modification by trawling on fauna will increase our knowledge of fishing impacts on benthic fauna. Consequently, the combined outputs of the thesis promoted the inclusion of true multi-resolution environmental data, to capture the spatial heterogeneity in environmental conditions encountered in complex seafloor settings, when modelling faunal distributions, diversity and assemblage structure.

Lastly the thesis provided further ecological characterisation of the fauna and assemblages within Whittard, Dangaard and Explorer Canyons, North-East Atlantic and the developed morphospecies catalogue contributed to the development of a standardised database format and ongoing morphospecies guide for deep-sea taxa of the North-East Atlantic (Howell et al., 2019).

#### 5.3.1.1 Contributions toward cold-water coral habitat mapping in submarine canyons

The thesis advanced CWC habitat mapping in submarine canyons by contributing to our understanding of the links between environmental heterogeneity and CWC distributions in submarine canyons. The thesis showed both how environmental heterogeneity influences CWC distributions, but also how the increased structural complexity provided by CWC framework and rubble in turn creates fine scale environmental heterogeneity. The thesis illustrated that in order to produce accurate CWC habitat maps it is necessary to quantify and map ecologically relevant environmental heterogeneity (i.e. include correct parameters and map at the correct spatial scale). Within canyon

settings, this includes incorporating internal tide data, and this work has demonstrated that internal tides interacting with complex topography are key phenomena that can generate environmental heterogeneity in food supply and physical oceanography to influence CWC distributions. The thesis also demonstrated how environmental heterogeneity and structural complexity created by CWC framework and rubble acts as a driver for species assemblage composition and diversity. While it is often of too fine a scale to be detected by standard acoustic surveying techniques, this fine-scale heterogeneity should be kept in mind when evaluating the status of benthic ecosystems and accuracy of CWC habitat maps.

## 5.4 Limitations of the work

The thesis was principally aimed at modelling species–environment relationships for predictive mapping and ecological insights. However, model outputs are always constrained by the data inputs (Lecours et al., 2015, Miyamoto et al., 2017, Misiuk et al., 2018, Porskamp et al., 2018) and unfortunately deep-sea datasets are often acquired at broad resolutions, reflecting technological constrains rather than being ecologically intuitive (Verfaillie et al., 2009; Huvenne and Davies, 2014; Ismail et al., 2015; Lecours et al., 2015; Porskamp et al., 2018). When coupled with small sample sizes of ground-truthed data points and lack of robust replication across a highly heterogeneous landscape it can affect the statistical robustness and applicability of models beyond the data used to build them. Consequently caution should be applied not to over-interpret results, (Anderson et al., 2016b), especially in canyon settings that exhibit high spatial heterogeneity in environmental conditions and localised faunal distributions (Anderson et al., 2016b). To this end predictive habitat maps should be viewed as representing suitable locations rather than actual distributions. Ecological models should be viewed as simplifications of reality that provide insight but not absolute truth and should be used to guide further hypothesis or sampling designs.

The dependence of model performance on data resolution represents a limitation for all deep-sea models (Lecours et al., 2015, Miyamoto et al., 2017, Misiuk et al., 2018, Porskamp et al., 2018). Consequently, increased sample size, data resolution of the environmental variables and the inclusion of environmental variables that directly influence fauna will further enable more precise characterising of environmental heterogeneity which would improve our ability to resolve, model and predict relationships between faunal diversity/assemblage and environmental variables, and increase our understanding of which and at what scale heterogeneity in environmental variables influence deep-sea fauna.

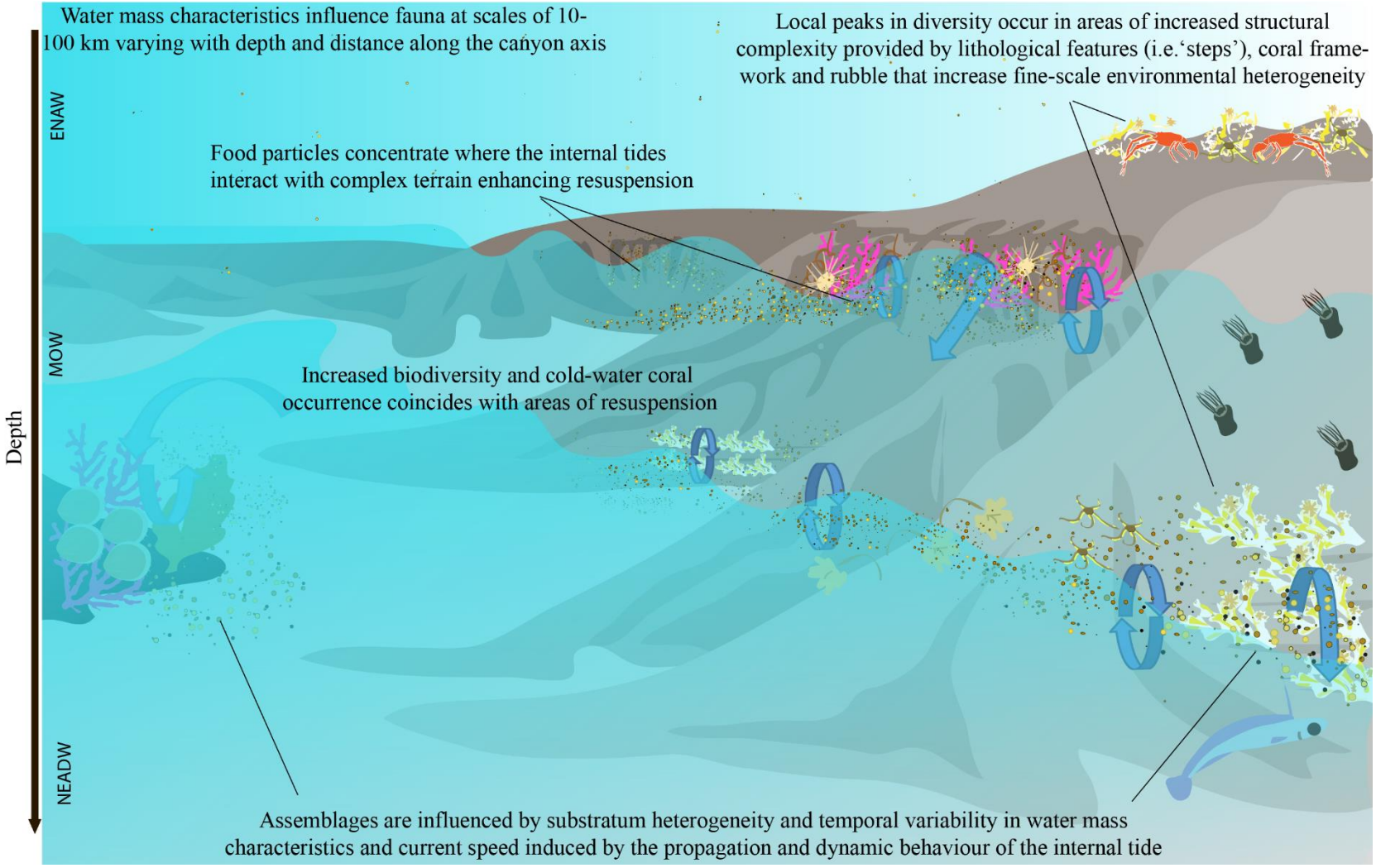
Water mass characteristics influence fauna at scales of 10-100 km varying with depth and distance along the canyon axis
Local peaks in diversity occur in areas of increased structural complexity provided by lithological features (i.e.'steps'), coral framework and rubble that increase fine-scale environmental heterogeneity
ENAW
Food particles concentrate where the internal tides interact with complex terrain enhancing resuspension
MOW
Increased biodiversity and cold-water coral occurrence coincides with areas of resuspension
Depth
NEADW
Assemblages are influenced by substratum heterogeneity and temporal variability in water mass characteristics and current speed induced by the propagation and dynamic behaviour of the internal tide

Figure 5.2 Schematic of thesis synthesis (Page 137) showing how environmental heterogeneity generated by structural complexity and internal tides influences faunal patterns in a deep-sea canyon. Environmental heterogeneity is an important factor driving spatial patterns in canyon faunal diversity and assemblages. Water mass characteristics influence fauna at spatial scales of 10 - 1000 km and vary with depth and distance along the canyon axis, with a reduced influence of the Mediterranean Outflow Water (MOW) and increased mixing toward the canyon head. Peaks in diversity and cold-water coral occurrence coincide with areas where the internal tide interacts with the broad-scale structural complexity of the canyon walls (i.e. ridges and escarpments), enhancing resuspension and the formation of nepheloid layers that represent an important food resource for deep-sea benthos. Local peaks in diversity also occur in areas of increased fine-scale structural complexity provided by lithologic features such as 'steps', coral framework and rubble that increase fine-scale environmental heterogeneity. Spatial patterns in assemblages, on the other hand, are influenced by patchiness in distribution of substratum characteristics (i.e. soft or hard) plus by temporal variability in water mass characteristics and current speed induced by the propagation and dynamic behaviour of the internal tide.

## 5.5 Future directions

Our understanding of the deep sea is intrinsically linked to technological advancements facilitating the acquisition of larger and higher resolution datasets (Danovaro et al., 2014; Huvenne and Davies, 2014). The thesis supports the increasingly advocated need for multi-scale approaches and understanding of how relationships change over scale to detect change and match hierarchal classification approaches applied in management (e.g. Deep-Ocean Stewardship Initiative) (Porskamp et al., 2018).

Although canyons are recognised as sites of intensified hydrodynamics (Hall et al., 2014; Aslam et al., 2018), which this thesis has shown to be influential to fauna, high-resolution hydrodynamic models for deep-sea canyons are scarce (Aslam et al., 2018; Bargain et al., 2018). Additionally, ship-borne acquired acoustic datasets struggle to resolve steep canyons walls that support the highest diversity (Hall and Carter, 2011; Huvenne et al., 2011; Robert et al., 2017; Robert et al., 2019). Together these factors limit our ability to adequately model habitats in other canyons with consequences for spatial management. Consequently, integrating data at an appropriate scale currently represents the main challenge of high-resolution canyon mapping. Therefore, future deep-sea canyon research and mapping should endeavour to incorporate physical oceanographic and acoustics datasets at ecologically relevant resolutions, apply multi-scale approaches to model selection and improve our understanding of how relationship change across scales.

Lastly, future modelling of internal tide dynamics and fauna in canyons or canyons branches where hydrodynamics differ to those studied here would enable comparisons and assist in determine the universality of the results.

## 5.6 Concluding remarks

Submarine canyons represent ecologically important geomorphological features that support and provide refuge for high biological diversity, productivity and VMES, such as CWC habitats. The spatial distributions of fauna in canyons, including CWCs are associated with environmental heterogeneity generated by internal tides and the structural complexity of the seafloor at various spatial scales. Effective management of canyons will require the integration of predictive modelling tools and the adoption of multi-scale approaches that incorporate high-resolution acoustic, physical oceanographic and internal tide data, to further our understanding of the processes driving spatial patterns in fauna.

# Appendix A Chapter 2 Supplementary materials

## 2.1 Methods supplementary materials

### 2.1.1 Annotator consistency between studies

Video Annotations from JC125 were combined with those from the previous cruises of JC010 and JC036 (Robert et al., 2015) and annotator consistency assessed following Durden et al. (2016).

Review of morphospecies catalogues from the two studies show that morphospecies discrimination was consistent between the annotators, with discrepancies relating to the level of classification rather than a misidentification. In such cases, the annotation in the combined matrix was assigned the lowest shared hierarchal classification.

Annotator consistency was assessed statistically using univariate statistics, T-test and Man Whitney of 1-*D*, that showed diversity differed between annotators (T-Test t = -4.435, df = 127.71, p-value = <0.001, Man Whitney W = 9378, p-value = <0.001). Annotator consistency was also assessed using multivariate analysis on Euclidean distance of a Chord transformed 50 m segment sample data matrix. This analysis found a difference between sample annotations by annotator (Permutational multivariate analysis of variance (PerMANOVA) $p < 0.005$, Supplementary materials Table 2.1). However, further analysis shows that the annotated data exhibit high variability in the morphospecies composition between samples from dives completed across different depths and substrates. Whittard Canyon is characterised by high spatial heterogeneity and beta diversity (Amaro et al., 2016), with authors reporting <40 % taxa shared between dives (Robert et al., 2015). Cluster analysis of our data shows that annotator annotations from dives covering similar environmental conditions fall within the same cluster (Supplementary materials Figure 2.1 and 2.3). We therefore conclude that differences between annotators reflect the inherent high beta-diversity resulting from habitat heterogeneity sampled by the different dives annotated by each annotator, rather than annotator bias. Consequently, annotations were combined.

Supplementary materials Table 2.1 Results from PERMANOVA analysis for differences in sample annotations between annotators.

| Factor | DF | Sum Sq | Pseudo-F | $R^2$ | P |
|---|---|---|---|---|---|
| Annotator | 1 | 10.52 | 12.371 | 0.02985 | <**0.005** |
| Residuals | 402 | 341.84 | | 0.97015 | |
| Total | 403 | 352.36 | | 1 | |

DF - degrees of freedom; Sum of Sq - sum of squares; Pseudo-F- F value by permutation, P-values based on 999 permutations. Bold indicating significant P value <0.05.

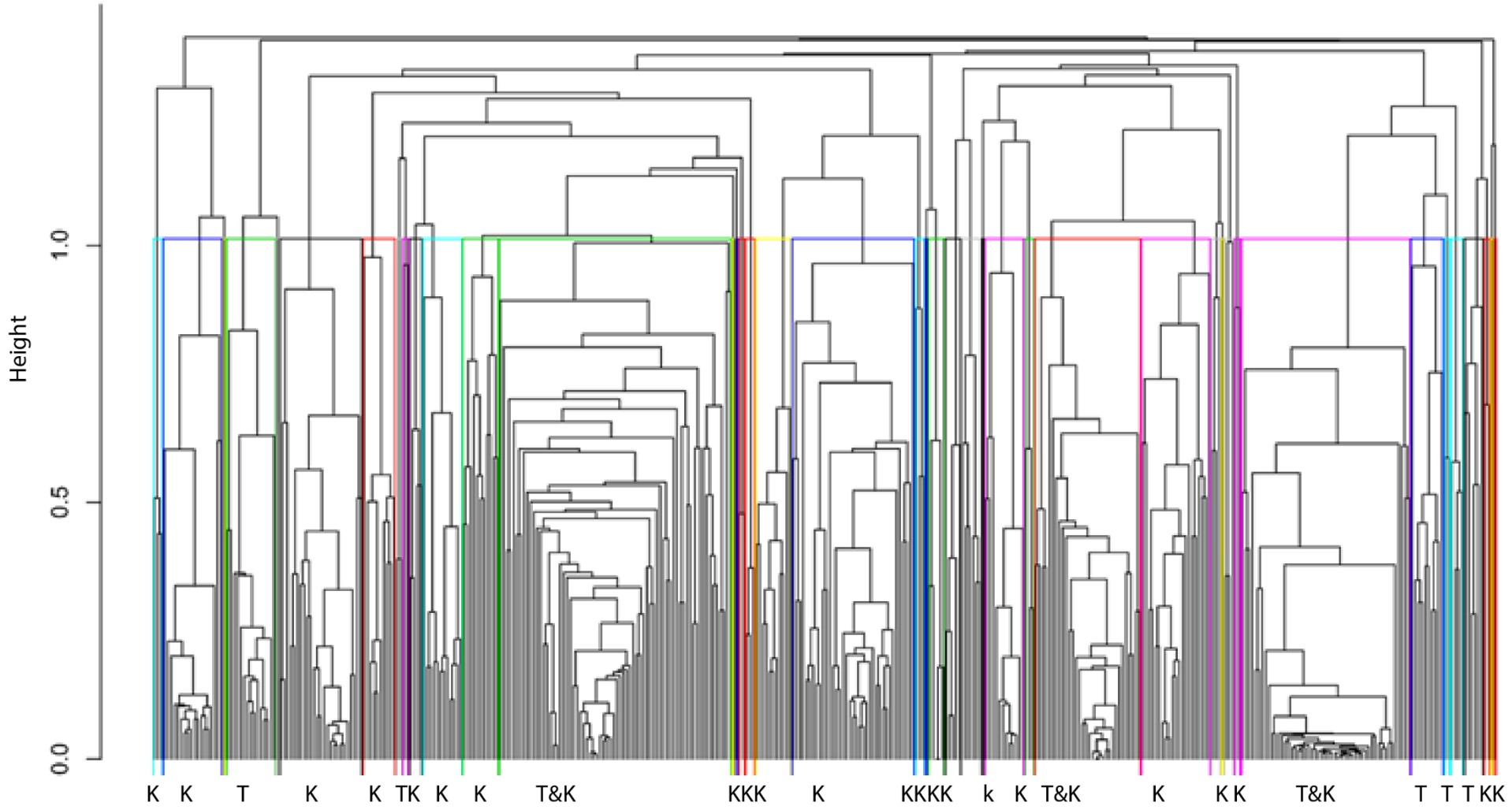


Supplementary materials Figure 2.1 Dendogram showing results of a reordered cluster analysis based upon 50 m segment samples. Each cluster allocated K or T representing the annotator of the samples within that cluster, where a cluster comprises samples from both annotators both prefixes are allocated. Samples from each annotator fall in the same cluster where annotations come from dives undertaken in similar environments within the canyon.

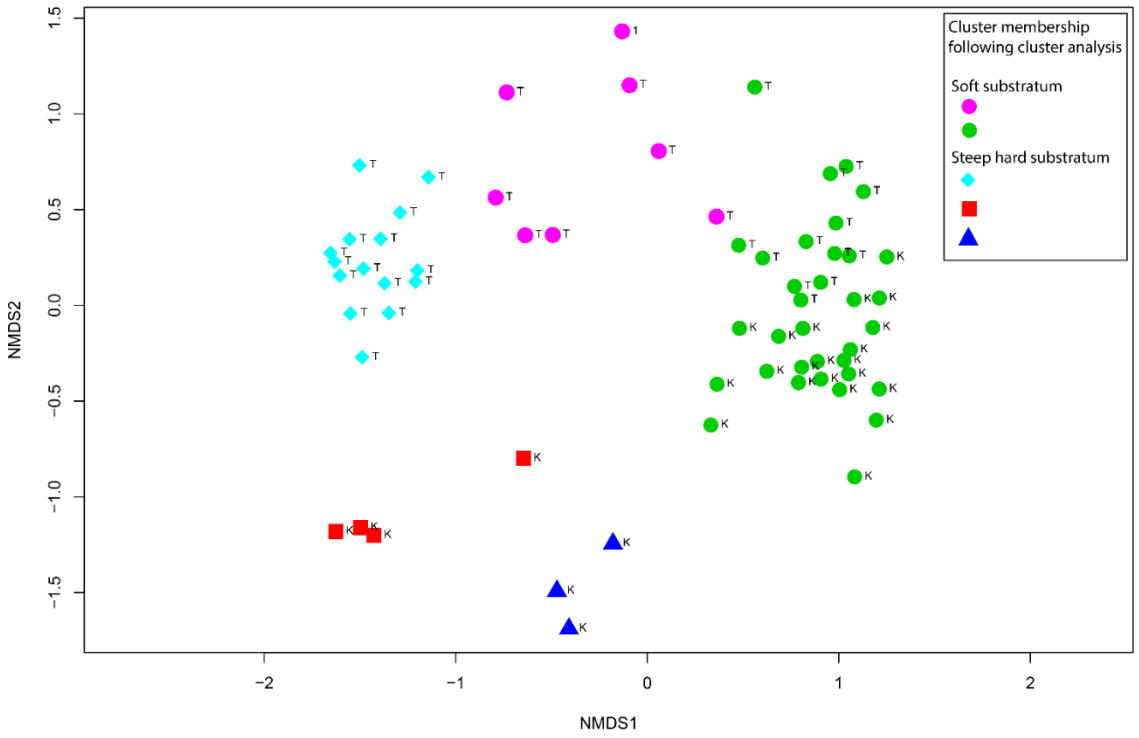


Supplementary materials Figure 2.2 A non-metric Multi-Dimensional Scaling (nMDS) plot with each 50 m segment sample coloured by cluster membership following cluster analysis. The plot shows a subset of the data (for ease of interpretation), comprising dive JC125_263 and JC036_117-118 that were undertaken from similar water depth but opposite flanks of the canyon. Each dive was annotated by a different annotator (T or K). The samples are spread across five clusters and overlap in one (denoted as green circles). Two clusters (denoted by pink and green circles) represent fauna characteristic of soft substratum and the other clusters represent fauna characteristic of steep hard substratum. Analysis of the characterising taxa of each cluster shows that they represent different taxonomic families, which are easily distinguishable from one another, suggesting that differences in sample annotations are not caused by inconsistent annotation but reflect the heterogeneous nature of the biota.

S.2.1.2 Multiscale analysis of terrain derivatives for predictive modelling

To capture the range of spatial scales at which the terrain derivatives may affect faunal distributions, a multi-resolution approach was implemented whereby terrain variables were derived from bathymetry gridded at 50, 100 and 500 m, and derivatives calculated at varying window sizes (Rugosity: 150 m, 750 m, 2350 m, BPI: 100 m, 150 m, 200 m, 1000 m). Statistical modelling was then applied to identify the most ecologically meaningful resolution to use for each variable, identified as those derivatives that produced the optimal model. Model performance was based upon comparing measures of variance explained and the Area Under the Receiver operating Curve (AUC) score for cold-water coral (CWC) presence-absence (Elith and Leathwick, 2009) and correlation coefficients (linear regression) for the remaining models. The AUC score (0 to 1) indicates how well

the model fits the data. An AUC score <0.5 indicates that the model is no better than random and an AUC score >0.7 can be considered as adequately fitting the data. For GAM models the Akaike's Information Criterion (AIC) score (Zuur et al., 2014a) was also used. The AIC score is commonly applied to compare model performance and measures the goodness of fit and model complexity reflecting the variance explained penalised by number of explanatory variables, with a lower AIC score indicting a better model fit (Zuur et al., 2014a). The results from this analysis indicated that terrain derivatives from bathymetry gridded at 50 m were found to be optimal. A subset of this analysis for CWC occurrence is shown in Supplementary materials Table 2.2.

Supplementary materials Table 2.2 Modelling performance for the probability of cold-water coral (CWC) occurrence is optimal utilising terrain variables derived from bathymetry gridded at 50 m. For each of the modelling algorithms used (Boosted Regression Tree (BRT), Random Forest (RF) and General Additive Models (GAMs)) variance explained in the training data and AUC scores are highest or equal for models utilising terrain variables derived from bathymetry gridded at 50 m. The Area Under the Receiver operating Curve (AUC) score indicates how well the model fits the data (0 - 1). An AUC score <0.5 indicates that the model is no better than random and an AUC score >0.7 can be considered as adequately fitting the data.

| Model | Variable importance | Variance explained Adj $R^2$ (Train) | AIC | AUC (Train) | AUC (Test) |
|---|---|---|---|---|---|
| Species Richness | | | | | |
| CWC_BRT_50 | Depth, Slope, Rugosity, Eastness | 29% | | 0.97 | 0.90 |
| CWC_RF_50 | Depth, Slope, Rugosity, Eastness | 32% | | 0.99 | 0.89 |
| CWC_GAM_50 | Depth, Slope, Rugosity, Eastness | 38% | 167 | 0.92 | 0.87 |
| CWC_BRT_100 | Depth, Slope, Rugosity | 25% | | 0.95 | 0.87 |
| CWC_RF_100 | Depth, Slope, Rugosity | 21% | | 0.98 | 0.87 |
| CWC_GAM_100 | Depth, Slope, Rugosity | 33% | 151 | 0.89 | 0.90 |
| CWC_BRT_500 | Depth, BBPI, Northness | 27% | | 0.94 | 0.90 |
| CWC_RF_500 | Depth, BBPI, Northness | 29% | | 0.94 | 0.90 |
| CWC_GAM_500 | Depth, BBPI, Northness | 37% | 169 | 0.91 | 0.82 |

2.1.3. Calculation of the bathymetric slope criticality to the dominate semi diurnal tide ($M_2$ internal tide)

$$\alpha = \frac{\partial H/\partial x}{[(\omega^2 - f^2)/(N^2 - \omega^2)]^{\frac{1}{2}}}$$

Where: $x$ is across-slope distance (m), $H$ is the total depth (m), ω is the angular frequency of the wave (Hz), $f$ is the inertial frequency (Hz), and $N$ is the buoyancy frequency (Hz), calculated from the ship's CTD cast.

**2.2 Data exploration supplementary materials**

2.2.1 Data exploration

The pair plots, Pearson's correlation matrix and variance inflation factor (VIF) scores indicate collinearity between environmental variables and no strong correlations between the response variables and the environmental predictor variables (Supplementary materials 2.3 and Supplementary materials Tables 2.3 and 2.4).

Supplementary materials Table 2.3 Correlation variance inflation factors for each of the environmental variables.

| Variance inflation factors | VIF Score |
|---|---|
| Northness | 1.144411 |
| Rugosity | 1.457108 |
| Slope | 1.553037 |
| Eastness | 1.823179 |
| Slope Criticality to the $M_2$ tide | 2.029585 |
| Planar Curvature | 2.692182 |
| Broad Bathymetric Position Index | 3.078473 |
| Profile Curvature | 3.102408 |
| Fine Bathymetric Position Index | 3.53757 |
| Barotropic Current Speed | 5.865172 |
| Baroclinic Current Speed | 6.139925 |
| Depth | 9.857295 |
| Temperature | 189.2233 |
| Salinity | 214.7065 |

Appendix A

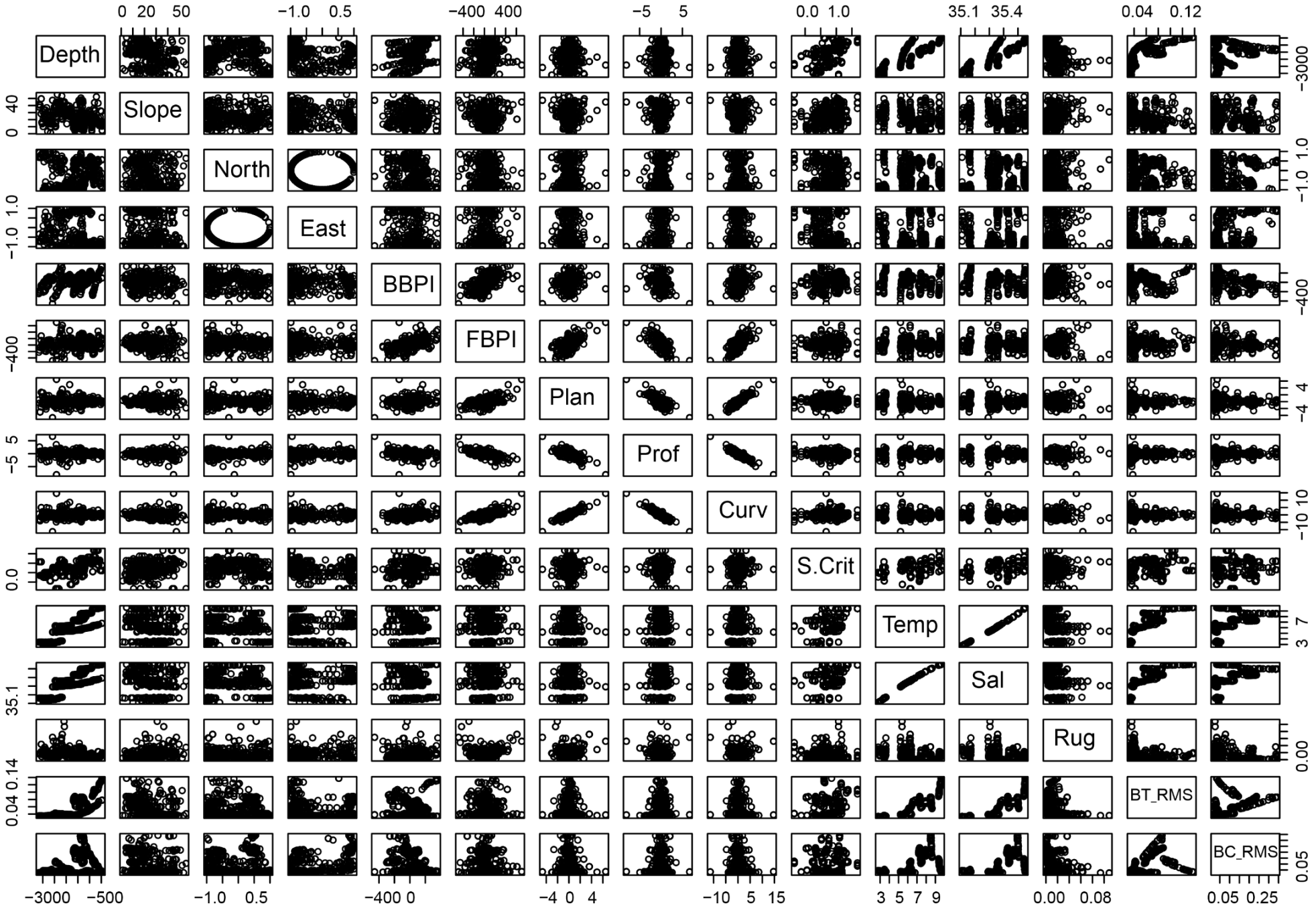
Depth
Slope
North
East
BBPI
FBPI
Plan
Prof
Curv
S.Crit
Temp
Sal
Rug
BT_RMS
BC_RMS

Supplementary materials Figure 2.3 (Page 146) Pair plots between the environmental predictor variables indicate that many environmental variables are collinear. Label abbreviations: North = Northness, East = Eastness, BBPI = Broad Bathymetric Position Index, FBPI = Fine Bathymetric Position Index, Slope Criticality = criticality of the slope to the dominate semi diurnal tide (M2), S.Crit = criticality of the slope to the dominate semi diurnal tide (M2), Temp = Temperature ° C, Sal = Salinity (PSU) Curve = Curvature, Plan = Planar Curvature, Prof = Profile Curvature, Rug = Rugosity, BT_RMS = Root mean squared current speed of the barotropic tide, BC_RMS = Root mean squared current speed of the baroclinic tide.

Supplementary materials Table 2.4 Pearson's correlation between the environmental predictor variables. Label abbrevtaions: BBPI = Broad Bathymetric Position Index, FBPI = Fine Bathymetric Position Index, Slope Criticality = criticality of the slope to the dominate semi diurnal tide ($M_2$).

| | Depth | Slope | Northness | Eastness | BBPI | FBPI | Plan Curvature | Profile Curvature | Curvature | Slope Criticality | Temperature | Salinity | Rugosity | Baroclinic Current | Barotropic Current |
|---|---|---|---|---|---|---|---|---|---|---|---|---|---|---|---|
| Depth | 1 | -0.258 | -0.088 | -0.214 | 0.288 | 0.079 | 0.017 | 0.019 | -0.002 | 0.537 | 0.811 | 0.819 | -0.366 | 0.291 | 0.246 |
| Slope | -0.258 | 1 | -0.099 | -0.033 | -0.126 | -0.013 | 0.006 | -0.050 | 0.031 | 0.233 | -0.151 | -0.154 | 0.370 | -0.155 | -0.034 |
| Northness | -0.088 | -0.099 | 1 | 0.142 | -0.203 | -0.128 | -0.026 | 0.100 | -0.069 | -0.080 | -0.090 | -0.084 | -0.062 | 0.019 | 0.056 |
| Eastness | -0.214 | -0.033 | 0.142 | 1 | -0.224 | -0.118 | -0.033 | 0.099 | -0.072 | -0.316 | 0.087 | 0.085 | -0.010 | 0.447 | 0.490 |
| BBPI | 0.288 | -0.126 | -0.203 | -0.224 | 1 | 0.591 | 0.241 | -0.284 | 0.280 | 0.214 | -0.069 | -0.070 | -0.030 | -0.329 | -0.385 |
| FBPI | 0.079 | -0.013 | -0.128 | -0.118 | 0.591 | 1 | 0.655 | -0.709 | 0.727 | 0.180 | -0.050 | -0.046 | 0.031 | -0.129 | -0.169 |
| Plan Curvature | 0.017 | 0.006 | -0.026 | -0.033 | 0.241 | 0.655 | 1 | -0.766 | 0.934 | 0.081 | -0.006 | -0.006 | 0.038 | -0.051 | -0.048 |
| Profile Curvature | 0.019 | -0.050 | 0.100 | 0.099 | -0.284 | -0.709 | -0.766 | 1 | -0.945 | -0.111 | 0.048 | 0.048 | -0.080 | 0.075 | 0.096 |
| Curvature | -0.002 | 0.031 | -0.069 | -0.072 | 0.280 | 0.727 | 0.934 | -0.945 | 1 | 0.102 | -0.030 | -0.030 | 0.063 | -0.067 | -0.078 |
| Slope Criticality | 0.537 | 0.233 | -0.080 | -0.316 | 0.214 | 0.180 | 0.081 | -0.111 | 0.102 | 1 | 0.383 | 0.381 | -0.026 | -0.004 | 0.045 |
| Temperature | 0.811 | -0.151 | -0.090 | 0.087 | -0.069 | -0.050 | -0.006 | 0.048 | -0.030 | 0.383 | 1 | 0.997 | -0.279 | 0.603 | 0.588 |
| Salinity | 0.819 | -0.154 | -0.084 | 0.085 | -0.070 | -0.046 | -0.006 | 0.048 | -0.030 | 0.381 | 0.997 | 1 | -0.278 | 0.612 | 0.586 |
| Rugosity | -0.366 | 0.370 | -0.062 | -0.010 | -0.030 | 0.031 | 0.038 | -0.080 | 0.063 | -0.026 | -0.279 | -0.278 | 1 | -0.294 | -0.193 |
| Baroclinic Current Speed | 0.291 | -0.155 | 0.019 | 0.447 | -0.329 | -0.129 | -0.051 | 0.075 | -0.067 | -0.004 | 0.603 | 0.612 | -0.294 | 1 | 0.881 |
| Barotropic Current Speed | 0.246 | -0.034 | 0.056 | 0.490 | -0.385 | -0.169 | -0.048 | 0.096 | -0.078 | 0.045 | 0.588 | 0.586 | -0.193 | 0.881 | 1 |

## 2.3. Modelling supplementary materials

### 2.3.1. Model outputs

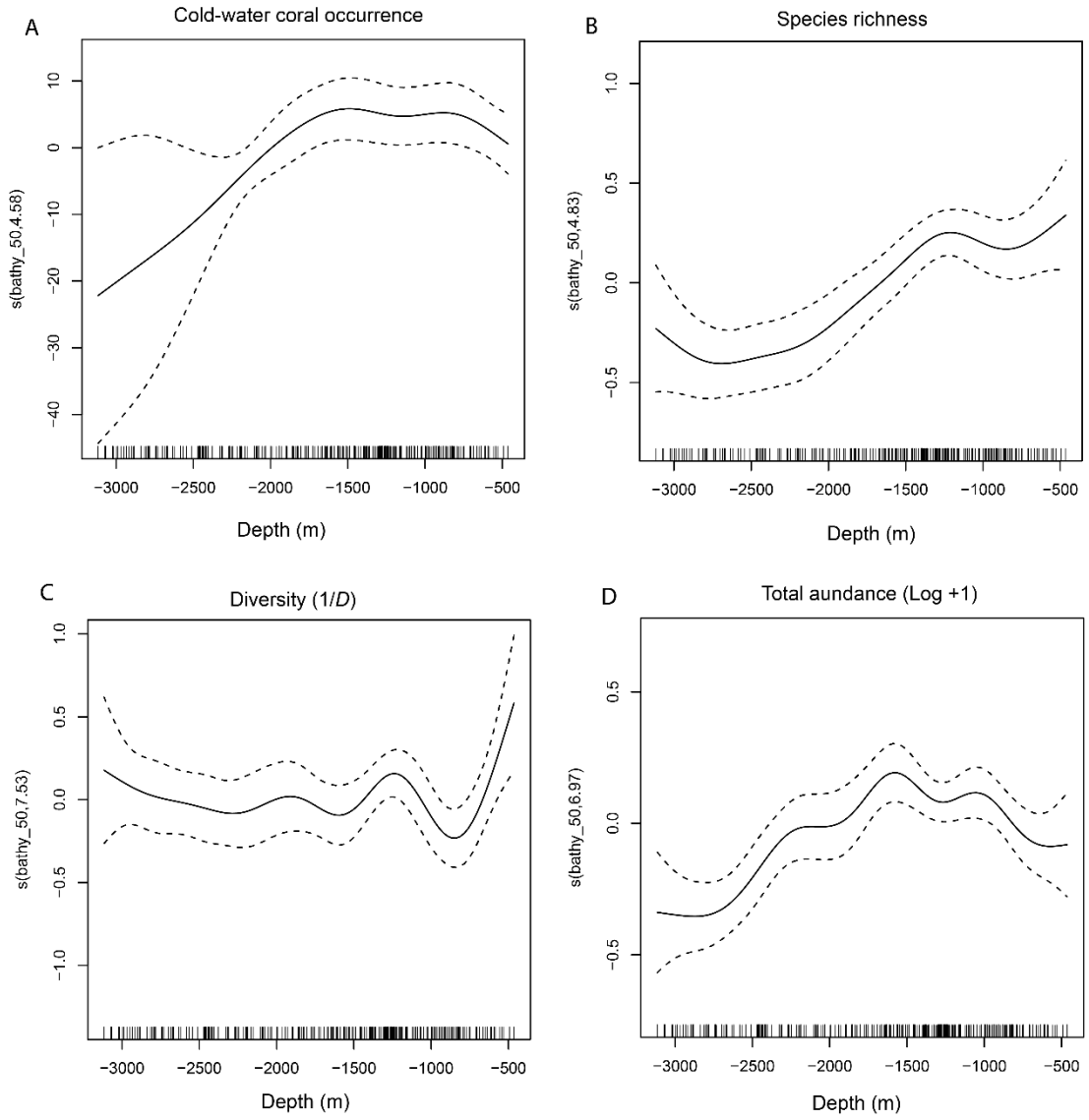


Supplementary materials Figure 2.4 GAM smoother outputs showing the relationship between depth (m) and (A) Cold-water coral occurrence, (B) Species richness, (C) Diversity (1/*D*) and (D) Total abundance (Log+1).

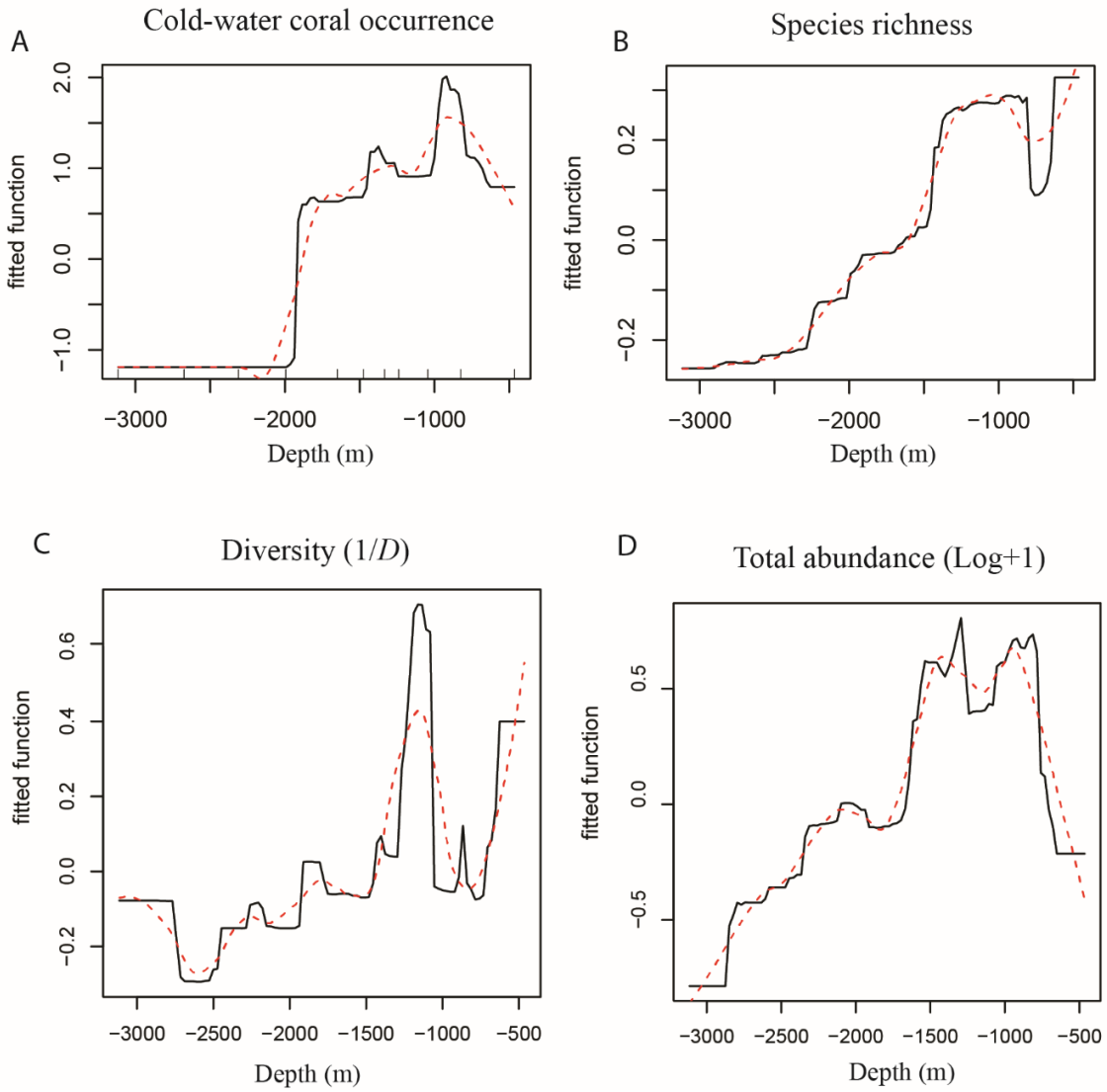


Supplementary materials Figure 2.5 Fitted function of BRT outputs showing the relationship between depth (m) and (A) Cold-water coral occurrence, (B) Species richness, (C) Diversity (1/*D*) and (D) Total abundance (Log+1).

# Appendix B Chapter 3 Supplementary materials

### 3.1 Methods supplementary materials

3.1.1 Calculation of the bathymetric slope criticality to the dominate semi diurnal tide ($M_2$ internal tide)

$$\alpha = \frac{\partial H/\partial x}{[(\omega^2 - f^2)/(N^2 - \omega^2)]^{\frac{1}{2}}}$$

Where: $x$ is across-slope distance (m), $H$ is the total depth (m), ω is the angular frequency of the wave (Hz), $f$ is the inertial frequency (Hz), and $N$ is the buoyancy frequency (Hz), calculated from the ship's CTD cast.

3.1.2 Environmental rasters

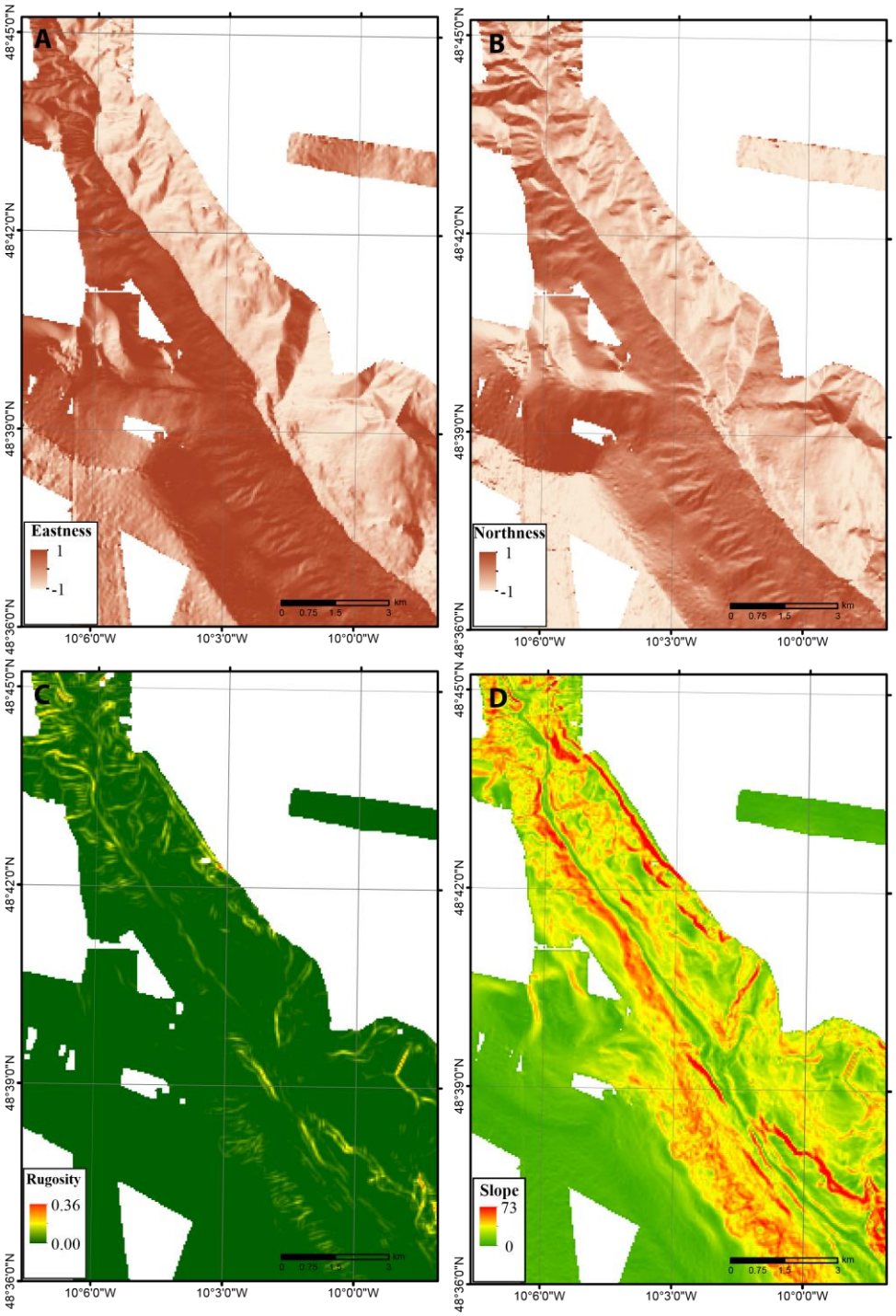


Supplementary materials Figure 3.1 Maps (50 m pixel resolution) of the bathymetric derivatives used as environmental variables in the model selectin. (A): Rugosity, (B): Slope (˚), (C): Eastness (D): Northness.

Appendix B

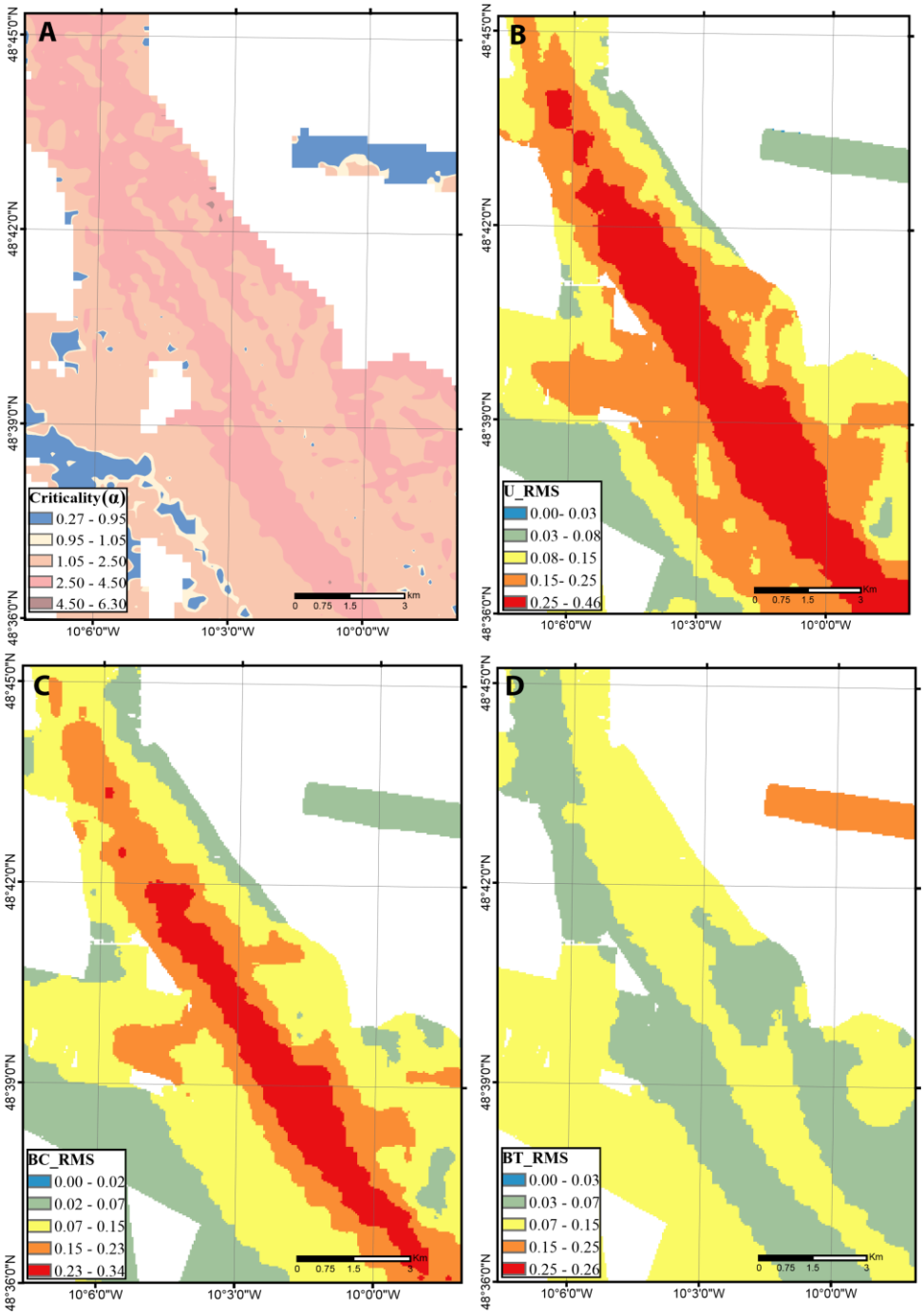


Supplementary materials Figure 3.2 Maps (50 m pixel resolution) of the oceanographic derivatives used as environmental variables in model selection. (A): Bathymetric slope criticality to the dominant semi-diurnal internal tide (α), (B): Root mean squared current speed of the sum of baroclinic and barotropic tide (m $s^{-1}$) (C): Root mean squared current speed of baroclinic tide (m $s^{-1}$) (D): Root mean squared current speed of barotropic tide (m $s^{-1}$).

3.1.3

Assessment of variability between profiles prior to deriving physical oceanographic variables

CTD data from the JC125, 64PE421 and PE453 cruises were compared to assess temporal and spatial variability. The temperature-salinity plots show temporal and spatial variability between profiles with increased consistency below the seasonal thermocline (Supplementary materials Figure 3.3 and 3.5). Depth profiles show that data collected during the same cruise are more consistent than data collected from different cruises but in closer proximity (Supplementary materials Figure 3.3 – 3.6). Although temporal variability is observed, the profiles converge below the seasonal thermocline (Supplementary materials Figure 3.3 - 3.6) justifying the combining of profiles within proximity of dives and for the local extrapolation from CTD data to dive sites all of which occur below the seasonal thermocline.

Appendix B

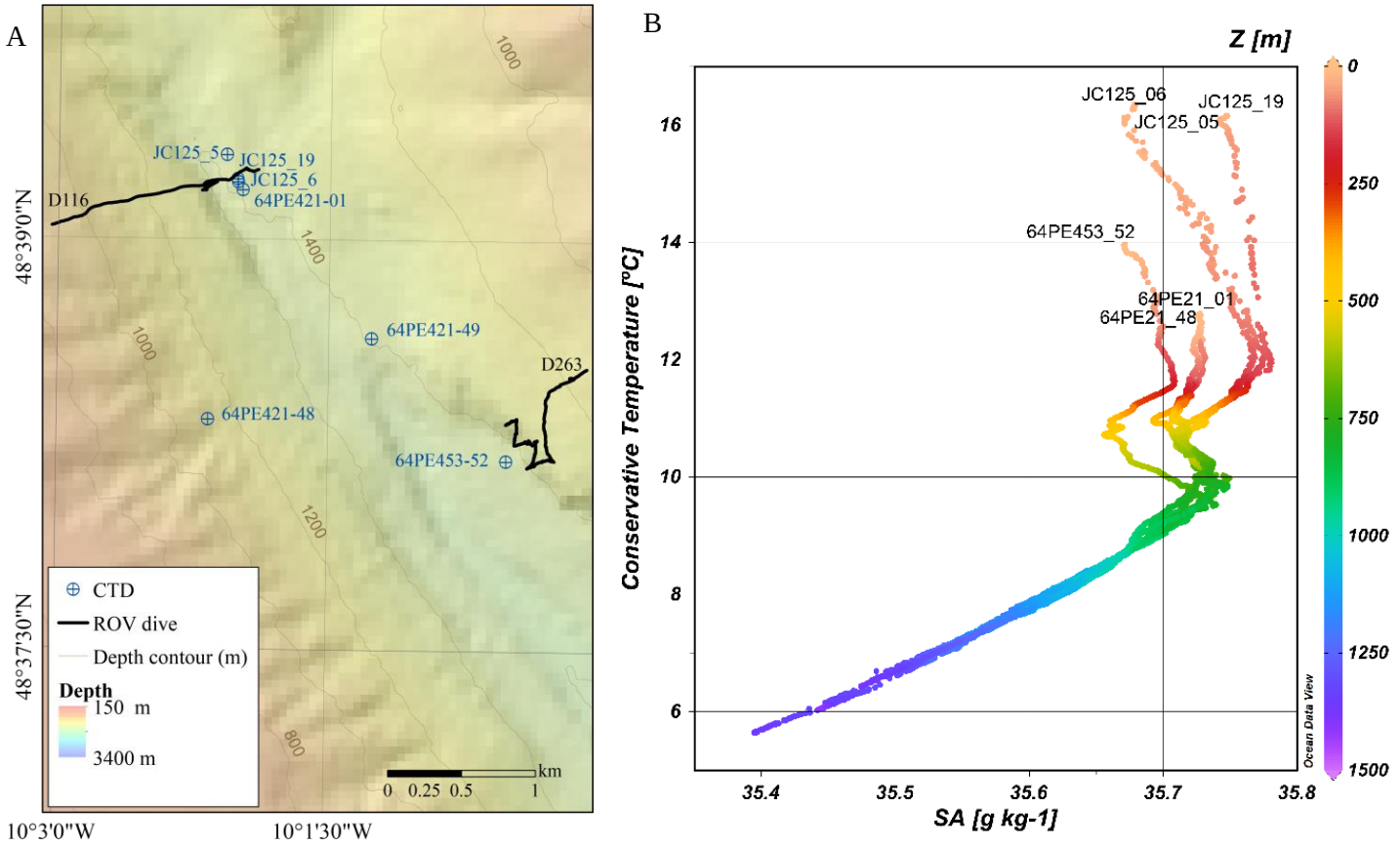


Supplementary materials Figure 3.3. (A) Location of CTD casts from the JC125, 64PE421 and 64PE453 cruises combined to obtain mean values for the fauna samples from Dives D116 and D263. The JC125 CTD casts were used to calculate vertical displacement of the $M_2$ tide. (B) Temperature-Salinity Plot. CTD casts come from the JC125, 64PE421 and 64PE453 cruises.

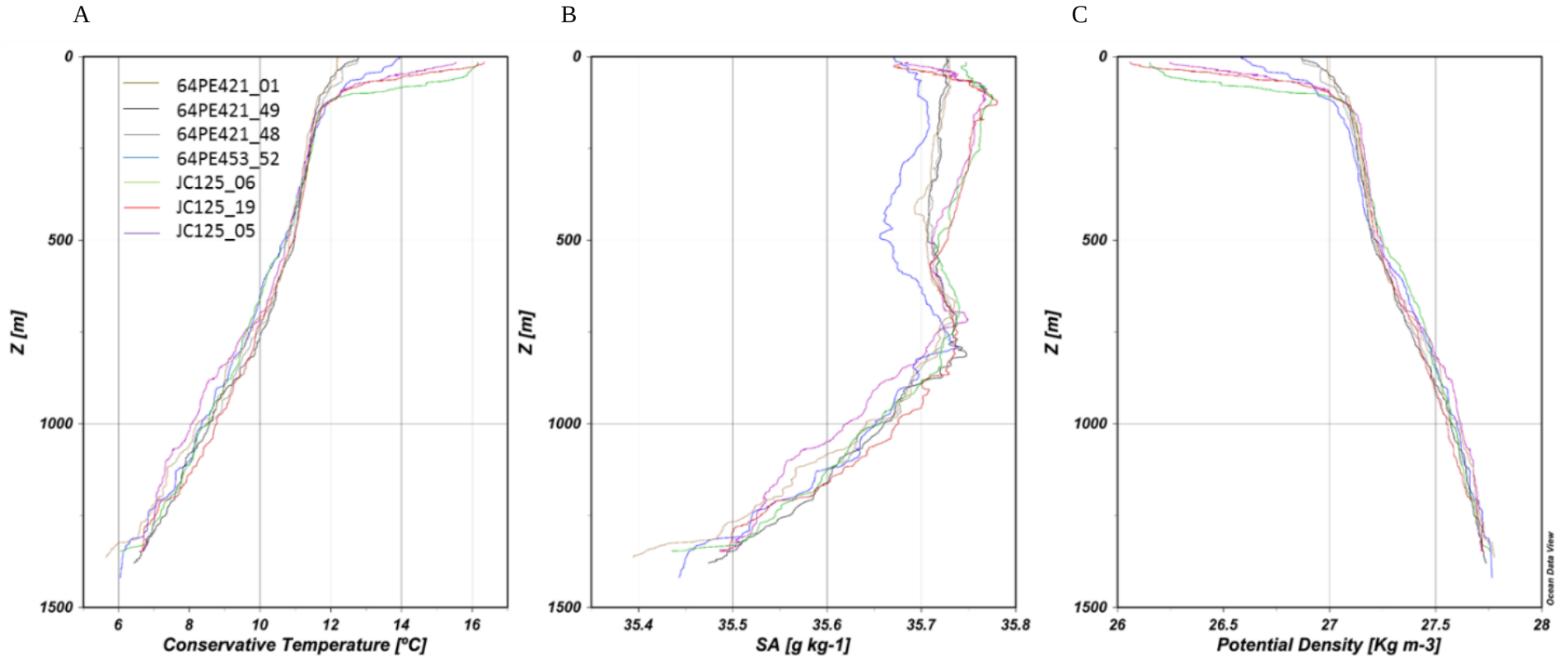


Supplementary materials Figure 3.4. Depth Profiles for (A) conservative temperature (ºC), (B) absolute salinity (g $kg^{-1}$), and (C) potential density (kg/ $m^3$). Profiles represent CTD casts from the JC125, 64PE421 and 64PE453 cruises. Data collected during the same cruise are more consistent that data collected from different cruises but in closer proximity. Temporal variability is observed however, the profiles converge below the seasonal thermocline.

Appendix B

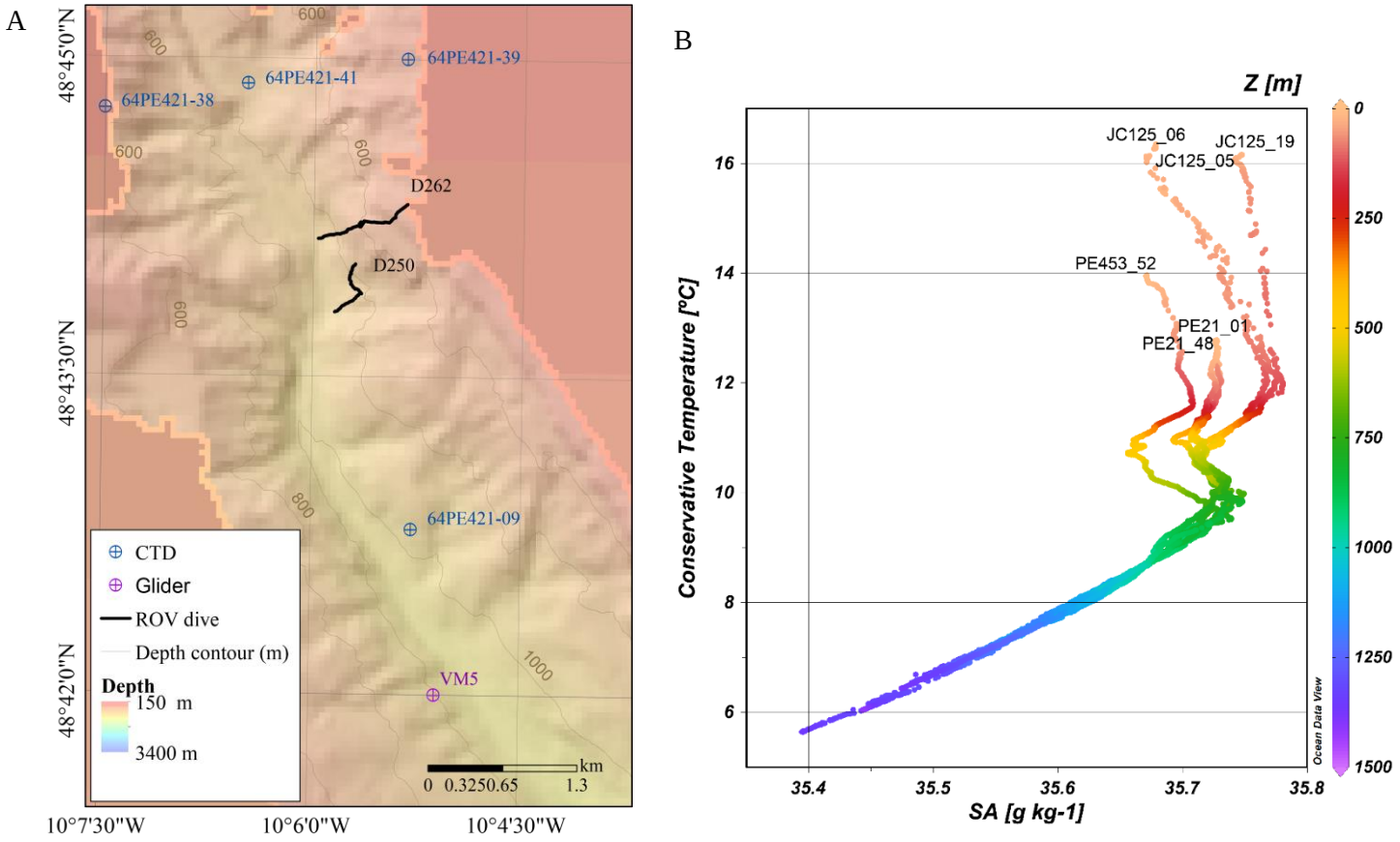


Supplementary materials Figure 3.5 (A) Location of CTD casts combined from the 64PE421 cruise to obtain mean values for the fauna samples from Dives D262 and D250. Location of glider station VM5 from which vertical amplitude displacement of the $M_2$ tide was calculated. (B) Temperature-Salinity Plot. Profiles represent four CTD casts from the 64PE421 cruise.

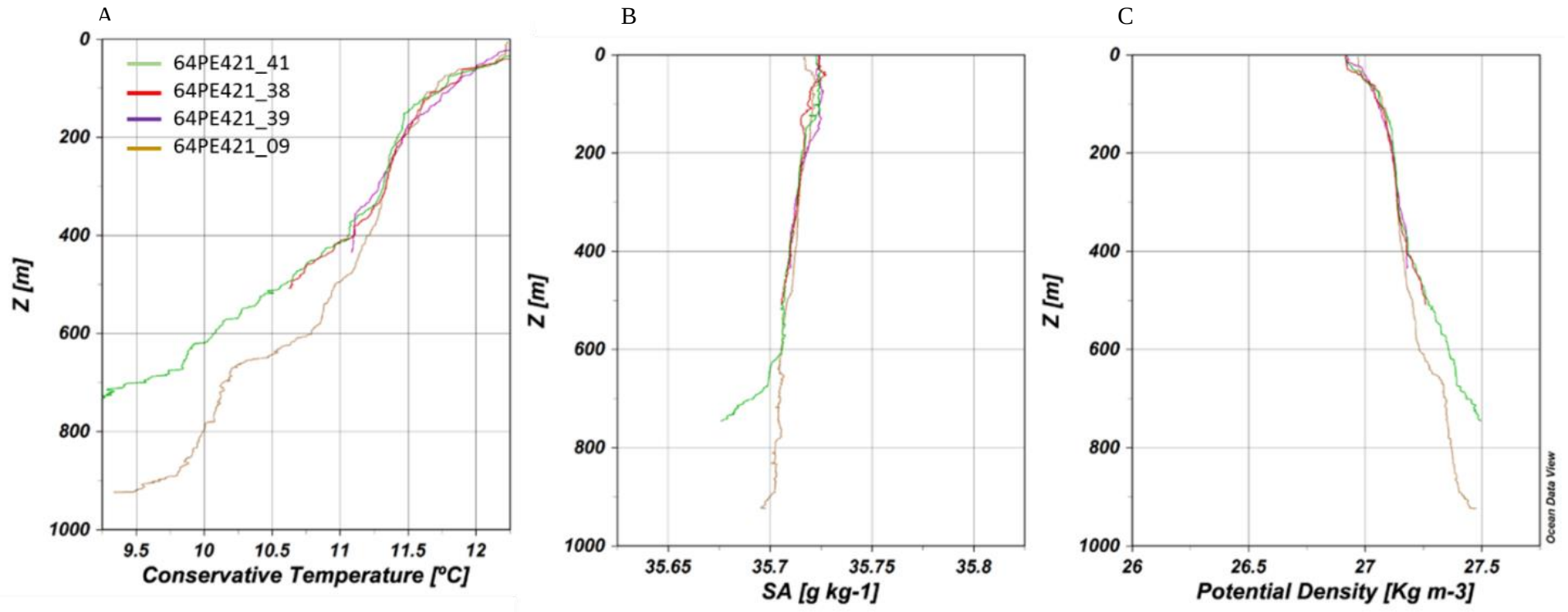


Supplementary materials Figure 3.6 Depth Profiles for (A) conservative temperature (ºC), (B) absolute salinity (g $kg^{-1}$) and (C) potential density (kg/ $m^3$). Profiles represent 4 CTD casts from the 64PE421 cruise.

Appendix B

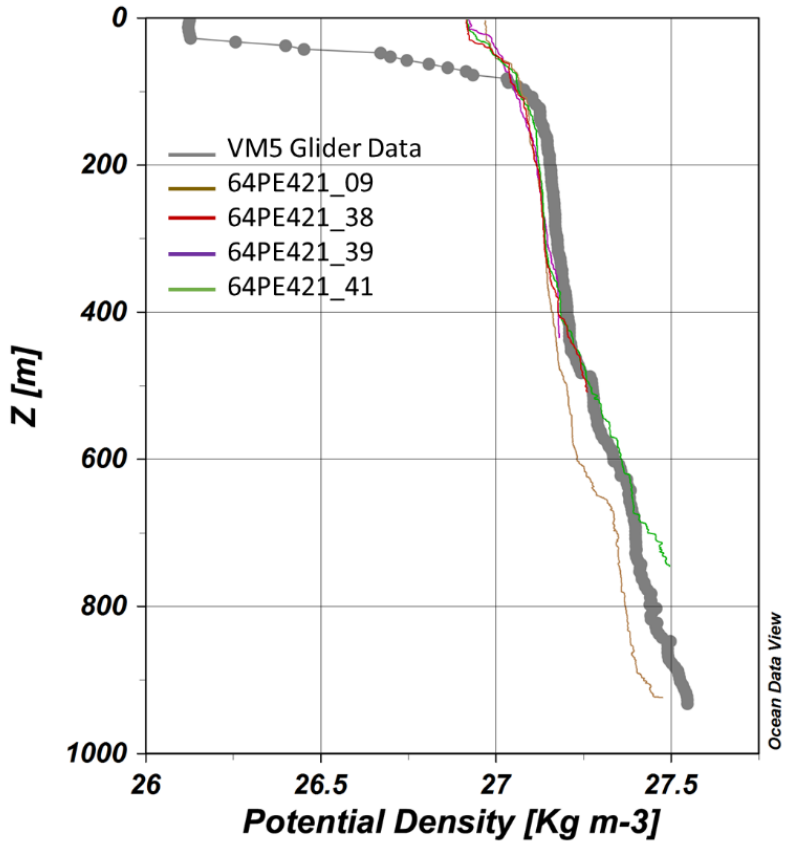


Supplementary materials Figure 3.7 Depth profiles for potential density (kg/ $m^3$) from CTD casts 64PE421_38, _39 , _41, _09 and glider data from VM5 (thick grey line). The profiles are consistent beyond a depth of ca 150 m for the glider and CTD data.

3.1.4

Example images of substratum types annotated from ROV still images

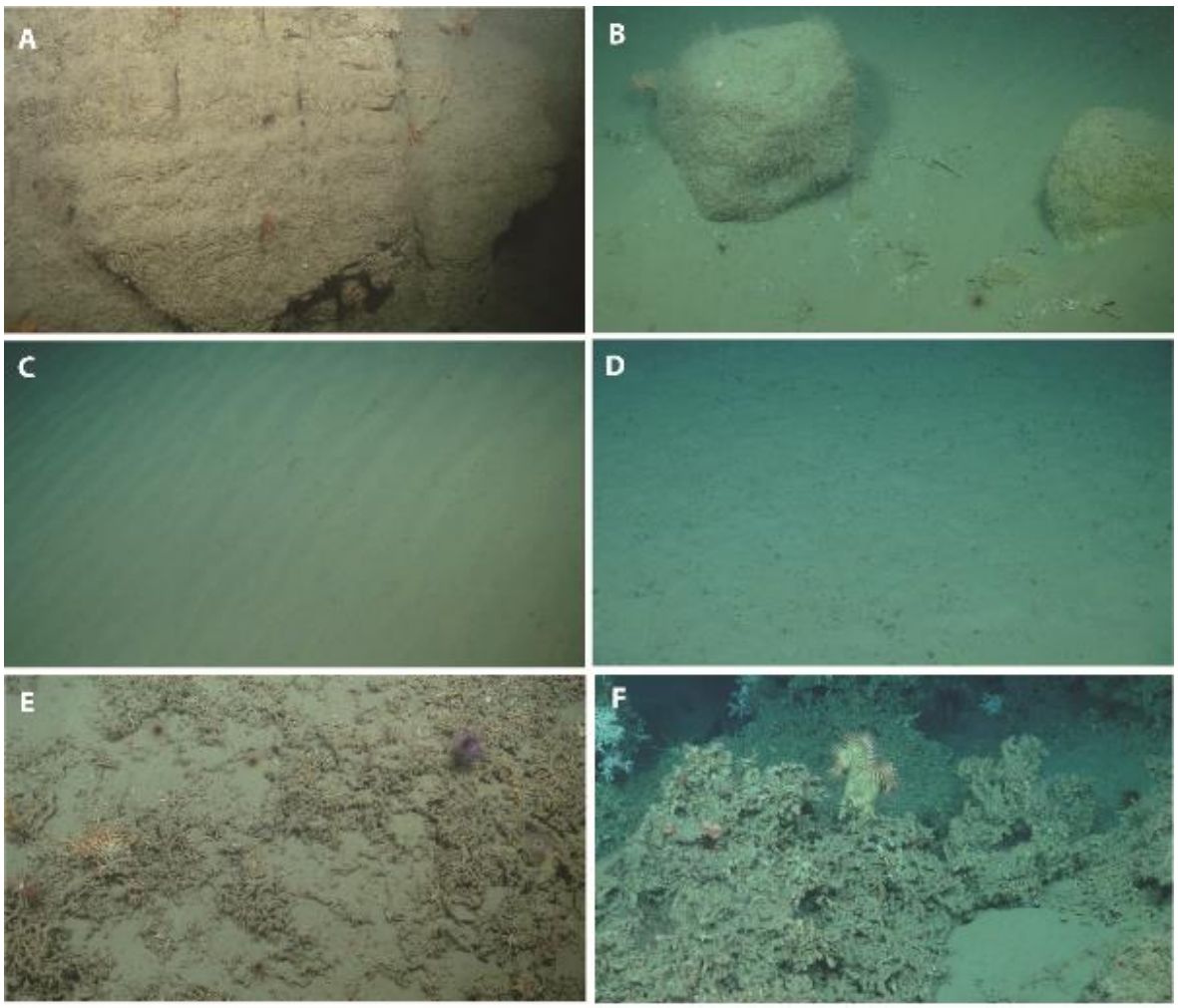


Supplementary materials Figure 3.8 ROV images representing the different substrata classified under the CATAMI classification. (A) H_V.M, Hard substratum with veneer of mud: rock (B) H_MS, Hard substratum with muddy sand (C) S, Sand (D) M, Mud (E) CR, Coral rubble (F) CRF, Coral reef framework.

Appendix B

**3.2 Results supplementary materials**

3.2.1

Spatial and temporal variability within the canyon was assessed by plotting CTD and glider data.

Profiles from cruises JC125, 64PE421, 64PE453 and 64PE437

Profiles from the 64PE421 cruise cover the greatest spatial extent of the canyon (Supplementary materials Figure 3.9). Section plots of the data show spatial variability of the physical oceanographic variables along the canyon axis.

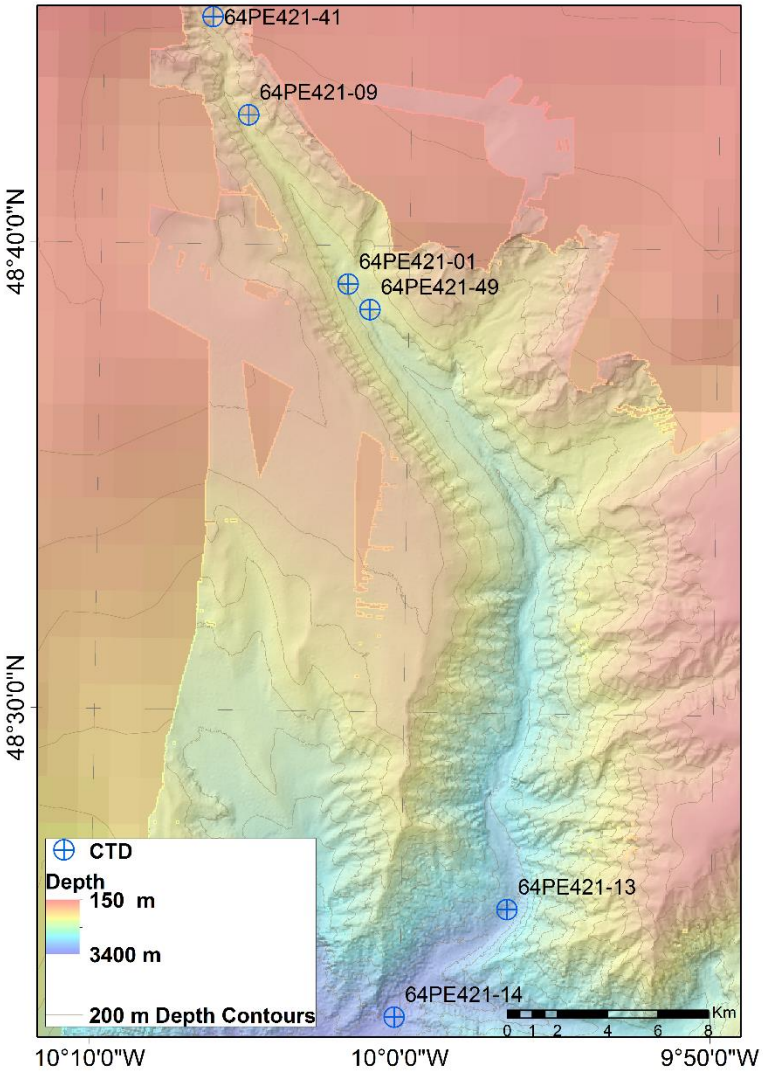


Supplementary materials Figure 3.9 Profile locations from the 64PE421 cruise.

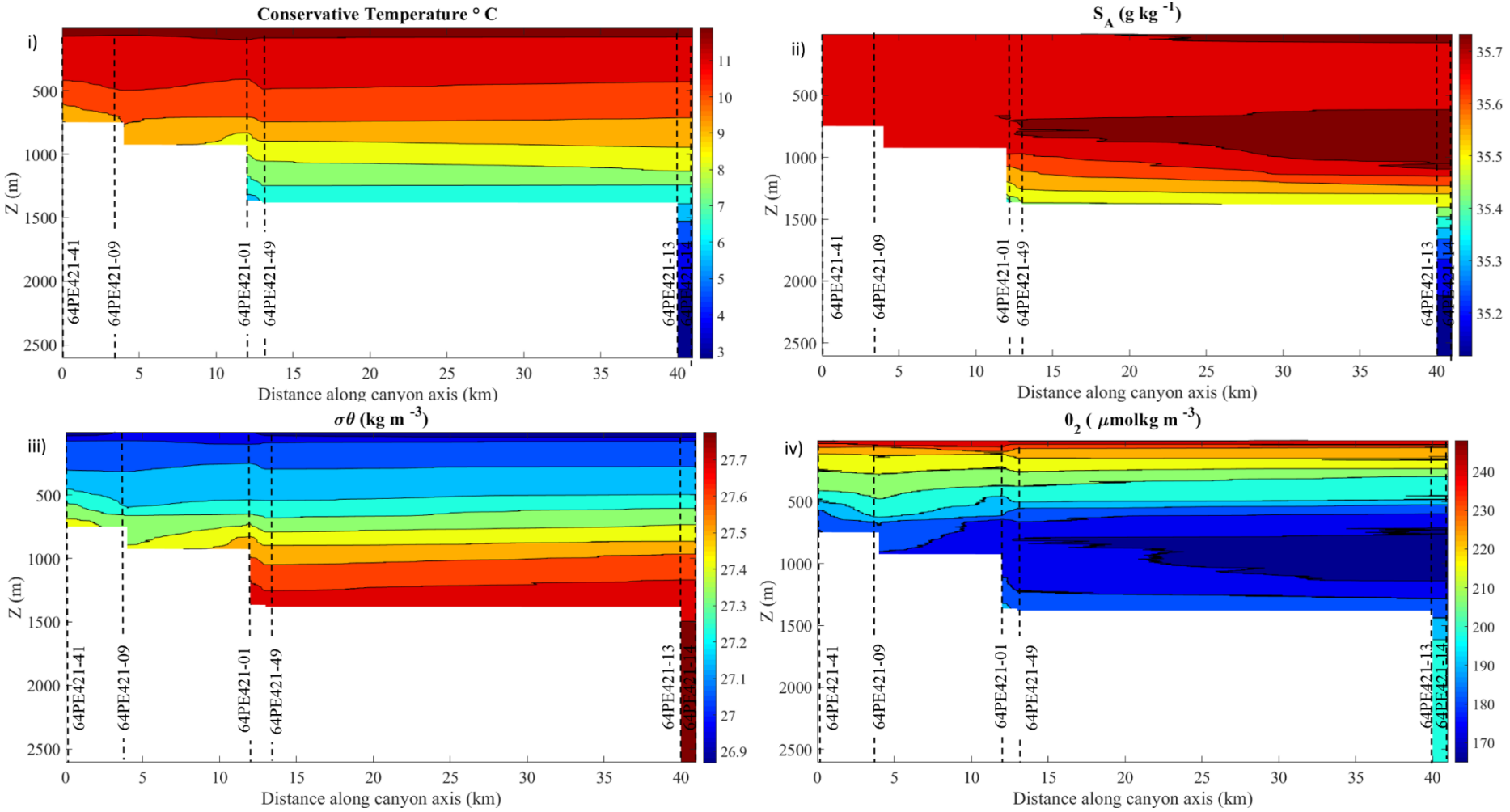
i)
Conservative Temperature ° C
ii)
$S_A$ (g kg $^{-1}$)
iii)
$\sigma\theta$ (kg m $^{-3}$)
iv)
$0_2$ ( $\mu$molkg m $^{-3}$)
Z (m)
Distance along canyon axis (km)
64PE421-41
64PE421-09
64PE421-01
64PE421-49
64PE421-13
64PE421-14

Appendix B

Supplementary materials Figure 3.10 (Page 162) Section plots of Conservative Temperature, Absolute Salinity, Potential Density and Oxygen plotted against z (m) and latitude. The data come from 6 CTD casts (denoted by dashed lines) collected along Whittard Eastern branch canyon axis during the 64PE421 cruise. The data exhibit spatial variability along the canyon axis. The influence of the Mediterranean Outflow Water (MOW), expressed as increased salinity, can be observed from measurements taken lower down the canyon axis but is absent toward the canyon head.

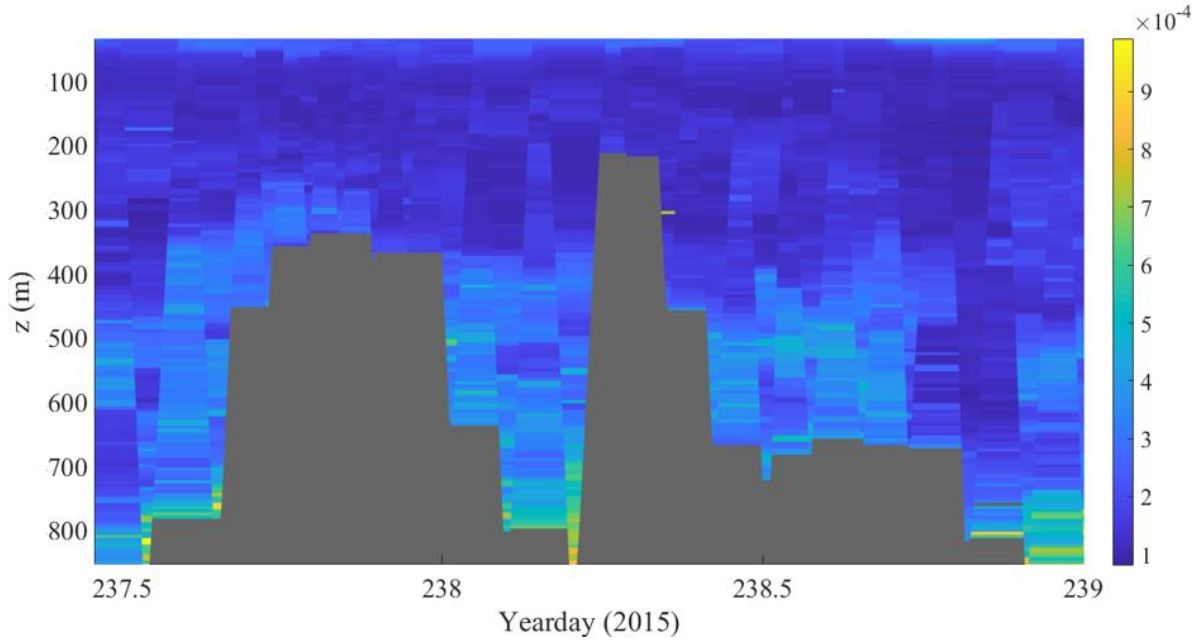


Supplementary materials Figure 3.11 Particulate backscatter $b_{pb}$ at 700 nm ($m^{-1}$) at VM5.

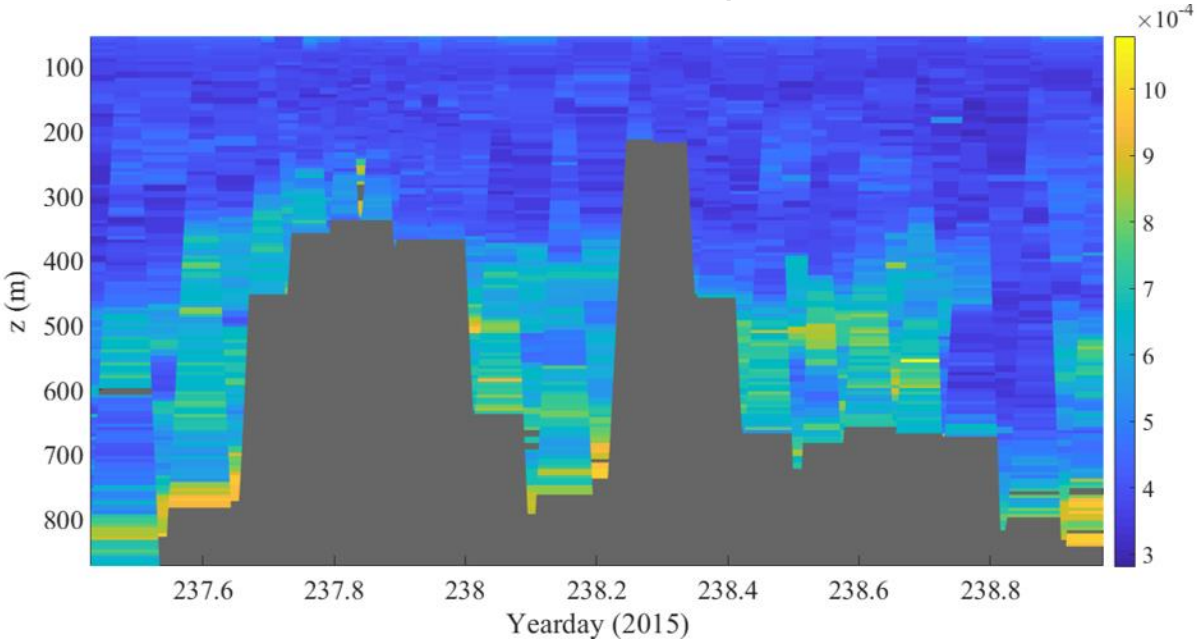


Supplementary materials Figure 3.12 Particulate backscatter $b_{pb}$ at 470 nm ($m^{-1}$) at VM5.

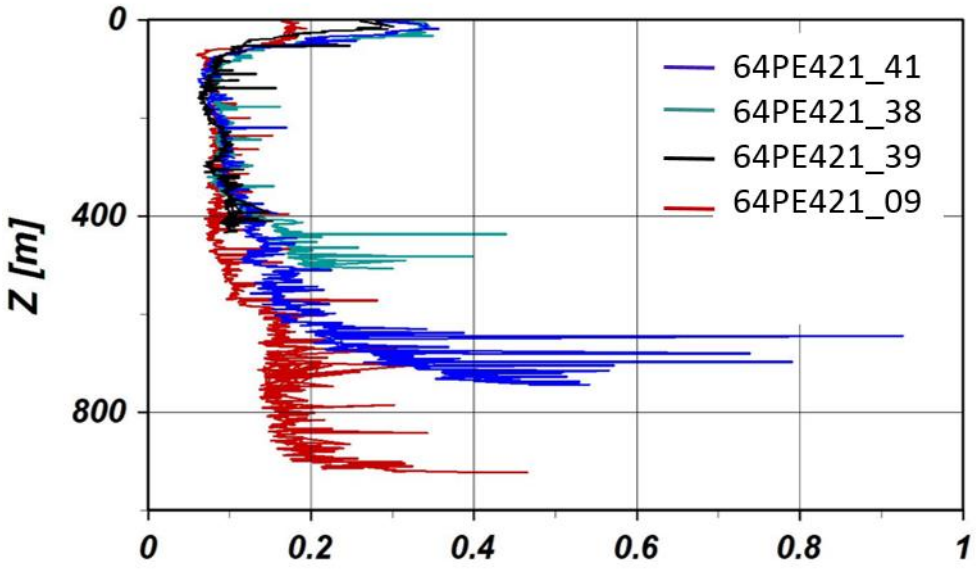


Supplementary materials Figure 3.13 Turbidity measured from CTD casts 64PE421_41, 64PE421_39, 64PE421_38, 64PE421_09.

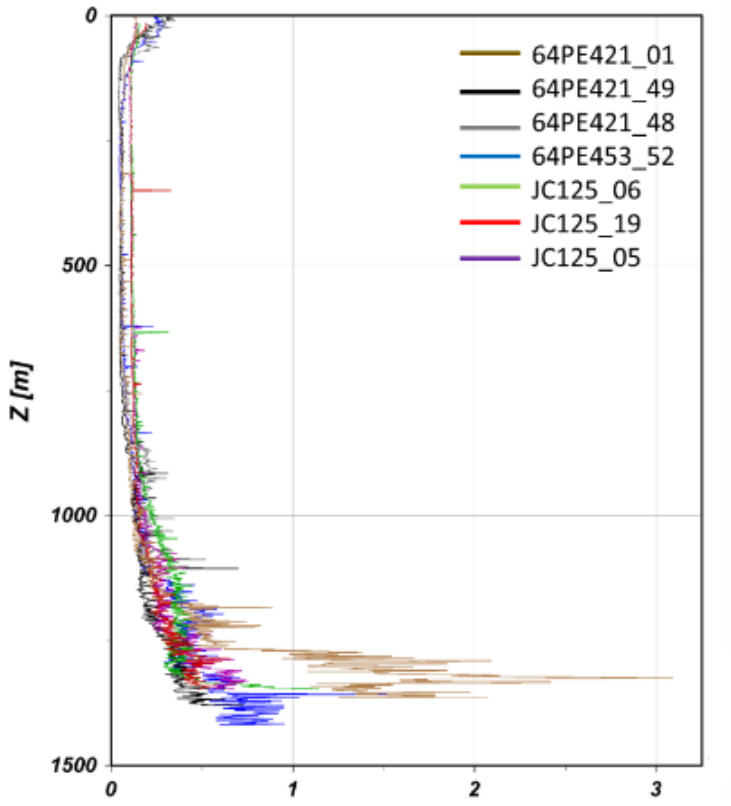


Supplementary materials Figure 3.14 Turbidity measured from CTD casts 64PE421_01, 64PE421_49, 64PE421_48, 64PE453_52, JC125_06, JC125_05 and JC125_19.

Appendix B

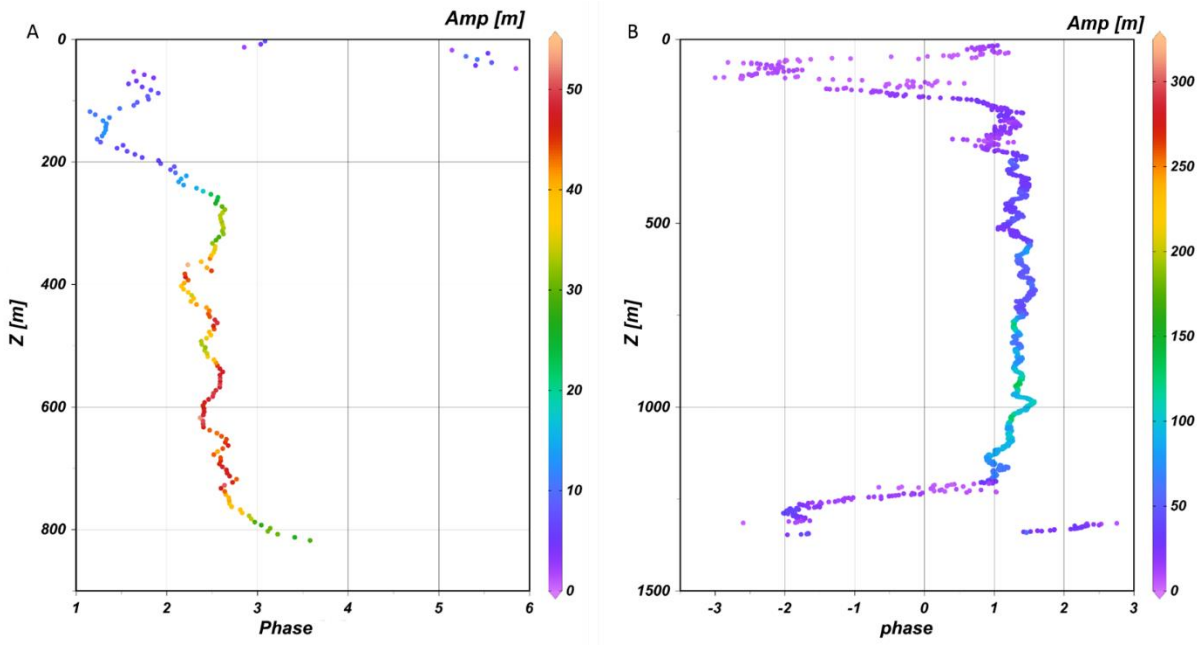


Supplementary materials Figure 3.15. A) $M_2$ vertical isopycnal displacement phase at VM5 with displacement amplitude indicated by colour. B) $M_2$ vertical isopycnal displacement phase at calculated from combined CTD casts.

3.2.2 Supplementary faunal analysis results

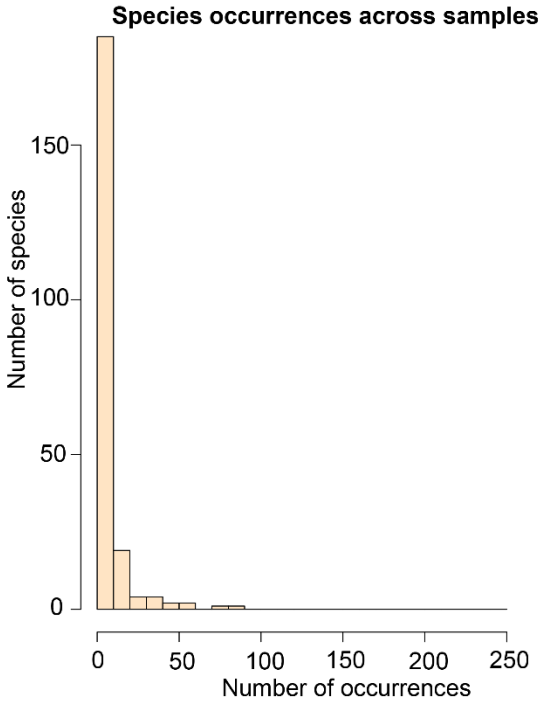


Supplementary materials Figure 3.16. Histogram of species occurrences across samples from all the dives.

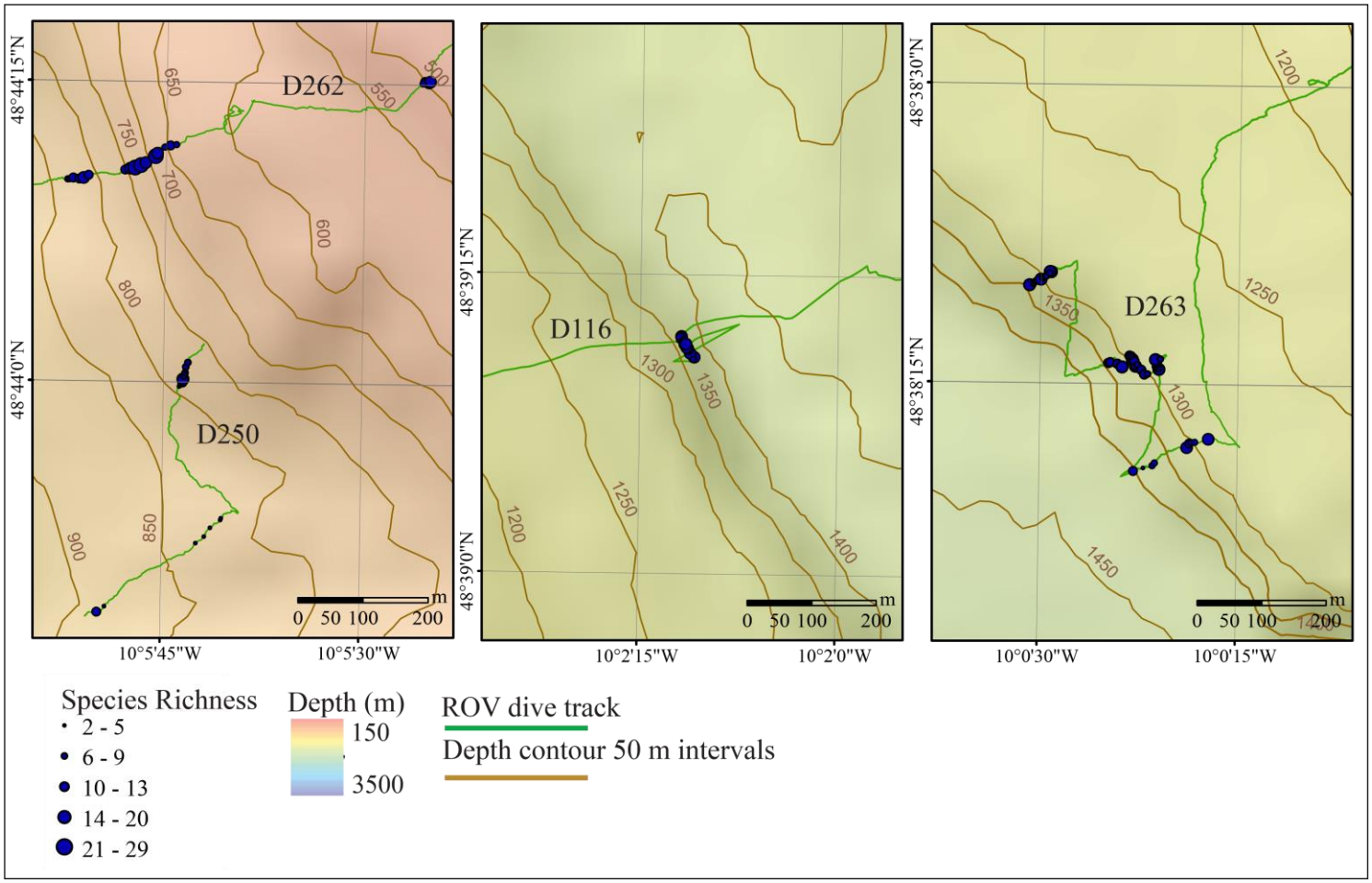


Supplementary materials Figure 3.17 Spatial plot of species richness of vertical wall sample plotted on bathymetry.

Appendix B

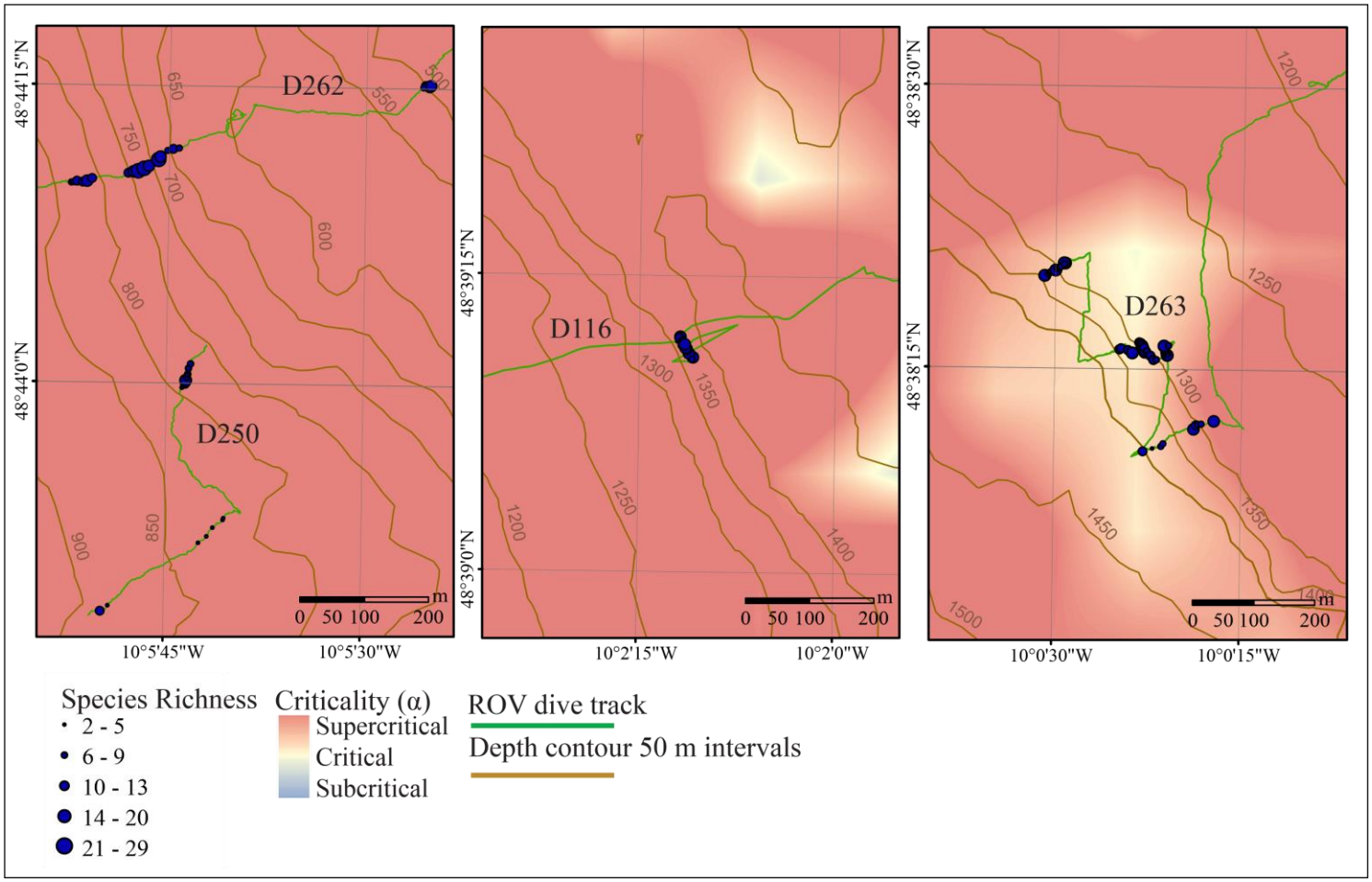


Supplementary materials Figure 3.18 Spatial plot of species richness of vertical wall sample plotted on bathymetric criticality to the $M_2$ tide.

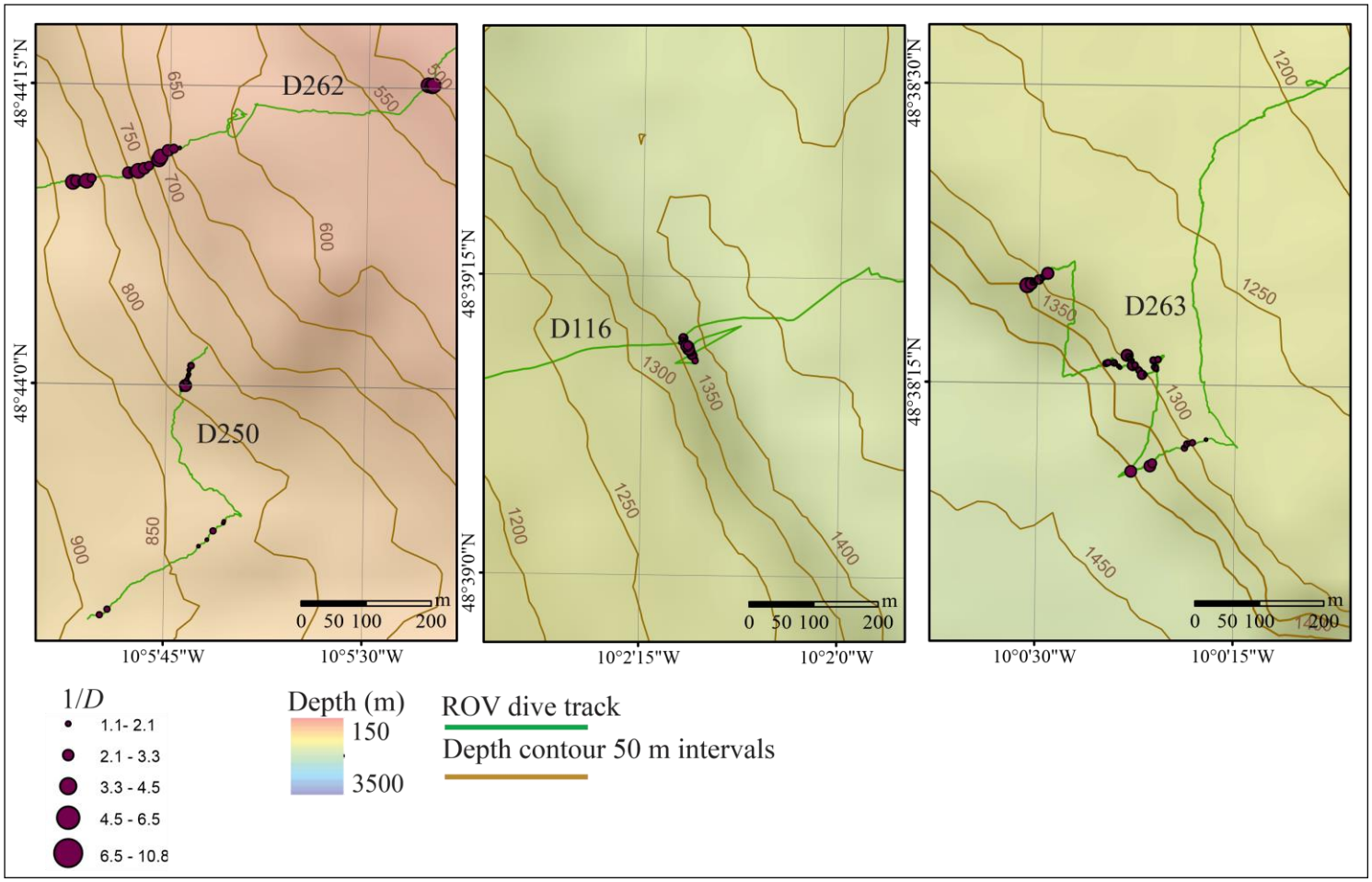


Supplementary materials Figure 3.19 Spatial plot of Simpson's Reciprocal Index (1/*D*) of vertical wall sample plotted on bathymetry.

Appendix B

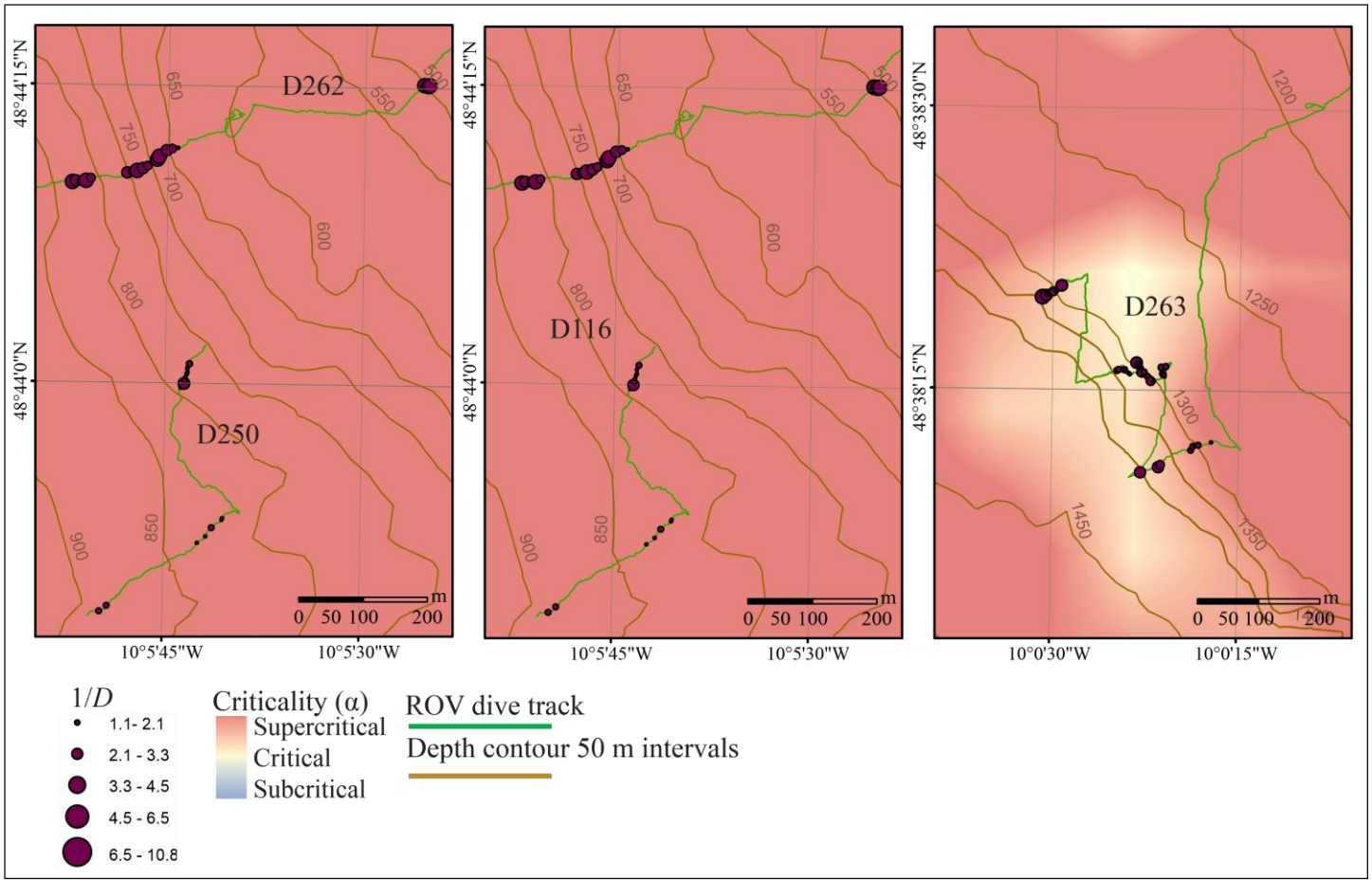


Supplementary materials Figure 3.20 Spatial plot of Simpson's Reciprocal Index (1/*D*) of vertical wall sample plotted on bathymetric criticality to the $M_2$ tide.

Supplementary materials Table 3.1 SIMPER results: Average abundance, their contribution (%) to within group similarity, cumulative total (%) of contributions (90 % cut off).

Group 1
Average similarity: 62.64

| Species | Av.Abund | Contrib% | Cum.% |
|---|---|---|---|
| *Desmophyllum pertusum* | 10.06 | 34.43 | 34.43 |
| *Acesta excavata* | 5.12 | 16.11 | 50.54 |
| Actinaria sp. 10 | 4.34 | 14.37 | 64.9 |
| Cnidaria sp. I29 | 2.55 | 7.64 | 72.55 |
| Red Coral sp. 2 | 2.58 | 5.64 | 78.18 |
| Cnidaria sp. I4 | 1.58 | 4.6 | 82.78 |
| Crinoidea sp. 11 | 2.5 | 3.77 | 86.55 |
| Caryophylliidae sp. | 1.21 | 2.12 | 88.66 |
| *Echinus* sp. 1 | 0.94 | 2.1 | 90.76 |

Group 2
Average similarity: 48.60

| Species | Av.Abund | Contrib% | Cum.% |
|---|---|---|---|
| Brachiopoda sp. 1 | 8.43 | 46.97 | 46.97 |
| Caryophylliidae sp. | 2.75 | 15.45 | 62.42 |
| *Psolus squamatus* | 2.89 | 12.15 | 74.57 |
| Isididae sp. 3 | 2.06 | 8.02 | 82.59 |
| Porifera (Chalice) | 1.23 | 4.94 | 87.53 |
| *Desmophyllum pertusum* | 1.3 | 4.22 | 91.75 |

Group 3
Average similarity: 34.32

| Species | Av.Abund | Contrib% | Cum.% |
|---|---|---|---|
| Cerianthidae sp. | 4.55 | 70.2 | 70.2 |
| *Cidaris cidaris* | 0.84 | 6.51 | 76.71 |
| Antipathidae sp. 1 | 0.83 | 3.3 | 80 |
| Ophiuroidea sp. 1 | 0.69 | 3.01 | 83.01 |
| Caryophylliidae sp. | 0.51 | 2.89 | 85.9 |
| Brisingidae sp. 1 | 0.72 | 2.16 | 88.05 |
| *Desmophyllum pertusum* | 0.57 | 2.1 | 90.16 |

Group 4
Average similarity: 21.72

| Species | Av.Abund | Contrib% | Cum.% |
|---|---|---|---|
| Caryophylliidae sp. | 1.57 | 100 | 100 |

Group 5
Average similarity: 40.80

| Species | Av.Abund | Contrib% | Cum.% |
|---|---|---|---|
| *Echinus* sp. 1 | 1.63 | 55.02 | 55.02 |
| *Acanella* sp. 1 | 0.67 | 12.29 | 67.31 |
| Caryophylliidae sp. | 0.8 | 12.29 | 79.6 |
| *Desmophyllum pertusum* | 0.67 | 10.2 | 89.8 |
| Asteroidea sp. 8 | 0.91 | 10.2 | 100 |

Appendix B

Group 6
Average similarity: 49.87

| Species | Av.Abund | Contrib% | Cum.% |
|---|---|---|---|
| Porifera sp. 13 | 6.19 | 16.82 | 16.82 |
| Antipathidae sp. 1 | 3.74 | 10.77 | 27.58 |
| Actinaria sp. 14 | 3.4 | 9.7 | 37.28 |
| *Cidaris* | 2.18 | 7.72 | 45 |
| Serpulidae | 1.7 | 6.36 | 51.37 |
| Cyclostomatida | 1.97 | 5.55 | 56.92 |
| Cerianthidae sp. | 3.11 | 5.39 | 62.31 |
| Porifera sp. 18 | 2.24 | 4.65 | 66.96 |
| Actinaria sp. 19 | 1.8 | 4.06 | 71.02 |
| *Psolus squamatus* | 2.05 | 2.85 | 73.87 |
| Caryophylliidae sp. | 1.21 | 2.63 | 76.51 |
| Sabellidae | 1.11 | 2.48 | 78.99 |
| Turbinidae sp. 1 | 1 | 2.36 | 81.35 |
| Alcyonacea sp. 7 | 1.16 | 2.28 | 83.63 |
| *Bathynectes* sp. 1 | 0.75 | 2.06 | 85.68 |
| Actinaria sp. 13 | 0.85 | 1.86 | 87.55 |
| Asterinidae sp. 1 | 0.75 | 1.86 | 89.41 |

Group 7
Average similarity: 50.50

| Species | Av.Abund | Contrib% | Cum.% |
|---|---|---|---|
| *Neopycnodonte* sp. | 3.5 | 14.43 | 14.43 |
| *Leptometra celtica* | 3.26 | 11.06 | 25.48 |
| Munididae sp. 1 | 2.51 | 9.76 | 35.25 |
| Caryophylliidae sp. | 2.67 | 7.47 | 42.72 |
| *Cidaris cidaris* | 2.21 | 7.32 | 50.04 |
| *Madrepora oculata* | 2.12 | 7.08 | 57.12 |
| Asterinidae sp. 1 | 1.33 | 7.04 | 64.16 |
| Porifera sp. 11 | 1.39 | 6.88 | 71.04 |
| Zoanthidea | 1.52 | 4.35 | 75.39 |
| Crinoidea sp. | 1.97 | 3.92 | 79.31 |
| *Desmophyllum pertusum* | 1.03 | 3.76 | 83.07 |
| Porifera sp. 14 | 0.97 | 3.69 | 86.76 |
| *Bathynectes* sp. 1 | 0.88 | 3.54 | 90.3 |

Group 8
Less than 2 samples in group

Group 9
Less than 2 samples in group

4.2.3 Modelling results

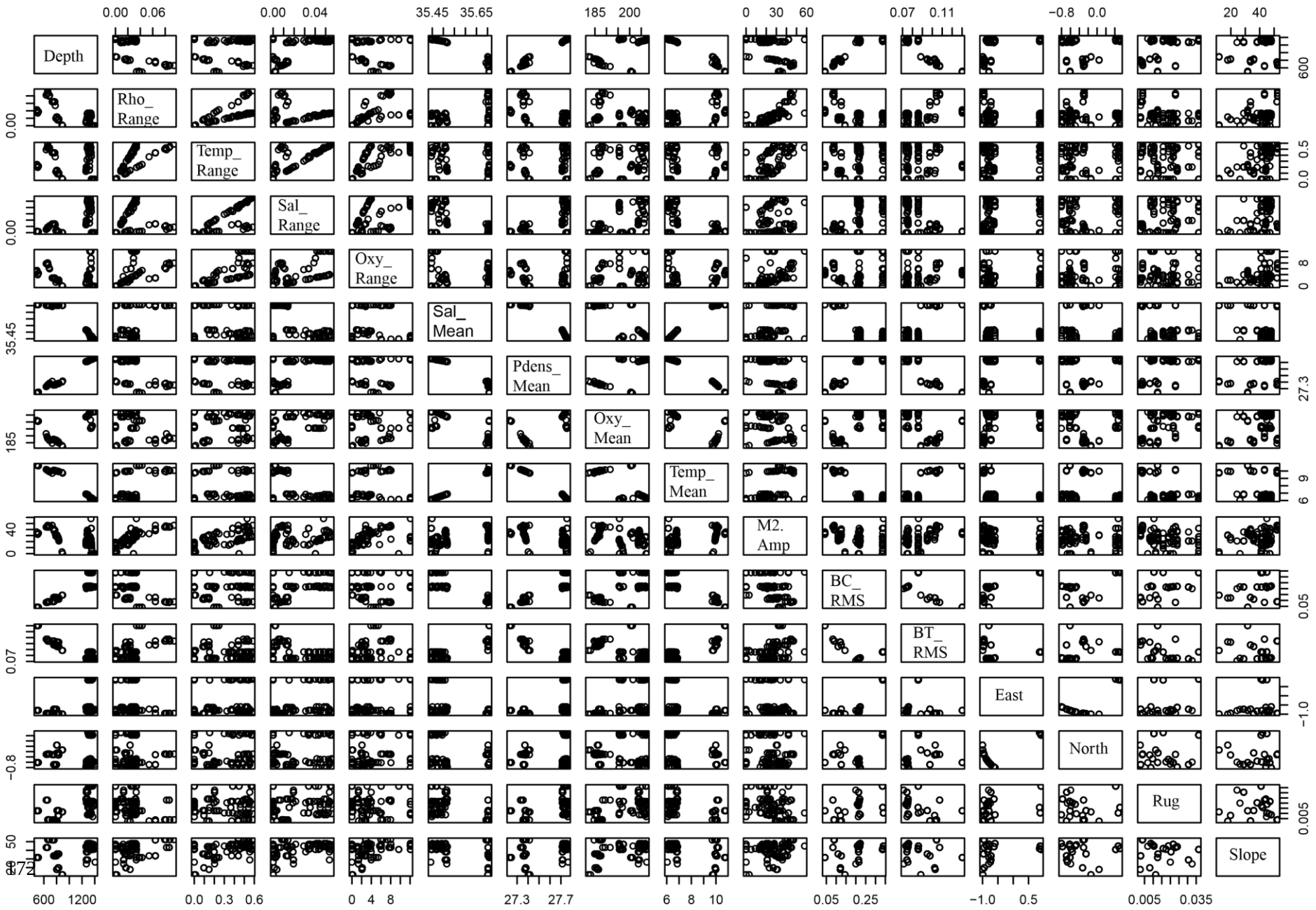
Depth
Rho_ Range
Temp_ Range
Sal_ Range
Oxy_ Range
Sal_ Mean
Pdens_ Mean
Oxy_ Mean
Temp_ Mean
M2. Amp
BC_ RMS
BT_ RMS
East
North
Rug
Slope

Appendix B

Supplementary materials Figure 3.21 (Page 172) Pairs plot for environmental variables used in model selection. Rho_Range = Range in density, Temp_Range = Range in temperature, Sal_Range = Range in Salinity, Oxy_Range= Range in oxygen, Sal_Mean = Mean salinity, Pdens_Mean = means density, Oxy_Mean = mean oxygen, Temp_Mean = Mean temperature, M2. Amp = Amplitude of the M2 internal tide, BC_RMS = Root mean current speed of baroclinic tide, BT_RMS = Root mean squared current speed of barotorpic tide, East = Eastness, North = Northness, Rug = Rugosity.

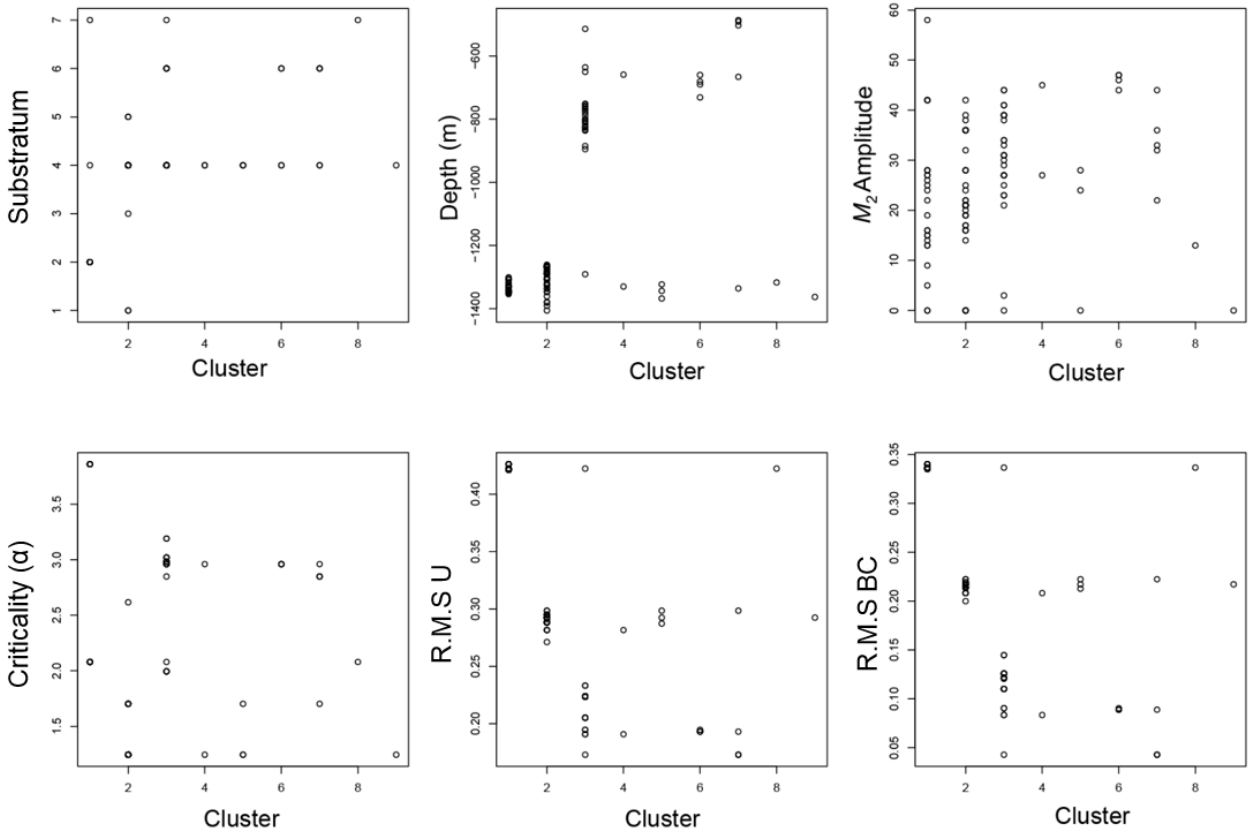


Supplementary materials Figure 3.22. The nine assemblages identified from multivariate hierarchal clustering analysis plotted against environmental variables identified by RDA analysis as key factors driving assemblage patterns (Substratum, depth (m), $M_2$ Amplitude (m), bathymetric criticality to the $M_2$ tide. Additionally assemblages have also been plotted against root mean current speed of the summed barotropic and baroclinic tide, U (m $s^{-1}$) and root mean current speed of the baroclinic $M_2$ tide. BC (m $s^{-1}$).

Supplementary materials Table 3.2 Results from RDA performed on Hellinger transformed species data and spatial coordinates reveal that there is a spatial trend in the species data. Significance ***p ≤ 0.001, **p ≤ 0.01, *p ≤ 0.05, •p ≤ 0.1

| Significance of individual terms by ANOVA | Adjusted $R^2$ | Significance of RDA plot by ANOVA | |
|---|---|---|---|
| | | F-value | p-value |
| X coordinate **, Y coordinate ** | 45% | 49.331, df=2, 115 | 0.001 |

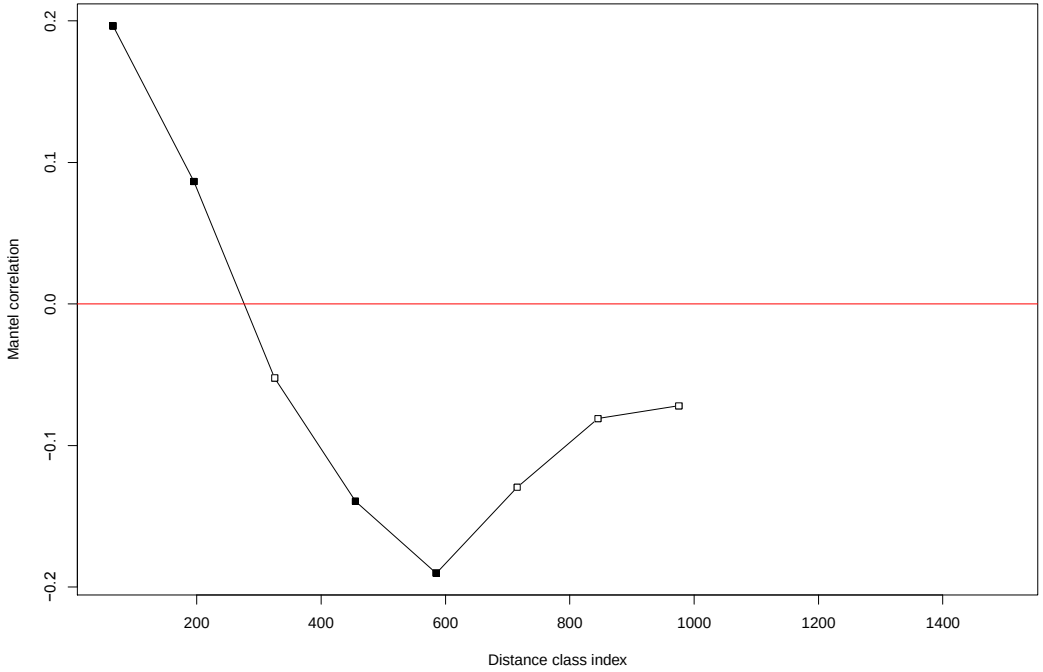


Supplementary materials Figure 3.23 Mantel correlogram of detrended species data for vertical walls Holm correction for multiple testing. The Mantel correlogram of the detrended species data shows significant positive spatial correlation in the first two distance classes (i.e. <200 m) and negative significant spatial correlation between the fourth and fifth distances classes (>450 m).

# Appendix C Chapter 4 Supplementary materials

### 4.1 Methods supplementary materials

4.1.1. Derivation of terrain variables

Supplementary materials Figure 4.1(Page 176) Maps (25 m pixel resolution) of the bathymetric derivatives used as environmental variables in the model selection coinciding with spatial extent of sidescan sonar collected from the Explorer interfluve. (A): Depth (m), (B): Slope ($^{o}$), (C): General curvature (D): Planar curvature (E): Profile curvature (F): Northness (F): Eastness (G): Fine scale bathymetric position index (FBPI) with an inner radius of one and outer radius of three.

Supplementary materials Figure 4.2 (Page 177) Maps (25 m pixel resolution) of the bathymetric derivatives used as environmental variables in the model selection coinciding with spatial extent of sidescan sonar collected from the Explorer interfluve. (A): Ruggedness derived with window size of 33, (B): Ruggedness derived with window size of 17 (C): Ruggedness derived with window size of nine (D): Ruggedness derived with window size of five (E): Ruggedness derived with window size of three (F): Bathymetric position index (BPI) with an inner radius of one and outer radius of 33 (G): Bathymetric position index (BBPI) with an inner radius of one and outer radius of 17 (H): Bathymetric position index (BBPI) with an inner radius of one and outer radius of nine (I): Fine scale bathymetric position index (BBPI) with an inner radius of one and outer radius of five.

Supplementary materials Figure 4.3 (Page 178) Maps (25 m pixel resolution) of the bathymetric derivatives used as environmental variables in the model selection coinciding with spatial extent of sidescan sonar collected from the Dangaard interfluve. (A): Depth (m), (B): Slope ($^{o}$), (C): General curvature (D): Planar curvature (E): Profile curvature (F): Northness (F): Eastness (G): Fine scale bathymetric position index (BBPI) with an inner radius of one and outer radius of three.

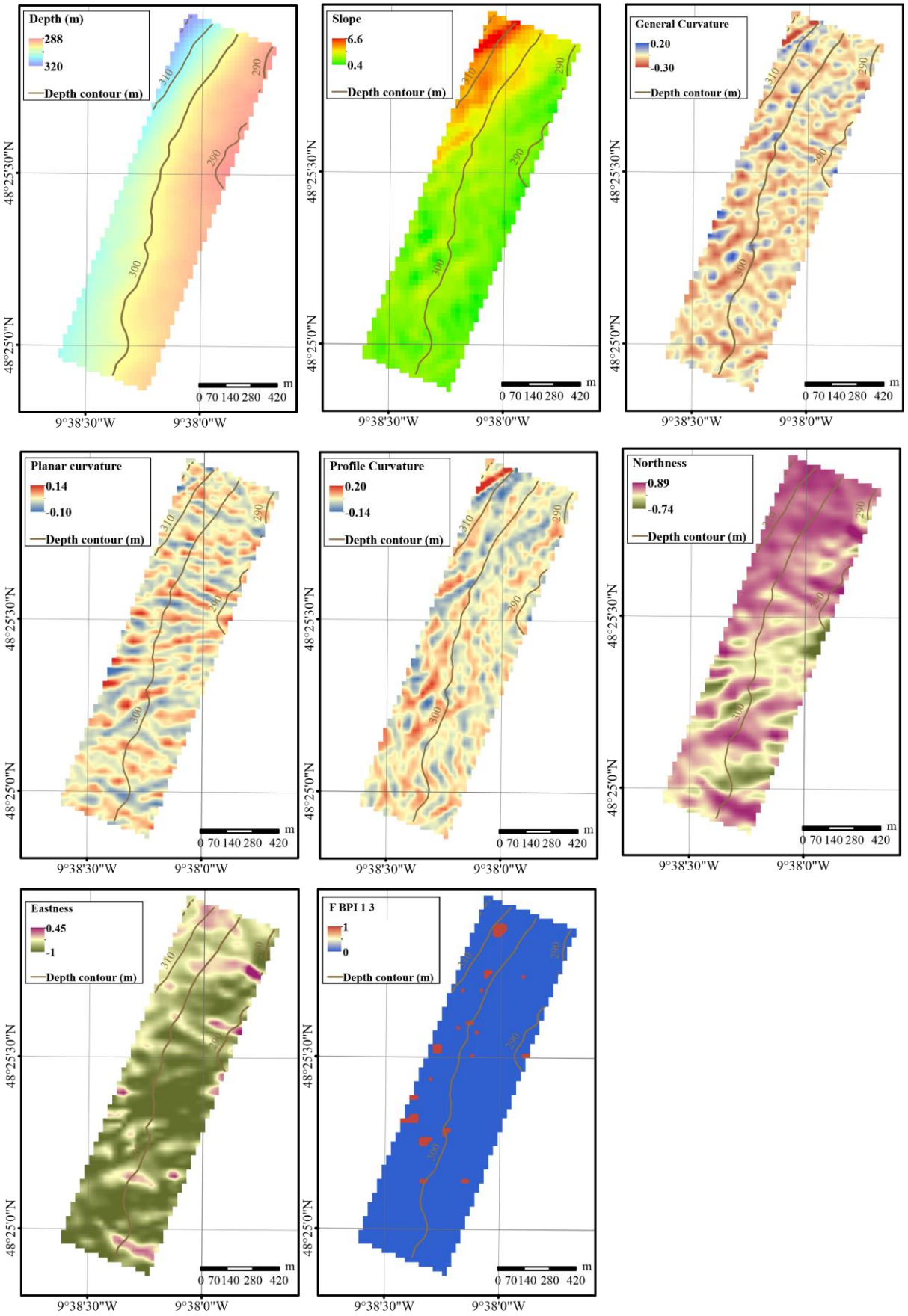
Depth (m)
288
320
Depth contour (m)
Slope
6.6
0.4
Depth contour (m)
General Curvature
0.20
-0.30
Depth contour (m)
Planar curvature
0.14
-0.10
Depth contour (m)
Profile Curvature
0.20
-0.14
Depth contour (m)
Northness
0.89
-0.74
Depth contour (m)
Eastness
0.45
-1
Depth contour (m)
F BPI 1 3
1
0
Depth contour (m)
48°25'30"N
48°25'0"N
9°38'30"W
9°38'0"W
0 70 140 280 420
m

Appendix C

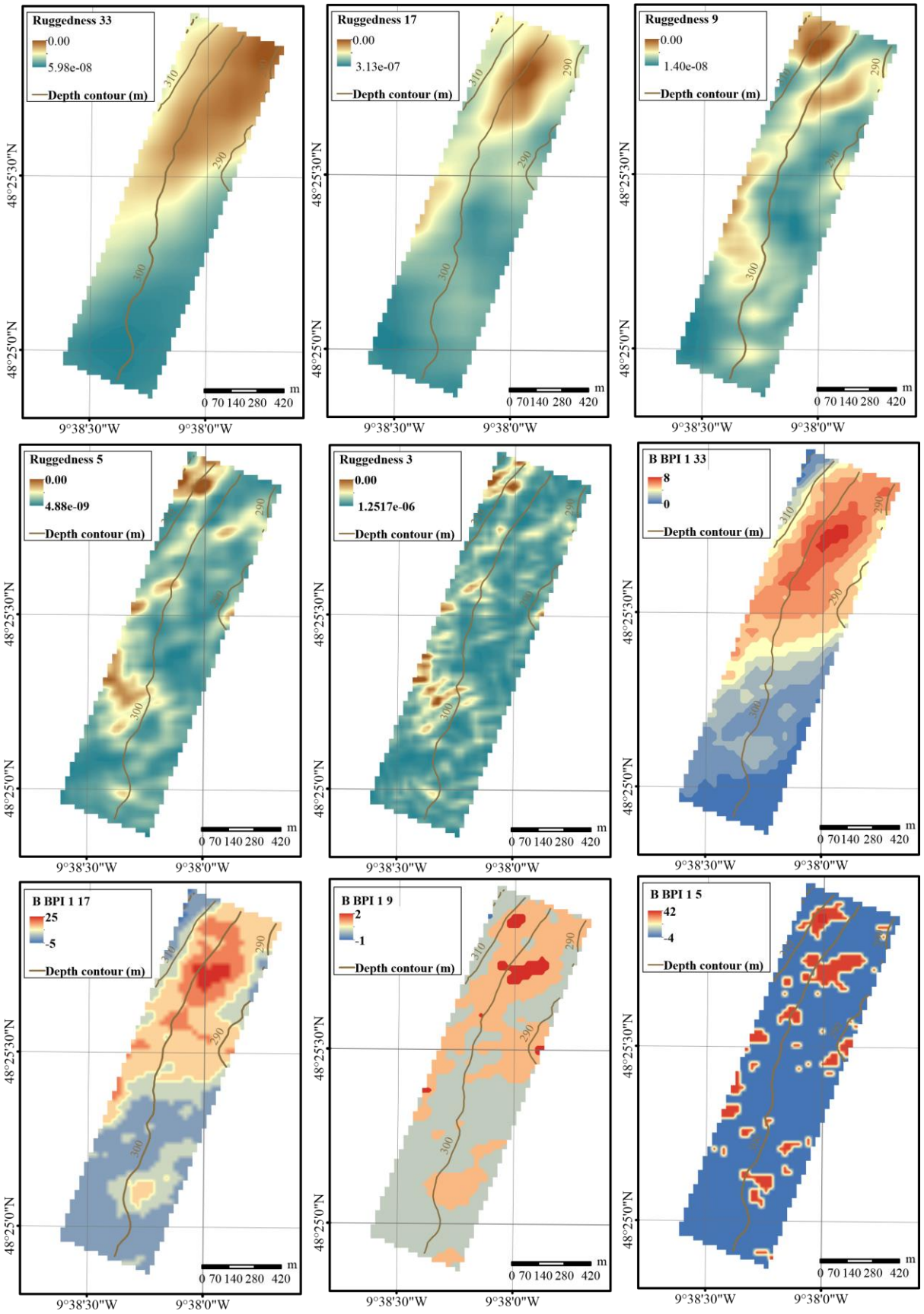
Ruggedness 33
0.00
5.98e-08
Depth contour (m)
Ruggedness 17
0.00
3.13e-07
Depth contour (m)
Ruggedness 9
0.00
1.40e-08
Depth contour (m)
Ruggedness 5
0.00
4.88e-09
Depth contour (m)
Ruggedness 3
0.00
1.2517e-06
Depth contour (m)
B BPI 1 33
8
0
Depth contour (m)
B BPI 1 17
25
-5
Depth contour (m)
B BPI 1 9
2
-1
Depth contour (m)
B BPI 1 5
42
-4
Depth contour (m)
48°25'30"N
48°25'0"N
9°38'30"W
9°38'0"W
0 70 140 280 420
m

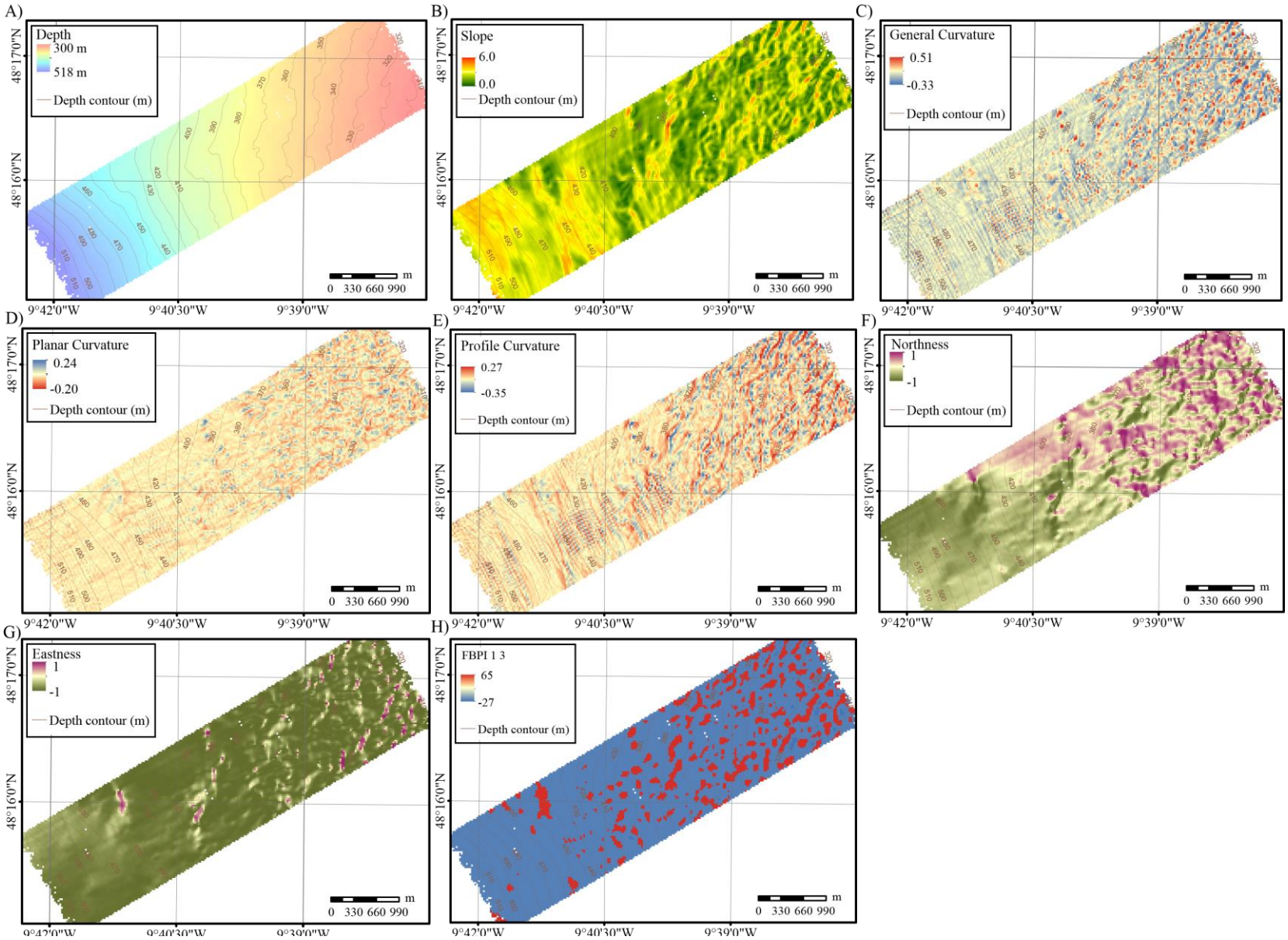
A)
Depth
300 m
518 m
Depth contour (m)
B)
Slope
6.0
0.0
Depth contour (m)
C)
General Curvature
0.51
-0.33
Depth contour (m)
D)
Planar Curvature
0.24
-0.20
Depth contour (m)
E)
Profile Curvature
0.27
-0.35
Depth contour (m)
F)
Northness
1
-1
Depth contour (m)
G)
Eastness
1
-1
Depth contour (m)
H)
FBPI 1 3
65
-27
Depth contour (m)
48°17'0"N
48°16'0"N
9°42'0"W
9°40'30"W
9°39'0"W
m
0 330 660 990

Appendix C

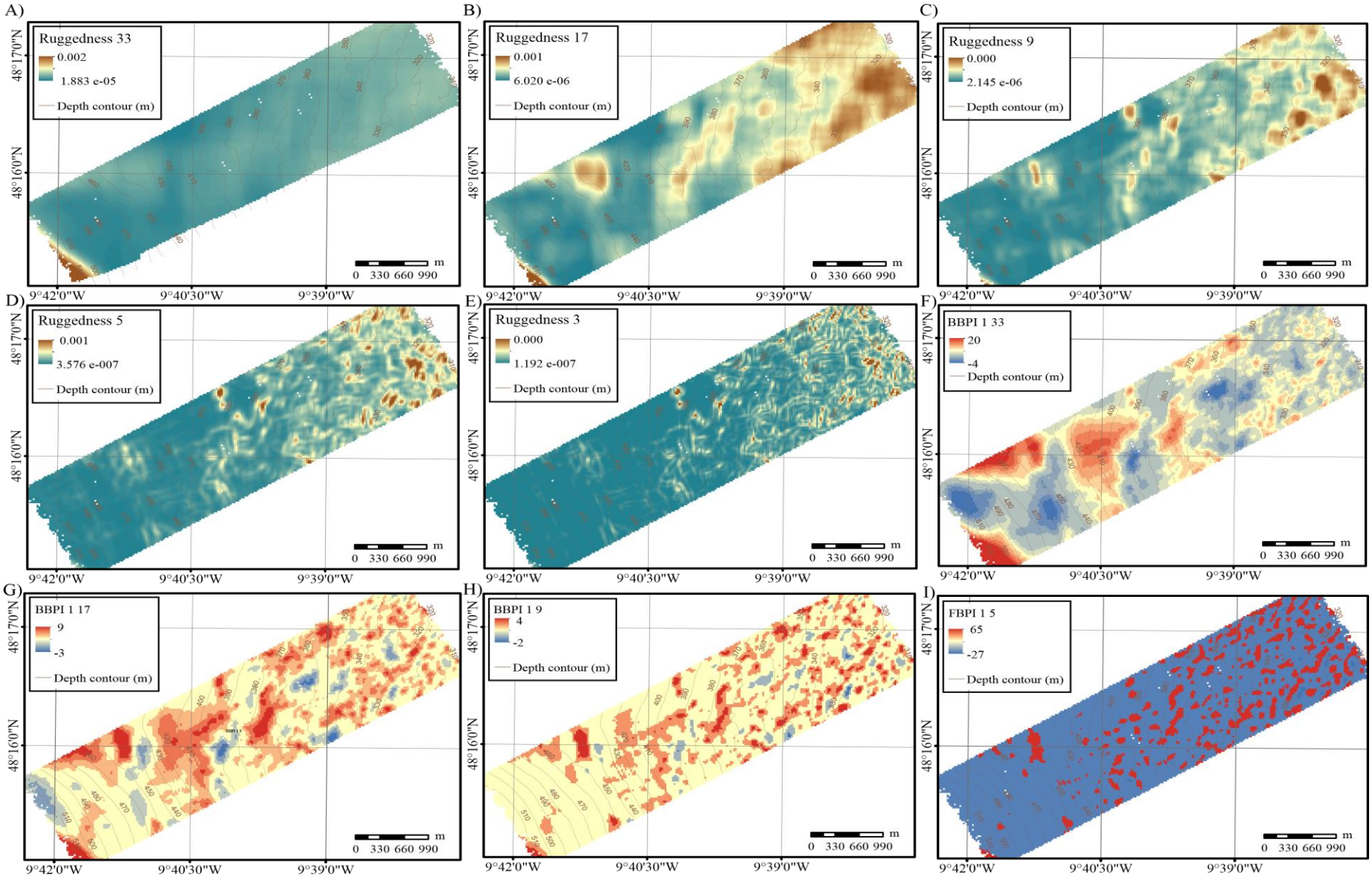
A)
Ruggedness 33
0.002
1.883 e-05
Depth contour (m)
B)
Ruggedness 17
0.001
6.020 e-06
Depth contour (m)
C)
Ruggedness 9
0.000
2.145 e-06
Depth contour (m)
D)
Ruggedness 5
0.001
3.576 e-007
Depth contour (m)
E)
Ruggedness 3
0.000
1.192 e-007
Depth contour (m)
F)
BBPI 1 33
20
-4
Depth contour (m)
G)
BBPI 1 17
9
-3
Depth contour (m)
H)
BBPI 1 9
4
-2
Depth contour (m)
I)
FBPI 1 5
65
-27
Depth contour (m)
48°17'0"N
48°16'0"N
9°42'0"W
9°40'30"W
9°39'0"W
m
0 330 660 990

Supplementary materials Figure.4.4 (Page 179) Maps (25 m pixel resolution) of the bathymetric derivatives used as environmental variables in the model selection coinciding with spatial extent of sidescan sonar collected from the Dangaard interfluve. (A): Ruggedness derived with window size of 33, (B): Ruggedness derived with window size of 17 (C): Ruggedness derived with window size of nine (D): Ruggedness derived with window size of five (E): Ruggedness derived with window size of three (F): Bathymetric position index (BPI) with an inner radius of one and outer radius of 33 (G): Bathymetric position index (BBPI) with an inner radius of one and outer radius of 17 (H): Bathymetric position index (BBPI) with an inner radius of one and outer radius of nine (I): Fine scale bathymetric position index (BBPI) with an inner radius of one and outer radius of five.

4.1.2 Multi Scale Analysis

To further our understanding of the resolution at which structural complexity influences faunal assemblages, derivatives of bathymetric position index (BPI) and ruggedness were created at neighbourhoods ($_{nh}$) of 3, 5, 9, 17 and 33 and a multi-scale analysis performed to identify which resolution explains most variation in fauna data (Misiuk et al., 2018, Porskamp et al., 2018).

Two approaches were adopted for the multi-scale analysis. First, all terrain derivative variables were modelled simultaneously by canonical Redundancy Analysis (RDA) (Supplementary materials Figure 4.6) with Hellinger transformed species data, using forward selection and variance inflation factor (VIF) scores, with the highest ranking variables that were <0.7 correlated retained (Supplementary materials Figures 4.6 and Supplementary materials Tables 4.1- 4.4). Second, Random forests (RF) and Boosted Regression Trees (BRT) were used to model cluster membership, following cluster analysis of the species data (detailed in chapter 4 of this thesis section 4.3.6). RF and BRT were used to account for any non-linear relationships among environmental variables. The terrain derivatives were modelled separately but at all resolutions in order to rank the contribution of each variable at the different resolutions (Supplementary materials Figure 4.7 and 4.8 following the protocol in Misiuk et al., (2018). Additionally, all the terrain variables were assessed simultaneously to account for potential interactions or correlation between the variables (Supplementary materials Figure 4.9). Terrain variables that contributed > 10 % to overall variance explained by the model and were < 0.7 correlated were retained (Supplementary materials Figures 4.7-4.9 and Supplementary materials Table 4.1). Results show high collinearity present among many of the terrain derivatives (Supplementary materials Table 4.1. and Supplementary materials Figure 4.5). The terrain derivatives BPI and ruggedness were collinear, as were measures of curvature. In each correlated group the terrain derivative that explained the greatest variance was retained (Supplementary materials Figure 4. 9).

Following the multi scale analysis the terrain derivatives depth, slope, Northness, Eastness, ruggedness created from neighbourhoods of 17 and three were retained.

Appendix C

Supplementary materials Table 4.1 Pearson's correlation between terrain derivatives. Abbreviations: FBPI = Fine bathymetric position index, BBPI = Broad bathymetric position index, created at neighbourhoods of 3, 5, 9, 17 and 33, Rug = Ruggedness created at neighbourhoods of 3, 5, 9, 17 and 33, North= Northness, East = Eastness, Curv= Curvature.

| | Depth | Slope | Curv | Planar Curv | Profile Curv | North | East | FBPI 1 3 | FBPI 1 5 | BBPI 1 17 | BBPI 1 9 | BPI 1 33 | Rug 3 | Rug 5 | Rug 9 | Rug 17 | Rug 33 |
|---|---|---|---|---|---|---|---|---|---|---|---|---|---|---|---|---|---|
| Depth | 1 | | | | | | | | | | | | | | | | |
| Slope | -0.11 | 1.00 | | | | | | | | | | | | | | | |
| Curv | 0.01 | 0.12 | 1.00 | | | | | | | | | | | | | | |
| Planar Curv | 0.04 | 0.14 | 0.84 | 1.00 | | | | | | | | | | | | | |
| Profile Curv | 0.00 | -0.08 | -0.92 | -0.55 | 1.00 | | | | | | | | | | | | |
| North | -0.55 | 0.47 | 0.06 | 0.06 | -0.04 | 1.00 | | | | | | | | | | | |
| East | 0.25 | -0.15 | -0.12 | -0.19 | 0.05 | -0.23 | 1.00 | | | | | | | | | | |
| FBPI 1 3 | 0.10 | 0.03 | 0.69 | 0.68 | -0.55 | 0.08 | -0.14 | 1.00 | | | | | | | | | |
| FBPI 1 5 | 0.10 | 0.01 | 0.78 | 0.70 | -0.69 | -0.01 | 0.04 | 0.71 | 1.00 | | | | | | | | |
| BBPI 1 17 | -0.12 | 0.29 | 0.39 | 0.21 | -0.44 | 0.27 | 0.13 | 0.17 | 0.37 | 1.00 | | | | | | | |
| BBPI 1 9 | -0.01 | 0.16 | 0.62 | 0.40 | -0.65 | 0.15 | 0.18 | 0.37 | 0.64 | 0.79 | 1.00 | | | | | | |
| BPI 1 33 | -0.18 | 0.45 | 0.19 | 0.04 | -0.26 | 0.40 | 0.15 | 0.02 | 0.14 | 0.87 | 0.57 | 1.00 | | | | | |
| Rug 3 | 0.12 | -0.01 | 0.14 | 0.40 | 0.07 | 0.04 | -0.13 | 0.54 | 0.29 | -0.18 | -0.12 | -0.20 | 1.00 | | | | |
| Rug 5 | 0.05 | 0.07 | -0.01 | 0.26 | 0.20 | 0.02 | -0.07 | 0.34 | 0.12 | -0.30 | -0.25 | -0.28 | 0.91 | 1.00 | | | |
| Rug 9 | 0.06 | 0.12 | -0.05 | 0.20 | 0.21 | 0.00 | 0.03 | 0.22 | 0.11 | -0.30 | -0.23 | -0.27 | 0.77 | 0.94 | 1.00 | | |
| Rug 17 | 0.17 | 0.25 | 0.08 | 0.17 | 0.00 | 0.04 | 0.25 | 0.25 | 0.22 | 0.11 | 0.11 | 0.14 | 0.60 | 0.71 | 0.81 | 1.00 | |
| Rug 33 | 0.19 | 0.39 | 0.05 | 0.11 | 0.00 | 0.25 | 0.24 | 0.18 | 0.11 | 0.34 | 0.17 | 0.52 | 0.41 | 0.45 | 0.51 | 0.81 | 1.00 |

Supplementary material Figure 4.5 (Page 182) Pairs plot for environmental variables used in model selection of terrain variables, FBPI = Fine Bathymetric position index, BPI = Bathymetric position index created at neighbourhoods of 3, 5, 9, 17 and 33, R = Ruggedness created at neighbourhoods of 3, 5, 9, 17 and 33, Curv = Curvature and Plan = Planar Curvature.

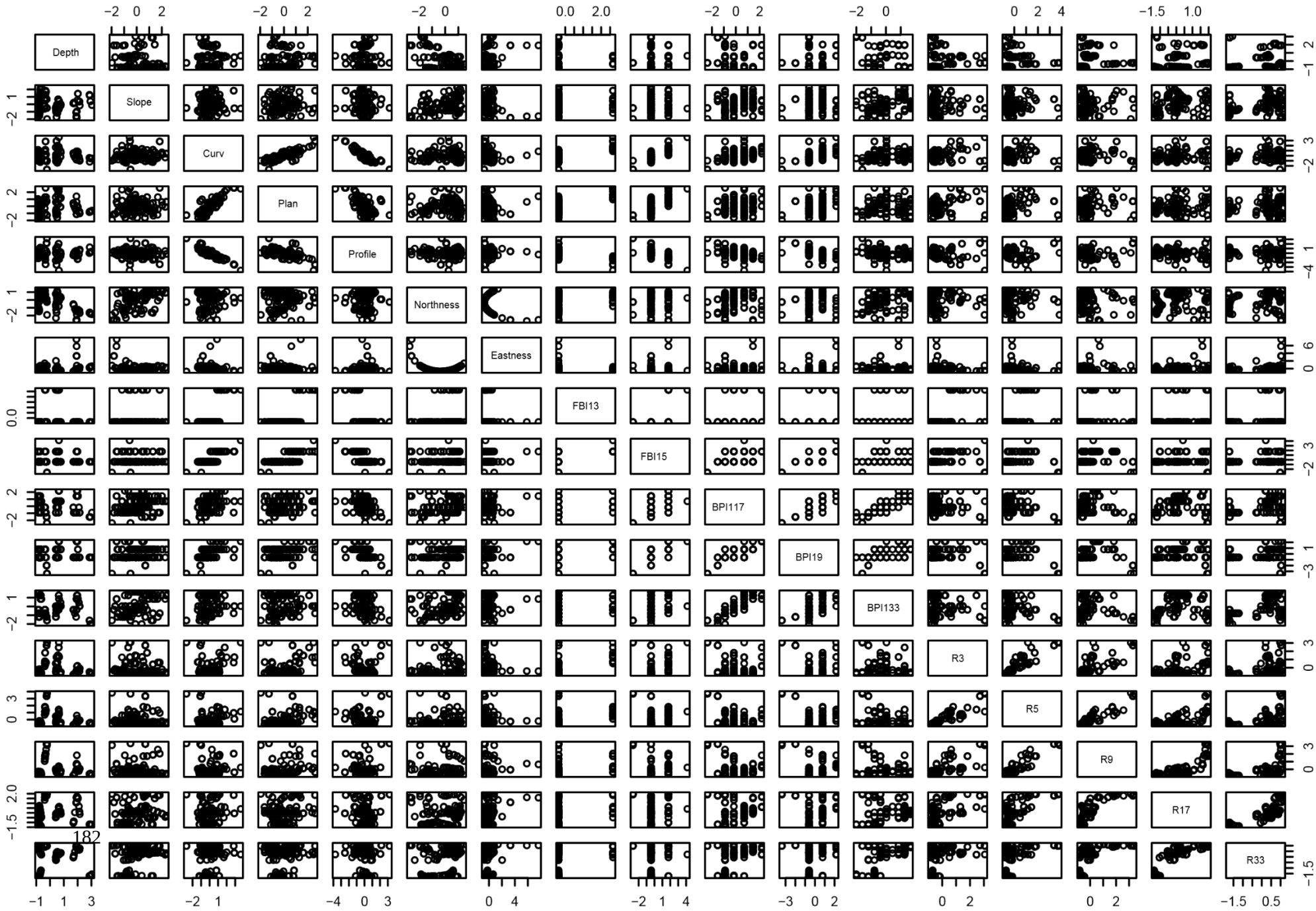
Depth
Slope
Curv
Plan
Profile
Northness
Eastness
FBI13
FBI15
BPI117
BPI19
BPI133
R3
R5
R9
R17
R33

Appendix C

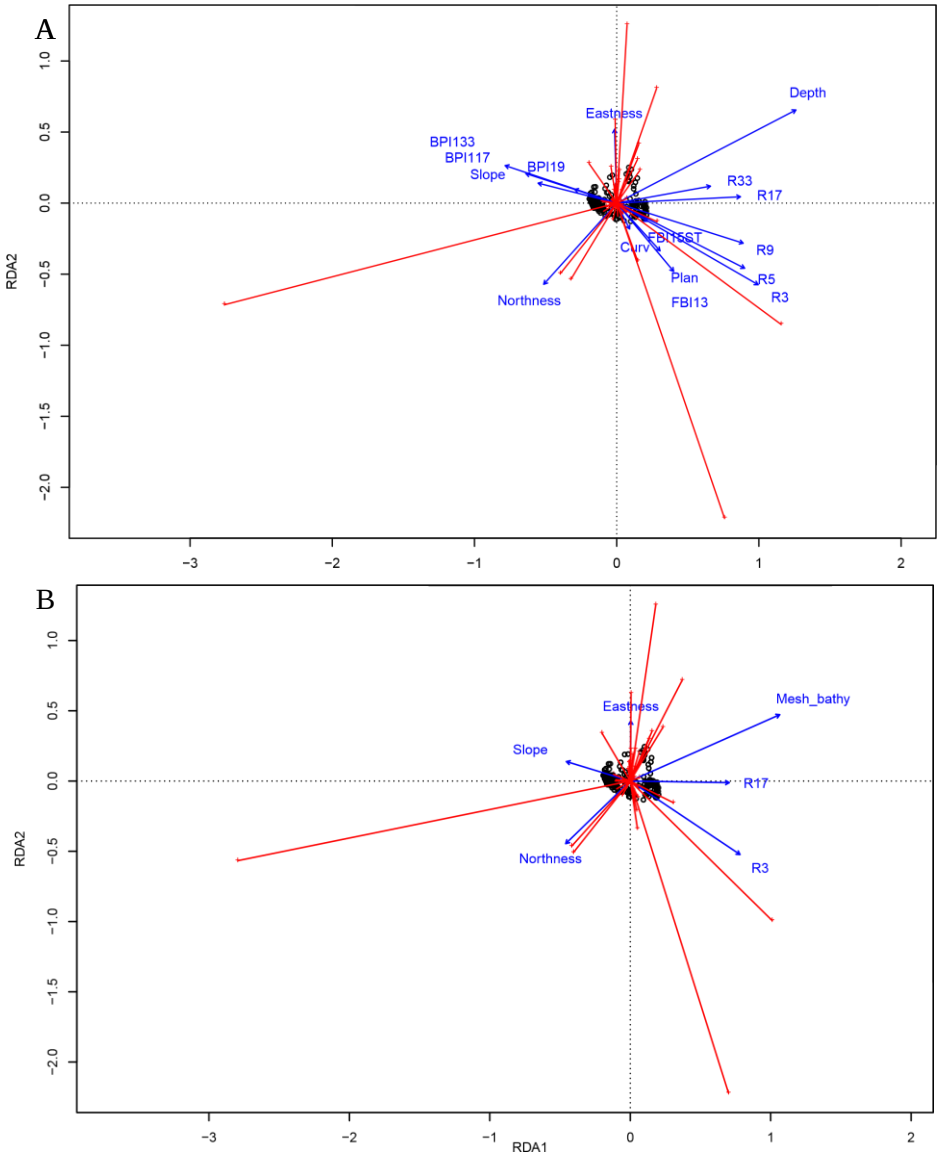


Supplementary materials Figure 4.6 (A) Triplot showing results from a canonical redundancy analysis (RDA) of species data and all the derived terrain variables. Terrain variables codes: BPI = Bathymetric position index created at neighbourhoods of 3, 5, 9, 17 and 33, R = Ruggedness created at neighbourhoods of 3, 5, 9, 17 and 33, Curv = Curvature and Plan = Planar Curvature. (B) Triplot showing results from a RDA of species data and all the derived terrain variables. Terrain variables codes: R = Ruggedness created at neighbourhoods of 3 and 17. The blue vector arrowheads represent high, the origin averages, and the tail (when extended through the origin) low values of the selected continuous derived terrain variables. The red vector arrowheads represent high, the origin averages, and the tail (when extended through the origin) low values of the species data. Circles represent sites. Sites close to one another tend to have similar faunal structure than those further apart.

Supplementary materials Table 4.2 Results from RDA performed on Hellinger transformed species data and final terrain derivatives, after forward selection of all terrain derivatives. Significance ***$p \leq 0.001$, **$p \leq 0.01$, *$p \leq 0.05$, •$p \leq 0.1$

| Model | Environmental Variables - Significance of individual terms by ANOVA | Adjusted $R^2$ | Significance of RDA Plot by ANOVA | |
|---|---|---|---|---|
| | | | F-value | p- value |
| Terrain Derivatives | Depth***, Slope ***, Northness ***, Eastness***, Ruggedness $17_{nh}$ ***, Ruggedness $3_{nh}$ ** | 22 | 9.39, df= 6,171 | 0.001 |

Supplementary materials Table 4.3 Pearson's correlation for terrain derivatives included in final RDA

| | Depth | Slope | Northness | Eastness | Ruggedness $17_{nh}$ | Ruggedness $3_{nh}$ |
|---|---|---|---|---|---|---|
| Depth | 1.00 | | | | | |
| Slope | -0.11 | 1.00 | | | | |
| Northness | -0.55 | 0.47 | 1.00 | | | |
| Eastness | 0.25 | -0.15 | -0.23 | 1.00 | | |
| Ruggedness $17_{nh}$ | 0.17 | 0.25 | 0.04 | 0.25 | 1.00 | |
| Ruggedness $3_{nh}$ | 0.12 | -0.01 | 0.04 | -0.13 | 0.60 | 1.00 |

Supplementary materials Table 4.4 Covariance inflation scores for terrain derivatives included in final RDA

| Terrain derivatives | Covariance inflation factor score |
|---|---|
| Depth | 1.6 |
| Slope | 1.6 |
| Northness | 1.9 |
| Eastness | 1.4 |
| Ruggedness $17_{nh}$ | 2.3 |
| Ruggednes $3_{nh}$ | 2.0 |

Appendix C

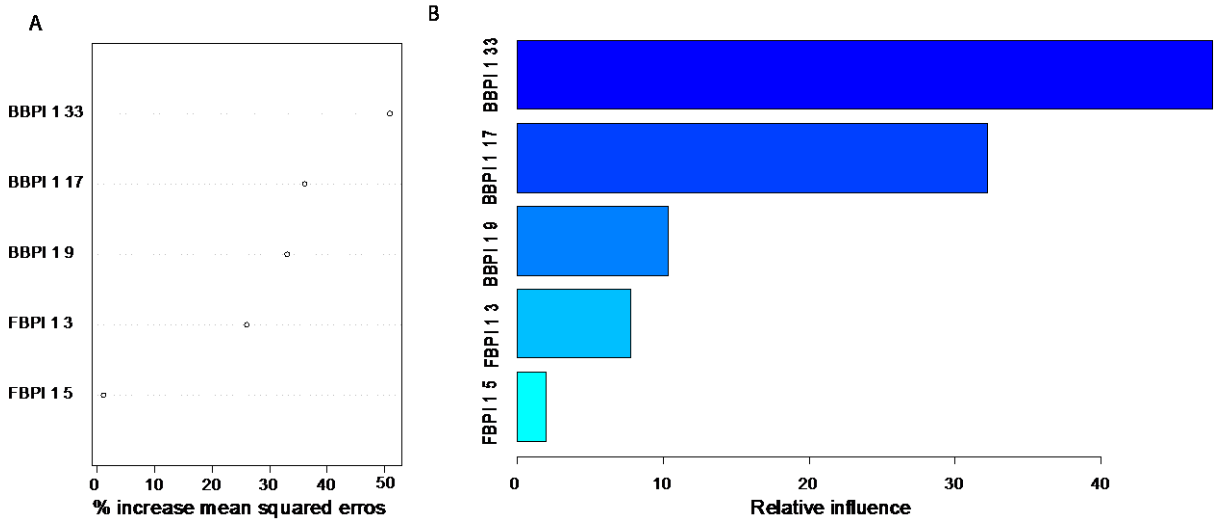


Supplementary materials Figure 4.7 Variable importance (percentage increase in mean squared errors) of derivatives of BPI (created at neighbourhoods of 3, 5, 9, 17 and 33 for (A) random forest and (B) Boosted Regression Trees of the eight faunal clusters identified from cluster analysis.

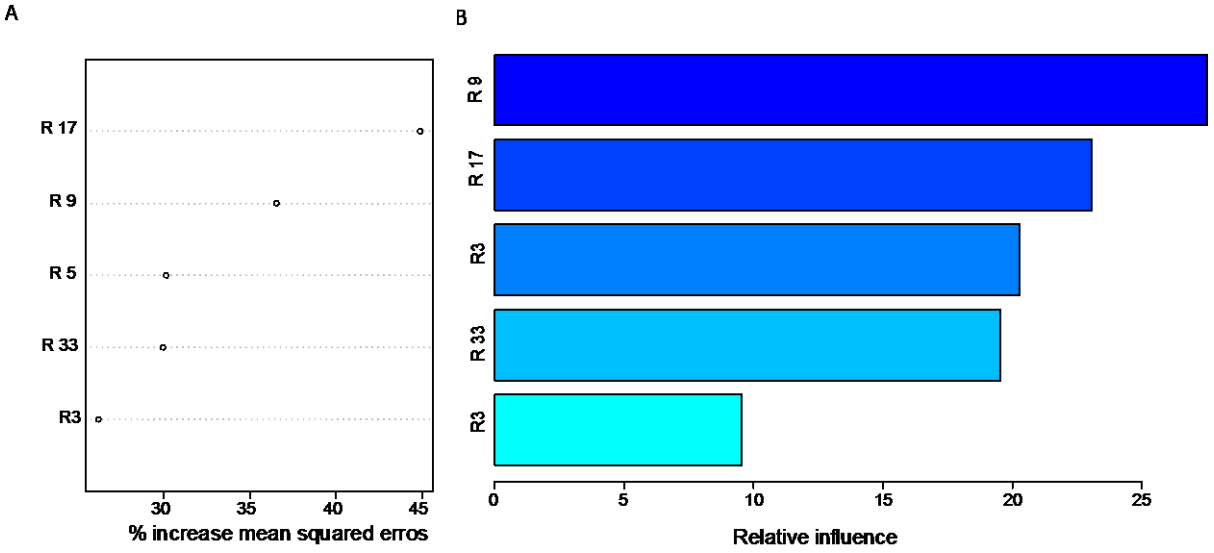


Supplementary materials Figure 4.8 Variable importance (percentage increase in mean squared errors) of derivatives of ruggedness (R) (created at neighbourhoods of 3, 5, 9, 17 and 33 for (A) random forest and (B) Boosted Regression Trees of the eight faunal assemblages identified from cluster analysis.

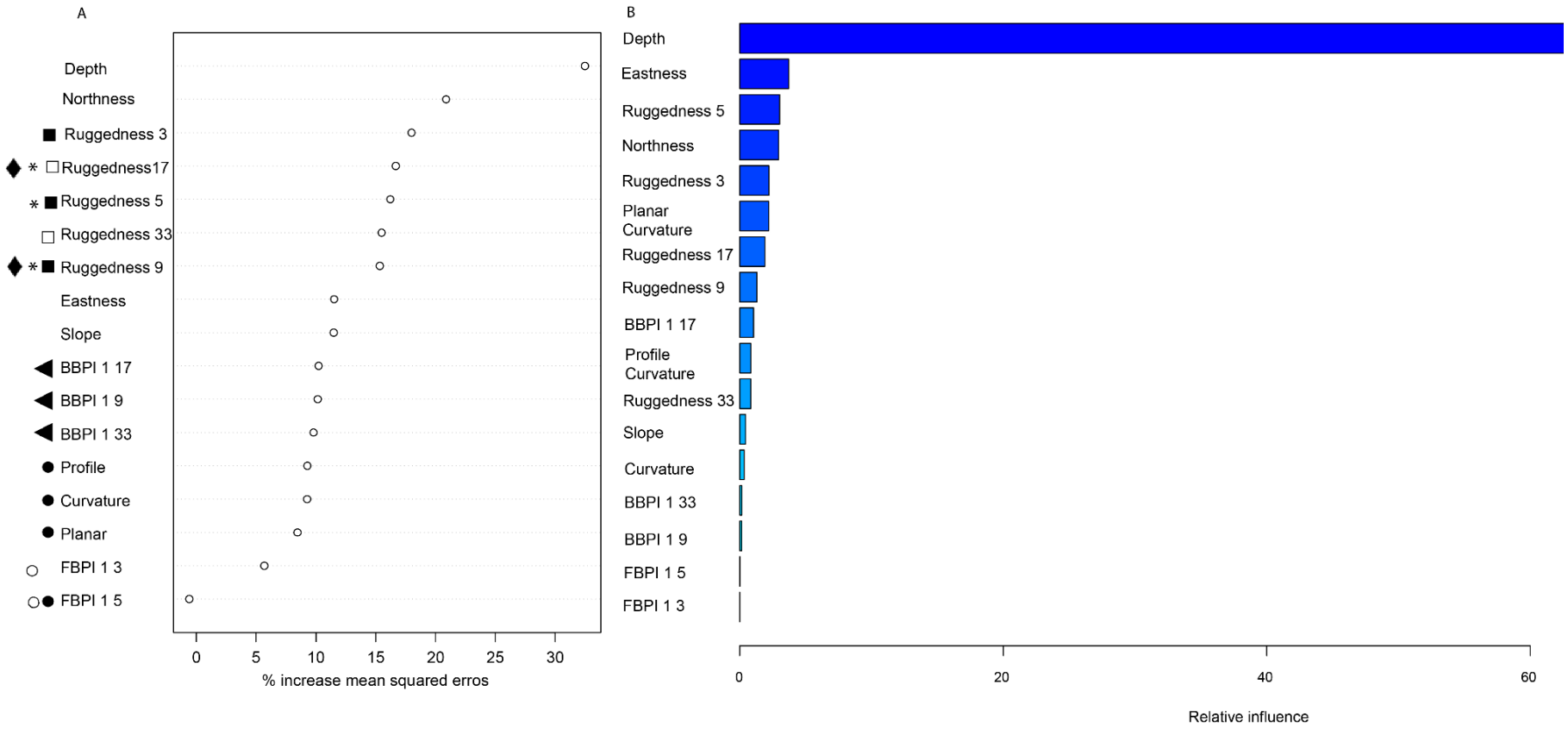


Supplementary materials Figure 4.9 Variable importance (percentage increase in mean squared errors) for (A) random forest and (B) Boosted Regression Trees of the eight faunal assemblages identified from cluster analysis. Symbols denote groups of correlated terrain derivative (Pearson's correlation > 0.7). In each correlated group the terrain derivative that explained > 10 % variance was retained = Depth, slope, Northness, Eastness, ruggedness $17_{nh}$ and ruggedness $3_{nb}$.

Appendix C

4.1.3 Multiscale analysis of textural indices

To capture the different resolutions of textural variation across the sidesacn sonar (SSS) and to further our understanding of the resolution at which seafloor complexity influences faunal assemblages, derivatives of texture (entropy, homogeneity, contrast and correlation ) were calculated from GLCM calculated at range of pixel distances (5 up to half of the window size) and window sizes (11, 21 and 51) across all directions (Supplementary materials Table 4.5 and Supplementary materials Figure 4.10) and a multi scale analysis performed to identify which resolution explains most variation (Misiuk et al., 2018, Porskamp et al., 2018).

Two approaches were adopted for the multi-scale analysis. First, all textural variables were modelled with Hellinger transformed species data by RDA, using forward selection and VIF scores, with the highest ranking textural variables that had Pearson's correlation coefficient <0.7 retained (Supplementary materials Figure 4. 11and Supplementary materials Table 4.6).

Second, Random forests (RF) and Boosted Regression Trees (BRT) were used to model cluster membership, following cluster analysis of the species data (detailed in chapter 4 of this thesis section 4.3.6). RF and BRT were used to account for any non-linear relationships among environmental variables. The textural indices were modelled separately but at all resolutions in order to rank the contribution of each variable at the different resolutions (Supplementary materials Figure 4.12 and 4.16 following the protocol in Misiuk et al., (2018). Additionally, all the textural variables were assessed simultaneously to account for potential interactions or correlation between the variables (Supplementary materials Figure 4.17). Textural variables that contributed > 10 % to overall variance explained by the model and were < 0.7 correlated were retained (Supplementary materials Figures 4.17). Results show high collinearity present among many of the textural derivatives (Supplementary. and Supplementary materials Figure 4.17). In each correlated group the terrain derivative that explained the greatest variance was retained (Supplementary materials Figure 4. 17).

Following the multi scale analysis the textural indices correlation (window size 51 inter-pixel distance 20) and homogeneity (window size 51 inter-pixel distance 25) were retained.

Supplementary materials Table 4.5 Window sizes and inter-pixel distances over which GLCMs for each textural indices were calculated. GLCMs were calculated from sidescan sonar at 0.5 m pixel resolution, resulting in inter-pixel distances (m) of 5 = 2.5, 10 = 5, 15 = 7.5, 20 = 10 and 25 = 12.5.

| Window size ($_{ws}$) | Area ($m^2$) | Inter-pixel distances calculated ( $_{ipd}$) |
|---|---|---|
| 1 | 5.5 | 5 |
| 21 | 10.5 | 5,10 |
| 51 | 25.5 | 5, 10, 15, 20, 25 |

Textural indices calculated from GLCMs with window sizes of 11 capture variation between approximately 5 $m^2$ patches and those calculated from window sizes capture variation at 10 $m^2$ comparable with variation captured in the video still data that was sub sampled at > 7 m intervals. While the Textural indices calculated from GLCMs with window sizes of 51 capture variation between approximately 25 $m^2$ patches comparable with variation captured by the terrain derivatives.

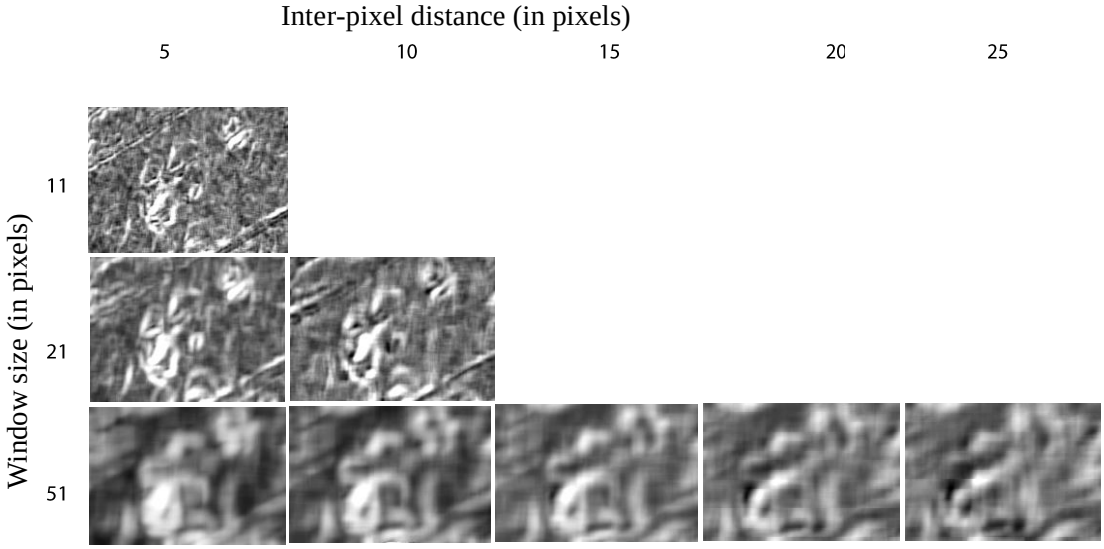


Supplementary materials Figure 4.10 Example of different windows sizes and inter-pixel distances used in GLCM to derive correlation.

Appendix C

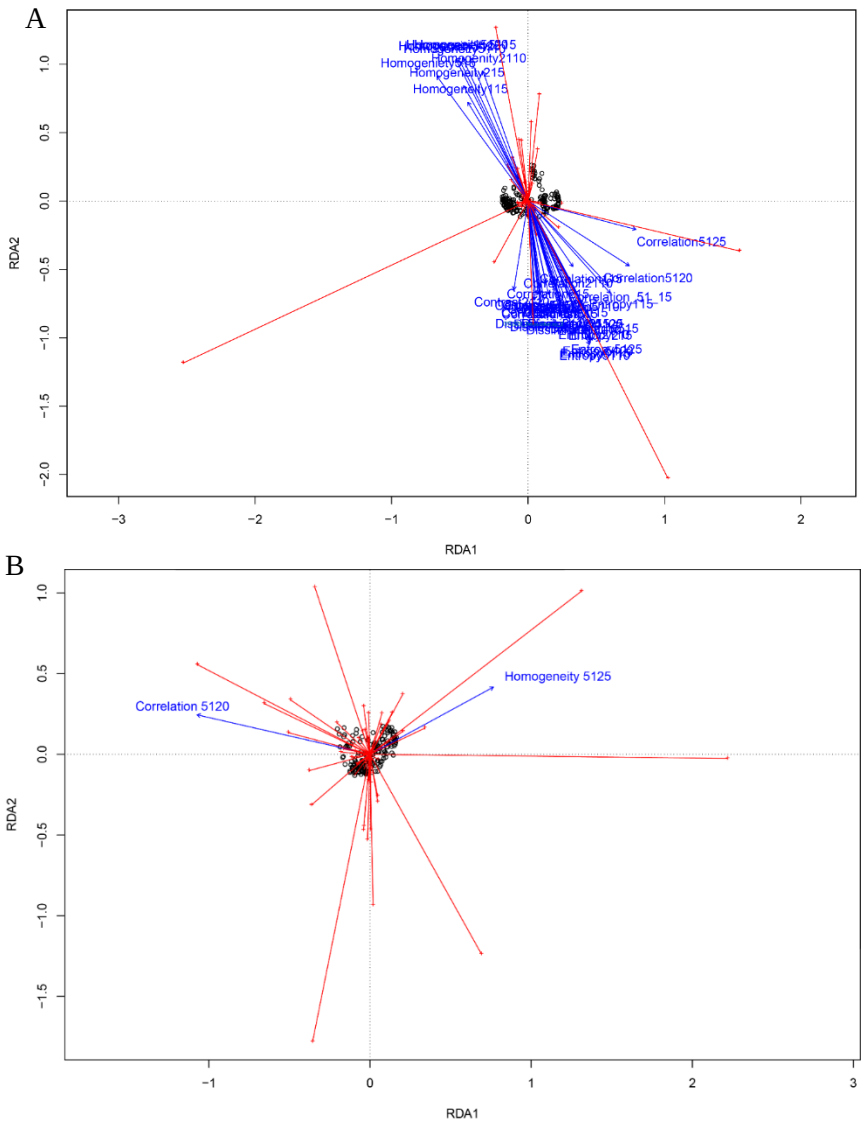


Supplementary materials Figure 4.11 (A) Triplot showing results from a canonical Redundancy Analysis (RDA) of species data and all the derived textual indices. The textural indices homogeneity, correlation, entropy and contrast were derived from GLCM matrices calculated at window seizes of 11, 21 and 51 with inter pixel distances of five up to half the window size increasing by increments of five. (B) Triplot showing results from a RDA of species data and all the final textual indices. The textural indices homogeneity and correlation were derived from GLCM matrices calculated at window seizes of 51 with inter pixel distances of 20 and 25. The blue vector arrowheads represent high, the origin averages, and the tail (when extended through the origin) low values of the selected continuous derived terrain variables. The red vector arrowheads represent high, the origin averages, and the tail (when extended through the origin) low values of the species data. Circles represent sites. Sites close to one another tend to have similar faunal structure than those further apart.

Supplementary materials Table 4.6 Model selection for canonical Redundancy Analysis (RDA) of the textural indices. Textural indices were modelled simultaneously at all resolutions with species data using with forward selection and variance inflation factor (VIF) scores to identify the most informative textural variables. To determine which correlated textural variables to retain, from those identified as being most informative, each textural index was modelled separately but at all resolutions with species data and the resolution for each textual index that explained the greatest variation was retained. Collinearity between indices was checked with VIF scores and Pearson's correlation coefficient and uncorrelated indices retained in the final parsimonious model. $_w$ denotes window size and $_{ipd}$ denotes inter pixel distance.

| RDA by textural index | RDA with forward selection all textural indices | Parsimonious RDA (correlated variables removed) |
|---|---|---|
| Correlation $51_w20_{ipd}$ | Correlation $\underline{51_w20_{ipd}}$, $11_w5_{ipd}$ | Correlation $51_w20_{ipd}$ |
| Contrast $51_w5_{ipd}$* | Contrast $21_w10_{ipd}$* | Removed as explained least variance |
| Dissimilarity $51_w5_{ipd}$* | Dissimilarity $51_w5_{ipd}$, $\underline{51_w15_{ipd}}$* | Removed as had highest correlation inflation factor value |
| Homogeneity $51_w25_{ipd}$* | Homogeneity $51_w5_{ipd}$, $51_w10_{idp}$,$\underline{51_w25_{ipd}}$* | Homogeneity $51_w25_{ipd}$ |
| Entropy $51_w10_{ipd}$* | | |

Supplementary materials Table 4.7 Results from RDA performed on Hellinger transformed species data and final textural derivatives, after forward selection of all textural indices. Significance ***p ≤ 0.001, **p ≤ 0.01, *p ≤ 0.05, •p ≤ 0.1

| Model | Environmental Variables - Significance of individual terms by ANOVA | Adjusted $R^2$ | Significance of RDA Plot by ANOVA | |
|---|---|---|---|---|
| | | | F-value | p- value |
| Textural indices | Homogeneity $51_w25_{ipd}$ **, Correlation $51_w20_{ipd}$ ** | 2 | 3.26, df= 2,167 | 0.003 |

Appendix C

Supplementary materials Table 4.8 Pearson's correlation for textural derivatives included in final RDA

| | Correlation $51_w20_{ipd}$ | Homogeneity $51_w25_{ipd}$ |
|---|---|---|
| Correlation $51_w20_{ipd}$ | 1 | |
| Homogeneity $51_w25_{ipd}$ | -0.21 | 1 |

Supplementary materials Table 4.9 Covariance inflation scores for textural derivatives included in final RDA

| Terrain derivatives | Covariance inflation factor score |
|---|---|
| Correlation $51_w20_{ipd}$ | 1.04 |
| Homogeneity $51_w25_{ipd}$ | 1.04 |

The RF and BRT identified correlation at window size of 51 and inter pixel distance of 10 (Supplementary materials Figure 4.13 and 4.17) but as this is highly correlated with correlation calculated with a window size of 51 and inter pixel distance of 20 (Pearson's correlation 0.8), which was identified as more informative by RDA (Supplementary materials Table 4.6), the latter was retained. Contrast was also identified as a significant explanatory variable in the RF and BRT (Supplementary materials Figure 4.17). However, the RDA showed that contrast explained less variance in the species data than the other textural indices with which it was > 70 % correlated (Supplementary materials Table 4.6) and so it was not retained.

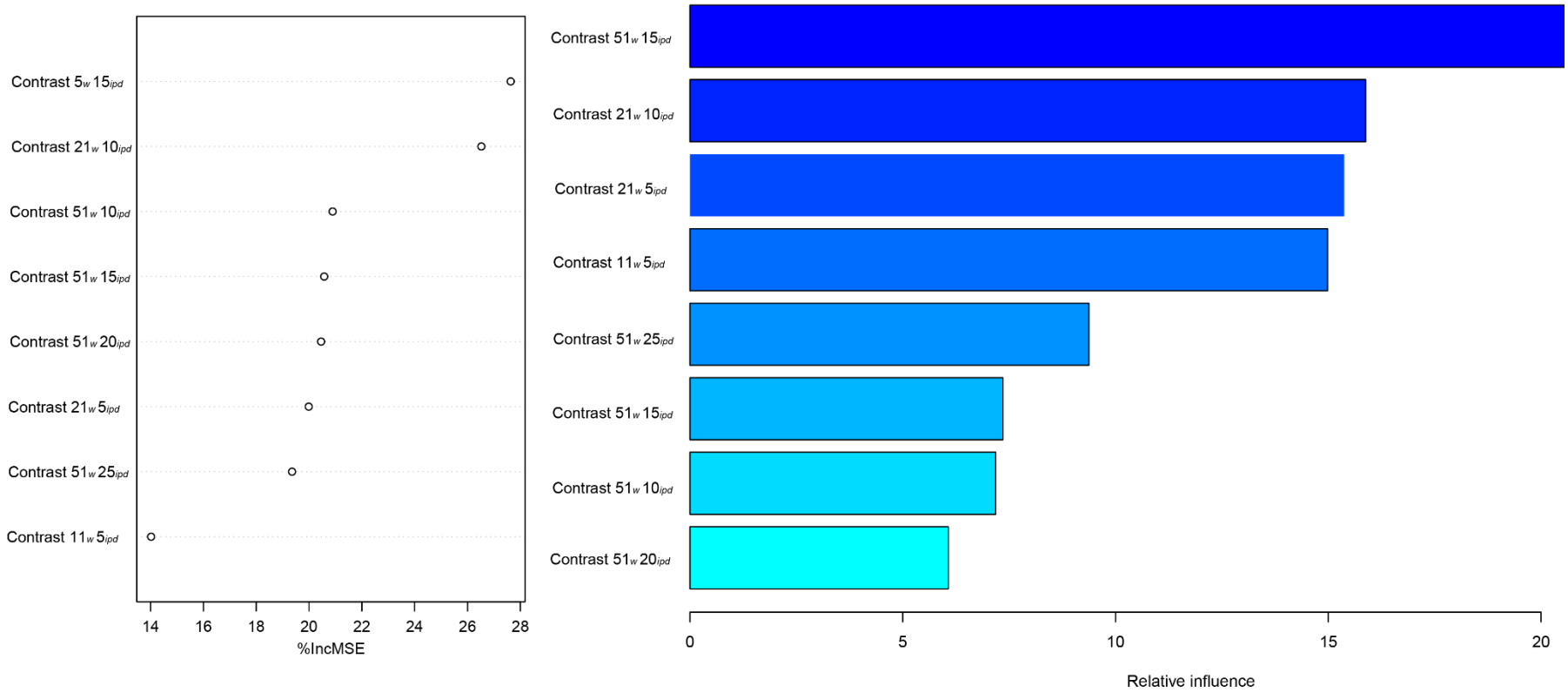


Supplementary materials Figure 4.12 Variable importance (percentage increase in mean squared errors) of textural index contrast (created at window sizes of 11, 21 and 51 with inter pixel distances of five up to half the window size in increments of five) for (A) random forest and (B) Boosted Regression Trees of the eight faunal assemblages identified from cluster analysis.

Appendix C

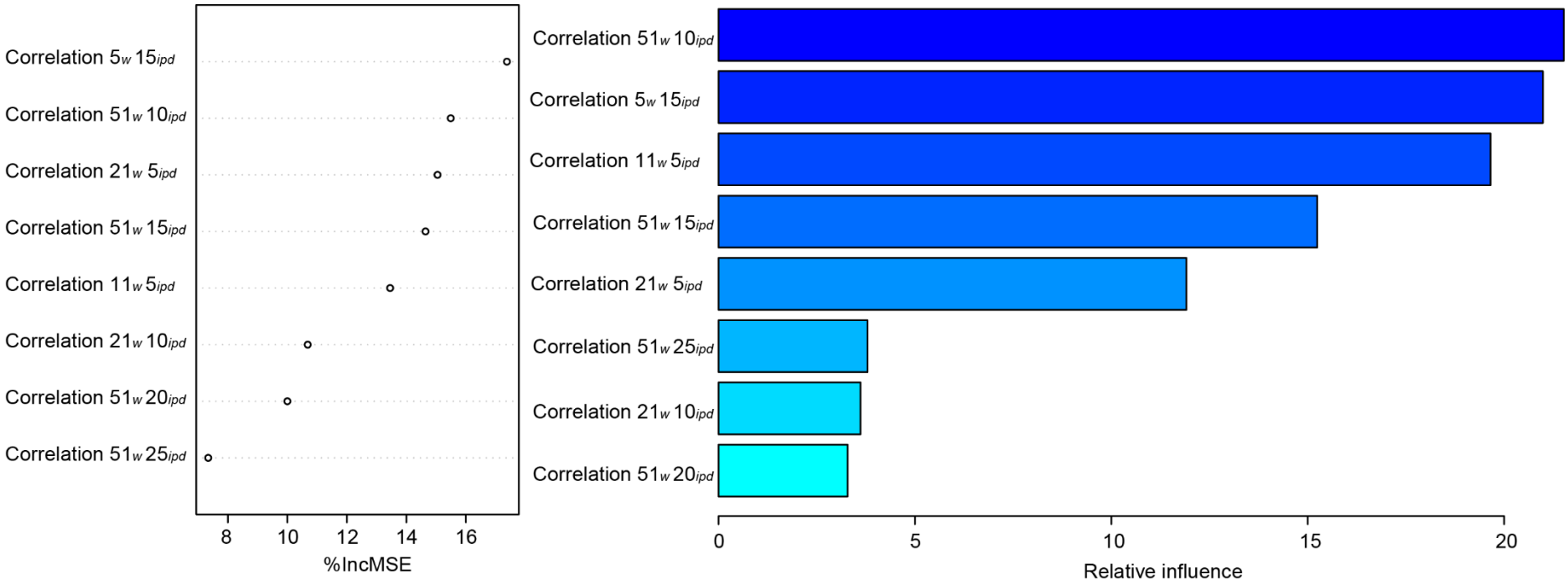


Supplementary materials Figure 4.13 Variable importance (percentage increase in mean squared errors) of textural index correlation (created at window sizes of 11, 21 and 51 with inter pixel distances of five up to half the window size in increments of five) for (A) random forest and (B) Boosted Regression Trees of the eight faunal assemblages identified from cluster analysis.

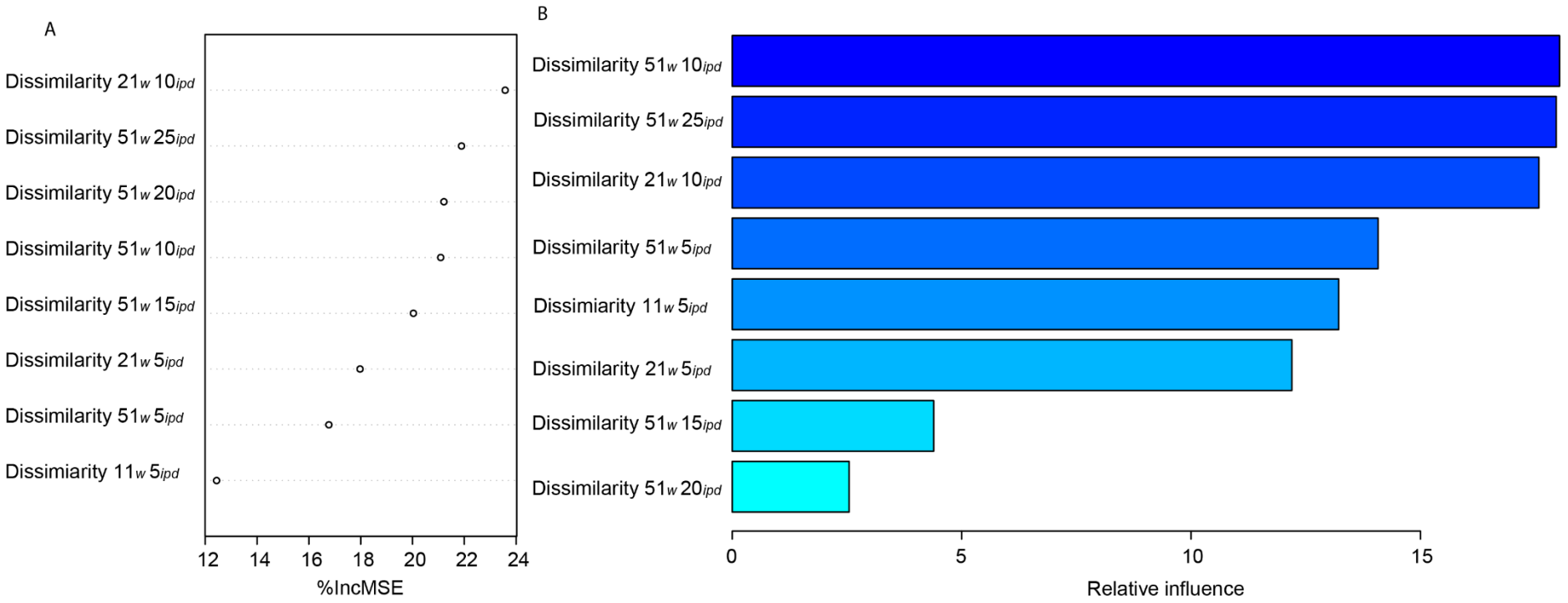


Supplementary materials Figure 4.14 Variable importance (percentage increase in mean squared errors) of textural index dissimilarity (created at window sizes of 11, 21 and 51 with inter pixel distances of five up to half the window size in increments of five) for (A) random forest and (B) Boosted Regression Trees of the eight faunal assemblages identified from cluster analysis.

Appendix C

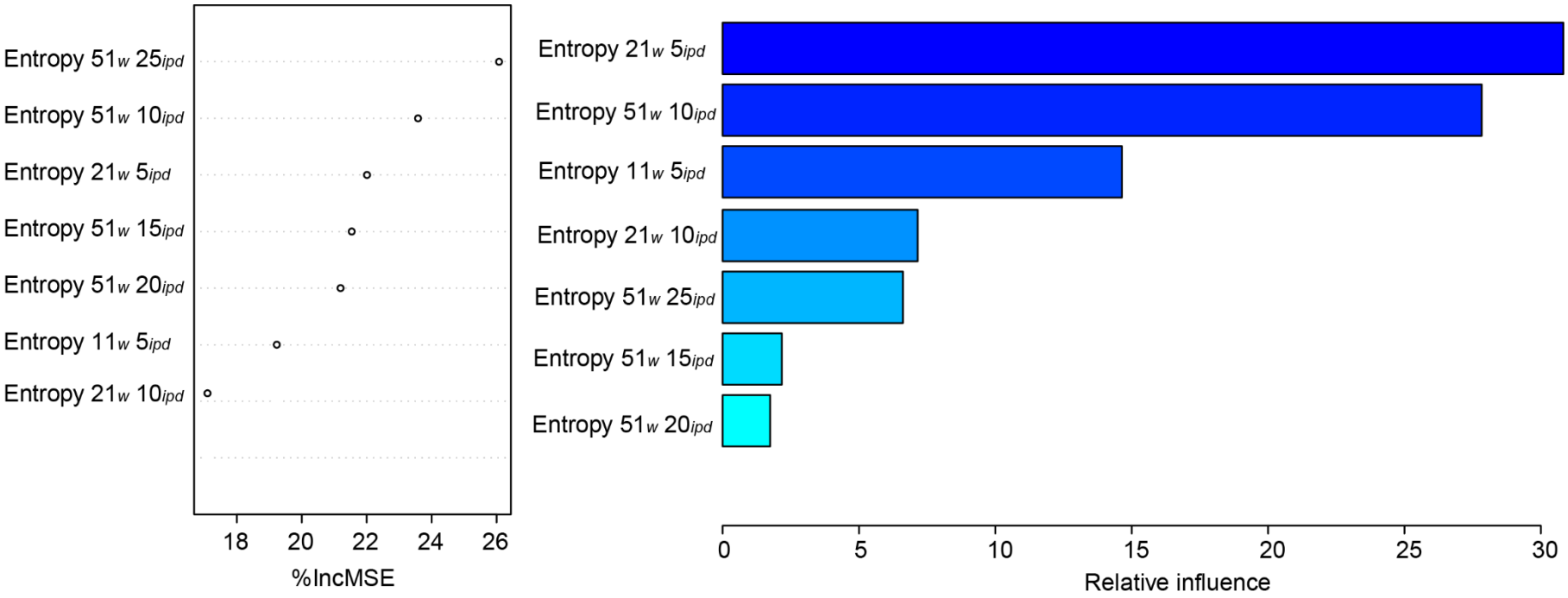


Supplementary materials Figure 4.15 Variable importance (percentage increase in mean squared errors) of textural index entropy (created at window sizes of 11, 21 and 51 with inter pixel distances of five up to half the window size in increments of five) for (A) random forest and (B) Boosted Regression Trees of the eight faunal assemblages identified from cluster analysis.

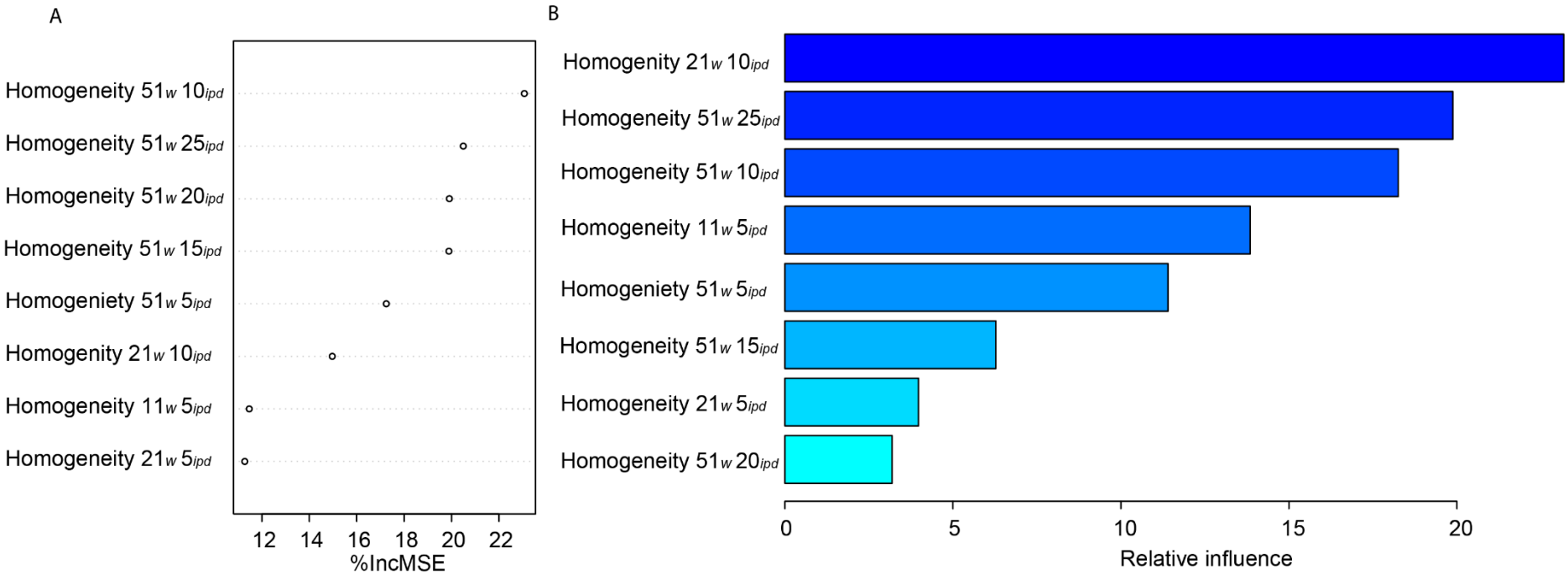


Supplementary materials Figure 4.16 Variable importance (percentage increase in mean squared errors) of textural index homogeneity (created at window sizes of 11, 21 and 51 with inter pixel distances of five up to half the window size in increments of five) for (A) random forest and (B) Boosted Regression Trees of the eight faunal assemblages identified from cluster analysis.

Appendix C

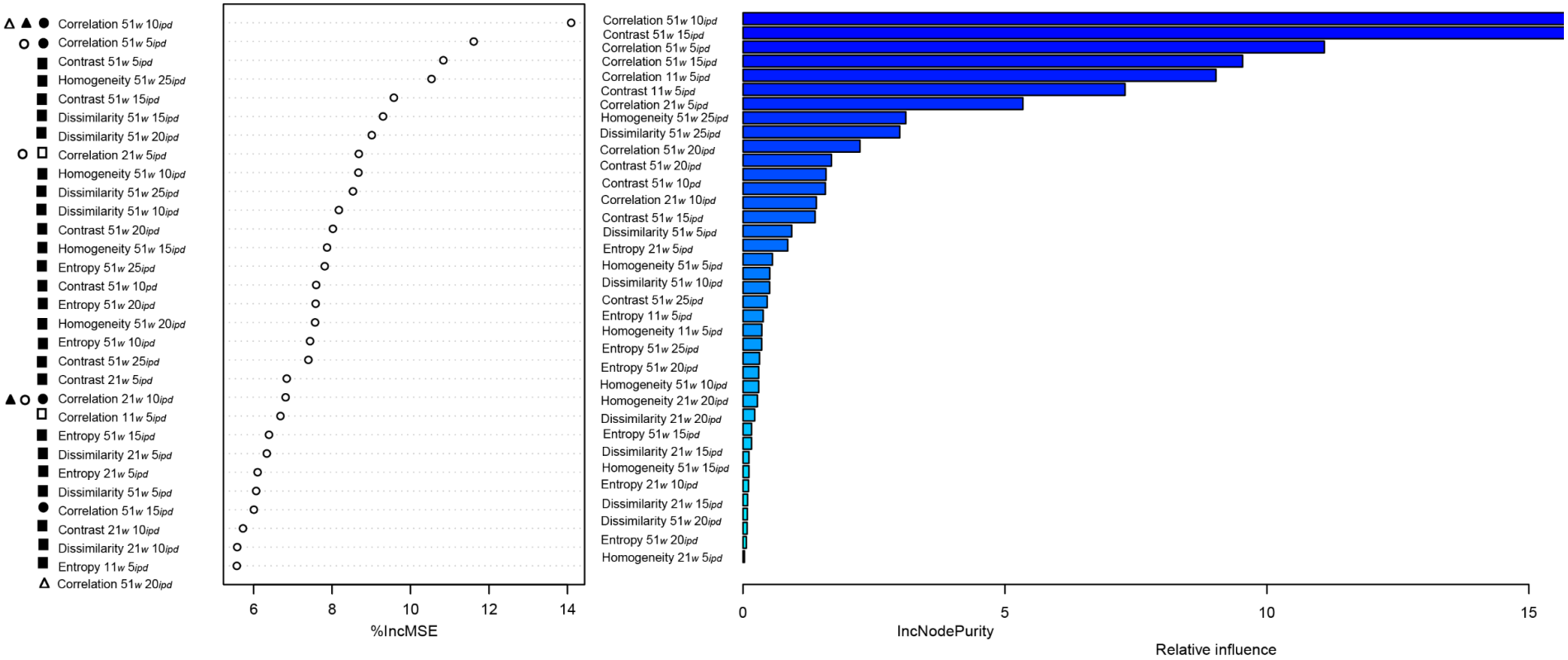


Supplementary materials Figure 4.17 Variable importance (percentage increase in mean squared errors) for (A) random forest and (B) Boosted Regression Trees of the eight faunal assemblages identified from cluster analysis. Symbols denote groups of correlated terrain derivative (Pearson's correlation > 0.7). In each correlated group the terrain derivative that explained > 10 % variance was retained = Correlation at a window size of 51 and inter-pixel distance of 10 and homogeneity window size of 51 and inter-pixel distance of 25. Homogeneity was retained over contrast because it is more ecologically intuitive to interoperate.

Supplementary materials Figure 4.18 Maps (~25 m pixel resolution) of the textural indices used as environmental variables in the model selection coinciding with spatial extent of sidescan sonar collected for homogeneity $51_w$ $25_{ipd}$ from the (A) Explorer interfluve and (B) Dangaard interfluve and correlation $51_w$ $20_{ipd}$ from the (C) Explorer interfluve and (D) Dangaard interfluve.

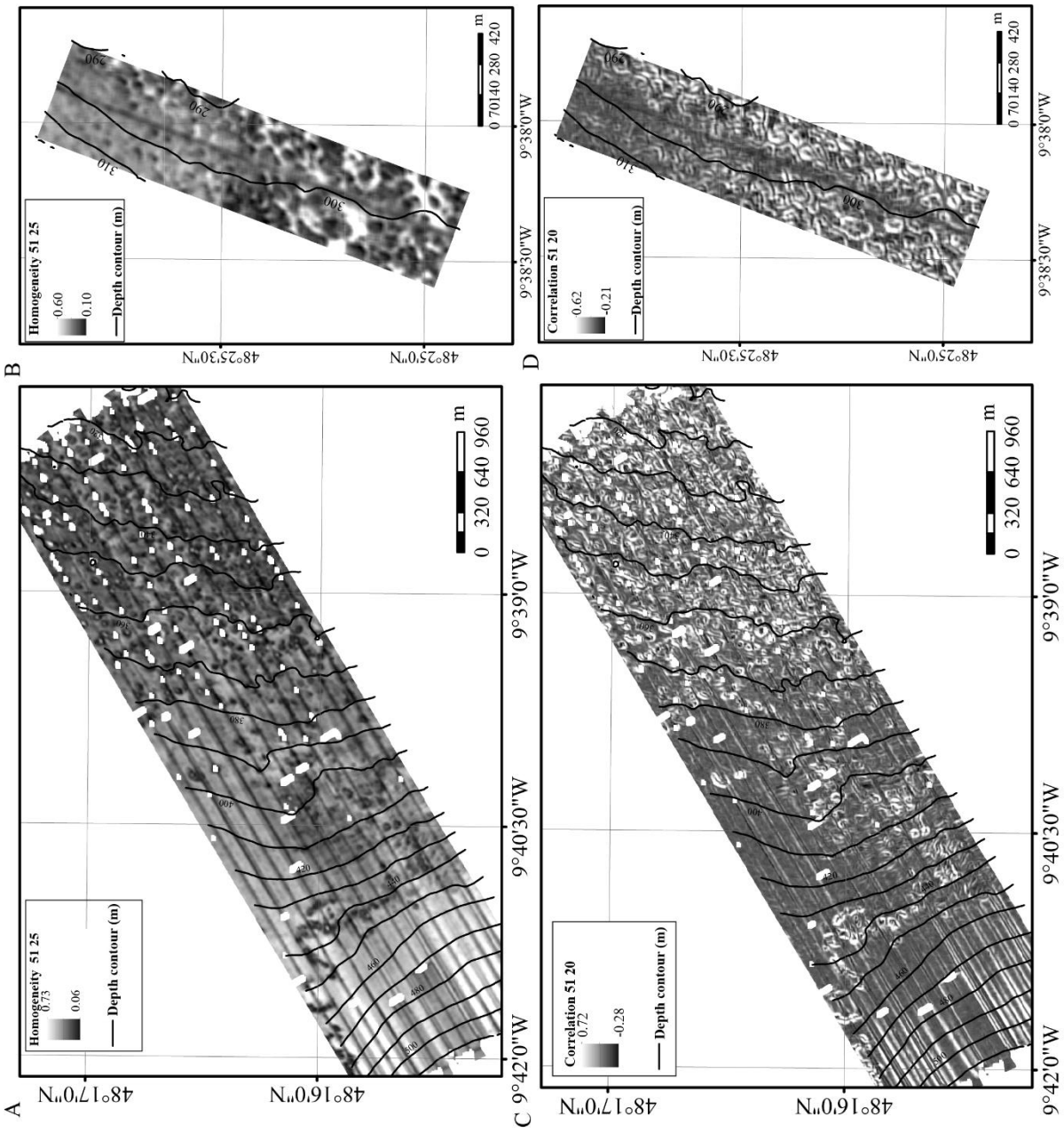

Appendix C

4.1.4 Imagery data

4.1.4.1 Calculation of image area

Video stills data were acquired during the CEND0917 and JC166 cruises.

The approximate field of view of each image, and therefore the area sampled, was calculated in accordance with a JNCC procedure implemented in the annotation of the CEND0917 still images (Turner et al., 2006).

Field of view approximate width in mm = (measured total width in pixels/measured laser width in pixels)* actual laser width mm

Field of view approximate height in mm = (measured total height in pixels/measured laser height in pixels)* actual laser width mm

Approximate field of view $m^2$ = (Field of view approximate width/1000)*(Field of view approximate height/1000)

4.1.4.2 Compilation of image data

To ensure consistency between the datasets an analysis of similarity (ANOSIM) with cruise as a factor was performed on the data matrix (Supplementary materials Table 4.10). Consistency was also assessed visually via a non-metric multidimensional scaling plot (Supplementary materials Figure 4.19). The results from these analysis show that the image samples do not differentiate according to cruise (ANOSIM R value of 0.25) justifying the complication of the two datasets.

Supplementary materials Table 4.10 Results of analysis of similarity (ANOSIM) calculated between groups based upon cruise on a Helligner transformed distance species matrices. Each pairwise comparion of two groups was performed using 999 permutations. R values >0.75 are generally interpreted as clesrly seperated, R >0.5 as seperaed and R <0.25 as groups that are hardly seperated.

| Factor | R | P |
|---|---|---|
| Cruise | 0.25 | 0.01 |

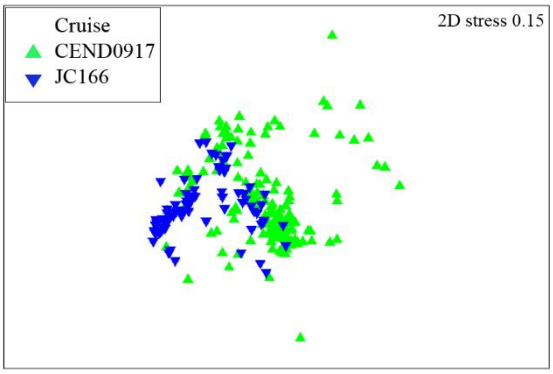


Supplementary materials Figure 4.19 – A non-metric multidimensional scaling (NMDS) plot with image samples coloured by the factor ‘cruise’. Samples positioned closer to one another on the plot are more similar. Image samples from each cruise overlap in the central and left hand side of the plot.

## 4.2 Results supplementary materials

### 4.2.1 Fauna results

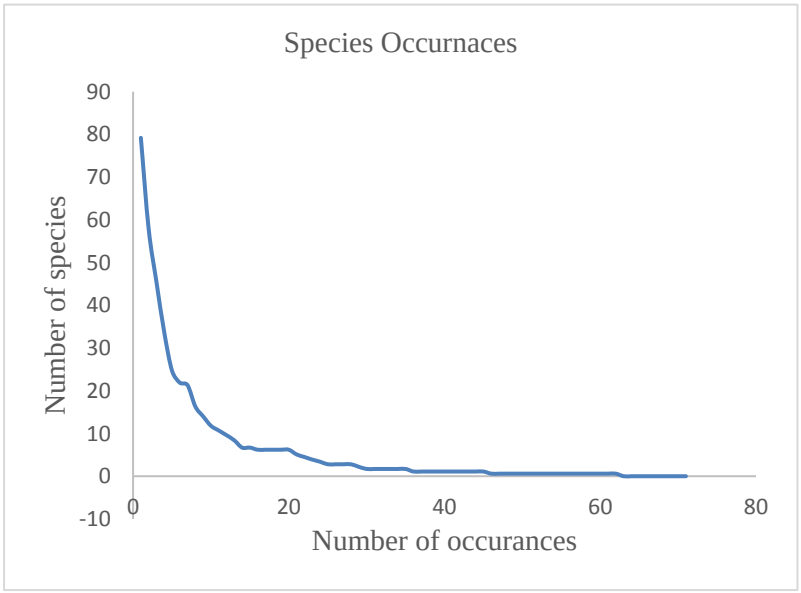


Supplementary materials Figure 4.20 Histogram of species occurrences across samples from all the dives.

Supplementary materials Table 4.11 SIMPER results: Average abundance, their contribution (%) to within group similarity, cumulative total (%) of contributions (90 % cut off).

| | | | |
|---|---|---|---|
| Group 1 | | | |
| Average similarity: 34.95 | | | |
| Species | Av.Abund | Contrib% | Cum.% |
| OTU499 *Actinauge richardi* | 1.71 | 80.32 | 80.32 |
| OTU500 *Caryophyllia smithii* | 0.43 | 7.11 | 87.44 |
| OTU2 Cerianthidae sp. 1 | 0.39 | 5.21 | 92.65 |
| Group 2 | | | |
| Average similarity: 42.54 | | | |
| Species | Av.Abund | Contrib% | Cum.% |
| OTU246 *Ophiactis* | 4.57 | 56.63 | 56.63 |
| OTU499 *Actinauge richardi* | 1.5 | 21.9 | 78.53 |
| OTU228 Serpulidae sp. 2 | 1.06 | 9.13 | 87.65 |
| OTU200 *Munida* sp. | 0.71 | 5.19 | 92.85 |
| Group 3 | | | |
| Average similarity: 47.88 | | | |
| Species | Av.Abund | Contrib% | Cum.% |
| OTU6 *Caryophyllia* sp. 2 | 2.45 | 56.93 | 56.93 |
| OTU499 *Actinauge richardi* | 1.08 | 32.09 | 89.02 |
| OTU228 Serpulidae sp. 2 | 0.58 | 9.29 | 98.31 |
| Group 4 | | | |
| Average similarity: 26.68 | | | |
| Species | Av.Abund | Contrib% | Cum.% |
| OTU605 Actiniaria sp. 20 | 2.55 | 100 | 100 |
| Group 5 | | | |
| Average similarity: 32.13 | | | |
| Species | Av.Abund | Contrib% | Cum.% |
| Unidentified Actiniaria sp. | 1.98 | 80.87 | 80.87 |
| OTU1219 Bivalvia sp. 3 | 0.77 | 8 | 88.87 |
| OTU499 *Actinauge richardi* | 0.65 | 6.25 | 95.12 |
| Group 6 | | | |
| Less than 2 samples in group | | | |
| Group 7 | | | |
| Average similarity: 47.36 | | | |
| Species | Av.Abund | Contrib% | Cum.% |
| OTU1255 Actiniaria sp. 32 | 1.85 | 41.06 | 41.06 |
| OTU510 Actiniaria sp. 17 | 1.39 | 35.79 | 76.85 |
| Unidentified Actiniaria sp. | 0.94 | 20.87 | 97.72 |

| |
|---|
| Group 8 |
| Less than 2 samples in group |

Supplementary materials Table 4.12 SIMPER results: Distances between cluster classes

| Class comparison | Average dissimilarity % |
|---|---|
| 1 and 2 | 79.26 |
| 1 and 3 | 75.14 |
| 1 and 4 | 96.11 |
| 1 and 5 | 87.61 |
| 1 and 6 | 92.2 |
| 1 and 7 | 92.03 |
| 1 and 8 | 96.58 |
| 2 and 3 | 82.55 |
| 2 and 4 | 96.44 |
| 2 and 5 | 86.48 |
| 2 and 6 | 94.95 |
| 2 and 7 | 86.72 |
| 2 and 8 | 95.54 |
| 3 and 4 | 99.69 |
| 3 and 5 | 90.22 |
| 3 and 6 | 99.65 |
| 3 and 7 | 94.67 |
| 3 and 8 | 98.57 |
| 4 and 5 | 87.74 |
| 4 and 6 | 94.25 |
| 4 and 7 | 89.51 |
| 4 and 8 | 100 |
| 5 and 6 | 92.22 |
| 5 and 7 | 78.16 |
| 5 and 8 | 92.86 |
| 6 and 7 | 81.05 |
| 6 and 8 | 71.69 |
| 7 and 8 | 96.77 |

Appendix C

4.2.3 Modelling results

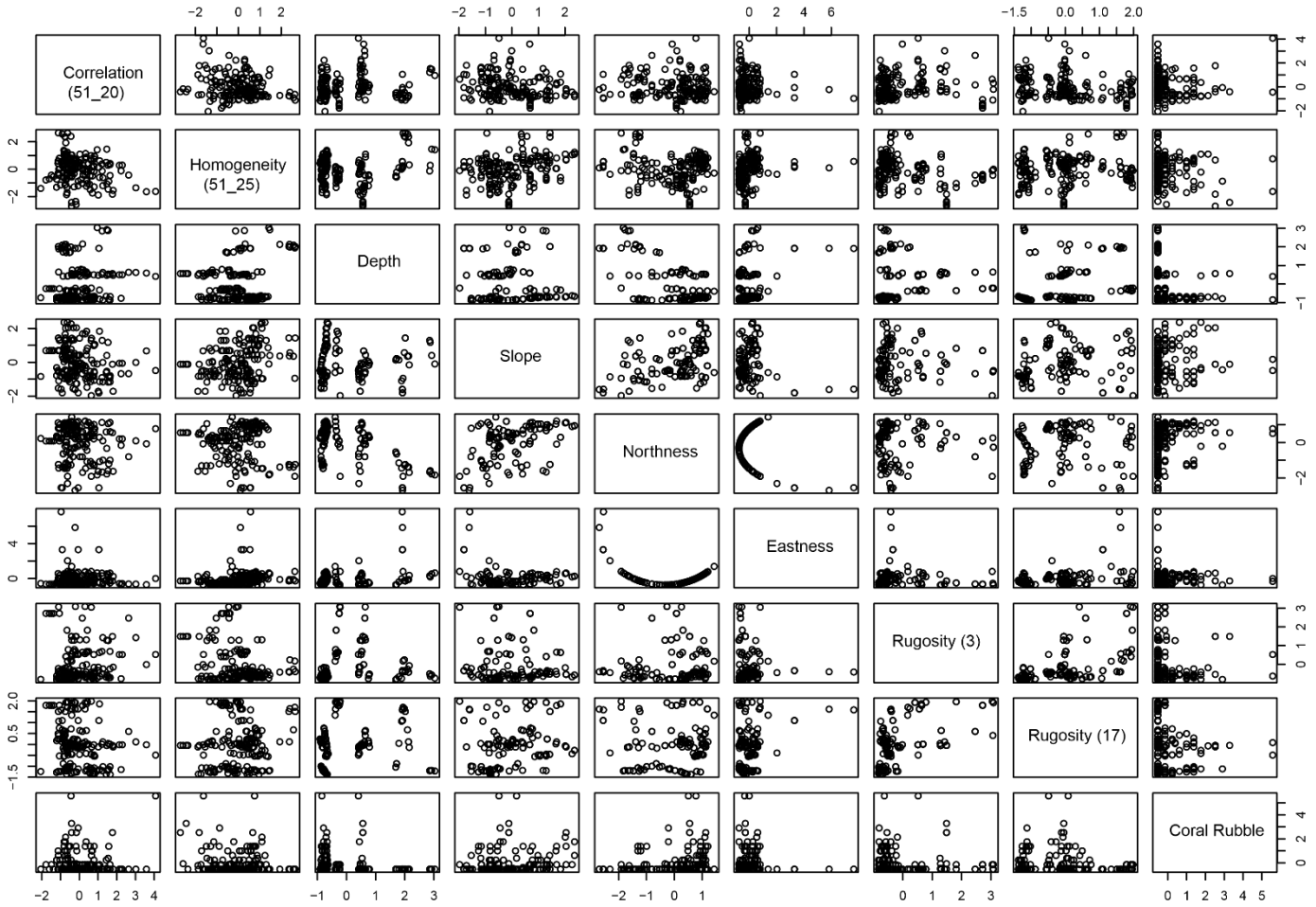


Supplementary materials Figure 4.21 Pairs plot for environmental variables used in model selection of redundancy analysis after multiscale analysis.

Supplementary materials Table 4.13 Results from RDA performed on Hellinger transformed species data and spatial coordinates reveal that there is a spatial trend in the species data. Significance ***p ≤ 0.001, **p ≤ 0.01, *p ≤ 0.05, •p ≤ 0.1

| Model | Environmental Variables - Significance of individual terms by ANOVA | Adjusted $R^2$ | Significance of RDA Plot by ANOVA | |
|---|---|---|---|---|
| | | | F-value | p- value |
| RDA | Latitude ***, Longtitude *** | 22 | 25.01, df= 1,167 | 0.001 |

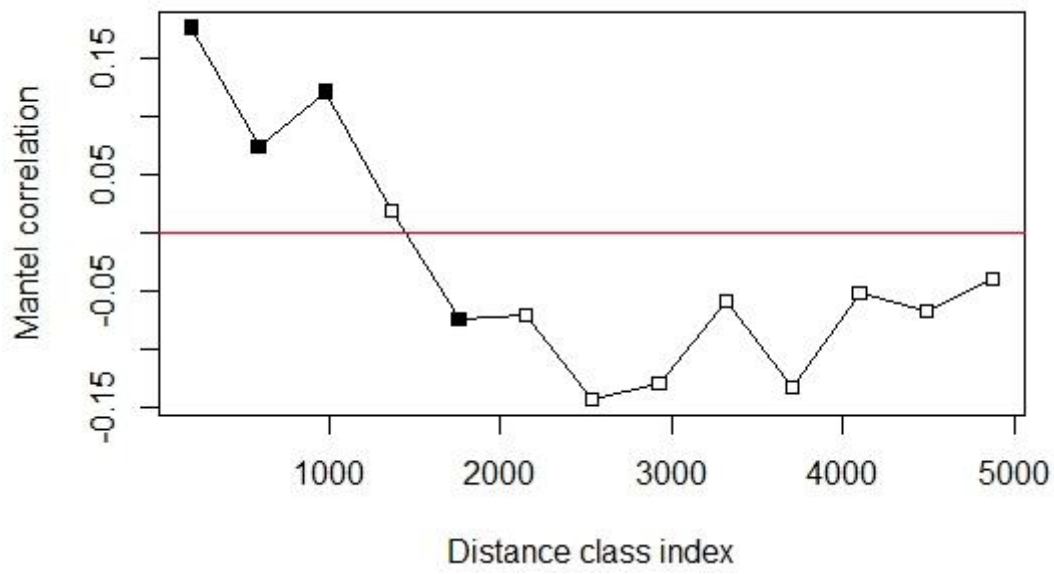


Supplementary materials Figure 4.22 Mantel correlogram of detrended species data from samples taken across the canyon interfluves with Holm correction for multiple testing. The Mantel correlogram of the detrended species data shows significant positive spatial correlation in the first three distance classes (i.e. < 14 m) and negative significant spatial correlation in the firth distances classes (i.e. > 2.7 km).

Appendix C

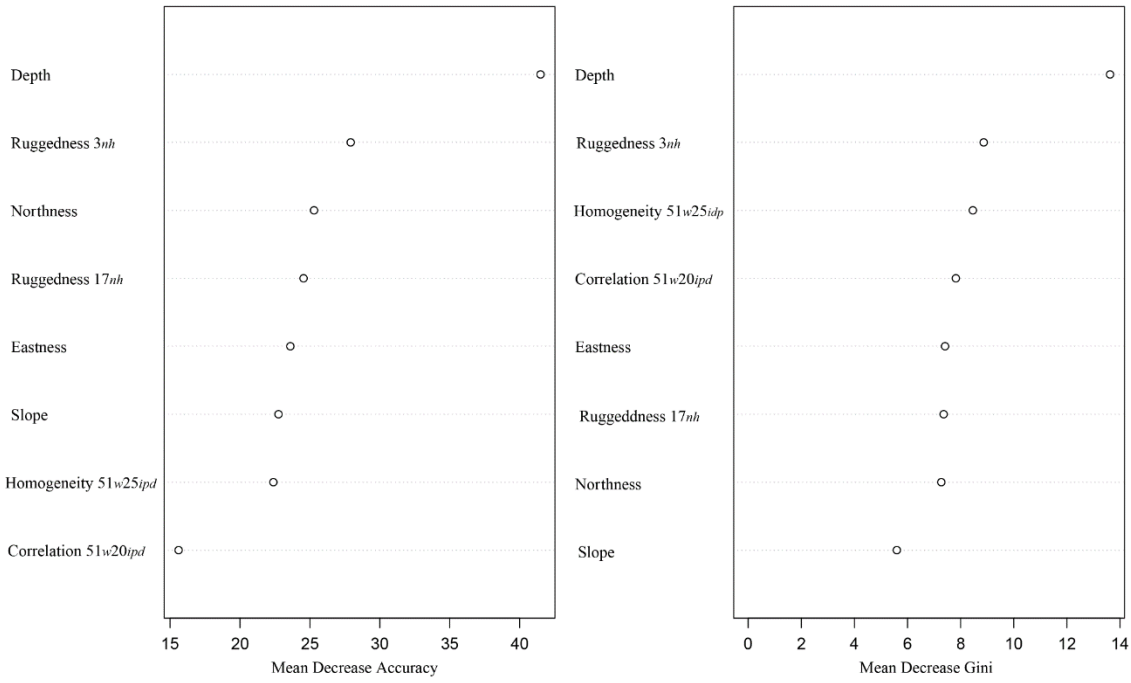


Supplementary materials Figure 23 Variable importance from Random Forests.

4.2.4

Relationship between broad-scale structural complexity captured by ruggedness $17_{nh}$ (350 m resolution) and that captured by the textual index correlation $51_w$ $20_{ipd}$ (25 m resolution) in relation to the distribution of mounds on the Dangaard interfluve.

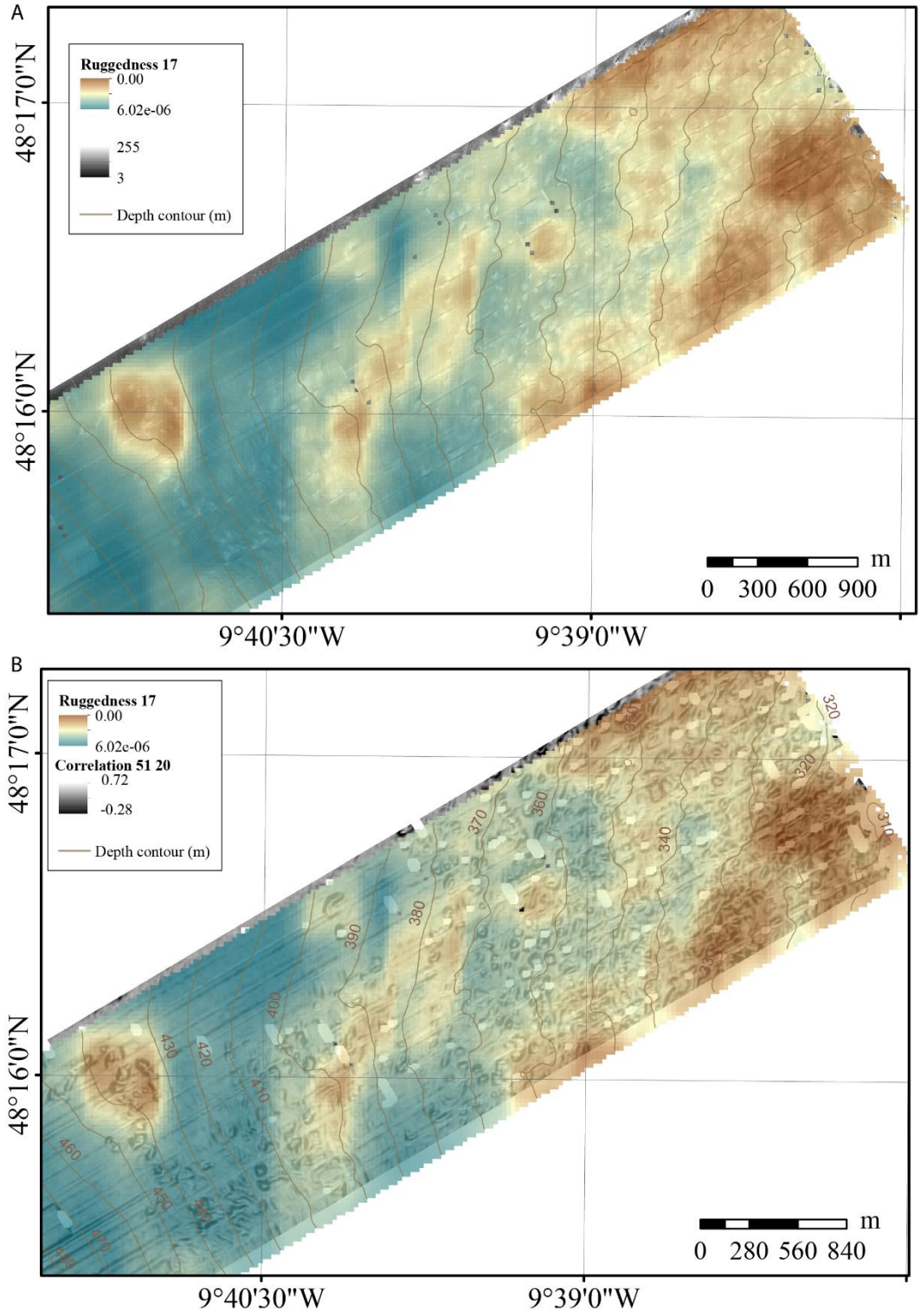


Supplementary materials Figure 4.24 Map of the mini-mounds surveyd on the Dangaard interfluve. (A) Ruggedness $17_{nh}$ is overlain on to side-scan sonar. (B) Ruggedness $17_{nh}$ is overlain on to correlation $51_{w}$ $20_{ipd}$.

# Appendix D Whittard Canyon morphospecies catalogue

Morphospecies catalogue developed for image analysis within Whittard Canyon, North-East Atlantic based upon the CATAMI classification and cross referenced against the Howell and Davies (2010) morphospecies catalogue.

The catalogue name is given followed by any other cross referenced name from the morphospecies guides developed by Howell and Davies (2010) https://deepseacru.org/2016/12/16/deep-sea-species-image-catalogue/, Davies (2017) for the annotation of CEND0917 image data and Robert (2014) for PhD Thesis, Evaluation of local- and medium-scale habitat heterogeneity as proxy for biodiversity in deep-sea habitats.

Appendix D

## 1. BRYOZOA

Bryozoa sp. 1

Bryozoa sp. 2

Bryozoa sp. 3

Cyclostomatida sp. 1 (Howell & Davies 2010 OTU 253)

## 2. ANNELIDIA

### 2.1 Polychaeta (Class)

Sabellidae sp. 1 (Howell & Davies 2010 OTU 54)

Serpulidae sp. 1

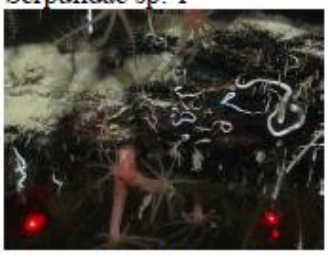

Echiura sp. 1 (Howell & Davies 2010 OTU 297)

## 3. ARTHROPODA

### 3.1 Pycnogonida (Class)

Pycnogonidae sp. 1

### 3.2 Cirripedia (Infraclass)

Balanmorpha sp. 1

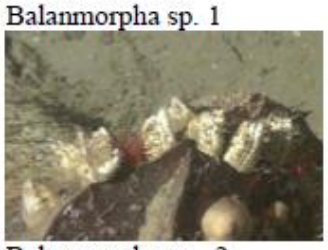

Balanmorpha sp. 2

### 3.3 Decopoda (Order)

#### 3.3.1 Anomura (Infraorder)

##### 3.3.1.1 Galathoidea

Galathoide sp. 1

Galathoide sp. 2

Appendix D

#### 3.3.1.1 Paguroidea

Paguroidea sp. 1 (Robert 2014 PAGU, Davies 2017 OTU 205)

Paguroidea sp. 2

### 3.3.2 Caridae (Infraorder)

*Pandalus borealis* (Davies 2017 OTU 57)

Prawn sp. 2

Prawn sp. 3

Red prawn sp. 1

Prawn sp. 4

Prawn sp. 5

### 3.3.3 Brachyura (Infraorder)

#### 3.3.3.1 Portunidae

*Bathynectes* sp. 1 (Howell & Davies 2010 OTU 235)

Portunidae sp. 1

#### 3.3.3.1 Geryonidae

Geryonidae sp. 1

#### 3.3.3.1 Progeryonidae

Progeryon sp. 1

Brachyura sp. 2

#### 3.3.3.1 Lithodidae

Lithodidae sp. 1

#### 3.3.3.1 Homolidae

*Paromola cuvieri* (Robert 2014 DECA8, Davies 2017 OTU 304)

Homolidae sp. 2

Homolidae sp. 3

**3.3.3.1 Majidae**

Majidae sp. 1

**3.4 Isopoda (Order)**

Isopoda sp. 1

**4. CNIDARIA**

**4.1 ANTHOZOA (Class)**

Anthozoa sp. 1

**4.1.1 Hexacorallia (Subclass)**

**4.1.1.1 Actiniaria (Order)**

Actinaria sp. 2 (Davies 2017 OTU 605)

Actinaria sp. 7

Actinaria_Orange sand anemone

Actinaria sp. 10 (Robert 2014 CNI71)

Actinaria sp.13 (Robert 2014 CNI71, Howell & Davies 2010 OTU 111?)

*Actinernus michaelsarsi* (Robert 2014 9455, Howell & Davies 2010 OTU 554)

Actinaria sp. 19

Actinaria (Howell & Davies 2010 OTU 976)

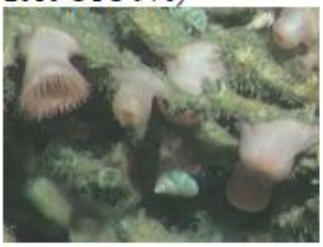

Appendix D

Actinaria sp. 18 (*Calliactis parasitica*, Howell & Davies 2010 OTU 605, Davies 2017 Actinaria sp. 20)

#### 4.1.1.2 Sagartiidae

Sargartiidae sp. 1 (Robert 2014 CNI12, Howell & Davies 2010 OTU 41)

#### 4.1.1.3 Actinoscyphiidae

*Actinoscyphia* sp. 1 (Robert 2014 ACTI)

#### 4.1.1.4 Hormathiidae

*Phelliactis* sp. 1 (Robert 2014 PHELI, Howell & Davies 2010 OTU 255)

*Actinauge richardi* (Howell & Davies 2010 OTU 499)

#### 4.1.1.1 Ceriantharia (Order)

#### 4.1.1.2 Cerianthidae

*Pachycerianthus multiplicatus* (Howell & Davies 2010 OTU 458)

Cerianthidae sp. 4 (Howell & Davies 2010 OTU 2)

Cerianthiidae (Robert 2014 CERI)

Cerianthidae sp. 5

Cerianthidae sp. 6

#### 4.1.2 Zoanthidea (Order)

Zoanthidae sp. 1(Davies 201 OTU 586)

Zoanthidae sp. 2 (Davies 2017 OTU 1041c)

*Epizoanthus paguriphilus*

#### 4.1.3 Corallimorpharia (Order)

Coralliomorpha sp. 1

#### 4.1.4 Scleractinia (Order)

##### 4.1.4.1 Oculinidae

*Madrepora oculata* (Robert 2014 MAD)

##### 4.1.4.2 Caryophylliidae

*Desophyllum pertusum* (Robert 2014 CORA)

Caryophyllidae sp.

*Coryaphyllia* sp. 2 (Davies 2017 OUT 6)

#### 4.1.5 Antipatharia (Order)

##### 4.1.5.1 Schizopathidae

*Bathypathes* sp.1 (Robert 2014 CNI54)

*Parantipathes* sp.1

##### 4.1.5.2 Antipathidae

*Stichopathes* sp. 1 (*Stichopathes* cf. *gravieri*, Howell & Davies 2010 OTU 283, Robert 2014WHIP4)

*Antipathes* sp.1

Antipatharian sp. 1(Robert 2014 CNI50)

Appendix D

**4.1.5.3 Protoptilidae**

*Distichoptilum gracile*

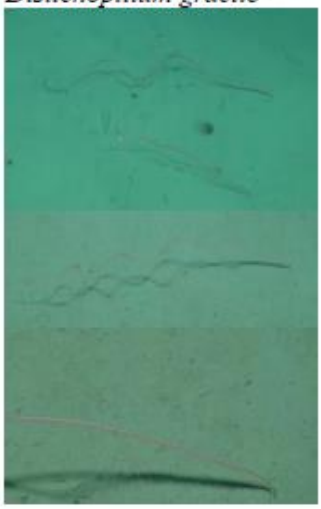

**4.1.6 Octocorallia (Subclass)**

**4.1.7 Alcyonacea (Order)**

**4.1.7.1 Alcyoniidae**

*Anthomastus* sp. 1 (Robert 2014 ANTHO, Howell & Davies 2010 OTU 278)

*Clavularia* sp.1

**4.1.7.2 Primnoidae**

*Primnoa* sp. 1

Primnoidea sp. 2

**4.1.7.3 Plexauridae**

*Swiftia* sp. 1

*Swiftia* sp. (Robert 2014 CNI28)

**4.1.7.4 Isididae**

Isididae sp.1 (Robert 2014 CNI130, Howell & Davies 2010 OTU 334)

*Acanella* sp. 1 (Robert 2014 ACAN)

*Acanella* sp. 2 (Howell & Davies 2010 OTU 282)

Isididae sp. 2

Isididae sp. 3

Isididae sp. 5

Isididae sp. 6

#### 4.1.7.5 Paragorgiidae

*Paragorgia* sp. 1

#### 4.1.7.6 Chrysogorgiidae

Chrysogorgiidae sp. 1

Unknown coral sp.

Red coral sp. 1

Red coral sp. 2 (Robert 2014 CNI27)

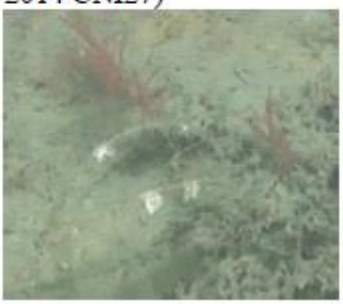

### 4.1.8 Pennatulacea (Order)

*Pennatula* sp.1 (Howell & Davies 2010 OTU 486)

Pennatulacea sp. 2 (*Funiculina* sp.)

Umbellula sp. 1 (Howell & Davies 2010 OTU 581)

*Umbellula* sp. 2

*Umbellula* sp. 3

Pennatulacea (Unsure of ID)

Appendix D

## 4.2 HYDROZOA (Class)

#### 4.2.1.1 Stylasteridae

*Stylaster* sp. 1

Hydrozoa sp. 1

Hydrozoa sp. 2

Hydrozoa sp. 11

## 5. ECHINODERMATA

## 5.1 Ophiuroidea (Class)

Ophiuroidea sp. 1

Ophiuroidea sp. 2

Ophiuroidea sp. 3

Ophiuroidea sp. 4

#### 5.1.1.1 Ophiuridae

Ophiuridae sp. 1

#### 5.1.1.1 Gorgonocephalidae

*Gorgonocephalus* sp. 1 (Robert 2014 Gorgonocephalidae, Howell & Davies 2010 OTU 214)

## 5.2 Crinoidea (Class)

### 5.2.1 Sessile crinoids

*Leptometra celtica*

Crinoid sp. 1

Crinoid sp .2 Red/brown crinoid (Robert 2014 FSTAI

Crinoid sp. 4 (Howell & Dav 2010 OTU 131)

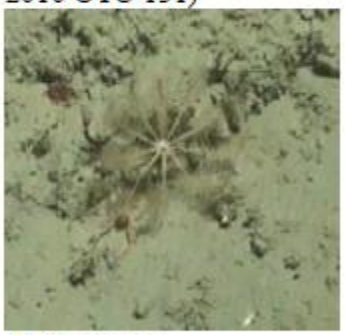

Crinoid sp. 7

Crinoid sp. 8 (Robert 2014 FSTAR6, Howell & Davies 2010 OUT 135)

*Pentametrocrinus atlanticus* (Robert 2014 PENTA)

### 5.2.2 Stalked crinoids

*Bathycrinus carpenterii*

Crinoid sp. 3

Crinoid sp. 4

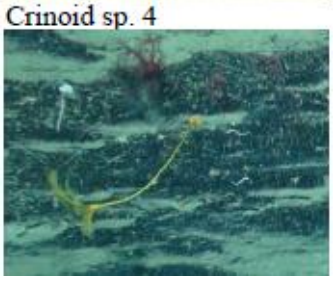

Crinoid sp. 5

Crinoid sp. 10

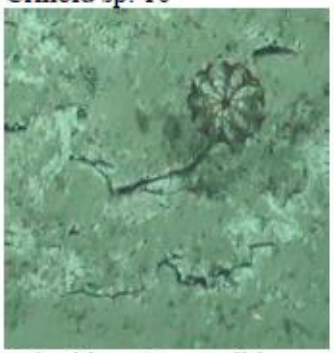

Crinoid sp. 6 - possibly *Endoxocrinus wyvillethomsoni* (Robert 2014 LILY6)

### 5.3 Asteroidea (Class)

Asteroidea sp. 2

Asteroidea sp. 6

### 5.3.1 Forcipulatida (Order)

*Stichastrella rosea* (Howell & Davies 2010 OTU198 )

Asteroidea sp. 11 ( *Zoroaster fulgens*, Robert 2014 ASTER3)

### 5.3.2 Paxillosida (Order)

*Nymphaster* sp. 1 (Robert 2014 NYMPH, Howell & Davies 2010 OTU 433)

Appendix D

**5.3.3 Valvatida (Order)**

**5.3.4 Spinulosia (Order)**

*Henricia sanguinolenta*

**5.3.5 Brisingida (Order)**

*Brisingida* sp. (Robert 2014 BRIS, Howell & Davies 2010 OTU 274)

**5.4 Echinoidea (Class)**

*Cidaris cidaris* (Robert 2014 CID, Howell & Davies 2010 OTU 211)

**5.4.1.1 <u>Echinoidea</u>**

*Echinus* sp. 1 (Robert 2014 URCH3, Howell & Davies 2010 OTU 194)

*Echinus acutus*

*Echinus* sp. 5

*Echinus* sp. 3 (Howell & Davies 2010 OTU 445)

Echinoidea sp. 1 (*Calveriosoma fenestratum*, Howell & Davies 2010 OTU 188?)

*Phormosoma placenta* (Robert 2014 PHORMO)

Spatangoidea sp. 2

**5.5 Holothuroidea (Class)**

*Benthogone* sp. (Robert 2014 HOLO15)

Holothuroidea sp. 1

Holothuroidea sp. 2

Holothuroidea sp. 3

Holothuroidea sp. 4

Holothuroidea sp. 5

Holothuroidea sp. 6

*Parastichopus tremulus* (Howell & Davies 2010 OTU 266)

Holothuroidea sp. 8

Holothuroidea sp. 9

*Mesothuria intestinalis*

*Psolus squamatus* (Howell & Davies 2010 OTU 252)

## 6. MOLLUSCA

### 6.1.1 Bivalvia (Class)

*Neopycnodonte* sp. 1 sp

*Acesta excavata*

### 6.1.2 Gastropoda (Class)

Turbinidae sp. 1 (*Margarites* sp. 1, Howell & Davies 2010 OTU 277?)

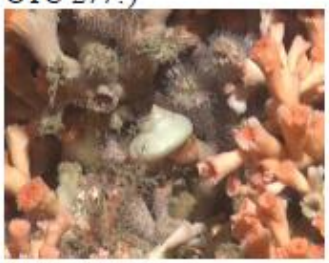

Buccinidae sp. 1

Buccinidae sp. 2

## 7. BRACHIOPODA

Brachiopoda sp. 1 (*Gryphus vitreus*?)

## 8. PORIFERA

#### 8.1.1.1 Erect Sponges

Porifera sp.1

Appendix D

**6.1.2 Gastropoda (Class)**

Turbinidae sp. 1 (*Margarites* sp. 1, Howell & Davies 2010 OTU 277?)

Buccinidae sp. 1

Buccinidae sp. 2

7. **BRACHIOPODA**

Brachiopoda sp. 1 (*Gryphus vitreus*?)

8. **PORIFERA**

**8.1.1.1 Erect Sponges**

Porifera sp.1

Morpospecies- Chalice sponge

*Hyalonema apertum* (Robert 2014 PORI4) – Stem covered in *Epizoanthus* sp.

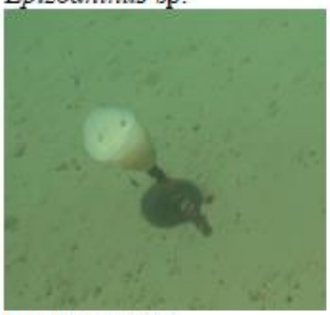

Porifera sp. 15

**8.1.1.1 Encrusting Sponge**

Porifera sp. 11 (Hexadella sponge)

Porifera sp.14

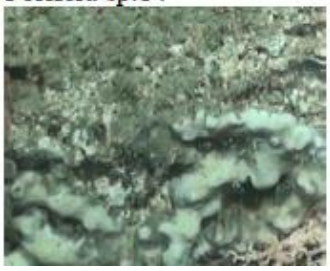

9. **FORMANIFERA**

**9.1.1.1 Xenophyophoroidea**

*Syringammina* sp. 1 (Howell & Davies 2010 OTU 261)

10. **CHORDATA**

**10.1 Ascidacea (Class)**

Tunicate sp. 1

# Appendix E Research papers co-authored during the course of this PhD

This appendix consists of two additional peer-reviewed papers that were co-authored during the course of the PhD. They are included in chronological order.

HOWELL, K. L., DAVIES, J. S., ALLCOCK, A. L., BRAGA-HENRIQUES, A., BUHL-MORTENSEN, P., CARREIRO-SILVA, M., DOMINGUEZ-CARRIO, C., DURDEN, J. M., FOSTER, N. L., GAME, C. A., HITCHIN, B., HORTON, T., HOSKING, B., JONES, D. O. B., MAH, C., LAGUIONIE MARCHAIS, C., MENOT, L., MORATO, T., PEARMAN, T. R. R., PIECHAUD, N., ROSS, R. E., RUHL, H. A., SAEEDI, H., STEFANOUDIS, P. V., TARANTO, G. H., THOMPSON, M. B., TAYLOR, J. R., TYLER, P., VAD, J., VICTORERO, L., VIEIRA, R. P., WOODALL, L. C., XAVIER, J. R. & WAGNER, D. 2019. A framework for the development of a global standardised marine taxon reference image database (SMarTaR-ID) to support image-based analyses. PLoS One, 14, e0218904.

ROWDEN, A. A., PEARMAN, T. R. R., BOWDEN, D. A., ANDERSON, O. F. & CLARK, M. R. 2020. Determining Coral Density Thresholds for Identifying Structurally Complex Vulnerable Marine Ecosystems in the Deep Sea. Frontiers in Marine Science, 7.

Appendix E

PLOS ONE

RESEARCH ARTICLE

# A framework for the development of a global standardised marine taxon reference image database (SMarTaR-ID) to support image-based analyses

**Kerry L. Howell[1]*, Jaime S. Davies[1], A. Louise Allcock[2], Andreia Braga-Henriques[3,4], Pål Buhl-Mortensen[5], Marina Carreiro-Silva[6,7], Carlos Dominguez-Carrió[6,7], Jennifer M. Durden[8], Nicola L. Foster[1], Chloe A. Game[9], Becky Hitchin[10], Tammy Horton[8], Brett Hosking[8], Daniel O. B. Jones[8], Christopher Mah[11], Claire Laguionie Marchais[2], Lenaick Menot[12], Telmo Morato[6,7], Tabitha R. R. Pearman[8], Nils Piechaud[1], Rebecca E. Ross[1,5], Henry A. Ruhl[8,13], Hanieh Saeedi[14,15,16], Paris V. Stefanoudis[17,18], Gerald H. Taranto[6,7], Michael B. Thompson[19], James R. Taylor[20], Paul Tyler[21], Johanne Vad[22], Lissette Victorero[23,24,25], Rui P. Vieira[20,26], Lucy C. Woodall[16,17], Joana R. Xavier[27,28], Daniel Wagner[29]**

**1** School of Biological and Marine Science, Plymouth University, Drake Circus, Plymouth, United Kingdom, **2** Zoology, School of Natural Sciences, and Ryan Institute, National University of Ireland, Galway, Galway, Ireland, **3** MARE-Marine and Environmental Sciences Centre, Estação de Biologia Marinha do Funchal, Cais do Carvão, Funchal, Madeira Island, Portugal, **4** ARDITI-Regional Agency for the Development of Research, Technology and Innovation, Oceanic Observatory of Madeira (OOM), Madeira Tecnopolo, Caminho da Penteada, Funchal, Portugal, **5** Institute of Marine Research,Nordnes, Bergen, Norway, **6** Okeanos Research Centre, Universidade dos Açores, Departamento de Oceanografia e Pesca, Horta, Portugal, **7** IMAR Instituto do Mar, Marine and Environmental Sciences Centre (MARE), Universidade dos Açores, Horta, Portugal, **8** National Oceanography Centre, University of Southampton Waterfront Campus, European Way, Southampton, United Kingdom, **9** School of Computing Sciences, University of East Anglia, Norwich, United Kingdom, **10** JNCC, Inverdee House, Aberdeen, United Kingdom, **11** Dept. of Invertebrate Zoology, National Museum of Natural History, Smithsonian Institution, Washington D.C., United States of America, **12** Ifremer, Centre de Bretagne, Plouzané, France, **13** Monterey Bay Aquarium Research Institute, Moss Landing, CA, United States of America, **14** Senckenberg Research Institute and Natural History Museum; Department of Marine Zoology, Frankfurt am Main, Germany, **15** Goethe University Frankfurt, Institute for Ecology, Diversity and Evolution, Frankfurt am Main, Germany, **16** OBIS Data Manager, Deep-Sea Node, **17** Nekton Foundation, Begbroke Science Park, Begbroke Hill, Begbroke, Oxfordshire, United Kingdom, **18** Department of Zoology, University of Oxford, Zoology Research and Administration Building, Oxford, United Kingdom, **19** Gardline Limited, Endeavour House, Great Yarmouth, Norfolk, United Kingdom, **20** Senckenberg am Meer, German Centre for Marine Biodiversity Research (DZMB), Martin-Luthur-King-Platz, Hamburg, Germany, **21** School of Ocean and Earth Science National Oceanography Centre, University of Southampton Waterfront Campus, European Way, Southampton, United Kingdom, **22** Grant Institute, School of Geosciences, The University of Edinburgh, The King's Buildings, Edinburgh, United Kingdom, **23** Institut de Systématique, Évolution, Biodiversité (ISYEB), CNRS, Muséum national d'Histoire naturelle,Sorbonne Université, Ecole Pratique des Hautes Etudes, Paris, France, **24** Biologie des Organismes et Ecosystèmes Aquatiques (BOREA), CNRS, Muséum national d'Histoire naturelle,Sorbonne Université, Université de Caen Normandie, Université des Antilles, IRD, Paris, France, **25** Centre d'Écologie et des Sciences de la Conservation (CESCO), CNRS, Muséum national d'Histoire naturelle,Sorbonne Université, Paris, France, **26** Centre for Environment, Fisheries & Aquaculture Science, Lowestoft Laboratory, Lowestoft, Suffolk, United Kingdom, **27** CIIMAR–Interdisciplinary Centre of Marine and Environmental Research of the University of Porto, Matosinhos, Portugal, **28** University of Bergen, Department of Biological Sciences and KG Jebsen Centre for Deep-Sea Research, Bergen, Norway, **29** NOAA Office of Ocean Exploration and Research, Charleston, South Carolina, United States of America

* kerry.howell@plymouth.ac.uk





**Citation:** Howell KL, Davies JS, Allcock AL, Braga-Henriques A, Buhl-Mortensen P, Carreiro-Silva M, et al. (2019) A framework for the development of a global standardised marine taxon reference image database (SMarTaR-ID) to support image-based analyses. PLoS ONE 14(12): e0218904. https://doi.org/10.1371/journal.pone.0218904

**Editor:** Vincent Lecours, University of Florida, UNITED STATES

**Received:** June 6, 2019

**Accepted:** December 9, 2019

**Published:** December 31, 2019



**Data Availability Statement:** All relevant data are within the paper.

**Funding:** KH, NP, RR, NF was supported by the Natural Environment Research Council funded DeepLinks project NE/K011855/1, https://nerc.ukri.org/. The workshop was funded by the Deep Sea Biology Society's Lounsbery Workshop Award https://dsbsoc.org/. ALA and CLM are supported by Grant Number SFI/15/IA/3100 to ALA from Science Foundation Ireland http://www.sfi.ie/ and

the Marine Institute https://www.marine.ie/Home/home under the Investigators Programme co-funded under the European Regional Development Fund 2014-2020, https://ec.europa.eu/regional_policy/en/funding/erdf/. AB-H was supported by the Oceanic Observatory of Madeira project (M1420-01-0145-FEDER-000001-Observatório Oceânico da Madeira- OOM) co-financed by the Madeira Regional Operational Programme (Madeira 14-20) under the Portugal 2020 strategy through the European Regional Development Fund https://ec.europa.eu/regional_policy/en/funding/erdf/, and the Portuguese Foundation for Science and Technology (FCT, Portugal) https://www.fct.pt/, through the strategic project UID/MAR/04292/2013 granted to MARE. JV is supported by Oil and Gas UK https://oilandgasuk.co.uk/ and the ATLAS project funded by the European Commission's H2020 Scheme https://ec.europa.eu/programmes/horizon2020/en through Grant Agreement 678760. HAR was supported by the CeNCOOS Partnership: Ocean Information for Decision Makers (award number NA16NOS0120021) https://www.cencoos.org/about/program/funding. DOBJ was supported by the UK Natural Environment Research Council National Capability funding: "Climate Linked Atlantic Section Science" (CLASS), grant number NE/R015953/1 https://nerc.ukri.org/. DW was supported by NOAA Deep Sea Coral Research and Technology Program https://deepseacoraldata.noaa.gov/. LW and PS were supported by the Garfield Weston Foundation https://garfieldweston.org/. TM was supported by Program Investigador FCT (IF/01194/2013), IFCT Exploratory Project (IF/01194/2013/CP1199/CT0002) from the Fundação para a Ciência e Tecnologia (POPH and QREN) https://www.fct.pt/, PO2020 MapGes (Acores-01-0145-FEDER-000056) http://www.azores.gov.pt/Portal/en/principal/, and H2020 ATLAS (grant agreement no. 678760) https://ec.europa.eu/programmes/horizon2020/en. RV was funded by the Fundação para a Ciência e a Tecnologia (FCT/SFRH/BD/84030/2012) https://www.fct.pt/, with additional support provided by Cefas through the Science Futures programme https://www.cefas.co.uk/. JRX research is funded by the H2020 EU Framework Programme for Research and Innovation through the SponGES project (grant agreement No. 679849) https://ec.europa.eu/programmes/horizon2020/en and partially supported by the Strategic Funding UID/Multi/04423/2019 through national funds provided by the Foundation for Science and Technology (FCT) https://www.fct.pt/ and the European Regional Development Fund (ERDF) https://ec.europa.eu/regional_policy/en/funding/erdf/, in the framework of the programme PT2020. We would like to make

## Abstract

Video and image data are regularly used in the field of benthic ecology to document biodiversity. However, their use is subject to a number of challenges, principally the identification of taxa within the images without associated physical specimens. The challenge of applying traditional taxonomic keys to the identification of fauna from images has led to the development of personal, group, or institution level reference image catalogues of operational taxonomic units (OTUs) or morphospecies. Lack of standardisation among these reference catalogues has led to problems with observer bias and the inability to combine datasets across studies. In addition, lack of a common reference standard is stifling efforts in the application of artificial intelligence to taxon identification. Using the North Atlantic deep sea as a case study, we propose a database structure to facilitate standardisation of morphospecies image catalogues between research groups and support future use in multiple front-end applications. We also propose a framework for coordination of international efforts to develop reference guides for the identification of marine species from images. The proposed structure maps to the Darwin Core standard to allow integration with existing databases. We suggest a management framework where high-level taxonomic groups are curated by a regional team, consisting of both end users and taxonomic experts. We identify a mechanism by which overall quality of data within a common reference guide could be raised over the next decade. Finally, we discuss the role of a common reference standard in advancing marine ecology and supporting sustainable use of this ecosystem.

## Introduction

There is a long history of using images in marine ecological studies. The first underwater photograph was taken in 1856 in UK seas [1] but it took until 1893, on the sunlit Mediterranean seabed, for the first clear images to be produced [2]. Following this, the use of underwater photography became widespread in shallow seas, opening up this environment to a wider public (e.g. [3]). The first deep-sea photograph was taken from the porthole of a bathysphere in the early 1930s [4] and shortly after, the first self-contained deep-sea photographic systems were developed in the 1940s at the Woods Hole Oceanographic Institution [5,6]. Whilst there were many good deep-sea photographs available between this time and the early 1970s [7,8], few biologists studied them, as often no corresponding samples of animals were taken, making identification difficult [9]. The notable exceptions to this [9, 10, 11, 12, 13, 14] paved the way for photography to become established as an important tool for the study of deep-water environments [15, 16, 17, 18, 19]. Today, with the routine use of seafloor cameras, towed camera platforms, remotely operated and autonomous underwater vehicles (ROVs and AUVs), photographic assessment of marine fauna and faunal assemblages is a vital tool for research used by both scientists and industry [20, 21, 22].

Imaging is an important non-destructive tool for studying marine geology and biodiversity at a wide range of spatial scales (from millimetres to tens of km) [21, 23]. It enables a rapid assessment of wide areas while retaining valuable ecological information, such as spatial distribution and associations between organisms and with the landscape. Photographic and video assessment is particularly useful in complex terrain or sensitive areas [24, 25], where direct sampling is challenging or undesirable. Imaging is generally used to provide both qualitative

Appendix E



it clear that one of the co-authors is employed by a commercial company (Gardline Limited). This company provided support in the form of salary, travel and subsistence for Michael Thompson to attend the workshop held to discuss end user needs and database structure, as well as to contribute to the preparation of the manuscript. We would also like to make clear that this commercial affiliation does not alter our adherence to all PLOS ONE policies on sharing data and materials.

**Competing interests:** We would like to make it clear that one of the co-authors is employed by a commercial company (Gardline Limited). We would also like to make clear that this commercial affiliation does not alter our adherence to all PLOS ONE policies on sharing data and materials.

and quantitative information on the marine environment (e.g. sediment type [26]; hyperbenthic (living immediately above the seafloor) and midwater organisms [27]; benthic epifauna (the organisms living on the sediment surface [24, 28, 29]); and faunal activity or behaviour (through visible life traces or video/time-lapse images [30, 31, 32]). As a non-destructive tool, imaging is also paramount in the identification of Vulnerable Marine Ecosystems (VMEs) [33, 34]. It has also been widely used to access the impact of human activities on benthic communities e.g. [35, 36] and to evaluate the distribution of marine litter on the seafloor e.g. [37, 38]. Imaging has also been applied to detecting and assessing temporal variation [22, 39]. Estimates of organism densities from seafloor imagery have proven more accurate than those obtained by physical sampling methods, such as trawling. For instance, densities derived from seafloor imagery provided a 10-50 fold increase in accuracy in comparison to trawling in the Porcupine Abyssal Plain in the North East Atlantic [40]. However, it is likely that diversity is underestimated as a result of difficulties of identification of the taxa to lower taxonomic levels from imagery [21].

The use of images to collect faunal data brings with it the challenge of identifying taxa from image data. Identification of physical specimens is usually achieved using taxonomic keys that have been developed by experts working on specific taxonomic groups. These keys are developed based on thorough study of preserved specimens, incorporating a systematic analysis of characteristic morphological features, followed by the development of a dichotomous key. While traditional taxonomic keys may be useful in the identification of some taxonomic groups from imagery (e.g. fish), many such keys rely on characteristics that are not visible in imagery (e.g. the arrangement of mesenteries in anemones, spicule shape in sponges, sclerite morphology in gorgonians, and the ossicles of holothurians). Therefore, for many taxonomic groups the development of field guides are essential to support taxon identification from image data. Many field guides have been developed for shallow-water marine species for use by SCUBA divers. These rely heavily on image data to show form, function and details of anatomy that can be used for accurate identification e.g. [41, 42], but they are rare for depths beyond recreational SCUBA diving capability (>30 m) (hereinafter referred to as deep-water species). Good field guides are usually underpinned by a comprehensive understanding of the species pool for the region of study. For most deep-water regions, this understanding is lacking. Notable exceptions include the Monterey Canyon [43] and the soft sediment (trawlable) habitats of the North Atlantic. The lack of comprehensive field guides for deep-water marine organisms presents a significant challenge to those faced with the interpretation of image data from poorly known regions or habitats, such as seamounts, ridges, or other areas of hard and high-relief substrates that are not conducive to trawling surveys.

In the absence of a good knowledge of the taxonomy of many groups and regional field guides, a common practice in the interpretation of image data is the development of a morphospecies reference image dataset (Fig 1) and the use of operational taxonomic unit (OTU) numbers. The OTU numbers are used in place of taxon names for organisms for which a species name has not yet been assigned owing to the lack of physical specimens to corroborate the observation [24, 43, 44, 45, 46, 47, 48, 49, 50]. These morphospecies reference image catalogues provide a permanent reference of what has been observed in the study. But perhaps more importantly, allow the user to differentiate between taxa below the lowest level of the taxonomic hierarchy to which the observed organism can be identified, using traditional taxonomic features, and thus preserve important information on biodiversity. For example, taxonomic identification of many sponge and soft coral species is impossible from image data alone, since their taxonomy is based on the arrangement, size and shape of microscopic structures in their skeletons. Thus, following traditional methods of sample analysis, all observed species would be assigned the level Porifera or Alcyonacea, resulting in a significant loss of

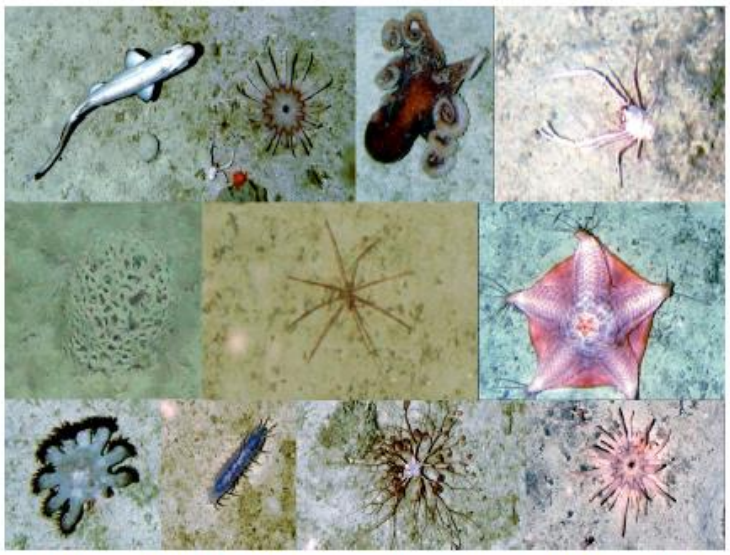

**Fig 1. Example of a reference image catalogue where representatives of each taxa observed are cropped from an image, and assigned an OTU number that is subsequently used in image analysis in place of a standard latin name.**

https://doi.org/10.1371/journal.pone.0218904.g001

resolution in the data. However, use of a morphospecies reference image catalogue allows the observer to assign morphologically different (and in most cases, likely taxonomically distinct) forms to a unique OTU number, which can then be assigned to the taxon (e.g. Porifera msp. 1, Porifera msp 2 etc.) if needed, thereby retaining taxonomic resolution in the data.

The problem with this approach is that each study or group uses a different naming convention for morphospecies. It then becomes impossible to compare or combine datasets between studies. Morphospecies catalogues are not usually published, making it difficult for researchers to compare data or check identifications. Comparison between research studies or industry-gathered data (for example from environmental impact assessments or site monitoring) are also impaired by this issue. In addition, both field guides and morphospecies reference image catalogues fail to document explicitly the visual characteristics used to differentiate taxa. They generally provide little more than a visual idea of what a taxon looks like. This compounds problems of observer biases that are well documented in biological sample analysis [51, 52, 53). When identifying taxa from image data, it is necessary to use a combination of traditional taxonomic features and ecological data (e.g. depth, location, habitat, knowledge of the local species pool) to arrive at an identification. This skill in 'field identification' is often acquired through an 'oral tradition' with little in the way of formalised training materials provided to new researchers entering the field or new consultants provided with image data to analyse.

Developments in autonomous and robotic technology, and the increased use of them across different fields, are increasing the amount of image-based data that can be collected [54, 55, 56]. For example, a single 22-hour AUV mission returned over 150,000 seafloor images [40, 56]. Manual image analysis is a time-consuming process, which forms the current bottleneck in image-based ecological sampling [21, 57, 58, 59]. As a result, a number of research teams are investigating the use of artificial intelligence (AI) and computer vision (CV) as potential means to accelerate and standardise the interpretation of ecological image data [51, 52, 53, 56,

Appendix E



60]. The most promising of these techniques is supervised machine learning to automatically detect and classify taxa [53, 58, 61]. However, consistent interpretations by humans are initially required, providing 'gold standard' classifications, with as much data as possible, which can be used to train these algorithms. Moving forward, developments in AI and CV approaches that combine the use of visible morphological characteristics with deep learning, would benefit significantly from the development of a standard image-reference dataset. For those taxonomic groups in which the morphological characteristics commonly used to differentiate taxa are not discernible in images (e.g. sponges, anemones, zoanthids and plexaurid gorgonians), these types of combined approaches will first require development of novel visual multi-access keys, which themselves can only be created from a high-quality reference image dataset and skilful determination of characteristics differentiating taxa.

While there are a variety of on-line open-access databases that are designed to archive biological and ecological information, including genetic data (for example GenBank), species occurrence records (for example the Global Biodiversity Information Facility GBIF) and even images of taxa (for example Morphbank), there are few that provide a reference guide to support the interpretation of image-based datasets. Table 1 provides a list of existing field guides and morphospecies reference image catalogues for deep-water species of the Atlantic Ocean that are currently publicly available. However, many more are un-published or inaccessible to others, and are held as a mixture of printed and electronic materials. Recently there have been attempts to make morphospecies reference image catalogues associated with specific research programmes or projects available to others (for example [43, 47, 62, 63, 64, 65, 66] to mention a few). In addition classification based approaches to this issue have also been developed [67]. While useful, this 'piece-meal' approach will not solve the challenges outlined above.

There is a clear need for the development of a standard reference guide to support the use of image-based sampling. Failure to develop appropriate tools will ultimately hinder progress in marine ecology, particularly in deep-sea marine ecology where images are frequently one of the few collected datasets. In order to improve data quality and comparability, realise the benefits of new technologies in both image data collection and interpretation, and ultimately raise standards of taxonomic identification within academia, government, and industry, we must move towards the use of standard reference guides, quality controlled and curated by experts in both taxonomy and field identification.

Our aims were to develop 1) a database structure to facilitate the standardisation (and ultimately pooling) of morphospecies reference image catalogues between individuals and groups, supporting onward use in multiple applications; and 2) a framework for coordination of international efforts to develop reference guides for the identification of deep-water species from image-based data.

## Methods

The initial stages of developing the framework for the database consisted of assessing the requirements of those working with image-based data through end user group discussions, both informally and as part of an international workshop. This included the need for both online and offline databases and printable catalogues for use in making identifications at sea.

We reviewed current relevant databases and database standards. These were focused around the Darwin Core standard, the Ocean Biogeographic Information System (OBIS), and the World Register of Marine Species databases (WoRMS), which are all used regularly by the end user community.

The Darwin Core is an international standard set of terms and definitions that facilitates sharing biodiversity data [84]. The Darwin Core quick reference guide (http://rs.tdwg.org/

**Table 1. List of available image catalogues and identification guides of the deep-sea fauna off the Atlanto-Mediterranean region.**

| Name of resource | Geographical scope | Taxonomic scope | Type of resource | Developer;reference | Available at: |
|---|---|---|---|---|---|
| Deep Sea ID (v1.2) | Global | All groups | Smartphone application | NHM, NOC, WORMS; [68] | http://www.marinespecies.org/deepsea |
| NOAA Office of Ocean Exploration and Research Benthic Deepwater Animal Identification Guide | Global | All groups | Online portal | NOAA [69] | https://oceanexplorer.noaa.gov/okeanos/animal_guide/animal_guide.html |
| Sharks, batoids, and chimaeras of the North Atlantic | NA | Sharks, batoids and chimaeras | Book and digital file | FAO; [70] | http://www.fao.org/docrep/017/i3178e/i3178e.pdf |
| Catalogue of Atlantic Deep-Sea fauna | NEA | All groups | Online portal | University of Plymouth, IFREMER, NOAA; [71] | http://www.deepseacatalogue.fr |
| SERPENT Media Archive | NEA | All groups | Online portal | National Oceanography Centre ; [72] | http://archive.serpentproject.com |
| Holothuroidea of the Charlie Gibbs Fracture Zone area, northern Mid-Atlantic Ridge | NEA | Holothurians | Peer-reviewed journal article | [73] | https://doi.org/10.1080/17451000.2012.750428 |
| An identification guide to sharks, skates and rays in Northern English waters | NEA | Sharks, skates and rays | Digital file | Shark Trust | https://www.sharktrust.org/shared/downloads/projects/id_guide_sharks_skates_rays_northern_england.pdf |
| Deep-sea life of Scotland and Norway | NEA (Cold water Faroe-Shetland Channel and Norwegian Sea only) | All groups | Book | [63] | Book |
| A photographic guide of the species of the Gorringe Bank | NEA (Gorringe Bank only) | All groups | Digital file | CCMAR, OCEANA; [74] | https://www.ccmar.ualg.pt/sites/ccmar.ualg.pt/files/files/Docs_ASP/Events_2017/Gorringe/a_photographic_guide_of_the_species_of_the_gorringe_bank.pdf |
| Coral identification guide, NAFO area | NWA | Corals | Digital file | NAFO; [75] | https://archive.nafo.int/open/studies/s42/S42-final.pdf |
| Sponge identification guide, NAFO area | NWA | Sponges | Digital file | NAFO; [76] | https://archive.nafo.int/open/studies/s43/S43.pdf |
| Coral, Sponge, and Other Vulnerable Marine Ecosystem Indicator Identification Guide, NAFO Area | NWA | Sponges and corals | Digital file | NAFO; [77] | https://www.nafo.int/Portals/0/PDFs/Studies/s47/s47-print.pdf |
| Identification sheets for the common deep-sea corals off the Northeast and Mid-Atlantic US (v1.0) | NWA | Corals | Digital file | NOAA; [78] | https://www.nefsc.noaa.gov/fsb/training/NortheasternU.SDeepsea_Coral_Guide.pdf |
| Deep Reef Benthos of Bermuda: Field Identification Guide. | NWA | All groups | Book and digital file | Nekton; [66] | https://doi.org/10.6084/m9.figshare.7333838 |
| Field identification guide to the sharks and rays of the Mediterranean and Black Sea | MED and BS | Sharks and rays | Book and digital file | FAO; [79] | http://www.fao.org/3/a-y5945e.pdf |
| Guide de la faune profonde de la mer Méditerranée | MED | All groups | Book | MNHN; [80] | http://sciencepress.mnhn.fr/fr/collections/patrimoines-naturels/guide-de-la-faune-profonde-de-la-mer-mediterranee |
| Deep-sea sponges of the Mediterranean Sea | MED | Sponges | Poster and digital file | FAO; [81] | http://www.fao.org/3/a-i6945e.pdf |
| Deep-sea corals of the Mediterranean Sea | MED | Corals | Poster and digital file | FAO; [82] | http://www.fao.org/3/a-i7256e.pdf |

(*Continued*)

Appendix E



Table 1. (Continued)

| Name of resource | Geographical scope | Taxonomic scope | Type of resource | Developer;reference | Available at: |
|---|---|---|---|---|---|
| On the Benthic Invertebrate Megafauna at the Mid-Atlantic Ridge, in the Vicinity of the Charlie-Gibbs Fracture Zone (Appendix) | NEA | Invertebrates | PhD thesis | [83] | https://eprints.soton.ac.uk/id/eprint/351272 |

MED–Mediterranean Sea; NA–North Atlantic; NEA–Northeast Atlantic; NWA–Northwest Atlantic; BS–Black Sea

https://doi.org/10.1371/journal.pone.0218904.t001

dwc/terms/), provides a comprehensive glossary of terms (standardised fields with descriptors and examples) to ensure data concerned with the occurrence of organisms, the physical existence of specimens in collections, and related environmental information can be standardised. Darwin Core forms the basis of a number of existing online open-source relevant databases (e.g. [85, 86, 87, 88]), and, thus, is the internationally agreed standard upon which further database development should be based. Darwin Core Archives (DwC-A) comprise a set of text files, including both the dataset (.csv) and a document (.xml) which describes the included files, fields, and their relationships. This offers a standard format used to describe biodiversity data and is being commonly employed to share more complex and structured datasets.

OBIS [87] was originally developed as the information management component of the Census of Marine Life (2000–2010) programme. OBIS founder, Dr. J. F. Grassle, articulated the vision of OBIS as "an online, worldwide atlas for accessing, modelling and mapping marine biological data in a multidimensional geographic context". The OBIS database currently consists of over 55 million observations of nearly 124,000 marine species. In 2009, OBIS was adopted as a project by the International Oceanographic Data and Information Exchange (IODE) programme of the Intergovernmental Oceanographic Commission (IOC) of UNESCO. It represents an internationally important archive for species distribution data. OBIS is closely linked with WoRMS, which provides the taxonomic backbone, and geospatial data are provided by the Marine Regions database. Additional functionality includes the taxon match tool for resolving names used by other similar platforms, providing crucial quality control support for taxonomic data among the research community and biodiversity platforms [89].

WoRMS is an authoritative classification and catalogue of marine names including information on synonymy, and is curated by around 400 taxonomists globally, in accordance with best practice [88, 89, 90]. The content of WoRMS is managed by taxonomic and thematic experts, who are responsible for controlling the quality of the information contained within the database [89]. WoRMS is underpinned by the Aphia platform, which is a Microsoft Structured Query Language (MS SQL) database, containing over 400 fields spread over more than 80 related tables. This infrastructure is designed to capture taxonomic and related data and information. WoRMS is also the basis of the World Register of Deep-Sea Species (WoRDSS), which, through its app, Deep Sea ID [68], represents one of the few existing image-based deep-sea species guides (but see Table 1).

The Marine Regions database [91] provides a standard, relational list of geographic names, coupled with information and maps of the geographic location of these features. All geographic objects of the Marine Regions database have a unique ID, called the Marine Regions Geographic Identifier (MRGID). The different geographic objects are determined by a place-type and coordinates. While the coordinates are represented as different vector data types

being a point, a line or a polygon, a placetype provides contextual information to the geographic objects, for example a sea, a bay, a ridge, a sandbank or an undersea trench.

Following the initial review of relevant databases and database standards, a strawman database architecture, to facilitate the standardisation of morphospecies reference image catalogues between individuals / groups, was proposed and circulated to an international team of end users, database specialists and programmers. An international workshop funded by the Deep-Sea Biology Society was held at Plymouth University, UK, on the 4th-5th December 2017, where the draft structure was reviewed and refined. The workshop consisted of a cross section of attendees including major dataset holders, computer scientists, taxonomists, benthic ecologists, and representatives from WoRMS / WoRDSS. Following the workshop, the refined structure was tested by both workshop participants and members of the wider community, who input their existing morphospecies reference image catalogues into the proposed format. This resulted in further minor changes and the development of the final data-sharing structure.

Workshop participants also considered how to coordinate international efforts to develop reference guides to the identification of deep-water species from images. The following questions were considered by the workshop attendees, how can we: 1) merge existing published and unpublished catalogues? 2) manage new submissions to a merged catalogue? 3) improve the scope and quality of the image data within a merged catalogue? and 4) improve and classify the quality of identification from images?

## Results

### End product needs

Workshop participants, and specifically those engaged in image-based analysis, felt the most critical tools urgently required to support their work were *in-situ* photo-guides in book format (hard copy or e-book), a standard reference morphospecies taxonomic tree (or annotation scheme) that can be imported into different annotation software, and on-line user-friendly image reference catalogues that include information on characteristics used to classify animals as belonging to a particular OTU. The final database structure must therefore be such that these end-use products can be easily created from the database by a query using purpose-built web-accessible software as part of future developments.

### Database structure

The final database structure consists of two tables that contain fields that map onto Darwin Core fields, together with additional fields for which no Darwin Core equivalent could be established. Table 2 is the OTU table. It documents the OTU, and primarily maps to fields from the Darwin Core classes "Taxon" and "Identification". Table 3 is the image table. It documents the individual image file and maps onto fields from multiple Darwin Core classes, including "Occurrence", "Identification", "Event", "Location", "Record-level", and "Organism". The two tables are related via the "OTU" field. This structure allows a single OTU (one entry into Table 2) to be related to multiple example images of the OTU (many entries in Table 3).

The OTU table (Table 2) consists of a GUID field "Number", the inclusion of which is standard practice in database tables. The "OTU" field is a unique number given to this taxon and is initially assigned by the user. The subsequent four fields: "scientificName", "scientificNameID", "scientificNameAuthorship", "taxonRank", provide the link to the WoRMS database. The link is via the "scientificNameID" field, which requires the user to input the appropriate Life Science Identifier (LSID) for the OTU drawn from the WoRMS database. Each taxon in

Appendix E



**Table 2. The Operational Taxonomic Unit (OTU) table, one of two tables that make up the final database.**

| Field name | Field required | Instructions for field use | DarwinCoreClass |
|---|---|---|---|
| Number | required | GUID (to be assigned by database manager) | n/a |
| OTU | required | Operational taxonomic unit number—number assigned to that taxa—no order needed, simply used as a reference number for the taxon. | n/a |
| scientificName | autopopulate from WoRMS | scientificName should contain the name of the lowest possible taxon rank that refers to the most accurate identification. E.g. if the specimen was accurately identified down to family level, but not lower, then the scientificName should contain the name of the family. This field should always contain the originally recorded scientific name, even if the name is currently a synonym. This is necessary to be able to track back records to the original dataset. Do not add sp, spp, cf or any other extras. | Taxon |
| scientificNameID | required | The WoRMS LSID for the corresponding scientificName | Taxon |
| scientificNameAuthorship | autopopulate from WoRMS | Taxonomic authority for the corresponding scientificName | Taxon |
| taxonRank | autopopulate from WoRMS | Level of taxonomic hierarchy given in scientificName, e.g. "family" | Taxon |
| Morphospecies (maps onto identificationQualifier in Darwin Core) | required | Allows the extra detail distinguishing between different morphs e.g. msp1, msp2, msp3, or in the case of sponges: encrusting, vase, fig, sponge, massive globose etc. | Identification |
| CombinedNameID (maps onto TaxonConceptID in Darwin Core) | autopopulate | scientificName + Morphospecies | Taxon |
| PreviousName | optional | This field is intended to capture previous CombinedNameID. A list (concatenated and separated) of previous assignments of names to the Organism. The recommended best practice is to separate the values with a vertical bar (' \| '). | n/a |
| IdentificationFeatures (maps onto TaxonRemarks in Darwin Core) | optional | Free text remarks on why the taxon is what it is. | Taxon |
| IconicImage | optional | The best example of image(s) of this OTU. | |

https://doi.org/10.1371/journal.pone.0218904.t002

WoRMS receives a unique and persistent identifier, known as the AphiaID. This AphiaID can be expanded to a LSID. WoRMS has implemented LSIDs for all its taxonomic names and they are displayed on each taxon page. The LSID integrates the AphiaID and so is the preferred option, of the two possible fields, to use as a link. The appropriate LSID for an OTU is the lowest formal taxonomic rank that can be assigned to an image. For some taxa, this may be at the species level; however, for many image-based identifications it will be at a higher taxonomic level, such as Family, Class or Phylum level. Use of the LSID field ensures that the OTU can be linked to standard taxonomic nomenclature and the related taxonomic hierarchy. Using this LSID, the other three fields within the database ("scientificName", "scientificNameAuthorship", "taxonRank") can be auto-populated from WoRMS.

The "Morphospecies" field maps onto the "identificationQualifier" field in Darwin Core and allows the input of extra details distinguishing between different morphotypes; for example, Brisingidae msp1, or in the case of sponges, Porifera encrusting msp1, Porifera branching msp1. Thus, entries into this field will be of the form msp1, msp2, encrusting msp1, branching msp1, etc. The "CombinedNameID" field is then autopopulated by adding the "scientificName" and "Morphospecies" fields to give, for example, Brisingidae msp1, Porifera branching msp1. The "CombinedNameID" field can be mapped onto the "taxonconceptID" Darwin Core field. A recommended best practice for the standardisation of entries to the "identificationQualifier" field, specifically related to nomenclatural qualifiers used in image analyses is now in preparation. The "PreviousName" field is not intended to document recombinations of taxonomic nomenclature as this is captured and managed in WoRMS [90]. Rather, this field is to capture changes to the assigned identity of the OTU. For example, where Brisingidae

**Table 3. The image table, one of two tables that make up the final database.**

| Field name | Field required | Instructions for field use | DarwinCoreClass | Field name in Darwin Core if different |
|---|---|---|---|---|
| Number | required | GUID (assigned by database manager) | n/a | |
| OTU | required | Operational Taxonomic Unit number | n/a | |
| InsituImageName | required | Name of *in-situ* Image including file extension. If more than one image the recommended best practice is to separate the values with a vertical bar (' \| '). | Occurrence | associatedMedia |
| ExsituImageName | optional | Name of *ex-situ* Image including file extension. If more than one image the recommended best practice is to separate the values with a vertical bar (' \| '). | Occurrence | |
| PhysicalSample (Potentially could map to 'basis of record' field.) | required | This is a Yes / No field | n/a | |
| ImageCredits | required | The credit for the image, how it should read in a display. | Occurrence | associatedReferences |
| identifiedBy | required | Who provided the identification | Identification | |
| dateIdentified | optional | Use the ISO 8601:2004(E) standard for date and time e.g. 1973-02-28T15:25:00 | Identification | |
| identificationRemarks | optional | Free text notes field | Identification | |
| identificationVerificationStatus | required | Score of the quality of the identification. 1 = identified from image only, 2 = identified from image and physical specimens sampled from the same region, 3 = identified from image and that specific physical specimen | Identification | |
| typeStatus | optional | Holotype, syntype, etc | Identification | |
| RawImage | required | This is the number / name of the original image from which the species was cut. Generate your own. E.g CruiseNumber_StationNumber_timestamp | Event | eventID |
| locality | required | Use established MarineRegions and corresponding coordinates. http://www.marineregions.org/gazetteer.php?p=search | Location | |
| locationID | required | | Location | |
| locationRemarks | optional | Free text field for more detailed location data | Location | |
| decimalLatitude | optional | In decimal degrees N | Location | |
| decimalLongitude | optional | In decimal degrees E | Location | |
| minimumDepthInMeters | required | Value in meters of the depth the image was taken at. Use positive values. If exact depth known please put same value in both fields | Location | |
| maximumDepthInMeters | required | | Location | |
| institutionID | required | An identifier for the institution having custody of the object(s) or information referred to in the record. | Record-level | |
| collectionID | optional | Identifies the collection or dataset within that institute This could identify a specific catalogue e.g. Howell & Davies 2010. | Record-level | |
| bibliographicCitation | optional | Citation for the original image database e.g. Howell & Davies, 2010. | Record-level | |
| modified | autopopulate | The most recent date-time on which the resource was changed. It is required to use the ISO 8601:2004(E) standard | Record-level | |
| dcterms:license | required | A legal document giving official permission to do something with the resource. | Record-level | |
| dcterms:rightsHolder | required | A person or organization owning or managing rights over the resource. | Record-level | |
| dcterms:accessRights | required | Information about who can access the resource or an indication of its security status. Access Rights may include information regarding access or restrictions based on privacy, security, or other policies. | Record-level | |
| previousIdentifications | optional | This field is intended to capture changes in opinion on the OTU number of the animal in the image. A list (concatenated and separated) of previous assignments of OTU to the organism in the specific image. The recommended best practice is to separate the values with a vertical bar (' \| '). | Organism | |
| catalogNumber | optional | Museum collection | Occurrence | |

(*Continued*)

Appendix E



Table 3. (Continued)

| Field name | Field required | Instructions for field use | DarwinCoreClass | Field name in Darwin Core if different |
|---|---|---|---|---|
| associatedSequences | optional | For example Genbank ID | Occurrence | |
| habitat | optional | A category or description of the habitat in which the Event occurred (e.g. seamount, hydrothermal vent, abyssal hill, etc.). Where possible use classes given in Greene et al., 1999. A classification scheme for deep seafloor habitats. Oceanologica acta, 22(6), pp.663-678. | Event | |
| SubstrateType | optional | There is no consensus on the way in which substrate is interpreted from image data. Some use EUNIS, others use modified Folk classification or % of Wentworth classes. It is recommended to use the Wentworth scale, if more than one category is used, recommended best practice is to separate the classes and their respective % with a vertical bar (' \| '). | n/a | |
| Size | optional | Approximate size of animal in cm | n/a | |
| SubstrateMethod | optional | e.g. Folk, Wenthworth, EUNIS, Other. | n/a | |
| ProjectName | optional | e.g. DeepLinks, CoralFish, SponGES. | n/a | |
| Link to external database | optional | For example link to another non merged online species guide | n/a | |

https://doi.org/10.1371/journal.pone.0218904.t003

msp1 was later confidently identified to a lower taxonomic level (e.g. *Brisinga* msp4). This field would capture its former "CombinedNameID". The inclusion of the "IdentificationFeatures" free text field is intended to provide insight into the visual characteristics that observers are using to distinguish between morphospecies. It is hoped that over time this field will provide the material to start developing novel visual keys. The "IdentificationFeatures" free text field may map onto the Darwin Core "TaxonRemarks" field. Finally, the "IconicImage" field is used to identify the best example image of the OTU present in the database. This field determines the image that is supplied back to the WoRMS database for use on the appropriate taxon page.

The Image table (Table 3) also has a GUID field "Number", followed by the "OTU" field, which provides the relational link to the OTU table (Table 2). The fields "InsituImageName" and "ExsituImageName" provide the relational link to the images that make up the morphospecies reference image catalogue, and are the name of the image file including the file extension (e.g. IMG10542.jpg). The "ImageCredits" field ensures the owners of the image are identified. We discussed at length how best to include *in-situ* and associated *ex-situ* images. While a strong argument was made around the need for good *ex-situ* images of taxa for use in developing guides for fisheries observer monitoring of bycatch, the group felt the focus of the database should be to provide a tool for the interpretation of *in-situ* image and video data. Therefore, *ex-situ* images should only be included in the database together with an accompanying *in-situ* image of the same individual. As a result, the "InsituImageName" field is required, while the "ExsituImageName" is optional. Where a physical sample has also been taken, this should be indicated in the "PhysicalSample" field as a simple yes or no. If this physical sample has been archived in a museum collection, the catalogue number should be included in the "catalogNumber" field. If it has been identified using molecular techniques, the Genbank or similar ID should be included in the "associatedSequences" field.

The fields pertaining to the Darwin Core class "Identification" concern the identification of the individual in the image, and are self-explanatory ("identifiedBy", "dateIdentified", "identificationRemarks"). The "identificationVerificationStatus" field is the indicator of the quality of the identification provided. Durden et al. [21] suggest three categories of image quality: 1 = Unconfirmed: the status of the organism is uncertain, pending field collection and further taxonomic investigation, or the description and naming of a new species, 2 = Provisional: the

organism is very likely this species/taxon based on investigation (literature search, consultation with outside taxonomic experts, 3 = Certain: the organism has been collected and has been definitively identified by a taxonomic expert. We have modified these categories as follows: 1 = identified from image only, 2 = identified from image and physical specimens sampled from the same region, 3 = identified from image and physical specimen of the actual individual in the image. There are often instances where an organism has been identified from an image and a specimen collected that has not yet been identified. Under these circumstances the quality score would be 1, but the existence of a specimen noted in the "PhysicalSample" field. Once a specimen is identified the quality score for the image could be changed to 2 or 3.

The fields pertaining to the Darwin Core class "Location" concern where the image was taken. We recognise that for older image data archives, exact position data may not have been recorded. However, the importance of location and depth to field identification of taxa cannot be understated. We feel it is important to ensure that the terminology used to define location is consistent with a published standard. In addition, we want to ensure that, in the future, users will be able to construct local morphospecies reference image catalogues based on selection of an area through mapping software. The Marine Regions database [91] is ideally placed to provide this geospatial standard. Its use will also ensure compatibility with OBIS such that this database can share data with OBIS and vice versa. The required fields "locality" and "locationID" provide the link to the Marine Regions database. The user must input the appropriate "locality" and "locationID" for the image drawn from the Marine Regions database. The "locationRemarks" field is an optional free text field that allows users to capture more detailed location information that is not captured by the options available in the Marine Regions database. The fields "minimumDepthInMeters", "maximumDepthInMeters" are also required as species distributions are structured with depth [92] and this characteristic is likely to be important in the development of future field guides. The remaining fields, "decimalLatitude", "decimalLongitude", are optional so as to accommodate older data and / or sensitive data, for example, from industry partners.

The fields pertaining to the Darwin Core class "Record-level" focus on ownership and origin of the image. Required information includes the name of the institution that owns the image ("institutionID"), a licence document ("dcterms:license"), the name of the person / institution managing right over the image ("dcterms:rightsHolder"), and the terms of access to the image ("dcterms:accessRights"). It is anticipated that a standard licencing arrangement can be agreed to upon submission of material to the database, whereby image ownership is retained by the organisation / individual submitting but use for scientific purposes is freely granted. Use of images for commercial gain would be prohibited. There are existing licencing models for WoRDSS and these can be replicated here. Optional fields allow the identification ("collectionID") and citation ("bibliographicCitation") of any previously published or in-house morphospecies reference image catalogues from which the image data have been drawn. The modified field is autopopulated and is the most recent date-time on which the resource was changed.

There are just two fields that relate to the image collection event via the Darwin Core class "Event". These are the fields "RawImage", which maps to the Darwin Core "eventID" field, and "habitat". It is not the intention of this database to capture details of the research cruises, ROV dives, etc., on which the organism images were taken. These details are not overly important to the creation of a field guide. However, should this information be viewed as important in the future, we suggest that images are given the name of the original image from which the organism was cropped, and that this name be extended to consist of the following elements: CruiseNumber_StationNumber_timestamp_imagename. The "habitat" field is able to capture the geomorphological setting in which the organism was observed, e.g. seamount, canyon,

Appendix E



mid-ocean ridge. We felt this information might be useful in the development of a field guide. The ideal situation would be to use standardised terms to describe these settings. We suggest the use of Greene et al. [93] as a standard reference; however, the European Nature Information System (EUNIS) [94, 95] or other classification systems may also provide a reasonable standard and the standard used could be indicated when data are submitted. One final field maps to the Darwin Core class "Organism" and is used to capture previous names that have been assigned to the organism in the image ("previousIdentifications"). As with the "PreviousName" field in the OTU table, this field is not used to capture taxonomic name changes, which are well recorded by WoRMS. It is used to capture changes in opinion on the identity of the organism in the image.

The remaining fields in the Image table do not map to Darwin Core fields but do provide additional information that is important to record. The "SubstrateType" field allows details of the substrate on which the organism was observed to be logged. Substrate is an important environmental factor that determines the distribution of species and can play a role in the field identification of taxa. As always though, it is preferable to use standard terminology to record substrate and there are many standards available. Among workshop participants, there was no consensus on methods of substrate interpretation from image data, and the terminology standards used. Some use EUNIS [94, 95], some a modified Folk [96] classification and others percentage of Wentworth [97] sediment size classes. The "SubstrateMethod" field allows the user to indicate the standard they have followed. The "Size" field, standardised to centimetres, is self-explanatory and may be useful in the future development of a field guide. The "ProjectName" field offers the opportunity to credit specific projects with provision of imagery, while the "Link to external database" field enables links to be made to source on-line morphospecies reference image catalogues.

The images are not stored within the table itself but should be provided as separate image files. Those with existing morphospecies reference image catalogues have tended to either paste images into Word or Power Point files, organise their data as Apple ibooks, or organise their images into Phylum or Class level folders. While this is useful at an individual level, and provides the end product required, it limits onward use and is not the appropriate format for a database.

## A framework for coordination

While the database structure outlined above provides the means to archive data, the development of a unified morphospecies reference image catalogue requires a management structure to curate the database and manage new data submissions. The WoRMS database provides a model that can be adapted for use with this database. WoRMS is curated by teams who are responsible for different taxonomic groups. Each team is led by an editor who takes overall responsibility for that group. We suggest that the morphospecies reference image database is similarly managed by teams focused at the taxonomic grouping level. The appropriate taxonomic grouping will vary depending on variety represented by each phylogenetic level of the group, and expertise available. For example, Hexacorallia may have separate teams grouped at the Order level (e.g. Scleractinia, Actiniaria, Antipatharia), whereas Echinodermata may have separate teams grouped at Class level (e.g. Asteroidea, Echinoidea, etc.). Each team will consist of experts in taxonomy of the group plus ecologists engaged in field identification of organisms from imagery. We felt it was important to have both taxonomists and field ecologists working together, to ensure that the final database considers both taxonomic rigor and the practical use of the images. Each team will have a nominated lead, and leads will come together, as a steering committee, to ensure that a standard approach to data organisation and curation is achieved across the entire database.

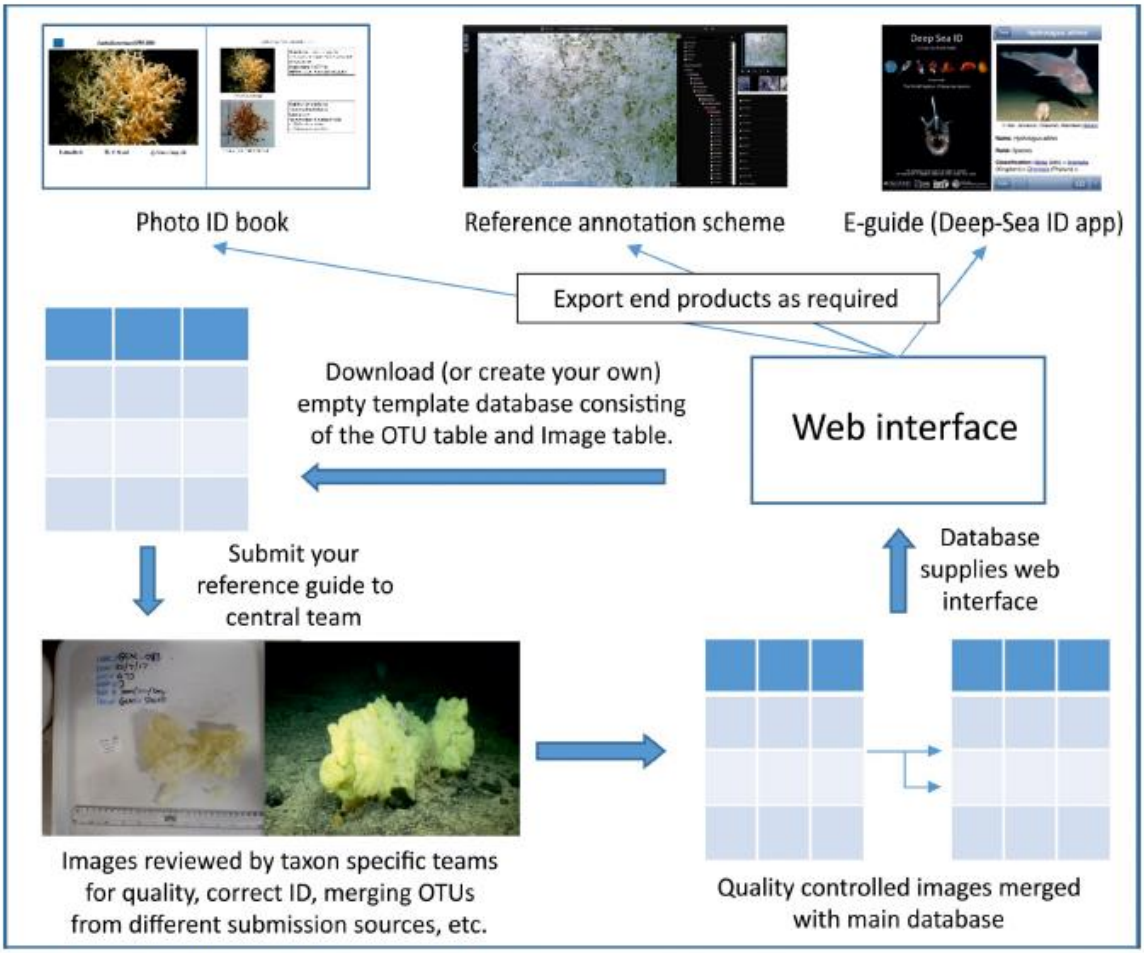


**Fig 2. A conceptual model for how the developed framework will operate.**

https://doi.org/10.1371/journal.pone.0218904.g002

We anticipate a two-stage process whereby an initial effort is made to collate and compile existing morphospecies reference image catalogues at a regional level using the new database structure described above as a data transfer format. In this format not all fields will need to be populated by those submitting data, for example the GUID fields, and other autopopulated fields. This initial effort to compile existing catalogues would be followed by new and on-going submissions of data, including from those encountering new organisms not in the existing database, and from those with higher quality images of organisms already listed in the database (Fig 2). We have committed to stage 1 of this process and morphospecies reference image databases held by all authors have been entered into this new database format and submitted to a central repository. Curation teams are now bringing these data submissions together into a single database.

Appendix E



Stage 2 of this process will involve the effort of the global community and could potentially be a focus for the up-coming UN Decade of Ocean Science for Sustainable Development (2021–2030). This could be a very light-touch involvement, where end users simply submit images of new organisms not currently present in the database to the database for inclusion (Fig 2). Or it could be a more targeted and active involvement aimed at raising the quality of the data already in the database. For example, principal investigators of research cruises could actively help to move taxa from "identificationVerificationStatus" 1 to level 3 by targeted *in-situ* imaging and collection of organisms on an opportunistic basis. Raising the quality of the data in the database should be a priority over the next decade, and with that the recognition of the importance of skills in taxonomy and species identification. A concerted effort to ground truth species identified from imagery only, should be made in order to provide robust tools with which to monitor ecosystems.

Ultimately, it is not the database per-se that end users require, but the end products (photo-guides in book format, taxonomic tree for annotation software, etc.) that can be pulled from the database. This will require the development of a web interface that draws on the underlying database to produce multiple end use formats (Fig 2). This aspect of the project represents the next stage of development and is anticipated to take place over the next two years.

## Discussion

### Immediate advances enabled by the development of a common reference standard

We have proposed a common structure for a database from which a morphospecies reference image catalogue can be built. Our initial development is focused on the North Atlantic deep-sea benthos as a case study. However, the structure developed is applicable to any marine region or habitat, and may also be used for terrestrial ecosystems. Individuals need only adopt the structure and populate the tables with their own data. The Standardised Marine Taxon Reference Image Database (SMarTaR-ID) will enable different researchers to bring their data together in a common morphospecies reference image catalogue at an appropriate time. Within the North Atlantic deep sea that time is now. The implementation of coherent monitoring programmes to assess biological biodiversity in marine waters are mandatory under the EU Marine Strategy Framework Directive (MSFD 2008/56/EC), and all European nations are required to monitor sites of community importance every six years. An image catalogue, such as the one herein proposed, will be a powerful instrument to support monitoring efforts, particularly in poorly surveyed regions. We have outlined a framework by which data can be brought together, curated, and new submissions managed going forward, which follows a successful model already applied by WoRMS.

We anticipate the introduction of a common reference standard for the deep sea to enhance significantly our understanding of megafaunal biodiversity by enabling multiple researchers to combine existing datasets to address long-standing ecological questions. This is particularly the case for hard substrate habitats that dominate features, such as seamounts, ridges, banks, abyssal hills, canyons, and areas of the continental slope, and for which image-based techniques remain the only effective means of survey. Past exploration of the deep-sea epibenthic megafauna generated many paradigms, but these were largely built on data obtained using trawls and sledges. Video and still image-based tools have facilitated quantitative sampling of previously inaccessible habitats; and the resulting new findings are challenging the prevailing view of deep-sea ecosystems [98]. However, these new datasets are often limited to individual features or feature types (e.g. seamounts: [99, 100], abyssal hills: [101] slopes: [66, 102, 103] canyons: [48, 64, 104, 105, 106]; ridges: [107], fracture zones: [100], and hydrothermal vents:

[108]) and thus limit our ability to generalise findings. In their review of major outstanding questions in deep-sea biogeography [109] concluded, among other things, that an integrated biogeographic framework of hard-substrate areas of the deep sea was required to yield more realistic estimates of endemism/cosmopolitanism. It has been repeatedly argued that concerted efforts to link existing independent data streams together to examine long-standing questions of deep-sea diversity are very much needed in order to move the field forward [109, 110]. The proposed database will facilitate these advances.

We anticipate that this common reference standard will provide an invaluable tool for environmental managers, industry and wider stakeholders. For environmental managers, it will, for example, enable the development of clearer descriptions and definitions of habitats of conservation concern. For example, deep-sea sponge aggregations potentially qualify as Vulnerable Marine Ecosystems (VME) under the United Nations General Assembly (UNGA) Resolution 61/105. They are also classed as a threatened and declining ecosystem under Annex V of the Oslo-Paris (OSPAR) Convention for the Protection of the Marine Environment of the North East Atlantic. However, comprehensive descriptions of deep-sea sponge aggregations, and specifically the component taxa that compose different types of aggregation, are lacking. In addition, basin-wide data on the distribution of sponge VME indicator taxa are only available for those species / genera whose appearance both *in-situ* and *ex-situ* are similar (e.g. Geodia, Hyalonema, Pheronema). For many sponge species, the lack of taxonomic resolution possible when identifying sponges from image data hinders progress in management and conservation of these taxa by limiting our ability to 1) effectively describe sponge VME composition and diversity, and 2) pool data to determine basin-wide distributions. A common morphospecies reference image catalogue will provide a standard reference to use in VME descriptions in the absence of confirmed taxonomic identification of species from physical samples. It will also facilitate the production of basin-wide models of the distribution of habitat forming sponge taxa to support spatial management decisions [111].

For industry, implementation of a standard approach to referencing morphospecies between industry and regulators will facilitate a much more effective impact assessment associated with licensing and consent processes, as well as subsequent monitoring approaches. Often in industry, a range of sub-contractors are used for routine survey and monitoring work by the various industry bodies. Therefore, morphotypes are produced per project with no consistency between sub-contractor or between years in long-term monitoring as data are rarely shared. This standardisation would increase industry and regulatory comparison across applications and across industries to facilitate cumulative impact assessments, thus allowing better understanding of impact at feature and site levels, as required in nature conservation legislation. For industry, this could also decrease levels of risk associated with the assessments as well as decreased analysis time and costs for survey data, and would be a particularly powerful tool if industry could include their own data in the database and play an active role in providing images and survey data.

The need for a standard approach in industry was recently highlighted by the development of the deep-sea mining industry in the Clarion Clipperton Zone (CCZ) of the central Pacific. Here, baseline data collection is taking place, commonly including seabed imaging-based assessments of megafauna [29, 47, 65, 112, 113]. Without a consistent morphospecies reference image catalogue it is difficult to compare studies and generate regional syntheses. This greatly hampers conservation and management efforts, which commonly rely on information on biodiversity, species ranges and behaviour–ecological properties that are difficult to assess without good quality and consistent identifications. Recent work to document megafaunal diversity will help (e.g. 47, 65), but widely adopted and regularly updated catalogues will be vital for improving scientific understanding and effective environmental management.

Appendix E



A common morphospecies reference image catalogue may also serve as a tool to support the identification of taxa from fisheries bycatch by fisheries observers (e.g. [114]. While our proposed database focuses on *in-situ* images of taxa, we advocate, and have provided for within the proposed database structure, the collection of *ex-situ* images of taxa. There are a number of existing image guides designed for use by fisheries observers that provide *ex-situ* images of VME indicator taxa (Table 1). This database could supplement existing guides by providing additional imagery. Interestingly, it may also provide a link between *in-situ* and *ex-situ* taxon identification, which may ultimately allow fisheries bycatch data to be pooled with *in-situ* image data, again broadening our understanding of species distributions (e.g. [115]).

Finally, the simple act of combining multiple existing morphospecies reference image catalogues will advance the overall quality of current identifications. It is important to remember that image data is no substitute for a physical sample, and a long term goal in this endeavour is that all image reference material has been ground truthed by a physical specimen identified by a professional taxonomist. At present different research groups have images of different species for which the "identificationVerificationStatus" level is 3 (the highest level, confirmed by physical specimen). By bringing these reference image sets together, we will collectively have more species that can be identified by reference to images in which we have the highest level of confidence of the animal's identification.

## Future advances enabled by the development of a common reference standard

The development of a common reference standard has the potential to advance significantly the field of offshore and deep-sea marine ecology. The ability to pool datasets across time and space will allow us to address a greater range of questions about the offshore and deep-sea benthic ecosystem than is currently possible. Critically, it will enable us to raise standards of identification from image data through the development of training materials and quality control measures. Efforts to develop such tools for shallow water have been undertaken by the UK's National Marine Biological Association Quality Control scheme (NMBAQC). This programme is steered by a range of academic and governmental organisations, and provides guidance on best practice, as well as identification guides, taxonomic workshops, training exercises and quality control ring tests.

There will remain some potential shortcomings on the use of such catalogues related to uncertainties in species identification due to the method of image collection and scale. The ability to zoom-in on specific features of species with ROV cameras means ROVs may provide better imagery for identification than AUVs or drop-down cameras, particularly in cases where species look remarkably similar and occupy overlapping environmental niches. For example, the octocorals *Acanthogorgia armata* and *Acanthogorgia hirsuta* can only be distinguished if close up images of the polyps are taken, otherwise identifications have to be left at genus level. Nevertheless, the development of a common reference standard will expose these limitations to a wider audience, and help develop agreed international guidance around the taxonomic levels to which it is appropriate to identify when interpreting image data.

In the longer term, regional field keys are required for use in survey and monitoring of the deep-sea ecosystem. The construction of tools that allow others to identify taxa reliably and consistently in the field is perhaps one of the most underappreciated roles for taxonomists. It is also one of the most challenging roles as taxonomists are often not engaged in field identification, and therefore a gap exists between the generator and end user of a key [116]. The starting point for the development of any key is a standard reference against which to compare new observations. In traditional taxonomy, this is the type specimen, a physical specimen

from which a species is described, that is subsequently archived in a museum. The development of dichotomous or polytomous keys is then achieved by measuring the variability in observable characteristics within examples of a taxon and between taxa, then selecting characteristics that best discriminate between taxa for a given region / group. These characteristics are then organised into pathways of character state choices (steps) that lead to identifications.

In order to move forward with the development of much-needed field keys to deep-water taxa, we must first develop an appropriate standard reference against which to assess new observations. This reference point remains the holotype specimen. Our proposed database will establish an image 'similitype' (or a series of images that contribute to the similitype) to accompany a physical specimen that has been identified with reference to the holotype of a species, or through matching DNA sequences to other specimens identified with reference to the holotype of a species, and thus link traditional taxonomy to field identification. This approach will provide a much-needed strategy to advance the taxonomic description of species based on multisource information collected by both ecologists and taxonomists [117, 118]. If researchers use and contribute to this common reference standard, a library of images with examples of each taxon will be built up over time. This library of image examples can then be used to understand both the observable characteristics within a species or higher taxonomic level grouping, and the variability in these characteristics in image-based data. Where possible it is desirable for these characteristics to be those used in traditional taxonomic keys. However, this will not be possible for all groups to all levels of the taxonomic hierarchy. For example, while it is possible to use traditional taxonomic features to determine the order of some coral taxa from image data, it is not possible to do this for anemone taxa, which rely on internal characteristics for positive identification. It is likely that novel characteristics, combinations of characteristics, as well as the use of circumstantial information (e.g. environmental characteristics), will be required to enable reliable and consistent field identification of organisms, but even then some morphotypes will remain as morphotypes.

Multi-access keys (also known as matrix based or free-access keys) may be more appropriate than dichotomous or polytomous keys (also known as single-access keys) for use with image data as they, by their nature, have multiple access points [116, 119]. Single-access keys place a logical order on the use of characteristics, with each step in the decision tree taking the user along a predefined pathway that progressively narrows the number of possibilities for the identification of the animal. If a characteristic is not visible at any step along this pathway, the choice required by the user is unanswerable and further progression is not possible. Views of organisms in *in-situ* image data can be highly variable, and it is likely that in any one image only some features will be visible. This may limit the utility of single-access keys with image data. Multi-access keys enable the user to determine the sequence of choices where the user can select from the list of characteristics offered in order to arrive at an identification. In the context of image data, this would allow the user to employ all visible characteristics (and potentially environmental information) to arrive at an identification. Multi-access keys are more suitable for computer-aided identification tools [116, 119]. This also makes them a promising tool to use with image data where analysis is computer based.

If we are to move forward with the application of AI and CV to the identification of taxa, we must have a common reference standard. Our proposed database aims to meet this need through future development that will enable the database to interface with image annotation software, such as Squidle [120] and BIIGLE 2.0 [121,122]. These annotation softwares enable users to mark the x,y position of organisms within an image and attribute this point / polygon with a taxon identification. This process of image annotation is the means by which ecologists extract semantic data from an image in order to then apply numerical and statistical analysis to these data and answer ecological questions. This annotated dataset is also the base data

Appendix E



needed in the development of AI and CV algorithms. These algorithms require large numbers of images to "learn" the features that distinguish the different OTUs to which they have been exposed, and which of these features are characteristic of each OTU [123, 124]. If researchers are able to use a common reference standard, thus extracting the same information from an image regardless of who is annotating it, then collated datasets from various origins could reach the size needed to train and test CV algorithms (acknowledging challenges of observer bias). Their use within the field of deep-sea benthic ecology, will then increase exponentially through accumulation of data, skill and experience. This can only serve to facilitate the development of CV and bring us closer to automation of image annotation and data extraction.

Ultimately, standardisation of tools and methods is central to long-term monitoring and assessments of ocean health. Woodall et al. [125] recognised this and produced GOSSIP (General Ocean Survey and Sampling Iterative Protocol), which outlines a framework of 20 biological, chemical, physical, and socioeconomic parameters that allow marine scientists to generate comparable data on the function, health and resilience of the ocean. There are several international efforts underway to try and harmonise ocean observing in the areas of biology and ecology, including the efforts of the Group on Earth Observation–Biodiversity Observing Network (GEO-BON) and the Global Ocean Observing System (GOOS) panel on biology and ecosystem–Essential Ocean Variables (EOVs). These efforts are also being informed by international efforts, such as the Deep Ocean Observing Strategy (http://www.deepoceanobserving.org/), which is adding deep ocean context to GOOS EOV specifications. There are more than a dozen regional alliances internationally, which are implementing the GOOS vision with international coordination by the IOC. Together these organisations are forming a means for efforts from individual observers, as well as local to international bodies, to join together to realise the power of 'big data' in observing and understanding change. National-level data management and communications groups affiliated with GOOS are now working to include tools, such as automated image classification, into their information technology systems. The common reference image standard described above will therefore contribute to global efforts under GOOS.

## Conclusions

We have developed a database structure (and data transfer format) to facilitate the standardisation of morphospecies image catalogues between individuals, research groups, and nations. We have also proposed a framework for coordination of international efforts to develop reference guides for the identification of deep-sea species from images. We have highlighted the potential gains to be made through the use of this database structure by the deep-sea community in: increasing the quality and quantity of data available to researchers, improvement of overall understanding of the deep-sea ecosystem, more effective management and monitoring by statutory bodies and industry alike, and realising the potential benefits of emerging AI and CV approaches. To make these gains it is critical there is now uptake of this database format by the community, and additional funding is found to contribute to stage two development.

## Acknowledgments

We would like to thank the Deep Sea Biology Society for supporting this project.

## Author Contributions

**Conceptualization:** Kerry L. Howell.

**Data curation:** Kerry L. Howell, Jaime S. Davies, A. Louise Allcock, Andreia Braga-Henriques, Pål Buhl-Mortensen, Marina Carreiro-Silva, Jennifer M. Durden, Nicola L. Foster, Chloe A. Game, Tammy Horton, Claire Laguionie Marchais, Lenaick Menot, Tabitha R. R. Pearman, Nils Piechaud, Rebecca E. Ross, Paul Tyler, Rui P. Vieira, Daniel Wagner.

**Funding acquisition:** Kerry L. Howell, Lenaick Menot.

**Investigation:** Kerry L. Howell.

**Methodology:** Kerry L. Howell.

**Project administration:** Kerry L. Howell.

**Resources:** Jaime S. Davies, A. Louise Allcock, Pål Buhl-Mortensen, Marina Carreiro-Silva, Jennifer M. Durden, Nicola L. Foster, Chloe A. Game, Becky Hitchin, Tammy Horton, Brett Hosking, Daniel O. B. Jones, Claire Laguionie Marchais, Lenaick Menot, Tabitha R. R. Pearman, Nils Piechaud, Rebecca E. Ross, Hanieh Saeedi, Michael B. Thompson, James R. Taylor, Paul Tyler, Johanne Vad, Lissette Victorero, Rui P. Vieira, Joana R. Xavier, Daniel Wagner.

**Validation:** Andreia Braga-Henriques.

**Writing – original draft:** Kerry L. Howell, Becky Hitchin, Tammy Horton, Daniel O. B. Jones, Claire Laguionie Marchais, Lenaick Menot, Nils Piechaud, Rebecca E. Ross, Hanieh Saeedi, Michael B. Thompson, James R. Taylor, Paul Tyler, Rui P. Vieira, Joana R. Xavier.

**Writing – review & editing:** Kerry L. Howell, Jaime S. Davies, A. Louise Allcock, Andreia Braga-Henriques, Pål Buhl-Mortensen, Marina Carreiro-Silva, Carlos Dominguez-Carrió, Jennifer M. Durden, Nicola L. Foster, Chloe A. Game, Tammy Horton, Brett Hosking, Daniel O. B. Jones, Christopher Mah, Claire Laguionie Marchais, Telmo Morato, Tabitha R. R. Pearman, Nils Piechaud, Rebecca E. Ross, Henry A. Ruhl, Hanieh Saeedi, Paris V. Stefanoudis, Gerald H. Taranto, Michael B. Thompson, James R. Taylor, Paul Tyler, Johanne Vad, Lissette Victorero, Rui P. Vieira, Lucy C. Woodall, Joana R. Xavier, Daniel Wagner.

## References

1. Ruppé CV, Barstad JF, editors. International handbook of underwater archaeology. Berlin: Springer Science & Business Media; 2013.
2. Boutan L. La photographie sous-marine. Arch Zool Exp. 1893; 3: 281–324.
3. Cousteau JY. The living sea. London: H. Hamilton; 1963.
4. Beebe W. Half mile down. Duell, Sloan and Pearce; 1951.
5. Ewing M, Vine A, Worzel JL. Photography of the ocean bottom. JOSA. 1946 Jun 1; 36(6):307–21.
6. Ewing M, Worzel JL, Vine AC. Early development of ocean-bottom photography at Woods Hole Oceanographic Institution and Lamont Geological Observatory. The John Hopkins Oceanographic Studies. 1967.
7. Schenck HJ, Kendall H. Underwater photography. Maryland: Cornell Maritime Press; 1954.
8. Thorndike EM. Deep-sea cameras of the Lamont Observatory. Deep Sea Research (1953). 1958 Jan 1; 5(2–4):234–7.
9. Fell HB. Biological applications of sea-floor photography. In: Hersey JB, editor. Deep-sea photography. Baltimore: John Hopkins Press. 1967. pp 207–221.
10. Vevers HG. Photography of the sea floor. J Mar Biol Assoc UK 1951; 30: 101–111.
11. Clark HES. Fauna of the Ross Sea Part 3: Asteroidea. Mem N Z Oceanogr Inst 1963; 21: 1–84.
12. Marshall NB, Bourne DW. A photographic survey of benthic fishes in the Red Sea and Gulf of Eden, with observations on their population density, diversity and habitats. Bull Mus Comp Zool 1964; 132: 225–244.
13. Hersey JB. Deep-sea photography. Baltimore: John Hopkins Press; 1967.

Appendix E




14. Heezen BC, Hollister CD. The face of the deep. London: Oxford University Press; 1971.
15. Grassle JP, Sanders RR, Hessler GT, Rowe GT, McLellan T. Pattern and zonation: a study of the bathyal megafauna using the research submersible Alvin. Deep Sea Res I 1975; 22: 457–481.
16. Rice AL, Aldred G, Darlington E, Wild RA. The quantitative estimation of the deep-sea megabenthos: a new approach to an old problem. Oceanol Acta 1982; 5: 63–72.
17. Rowe GT, Sibuet M, Vangriesheim A. Domains of occupation of abyssal scavengers inferred from baited cameras and traps on the Demerara Abyssal Plain. Deep Sea Res Part I 1986; 33: 501–522.
18. Smith KL, Kaufmann RS, Wakefield WW. Mobile megafaunal activity monitored with a time-lapse camera in the abyssal North Pacific. Deep Sea Res I 1993; 40: 2307–2324.
19. Thurston MH, Bett BJ, Rice AL, Jackson PAB. Variations in the invertebrate abyssal megafauna in the North Atlantic Ocean. Deep Sea Res I 1994; 41: 1321–1348.
20. Howell KL, Davies J, Hughes DJ, Narayanaswamy BE. Strategic Environmental Assessment / Special Area for Conservation Photographic Analysis Report. London: Department of Trade and Industry; 2007.
21. Durden JM, Schoening T, Althaus F, Friedman A, Garcia R, Glover AG, et al. Perspectives in visual imaging for marine biology and ecology: from acquisition to understanding. Oceanogr Mar Biol Annu Rev 2016; 54: 1–72.
22. Taylor J, Krumpen T, Soltwedel T, Gutt J, Bergmann M. Dynamic benthic megafaunal communities: Assessing temporal variations in structure, composition and diversity at the Arctic deep-sea observatory HAUSGARTEN between 2004 and 2015. Deep-Sea Res I 2017; 122: 81–94.
23. Taylor J, Krumpen T, Soltwedel T, Gutt J, Bergmann M. Regional- and local- scale variations in benthic megafaunal composition at the Arctic deep-sea observatory HAUSGARTEN. Deep Sea Res I 2016; 108: 58–72.
24. Howell KL, Davies JS, Narayanaswamy BE. Identifying deep-sea megafaunal epibenthic assemblages for use in habitat mapping and marine protected area network design. J Mar Biol Assoc UK 2010a; 90: 33–68.
25. Huvenne VAI, Bett BJ, Masson DG, Le Bas TP, Wheeler AJ. Effectiveness of a deep-sea cold-water coral Marine Protected Area, following eight years of fisheries closure. Biol Conserv 2016; 200: 60–69.
26. Escartin J, Barreyre T, Cannat M, Garcia R, Gracias N, Deschamps A, et al. Hydrothermal activity along the slow-spreading Lucky Strike ridge segment (Mid-Atlantic Ridge): Distribution, heatflux, and geological controls. Earth Planet Sci Lett 2015; 431: 173–185.
27. Hirai J, Jones DOB. The temporal and spatial distribution of krill (Meganyctiphanes norvegica) at the deep seabed of the Faroe–Shetland Channel, UK: A potential mechanism for rapid carbon flux to deep sea communities. Mar Biol Res 2011; 8: 48–60.
28. Olu K, Lance S, Sibuet M, Henry P, Fiala-Médioni A, Dinet A. Cold seep communities as indicators of fluid expulsion patterns through mud volcanoes seaward of the Barbados accretionary prism. Deep Sea Res I 1997; 44: 811–819.
29. Simon-Lledó E, Bett BJ, Huvenne VAI, Schoening T, Benoist NMA, Jeffreys RM, et al. Megafaunal variation in the abyssal landscape of the Clarion Clipperton Zone. Prog Oceanogr 2019a; 170: 119–133.
30. Laurenson C, Hudson IR, Jones DOB, Preide IM. Deep water observations of Lophius piscatorius in the north-eastern Atlantic Ocean by means of a Remotely Operated Vehicle. Fish Biol 2004; 65: 947–960.
31. Jones DOB, Bett BJ, Tyler PA. Megabenthic ecology of the Faroe-Shetland Channel: a photographic study. Deep Sea Res I. 2007; 54: 1111–1128.
32. Durden JM, Bett BJ, Ruhl HA. The hemisessile lifestyle and feeding strategies of Iosactis vagabunda (Actiniaria, Iosactiidae), a dominant megafaunal species of the Porcupine Abyssal Plain. Deep Sea Res I. 2015a; 102: 72–77.
33. Bullimore RD, Foster NL, Howell KL. Coral-characterized benthic assemblages of the deep Northeast Atlantic: defining "Coral Gardens" to support future habitat mapping efforts. ICES J Mar Sci. 2013; 70: 511–522.
34. Morato TM, Pham CK, Pinto C, Golding N, Ardron JA, Durán Muñoz P, et al. A multi criteria assessment method for identifying Vulnerable Marine Ecosystems in the North-East Atlantic. Front Mar Sci. 2018; 5: 460.
35. Pham CK, Diogo H, Menezes G, Porteiro F, Braga-Henriques A, Vandeperre F, et al. Deep-water longline fishing has reduced impact on Vulnerable Marine Ecosystems. Sci Rep. 2014a; 4:4837.
36. Buhl-Mortensen P. Coral reefs in the Southern Barents Sea: habitat description and the effects of bottom fishing. Mar Biol Res. 2017; 13: 1027–1040.

37. Pham CK, Ramirez-Llodra E, Alt CHS, Amaro T, Bergmann M, Canals M, et al. Marine litter distribution and abundance in European Seas, from the shelf to deep basins. PLOS ONE. 2014b; 9: e95839.
38. Buhl-Mortensen P, Buhl-Mortensen L. Impacts of Bottom Trawling and Litter on the Seabed in Norwegian Waters. Front Mar Sci. 2018; 5:42 https://doi.org/10.3389/fmars.2018.00042
39. Billett DSM, Bett BJ, Reid WDK, Boorman B, Priede IG. Long-term change in the abyssal NE Atlantic: the 'Amperima Event' revisited. Deep Sea Res II 2010; 57: 1406–1417.
40. Morris KJ, Bett BJ, Durden JM, Huvenne VAI, Milligan R, Jones DOB, et al. A new method for ecological surveying of the abyss using autonomous underwater vehicle photography. Limnol Oceanogr Methods. 2014; 12: 795–809.
41. Edgar GJ. Australian marine life: the plants and animals of temperate waters. Sydney: Reed New Holland; 2008.
42. Wood C. Sea anemones and corals of Britain and Ireland. Plymouth: Wild Nature Press; 2013.
43. Jacobsen Stout N, Kuhnz L, Lundsten L, Schlining B, Schlining K, von Thun S. The Deep-Sea Guide (DSG). Monterey Bay Aquarium Research Institute (MBARI). 2015. Available from: http://dsg.mbari.org/dsg/home
44. Braga-Henriques A, Pereira JN, Tempera F, Porteiro FM, Pham C, Morato T, et al. Cold-water coral communities on Condor Seamount: initial interpretations. In: Giacomello E, Menezes G (eds) CONDOR observatory for long-term study and monitoring of azorean seamount ecosystems. Final Project Report, Arquivos do DOP, Série Estudos 1/2012, Horta. 2011. pp 105–114.
45. Braga-Henriques A, Carreiro-Silva M, Tempera F, Porteiro FM, Jakobsen K, Jakobsen J, et al. Carrying behavior in the deep-sea crab Paromola cuvieri (Northeast Atlantic). Mar Biodiv. 2012; 42: 37–46
46. Narayanaswamy BE, Hughes DJ, Howell KL, Davies J, Jacobs C. First observations of megafaunal communities inhabiting George Bligh Bank, northeast Atlantic. Deep Sea Res II. 2013; 92: 79–86.
47. Amon DJ, Ziegler A, Kremenetskaia A, Mah C, Mooi R, O'Hara T, et al. Megafauna of the UKSRL exploration contract area and eastern Clarion-Clipperton Zone in the Pacific Ocean: Echinodermata. Biodivers Data J. 2017a; 5: e11794.
48. van den Beld IMJ, Bourillet JF, Arnaud-Haond S, de Chambure L, Davies JS, Guillaumont B, et al. Cold-water coral habitats in submarine canyons of the Bay of Biscay. Front Mar Sci. 2017; 4: 10.3389/fmars.2017.00118
49. Alt CHS, Kremenetskaia A, Gebruk AV, Gooday AJ, Jones DOB. Bathyal benthic megafauna from the Mid-Atlantic Ridge in the region of the Charlie-Gibbs fracture zone based on remotely operated vehicle observations. Deep Sea Res I. 2019; 145: 1–12.
50. Hawkes N, Korabik M, Beazley L, Rapp HT, Xavier JR, Kenchington E. Glass sponge grounds on the Scotian Shelf and their associated biodiversity. Mar Ecol Prog Ser. 2019; 614: 91–109.
51. Culverhouse PF, Williams R, Reguera B, Herry V, Gonzalez-Gils. Do experts make mistakes? A comparison of human and machine identification of dinoflagellates. Mar Ecol Prog Ser. 2003; 247: 17–25.
52. MacLeod N, Benfield M, Culverhouse P. Time to automate identification. Nature. 2010; 467: 154–155. https://doi.org/10.1038/467154a PMID: 20829777
53. Schoening T, Bergmann M, Ontrup J, Taylor J, Dannheim J, Gutt J, et al. Semi-automated image analysis for the assessment of megafaunal densities at the Arctic deep-sea observatory HAUSGARTEN. PLOS ONE. 2012; 7: e38179. https://doi.org/10.1371/journal.pone.0038179 PMID: 22719868
54. Wynn RB, Huvenne VAI, Le Bas TP, Murton BJ, Connelly DP, Bett BJ, et al. Autonomous Underwater Vehicles (AUVs): their past, present and future contributions to the advancement of marine geoscience. Mar Geol. 2014; 352: 451–468.
55. Jones DOB, Gates AR, Huvenne VAI, Phillips AB, Bett BJ. Autonomous marine environmental monitoring: Application in decommissioned oil fields. Sci Total Environ. 2019; 668: 835–853. https://doi.org/10.1016/j.scitotenv.2019.02.310 PMID: 30870752
56. Piechaud N, Hunt C, Culverhouse PF, Foster NL, Howell KL. Automated identification of benthic epifauna with computer vision. Mar Ecol Prog Ser. 2019; 615: 15–30.
57. Edgington DR, Cline DE, Davis D, Kerkez I, Mariette J. Detecting, tracking and classifying animals in underwater video. Proc Oceans IEEE. 2006.
58. Beijbom O, Edmunds PJ, Roelfsema C, Smith J, Kline DI, Neal BP, et al. Towards automated annotation of benthic survey images: Variability of human experts and operational modes of automation. PLOS ONE. 2015; 10:e0130312. https://doi.org/10.1371/journal.pone.0130312 PMID: 26154157
59. Schoening T, Durden J, Preuss I, Albu AB, Purser A, De Smet B,et al. Report on the marine imaging workshop 2017. Res Ideas Outcomes. 2017; 3:e13820.
60. Favret C, Sieracki JM. Machine vision automated species identification scaled towards production levels. Syst Entomol. 2016; 41: 133–143.

Appendix E




61. Langenkämper D, Nattkemper TW. COATL—A learning architecture for online real-time detection and classification assistance for environmental data. IEEE Int Conf Pattern Recognit, IEEE, 2017a. pp 597–602.
62. Howell KL, Davies JS. Deep-sea species image catalogue, On-line version 2. 2016. Available from: https://deepseacruorg/2016/12/16/deep-sea-species-image-catalogue/
63. Jones DOB, Gates AR. Deep-sea life of Scotland and Norway. UK: Ophiura; 2010.
64. Robert K, Jones DOB, Tyler PA, Van Rooji D, Huvenne VAI. Finding the hotspots within a biodiversity hotspot: fine-scale biological predictions within a submarine canyon using high-resolution acoustic mapping techniques. Mar Ecol. 2014; 36: 1256–1276.
65. Amon DJ, Ziegler AF, Drazen JC, Grischenko AV, Leitner AB, Lindsay DJ,et al. Megafauna of the UKSRL exploration contract area and eastern Clarion-Clipperton Zone in the Pacific Ocean: Annelida, Arthropoda, Bryozoa, Chordata, Ctenophora, Mollusca. Biodivers Data J. 2017b; 5: e14598–e14598
66. Stefanoudis P, Smith S, Schneider C, Wagner D, Goodbody-Gringley G, Xavier J,et al. Deep Reef Benthos of Bermuda: Field Identification Guide. Figshare Book. 2018. Available from: https://doi.org/10.6084/m9.figshare.7333838.v1
67. Althaus F, Hill N, Ferrari R, Edwards L, Przeslawski R, Schönberg CH, et al. A standardised vocabulary for identifying benthic biota and substrata from underwater imagery: the CATAMI classification scheme. PLOS ONE. 2015; 10:e0141039 https://doi.org/10.1371/journal.pone.0141039 PMID: 26509918
68. Glover AG, Higgs ND, Horton T, Porrer A. Deep Sea ID v.1.2 A Field Guide to the Marine Life of the Deep Sea 2015. Available from http://www.marinespecies.org/deepsea
69. NOAA Office of Ocean Exploration and Research Benthic Deepwater Animal Identification Guide. 2018. Available from: https://oceanexplorer.noaa.gov/okeanos/animal_guide/animal_guide.html
70. Ebert DA, Stehmann MFW. Sharks, batoids, and chimaeras of the North Atlantic. FAO Species Catalogue for Fishery Purposes. No. 7. FAO, Rome; 2013.
71. Howell KL, Davies JS, van den Beld I. Deep-sea species image catalogue. University of Plymouth, Ifremer, NOAA. 2017; Available from: http://www.deepseacatalogue.fr/
72. Jones DOB, Gates AR, Curry RA, Thomson M, Pile A, Benfield M editors. SERPENT project. Media database archive. 2009; Available online: http://archive.serpentproject.com/
73. Rogacheva A, Gebruk A, Alt CH. Holothuroidea of the Charlie Gibbs Fracture Zone area, northern Mid-Atlantic Ridge. Mar Biol Res 2013; 9: 587–623.
74. Oliveira F, Aguilar R, Monteiro P, Bentes L, Afonso CML, García S,et al. A photographic guide of the species of the Gorringe. Centro de Ciências do Mar/Oceana, Faro. 2017.
75. Kenchington E, Best M, Cogswell A, MacIsaac K, Murillo-Perez FJ, MacDonald B,et al. Coral Identification Guide NAFO Area. NAFO Scientific Council Studies, Nova Scotia. 2009.
76. Best M, Kenchington E, MacIsaac K, Wareham VE, Fuller SD, Thompson AB Sponge Identification Guide NAFO Area. NAFO Scientific Council Studies, Nova Scotia. 2010; pp 43–50.
77. Kenchington E, Beazley L, Murillo FJ, Tompkins MacDonald G, Baker E. Coral, Sponge, and Other Vulnerable Marine Ecosystem Indicator Identification Guide, NAFO Area. NAFO Scientific Council Studies, Nova Scotia. 2015.
78. Packer D, Drohan A. Identification sheets for the common deep-sea corals off the Northeast and Mid-Atlantic US (v1.0). NOAA. 2013. Available from: https://www.nefsc.noaa.gov/fsb/training/NortheastemU.SDeepsea_Coral_Guide.pdf
79. Serena F. Field identification guide to the sharks and rays of the Mediterranean and Black Sea. FAO Species Catalogue for Fishery Purposes. FAO, Rome; 2005.
80. Fourt M, Goujard A, Pérez T, Chevaldonné P. Guide de la faune profonde de la mer Méditerranée: Explorations des roches et canyons sous-marins des côtes françaises. Muséum national d'Histoire naturelle, Paris; 2017.
81. Xavier JR, Bo M. Deep-sea sponges of the Mediterranean Sea; 2017. Available from http://www.fao.org/3/a-i6945e.pdf
82. Bo M. Deep-sea corals of the Mediterranean Sea; 2017. Available from http://www.fao.org/3/a-i7256e.pdf
83. Alt CHS. On the benthic invertebrate megafauna at the Mid-Atlantic Ridge, in the vicinity of the Charlie-Gibbs Fracture Zone. PhD Thesis, University of Southampton. 2012.
84. Wieczorek J, Bloom D, Guralnick R, Blum S, Doring M, Giovanni R, et al. Darwin Core: an evolving community-developed biodiversity data standard. PLOS ONE. 2012; 7: e2971569.
85. Encyclopedia of Life. Available from http://www.eol.org

86. GBIF.org. GBIF Home Page. 2018. Available from https://www.gbif.org
87. OBIS. Ocean Biogeographic Information System. Intergovernmental Oceanographic Commission of UNESCO. 2018. Available from www.iobis.org.
88. WoRMS Editorial Board. World Register of Marine Species. 2018. Available from http://www.marinespecies.org.
89. Vandepitte L, Vanhoorne B, Decock W, Vranken S, Lanssens T, Dekeyzer S, et al. A decade of the World Register of Marine Species—General insights and experiences from the Data Management Team: Where are we, what have we learned and how can we continue? PLOS ONE 2018; 13: e0194599 https://doi.org/10.1371/journal.pone.0194599 PMID: 29624577
90. Horton T, Gofas S, Kroh A, Poore GCB, Read G, Rosenberg G, et al. Improving nomenclatural consistency: a decade of experience in the World Register of Marine Species. Eur J Taxon. 2017; 389: 1–24.
91. Claus S, De Hauwere N, Vanhoorne B, Souza Dias F, Oset García P, Schepers L, et al. MarineRegions.org. 2018. Available from http://www.marineregions.org
92. Howell KL, Billett DSM, Tyler PA. Depth-related distribution and abundance of seastars (Echinodermata: Asteroidea) in the Porcupine Seabight and Porcupine Abyssal Plain, NE Atlantic. Deep Sea Res I. 2002; 49: 1901–1920.
93. Greene HG, Yoklavich MM, Starr RM, O'Connell VM, Wakefield WW, Sullivan DE, et al. A classification scheme for deep seafloor habitats. Oceanol Acta 1999; 22: 663–678.
94. Davies CE, Moss D. EUNIS Habitat Classification. Final Report to the European Topic Centre on Nature Conservation, European Environment Agency, Copenhagen; 1998.
95. Davies CE, Moss D, Hill MO. EUNIS Habitat Classification Revised 2004. Report to the European Topic Centre on Nature Protection and Biodiversity, European Environment Agency, Copenhagen; 2004.
96. Folk RL. The distinction between grain size and mineral composition in sedimentary rock nomenclature. J Geol. 1954; 62: 344–359.
97. Wentworth CK. A scale of grade and class terms for clastic sediments. J Geol. 1922; 30: 377–392.
98. Danovaro R, Snelgrove PV, Tyler P. Challenging the paradigms of deep-sea ecology. Trends Ecol Evol. 2014; 29: 465–475. https://doi.org/10.1016/j.tree.2014.06.002 PMID: 25001598
99. Howell KL, Mowles SL, Foggo A. Mounting evidence: near-slope seamounts are faunally indistinct from an adjacent bank. Mar Ecol—Evol Persp. 2010b; 31: 52–62.
100. Victorero L, Robert K, Robinson LF, Taylor ML, Huvenne VAI. Species replacement dominates megabenthos beta diversity in a remote seamount setting. Sci Rep. 2018; 8: 4152. https://doi.org/10.1038/s41598-018-22296-8 PMID: 29515196
101. Durden JM, Bett BJ, Jones DOB, Huvenne VAI, Ruhl HA. Abyssal hills a hidden source of increased habitat heterogeneity, benthic megafaunal biomass and diversity in the deep sea. Prog Oceanogr. 2015b; 137: 209–218.
102. Buhl-Mortensen L, Buhl-Mortensen P, Dolan MFJ, Dannheim J, Bellec V, Holte B. Habitat complexity and bottom fauna composition at different scales on the continental shelf and slope of northern Norway. Hydrobiologia. 2012; 685:191–219.
103. Fonseca P, Abrantes F, Aguilar R, Campos A, Cunha M, Ferreira D, et al. A deep-water crinoid Leptometra celtica bed off the Portuguese south coast. Mar Biodivers. 2014; 44: 223–228.
104. Huvenne VAI, Tyler PA, Masson DG, Fisher EH, Hauton CH, Hühnerbach V,et al. A picture on the wall: Innovative mapping reveals cold-water coral refuge on submarine canyon. PLOS ONE. 2011; 6: e28755. https://doi.org/10.1371/journal.pone.0028755 PMID: 22194903
105. Johnson MP, White M, Wilson A, Würzberg L, Schwabe E, Folch H, et al. A vertical wall dominated by Acesta excavata and Neopycnodonte zibrowii, part of an undersampled group of deep-sea habitats. PLOS ONE. 2013; 8: e79917 https://doi.org/10.1371/journal.pone.0079917 PMID: 24260319
106. Davies JS, Howell KL, Stewart HA, Guinan J, Golding N. Defining biological assemblages (biotopes) of conservation interest in the submarine canyons of the South West Approaches (offshore United Kingdom) for use in marine habitat mapping. Deep Sea Res II. 2014;104: 208–229.
107. Bell JB, Alt CHS, Jones DOB. Benthic megafauna on steep slopes at the Northern Mid-Atlantic Ridge. Mar Ecol. 2016; 37: 1290–1302.
108. Marsh L, Copley JT, Huvenne VAI, Tyler PA and the Isis ROV Facility. Getting the bigger picture: Using precision Remotely Operated Vehicle (ROV) videography to acquire high-definition mosaic images of newly discovered hydrothermal vents in the Southern Ocean. Deep Sea Res II. 2013; 92: 124–135.
109. McClain CR, Hardy SM. The dynamics of biogeographic ranges in the deep sea. Proc R Soc Lond [Biol]. 2010; 277: 3533–3546.

Appendix E




110. McClain CR, Schlacher TA. On some hypotheses of diversity of animal life at great depths on the sea floor. Mar Ecol. 2015; 36: 849–872.

111. Howell KL, Pfechaud N, Downie AL, Kenny A. The distribution of deep-sea sponge aggregations in the North Atlantic and implications for their effective spatial management. Deep Sea Res I. 2016; 115: 309–320.

112. Vanreusel A, Hilario A, Ribeiro PA, Menot L, Arbizu PM. Threatened by mining, polymetallic nodules are required to preserve abyssal epifauna. Sci Rep. 2016; 6: 26808 https://doi.org/10.1038/srep26808 PMID: 27245847

113. Simon-Lledó E, Bett BJ, Huvenne VAI, Schoening T, Benoist NMA, Jones DOB. Ecology of a polymetallic nodule occurrence gradient: Implications for deep-sea mining. Limnol Oceanogr 2019b.

114. CCAMLR. VME Taxa Classification Guide. Commission for the Conservation of Antarctic Marine Living Resources, Hobart, Tasmania, 2009; 4pp

115. Vieira RP, Cunha MR. *In situ* observation of chimaerid species in the Gorringe Bank: new distribution records for the north-east Atlantic Ocean. J Fish Biol. 2014; 85: 927–932. https://doi.org/10.1111/jfb.12444 PMID: 24976453

116. Walter DE, Winterton S. Keys and the crisis in taxonomy: extinction or reinvention? Annu Rev Entomol. 2007; 52: 193–208. https://doi.org/10.1146/annurev.ento.51.110104.151054 PMID: 16913830

117. Grandcolas P. Loosing the connection between the observation and the specimen: a by-product of the digital era or a trend inherited from general biology? Bionomina. 2017; 12: 57–62.

118. Thomson SA, Pyle RL, Ahyong ST, Alonso-Zarazaga M, Ammirati J, Araya JF, et al. Taxonomy based on science is necessary for global conservation. PLOS Biol. 2018; 16: e2005075 https://doi.org/10.1371/journal.pbio.2005075 PMID: 29538381

119. Hagedorn G, Rambold G, Martellos S. Types of identification keys. In Nimis PL, Vignes Lebbe R, editors. Tools for identifying biodiversity: progress and problems. Proc Int Cong Paris, Edizioni Università di Trieste 2012; pp 59–64.

120. Williams S, Friedman A. SQUIDLE+ 2018. Available from: http://squidle.acfr.usyd.edu.au.

121. Ontrup J, Ehnert N, Bergmann M, Nattkemper TW. BIIGLE—Web 2.0 enabled labelling and exploring of images from the Arctic deep-sea observatory HAUSGARTEN. In OCEANS 2009 N EUROPE. IEEE, Bremen, 2009; pp 1–7.

122. Langenkämper D, Zurowietz M, Schoening T, Nattkemper TW. BIIGLE 2.0—Browsing and Annotating Large Marine Image Collections. Front Mar Sci 2017b; 4: 1–10.

123. Krizhevsky A, Sutskever I, Hinton GE. Imagenet classification with deep convolutional neural networks. In Krizhevsky A, Sutskever I, Hinton GE, editors. Advances in neural information processing systems. 2012; pp 1097–1105.

124. LeCun Y, Bengio Y, Hinton G. Deep learning. Nature. 2015; 521:436. https://doi.org/10.1038/nature14539 PMID: 26017442

125. Woodall LC, Andradi-Brown DA, Brierley AS, Clark MR, Connelly D, Hall RA, et al. Multidisciplinary approach for generating globally consistent data on mesophotic, deep-pelagic, and bathyal biological communities. Oceanogr. 2018; 31: 3.

frontiers in Marine Science

ORIGINAL RESEARCH
published: 21 February 2020
doi: 10.3389/fmars.2020.00095

# Determining Coral Density Thresholds for Identifying Structurally Complex Vulnerable Marine Ecosystems in the Deep Sea

*Ashley A. Rowden[1,2]*, Tabitha R. R. Pearman[3], David Anthony Bowden[1], Owen F. Anderson[1] and Malcolm Ross Clark[1]*

[1] National Institute of Water and Atmospheric Research, Wellington, New Zealand, [2] Victoria University of Wellington, Wellington, New Zealand, [3] Ocean and Earth Science, University of Southampton, Southampton, United Kingdom

OPEN ACCESS

**Edited by:**
Sandra Brooke,
Florida State University, United States

**Reviewed by:**
Tina Molodtsova,
P.P. Shirshov Institute of Oceanology (RAS), Russia
Saskia Brix,
Senckenberg Museum, Germany

***Correspondence:**
Ashley A. Rowden
ashley.rowden@niwa.co.nz

**Specialty section:**
This article was submitted to Deep-Sea Environments and Ecology, a section of the journal Frontiers in Marine Science

**Received:** 03 October 2019
**Accepted:** 05 February 2020
**Published:** 21 February 2020

**Citation:**
Rowden AA, Pearman TRR, Bowden DA, Anderson OF and Clark MR (2020) Determining Coral Density Thresholds for Identifying Structurally Complex Vulnerable Marine Ecosystems in the Deep Sea. Front. Mar. Sci. 7:95. doi: 10.3389/fmars.2020.00095

Vulnerable marine ecosystems (VMEs) are at risk from the impacts of deep-sea trawling. Identifying the presence of VMEs in high seas fisheries management areas has to date relied mainly on presence records, or on habitat suitability models of VME indicator taxa (e.g., the stony coral species *Solenosmilia variabilis* Duncan, 1873) as proxies for the occurrence of VMEs (e.g., cold-water coral reefs). However, the presence or predicted presence of indicator taxa does not necessarily equate to the occurrence of a VME. There have been very few attempts to determine density thresholds of VME indicator taxa that relate to a "significant concentration" which supports a "high diversity" of associated taxa, as per the current criterion for identifying structurally complex VMEs (FAO, 2009). Without knowing such thresholds, identifications of VMEs will continue to be subjective, impeding efforts to design effective spatial management measures for VMEs. To address this issue, we used seafloor video and still image data from the Louisville Seamount Chain off New Zealand to model relationships between the densities of live *Solenosmilia variabilis* coral heads, as well as percent cover of live and dead coral matrix, and the number of other epifauna taxa present. Analyses were conducted at three spatial scales; 50 and 25 $m^2$ for video, and 2 $m^2$ for stills. Model curves exhibited initial steep positive responses reaching thresholds for the number of live coral heads at 0.11 $m^{-2}$ (50 $m^2$), 0.14 $m^{-2}$ (25 $m^2$), and 0.85 $m^{-2}$ (2 $m^2$). Both live and dead coral cover were positively correlated with the number of associated taxa up to about 30% cover, for all spatial scales (24.5–28%). We discuss the results in the context of past and future efforts to develop criteria for identifying VMEs.

**Keywords: *Solenosmilia variabilis*, cold-water coral reef, density threshold, VME, deep sea**

## INTRODUCTION

Deep-sea trawling impacts the structure and function of seafloor communities and habitats (see review by Clark et al., 2016). In 2006 and 2009, the United Nations General Assembly (UNGA) called upon regional fisheries management organizations (RFMOs) to develop and adopt binding conservation management measures requiring their members to protect vulnerable

Appendix E



marine ecosystems (VMEs) from significant adverse impacts of bottom fishing (Resolutions 61/105 and 64/72; UNGA, 2006, 2009). The Fisheries Agricultural Organisation (FAO) International Guidelines for the Management of Deep-sea Fisheries in the High Seas provides guidance for defining and identify VMEs (FAO, 2009). Although the guidelines have served as the principal means for RFMOs to define and identify VMEs, they did not provide any clear guidance on what constitutes evidence of an encounter with a VME during bottom fishing operations or analytical approaches for identifying areas containing VMEs.

Occurences of VME indicator taxa are routinely used by RFMOs as surrogates for VME identification and delimitation. VME indicator taxa may be recorded from trawling bycatch and used for encounter protocols [e.g., Parker et al., 2009 for the South Pacific Regional Fisheries Management Organisation (SPRFMO)] or their distribution may be predicted by habitat suitability modeling (also called species distribution modeling) (e.g., Georgian et al., 2019 for SPRFMO). However, the distribution of a VME indicator taxon does not necessarily correlate with the distribution of the VME itself. For example, Howell et al. (2011) noted that the observed distribution of a coral reef in the North Atlantic is a subset of the wider predicted distribution the indicator taxon *Desmophyllum pertusum* (Linnaeus, 1758) [formerly *Lophelia pertusa*] that can form such a VME when it occurs in sufficient density. Most methods used to date to distinguish VMEs involve some subjective judgment, and therefore the veracity of these methods depends upon a number of untested assumptions. For example, Rowden et al. (2017) used abundance-based habitat suitability models of a coral species and a subjective density-based definition of a coral reef to predict VME distribution. However, the definition used was not related directly to any of the criteria that the FAO guidelines specify for what constitutes a VME (FAO, 2009).

The FAO guidelines have 5 criteria for identifying VMEs, one of which is: "*Structural complexity – an ecosystem that is characterized by complex physical structures created by significant concentrations of biotic and abiotic features. In these ecosystems, ecological processes are usually highly dependent on these structured systems. Further, such ecosystems often have high diversity, which is dependent on the structuring organisms*" (FAO, 2009). This criterion emphasizes two obvious components that can be measured, and which can therefore be used to determine objectively a threshold for identifying a VME. That is, the threshold of the "significant concentrations" of the structure forming organism that supports a "high diversity" of the organisms that are dependent on the structuring organisms. Thresholds for identifying cold-water coral reefs are beyond the remit of the FAO guidelines, and of the few thresholds that have been published independently none are based on a quantitative analysis of the direct relationship between coral density and associated biodiversity. These threshold estimates for identifying distinct coral reef habitat range widely between 15 and >60% coral cover (Vertino et al., 2010; Rowden et al., 2017), presumably at least in part because of taxa and site/regional differences in the relationship between coral cover and the formation of a recognizable reef structure, but also potentially because of the subjective nature of the threshold estimate. Ideally, if habitat suitability models or even direct observation of VMEs are going to be used to inform spatial management of bottom trawling, then studies are required that objectively derive VME thresholds where VME indicator taxa densities are sufficient to provide specific ecological functions. Such studies will need to be specific to the taxa encountered in a RFMO area.

*Solenosmilia variabilis* is a stony coral VME indicator species that is structurally complex, long-lived, fragile, and widespread within the SPRFMO Convention Area (Anderson et al., 2016). This coral species can form structurally complex reef that provides habitat for diverse communities in the region, which can be impacted by bottom trawling (Koslow et al., 2001; Althaus et al., 2009; Clark and Rowden, 2009; Williams et al., 2010; Clark et al., 2019). The aim of the present study was to examine the relationship between the density of *S. variabilis* and the diversity of associated organisms, and to determine if it is possible to identify a density threshold at which a demonstrable elevated biodiversity is supported by the coral habitat, and which can be used practically to identify a VME. While a density threshold identified by the study may not be transferable to other taxa/regions, the methodology can be used for similar determinations in other RFMO areas. That is, our overall purpose is to operationalize one of the FAO's criteria for identifying VMEs so that it can be used as a basis for devising spatial management measures to prevent significant adverse impacts by fishing.

## MATERIALS AND METHODS

### Study Area and Sampling

Data used in the analysis were collected during a survey of six seamounts on the Louisville Seamount Chain to field test habitat suitability models for VME indicator taxa (Anderson et al., 2016). The Louisville Seamount Chain lies to the east of New Zealand in the SPRFMO Convention Area, the region of the South Pacific beyond areas of national jurisdiction. Analysis was conducted on data from one of these seamounts, Forde Guyot, situated at the North-West of the part of the Louisville Seamount Chain sampled by the survey (**Figure 1**). Forde Guyot was chosen for the analysis because historically it has received the least fishing pressure (of the six seamount features surveyed) and is now closed to bottom trawling (since May 2008), and thus represents an environment in which the coral reef habitat formed by *S. variabilis* is unlikely to have been modified by bottom trawling (no indication of trawling impacts – trawl net/door marks, discarded gear etc – were observed in the camera survey of this seamount). The survey used a towed camera system (Hill, 2009) with video (HD1080, 45° forward-orientation) and stills (24 mp DSLR, vertical orientation) cameras. The tow speed, camera and light settings, and transect length were optimized for imaging and quantifying benthic epifauna communities (see Anderson et al., 2016 for deployment details). Imagery from both cameras was analyzed to obtain data on the abundance and distribution of *S. variabilis* and all visible epifauna. These data were used to

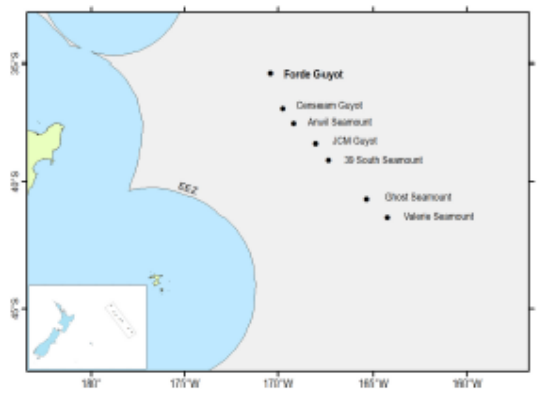


**FIGURE 1 |** Map showing the summit location of Forde Guyot (bolded feature name) in relation to other seamount features on part of the Louisville Seamount Chain. Inset map shows these seamounts in relation to New Zealand (modified from Rowden et al., 2017).

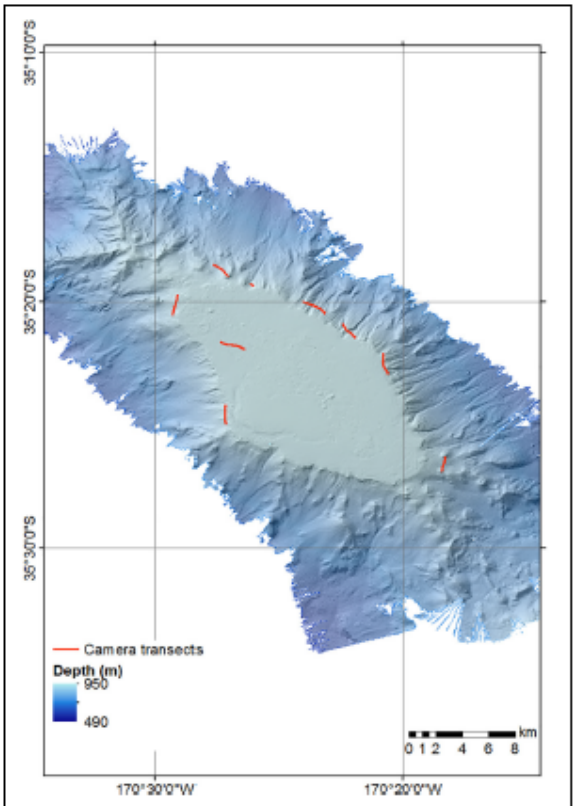


**FIGURE 2 |** Bathymetric map of Forde Guyot showing the location of the camera transects analyzed for this study.

not only test regional habitat suitability models, but to also make abundance-based models of *S. variabilis* (Rowden et al., 2017).

## Data and Data Processing

Video data from Rowden et al. (2017), detailing faunal occurrences and substrate types were reviewed, and nine transects from Forde Guyot in which *S. variabilis* was present were used in the analysis (**Figure 2** and **Table 1**). For the current study, still images from these transects were also analyzed (**Table 1**; after review to remove overlapping images, poor quality images, and images taken at >3 m altitude) with *S. variabilis* and all other visible epifauna ('morphospecies' > 10 mm) being counted (using the image annotation platform BIIGLE 2.0; Langenkämper et al., 2017). Because much of the *S. variabilis* matrix of colonies observed was evidently not alive (dark coloration with no live polyps visible in high resolution still imagery), which is apparently typical for such cold-water coral reef habitat (e.g., Clark and Rowden, 2009; Vertino et al., 2010, and see **Figure 3**), occurrence of this taxon was recorded in three ways: percent cover of the seabed for live and dead "intact coral" matrix, percent cover of dead broken-up matrix termed "coral rubble," and counts of distinct live coral colonies or "coral heads" on which live polyps were visible (**Figure 3**). A coral head was considered distinct if the separation between colonies with live polyps was visually obvious (typically > 5 cm). No minimum or maximum size criteria were used to identify a live coral head, but they were typically in the range of 15–40 cm in diameter.

Coral and other epifauna records were determined at three spatial scales: per 50 $m^2$ segment of video transect (~2 m transect image width × 24 m along the transect track), per 25 $m^2$ segment of video transect (~2 m transect image width × 12 m along the transect track) and from individual still frames per 2 $m^2$ (~ 2 m × 1 m still image view). Analyses at these spatial scales allow for an examination of whether any identified VME density thresholds were scale dependent, and allow for comparisons with previously published threshold estimates for coral reef habitat.

## Data Analysis

Welch's ANOVA was first used to test if coral habitat (live and dead intact coral and coral rubble) is associated with higher species richness (number of other epifaunal 'morphospecies') than non-coral habitat (mainly unconsolidated substrates such as sand and mud). Welch's ANOVA was used because data had unequal variances.

Data exploration indicated a lack of homogeneity and non-linear relationships within the datasets, which together with the nested structure of the data violate statistical assumptions of methods that fit curves to raw data (**Supplementary Figure S1**). Thus, general additive models (GAMs) were applied to the datasets to model the relationship between the coral density parameters noted above (predictor variables) and the species richness of other epifauna (response variable). GAMs are generalized models with smoothers and link functions based on an exponential relationship between the response variable and the predictor variables (Zuur et al., 2014b). GAMs have previously been used to model relationships between

Appendix E



**TABLE 1 |** Length of each camera transect, video duration, total number of still images taken and retained for analysis, and % of video transect represented by the retained images.

| Camera transect | Length (m) | Duration (hh:mm:ss) | Total images | Images retained | % Video sampled | Mid transect depth (m) |
|---|---|---|---|---|---|---|
| TAN1402/06 | 1268 | 01:02:43 | 251 | 217 | 34 | 1217 |
| TAN1402/09 | 1648 | 01:02:50 | 258 | 234 | 28 | 1105 |
| TAN1402/12 | 1734 | 00:28:05 | 258 | 206 | 24 | 1472 |
| TAN1402/13 | 335 | 00:11:22 | 100 | 34 | 20 | 1375 |
| TAN1402/18 | 1264 | 01:02:53 | 254 | 157 | 25 | 1483 |
| TAN1402/19 | 1550 | 00:55:30 | 228 | 210 | 27 | 1227 |
| TAN1402/20 | 1469 | 00:58:03 | 259 | 218 | 30 | 1234 |
| TAN1402/25 | 1151 | 00:47:42 | 199 | 192 | 33 | 1430 |
| TAN1402/27 | 1668 | 01:02:48 | 256 | 250 | 30 | 1053 |

environmental variables and species richness (Robert et al., 2015; Song and Cao, 2017) and to identify ecological response thresholds (Foley et al., 2015; Large et al., 2015). GAMs were chosen because they can accommodate non-linear relationships and produce ecologically intuitive outputs by identifying the shape and strength of the relationship between the response and predictor variables (Zuur et al., 2014a). Non-linear threshold responses are common in ecological systems, but some non-linear phenomena may not be of direct interest and need to be accounted for when making inferences about the variables in question. Depth and spatial proximity of data points to one another can influence biological responses and were integrated into models via the categorical variable 'transect.' To further account for inherent spatial autocorrelation in the data an additional predictor variable, the residual autocovariate (RAC) was calculated and added to the model. The RAC represents the similarity between the residuals from initial models at a location compared with those of neighboring locations. This method can account for spatial autocorrelation without compromising model performance (Crase et al., 2012).

The degree of smoothing in the fitting of the explanatory variables was based on the generalized cross validation (GCV) method and a log link function. For the 2 $m^2$ dataset smooth terms allowing up to 4 degrees of freedom were used, due to the low variability in the response values at this resolution. A negative binomial distribution with no transformation was chosen (in part because this provided better fits given the high proportion of zero values) after exploring several alternative distributions (Poisson, quasi-Poisson, zero inflated) and model set ups (different variable explanatory variables and optimized under parsimony). Significance of terms in the model were tested with ANOVA. Model accuracy was assessed by variance in species richness explained by each model (Adjusted $R^2$) and model fit by Akaike's Information Criterion score (AIC). All statistical analyses were conducted using the open source software R (R Core Team, 2014), packages "mgcv," "gbm," "raster" and "vegan."

Thresholds are characterized by a non-linear change in response to a predictor variable (Foley et al., 2015; Large et al., 2015). Based on ecological theory, we expect the relationship between coral density parameters and associated species richness to exhibit an initial relatively steep positive relationship before flattening off to a plateau or exhibiting a slight drop off as coral density increases. That is, as the amount or density of structurally complex habitat increases so does the number of species that can be supported by this habitat, up until a point where the concentration of habitat has reached a level where all physical niches are occupied by species that have become associated with the habitat (Rosenzweig, 1995, pp. 32–36, and references therein). As the density of the structural habitat increases beyond this threshold, it is possible that the number of associated species

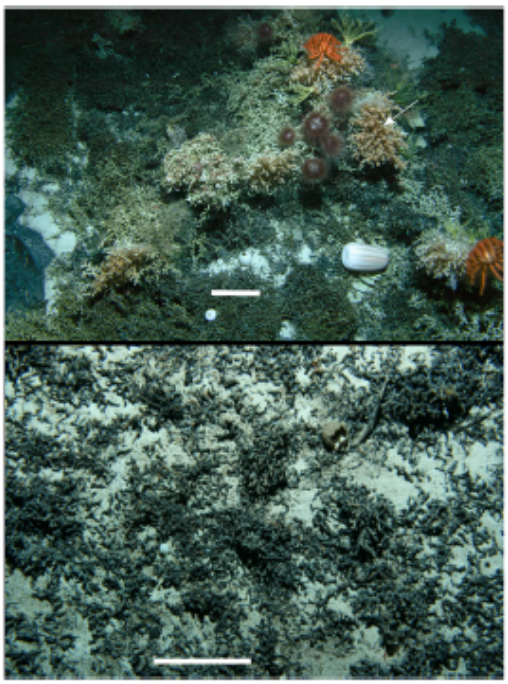

**FIGURE 3 |** Still images of the seafloor on Forde Guyot showing: **(top)** intact dead (brown)/live (white and pale orange) coral matrix with live coral heads (distinct pale orange colonies with live polyps; arrow indicates an example of a coral head) of *Solenosmilia variabilis*, and associated epifauna taxa; **(bottom)** broken-down dead coral matrix or coral rubble. Scale bar = 20 cm.

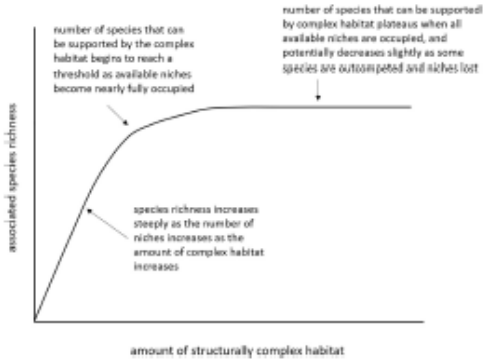


**FIGURE 4 |** Theoretical relationship between the amount of structurally complex habitat and associated species richness.

may decrease slightly as some species are outcompeted and the number of niches is reduced, assuming an increase in density is associated to some extent with an increase in time (Rosenzweig, 1995, pp. 186–189, and references therein) (**Figure 4**). Potential coral density thresholds for species richness were identified from the GAMs using four methods: (1) the intersections of linear regressions through the initial and final 5% of the data; (2) the intersection of a linear regression through the initial 5% of data with a horizontal line extended from the maximum cumulative value; (3) the point on a curve fit to the data that is closest to the top-left corner; and (4) the point that maximizes the distance between the curve and a line drawn between the extreme points on the curve (Youden Index) (**Supplementary Figure S2**). Where possible, all four threshold values were determined for each of the coral density parameters, and the average threshold for each spatial scale calculated.

## RESULTS

See **Supplementary Material** for species richness data for each spatial scale of the analysis.

One hundred and thirty-six epifaunal morphospecies were identified from the datasets. Epifauna exhibited a patchy distribution, reflected in the species richness counts that were relatively low, and which reached maximum values of 10 at 50 $m^2$, 8 at 25 $m^2$ and 9 at 2 $m^2$. *Solenosmilia variabilis* also exhibited a patchy distribution occurring at low density across the study transects (**Figure 5**).

At all spatial scales, average epifaunal species richness was significantly higher for the intact live and dead coral matrix (2.35 50 $m^{-2}$, 3.28 25 $m^{-2}$, 2.6 2 $m^{-2}$), compared to coral rubble (0.98 50 $m^{-2}$, 1.56 25 $m^{-2}$, 1.09 2 $m^{-2}$) and non-coral habitat (0.81 50 $m^{-2}$, 1.27 25 $m^{-2}$, 1.15 2 $m^{-2}$) (Welch's ANOVA for 50 $m^2$ F2, 168 = 61.49, $p < 0.001$; 25 $m^2$ F2, 258 = 77.886, $p < 0.001$; 2 $m^2$ F2, 227 = 20.51, $p < 0.001$).

The number of live *S. variabilis* coral heads had the greatest influence on the models for species richness, followed by % cover of intact coral, whilst coral rubble had no significant influence, except at the 50 $m^2$ spatial scale. This result is consistent across spatial scales (**Table 2**).

Species richness exhibited an initial shallow positive response to % intact coral, which flattened or dropped off after reaching thresholds of 26% (50 $m^2$), 24.5% (25 $m^2$) and 28% (2 $m^2$) (**Figure 5** and **Table 3**). The relationships between species richness and % coral rubble were too 'flat' to determine thresholds (**Figure 6**).

Species richness exhibited an initial steep positive relationship with the number of live coral heads of *S. variabilis*, before reaching an identifiable threshold beyond which the relationship flattened off in an undulating or slightly decreasing curve (**Figure 6**). The multimodal response beyond the threshold at the 50 and 25 $m^2$ spatial scales appears to reflect inter-transect variability driven by the high density of *S. variabilis* recorded from one transect (station TAN1402/18) which is responsible for the second maxima. The average density threshold for the number of *S. variabilis* live heads is similar for both 50 and 25 $m^2$ spatial scales of the analysis, when expressed as number of coral heads $m^{-2}$; 0.11 and 0.14 $m^{-2}$, respectively. The average density threshold for number of live coral heads was 0.85 $m^{-2}$ at the 2 $m^2$ spatial scale of the analysis (**Table 3**).

## DISCUSSION

We determined density thresholds that can be used to objectively identify structurally complex coral reef VMEs in the SPRFMO Convention Area. We used a methodology that operationalizes one of the criteria for identifying VMEs by determining the "significant concentrations" of a structure forming organism that supports a "high diversity" of associated fauna that are dependent on this structuring organism (FAO, 2009).

Our initial analysis of image data from Forde Guyot on the Louisville Seamount Chain demonstrated that cold-water coral reef habitat formed by the stony coral *Solenosmilia variabilis* supports elevated levels of biodiversity compared to less structurally complex substrates such as nearby mud and sand. Elevated levels of biodiversity associated with habitat formed by other stony coral species, compared to other deep-sea habitats, have been demonstrated previously in other ocean regions (e.g., *Desmophyllum pertusum* in the North Atlantic - Henry and Roberts, 2007). However, we are unaware of any published study that has examined the direct relationship between density parameters of cold-water coral reefs and the richness of associated species [but see acknowledgments, and Beazley et al. (2015) and Ashford et al. (2019) for examinations of the density/biomass of other VME indicatar taxa and associated species richness]. A study by Van Den Beld et al. (2017) examined the separate relationships between stony coral cover and the abundance (but not species richness) of solitary coral taxa, and no density threshold for the abundances of these taxa was observed.

Our modeling analysis demonstrated a relationship between coral density and associated species richness at three spatial scales, and identified density thresholds at which coral reef habitat supports relatively higher levels of associated biodiversity.

Appendix E



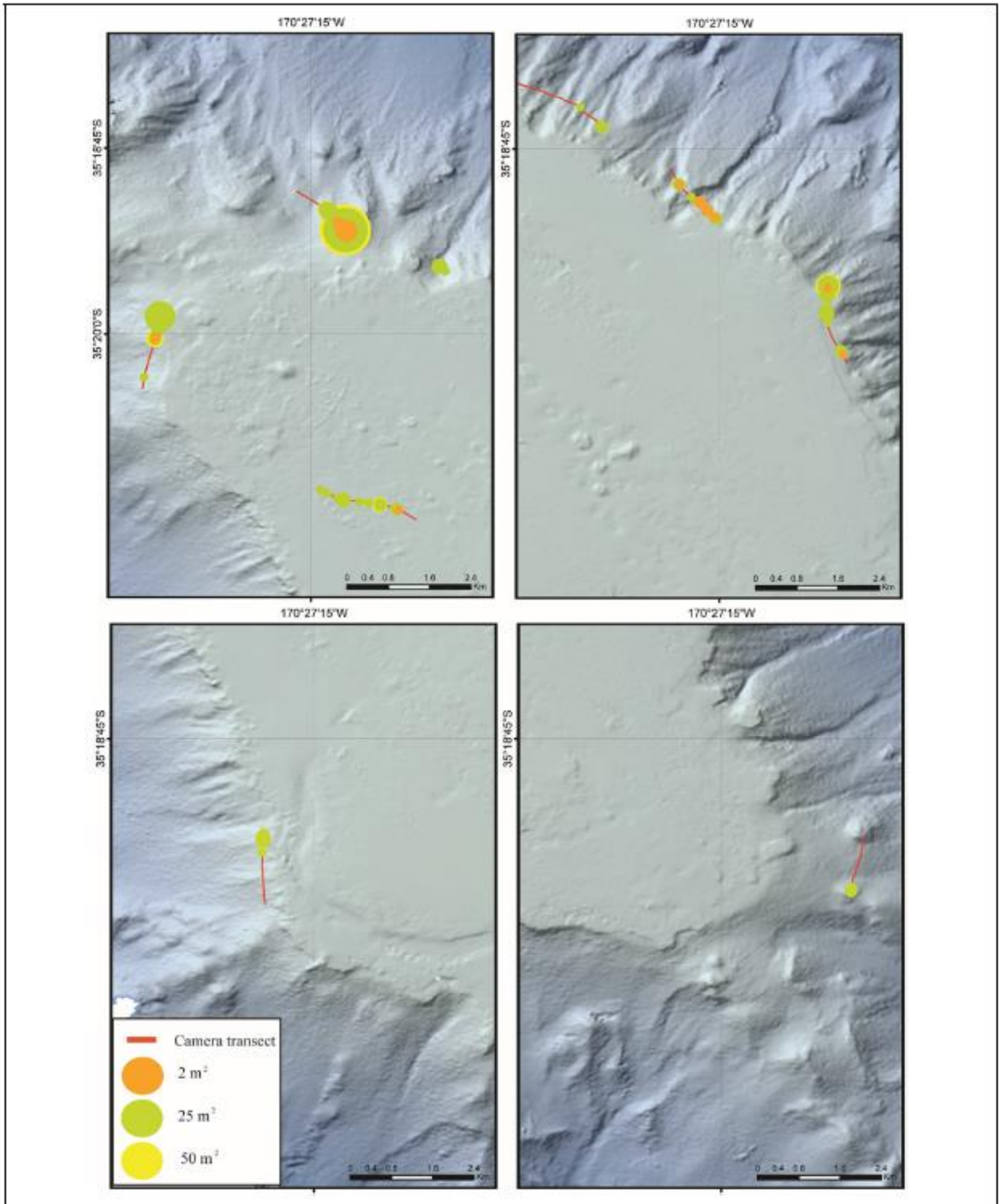


**FIGURE 5 |** Maps showing the distribution of the abundance of the stony coral *Solenosmilia variabilis* at three spatial scales (50, 25, and 2 $m^2$). Relative abundance expressed by expanding circles (see key for values). Symbols plotted at the midpoints of the 50 $m^2$, 25 $m^2$ sections of the camera transects, and at the exact image location for 2 $m^2$.

Appendix E



**TABLE 2 |** Results of the GAM models at three spatial scales.

| | Spatial scale | | |
|---|---|---|---|
| | **50 m²** | **25 m²** | **2 m²** |
| **Variable** | **Approximate significance of smoother terms (ANOVA)** | | |
| Number of live coral heads | 3 (4), 580 = 2e-16*** | 4 (5), 1153 ≤ 2e-16*** | 2 (3), 1658 = 1.24e-08*** |
| % intact coral | 2 (9), 580 = 0.00586** | 2 (9), 1153 = 0.00096*** | 2 (3), 1658 = 6.47-06*** |
| % coral rubble | 2 (9), 580 = 0.00461** | 1 (9), 1153 = 0.0982 | 1 (3), 1658 = 0.273 |
| Transect | 8,580 ≤ 2e-16*** | 8,1153 ≤ 2e-16*** | 8, 1658 ≤ 2e-16*** |
| RAC | 1,580 ≤ 2e-16*** | 1,1153 ≤ 2e-16*** | 1,1658 ≤ 2e-16*** |
| Adjusted $R^2$ | 48% | 36% | 26% |
| AIC | 1723 | 2793 | 4550 |

*Explanatory contribution of each variable indicated by approximate significance of the smoother terms. Model accuracy assessed by variance in species richness explained by each model (Adjusted $R^2$) and model fit by Akaike's Information Criterion score (AIC).*

The non-linear relationship conformed to the theoretical expectation on which our study was based (see section Materials and Methods). We acknowledge that a possible alternative explanation, in addition to competition, for any apparent decrease in the number of species associated with coral densities above the thresholds could be related to lower detection probability as habitat-forming taxa become more abundant and increase in complexity. Somewhat surprisingly, the density thresholds for the % cover of the intact coral matrix were similar across all spatial scales (ranging from 24.5 to 28%), as were the thresholds for the number of live coral heads at the 50 $m^2$ and 25 $m^2$ spatial scales (0.11 and 0.14 $m^{-2}$, respectively). The higher coral head density threshold observed for the 2 $m^2$ spatial scale (0.85 $m^{-2}$) could potentially be explained by a range of factors associated with the two camera systems, including: different observation viewpoints in video and still images; image resolution and lighting differences; and differing spatial scales of observation. The angled viewpoint of the video means that it is possible some coral heads may be obscured by coral matrix in front of them, whereas the vertical viewpoint of the still images will ensure that all live coral heads are observable, thereby resulting in a higher count. The still images are of higher resolution and more evenly lit than the video imagery, which could also result in higher detection rates of the live coral heads in the still images. It is also possible that the identification of thresholds for individual live coral heads are scale-dependent. The cold-water coral reefs were patchy, and because still images sample a smaller seabed area than does video, they are less likely to encounter coral reef patches, which will influence the counts of live coral heads. A further consequence of the smaller seabed area within individual still images (which is typically smaller than the coral patches) is that counts of live coral head density may be higher in still images because larger coral reef patches are more likely to be detected multiple times by the images than smaller habitat patches (assuming larger patches are more dense than smaller patches). Observations made by video at the 50 $m^2$ and 25 $m^2$ spatial scale will more likely capture whole coral reef patches, and thereby result in more stable and reliable density estimates. Thus, it is clear that scale-related sampling effects should be considered when attempting to determine reliable density estimates of fauna that generate patchy habitats (Andrew and Mapstone, 1987). However, the results for the two larger spatial scales, both derived from the same imaging system, suggest that the relationships and thresholds observed are ecologically fundamental. This finding provides support for the practical application of such objectively identified quantitative thresholds in the identification and mapping of structurally complex VME habitats.

**TABLE 3 |** Results of the analysis to determine coral density thresholds for identifying structurally complex vulnerable marine ecosystems at three spatial scales (see section Materials and Methods for description of numbered threshold methods).

| **Threshold method** | **Spatial scale** | | |
|---|---|---|---|
| | **50 m²** | **25 m²** | **2 m²** |
| **% Intact coral cover** | | | |
| 1 | NA | NA | NA |
| 2 | NA | NA | NA |
| 3 | 22 | 19 | 25 |
| 4 | 32 | 30 | 31 |
| Average | 24.5 | 26 | 28 |
| **Number of coral heads $m^{-2}$** | | | |
| 1 | 0.11 | NA | NA |
| 2 | 0.10 | 0.13 | 0.80 |
| 3 | 0.10 | 0.15 | 0.65 |
| 4 | 0.11 | 0.15 | 1.10 |
| Average | 0.11 | 0.14 | 0.85 |

Vertino et al. (2010) subjectively identified 20–40% coverage of live and/or dead coral colonies as a threshold at a spatial scale of 2.4 $m^2$ in the Mediterranean Sea. Their result, even though a different species in a different ocean was broadly similar to our objectively derived thresholds of 24.5 – 28% cover. For the one quantitative examination that we know of that examined the relationship between % coral cover and community structure (Price et al., 2019), the derived density threshold is also similar to the one we identify more directly for species richness. Price et al. (2019) found through multivariate analysis that the proportion

Appendix E



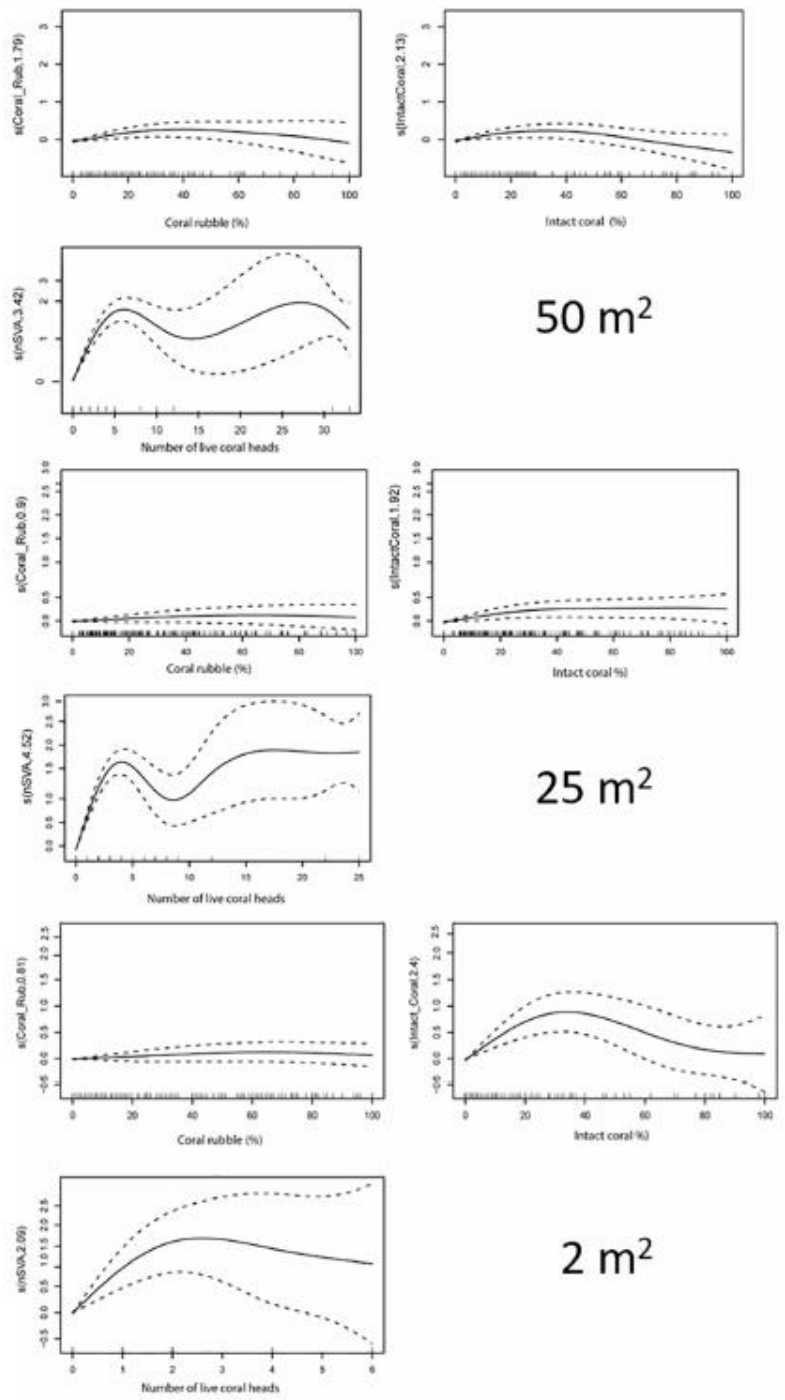


**FIGURE 6 |** General Additive Model smoother outputs showing the relationship between coral density (% coral rubble, % intact coral, number of live coral heads) and species richness at three spatial scales.

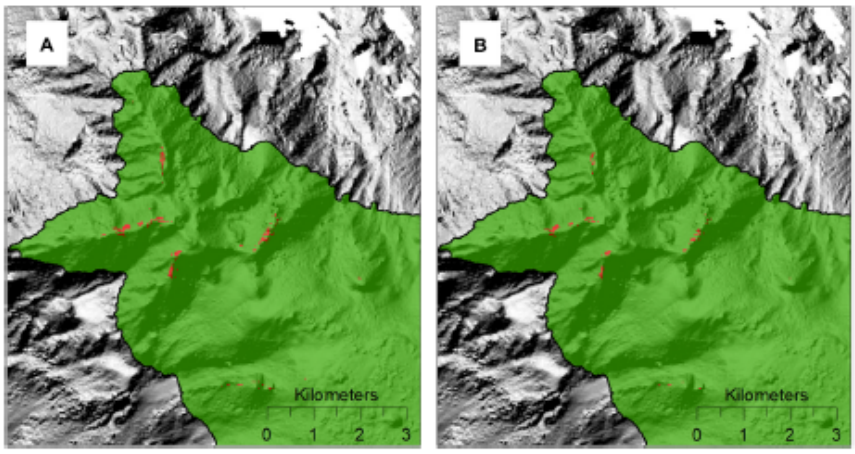


**FIGURE 7 |** Predicted coral reef VME habitat (red patches) on the north-west portion of Forde Guyot, identified by applying a density threshold for live coral heads to an abundance-based habitat suitability model for *Solenosmilia variabilis* (Rowden et al., 2017); **(A)** using the subjectively derived threshold of 2.78 live coral heads 25 $m^{-2}$ from Rowden et al. (2017), and **(B)** the objectively derived threshold of 3.5 live coral heads 25 $m^{-2}$ from the present study.

of live and dead coral cover of stony coral (predominantly *Madrepora oculata* Linnaeus, 1758 and *Desmophyllum pertusum*) in the Whittard Canyon (North East Atlantic) was apparently related to community structure, and that coral reef communities become distinct somewhere between a coral cover of 28 and 36% (they suggested 30% as an approximation) at a spatial scale of 10 s of meters. They demonstrated more directly using GAMs that species richness began to plateau at a particular level of structural complexity (0.7 vector ruggedness measure), which they reported (but did not show) as being equivalent to 30% coral cover.

The density thresholds we identified for live coral heads using video data, 0.11 $m^{-2}$ and 0.14 $m^{-2}$ (at 50 $m^2$ and 25 $m^2$, respectively), were the same or similar to the threshold of 0.11 $m^{-2}$ used previously to identify coral reef VME on the Lousiville Seamount Chain (coverted from 2.78 live heads per 25 $m^2$, Rowden et al., 2017). The density threshold used by Rowden et al. (2017) was from the same video data but derived by a different methodology, and based on a subjective definition of what constitutes a coral reef "sensitive environment" according to regulations devised to prevent impacts to such habitats by human activities in the New Zealand EEZ[1]. The similarity between the thresholds appears to offer some support for the subjective-based threshold. However, Rowden et al. (2017) urged caution of the use of the threshold they applied, describing it as a subjective regional translation of the "you will know when you see it" descriptions of cold-water coral reefs, and argued for the implementation of quantitative studies such as the present work to objectively identify VMEs. Having now established a quantitative-based threshold to identify VMEs, it is possible to re-map the coral reef habitat on the study seamounts of the Louisville Seamounts Chain. Although the objective and subjective-based thresholds were apparently similar, application of the new density threshold for 25 $m^2$ indicates that there is ~60% less coral reef VME habitat on Forde Guyot than previously estimated (Rowden et al., 2017; 0.12 $km^2$ compared to 0.20 $km^2$, **Figure 7**).

In the present study, low sample size and uneven sampling posed some limitations for modeling the relationship between coral density parameters and associated species richness. However, it appears that low coral density and a patchy distribution is inherent in the nature of the cold-water coral reefs on Forde Guyot, and indeed other seamounts on the Louisville Seamount Chain (Rowden et al., 2017). Future studies should endeavor to better accommodate such heterogeneity in analyses of the relationships that we examined. Despite the potential limitations, we hope our work will encourage future efforts to look further at the taxa/regional-specific or universal nature of the density thresholds determined here for identifying structural complex coral reef VMEs. Quantitative studies establishing the association between coral density parameters and the structural or functional attributes that distinguish VMEs are few, and this lack is currently hindering efforts to devise measures to protect VMEs from the impacts of fishing.

## CONCLUSION

Our data and previous findings suggest that approximately 30% intact coral cover represents a significant concentration which supports a high diversity of associated taxa. This threshold could be used broadly to distinguish deep-sea coral reef VMEs made by structurally complex stony coral species such as *Solenosmilia variabilis*, *Madrepora oculata*, and *Desmophyllum pertusum*. Furthermore, specific threshold density metrics for particular species and regions, such as we derived for number of live coral heads of *S. variabilis* for the South Pacific, can be used to threshold abundance-based habitat suitability model

[1]http://www.mfe.govt.nz/marine/legislation/regulations-under-eez-act

Appendix E



predictions to make maps that can be used by RFMOs to design spatial management measures to prevent significant adverse impacts to VMEs.

## DATA AVAILABILITY STATEMENT

All datasets generated for this study are included in the article/**Supplementary Material**.

## AUTHOR CONTRIBUTIONS

AR conceived of the study, led the writing, and drafted text for the manuscript. AR, MC, and DB designed the field survey. MC, DB, and OA collected the data from the field survey. TP analyzed the images, conducted the statistical analysis, and contributed draft text to the manuscript. All authors interpreted all data, revised and approved the final version of the manuscript.

## FUNDING

This work was based on data obtained during the NIWA-led South Pacific Vulnerable Marine Ecosystems Project funded by the New Zealand Ministry for Business, Innovation and Employment (C01X1229). AR, DB, OA, and MC's contribution to the research reported here was funded by NIWA's Fisheries Centre. TP's contribution to the research was funded by the Southampton Partnership for Innovative Training of Future Investigators Researching the Environment, which supported her internship at NIWA while a Ph.D. student at the University of Southampton.

## ACKNOWLEDGMENTS

We acknowledge that our study was partly inspired by the poster displayed by Lenaick Menot et al. at the 2018 Deep Sea-Biology Symposium in Monterey, United States (The ecological role of patchy cold-water coral habitats: Does coral density influence local biodiversity in submarine canyons in the Bay of Biscay? http://dsbsoc.org/wp-content/uploads/2014/12/15thDSBS_Abstracts.pdf). We thank Tom Ezard, from the National Oceanography Centre, for his discussions of statistical model validation plots.

## SUPPLEMENTARY MATERIAL

The Supplementary Material for this article can be found online at: https://www.frontiersin.org/articles/10.3389/fmars.2020.00095/full#supplementary-material

## REFERENCES

Althaus, F., Williams, A., Schlacher, T. A., Kloser, R. K., Green, M. A., Barker, B. A., et al. (2009). Impacts of bottom trawling on deep-coral ecosystems of seamounts are long-lasting. *Mar. Ecol. Progr. Ser.* 397, 279–294. doi: 10.3354/meps08248

Anderson, O. F., Guinotte, J. M., Rowden, A. A., Clark, M. R., Mormede, S., Davies, A. J., et al. (2016). Field validation of habitat suitability models for vulnerable marine ecosystems in the South Pacific Ocean: implications for the use of broad-scale models in fisheries management. *Ocean Coast. Manag.* 120, 110–126. doi: 10.1016/j.ocecoaman.2015.11.025

Andrew, N. L., and Mapstone, B. D. (1987). Sampling and the description of spatial pattern in marine ecology. *Oceanogr. Mar. Biol.* 25, 39–90.

Ashford, O. S., Kenny, A. J., Barrio Froján, C. R. S., Downie, A.-L., Horton, T., and Rogers, A. D. (2019). On the influence of Vulnerable Marine Ecosystem habitats on peracarid crustacean assemblages in the Northwest Atlantic Fisheries Organisation regulatory area. *Front. Mar. Sci.* 6:401. doi: 10.3389/fmars.2019.00401

Beazley, L., Kenchington, E., Yashayaev, I., and Murillo, F. J. (2015). Drivers of epibenthic megafaunal composition in the sponge grounds of the Sackville Spur, northwest Atlantic. *Deep Sea Res. Part I Oceanogr. Res. Pap.* 98, 102–114. doi: 10.1016/j.dsr.2014.11.016

Clark, M. R., Althaus, F., Schlacher, T. A., Williams, A., Bowden, D. A., and Rowden, A. A. (2016). The impacts of deep-sea fisheries on benthic communities: a review. *ICES J. Mar. Sci.* 73, i51–i69. doi: 10.1371/journal.pone.0022588

Clark, M. R., Bowden, D. A., Rowden, A. A., and Stewart, R. (2019). Little evidence of benthic community resilience to bottom trawling on seamounts after 15 Years. *Front. Mar. Sci.* 6:63. doi: 10.3389/fmars.2019.00063

Clark, M. R., and Rowden, A. A. (2009). Effect of deep water trawling on the macro-invertebrate assemblages of seamounts on the Chatham Rise. *New Zealand. Deep Sea Res. I* 56, 1540–1554. doi: 10.1016/j.dsr.2009.04.015

R Core Team, (2014). *R: A language and environment for statistical computing. R Foundation for Statistical Computing*. Vienna: R Core Team.

Crase, B., Liedloff, A. C., and Wintle, B. A. (2012). A new method for dealing with residual spatial autocorrelation in species distribution models. *Ecography* 35, 879–888. doi: 10.1111/j.1600-0587.2011.07138.x

Duncan, P. M. (1873). A description of the Madreporaria dredged up during the Expeditions of H.M.S. 'Porcupine' in 1869 and 1870. *Trans. Zool. Soc. London* 8, 303–344.

FAO, (2009). *Management of Deep-Sea Fisheries in the High Seas*. Rome: FAO.

Foley, M. M., Martone, R. G., Fox, M. D., Kappel, C. V., Mease, L. A., Erickson, A. L., et al. (2015). Using ecological thresholds to inform resource management: current options and future possibilities. *Front. Mar. Sci.* 2:95. doi: 10.3389/fmars.2015.00095

Georgian, S. E., Anderson, O. F., and Rowden, A. A. (2019). Ensemble habitat suitability modeling of vulnerable marine ecosystem indicator taxa to inform deep-sea fisheries management in the South Pacific Ocean. *Fish. Res.* 211, 256–274. doi: 10.1016/j.fishres.2018.11.020

Henry, L. A., and Roberts, J. M. (2007). Biodiversity and ecological composition of macrobenthos on cold-water coral mounds and adjacent off mound habitat in the bathyal Porcupine Seabight. *Ne Atlantic. Deep Sea Res I* 54, 654–672. doi: 10.1016/j.dsr.2007.01.005

Hill, P. (2009). Designing a deep-towed camera vehicle using single conductor cable. *Sea Technol.* 50, 49–51.

Howell, K. L., Holt, R., Endrino, I. P., and Stewart, H. (2011). When the species is also a habitat: comparing the predictively modelled distributions of Lophelia pertusa and the reef habitat it forms. *Biol. Conservat.* 144, 2656–2665. doi: 10.1016/j.biocon.2011.07.025

Koslow, J. A., Gowlett-Holmes, K., Lowry, J. K., O'hara, T., Poore, G. C. B., and Williams, A. (2001). Seamount benthic macrofauna off southern Tasmania: community structure and impacts of trawling. *Mar. Ecol. Progr. Ser.* 213, 111–125. doi: 10.3354/meps213111

Langenkämper, D., Zurowietz, M., Schoening, T., and Nattkemper, T. W. (2017). BIIGLE 2.0 - *Browsing and annotating large marine image collections. Front. Mar. Sci.* 4:83. doi: 10.3389/fmars.2017.00083

Appendix E



Large, S. I., Fay, G., Friedland, K. D., and Link, J. S. (2015). Critical points in ecosystem responses to fishing and environmental pressures. *Mar. Ecol. Progr. Ser.* 521, 1–17. doi: 10.3354/meps11165

Linnaeus, C. (1758). *Systema Naturae Per Regna Tria Naturae, Secundum Classes, Ordines, Genera, Species, Cum Characteribus, Differentiis, Synonymis, Locis*, 10th Edn, Vol. 1. Holmiae: Laurentius Salvius, 824. doi: 10.5962/bhl.title.542

Parker, S. J., Penney, A. J., and Clark, M. R. (2009). Detection criteria for managing trawl impacts to Vulnerable Marine Ecosystems in high seas fisheries of the South Pacific Ocean. *Mar. Ecol. Progr. Ser.* 397, 309–317. doi: 10.3354/meps08115

Price, D. M., Robert, K., Callaway, A., Lo Iacono, C., Hall, R. A., and Huvenne, V. A. I. (2019). Using 3D photogrammetry from ROV video to quantify cold-water coral reef structural complexity and investigate its influence on biodiversity and community assemblage. *Coral Reefs* 38, 1007–1021. doi: 10.1007/s00338-019-01827-3

Robert, K., Jones, D. O. B., Tyler, P. A., Van Rooij, D., and Huvenne, V. A. I. (2015). Finding the hotspots within a biodiversity hotspot: fine-scale biological predictions within a submarine canyon using high-resolution acoustic mapping techniques. *Mar. Ecol.* 36, 1256–1276. doi: 10.1111/maec.12228

Rosenzweig, M. L. (1995). *Species diversity in space and time*. Cambridge: Cambridge University Press.

Rowden, A. A., Anderson, O. F., Georgian, S. E., Bowden, D. A., Clark, M. R., Pallentin, A., et al. (2017). High-resolution habitat suitability models for the conservation and management of vulnerable marine ecosystems on the Louisville Seamount Chain, South Pacific Ocean. *Front. Mar. Sci.* 4:335. doi: 10.3389/fmars.2017.00335

Song, C., and Cao, M. (2017). Relationships between plant species richness and terrain in middle sub-tropical eastern China. *Forests* 8:344. doi: 10.3390/f8090344

UNGA, (2006). *United Nations General Assembly. Sustainable fisheries, including through the 1995 agreement for the implementation of the provisions of the United Nations convention on the law of the sea of 10 December 1982 relating to the conservation and management of straddling fish stocks and highly migratory fish stocks, and related instruments*. New York: UNGA.

UNGA, (2009). *United Nations General Assembly. Sustainable fisheries, including through the 1995 agreement for the implementation of the provisions of the United Nations convention on the law of the sea of 10 December 1982 relating to the conservation and management of straddling fish stocks and highly migratory fish stocks, and related instruments. General Assembly Resolution 64/72, 2009; A/RES/64/72*. New York: UNGA.

Van Den Beld, I. M. J., Bourillet, J.-F., Arnaud-Haond, S., De Chambure, L., Davies, J. S., Guillaumont, B., et al. (2017). Cold-water coral habitats in submarine canyons of the Bay of Biscay. *Front. Mar. Sci.* 4, 1–30. doi: 10.3389/fmars.2017.00118

Vertino, A., Savini, A., Rosso, A., Di Geronimo, I., Mastrototaro, F., Sanfilippo, R., et al. (2010). Benthic habitat characterization and distribution from two representative sites of the deep-water SML Coral Province (Mediterranean). *Deep Sea Res. Part II Top. Stud. Oceanogr.* 57, 380–396. doi: 10.1016/j.dsr2.2009.08.023

Williams, A., Schlacher, T. A., Rowden, A. A., Althaus, F., Clark, M. R., Bowden, D. A., et al. (2010). Seamount megabenthic assemblages fail to recover from trawling impacts. *Mar. Ecol.* 31, 183–199. doi: 10.1111/j.1439-0485.2010.00385.x

Zuur, A., Ieno, E., Walker, N., Saveliev, A., and Smith, G. (2014a). *Mixed effects models and extensions in ecology with R*. Berlin: Springer.

Zuur, A., Saveliev, A., and Ieno, E. (2014b). *A beginner's Guide to Generalised Additive Mixed Models with R*. United Kingdom: Kingdom.

**Conflict of Interest:** The authors declare that the research was conducted in the absence of any commercial or financial relationships that could be construed as a potential conflict of interest.

# List of References

92/43/EEC 1992. Council Directive 92/43/EEC of 21 May 1992 on the conservation of natural habitats and of wild fauna and flora. .

ADDAMO, A. M., VERTINO, A., STOLARSKI, J., GARCIA-JIMENEZ, R., TAVIANI, M. & MACHORDOM, A. 2016. Merging scleractinian genera: the overwhelming genetic similarity between solitary Desmophyllum and colonial Lophelia. *BMC Evolutionary Biology,* 16**,** 108.

AGASSIZ, A. 1888. A Contribution to American Thalassography. Three Cruises of the United States Coast and Geodetic Survey Steamer "Blake", in the Gulf of Mexico, in the Caribbean Sea, and along the Atlantic Coast of the United States from 1877 to 1880. 2 Volumes. *Boston: Houghton Mifflin & Co.*

ALLEN, S. E. & DURRIEU DE MADRON, X. 2009. A review of the role of submarine canyons in deep-ocean exchange with the shelf. *Ocean Science,* 5**,** 607-620.

ALLEN, S. E. & HICKEY, B. M. 2010. Dynamics of advection-driven upwelling over a shelf break submarine canyon. *Journal of Geophysical Research,* 115**,** C08018.

ALTHAUS, F., HILL, N., FERRARI, R., EDWARDS, L., PRZESLAWSKI, R., SCHONBERG, C. H., STUART-SMITH, R., BARRETT, N., EDGAR, G., COLQUHOUN, J., TRAN, M., JORDAN, A., REES, T. & GOWLETT-HOLMES, K. 2015. A Standardised Vocabulary for Identifying Benthic Biota and Substrata from Underwater Imagery: The CATAMI Classification Scheme. *PLoS One,* 10**,** e0141039.

AMARO, T., BIANCHELLI, S., BILLETT, D. S. M., CUNHA, M. R., PUSCEDDU, A. & DANOVARO, R. 2010. The trophic biology of the holothurian Molpadia musculus: implications for organic matter cycling and ecosystem functioning in a deep submarine canyon. *Biogeosciences,* 7**,** 2419-2432.

AMARO, T., HUVENNE, V. A. I., ALLCOCK, A. L., ASLAM, T., DAVIES, J. S., DANOVARO, R., DE STIGTER, H. C., DUINEVELD, G. C. A., GAMBI, C., GOODAY, A. J., GUNTON, L. M., HALL, R., HOWELL, K. L., INGELS, J., KIRIAKOULAKIS, K., KERSHAW, C. E., LAVALEYE, M. S. S., ROBERT, K., STEWART, H., VAN ROOIJ, D., WHITE, M. & WILSON, A. M. 2016. The Whittard Canyon – A case study of submarine canyon processes. *Progress in Oceanography,* 146**,** 38-57.

AMARO, T., STIGTER , H., LAVALEYE, M. & DUINEVELD, G. 2015. Organic matter enrichment in the Whittard Channel; its origin and possible effects on benthic megafauna. *Deep-Sea Research Part I: Oceanographic Research Papers,* 102**,** 90–100.

AMBLAS, D., CERAMICOLA, S., GERBER, T. P., CANALS, M., CHIOCCI, F. L., DOWDESWELL, J. A., HARRIS, P. T., HUVENNE, V. A. I., LAI, S. Y. J., LASTRAS, G., IACONO, C. L., MICALLEF, A., MOUNTJOY, J. J., PAULL, C. K., PUIG, P. & SANCHEZ-VIDAL, A. 2018. Submarine Canyons and Gullies. *Submarine Geomorphology***,** 251-272.

ANDERSON, O., GUINOTTE, J., ROWDEN, A., TRACEY, D., MACKAY, K. & CLARK, R. 2016a. Habitat suitability models for predicting the occurrence of vulnerable marine ecosystems in the seas around New Zealand. *Deep-Sea Research I,* 115**,** 265-292.

ANDERSON, O. F., GUINOTTE, J. M., ROWDEN, A. A., CLARK, M. R., MORMEDE, S., DAVIES, A. J. & BOWDEN, D. A. 2016b. Field validation of habitat suitability models

for vulnerable marine ecosystems in the South Pacific Ocean: Implications for the use of broad-scale models in fisheries management. *Ocean & Coastal Management,* 120**,** 110-126.

ARJONA-CAMAS, M., PUIG, P., PALANQUES, A., EMELIANOV, M. & DURÁN, R. 2019. Evidence of trawling-induced resuspension events in the generation of nepheloid layers in the Foix submarine canyon (NW Mediterranean). *Journal of Marine Systems,* 196**,** 86-96.

ARZOLA, R. G., WYNN, R. B., LASTRAS, G., MASSON, D. G. & WEAVER, P. P. E. 2008. Sedimentary features and processes in the Nazaré and Setúbal submarine canyons, west Iberian margin. *Marine Geology,* 250**,** 64-88.

ASLAM, T., HALL, R. & DYEA, S. 2018. Internal tides in a dendritic submarine canyon. *Progress in Oceanography,* 169**,** 20-32.

AUSTER, P. J., GJERDE, K., HEUPEL, E., WATLING, L., GREHAN, A. & ROGERS, A. D. 2011. Definition and detection of vulnerable marine ecosystems on the high seas: problems with the "move-on" rule. *ICES Journal of Marine Science,* 68**,** 254-264.

AZAROFF, A., MIOSSEC, C., LANCELEUR, L., GUYONEAUD, R. & MONPERRUS, M. 2020. Priority and emerging micropollutants distribution from coastal to continental slope sediments: A case study of Capbreton Submarine Canyon (North Atlantic Ocean). *Science of the Total Environment,* 703**,** 135057.

BAHN_MCGILL 2012. Testing the predictive performance of distribution models. *Oikos,* 122.

BAKER, K. D., SNELGROVE, P. V. R., FIFIELD, D. A., EDINGER, E. N., WAREHAM, V. E., HAEDRICH, R. L. & GILKINSON, K. D. 2019. Small-Scale Patterns in the Distribution and Condition of Bamboo Coral, Keratoisis grayi, in Submarine Canyons on the Grand Banks, Newfoundland. *Frontiers in Marine Science,* 6.

BAKER, K. D., WAREHAM, V. E., SNELGROVE, P. V. R., HAEDRICH, R. L., FIFIELD, D. A., EDINGER, E. N. & GILKINSON, K. D. 2012. Distributional patterns of deep-sea coral assemblages in three submarine canyons off Newfoundland, Canada. *Marine Ecology Progress Series,* 445**,** 235-249.

BARGAIN, A., FOGLINI, F., PAIRAUD, I., BONALDO, D., CARNIEL, S., ANGELETTI, L., TAVIANI, M., ROCHETTE, S. & FABRI, M. 2018. Predictive habitat modelling in two Mediterranean canyons including hydrodynamic variables. *Process in Oceanography,* 169**,** 151-168.

BEAZLEY, L. I., KENCHINGTON, E. L., MURILLO, F. J. & SACAU, M. D. M. 2013. Deep-sea sponge grounds enhance diversity and abundance of epibenthic megafauna in the Northwest Atlantic. *ICES Journal of Marine Science,* 70**,** 1471-1490.

BECK, M. 2000. Separating the elements of habitat structure: independent effects of habitat complexity and structural components on rocky intertidal gastropods. *Journal of Experimental Marine Biology and Ecology,* 249**,** 29–49.

BELL, J. J. & BARNES, D. K. A. 2001. Sponge morphological diversity: a qualitative predictor of species diversity? *Aquatic Conservation: Marine and Freshwater Ecosystems,* 11**,** 109-121.

BERTOLINO, M., RICCI, S., CANESE, S., CAU, A., BAVESTRELLO, G., PANSINI, M. & BO, M. 2019. Diversity of the sponge fauna associated with white coral banks from two Sardinian canyons (Mediterranean Sea). *Journal of the Marine Biological Association of the United Kingdom,* 99**,** 1735-1751.

BETT, B. 2001. UK Atlantic Margin Environmental Survey: Introduction and overview of bathyal benthic ecology. *Continental Shelf Research,* 21**,** 917-956.

BIANCHELLI, S. & DANOVARO, R. 2019. Meiofaunal biodiversity in submarine canyons of the Mediterranean Sea: A meta-analysis. *Progress in Oceanography,* 170**,** 69-80.

BLONDEL, P., MACLEOD, C. J., TYLER, P. A. & WALKER, C. L. 1996. Segmentation of the Mid-Atlantic Ridge south of the Azores, based on acoustic classification of TOBI data. *Geological Society Special Publication,* 118**,** 17-28.

BLONDEL, P., PARSON, L. M. & ROBIGOU, V. 1998. TexAn: textural analysis of sidescan sonar imagery and generic seafloor characterisation. *Oceans Conference Record (IEEE),* 1**,** 419-423.

BOEHLERT, G. W. 1988. Current-Topography Interactions at Mid-Ocean Seamounts and the Impact on Pelagic Ecosystems. *GeoJournal,* 16**,** 45-52.

BOND, N. R. & LAKE, P. S. 2003. Characterising fish-habitat associations in streams as the first step in ecological restoration. *Austral Ecology* 28**,** 611–621.

BORCARD, D., GILLET, F. & LEGENDRE, P. 2011. Numerical Ecology with R. *Springer-Verlag New York***,** 1-306.

BORTHAGARAY, A. I. & CARRANZA, A. 2007. Mussels as ecosystem engineers: their contribution to species richness in a rocky littoral community. . *Acta Oecologica* 31**,** 243–250.

BRAGA-HENRIQUES, A., PORTEIRO, F. M., RIBEIRO, P. A., DE MATOS, V., SAMPAIO, IACUTE, OCAÑA, O. & SANTOS, R. S. 2013. Diversity, distribution and spatial structure of the cold-water coral fauna of the Azores (NE Atlantic). *Biogeosciences,* 10**,** 4009-4036.

BRAULT, S., STUART, C. T., WAGSTAFF, M. C., MCCLAIN, C. R., ALLEN, J. A. & REX, M. A. 2013a. Contrasting patterns of α- and β-diversity in deep-sea bivalves of the eastern and western North Atlantic. *Deep Sea Research Part II: Topical Studies in Oceanography,* 92**,** 157-164.

BRAULT, S., STUART, C. T., WAGSTAFF, M. C. & REX, M. A. 2013b. Geographic evidence for source-sink dynamics in deep-sea neogastropods of the eastern North Atlantic: an approach using nested analysis. *Global Ecology and Biogeography,* 22**,** 433-439.

BREIMAN, L. 2001. Random Forests. *Machine Learning,* 45**,** 5-32.

BREIMAN, L. & CUTLER, A. 2018. Breiman and Cutler's Random Forests for Classification and Regression. *R Development Core Team,* 4**,** 6-10.

BROOKE, S., HOLMES, M. W. & YOUNG, C. M. 2009. Sediment tolerance of two different morphotypes of the deep-sea coral Lophelia pertusa from the Gulf of Mexico. *Marine Ecology Progress Series,* 390**,** 137–144.

BROOKE, S., ROSS, S., BANE, J., SEIM, H. & YOUNG, C. 2013. Temperature tolerance of the deep-sea coral Lophelia pertusa from the southeastern United States. *Deep Sea Research Part II: Topical Studies in Oceanography,* 92**,** 240–248.

BROOKE, S. & ROSS, S. W. 2014. First observations of the cold-water coral Lophelia pertusa in mid-Atlantic canyons of the USA. *Deep-Sea Research II,* 104**,** 245–251.

BROOKE, S. D., WATTS, M. W., HEIL, A. D., RHODE, M., MIENIS, F., DUINEVELDD, G. C. A., DAVIES, A. J. & C., S. W. R. 2017. Distributions and habitat associations of deep-water corals in Norfolk and Baltimore Canyons, Mid-Atlantic Bight, USA. *Deep-Sea Research II,* 137 131–147.

BROWN, A. & THATJE, S. 2014. Explaining bathymetric diversity patterns in marine benthic invertebrates and demersal fishes: physiological contributions to adaptation of life at depth. *Biol Rev Camb Philos Soc,* 89**,** 406-26.

BROWN, C. J., SMITH, S. J., LAWTON, P. & ANDERSON, J. T. 2011. Benthic habitat mapping: A review of progress towards improved understanding of the spatial ecology of the seafloor using acoustic techniques. *Estuarine, Coastal and Shelf Science,* 92**,** 502-520.

BRUUN, A. F. 1957. Deep sea and abyssal depths. In Treatise on Marine Ecology and Paleoecology. Vol. I. Ecology. *Geological Society of America***,** 641–672.

BUČAS, M., BERGSTRÖM, U., DOWNIE, A. L., SUNDBLAD, G., GULLSTRÖM, M., VON NUMERS, M., ŠIAULYS, A. & LINDEGARTH, M. 2013. Empirical modelling of benthic species distribution, abundance, and diversity in the Baltic Sea: evaluating the scope for predictive mapping using different modelling approaches. *ICES Journal of Marine Science,* 70**,** 1233-1243.

BUHL-MORTENSEN, L., DOLAN, M. & GONZALEZ-MIRELIS, G. 2015. Habitat mapping as a tool for conservation and sustainable use of marine resources: Some perspectives from the MAREANO Programme, Norway. *Journal of Sea Research* 100**,** 46–61.

BUHL-MORTENSEN, L., DOLAN, M. F. J., HOLTE, B., DANNHEIM, J., BUHL-MORTENSEN, P. & BELLEC, V. 2012. Habitat complexity and bottom fauna composition at different scales on the continental shelf and slope of northern Norway. *Hydrobiologia* 685**,** 191-219.

BUHL-MORTENSEN, L., VANREUSEL, A., GOODAY, A. J., LEVIN, L. A., PRIEDE, I. G., BUHL-MORTENSEN, P., GHEERARDYN, H., KING, N. J. & RAES, M. 2010. Biological structures as a source of habitat heterogeneity and biodiversity on the deep ocean margins. *Marine Ecology,* 31**,** 21-50.

CAIRNS, S. D. 2007. Deep-water corals: An overview with special reference to diversity and distribution of deep-water Scleractinian corals. *Bulletin Marine Science,* 81**,** 311-322.

CAMPANYÀ-LLOVET, N., SNELGROVE, P. V. R. & DE LEO, F. C. 2018. Food quantity and quality in Barkley Canyon (NE Pacific) and its influence on macroinfaunal community structure. *Progress in Oceanography,* 169**,** 106-119.

CANALS, M., PUIG, P., DURRIEU DE MADRON, X., HEUSSNER, S., PALANQUES, A. & FABRES, J. 2006. Flushing submarine canyons. *Nature,* 444**,** 354-7.

CARNEY, R. 2005. Zonation of Deep Biota on Continental Margins. 20051650**,** 211-278.

CARNEY, R. S., HAEDRICH, R. L. & ROWE, G. T. 1983. Zonation of fauna in the deep sea In The Sea Vol. 8: Deep-Sea Biology, G.T. Rowe (ed.). *New York: Wiley-Interscience***,** 97–122.

CARTER, G., HUVENNE, V., JENNIFER, G., LO IACONO, C., MARSH, L., OUGIER-SIMONINE, A., ROBERT, K. & WYNN, R. 2018. Ongoing evolution of submarine canyon rockwalls; examples from the Whittard Canyon, Celtic Margin (NE Atlantic). *Progress in Oceanography,* 169**,** 79-88.

CARUGATI, L., LO MARTIRE, M. & DANOVARO, R. 2019. Patterns and drivers of meiofaunal assemblages in the canyons Polcevera and Bisagno of the Ligurian Sea (NW Mediterranean Sea). *Progress in Oceanography,* 175**,** 81-91.

CARVALHO, L. R. S., LOIOLA, M. & BARROS, F. 2017. Manipulating habitat complexity to understand its influence on benthic macrofauna. *Journal of Experimental Marine Biology and Ecology,* 489**,** 48-57.

CAU, A., ALVITO, A., MOCCIA, D., CANESE, S., PUSCEDDU, A., RITA, C., ANGIOLILLO, M. & FOLLESA, M. C. 2017. Submarine canyons along the upper Sardinian slope (Central Western Mediterranean) as repositories for derelict fishing gears. *Marine Pollution Bulletin,* 123**,** 357-364.

CBD 2009. Azores scientific criteria and guidance for identifying ecologically or biologically signifi cant marine areas and designing representative networks of marine protected areas in open ocean waters and deep sea habitats.

CHAUVET, P., METAXAS, A., HAY, A. & MATABOS, M. 2018. Annual and seasonal dynamics of deep-sea megafaunal epibenthic communities in Barkley Canyon (British Columbia, Canada): A response to climatology, surface productivity and benthic boundary layer variation. *Progress in Oceanography***,** 89-105.

CHEN, Z., YAN, X.-H. & JIANG, Y. 2014. Coastal cape and canyon effects on wind-driven upwelling in northern Taiwan Strait. *Journal of Geophysical Research: Oceans,* 119**,** 4605–4625.

CLARK, M. R. & BOWDEN, D. 2015. Seamount biodiversity: high variability both within and between seamounts in the Ross Sea region of Antarctica. *Hydrobiologia,* 761**,** 161-180.

CLARK, M. R., ROWDEN, A., WILLIAMS, A., CONSALVEY, M., STOCKS, K., ROGERS, A., O'HARA , T., WHITE, M., SHANK, T. & HALL-SPENCER, J. 2010. The Ecology of Seamounts: Structure, Function, and Human Impacts. *Annual Review of Marine Science,* 2**,** 253-78.

CLARKE 1993. Non Parametrc multivariate analysis of change. *Australian Journal of Ecology,* 18**,** 117-143.

CLAVEL-HENRY, M., SOLÉ, J., AHUMADA-SEMPOAL, M.-Á., BAHAMON, N., BRITON, F., ROTLLANT, G. & COMPANY, J. B. 2019. Influence of the summer deep-sea circulations on passive drifts among the submarine canyons in the northwestern Mediterranean Sea. *Ocean Science,* 15**,** 1745-1759.

CLÉMENT, L. & THURNHERR, A. M. 2018. Abyssal Upwelling in Mid-Ocean Ridge Fracture Zones. *Geophysical Research Letters,* 45**,** 2424-2432.

COLLIN, A., ARCHAMBAULT, P. & LONG, B. 2011. Predicting species diversity of benthic communities within turbid nearshore using full-waveform bathymetric LiDAR and machine learners. *PLoS One,* 6**,** e21265.

CONLAN, K. E., CURRIE, D. R., DITTMANN, S., SOROKIN, S. J. & HENDRYCKS, E. 2015. Macrofaunal Patterns in and around du Couedic and Bonney Submarine Canyons, South Australia. *PLoS One,* 10**,** e0143921.

CORBERA, G., LO IACONO, C., GRÀCIA, E., GRINYÓ, J., PIERDOMENICO, M., HUVENNE, V. A. I., AGUILAR, R. & GILI, J. M. 2019. Ecological characterisation of a Mediterranean cold-water coral reef: Cabliers Coral Mound Province (Alboran Sea, western Mediterranean). *Progress in Oceanography,* 175**,** 245-262.

CORINALDESI, C., TANGHERLINI, M., RASTELLI, E., BUSCHI, E., LO MARTIRE, M., DANOVARO, R. & DELL'ANNO, A. 2019. High diversity of benthic bacterial and archaeal assemblages in deep-Mediterranean canyons and adjacent slopes. *Progress in Oceanography,* 171**,** 154-161.

COSTELLO, M. J. 2009. Distinguishing marine habitat classification concepts for ecological data management. *Marine Ecology Progress Series,* 397**,** 253-268.

COVAZZI HARRIAGUE, A., DANOVARO, R. & MISIC, C. 2019. Macrofaunal assemblages in canyon and adjacent slope of the NW and Central Mediterranean systems. *Progress in Oceanography,* 171**,** 38-48.

CRASE, B., LIEDLOFF, A. C. & WINTLE, B. A. 2012. A new method for dealing with residual spatial autocorrelation in species distribution models. *Ecography,* 35**,** 879-888.

CROOK, D. A. & ROBERTSON, A. I. 1999. Relationships between riverine fish and woody debris: implications for lowland rivers. . *Marine and Freshwater Research* 51**,** 941–953.

CUNHA, M. R., PATERSON, G. L. J., AMARO, T., BLACKBIRD, S., DE STIGTER, H. C., FERREIRA, C., GLOVER, A., HILÁRIO, A., KIRIAKOULAKIS, K., NEAL, L., RAVARA, A., RODRIGUES, C. F., TIAGO, Á. & BILLETT, D. S. M. 2011. Biodiversity of macrofaunal assemblages from three Portuguese submarine canyons (NE Atlantic). *Deep Sea Research Part II: Topical Studies in Oceanography,* 58**,** 2433-2447.

CUNNINGHAM, M. J., HODGSON, S., MASSON, D. G. & PARSON, L. M. 2005. An evaluation of along- and down-slope sediment transport processes between Goban Spur and Brenot Spur on the Celtic Margin of the Bay of Biscay. *Sedimentary Geology,* 179**,** 99-116.

CÚRDIA, J., CARVALHO, S., RAVARA, A., GAGE, J. & QUINTINO, V. 2004. Deep macrobenthic communities from Nazaré Submarine Canyon (NW Portugal). *Scientia Marina,* 68**,** 171-180.

CURRIE, D. R. & SOROKIN, S. J. 2013. Megabenthic biodiversity in two contrasting submarine canyons on Australia's southern continental margin. *Marine Biology Research,* 10**,** 97-110.

CUTLER, R., EDWARDS, T., BEARD, K., CUTLER, A., HESS, K., GIBSON, J. & LAWLER, J. 2007. Random Forest for Classification in Ecology. *Ecology,* 88**,** 2783-2792.

DALY, E., JOHNSON, M. P., WILSON, A. M., GERRITSEN, H. D., KIRIAKOULAKIS, K., ALLCOCK, A. L. & WHITE, M. 2018. Bottom trawling at Whittard Canyon: Evidence for seabed modification, trawl plumes and food source heterogeneity. *Progress in Oceanography,* 169**,** 227-240.

DANOVARO, R., COMPANY, J. B., CORINALDESI, C., D'ONGHIA, G., GALIL, B., GAMBI, C., GOODAY, A. J., LAMPADARIOU, N., LUNA, G. M., MORIGI, C., OLU, K., POLYMENAKOU, P., RAMIREZ-LLODRA, E., SABBATINI, A., SARDÀ, F., SIBUET, M. & TSELEPIDES, A. 2010. Deep-sea biodiversity in the Mediterranean Sea: the known, the unknown, and the unknowable. *PLoS One,* 8**,** e11832.

DANOVARO, R., SNELGROVE, P. V. & TYLER, P. 2014. Challenging the paradigms of deep-sea ecology. *Trends in Ecology & Evolution,* 29**,** 465-75.

DAVIES, A. J., DUIENVELD, G.C.A., LAVALEYE, M.S.S., BERGMAN, M.J.N., VAN HAREN, H., ROBERTS, J.M., 2009. Downwelling and deep-water currents as food supply mechanisms to the cold-water coral lophelia pertusa (Scleractinia) at the Mingulay reef complex. *Limnology and Oceanography,* 54**,** 620-629.

DAVIES, A. J. & GUINOTTE, J., M 2011. Global habitat suitability for framework-forming cold-water corals. *Plos one,* 6**,** e18483.

DAVIES, A. J., ROBERTS, J. M. & HALL-SPENCER, J. 2007. Preserving deep-sea natural heritage: emerging issues in offshore conservation and management. *Biological Conservation,* 138**,** 299–312.

DAVIES, A. J., WISSHAK, M., ORR, J. C. & ROBERTS, M. 2008a. Predicting suitable habitat for the cold-water coral Lophelia pertusa (Scleractinia). *Deep Sea Research Part I: Oceanographic Research Papers,* 55**,** 1048-1062.

DAVIES, J., GUINAN, J., HOWELL, K., STEWART, H. & VERLING, E. 2008b. MESH South west approaches canyons survey: Final report. *MESH Cruise 01-07-01*.

DAVIES, J. S., GUILLAUMONT, B., TEMPERA, F., VERTINO, A., BEUCK, L., ÓLAFSDÓTTIR, S. H., SMITH, C. J., FOSSÅ, J. H., VAN DEN BELD, I. M. J., SAVINI, A., RENGSTORF, A., BAYLE, C., BOURILLET, J. F., ARNAUD-HAOND, S. & GREHAN, A. 2017. A new classification scheme of European cold-water coral habitats: Implications for ecosystem-based management of the deep sea. *Deep Sea Research Part II: Topical Studies in Oceanography,* 145**,** 102-109.

DAVIES, J. S., HOWELL, K. L., STEWART, H. A., GUINAN, J. & GOLDING, N. 2014. Defining biological assemblages (biotopes) of conservation interest in the submarine canyons of the South West Approaches (offshore United Kingdom) for use in marine habitat mapping. *Deep Sea Research Part II: Topical Studies in Oceanography,* 104**,** 208-229.

DAVISON, J. J., VAN HAREN, H., HOSEGOOD, P., PIECHAUD, N. & HOWELL, K. L. 2019. The distribution of deep-sea sponge aggregations (Porifera) in relation to oceanographic processes in the Faroe-Shetland Channel. *Deep Sea Research Part I: Oceanographic Research Papers,* 146**,** 55-61.

DE FORGES, B. R., KOSLOW, A. & POORE, G. C. B. 2000. Diversity and endemismof the benthic seamount fauna in the southwest Pacifi. *Nature,* 405**,** 944–947.

DE LA TORRIENTE, A., SERRANO, A., FERNÁNDEZ-SALAS, L. M., GARCÍA, M. & AGUILAR, R. 2018. Identifying epibenthic habitats on the Seco de los Olivos Seamount: Species assemblages and environmental characteristics. *Deep Sea Research Part I: Oceanographic Research Papers,* 135**,** 9-22.

DE LEO, F. C., SMITH, C. R., ROWDEN, A. A., BOWDEN, D. A. & CLARK, M. R. 2010. Submarine canyons: hotspots of benthic biomass and productivity in the deep sea. *Proceedings of the Royal Society B: Biological Sciences,* 277**,** 2783-92.

DE LEO, F. C., VETTER, E. W., SMITH, C. R., ROWDEN, A. A. & MCGRANAGHAN, M. 2014. Spatial scale-dependent habitat heterogeneity influences submarine canyon macrofaunal abundance and diversity off the Main and Northwest Hawaiian Islands. *Deep Sea Research Part II: Topical Studies in Oceanography,* 104**,** 267-290.

DE MOL, B., VAN RENSBERGEN, P., PILLEN, S., VAN HERREWEGHE, K., VAN ROOIJ, D., MCDONNELL, A., HUVENNE, V., IVANOV, M., SWENNEN, R. & HENRIET, J. P. 2002. Large deep-water coral banks in the Porcupine Basin, southwest of Ireland. *Marine Geology,* 188**,** 193-231.

DE MOL, L., VAN ROOIJ, D., PIRLET, H., GREINERT, J., FRANK, N., QUEMMERAIS, F. & HENRIET, J.-P. 2011. Cold-water coral habitats in the Penmarc'h and Guilvinec Canyons (Bay of Biscay): Deep-water versus shallow-water settings. *Marine Geology,* 282**,** 40-52.

DE STIGTER, H. C., BOER, W., DE JESUS MENDES, P. A., JESUS, C. C., THOMSEN, L., VAN DEN BERGH, G. D. & VAN WEERING, T. C. E. 2007. Recent sediment transport and deposition in the Nazaré Canyon, Portuguese continental margin. *Marine Geology,* 246**,** 144-164.

DE STIGTER, H. C., JESUS, C. C., BOER, W., RICHTER, T. O., COSTA, A. & VAN WEERING, T. C. E. 2011. Recent sediment transport and deposition in the Lisbon–Setúbal and Cascais submarine canyons, Portuguese continental margin. *Deep Sea Research Part II: Topical Studies in Oceanography,* 58**,** 2321-2344.

DEAN, R. L. & CONNELL, J. H. 1987. Marine invertebrates in an algal succession III. Mechanisms linking habitat complexity with diversity. *Journal of Experimental Marine Biology and Ecology,* 109**,** 249–273.

DEFRA 2013. The Canyons Marine Conservation Zone Designation Order 2013 *(Ministerial Order 2013 No. 4)*

DEFRA 2019a. 2019 No.7 Environmental Protection Marine Management Wildlife - The Canyons Marine Conservation Zone Designation (Amendment) Order 2019 *Ministerial Order***,** 1-2.

DEFRA 2019b. The Canyons Marine Conservation Zone Designation (Amendment) Order 2019 *(Ministerial Order 2019 No.7)*

DEGEEST, A. L., MULLENBACH, B. L., PUIG, P., NITTROUER, C. A., DREXLER, T. M., DURRIEU DE MADRON, X. & ORANGE, D. L. 2008. Sediment accumulation in the western Gulf of Lions, France: The role of Cap de Creus Canyon in linking shelf and slope sediment dispersal systems. *Continental Shelf Research,* 28**,** 2031-2047.

DELL'ANNO, A., PUSCEDDU, A., CORINALDESI , C., CANALS, M., HEUSSNER, S., THOMSEN, L. & DANOVARO, R. 2013. Trophic state of benthic deep-sea ecosystems from two different continental margins off Iberia. *Biogeosciences,* 10**,** 2945−2957.

DEMOPOULOS, A. W. J., MCCLAIN-COUNTS, J., ROSS, S. W., BROOKE, S. & MIENIS, F. 2017. Food-web dynamics and isotopic niches in deep-sea communities residing in a submarine canyon and on the adjacent open slopes. *Marine Ecology Progress Series,* 578**,** 19-33.

DOMKE, L., LACHARITÉ, M., METAXAS, A. & MATABOS, M. 2017. Influence of an oxygen minimum zone and macroalgal enrichment on benthic megafaunal community composition in a NE Pacific submarine canyon. *Marine Ecology,* 38**,** e12481.

DOWNES, B. J., LAKE, P. S., SCHREIBER, E. S. G. & GLAISTER, A. 1998. Habitat structure and regulation of local species diversity in a stony upland stream. *Ecological Monographs,* 68**,** 237-257.

DU PREEZ, C., CURTIZ, J. & CLARKE, M. 2016. The Structure and Distribution of Benthic Communities on a Shallow Seamount (Cobb Seamount, Northeast Pacific Ocean). *PLoS ONE* 11.

DUINEVELD, G., C,A., JEFFREYS, R., M., LAVALEYE, M., S,S., DAVIES , A., J., BERGMAN, M., J,N., WATMOUGH, T. & WITBAARD, R. 2012. Spatial and tidal variation in food supply to shallow cold-water coral reefs of the Mingulay Reef complex (Outer Hebrides, Scotland). *Marine Ecology Progress Series,* 444**,** 97-115.

DUINEVELD, G., C,A., LAVALEYE , M., S,S., BERGMAN, M., J,N., DE STIGTER, H. & MIENIS, F. 2007. Trophic structure of a cold-water coral mound community (Rockall Bank, NE Atlantic) in relation to the near-bottom particle supply and current regime. *Bulletin Marine Science,* 81**,** 449-467.

DUINEVELD, G., LAVALEYE, M., BERGHUIS, E. & WILDE, P. D. 2001. Activity and composition of the benthic fauna in the Whittard Canyon and the adjacent continental slope (NE Atlantic). *Oceanologicaacta,* 24 69–83.

DULLO, W., FLÖGEL, S. & RÜGGEBERG, A. 2008. Cold-water coral growth in relation to the hydrography of the Celtic and Nordic European continental margin. *Marine Ecology Progress Series,* 371**,** 165-176.

DURDEN, J., SCHOENING, T., ALTHAUS, F., FRIEDMANN, A., GARICA, R., GLOVER, A., GREINERT, J., STOUT, N., JONES, D., JORDT, A., KAELI, J., KOSER, K., KUHNZ, L., LINDSAY, D., MORRIS, K., NATTKEMPER, T., OSTERLOFF, J., RUHL, H., SINGH, H., TRAN, M. & BETT, B. 2016. Perspectives in Visual Imaging for Marine Biology and Ecology: From Acquisition to Understanding. *Oceanography and Marine Biology,* 54**,** 1-72.

DURDEN, J. M., BETT, B. J., JONES, D. O. B., HUVENNE, V. A. I. & RUHL, H. A. 2015. Abyssal hills – hidden source of increased habitat heterogeneity, benthic megafaunal biomass and diversity in the deep sea. *Progress in Oceanography,* 137**,** 209-218.

EKMAN, S. 1953. Zoogeography of the Sea. *London: Didgewick and Jackson*.

ELITH, J. 2008. Blackwell Publishing Ltd A working guide to boosted regression trees. *Journal of Animal Ecology,* 77**,** 802-813.

ELITH, J. & LEATHWICK, J. R. 2009. Species Distribution Models: Ecological Explanation and Prediction Across Space and Time. *Annual Review of Ecology, Evolution, and Systematics,* 40**,** 677-697.

ELLIS, J. R., BURT, G. & ROGERS, S. I. 2007. Epifaunal sampling in the Celtic Sea. *Conference poster*.

EPPING, E., ZEE, C., SOETAERT, K. & HELDER, W. 2002. On the oxidation and burial of organic carbon in sediments of the Iberian Margin and Nazaré Canyon (NE Atlantic). *Progress in Oceanography,* 52**,** 399-431.

ETTER, R. J., REX, M. A., CHASE, M. R. & QUATTRO, J. M. 2005. Population differentiation decreases with depth in deep-sea bivalves. *Evolution,* 59**,** 1479-1491, 13.

EUNIS 2019. EUNIS marine habitat classification

FABRI, M. C., BARGAIN, A., PAIRAUD, I., PEDEL, L. & TAUPIER-LETAGE, I. 2017. Cold-water coral ecosystems in Cassidaigne Canyon: An assessment of their environmental living conditions. *Deep Sea Research Part II: Topical Studies in Oceanography,* 137**,** 436-453.

FABRI, M. C., PEDEL, L., BEUCK, L., GALGANI, F., HEBBELN, D. & FREIWALD, A. 2014. Megafauna of vulnerable marine ecosystems in French mediterranean submarine canyons: Spatial distribution and anthropogenic impacts. *Deep Sea Research Part II: Topical Studies in Oceanography,* 104**,** 184-207.

FANELLI, E., BIANCHELLI, S. & DANOVARO, R. 2018. Deep-sea mobile megafauna of Mediterranean submarine canyons and open slopes: Analysis of spatial and bathymetric gradients. *Progress in Oceanography,* 168**,** 23-34.

FAO 2008. Report of the Expert Consultation on International Guidelines for the Management of Deep-Sea Fisheries in the High Seas, Bangkok. 11–14 September, 2007. *FAO Fisheries Report No. 855*.

FAO 2009. Management of Deep-Sea Fisheries in the High Seas. Rome. *Food and Agriculture Organization of the United Nations*.

FERNANDEZ-ARCAYA, U., RAMIREZ-LLODRA, E., AGUZZI, J., ALLCOCK, A. L., DAVIES, J. S., DISSANAYAKE, A., HARRIS, P., HOWELL, K., HUVENNE, V. A. I., MACMILLAN-LAWLER, M., MARTÍN, J., MENOT, L., NIZINSKI, M., PUIG, P., ROWDEN, A. A., SANCHEZ, F. & VAN DEN BELD, I. M. J. 2017. Ecological Role of Submarine Canyons and Need for Canyon Conservation: A Review. *Frontiers in Marine Science,* 4.

FIRTH, L. B., THOMPSON, R. C., WHITE, F. J., SCHOFIELD, M., SKOV, M. W., HOGGART, S. P. G., JACKSON, J., KNIGHTS, A. M., HAWKINS, S. J. & DEFEO, O. 2013. The importance of water-retaining features for biodiversity on artificial intertidal coastal defence structures. *Diversity and Distributions,* 19**,** 1275-1283.

FLÖGEL, S., DULLO, W. C., PFANNKUCHE, O., KIRIAKOULAKIS, K. & RÜGGEBERG, A. 2014. Geochemical and physical constraints for the occurrence of living cold-water corals. *Deep Sea Research Part II: Topical Studies in Oceanography,* 99**,** 19-26.

FOLEY, M. M., MARTONE, R. G., FOX, M. D., KAPPEL, C. V., MEASE, L. A., ERICKSON, A. L., HALPERN, B. S., SELKOE, K. A., TAYLOR, P. & SCARBOROUGH, C. 2015. Using Ecological Thresholds to Inform Resource Management: Current Options and Future Possibilities. *Frontiers in Marine Science,* 2.

FONTANETO, D., SANCIANGCO, J. C., CARPENTER, K. E., ETNOYER, P. J. & MORETZSOHN, F. 2013. Habitat Availability and Heterogeneity and the Indo-Pacific Warm Pool as Predictors of Marine Species Richness in the Tropical Indo-Pacific. *PLoS ONE,* 8**,** e56245.

FOURNIERA, A., BARBET-MASSINA, M., ROMEB, Q. & COURCHAMP, F. 2017. Predicting species distribution combining multi-scale drivers. *Global ecology and conservation,* 12**,** 215-226.

FREDERIKSEN, JENSEN & WESTERBERG 1992. The distribution of the Scleractinian Coral Lophelia pertusa around the Faroe Islands and the relation to internal tidal mixing. *Sarsia North Atlantic Marine Science***,** 157-171.

FRUTOS, I. & SORBE, J. C. 2017. Suprabenthic assemblages from the Capbreton area (SE Bay of Biscay). Faunal recovery after a canyon turbidity disturbance. *Deep Sea Research Part I: Oceanographic Research Papers,* 130**,** 36-46.

GAGE, J. D. & TYLER, P. A. 1999. Deep-Sea Biology: A Natural History of Organisms at the Deep-Sea Floor. *Cambridge: Cambridge University Press*.

GAMBI, C. & DANOVARO, R. 2016. Biodiversity and life strategies of deep-sea meiofauna and nematode assemblages in the Whittard Canyon (Celtic margin, NE Atlantic Ocean). *Deep Sea Research Part I: Oceanographic Research Papers,* 108**,** 13-22.

GEBCO COMPILATION GROUP 2019. GEBCO 2019 Grid.

GENIN, A., DAYTON, P. K., LONSDALE, P. F. & SPIESS, F. N. 1986. Corals on seamount peaks provide evidence of current acceleration over deep-sea topography. *Nature,* 322**,** 59-61.

GORDEN, R. L. & MARSHALL, N. F. 1976. Submarine canyons: internal wave traps? *Geophysical Research Letters,* 116.

GORI, A., OREJAS, C., MADURELL, T., BRAMANTI, L., MARTINS, M., QUINTANILLA, E., MARTI-PUIG, P., LO IACONO, C., PUIG, P., REQUENA, S., GREENACRE, M. & GILI, J. M. 2013. Bathymetrical distribution and size structure of cold-water coral populations in the Cap de Creus and Lacaze-Duthiers canyons (northwestern Mediterranean). *Biogeosciences,* 10**,** 2049-2060.

GRAHAM, N. & NASH, K. 2013. The importance of structural complexity in coral reef ecosystems. *Coral Reefs* 32**,** 315–326.

GUIHEN, D., WHITE M & T, L. 2013. Boundary layer flow dynamics at a cold-water coral reef. *Journal of Sea Research,* 78**,** 36-44.

GUISAN, A. & THUILLER, W. 2005. Predicting species distribution: offering more than simple habitat models. *Ecology Letters,* 8**,** 993-1009.

GUISAN, A. & ZIMMERMANN, N. 2000. Predictive habitat distribution models in ecology. *Ecological Modelling,* 135 147-186.

GULLAGE, L., DEVILLERS, R. & EDINGER, E. 2017. Predictive distribution modelling of cold-water corals in the Newfoundland and Labrador region. *Marine Ecological Progress Series,* 582**,** 57-77.

GUNTON, L. M., GOODAY, A. J., GLOVER, A. G. & BETT, B. J. 2015a. Macrofaunal abundance and community composition at lower bathyal depths in different branches of the Whittard Canyon and on the adjacent slope (3500m; NE Atlantic). *Deep Sea Research Part I: Oceanographic Research Papers,* 97**,** 29-39.

GUNTON, L. M., NEAL, L., GOODAY, A. J., BETT, B. J. & GLOVER, A. G. 2015b. Benthic polychaete diversity patterns and community structure in the Whittard Canyon system and adjacent slope (NE Atlantic). *Deep Sea Research Part I: Oceanographic Research Papers,* 106**,** 42-54.

HALL, R. & CARTER, G. 2011. Internal Tides in Monterey Submarine Canyon. *Journal of Physical Oceanography* 41**,** 186-20.

HALL, R. A., ALFORD, M. H., CARTER, G. S., GREGG, M. C., LIEN, R.-C., WAIN, D. J. & ZHAO, Z. 2014. Transition from partly standing to progressive internal tides in Monterey Submarine Canyon. *Deep Sea Research Part II: Topical Studies in Oceanography,* 104**,** 164-173.

HALL, R. A., ASLAM, T. & HUVENNE, V. A. I. 2017. Partly standing internal tides in a dendritic submarine canyon observed by an ocean glider. *Deep Sea Research Part I: Oceanographic Research Papers,* 126**,** 73-84.

HALLENBECK, T. R., KVITEK, R. G. & LINDHOLM, J. 2012. Rippled scour depressions add ecologically significant heterogeneity to soft-bottom habitats on the continental shelf. *Marine Ecology Progress Series,* 468**,** 119-133.

HANZ, U., WIENBERG, C., HEBBELN, D., DUINEVELD, G., LAVALEYE, M., JUVA, K., DULLO, W.-C., FREIWALD, A., TAMBORRINO, L., REICHART, G.-J., FLÖGEL, S. & MIENIS, F. 2019. Environmental factors influencing benthic communities in the oxygen minimum zones on the Angolan and Namibian margins. *Biogeosciences,* 16**,** 4337-4356.

HARALICK, R. M., SHANMUGAM, K. & DINSTEIN, I. 1973. Textural Features for Image Classification. *IEEE Transactions on systems, man and cybernetics,* 3**,** 610–621.

HARGRAVE, B., KOSTYLEV, V. & HAWKINS, C. 2004. Benthic epifauna assemblages, biomass and respiration in The Gully region on the Scotian Shelf, NW Atlantic Ocean. *Marine Ecological Progress Series,* 270**,** 55-70.

HARRIS, P. T., MACMILLAN-LAWLER, M., RUPP, J. & BAKER, E. K. 2014. Geomorphology of the oceans. *Marine Geology,* 352**,** 4-24.

HARRIS, P. T. & WHITEWAY, T. 2011. Global distribution of large submarine canyons: Geomorphic differences between active and passive continental margins. *Marine Geology,* 285**,** 69-86.

HASEGAWA, D., LEWIS, M. R. & GANGOPADHYAY, A. 2009. How islands cause phytoplankton to bloom in their wakes. *Geophysical Research Letters,* 36.

HECK, K. L. J. & WETSTONE, G. S. 1977. Habitat complexity and invertebrate species richness and abundance in tropical seagrass meadows. *Journal of Biogeography,* 4**,** 135–142.

HEEZEN, B. C. & EWING, M. 1952. Turbidity currents and submarine slumps, and the 1929 Grand Banks earthquake. *American Journal of Science,* 250**,** 849-873.

HENRY, L.-A. & ROBERTS, J. M. 2007. Biodiversity and ecological composition of macrobenthos on cold-water coral mounds and adjacent off-mound habitat in the bathyal

Porcupine Seabight, NE Atlantic. *Deep Sea Research Part I: Oceanographic Research Papers,* 54**,** 654-672.

HENRY, L. A. & MURRAY, R. A. 2017. Global Biodiversity in Cold-Water Coral Reef Ecosystems. *Marine Animal Forests***,** 235-256.

HENRY, L. A., VAD, J. & ROBERTS, J. M. 2014. Environmental variability and biodiversity of megabenthos on the Hebrides Terrace Seamount (Northeast Atlantic). *Scientific reports,* 4**,** 5589.

HERNÁNDEZ-ÁVILA, I., GUERRA-CASTRO, E., BRACHO, C., RADA, M., OCAÑA, F. A. & PECH, D. 2018. Variation in species diversity of deep-water megafauna assemblages in the Caribbean across depth and ecoregions. *PLOS ONE,* 13**,** e0201269.

HIJMANS, R., J. & ELITH, J. 2017. Species distribution modelling with R. *Cran.r-project***,** 1-79.

HIXON, M. A. & MENGE, B. A. 1991. Species diversity: Prey refuges modify the interactive effects of predation and competition. *Theoretical Popoulation Biology,* 39**,** 178-200.

HOOKER, S. K., WHITEHEAD, H. & GOWANS, S. 1999. Marine Protected Area Design and the Spatial and Temporal Distribution of Cetaceans in a Submarine Canyon. *Conservation Biology,* 13**,** 592–602.

HOTCHKISS, F. S. & WUNSCH, C. 1982. Internal waves in Hudson Canyon with possible geological implications. *Deep-Sea Research Part I: Oceanographic Research Papers,* 29**,** 415-442.

HOWELL, K., BILLETT, D. S. M. & TYLER, P. 2002. Depth-related distribution and abundance of seastars (Echinodermata:Asteroidea) in the Porcupine Seabight and Porcupine Abyssal Plain, N.E. Atlantic. *Deep-Sea Research I* 49**,** 1901–1920.

HOWELL, K. L. & DAVIES, J. 2010. Morphospecies Guide.

HOWELL, K. L., DAVIES, J. S. & NARAYANASWAMY, B. E. 2010. Identifying deep-sea megafaunal epibenthic assemblages for use in habitat mapping and marine protected area network design. *Journal of the Marine Biological Association of the United Kingdom,* 90**,** 33-68.

HOWELL, K. L., HOLT, R., ENDRINO, I. P. & STEWART, H. 2011. When the species is also a habitat: Comparing the predictively modelled distributions of Lophelia pertusa and the reef habitat it forms. *Biological Conservation,* 144**,** 2656-2665.

HUNTER, W. R., JAMIESON, A., HUVENNE, V. A. I. & WITTE, U. 2013. Sediment community responses to marine vs. terrigenous organic matter in a submarine canyon. *Biogeosciences,* 10**,** 67-80.

HUTCHINS, L. W. 1947. The Bases for Temperature Zonation in Geographical Distribution. *Ecological Society of America,* 17**,** 325-335.

HUTCHINSON, G. E. & MACARTHUR, R. J. 1959. A theoretical ecological model of size distributions among species of animals. *American Naturalist,* 93**,** 117-125.

HUVENNE, V. & FURLONG, M. 2019. RRS James Cook Cruise 166-167, 19 June – 6 July 2018. Haig Fras Marine Conservation Zone AUV habitat monitoring, equipment trials and staff training. *National Oceanography Centre Cruise Report,* 56.

HUVENNE, V., HÜHNERBACH, V., BLONDEL, P., GÓMEZ SICHI, O. & LE BAS, T. 2007. Detailed Mapping of Shallow-water Environments Using Image Texture Analysis on Sidescan Sonar and Multibeam Backscatter Imagery. *In Proceedings of the International Conference "Underwater Acoustic Measurements: Technologies & amp; Results".* **,** 879-886.

HUVENNE, V., TYLER, P., D, M., FISHER, D., HAUTON, C., HUHNERBACH, V., LE BAS, T. & WOLFF, G. 2011. A Picture on the Wall: Innovative Mapping Reveals Cold-Water Coral Refuge in Submarine Canyon. *PLoS ONE* 6.

HUVENNE, V., WYNN, R. & GALES, J. 2016. RRS James Cook Cruise 124-125-126 09 Aug-12 Sep 2016. CODEMAP2015: Habitat mapping and ROV vibrocorer trials around Whittard Canyon and Haig Fras. *National Oceanography Centre Cruise Report,* 36.

HUVENNE, V. A. I., BLONDEL, P. & HENRIET, J. P. 2002. Textural analyses of sidescan sonar imagery from two mound provinces in the Porcupine Seabight. *Marine Geology,* 189**,** 323-341.

HUVENNE, V. A. I. & DAVIES, J. S. 2014. Towards a new and integrated approach to submarine canyon research. *Deep Sea Research Part II: Topical Studies in Oceanography,* 104**,** 1-5.

HUVENNE, V. A. I., PATTENDEN, A. D. C., MASSON, D. G. & TYLER, P. A. 2012. Habitat Heterogeneity in the Nazaré Deep-Sea Canyon Offshore Portugal. 691-701.

HYMAN, A. C., FRAZER, T. K., JACOBY, C. A., FROST, J. R. & KOWALEWSKI, M. 2019. Long-term persistence of structured habitats: seagrass meadows as enduring hotspots of biodiversity and faunal stability. *Proc Biol Sci,* 286**,** 20191861.

IERODIACONOU, D., LAURENSON, L., BURQ, S. & RESTON, M. 2007. Marine benthic habitat mapping using Multibeam data, georeferencedvideo and image classification techniques in Victoria, Australia. *Journal of Spatial Science,* 52**,** 93-104.

IERODIACONOU, D., SCHIMEL, A. C. G., KENNEDY, D., MONK, J., GAYLARD, G., YOUNG, M., DIESING, M. & RATTRAY, A. 2018. Combining pixel and object based image analysis of ultra-high resolution multibeam bathymetry and backscatter for habitat mapping in shallow marine waters. *Marine Geophysical Research,* 39**,** 271-288.

INGELS, J., KIRIAKOULAKIS, K., WOLFF, G. A. & VANREUSEL, A. 2009. Nematode diversity and its relation to the quantity and quality of sedimentary organic matter in the deep Nazaré Canyon, Western Iberian Margin. *Deep Sea Research Part I: Oceanographic Research Papers,* 56**,** 1521-1539.

INGELS, J., VANREUSEL, A., ROMANO, C., COENJAERTS, J., MAR FLEXAS, M., ZÚÑIGA, D. & MARTIN, D. 2013. Spatial and temporal infaunal dynamics of the Blanes submarine canyon-slope system (NW Mediterranean); changes in nematode standing stocks, feeding types and gender-life stage ratios. *Progress in Oceanography,* 118**,** 159-174.

ISMAIL, K., HUVENNE, V. & ROBERT, K. 2018. Quantifying spatial heterogeneity in submarine canyons. *Progress in Oceanography,* 169**,** 181-198.

ISMAIL, K., HUVENNE, V. A. I. & MASSON, D. G. 2015. Objective automated classification technique for marine landscape mapping in submarine canyons. *Marine Geology,* 362**,** 17-32.

JAMES, M. A., ANSELL, A. D., COLLINS, M. J., CURRY, G. B., PECK, L. S. & RHODES, M. C. 1992. Biology of Living Brachiopods. *Advances in Marine Biology* 28**,** 175-387.

JANOWSKI, L., TRZCINSKA, K., TEGOWSKI, J., KRUSS, A., RUCINSKA-ZJADACZ, M. & POCWIARDOWSKI, P. 2018. Nearshore Benthic Habitat Mapping Based on Multi-Frequency, Multibeam Echosounder Data Using a Combined Object-Based Approach: A Case Study from the Rowy Site in the Southern Baltic Sea. *Remote Sensing,* 10**,** 1983.

JANTZEN, C., SCHMIDT, G., WILD, C., RODER, C. & KHOKIATTIWONG , S. 2013. Benthic Reef Primary Production in Response to Large Amplitude Internal Waves at the Similan Islands (Andaman Sea, Thailand). *PLoS ONE* 8.

JÄRNEGREN, J. & ALTIN, D. 2006. Filtration and respiration of the deep living bivalve Acesta excavata (J.C. Fabricius, 1779) (Bivalvia; Limidae). *Journal of Experimental Marine Biology and Ecology,* 334**,** 122-129.

JEFFREE, E. P. & JEFFREE, C. E. 1994. Temperature and the Biogeographical Distributions of Species. *Functional Ecology,* 8**,** 640-650.

JOHNSON, M. P., WHITE, M., WILSON, A., WURZBERG, L., SCHWABE, E., FOLCH, H. & ALLCOCK, A. L. 2013. A vertical wall dominated by Acesta excavata and Neopycnodonte zibrowii, part of an undersampled group of deep-sea habitats. *PLoS One,* 8**,** e79917.

JONES, C. G., GUTIÉRREZ, J. L., BYERS, J. E., CROOKS, J. A., LAMBRINOS, J. G. & TALLEY, T. S. 2010. A framework for understanding physical ecosystem engineering by organisms. *Oikos,* 119**,** 1862-1869.

KÄMPF, J. 2007. On the magnitude of upwelling fluxes in shelf-break canyons. *Continental Shelf Research,* 27**,** 2211-2223.

KÄMPF, J. 2018. On the Dynamics of Canyon–Flow Interactions. *Journal of Marine Science and Engineering,* 6**,** 129.

KANE, A. I., CLARE, M. A., MIRAMONTES, E., WOGELIUS, R., ROTHWELL, J. J., GARREAU, P. & POHL, F. 2020. Seafloor microplastic hotspots controlled by deep-sea circulation. *Science,* 368**,** 1140–1145

KAUFMANN, R., WAKEFIELD, W. & GENIN, A. 1989. Distribution of epibenthic megafauna and lebensspuren on two central North Pacific seamounts. *Deep Sea Research,* 36**,** 1863-1896.

KAZANIDIS, G., HENRY, L.-A., ROBERTS, J. M. & WITTE, U. F. M. 2015. Biodiversity of Spongosorites coralliophaga (Stephens, 1915) on coral rubble at two contrasting cold-water coral reef settings. *Coral Reefs,* 35**,** 193-208.

KELLY, N. E., SHEA, E. K., METAXAS, A., HAEDRICH, R. L. & AUSTER, P. J. 2010. Biodiversity of the deep-sea continental margin bordering the Gulf of Maine (NW Atlantic): relationships among sub-regions and to shelf systems. *PLoS One,* 5**,** e13832.

KENCHINGTON, E. L., COGSWELL, A. T., MACISAAC, K. G., BEAZLEY, L., LAW, B. A. & KENCHINGTON, T. J. 2014. Limited depth zonation among bathyal epibenthic megafauna of the Gully submarine canyon, northwest Atlantic. *Deep Sea Research Part II: Topical Studies in Oceanography,* 104**,** 67-82.

KHRIPOUNOFF, A., VANGRIESHEIM, A., CRASSOUS, P., SEGONZAC, M., COLAÇO, A., DESBRUYÉRES, D. & BARTHELÉMY, R. 2001. Particle fux in the Rainbow hydrothermal vent field (Mid-Atlantic Ridge): Dynamics, mineral and biological composition. *Journal of Marine Research* 59**,** 633-656.

KOSTYLEV, V. E., TODD, B. J., FADER, G. B. J., COURTNEY, R. C., CAMERON, G. D. M. & PICKRILL, R. A. 2001. Benthic habitat mapping on the Scotian Shelf based on multibeam bathymetry, surficial geology and sea floor photographs. *Marine Ecological Progress Series,* 219**,** 121-137.

KOVALENKO, K. E., THOMAZ, S. M. & WARFE, D. M. 2011. Habitat complexity: approaches and future directions. *Hydrobiologia,* 685**,** 1-17.

LACHARITÉ, M. & METAXAS, A. 2017. Hard substrate in the deep ocean: How sediment features influence epibenthic megafauna on the eastern Canadian margin. *Deep Sea Research Part I: Oceanographic Research Papers,* 126**,** 50-61.

LACHARITÉ, M., METAXAS, A. & LAWTON, P. 2015. Using object-based image analysis to determine seafloor fine-scale features and complexity. *Limnology and Oceanography: Methods,* 13**,** 553-567.

LAMB, K. G. 2014. Internal Wave Breaking and Dissipation Mechanisms on the Continental Slope/Shelf. *Annual Review of Fluid Mechanics,* 46**,** 231-254.

LAMPITT, R. S., BILLETT, D. & RICE, L. A. 1986. Biomass of the invertebrate megabenthos from 500 to 4100 m in the northeast Atlantic Ocean. *Marine Biology,* 93**,** 69-81.

LARGE, S. I., FAY, G., FRIEDLAND, K. D. & LINK, J. S. 2015. Critical points in ecosystem responses to fishing and environmental pressures. *Marine Ecology Progress Series,* 521**,** 1-17.

LAURENT, L. S., FERRARI, R. & IJICHI, T. 2020. Transformation and upwelling of bottom water in fracture zone valleys. *Journal of Physical Oceanography,* 50**,** 715-726.

LAURENT, S. L. C. & THURNHERR, A. M. 2007. Intense mixing of lower thermocline water on the crest of the Mid-Atlantic Ridge. *Nature,* 448**,** 680-3.

LAWTON, J. H. 1983. Plant architecture and the diversity of phytophagous insects. *Annual Review of Entomology,* 28**,** 23-39.

LE BAS, T. 2002. PRISM - Processing of Remotely-sensed Imagery for Seafloor Mapping. *Southampton Oceanography Centre:***,** 196.

LECOURS, V., DEVILLERS, R., SCHNEIDER, D. C., LUCIEER, V. L., BROWN, C. J. & EDINGER, E. N. 2015. Spatial scale and geographic context in benthic habitat mapping: review and future directions. *Marine Ecology Progress Series,* 535**,** 259-284.

LEE, I. H., LIEN, R.-C., LIU, J. T. & CHUANG, W.-S. 2009. Turbulent mixing and internal tides in Gaoping (Kaoping) Submarine Canyon, Taiwan. *Journal of Marine Systems,* 76**,** 383-396.

LEGENDRE, P. & GALLAGHER, E. 2001. Ecologically meaningful transformations for ordination of species data. *Oecologia,* 129**,** 271–280.

LEGENDRE, P. & LEGENDRE, L. 2012. Numerical Ecology. *Elsevier,* 24.

LEITNER, A. B., NEUHEIMER, A. B. & DRAZEN, J. C. 2020. Evidence for long-term seamount-induced chlorophyll enhancements. *Sci Rep,* 10**,** 12729.

LESSARD-PILON, S. A., PODOWSKI, E. L., CORDES, E. E. & FISHER, C. R. 2010. Megafauna community composition associated with Lophelia pertusa colonies in the Gulf of Mexico. *Deep Sea Research Part II: Topical Studies in Oceanography,* 57**,** 1882-1890.

LEVIN, L. & SIBUET, M. 2012. Understanding Continental Margin Biodiversity: A New Imperative. *Annual Review of Marine Science,* 4**,** 79-112.

LEVIN, L., SIBUET, M., GOODAY, A., SMITH, C. & VANREUSEL, A. 2010. The roles of habitat heterogeneity in generating and maintaining biodiversity on continental margins: an introduction. *Marine Ecology,* 31 1-5.

LEVIN, L. A., JETTER, R., REX, M., GOODDAY, R., SMITH, C., PINEDA, J., STUART, C., ROBERT, R., HESSLER, R. & PAWSON 2001. Enviornemntal influences on regional deep-sea species diversity. *Annual Review of Ecology, Evolution, and Systematics,* 32**,** 51–93.

LIAO, J.-X., CHEN, G.-M., CHIOU, M.-D., JAN, S. & WEI, C.-L. 2017. Internal tides affect benthic community structure in an energetic submarine canyon off SW Taiwan. *Deep-Sea Research Part I 1,* 25**,** 147–160.

LINGO, M. E. & SZEDLMAYER, S. T. 2006. The influence of habitat complexity on reef fish communities in thenortheastern Gulf of Mexico. *Environmental Biology of Fishes,* 76**,** 71–80.

LIU, J. T., WANG, Y. H., LEE, I. H. & HSU, R. T. 2010. Quantifying tidal signatures of the benthic nepheloid layer in Gaoping Submarine Canyon in Southern Taiwan. *Marine Geology,* 271**,** 119-130.

LO IACONO, C., GUILLÉN, J., GUERRERO, Q., DURÁN, R., WARDELL, C., HALL, R. A., ASLAM, T., CARTER, G. D. O., GALES, J. A. & HUVENNE, V. A. I. 2020. Bidirectional bedform fields at the head of a submarine canyon (NE Atlantic). *Earth and Planetary Science Letters,* 542**,** 116321.

LO IACONO, C., ROBERT, K., GONZÁLEZ-VILLANUEVA, R., GORI, A., GILI, J.-M. & OREJAS, C. 2018. Predicting cold-water coral distribution in the Cap de Creus Canyon (NW Mediterranean): Implications for marine conservation planning. *Progress in Oceanography,* 169**,** 169-180.

LOBO, J. M., JIMÉNEZ-VALVERDE, A. & REAL, R. 2008. AUC: a misleading measure of the performance of predictive distribution models. *Global Ecology and Biogeography,* 17**,** 145–151.

LOKE, L. & TODD, P. 2016. Structural complexity and component type increase intertidal biodiversity independently of area. *Ecology,* 97**,** 383-393.

LONGHURST, A. R. 1998. Ecological Geography of the Sea. *San Diego, CA: Academic Press*.

LOPEZ-FERNANDEZ, P., CALAFAT, A., SANCHEZ-VIDAL, A., CANALS, M., MAR FLEXAS, M., CATEURA, J. & COMPANY, J. B. 2013. Multiple drivers of particle fluxes in the Blanes submarine canyon and southern open slope: Results of a year round experiment. *Progress in Oceanography,* 118**,** 95-107.

LÓPEZ, P., BIANCHELLI, S., PUSCEDDU, A., CALAFAT, A., SANCHEZ-VIDAL, A. & DANOVARO, R. 2012. Bioavailability of sinking organic matter in the Blanes canyon and the adjacent open slope (NW Mediterranean Sea). *Biogeosciences Discussions,* 9**,** 18295-18330.

LUCKHURST, B. E. & LUCKHURST, K. 1978. Analysis of the influence of substrate variables on coral reef fish communities. *Marine Biology,* 49**,** 317–323.

LUTZ, M. J., CALDEIRA, K., DUNBAR, R. B. & BEHRENFELD, M. J. 2007. Seasonal rhythms of net primary production and particulate organic carbon flux to depth describe the efficiency of biological pump in the global ocean. *Journal of Geophysical Research: Oceans,* 112**,** C10011.

MA 2005. "Ecosystems and human well-being: current state and trends" in Millennium Ecosystem Assessment, Global Assessment Reports (Washington,DC).

MACARTHUR, R. H. & MACARTHUR, J. W. 1961. On bird species diversity. *Ecology,* 42**,** 594-598.

MACIOLEK, N., GRASSLE, J., HECKER, B., BROWN, B. & BLAKE, J. 1987. Study of biological processes on the US North Atlantic slope and rise. *Final report prepared for U.S Department of the Interior, Minerals Management Service,* 2.

MAIER, S. R., KUTTI, T., BANNISTER, R. J., VAN BREUGEL, P., VAN RIJSWIJK, P. & VAN OEVELEN, D. 2019. Survival under conditions of variable food availability: Resource utilization and storage in the cold-water coral Lophelia pertusa. *Limnology and Oceanography,* 64**,** 1651-1671.

MARTÍN, J., PALANQUES, A. & PUIG, P. 2006. Composition and variability of downward particulate matter fluxes in the Palamós submarine canyon (NW Mediterranean). *Journal of Marine Systems,* 60**,** 75-97.

MARTÍN, J., PALANQUES, A., VITORINO, J., OLIVEIRA, A. & DE STIGTER, H. C. 2011. Near-bottom particulate matter dynamics in the Nazaré submarine canyon under calm and stormy conditions. *Deep Sea Research Part II: Topical Studies in Oceanography,* 58**,** 2388-2400.

MARTÍN, J., PUIG, P., MASQUÉ, P., PALANQUES, A. & SÁNCHEZ-GÓMEZ 2014a. Impact of bottom trawling on deep-sea sediment properties along the flanks of a submarine canyon. *PloS one,* 9**,** e104536.

MARTÍN, J., PUIG, P., PALANQUES, A. & GIAMPORTONE, A. 2014b. Commercial bottom trawling as a driver of sediment dynamics and deep seascape evolution in the Anthropocene. *Anthropocene,* 7**,** 1-15.

MARTÍN, J., PUIG, P., PALANQUES, A. & RIBO, M. 2014c. Trawling-induced daily sediment resuspension in the flank of a Mediterranean submarine canyon. *Deep Sea Research Part II: Topical Studies in Oceanography,* 104**,** 174–183.

MASSON, D. G. 2009. RRS James Cook Cruise 36, 19 Jul-28 Jul 2009. The Geobiology of Whittard Submarine Canyon. *National Oceanography Centre Southampton Cruise Report* 41.

MASSON, D. G., HUVENNE, V. A. I., DE STIGTER, H. C., WOLFF, G. A., KIRIAKOULAKIS, K., ARZOLA, R. G. & BLACKBIRD, S. 2010. Efficient burial of carbon in a submarine canyon. *Geology,* 38**,** 831-834.

MATIAS, M. G., UNDERWOOD, A. J., HOCHULI, D. F. & COLEMAN, R. A. 2010. Independent effects of patch size and structural complexity on diversity of benthic invertebrates. *Ecology,* 91**,** 1908-1915.

MAZZUCO, A. C. A., STELZER, P. S. & BERNARDINO, A. F. 2020. Substrate rugosity and temperature matters: patterns of benthic diversity at tropical intertidal reefs in the SW Atlantic. *PeerJ,* 8**,** e8289.

MCCLAIN, C. & BARRY, J. 2010. Habitat heterogeneity, disturbance, and productivity work in concert to regulate biodiversity in deep submarine canyons. *Ecology,* 91**,** 964-976.

MCCLAIN, C., LUNDSTEN, L. & BARRY, J. 2010. Assemblage structure, but not diversity or density, change with depth on a northeast Pacific seamount. *Marine Ecology,* 31**,** 14-25.

MCCLAIN, C. R. & HARDY, S. M. 2010. The dynamics of biogeographic ranges in the deep sea. *Proc Biol Sci,* 277**,** 3533-46.

MCCLAIN, C. R. & LUNDSTEN, L. 2015. Assemblage structure is related to slope and depth on a deep offshore Pacific seamount chain. *Marine Ecology,* 36**,** 210-220.

MCQUAID, C. D. & DOWER, K. M. 1990. Enhancement of habitat heterogeneity and species richness on rocky shores inundated by sand. *Oecologia,* 84**,** 142-144.

MEAGER, J. J. & SCHLACHER, T. A. 2013. New metric of microhabitat complexity predicts species richness on a rocky shore. *Marine Ecology,* 34**,** 484-491.

MELLIN, C., MENGERSEN, K., BRADSHAW, C. J. A. & CALEY, M. J. 2014. Generalizing the use of geographical weights in biodiversity modelling. *Global Ecology and Biogeography,* 23**,** 1314–1323.

MENGE, B., A. & SUTHERLAND, J., P. 1976. Species-diversity gradients: synthesis of roles of predation, competition, and temporal heterogeneity. *American Naturalist,* 110**,** 351–369.

MENGE, B. A., LUBCHENKO, J. & ASHKENAS, L. R. 1985. Diversity, heterogeneity and consumer pressure in a tropical rocky intertidal community. *Oecologia,* 65**,** 394–405.

MENZIES, R., & GEORGE, R. 1972. Hydrostatic Pressure—Temperature effects on Deep-sea Colonisation. *Proceedings of the Royal Society of Edinburgh. Section B. Biology,* 73**,** 195-202.

MENZIES, R. J., GEORGE, R.Y. & ROWE, G.T. 1973. Abyssal Environment and Ecology of the World Oceans. *New York: John Wiley & Sons.*

MESH 2008. http://www.emodnet-seabedhabitats.eu/.

METAXAS, A., LACHARITÉ, M. & DE MENDONÇA, S. N. 2019. Hydrodynamic Connectivity of Habitats of Deep-Water Corals in Corsair Canyon, Northwest Atlantic: A Case for Cross-Boundary Conservation. *Frontiers in Marine Science,* 6.

MICHAELIS, R., HASS, H. C., MIELCK, F., PAPENMEIER, S., SANDER, L., GUTOW, L. & WILTSHIRE, K. H. 2019. Epibenthic assemblages of hard-substrate habitats in the German Bight (south-eastern North Sea) described using drift videos. *Continental Shelf Research,* 175**,** 30-41.

MIENIS, F., DE STIGTER, H. C., DE HAAS, H., VAN DER LAND, C. & VAN WEERING, T. C. E. 2012. Hydrodynamic conditions in a cold-water coral mound area on the Renard Ridge, southern Gulf of Cadiz. *Journal of Marine Systems,* 96-97**,** 61-71.

MIENIS, F., DE STIGTER, H. C., DE HAAS, H. & VAN WEERING, T. C. E. 2009. Near-bed particle deposition and resuspension in a cold-water coral mound area at the Southwest Rockall Trough margin, NE Atlantic. *Deep Sea Research Part I: Oceanographic Research Papers,* 56**,** 1026-1038.

MIENIS, F., DE STIGTER, H. C., WHITE, M., DUINEVELD, G., DE HAAS, H. & VAN WEERING, T. C. E. 2007. Hydrodynamic controls on cold-water coral growth and carbonate-mound development at the SW and SE Rockall Trough Margin, NE Atlantic Ocean. *Deep Sea Research Part I: Oceanographic Research Papers,* 54**,** 1655-1674.

MILLER, R. J., HOCEVAR, J., STONE, R. P. & FEDOROV, D. V. 2012. Structure-forming corals and sponges and their use as fish habitat in Bering Sea submarine canyons. *PLoS One,* 7**,** e33885.

MILLER, R. J., JUSKA, C. & HOCEVAR, J. 2015. Submarine canyons as coral and sponge habitat on the eastern Bering Sea slope. *Global Ecology and Conservation,* 4**,** 85-94.

MISIUK, B., LECOURS, V. & BELL, T. 2018. A multiscale approach to mapping seabed sediments. *PLoS One,* 13**,** e0193647.

MIYAMOTO, M., KIYOTA, M., NAKAMURA, T. & HAYASHIBARA, T. 2017. Effects of Bathymetric Grid-Cell Sizes on Habitat Suitability Analysis of Cold-water Gorgonian Corals on Seamounts. *Marine Geodesy,* 40**,** 1-19.

MOHN, C., RENGSTORF, A., WHITE, M., DUINEVELD, G., MIENIS, F., SOETAERT, K. & GREHAN, A. 2014. Linking benthic hydrodynamics and cold-water coral occurrences: A high-resolution model study at three cold-water coral provinces in the NE Atlantic. *Progress in Oceanography,* 122**,** 92-101.

MONTEREALE-GAVAZZI, G., MADRICARDO, F., JANOWSKI, L., KRUSS, A., BLONDEL, P., SIGOVINI, M. & FOGLINI, F. 2016. Evaluation of seabed mapping methods for fine-scale classification of extremely shallow benthic habitats – Application to the Venice Lagoon, Italy. *Estuarine, Coastal and Shelf Science,* 170**,** 45-60.

MONTEREALE-GAVAZZI, G., ROCHE, M., LURTON, X., DEGRENDELE, K., TERSELEER, N. & VAN LANCKER, V. 2017. Seafloor change detection using multibeam echosounder backscatter: case study on the Belgian part of the North Sea. *Marine Geophysical Research,* 39**,** 229-247.

MOORE, E. C. & HOVEL, K. A. 2010. Relative influence of habitat complexity and proximity to patch edges on seagrass epifaunal communities. *Oikos,* 119**,** 1299–1311.

MORATO, T., HOYLE, S. D., ALLAIN, V. & NICOL, S. J. 2010. Seamounts are hotspots of pelagic biodiversity in the open ocean. *Proc Natl Acad Sci U S A,* 107**,** 9707-11.

MORENO NAVAS, J., MILLER, P. I., HENRY, L. A., HENNIGE, S. J. & ROBERTS, J. M. 2014. Ecohydrodynamics of cold-water coral reefs: a case study of the Mingulay Reef Complex (western Scotland). *PLoS One,* 9**,** e98218.

MORGAN, N. B., GOODE, S., ROARK, E. B. & BACO, A. R. 2019. Fine Scale Assemblage Structure of Benthic Invertebrate Megafauna on the North Pacific Seamount Mokumanamana. *Frontiers in Marine Science,* 6.

MORRIS, K. J., TYLER, P. A., MASSON, D. G., HUVENNE, V. I. A. & ROGERS, A. D. 2013. Distribution of cold-water corals in the Whittard Canyon, NE Atlantic Ocean. *Deep Sea Research Part II: Topical Studies in Oceanography,* 92**,** 136-144.

MORTENSEN, P. B. & BUHL-MORTENSEN, L. 2005. Deep-water corals and their habitats in The Gully, a submarine canyon off Atlantic Canada. *Cold-Water Corals and Ecosystems***,** 247-277.

MORTENSEN, P. B., HOVLAND, M., BRATTEGARD, T. & FARESTVEIT, R. 1995. Deep water bioherms of the scleractinian coral Lophelia pertusa (L.) at 641N on thet heegian shelf: structure and associated megafauna. *Sarsia North Atlantic Marine Science,* 80**,** 145–158.

MOUNTJOY, J., HOWARTH, J., ORPIN, A., BARNES, P., BOWDEN, D., ROWDEN, A., SCHIMEL, A., HOLDEN, C., HORGAN, H., NODDER, S., PATTON, J., LAMARCHE, G., GERSTENBERGER, M., MICALLEF, A., PALLENTIN, A. & KANE, T. 2018. Earthquakes drive large-scale submarine canyon development and sediment supply to deep-ocean basins. Science Advances. *Science Advances,* 4**,** eaar3748

MUELLER, C. E., LARSSON, A. I., VEUGER, B., MIDDELBURG, J. J. & VAN OEVELEN, D. 2014. Opportunistic feeding on various organic food sources by the cold-water coral Lophelia pertusa. *Biogeosciences,* 11**,** 123-133.

MULLINEAUX, L. S. & MILLS, S. W. 1997. A test of the larval retention hypothesis in seamount-generated flows. *Deep-Sea Research I,* 44**,** 745-770.

MUMBY, P. J. 2001. Beta and habitat diversity in marine systems: a new approach to measurement, scaling and interpretation. *Oecologia,* 128**,** 274-280.

MURRAY, J. 1895. A summary of the scientific results obtained at the soundings, dredging, and trawling stations of the HMS Challenger. In Report on the Scientific Results of the Voyage of the H.M.S. Challenger during the Years 1873–1876. *Edinburgh: Neill and Company.*

MURRAY, J. & HJORT, J. 1912. The Depths of the Ocean. *London: MacMillan*.

NAUMANN, M., OREJAS, C. & FERRIER-PAGÈS, C. 2014. Species-specific physiological response by cold-water corals Lophelia pertusa and Madrepora oculata to variations within their natural temperature range. *Deep-Sea Research II,* 99**,** 36-41.

O'NEILL, F. & SUMMERBELL, K. 2011. The mobilisation of sediment by demersal otter trawls. *Marine pollution bulletin,* 62**,** 1088-1097.

O'CONNOR, N. A. 1991. The effects of habitat complexity on the macroinvertebrate colonizing wood substrates in lowland stream. *Oecologia* 85**,** 504–512.

O'DEA, E. J., ARNOLD, A. K., EDWARDS, K. P., FURNER, R., HYDER, P., MARTIN, M. J., SIDDORN, J. R., STORKEY, D., WHILE, J., HOLT, J. T. & LIU, H. 2014. An operational ocean forecast system incorporating NEMO and SST data assimilation for the tidally driven European North-West shelf. *Journal of Operational Oceanography,* 5**,** 3-17.

O'HARA, T. D. & TITTENSOR, D. P. 2010. Environmental drivers of ophiuroid species richness on seamounts. *Marine Ecology* 31 26-38.

OBELCZ , J., BROTHERS, D., CHAYTOR, J., BRINK, U., ROSS, S. & BROOKE, S. 2014. Geomorphic characterization of four shelf-sourced submarine canyons along the U.S. Mid-Atlantic continental margin. *Deep-Sea Research II,* 104**,** 106-119.

OLABARRIA, C. 2005. Patterns of bathymetric zonation of bivalves in the Porcupine Seabight and adjacent abyssal plain, N.E. Atlantic. *Deep-Sea Research I,* 52**,** 15-31.

OREJAS, C., GORI, A., RAD-MENÉNDEZ, C., LAST, K. S., DAVIES, A. J., BEVERIDGE, C. M., SADD, D., KIRIAKOULAKIS, K., WITTE, U. & ROBERTS, J. M. 2016. The effect of flow speed and food size on the capture efficiency and feeding behaviour of the cold-water coral Lophelia pertusa. *Journal of Experimental Marine Biology and Ecology,* 481**,** 34-40.

OSPAR 2008. OSPAR List of Threatened and/or Declining Species and Habitats Reference Number: 2008-6.

PALANQUES, A., DURRIEU DE MADRON, X., PUIG, P., FABRES, J., GUILLÉN, J., CALAFAT, A., CANALS, M., HEUSSNER, S. & BONNIN, J. 2006. Suspended sediment fluxes and transport processes in the Gulf of Lions submarine canyons. The role of storms and dense water cascading. *Marine Geology,* 234**,** 43-61.

PARRY, M. E. V., HOWELL, K. L., NARAYANASWAMY, B. E., BETT, B. J., JONES, D. O. B., HUGHES, D. J., PIECHAUD, N., NICKELL, T. D., ELLWOOD, H., ASKEW, N., J, ENKINS, C. & MANCA, E. 2015. A Deep-sea Section for the Marine Habitat Classification of Britain and Ireland. Joint Nature Conservation Committee, Peterborough. JNCC report No. 530.

PATERSON, G. L. J., GLOVER, A. G., CUNHA, M. R., NEAL, L., DE STIGTER, H. C., KIRIAKOULAKIS, K., BILLETT, D. S. M., WOLFF, G. A., TIAGO, A., RAVARA, A., LAMONT, P. & TYLER, P. 2011. Disturbance, productivity and diversity in deep-sea canyons: A worm's eye view. *Deep Sea Research Part II: Topical Studies in Oceanography,* 58**,** 2448-2460.

PAWLOWICZ, R., BEARDSLEY, B. & LENTZ, R. 2002. Classical tidal harmonic analysis including error estimates in MATLAB using T TIDE. 28**,** 929-937.

PEARMAN, T. R. R., ROBERT, K., CALLAWAY, A., HALL, R., LO IACONO, C. & HUVENNE, V. A. I. 2020. Improving the predictive capability of benthic species distribution models by incorporating oceanographic data – towards holistic ecological modelling of a submarine canyon. *Progress in Oceanography,* 184.

PIECHAUD, N., DOWNIE, A., STEWART, H. A. & HOWELL, K. L. 2015. The impact of modelling method selection on predicted extent and distribution of deep-sea benthic assemblages. *Earth and Environmental Science Transactions of the Royal Society of Edinburgh,* 105**,** 251-261.

PIERDOMENICO, M., CARDONE, F., CARLUCCIO, A., CASALBORE, D., CHIOCCI, F., MAIORANO, P. & D'ONGHIA, G. 2019. Megafauna distribution along active submarine

canyons of the central Mediterranean: Relationships with environmental variables. *Progress in Oceanography,* 171**,** 49-69.

PIERDOMENICO, M., GORI, A., GUIDA, V. G. & GILI, J.-M. 2017. Megabenthic assemblages at the Hudson Canyon head (NW Atlantic margin): Habitat-faunal relationships. *Progress in Oceanography,* 157**,** 12-26.

PIERDOMENICO, M., MARTORELLI, E., DOMINGUEZ-CARRIÓ, C., GILI, J. M. & CHIOCCI, F. L. 2016. Seafloor characterization and benthic megafaunal distribution of an active submarine canyon and surrounding sectors: The case of Gioia Canyon (Southern Tyrrhenian Sea). *Journal of Marine Systems,* 157**,** 101-117.

PINGREE, R. & CANN, B. L. 1990. Structure, strength and seasonality of the slope currents in the Bay of biscay region. *Journal of the Marine Biological Association of the United Kingdom,* 70**,** 857–885.

POLLARD, R. T., GRIFFRRHS, M. J., CUNNINGHAM, S. A., READ, J. F., IREZ, F. F. & RLOS, A. F. 1996. Vivaldi 1991 - A study of the formation, circulation and ventilation of Eastern North Atlantic Central Water. *Progress in Oceanography,* 37**,** 167-172.

PORSKAMP, P., RATTRAY, A., YOUNG, M. & IERODIACONOU, D. 2018. Multiscale and Hierarchical Classification for Benthic Habitat Mapping. *Geosciences,* 8**,** 119.

POST, A. L., LAVOIE, C., DOMACK, E. W., LEVENTER, A., SHEVENELL, A. & FRASER, A. D. 2016. Environmental drivers of benthic communities and habitat heterogeneity on an East Antarctic shelf. *Antarctic Science,* 29**,** 17-32.

PRAMPOLINI, M., BLONDEL, P., FOGLINI, F. & MADRICARDO, F. 2018. Habitat mapping of the Maltese continental shelf using acoustic textures and bathymetric analyses. *Estuarine, Coastal and Shelf Science,* 207**,** 483-498.

PRASAD, A. M., IVERSON, L. R. & LIAW, A. 2006. Newer Classification and Regression Tree Techniques: Bagging and Random Forests for Ecological Prediction. *Ecosystems,* 9**,** 181-199.

PRATSON, L. F., NITTROUER, C. A., WIBERG, P. L., STECKLER, M. S., SWENSON, J. B., CACCHIONE, D. A., KARSON, J. A., MURRAY, A. B., WOLINSKY, M. A., GERBER, T. P., MULLENBACH, B. L., SPINELLI, G. A., FULTHORPE, C. S., O'GRADY, D. B., PARKER, G., DRISCOLL, N. W., BURGER, R. L., PAOLA, C., ORANGE, D. L., FIELD, M. E., FRIEDRICHS, C. T. & FEDELE, J. J. 2007. Seascape Evolution on Clastic Continental Shelves and Slopes. 339-380.

PRICE, D. M., ROBERT, K., CALLAWAY, A., LO LACONO, C., HALL, R. A. & HUVENNE, V. A. I. 2019. Using 3D photogrammetry from ROV video to quantify cold-water coral reef structural complexity and investigate its influence on biodiversity and community assemblage. *Coral Reefs*.

PRIEDE, I. G., BERGSTAD, O. A., MILLER, P. I., VECCHIONE, M., GEBRUK, A., FALKENHAUG, T., BILLETT, D. S. M., CRAIG, J., DALE, A. C., SHIELDS, M. A., TILSTONE, G. H., SUTTON, T. T., GOODAY, A. J., INALL, M. E., JONES, D. O. B., MARTINEZ-VICENTE, V., MENEZES, G. M., NIEDZIELSKI, T., SIGURÐSSON, Þ., ROTHE, N., ROGACHEVA, A., ALT, C. H. S., BRAND, T., ABELL, R., BRIERLEY, A. S., COUSINS, N. J., CROCKARD, D., HOELZEL, A. R., HØINES, Å., LETESSIER, T. B., READ, J. F., SHIMMIELD, T., COX, M. J., GALBRAITH, J. K., GORDON, J. D. M., HORTON, T., NEAT, F. & LORANCE, P. 2013. Does Presence of a Mid-Ocean Ridge Enhance Biomass and Biodiversity? *PLOS ONE,* 8**,** e61550.

PUIG, P., CANALS, M., COMPANY, J. B., MARTIN, J., AMBLAS, D., LASTRAS, G. & PALANQUES, A. 2012. Ploughing the deep sea floor. *Nature,* 489**,** 286-9.

PUIG, P., DURÁN, R., MUÑOZ, A., ELVIRA, E. & GUILLÉN, J. 2017. Submarine canyon-head morphologies and inferred sediment transport processes in the Alías-Almanzora canyon system (SW Mediterranean): On the role of the sediment supply. *Marine Geology,* 393**,** 21-34.

PUIG, P., PALANQUES, A. & MARTÍN, J. 2014. Contemporary Sediment-Transport Processes in Submarine Canyons. *Annual Review of Marine Science,* 6**,** 53-77.

PUSCEDDU, A., BIANCHELLI, S., MARTIN, J., PUIG, P., PALANQUES, A., MASQUE, P. & DANOVARO, R. 2014. Chronic and intensive bottom trawling impairs deep-sea biodiversity and ecosystem functioning. *Proc Natl Acad Sci U S A,* 111**,** 8861-6.

PYRON, M. 2010. Characterizing Communities. *Nature Education Knowledge,* 3**,** 39.

R_CORE_TEAM 2014. R: A language and environment for statistical computing. R Foundation for Statistical Computing, Vienna, Austria.

RAMIREZ-LLODRA, E., BRANDT, A., DANOVARO, R., DE MOL, B., ESCOBAR, E., GERMAN, C. R., LEVIN, L. A., MARTINEZ ARBIZU, P., MENOT, L., BUHL-MORTENSEN, P., NARAYANASWAMY, B. E., SMITH, C. R., TITTENSOR, D. P., TYLER, P. A., VANREUSEL, A. & VECCHIONE, M. 2010. Deep, diverse and definitely different: unique attributes of the world's largest ecosystem. *Biogeosciences,* 7**,** 2851-2899.

RAMIREZ-LLODRA, E., TRANNUM, H. C., EVENSET, A., LEVIN, L. A., ANDERSSON, M., FINNE, T. E., HILARIO, A., FLEM, B., CHRISTENSEN, G., SCHAANNING, M. & VANREUSEL, A. 2015. Submarine and deep-sea mine tailing placements: A review of current practices, environmental issues, natural analogs and knowledge gaps in Norway and internationally. *Marine Pollution Bulletin,* 97**,** 13-35.

RAMIRO-SÁNCHEZ, B., GONZÁLEZ-IRUSTA, J. M., HENRY, L.-A., CLELAND, J., YEO, I., XAVIER, J. R., CARREIRO-SILVA, M., SAMPAIO, Í., SPEARMAN, J., VICTORERO, L., MESSING, C. G., KAZANIDIS, G., ROBERTS, J. M. & MURTON, B. 2019. Characterization and Mapping of a Deep-Sea Sponge Ground on the Tropic Seamount (Northeast Tropical Atlantic): Implications for Spatial Management in the High Seas. *Frontiers in Marine Science,* 6.

RAMOS, M., BERTOCCI, I., TEMPERA, F., CALADO, G., ALBUQUERQUE, M. & DUARTE, P. 2016. Patterns in megabenthic assemblages on a seamount summit (Ormonde Peak, Gorringe Bank, Northeast Atlantic). *Marine Ecology,* 37**,** 1057-1072.

RAYMORE, P. A. 1982. Photographic investigations on three seamounts in the Gulf of Alaska. *Pacific Science,* 36**,** 15-34.

REID, G. & HAMILTON, D. 1990. A Reconnaissance Survey of the Whittard Sea Fan, Southwestern Approaches, British Isles. *Marine Geology,* 92 69-86.

RENGSTORF, A. M., MOHN, C., BROWN, C., WISZ, M. S. & GREHAN, A. J. 2014. Predicting the distribution of deep-sea vulnerable marine ecosystems using high-resolution data: Considerations and novel approaches. *Deep Sea Research Part I: Oceanographic Research Papers,* 93**,** 72-82.

RENGSTORF, A. M., YESSON, C., BROWN, C., GREHAN, A. J. & CRAME, A. 2013. High-resolution habitat suitability modelling can improve conservation of vulnerable marine ecosystems in the deep sea. *Journal of Biogeography,* 40**,** 1702-1714.

REX, M. 1976. Deep-Sea Species Diversity: Decreased Gastropod Diversity at Abyssal Depths. *Science* 181**,** 1051–53.

REX, M., ETTER, R., MORRIS, J., CROUSE, J., MCCLAIN, C., JOHNSON, N., STUART, C., DEMING, J., THIES, R. & AVERY, R. 2006. Global bathymetric patterns of standing stock and body size in the deep-sea benthos. *Marine Ecological Progress Series,* 317**,** 1-8.

REX, M. A. 1973. Deep-sea species diversity: decreased gastropod diversity at abyssal depths. *Science,* 181**,** 1051–1053.

REX, M. A. 1981. Community structure in the deep-sea benthos. *Annual Review of Ecology and Systematics,* 12**,** 331-353.

REX, M. A. 1983. Geographical patterns of species diversity in the deep-sea benthos. *In The Sea Vol. 8: Deep-Sea Biology*.

REX, M. A., CRAME, A., STUART, C. T. & CLARKE, A. 2005a. Large-scale biogeographic patterns in marine mollusks: A confluence of history and productivity? *Ecology,* 86**,** 2288-2297.

REX, M. A. & ETTER, J. 2010. Deep-sea Biodiversity: Pattern and Scale. *Harvard University Press***,** 1-354.

REX, M. A., MCCLAIN, C. R., JOHNSON, N. A., ETTER, R. J., ALLEN, J. A., BOUCHET, P. & WARÉN, A. 2005b. A Source-Sink Hypothesis for Abyssal Biodiversity. *The American Naturalist,* 165**,** 136-178.

RISK, M., J. 1972. Fish diversity on a coral reef in the Virgin Islands. *Atoll Research Bulletin,* 23**,** 239-249.

ROBERT, K., HUVENNE, V. A. I., GEORGIOPOULOU, A., JONES, D. O. B., MARSH, L., CARTER, G. D. O. & CHAUMILLON, L. 2017. New approaches to high-resolution mapping of marine vertical structures. *Scientific Reports,* 7.

ROBERT, K., JONES, D., GEORGIOPOULOU, A. & HUVENNE, V. 2019. Cold-water coral assemblages on vertical walls from the Northeast Atlantic. *Biodiversity Research***,** 1-15.

ROBERT, K., JONES, D. O. B. & HUVENNE, V. A. I. 2014. Megafaunal distribution and biodiversity in a heterogeneous landscape: the iceberg-scoured Rockall Bank, NE Atlantic. *Marine Ecology Progress Series,* 501**,** 67-88.

ROBERT, K., JONES, D. O. B., ROBERTS, J. M. & HUVENNE, V. A. I. 2016. Improving predictive mapping of deep-water habitats: Considering multiple model outputs and ensemble techniques. *Deep Sea Research Part I: Oceanographic Research Papers,* 113**,** 80-89.

ROBERT, K., JONES, D. O. B., TYLER, P. A., VAN ROOIJ, D. & HUVENNE, V. A. I. 2015. Finding the hotspots within a biodiversity hotspot: fine-scale biological predictions within a submarine canyon using high-resolution acoustic mapping techniques. *Marine Ecology,* 36**,** 1256-1276.

ROBERTS, J. M., DAVIES, A. J., HENRY, L. A., DODDS, L. A., DUINEVELD, G. C. A., LAVALEYE, M. S. S., MAIER, C., VAN SOEST, R. W. M., BERGMAN, M. J. N., HÜHNERBACH, V., HUVENNE, V. A. I., SINCLAIR, D. J., WATMOUGH, T., LONG, D., GREEN, S. L. & VAN HAREN, H. 2009a. Mingulay reef complex: an interdisciplinary study of cold-water coral habitat, hydrography and biodiversity. *Marine Ecology Progress Series,* 397**,** 139-151.

ROBERTS, J. M., HENRY, L. A., LONG, D. & HARTLEY, J. P. 2008. Cold-water coral reef frameworks, megafaunal communities and evidence for coral carbonate mounds on the Hatton Bank, north east Atlantic. *Facies,* 54**,** 297-316.

ROBERTS, J. M., WHEELER, A. & FREIWALD, A. 2006. Reefs of the Deep: The Biology and Geology of Cold-Water Coral Ecosystems. *Science,* 312**,** 543-547.

ROBERTS, J. M., WHEELER, A., FREIWALD, A. & CAIRNS, S. 2009b. Cold-Water Corals. The Biology and Geology of Deep-Sea Coral Habitats. *NewYork,NY:Cambridge University Press.*

ROBERTSON, C. M., DEMOPOULOS, A. W. J., BOURQUE, J. R., MIENIS, F., DUINEVELD, G. C. A., LAVALEYE, M. S. S., KOIVISTO, R. K. K., BROOKE, S. D., ROSS, S. W., RHODE, M. & DAVIES, A. J. 2020. Submarine canyons influence macrofaunal diversity and density patterns in the deep-sea benthos. *Deep Sea Research Part I: Oceanographic Research Papers,* 159**,** 103249.

ROGERS, A. D., MORLEY, S., FITZCHARLES, E., JARVIS, K. & BELCHIER, M. 2000. Genetic structure of Patagonian toothfish (Dissostichus eleginoides) populations on the Patagonian Shelf and Atlantic and western Indian Ocean sectors of the Southern Ocean. *Marine Biology,* 149**,** 915-924.

ROMANO, C., COENJAERTS, J., FLEXAS, M. M., ZÚÑIGA, D., VANREUSEL, A., COMPANY, J. B. & MARTIN, D. 2013. Spatial and temporal variability of meiobenthic density in the Blanes submarine canyon (NW Mediterranean). *Progress in Oceanography,* 118**,** 144-158.

ROSS, R. E. & HOWELL, K. L. 2013. Use of predictive habitat modelling to assess the distribution and extent of the current protection of 'listed' deep-sea habitats. *Diversity and Distributions,* 19**,** 433-445.

ROWDEN, A. A., PEARMAN, T. R. R., BOWDEN, D. A., ANDERSON, O. F. & CLARK, M. R. 2020. Determining Coral Density Thresholds for Identifying Structurally Complex Vulnerable Marine Ecosystems in the Deep Sea. *Frontiers in Marine Science,* 7.

ROWE, G. & MENZIES, R., J. 1969. Zonation of large benthic invertebrates in the deep-sea off the Carolinas. *Deep Sea Research and Oceanographic Abstracts,* 16**,** 531-532.

ROWE, G. T. 1983. Biomass and production of the deep-sea macrobenthos. *In The Sea Vol. 8: Deep-Sea Biology***,** 97–121.

SALDÍAS, G. S. & ALLEN, S. E. 2020. The Influence of a Submarine Canyon on the Circulation and Cross-Shore Exchanges around an Upwelling Front. *Journal of Physical Oceanography,* 50**,** 1677-1698.

SANCHEZ, F., MORANDEAU, G., BRU, N. & LISSARDY, M. 2013. A restricted fishing area as a tool for fisheries management: Example of the Capbreton canyon, southern Bay of Biscay. *Marine Policy,* 42**,** 180-189.

SCHLACHER, T. A., SCHLACHER-HOENLINGER, M. A., WILLIAMS, A., ALTHAUS, F., HOOPER, J., N, A. & KLOSER, R. 2007. Richness and distribution of sponge megabenthos in continental margin canyons off southeastern Australia *Marine Ecological Progress Series,* 340**,** 73–88.

SCHLACHER, T. A., WILLIAMS, A., ALTHAUS, F. & SCHLACHER-HOENLINGER, M. A. 2010. High-resolution seabed imagery as a tool for biodiversity conservation planning on continental margins. *Marine Ecology,* 31**,** 200-221.

SCHNEIDERL, D. C., GAGNON, J. & GILKINSON, K. D. 1987. Patchiness of epibenthic megafauna on the outer Grand Banks of Newfoundland. *Marine Ecological Progress Series,* 39**,** 1-13.

SEED, R. 1996. Patterns of biodiversity in the macro-invertebrate fauna associated with mussel patches on rocky shores. *Journal of the Marine Biological Association (UK),* 76**,** 203-210.

SERRANO, A., GONZÁLEZ-IRUSTA, J., PUNZÓN, A., GARCÍA-ALEGRE, A., LOURIDO, A., RÍOS, P., BLANCO, M., BALLESTEROS, M., DRUET, M., CRISTOBO, J. & CARTES, J. 2017. Deep-sea benthic habitats modeling and mapping in a NE Atlantic seamount (Galicia Bank). *Deep Sea Research Part I: Oceanographic Research Papers,* 126**,** 115-127.

SHEPARD, F. P. 1981. Submarine canyons: multiple causes and long-time persistence. *American Association of Petroleum Geologists Bulletin,* 65**,** 1062–1077.

SIGLER, M. F., ROOPER, C. N., HOFF, G. R., STONE, R. P., MCCONNAUGHEY, R. A. & WILDERBUER, T. K. 2015. Faunal features of submarine canyons on the eastern Bering Sea slope. *Marine Ecology Progress Series,* 526**,** 21-40.

SIMPSON, E. H. 1949. Measurement of Diversity. *Nature,* 163**,** 688-688.

SOETAERT, K., MOHN, C., RENGSTORF, A., GREHAN, A. & VAN OEVELEN, D. 2016. Ecosystem engineering creates a direct nutritional link between 600-m deep cold-water coral mounds and surface productivity. *Scientific Reports,* 6**,** 35057.

SOUTHWARD, A. J., HAWKINS, S. J. & BURROWS, M. T. 1995. Seventy Years' observations of changes in distribution and abundance of zooplankton and intertidal organisms in the Western English Chaennel in relation to rising sea temperature. *Journal of thermal biology,* 20**,** 127-155.

STEIN, A., GERSTNER, K. & KREFT, H. 2014. Environmental heterogeneity as a universal driver of species richness across taxa, biomes and spatial scales. *Ecological Letters,* 17**,** 866-80.

STEVENSON, A., MITCHELL, F., J,G, & DAVIES, J., S ., 2015. Predation has no competition: factors influencing space and resource use by echinoids in deep-sea coral habitats, as evidenced by continuous video transects. *Marine Ecology - An Evolutionary Perspective,* 36**,** 1454–1467.

STEWART, H. A., DAVIES, J. S., GUINAN, J. & HOWELL, K. L. 2014. The Dangeard and Explorer canyons, South Western Approaches UK: Geology, sedimentology and newly discovered cold-water coral mini-mounds. *Deep Sea Research Part II: Topical Studies in Oceanography,* 104**,** 230-244.

STEWART, H. A. & GAFEIRA, J. 2016. Quantitative analysis of mini-mounds from the Explorer and Dangeard canyons area: an automated approach [Poster] In. *Marine Geological and Biological Habitat Mapping (GeoHab) 15th International Symposium, Winchester, UK, 2-6 May 2016,* British Geological Survey.

STROUD, J. T., BUSH, M. R., LADD, M. C., NOWICKI, R. J., SHANTZ, A. A. & SWEATMAN, J. 2015. Is a community still a community? Reviewing definitions of key terms in community ecology. *Ecology and Evolution,* 5**,** 4757-65.

STUART-SMITH, R. D., EDGAR, G. J. & BATES, A. E. 2017. Thermal limits to the geographic distributions of shallow-water marine species. *Nat Ecol Evol,* 1**,** 1846-1852.

STUART, C. T. & REX, M. A. 2009. Bathymetric patterns of deep-sea gastropod species diversity in 10 basins of the Atlantic Ocean and Norwegian Sea. *Marine Ecology,* 30**,** 164-180.

TANIGUCHI, H., NAKANO, S. & TOKESHI, M. 2003. Influences of habitat complexity on the diversity and abundance of epiphytic invertebrates on plants. *Freshwater Biology,* 48**,** 718–728.

TEWS, J., BROSE, U., GRIMM, V., TIELBÖRGER, K., WICHMANN, M., SCHWAGER, M. & JELTSCH, F. 2004. Animal species diversity driven by habitat heterogeneity/diversity: The importance of keystone structures. *Journal of Biogeography,* 31**,** 79-92.

THIEM, Ø., RAVAGNAN, E., FOSSÅ, J. H. & BERNTSEN, J. 2006. Food supply mechanisms for cold-water corals along a continental shelf edge. *Journal of Marine Systems,* 60**,** 207-219.

THISTLE, D. 2003. The deep-sea floor: an overview, in: Ecosystems of the World. *Elsevier***,** 5–39.

THOMSEN, L. & GUST, G. 2000. Sediment erosion thresholds and characteristics of resuspended aggregates on the western European continental margin. *Deep Sea Research Part I: Oceanographic Research Papers,* 47**,** 1881-1897.

TIETJEN, J. H. 1971. Ecology and distribution of deep-sea meiobenthos off North Carolina. *Deep Sea Research and Oceanographic Abstracts,* 18**,** 941-944.

TURNER, J. A., HITCHIN, R., VERLING, E. & VAN REIN, H. 2006. NMBQAC Epibiota Remote Monitoring from Digital Imagery: Interpretation Guidelines. *JNCC Technical report*.

TURNEWITSCH, R., DUMONT, M., KIRIAKOULAKIS, K., LEGG, S., MOHN, C., PEINE, F. & WOLFF, G. 2016. Tidal influence on particulate organic carbon export fluxes around a tall seamount. *Progress in Oceanography,* 149**,** 189-213.

UNGA 2006. United Nations General Assembly. Sustainable fisheries, including through the 1995 agreement for the implementation of the provisions of the United Nations convention on the law of the sea of 10 December 1982 relating to the conservation and management of straddling fish stocks and highly migratory fish stocks, and related instruments. New York: UNGA.

VALLS, M. 2017. Trophic Ecology in Marine Ecosystems from the Balearis Sea (Western Mediterranean). *PHD Thesis***,** 1-198.

VAN AKEN, H. 2000. The hydrography of the mid-latitude Northeast Atlantic Ocean II: The intermediate water masses. *Deep-Sea Research Part I: Oceanographic Research Papers*.

VAN DEN BELD, I. M. J., BOURILLET, J.-F., ARNAUD-HAOND, S., DE CHAMBURE, L., DAVIES, J. S., GUILLAUMONT, B., OLU, K. & MENOT, L. 2017. Cold-Water Coral Habitats in Submarine Canyons of the Bay of Biscay. *Frontiers in Marine Science,* 4.

VAN DEN HOEK, C. 1982. The distribution of benthic marine algae in relation to the temperature regulation of their life histories. *Biological Journal of the Linnean Society,* 18**,** 81-144.

VAN HAREN, H., HANZ, U., DE STIGTER, H., MIENIS, F. & DUINEVELD, G. 2017. Internal wave turbulence at a biologically rich Mid-Atlantic seamount. *PLoS One,* 12**,** e0189720.

VAN OEVELEN, D., MUELLER, C., E., LUNDÄLV, T. & MIDDELBURG, J., J. 2016. Food selectivity and processing by the cold-water coral Lophelia pertusa. *Biogeosciences,* 13**,** 5789-5798.

VAN ROOIJ, D., IGLESIAS, J., HERNÁNDEZ-MOLINA, F. J., ERCILLA, G., GOMEZ-BALLESTEROS, M., CASAS, D., LLAVE, E., DE HAUWERE, A., GARCIA-GIL, S., ACOSTA, J. & HENRIET, J. P. 2010. The Le Danois Contourite Depositional System: Interactions between the Mediterranean Outflow Water and the upper Cantabrian slope (North Iberian margin). *Marine Geology,* 274**,** 1-20.

VASSEUR, D., A., DELONG, J., P. , GILBERT, B., GREIG, H., S. , HARLEY, C., G. , MCCANN, K., S., SAVAGE, V., TUNNEY, T., D. & O'CONNOR, M., I. 2014. Increased temperature variation poses a greater risk to species than climate warming. *Proceedings of The Royal Society B,* 281**,** 20132612.

VERDONSCHOT, R. C. M., DIDDEREN, K. & VERDONSCHOT, P. F. M. 2012. Importance of habitat structure as a determinant of the taxonomic and functional composition of lentic macroinvertebrate assemblages. *Limnologica,* 42**,** 31-42.

VERFAILLIE, E., DEGRAER, S., SCHELFAUT, K., WILLEMS, W. & VAN LANCKER, V. 2009. A protocol for classifying ecologically relevant marine zones, a statistical approach. *Estuarine, Coastal and Shelf Science,* 83**,** 175-185.

VETTER, E. W. & DRAYTON, P. K. 1998 Macrofaunal communities within and adjacent to a detritus-rich submarine canyon system. *Deep-Sea Research II:Topical Studies in Oceanography,* 45**,** 25—54.

VETTER, E. W., SMITH, C. R. & DE LEO, F. C. 2010. Hawaiian hotspots: enhanced megafaunal abundance and diversity in submarine canyons on the oceanic islands of Hawaii. *Marine Ecology,* 31**,** 183-199.

VICTORERO, L., ROBERT, K., ROBINSON, L., TAYLOR, M. & HUVENNE, V. 2018. Species replacement dominates megabenthos beta diversity in a remote seamount setting. *Scientific Reports,* 8**,** 4152.

VLASENKO, V., STASHCHUK, N., INALL, M., E.,, PORTER, M. & ALEYNIK, D. 2016. Focusing of baroclinic tidal energy in a canyon. *Journal of Geophysical Research: Oceans,* 121**,** 2824–2840,.

WALBRIDGE, S., SLOCUM, N., POBUDA, M. & WRIGHT, D. 2018. Unified Geomorphological Analysis Workflows with Benthic Terrain Modeler. *Geosciences (Switzerland),* 8.

WANG, Y. H., LEE, I. H. & LIU, J. T. 2008. Observation of internal tidal currents in the Kaoping Canyon off southwestern Taiwan. *Estuarine, Coastal and Shelf Science,* 80**,** 153-160.

WARFE, D. M., BARMUTA, L. A. & WOTHERSPOON, S. 2008. Quantifying habitat structure: surface convolution and living space for species in complex environments. *Oikos,* 117**,** 1764-1773.

WARWICK, R. M. & DAVIES , J. R. 1977. The Distribution of Sublittoral Macrofauna Communities in the Bristol Channel in Relation to the Substrate. *Estuarine and Coastal Marine Science* 5**,** 267-288.

WATLING, L., GUINOTTE, J., CLARK, M. R. & SMITH, C. R. 2013. A proposed biogeography of the deep ocean floor. *Progress in Oceanography,* 111**,** 91-112.

WEI, C. L., ROWE, G. T., HUBBARD, G. F., SCHELTEMA, A. H., WILSON, G. D. F., PETRESCU, I., FOSTER, J. M., WICKSTEN, M. K., CHEN, M., DAVENPORT, R., SOLIMAN, Y. & WANG, Y. 2010. Bathymetric zonation of deep-sea macrofauna in relation to export of surface phytoplankton production. *Marine Ecology Progress Series,* 399**,** 1-14.

WEINBAUERA, M. & VELIMIROV, B. 1996. Population Dynamics and Overgrowth of the Sea Fan Eunicella cavolini (Coelenterata: Octocorallia). *Estuarine, Coastal and Shelf Science,* 42**,** 583–595.

WHEELER, A. J., BEYER, A., FREIWALD, A., DE HAAS, H., HUVENNE, V. A. I., KOZACHENKO, M., OLU-LE ROY, K. & OPDERBECKE, J. 2006. Morphology and environment of cold-water coral carbonate mounds on the NW European margin. *International Journal of Earth Sciences,* 96**,** 37-56.

WHITE, M., BASHMACHNIKOV, I., ARÍSTEGUI, J. & MARTINS, A. 2007. Physical Processes and Seamount Productivity. *Seamounts: Ecology, Fisheries and Conservation*.

WHITE, M. & DORSCHEL, B. 2010. The importance of the permanent thermocline to the cold water coral carbonate mound distribution in the NE Atlantic. *Earth and Planetary Science Letters,* 296**,** 395-402.

WHITE, M., MOHN, C., DE STIGTER, H. & MOTTRAM , G. 2005. Deep-water coral development as a function of hydrodynamics and surface productivity around the submarine banks of the Rockall Trough, NE Atlantic. *Cold-Water Corals and Ecosystems***,** 503-514.

WILLIS, S. C., WINEMILLER, K. O. & LOPEZ-FERNANDEZ, H. 2005. Habitat structural complexity and morphological diversity of fish assemblages in a Neotropical floodplain river. *Oecologia,* 142**,** 284-95.

WILSON, A., KIRIAKOULAKIS, K., RAINE, R., GERRITSEN, H., BLACKBIRD, S., ALLCOCK, A. & WHITE, M. 2015a. Anthropogenic influence on sediment transport in the Whittard Canyon, NE Atlantic. *Marine pollution bulletin,* 101.

WILSON, A. M., RAINE, R., MOHN, C. & WHITE, M. 2015b. Nepheloid layer distribution in the Whittard Canyon, NE Atlantic Margin. *Marine Geology,* 367**,** 130-142.

WILSON, G. D. F. 1999. Some of the deep-sea fauna is ancient. *Crustaceana,* 72**,** 1019-1030.

WILSON, M. F. J., O'CONNELL, B., BROWN, C., GUINAN, J. C. & GREHAN, A. J. 2007. Multiscale Terrain Analysis of Multibeam Bathymetry Data for Habitat Mapping on the Continental Slope. *Marine Geodesy,* 30**,** 3-35.

WRIGHT 2005. Survey Data Analysis for Hemptons Turbot Bank.

WUNSCH, C. 1975. Internal Tides in the Ocean. *Reviews of Geophysics and Space Physics,* 13**,** 167-182.

WYNN, R. B., HUVENNE, V. A. I., LE BAS, T. P., MURTON, B. J., CONNELLY, D. P., BETT, B. J., RUHL, H. A., MORRIS, K. J., PEAKALL, J., PARSONS, D. R., SUMNER, E. J., DARBY, S. E., DORRELL, R. M. & HUNT, J. E. 2014. Autonomous Underwater Vehicles (AUVs): Their past, present and future contributions to the advancement of marine geoscience. *Marine Geology,* 352**,** 451-468.

YANOVSKI, R., NELSON, P. A. & ABELSON, A. 2017. Structural Complexity in Coral Reefs: Examination of a Novel Evaluation Tool on Different Spatial Scales. *Frontiers in Ecology and Evolution,* 5.

YASUHARA, M. & DANOVARO, R. 2016. Temperature impacts on deep-sea biodiversity. *Biol Rev Camb Philos Soc,* 91**,** 275-87.

YOKLAVICH, M., GREENE, H., CAILLIET, G., SULLIVAN, D., LEA, R. & LOVE, M. 2000. Habitat associations of deep-water rockfishes in a submarine canyon: an example of a natural refuge. *Fishery Bulletin,* 98**,** 625-641.

ZARDUS, J. D., ETTER, R. J., CHASE, M. R., REX, M. A. & BOYLE, E. E. 2006. Bathymetric and geographic population structure in the pan-Atlantic deep-sea bivalve Deminucula atacellana (Schenck, 1939). *Mol Ecol,* 15**,** 639-51.

ZELADA LEON, A., HUVENNE, V. A. I., BENOIST, N. M. A., FERGUSON, M., BETT, B. J. & WYNN, R. B. 2020. Assessing the Repeatability of Automated Seafloor Classification Algorithms, with Application in Marine Protected Area Monitoring. *Remote Sensing,* 12**,** 1572.

ZEPPILLI, D., PUSCEDDU, A., TRINCARDI, F. & DANOVARO, R. 2016. Seafloor heterogeneity influences the biodiversity-ecosystem functioning relationships in the deep sea. *Sci Rep,* 6**,** 26352.

ZHANG, L., HUETTMANN, F., ZHANG, X., LIU, S., SUN, P., YU, Z. & MI, C. 2019. The use of classification and regression algorithms using the random forests method with presence-only data to model species' distribution. *MethodsX*, 6**,** 2281-2292.

ZUUR, A., IENO, E., WALKER, N., SAVELIEV, A. & SMITH, G. 2014a. Mixed effects models and extensions in ecology with R *Springer-Verlag New York*.

ZUUR, A., IENO, N. & ELPHICK, C. 2010. A protocol for data exploration to avoid common statistical problems. *Methods in Ecology and Evolution* 1**,** 3-14.

ZUUR, A., SAVELIEV, A. & IEN, E. 2014b. A beginner's Guide to Generalised Additive Mixed Models with R. *Highland Statistics Ltd*.